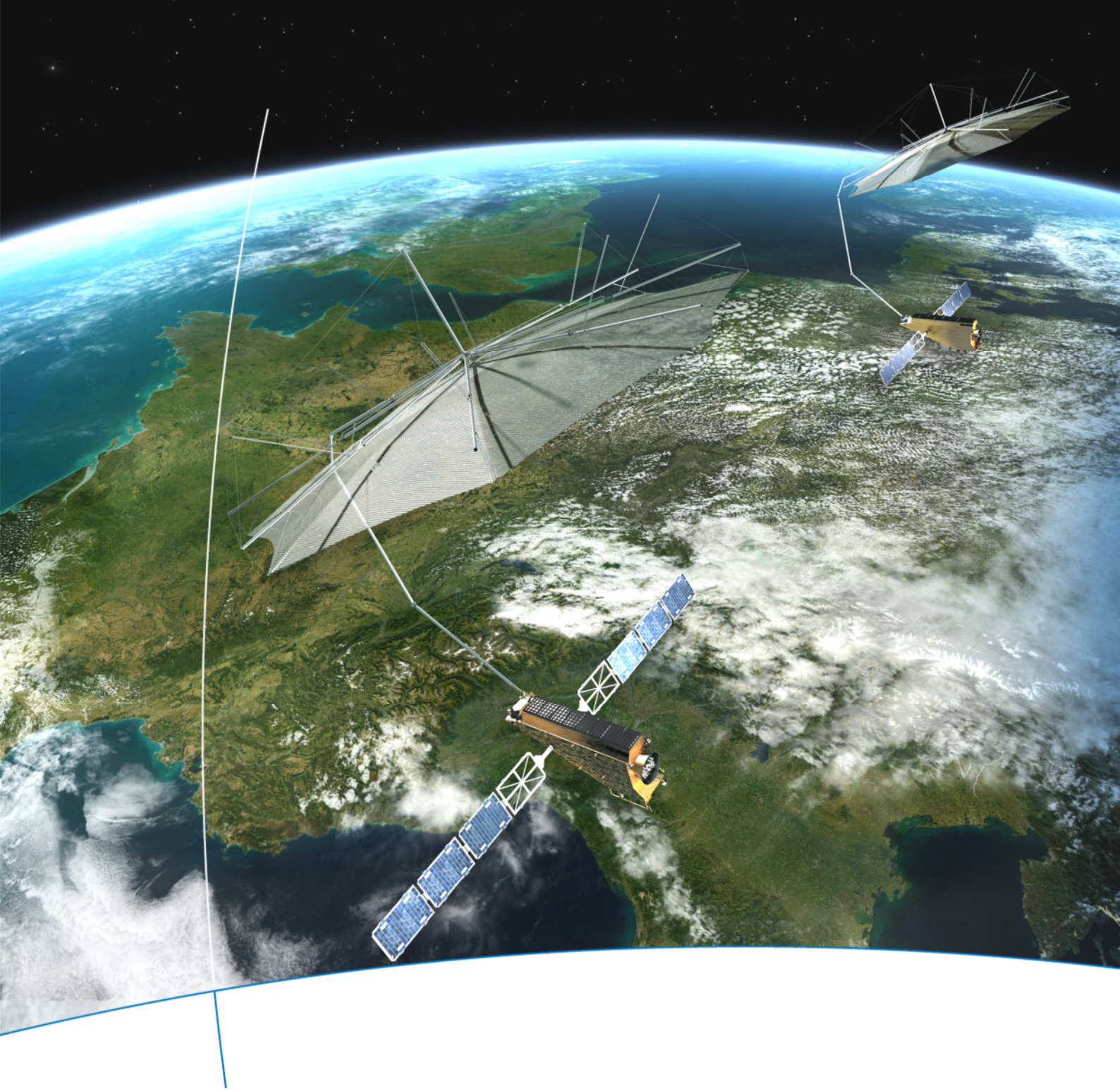

Research Results and Projects

Status Report 2011 - 2017

Microwaves and Radar Institute

DLR

German Aerospace Center
A member of the Helmholtz Association

Microwaves and Radar Institute

Director of the Institute Prof. Dr.-Ing. habil. Alberto Moreira

Address Oberpfaffenhofen
D-82234 Weßling
www.dlr.de/hr

Editorial Team A. Moreira
M. Zink
A. Reigber
Th. Neff
G. Krieger
K. Antesberger
M. Bachmann
J. Fischer
S. Middeler
R. Scheiber
E. Schreiber
M. Younis

Layout K. Antesberger

Printed by M & E Druckhaus
Weberstraße 7, 49191 Belm

October 2018

Images Cover page: Tandem-L satellite pair with 15-m deployable reflectors
Chapter 1 cover page: TanDEM-X digital elevation model of the Yamal peninsula, Russia
Chapter 2 cover page: TanDEM-X digital elevation model of Kalahari desert, Botswana
Chapter 2.1 cover page: TanDEM-X digital elevation model of the Atacama desert, Chile
Chapter 2.2 cover page: TanDEM-X digital elevation model of the Karakum desert, Turkmenistan
Chapter 2.3 cover page: F-SAR polarimetric X-band SAR image nearby Kaufbeuren, Germany
Chapter 2.4 cover page: Multi-temporal TerraSAR-X image of Munich
Chapter 3 cover page: TerraSAR-X image of a glacier in Antarctica

This document may be reprinted in whole or in part or otherwise
commercially used only with written permission from DLR.

Microwaves and Radar Institute

Status Report 2011 - 2017

Research Results and Projects

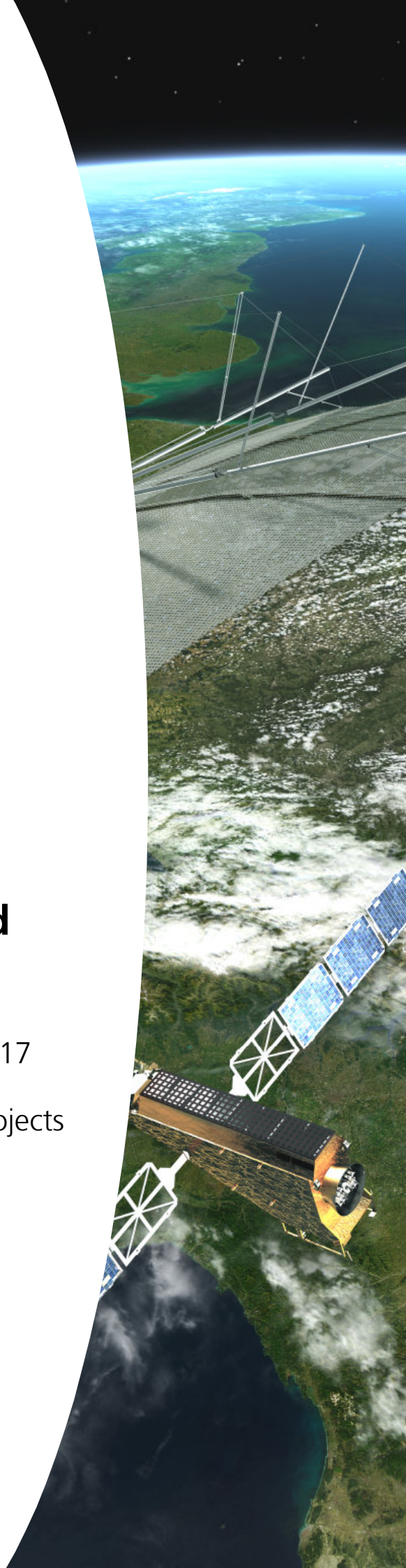

Preface

TanDEM-X has produced a new global topography of the Earth with unprecedented accuracy. We are proud to have initiated this challenging mission and to have made it a great success!

In the last decade we entered into a golden age for spaceborne synthetic aperture radar (SAR) systems with the number of satellites increasing in a quasi-exponential way. The reason for that is obvious: SAR data utilization and associated services are making a most important contribution in addressing societal challenges of global dimension since spaceborne SAR is the only sensor technology that is able to provide high-resolution images on a global scale independent of weather conditions and sun-light illumination. Due to a consistent radar technology program over more than four decades, Germany is playing today a leading role in SAR development worldwide. Our Institute participated and shaped this program from the very beginning with the project leadership and participation in the space shuttle missions Spacelab-1, SIR-C/X-SAR and SRTM. The golden age for the national radar program started, however, in 2006 and 2007 with the launch of the satellites SAR-Lupe and TerraSAR-X, respectively. At that time we started playing in the first league of the international arena of spaceborne SAR systems. Three years later, TanDEM-X was launched. Together with TerraSAR-X, it forms the first bistatic spaceborne SAR interferometer consisting of two satellites flying in close formation. The global digital elevation model of TanDEM-X became available in 2016 and surpassed all expectations. It has 99.9% coverage, 12-m posting, absolute height accuracy of approximately 1 m and a relative height error (standard deviation) of 0.8 m. This unique data set has been available since then for commercial and scientific applications. Besides the generation of a global digital elevation model, we could demonstrate a number of new imaging modes like bidirectional SAR and TOPS (Terrain Observation by Progressive Scans) as well as new technologies and techniques like digital beamforming and polarimetric SAR interferometry which play a key role for the conceptual design of the new generation of SAR systems. In 2017, we started new interferometric acquisitions with TanDEM-X to generate a global change layer which will register all the changes of the Earth topography occurred since the first acquisitions of TanDEM-X with unprecedented accuracy. The global change layer will be available by 2020.

Our Institute is very proud of TerraSAR-X and TanDEM-X. This year, these satellites commemorated 11 and 8 years of operation, respectively, and are still providing images with a superb quality: 0.35 dB absolute radiometric accuracy, a few decimeters geolocation accuracy without any reference points and an azimuth resolution as good as 20 cm by means of the new staring spotlight mode implemented in 2013. The vision of the mission TanDEM-X goes back to the beginning of the 90s, when we made the first demonstration of SAR interferometry in Europe with our airborne SAR. Holding the role of the leading principal investigator, the Institute submitted 2003 a proposal for the TanDEM-X mission to the national space administration in response to a call for Earth observation missions. Three years later we got the approval for realization and ten years later the generation of the global digital elevation model (DEM) was completed. It took about 20 years to get this vision realized. Working towards a vision is not easy; one needs not only to be able to forecast the future and move forward in the right direction, but also be able to shape the future by means of a solid strategy and with a highly motivated and competent team. When a vision becomes reality, it gives us a big piece of motivation to step into new challenges.

Europe took over the leadership role in Earth observation with the Copernicus program. Our Institute is participating in the complete series of the Sentinel-1 satellites, both as a partner in the industrial core team and in the scope of several studies and validation activities for ESA. It is also playing a major role in the radiometric and interferometric calibration and validation of Sentinel-1A/B data. Further, we are also involved in a number of studies for the Sentinel-1 next generation satellite as well as for the L-band extension in the scope of the Copernicus evolution program. Last but not least, we are delivering major contributions – both as a member of the industrial core team and as a member of the mission advisory group – for the ESA Earth Explorer mission BIOMASS, the first P-band SAR satellite to be launched in 2022. In the last years, we started a new research field in the Institute related to NewSpace SAR which uses disruptive technologies and concepts to drastically reduce the costs of spaceborne SAR. We foresee a fast development in this field and are providing innovative contributions with new multistatic concepts and applications which allow boosting the performance of low-cost NewSpace SAR systems in terms of image quality, resolution and imaging capacity as well as to widen their field of applications.

One of the main assets of our Institute is the end-to-end system expertise in microwave systems. In this context two facilities are

of utmost importance to our staff in order to expand its system expertise and to keep a step ahead in the demonstration of new technologies and sensor concepts: F-SAR, our airborne SAR sensor, and TechLab, a center for high-tech microwave sensor development with several measurement facilities including a Compact Test Range. The F-SAR system has been most successfully operated since 2009 with 58 calibration and measurement campaigns undertaken since then, including a forest tomography campaign in Gabon, an ice tomography campaign in Greenland, and – most recently in 2018 – a campaign in Canada dedicated to the study of permafrost. F-SAR can operate in 5 frequency bands in a fully polarimetric mode and is a most flexible and modular system, able to demonstrate advanced techniques, technologies, and applications, as well as to simulate data and to develop innovative applications for future spaceborne SAR systems. Just to mention a few highlights, the first demonstration of polarimetric circular SAR imaging and of SAR holography for natural targets have been carried out in the last few years, and the first test flights of the new digital beamforming SAR with up to 12 receive channels, each featuring 1.8 GHz bandwidth, have been successfully performed. Furthermore, polarimetric SAR interferometry and SAR tomography became now fully operational imaging modes. Besides the F-SAR system, several other active and passive microwave sensors have been developed in the TechLab. One highlight has been an ultra-wideband polarimetric MIMO radar placed on the cargo bay of a truck which allows an improved detection of buried mines and even the detection of thin wires by means of tomographic 3-D imaging.

Let us now take a look into the future. The Institute has initiated the Tandem-L proposal which is a highly innovative radar mission that enables the systematic and global monitoring of dynamic processes on the Earth's surface with unprecedented quality and resolution. Tandem-L will answer key scientific questions about the biosphere, geosphere, hydrosphere and cryosphere and will close essential gaps in climate research. Besides the scientific component, Tandem-L is distinguished by its high degree of innovation with respect to methodology (e.g., polarimetric SAR interferometry and coherence tomography) and technology (e.g., digital beamforming in combination with a large deployable reflector). The science and data utilization of Tandem-L is being prepared in the framework of the Helmholtz Alliance "Remote Sensing and Earth System Dynamics" which was initiated in 2012. In total, it includes 140 scientists from eight Helmholtz centers, Max Planck and Leibniz Institutes, as well as other national and international universities, organizations and research institutes. The Helmholtz Alliance is unique with its composition covering a comprehensive research spectrum in four Earth spheres.

As part of a review process of Tandem-L, the German Science Council evaluation report was published mid-2017 with the following statement: "The imaging technology in Tandem-L is expected to yield innovative geoinformation products and services, which can lay the foundation for future national and international observation and continuous monitoring of the Earth System and its changes." We have been working towards this vision with great enthusiasm and a great deal of innovation. Our Institute's staff is predestined to shape the future of synthetic aperture radar.

I wish you an enjoyable reading of this report.

Oberpfaffenhofen, October 2018

Prof. Dr.-Ing. habil. Alberto Moreira

Director
DLR Microwaves and Radar Institute (DLR-HR)

Professor
Karlsruhe Institute of Technology (KIT-IHE)

Table of Contents

1 Overview

2 Research and Project Results

2.1 Spaceborne SAR Missions

2.2 Microwave Systems and Techniques

2.3 Airborne SAR

2.4 Reconnaissance and Security

3 Documentation

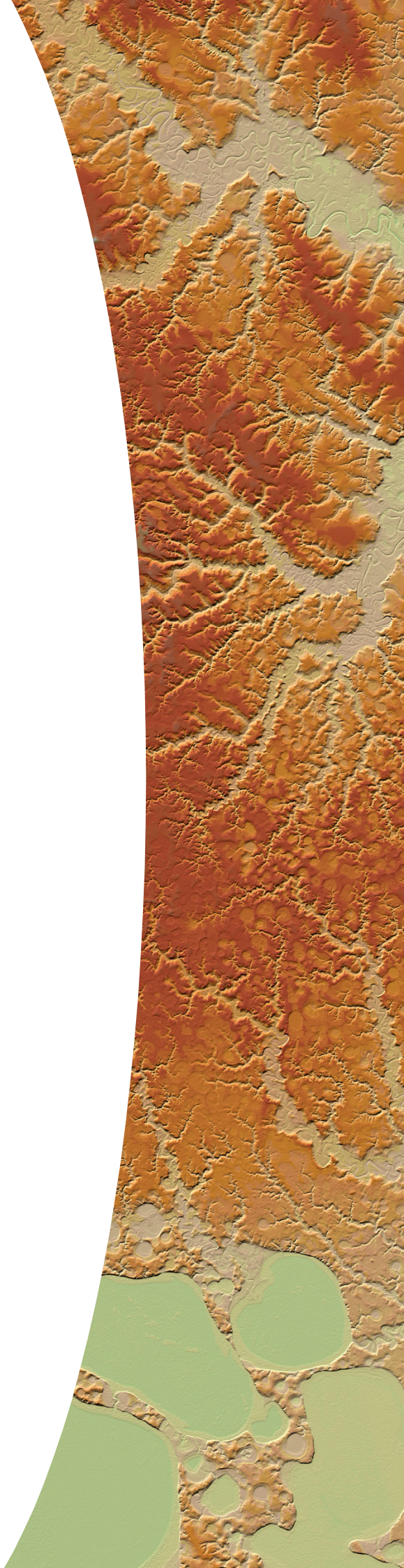

1 Overview

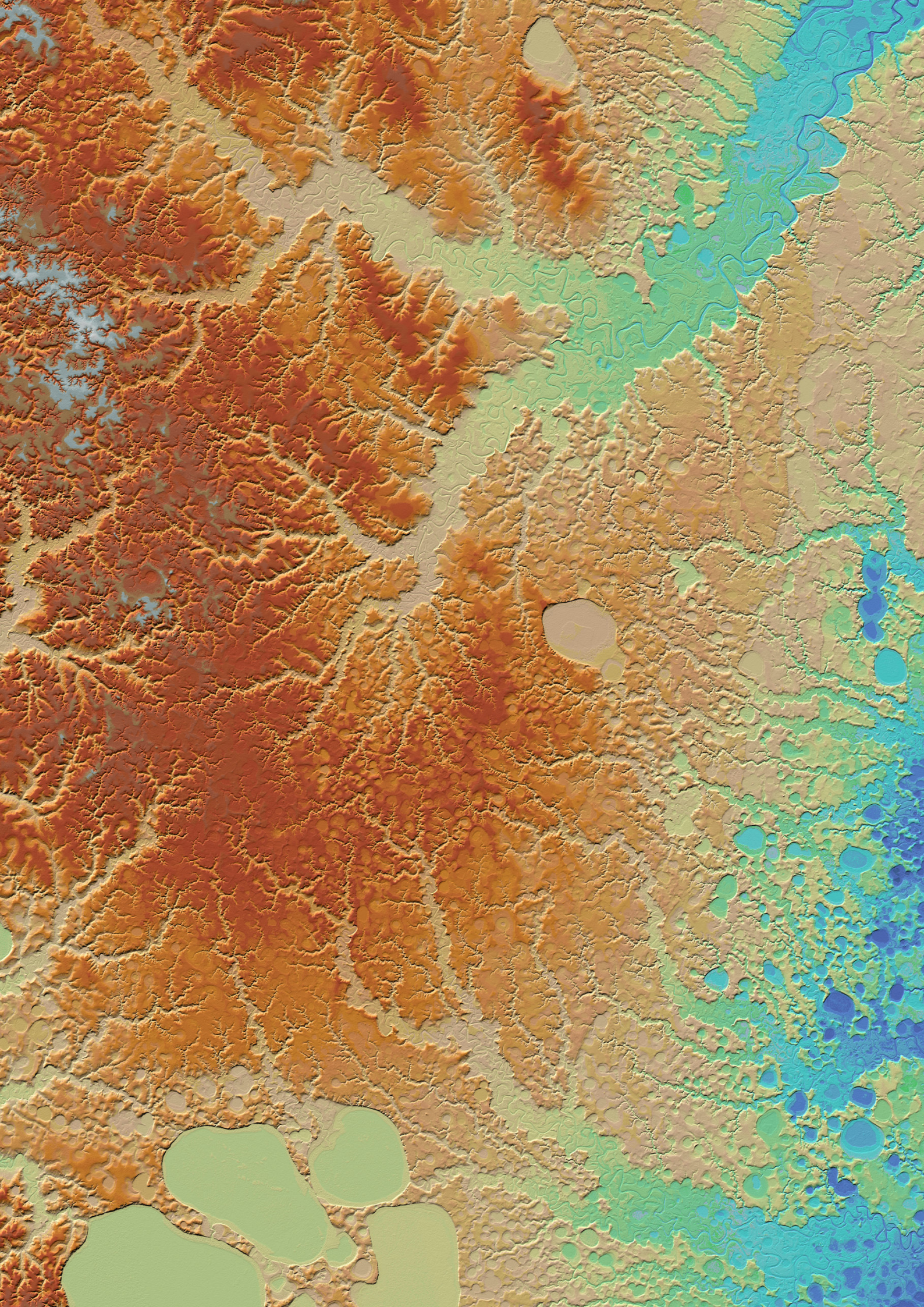

1. Overview

This report has been prepared for the evaluation of the Microwaves and Radar Institute (HR) of the German Aerospace Center (DLR). It summarizes the research activities and projects in the timeframe between 2011 and 2017. The Institute is located in Oberpfaffenhofen near Munich and has a long history dating back to the beginning of the last century. Today, the Institute focuses its research on active and passive microwave techniques, sensors and applications related to remote sensing, environmental monitoring, reconnaissance and surveillance, as well as road and maritime traffic monitoring. The Institute has about 160 researchers, engineers, technicians, and students and is the driving force for the synthetic aperture radar (SAR) activities at DLR. It is a leading institution in SAR remote sensing in Europe and worldwide.

1.1 Institute's Mission and Profile

With its know-how and expertise in passive and active microwave remote sensing, the Microwaves and Radar Institute contributes to the development and advancement of ground-based, airborne, and spaceborne sensors.
The focus of its research work is on the conception and development of innovative synthetic aperture radar (SAR) techniques and systems, as well as new sensor-specific applications for remote sensing of the Earth. By means of these research and engineering activities – and in particular with the conceptual design and participation in the development, instrument operation, and data exploitation of spaceborne SAR systems – our Institute's aim is to provide an essential contribution to existing and future SAR missions towards the vision of a radar observatory in space for continuous monitoring of the Earth surface. Spaceborne SAR is unique in addressing societal challenges of global dimension since it is the only sensor technology able to provide high-resolution imagery on a global scale independent of weather conditions and day-light illumination.
The Institute's strength is the execution of long-term research programs with applications in remote sensing, aeronautics, and traffic monitoring, as well as reconnaissance and security. In line with the German space program, the Institute works in close collaboration with several DLR institutes, the German Space Administration, the European Space Agency, German and European space industry, responsible ministries, and with several international research organizations and universities. The education of young scientists in the form of internships, as well as diploma and doctoral theses, is also an important part of the Institute's mission.

Institute's Expertise

The Institute's expertise encompasses the whole end-to-end system know-how in microwave remote sensing. This allows us to play a key role in the conception and specification of new sensors, including the development of new technologies, algorithms, and applications. In more than 40 years, a wide experience in overall system competence, reaching from the sensor and mission conception to sensor-related applications and information retrieval, has been established and is being actively maintained and expanded.
In the last 15 years, the Institute has provided major contributions to several SAR missions and research programs that are decisive for its long-term strategy. Important examples are TerraSAR-X, TanDEM-X, ALOS-1 and ALOS-2 (calibration and member of the Carbon & Kyoto science team), Sentinel-1A/B, and SAR-Lupe. It is also working on future remote sensing and reconnaissance systems, such as Tandem-L, HRWS (next generation X-band SAR with high-resolution wide-swath imaging capabilities and 3 passive satellites), Sentinel-1C/D, BIOMASS, Kompsat-6, and SARah (SAR-Lupe follow-on program). These projects are accompanied by research programs that ensure the Institute keeps a step ahead in the development of new research fields. Examples of such research programs are bistatic and multistatic SAR systems, signal processing, digital beamforming and MIMO, polarimetric SAR interferometry and tomography, information retrieval from multi-dimensional SAR data, calibration, radar signatures, propagation, antennas, metamaterials, as well as radiometry and imaging techniques for security-related applications. Since three years, we are also actively involved in a small SAR satellite program, exploring the advantages of the NewSpace activities in the commercial sector.

Figure 1.1-1 Microwaves and Radar Institute: main building (left) and TechLab (middle and right)

Figure 1.1-2 Employees of the Microwaves and Radar Institute (picture was taken at the courtyard of the main Institute's building in July 2018).

1.2 Organization

The Institute is composed of four research departments working in well-established research programs, projects, and external contracts. Figure 1.2-1 shows the organization chart with its research departments and a central unit which is responsible for the technical and scientific infrastructure activities. The Institute has about 165 employees, comprising scientists, engineers, technicians, support personnel, as well as internship, diploma and doctoral students, and guest scientists.

Three departments are mainly working on Earth observation and one on reconnaissance and security, including dual-use applications. The SAR Technology department is responsible for the development of the airborne SAR system F-SAR and its extension DBFSAR, and contributes to the spaceborne SAR projects with airborne campaigns to simulate new data products, validate and cross-calibrate the satellite data and demonstrate new techniques.

The Satellite SAR Systems department and the Radar Concepts department are engaged in spaceborne SAR missions. While pre-phase A and phase A studies are led by the Radar Concepts department, which is developing new sensor concepts and techniques for future radar systems, the Satellite SAR Systems department takes over the project leadership in phase B, or at the latest when a project is approved for realization. The Satellite SAR Systems department is also responsible for operation, performance monitoring and calibration of the radar

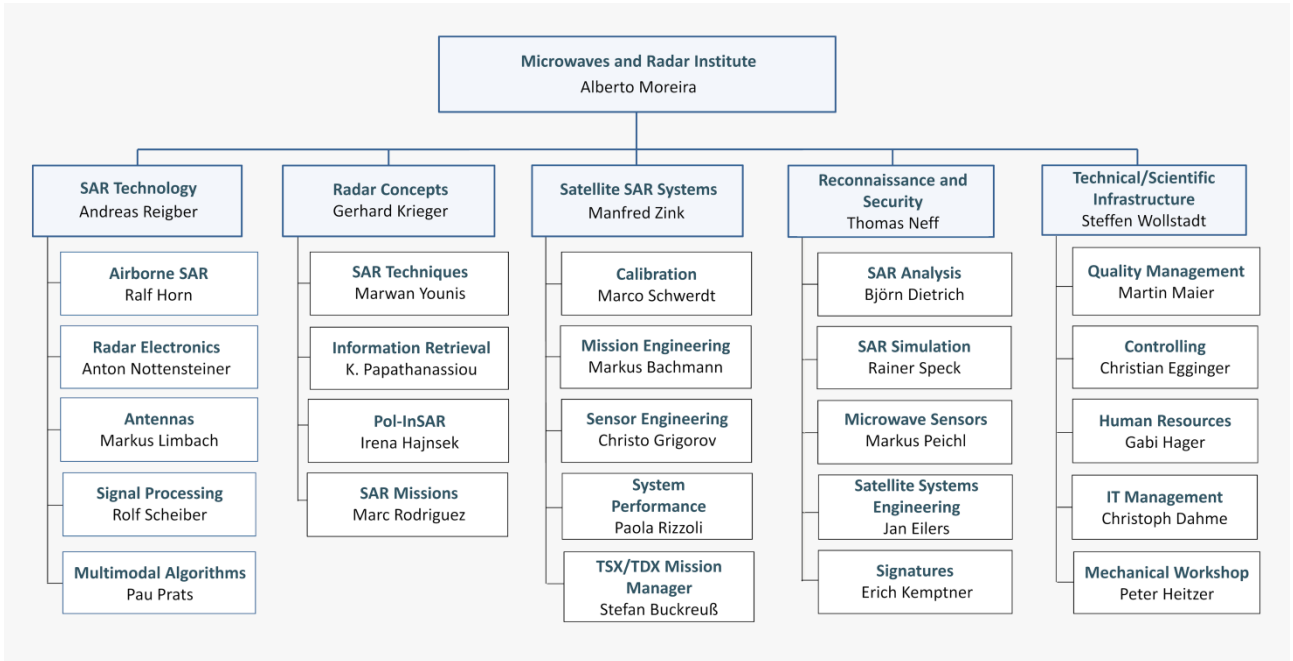

Figure 1.2-1 Organization of the Microwaves and Radar Institute with 4 research departments and a central unit for technical and scientific infrastructure support (October 2018).

Department	Competence	Research fields
SAR Technology	Airborne SAR	Airborne synthetic aperture radar technology and development, antennas, multimodal air- and spaceborne SAR signal processing, airborne campaigns for demonstration of new technologies, techniques, and applications
Radar Concepts	New radar concepts and techniques	New sensor concepts, spaceborne SAR mission conceptual design, digital beamforming, bistatic and multistatic systems, traffic monitoring with radar, and information retrieval
Satellite SAR Systems	Spaceborne SAR missions	Spaceborne SAR techniques, system concepts, SAR missions and instrument operations, system engineering and performance, calibration, SAR mission project leadership, and management
Reconnaissance and Security	Microwave sensors for reconnaissance and security applications	SAR data and mission simulation, mission planning, analysis and optimization, inverse SAR, radiometry, signatures, and synthetic aperture radiometry

Table 1.2-1 Institute's departments and their respective competence and research fields

instruments. For military spaceborne SAR activities, all major projects and activities are concentrated in the Reconnaissance and Security department. The Institute's expertise in passive microwave systems is also part of this department, as most of the passive microwave projects are presently related to security applications. The mechanical workshop is assigned to the central unit, as it supports the research projects of all departments.

Table 1.2-1 summarizes the expertise of each department in the Institute. Today, about 70 percent of the Institute's activities are concentrated on external contracts or DLR internal projects.

For many years, the Institute has established a matrix structure to allow the use of the expertise and personnel from different departments for the execution of large projects and research activities. The TerraSAR-X, TanDEM-X, and Tandem-L projects are notable examples; the project leadership for the Institute's contributions is under the responsibility of the Satellite SAR Systems department. In this department, approximately 60% of the personnel is allocated to these projects, including the project lead and mission manager; the remaining 40% is coming from two other departments in the Institute.

The Institute closely works with three other DLR institutes at Oberpfaffenhofen, especially within the framework of the SAR satellite projects: German Space Operations Center (GSOC), German Remote Sensing Data Center (DFD), and Remote Sensing Technology Institute (IMF). Airborne SAR campaigns are planned and conducted in close collaboration with DLR's Flight Operations (FX) facility.

The directorship of the Institute is linked to a full professorship at the Karlsruhe Institute of Technology (KIT), Institute of Radio Frequency Engineering and Electronics (IHE). Several joint projects have being carried out in cooperation with KIT-IHE in the fields of digital beamforming, calibration transponders for TerraSAR-X, and antenna development. With a new professorship being established in 2017, we want to reinforce the link to KIT-IHE by means of the research focused on small multichannel UAV radar systems. In total, 11 scientists of the Institute are engaged with regular lectures at universities; four of them have a joint professorship position with our Institute while two further professorship appointments are underway and should be established in the course of 2019. With these lecture activities, tutorials and short courses, as well as the hosting of internships, diploma and doctoral theses, the Institute enhances its cooperation with universities every year.

1.3 Large-Scale Facilities

The Institute owns a number of large-scale facilities to support its research activities in microwave sensor development and associated technologies. These facilities are essential to expand its know-how and expertise in microwave systems and techniques, to develop and demonstrate new microwaves technologies, concepts and applications, and to assist a number of internal and external projects. The operational airborne SAR system, F-SAR, is fully reconfigurable in 5 frequency bands and provides fully polarimetric and interferometric data. Its main objective is to support the development of innovative SAR operational modes, the demonstration of novel techniques and new applications, as well as to perform preparatory experiments for future SAR satellite systems. The new airborne DBFSAR system has 12 channels for digital beamforming on receive.

Since 2009, all Institute's facilities and technological developments have been concentrated in a new building – TechLab – a center for advanced microwave sensor development with several laboratories and measurement facilities, hosting approx. 40 employees. The main facility is a Compact Test Range (CTR) for highly accurate antenna characterization, as well as for radar cross-section measurements. Further facilities are a microwave chamber for measuring monostatic and bistatic radar signatures of scaled target models, a facility for determining the dielectric properties of material samples and a pool of corner reflectors, ground receivers and transponders for spaceborne SAR calibration. Also included in the TechLab are several research laboratories, especially equipped for development, optimization, integration, testing and calibration of radar and radiometer systems.

The Institute operates in its main building a microwave mechanical laboratory for the design, development and manufacturing of microwave components, instruments and models, using numerically controlled machines. This laboratory also provides valuable consultancy to the researchers and developers for the specification and design of microwave instruments and experimental setups.

Figure 1.3-1 F-SAR sensor on-board the Dornier DO228-212 aircraft: at the hangar of DLR in Oberpfaffenhofen (left), starting for a flight measurement campaign (right).

F-SAR/DBFSAR

The F-SAR (Figure 1.3-1) is an advanced modular airborne SAR system, used for scientific flight campaigns and for researching new SAR imaging modes and applications. It has a fully polarimetric operation in X, C, S, L and P band, with the possibility for simultaneous data acquisition in multiple frequency bands, as well as single-pass polarimetric interferometric acquisitions in X and S band. It supports several innovative imaging modes such as tomography, circular SAR, holography and bistatic SAR and has high spatial resolution of up to 25 cm in both range and azimuth, and excellent signal-to-noise ratio and calibration accuracy. New developments are the 12-channel receive-only DBFSAR system with digital beamforming (under test, finalization planned for 2019), the polarimetric and interferometric Ka-band system (under development, completion planned for 2020) and the DuoLIM, a bistatic L-band system as a demonstrator for Tandem-L (under development, finalization planned for 2021).

TechLab

The TechLab (Figure 1.3-2) is a center for high-tech microwave and radar hardware development, including several laboratories and facilities for sensor development, integration and testing of airborne radar, radiometers, antennas and calibration devices. Besides the CTR (see below), research laboratories, an anechoic chamber for measuring radar signatures, facilities for determining the dielectric material properties and the spaceborne SAR calibration facility are bundled in the TechLab.

Compact Test Range

The CTR facility (Figure 1.3-3) consists of a microwave anechoic chamber (24 m x 11.7 m x 9.7 m) with a dual cylindrical reflector configuration for highly accurate antenna characterization and radar cross-section measurements. It has a far field condition for precise real-time measurements within a frequency range from 300 MHz to 100 GHz and a quiet zone diameter of up to 3.4 m.

Figure 1.3-2 TechLab building – a center for advanced hardware and microwave sensor development (left). Measurements of a calibration transponder (upper right), tests of the airborne SAR system (bottom right).

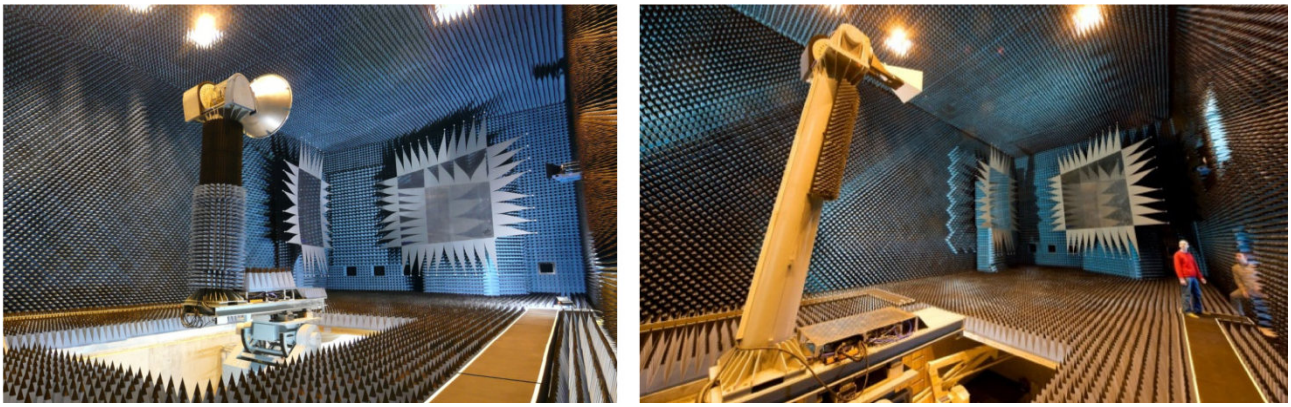

Figure 1.3-3 Compact Test Range (CTR) facility with a quiet zone of 3.4 m diameter

Figure 1.3-4 Calibration devices of the DLR calibration center: remote-controlled transponder in the laboratory (left) and deployed in the calibration field (center), and remote-controlled corner reflector (right) at one of the permanent sites within our calibration field covering a total area of 120 km x 40 km.

A six-axis positioner is used to handle devices under test of up to 300 kg. Advanced capabilities for control, post-processing and data analysis are available.

DLR SAR Calibration Center

The DLR SAR calibration center (Figure 1.3-4) is a facility for efficient and robust calibration – supporting extended field campaigns – for multimode SAR missions like TerraSAR-X, TanDEM-X or Sentinel-1A/B. It is well equipped with a large number of accurate passive and active reference targets and includes several analysis and evaluation tools based on precise algorithms. Within an area of 120 km x 40 km, 37 targets are deployed and maintained in South Germany at different sites. Six of these test sites are remotely controlled and operated from Oberpfaffenhofen.

Bistatic Signatures Chamber

The microwave anechoic chamber (8.5 m x 5.7 m x 5 m) (Figure 1.3-5) is used for measuring quasi monostatic and bistatic polarimetric radar signatures of canonical test objects as well as scaled target models operating in W band under stable temperature conditions.
The target is mounted on a turn table and aligned with high accuracy by using an optical camera and motor-controlled fine mechanical adjustment facilities. High-precision stepping motors rotate the turn table and the arm with the transmitting antenna. The facility is remotely controlled from a PC in a separate room, and data acquisition is automated.

Material Characterization Measurements

Material characterization setups (Figure 1.3-6) for free-space transmission and reflection measurements are operated at S, C, X, Ku, K, Ka, V and W band. Waveguide measurements are also provided for frequencies from 1.1 GHz up to 110 GHz. The materials that can be characterized include ceramic laminates, glasses, and special papers, mostly in the form of flat samples (plates). In addition to solid samples, also soft materials (e.g., powders, sand, fluids) can be characterized.

Mechanical Lab

The mechanical laboratory (Figure 1.3-7) is a highly specialized lab for design, development and manufacture of microwave components, instruments and models in machining and electroforming techniques, as well as mechanical drives, positioning systems and various racks and housings. Furthermore, 3-D printing capabilities and qualifications in adhesive technology and bonding techniques (European Adhesive Bonder and European Adhesive Specialist – EAS) are available. The mechanical lab is providing support and individual solutions to all research projects of the Institute and has dedicated knowledge for assembling hardware for DLR´s research aircraft DO228-212.

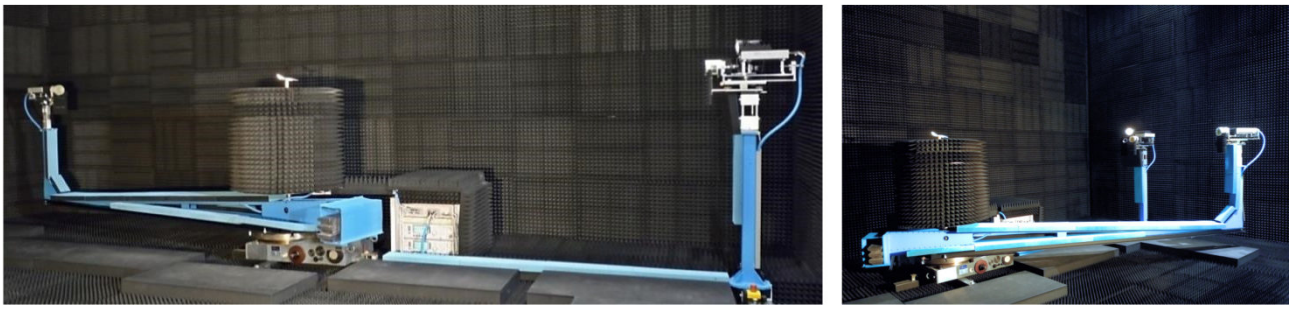

Figure 1.3-5 Microwave anechoic chamber for the measurement of monostatic and bistatic radar signatures

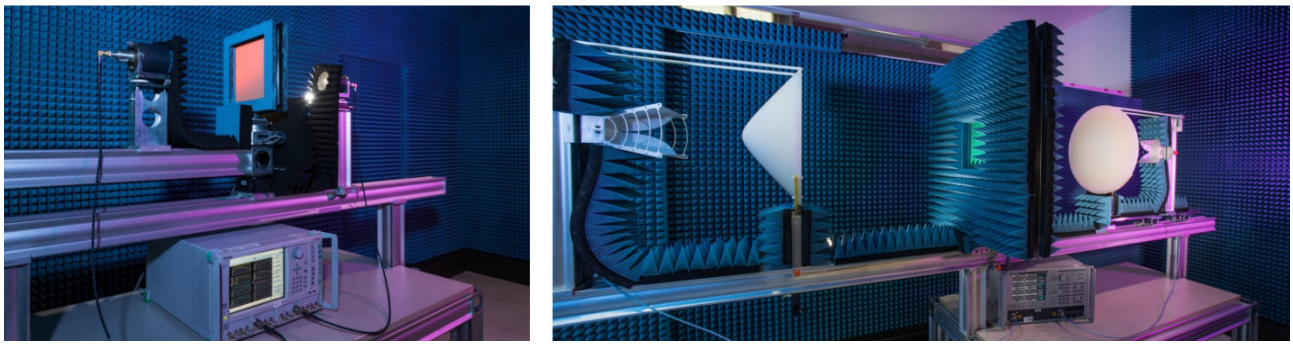

Figure 1.3-6 Material characterization setups for free-space transmission and reflection measurements

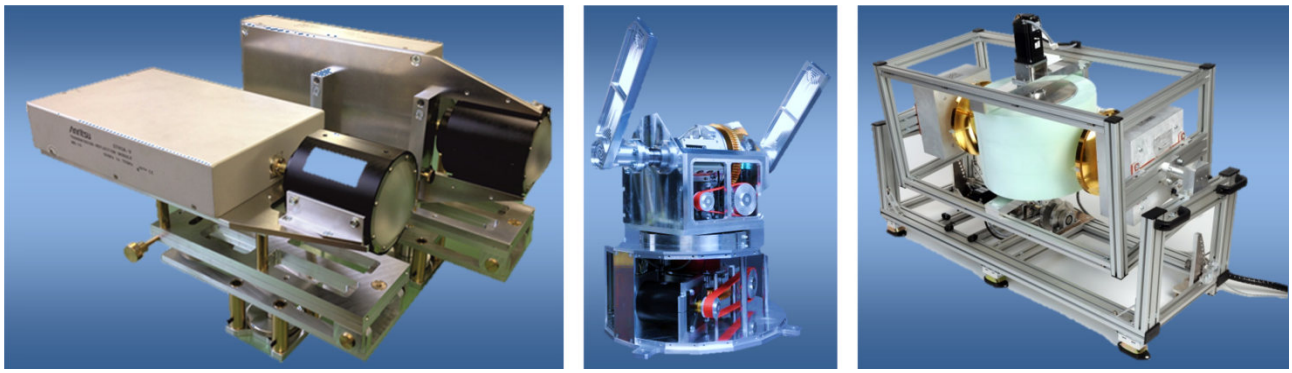

Figure 1.3-7 Developments at the Institute's mechanical laboratory: setup for material characteristics measurement in Ka band (left), transponder positioner for Sentinel-1 (middle), scanning radiometer SUMIRAD in W band (right).

1.4 Major Achievements

The last thirty years of the Institute were characterized by several highlights, particularly in the SAR field. The launches of TerraSAR-X and TanDEM-X in 2007 and 2010, respectively, marked the beginning of a new era for the national spaceborne radar program. The Institute has shaped this program since its beginning and aims at expanding its contributions in the scope of future missions both for the national and European program.

In the following summary, the major achievements and projects within the last seven years are summarized. Chapter 2 of this report complements this summary with a detailed description of the research activities and projects.

After more than 11 years in orbit, TerraSAR-X is still providing high-resolution SAR data of outstanding quality. Being well beyond its nominal life time of 5.5 years, the system is still fully operational without any performance degradation (Section 2.1.1). Due to the close involvement in the sensor development, the Institute established the required expertise to precisely calibrate the system and to fully exploit its capabilities, including the experimental demonstration of new imaging modes such as the TOPS mode. The staring spotlight mode, featuring 20 cm azimuth resolution and the wide ScanSAR mode, covering up to 260 km swath width, attracted such high interest, that they were implemented as new operational modes on the running in-orbit system. While investigating the staring spotlight mode, the bidirectional (BiDi) SAR mode has been invented. Azimuth patterns with steered lobes and an increased PRF are used to simultaneously acquire forward and backward looking images that can be used to detect fast moving objects or to infer ocean surface currents.

The geometric and radiometric accuracy of the TerraSAR-X image products is excellent: A localization accuracy of approximately 30 cm is achieved without the use of any tie points and a relative and absolute calibration accuracy of 0.2 and 0.35 dB, respectively, is guaranteed for all image products.

The focus of the spaceborne SAR activities since 2011 has been on the implementation of **TanDEM-X**, the first bistatic interferometer in space consisting of two satellites in close formation flight (Section 2.1.2). TanDEM-X is a truly innovative mission concept developed by the Institute. It has successfully achieved its primary mission objective, the generation of a global digital elevation model (DEM) with unprecedented accuracy. From the very beginning, we took the lead role in the mission design and development. Exemplary key achievements are the outstanding calibration of the interferometric system and radar synchronization link between both satellites, the implementation of a sophisticated data acquisition planning, including feedback loops from the DEM processing, and the monitoring and control of the final DEM performance (see also Figure 1.4-1 and Figure 1.4-2). Interferometric baselines at millimeter accuracy, synchronization between the two radar instruments at fractions of a picosecond, and precise characterization of differential internal delays enabled the generation of highly-accurate scene-based DEMs without the use of any external reference data. Residual errors in the order of a few meters were compensated in the final mosaicking step

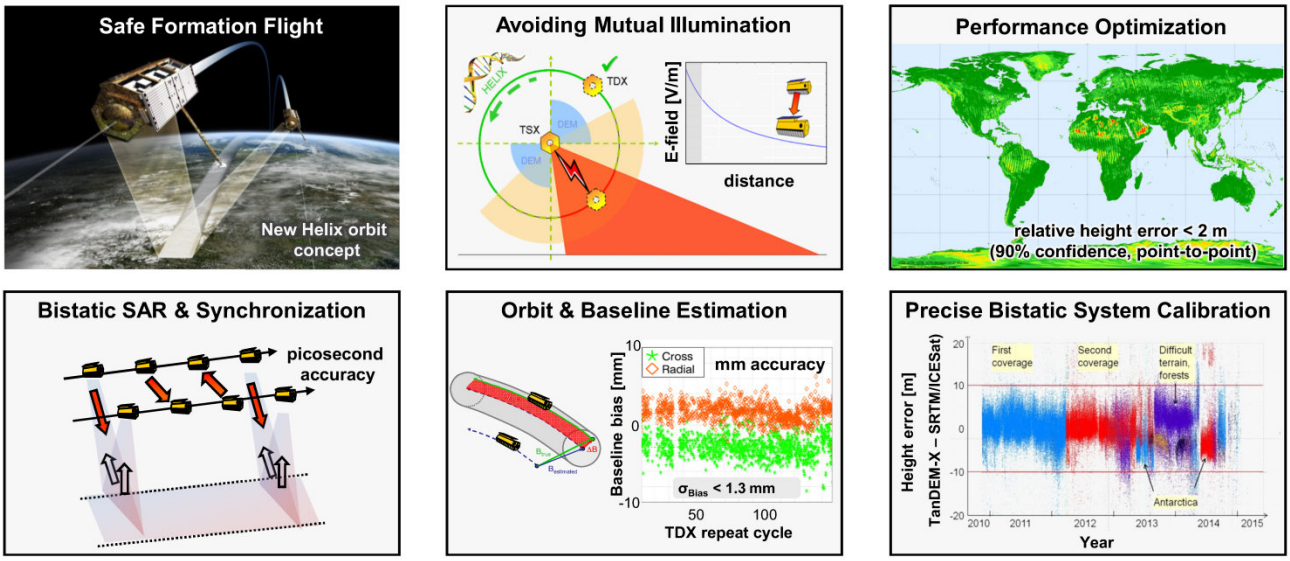

Figure 1.4-1 Key innovations of the TanDEM-X mission required for the generation of a high-resolution digital elevation model. Until 2016, 3000 Terabyte of data have been generated by the TanDEM-X mission, including the acquired radar raw data, intermediate interferometric and image products, as well as the final DEM data.

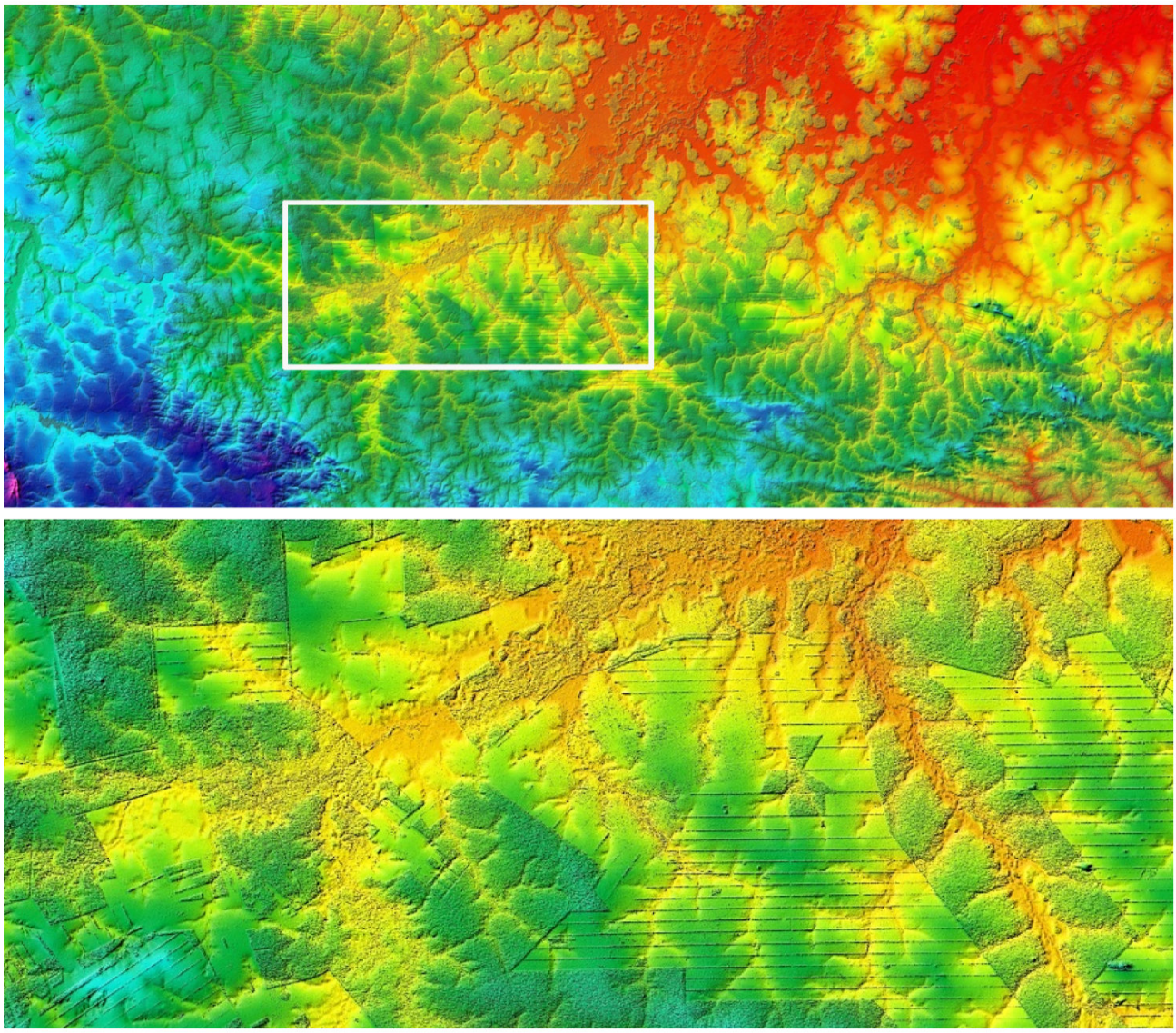

Figure 1.4-2 TanDEM-X DEM of the rain forest at the border between Brazil and Bolivia (top) and enlargement showing typical deforestation patterns (bottom). Topographic heights are shown in different colors.

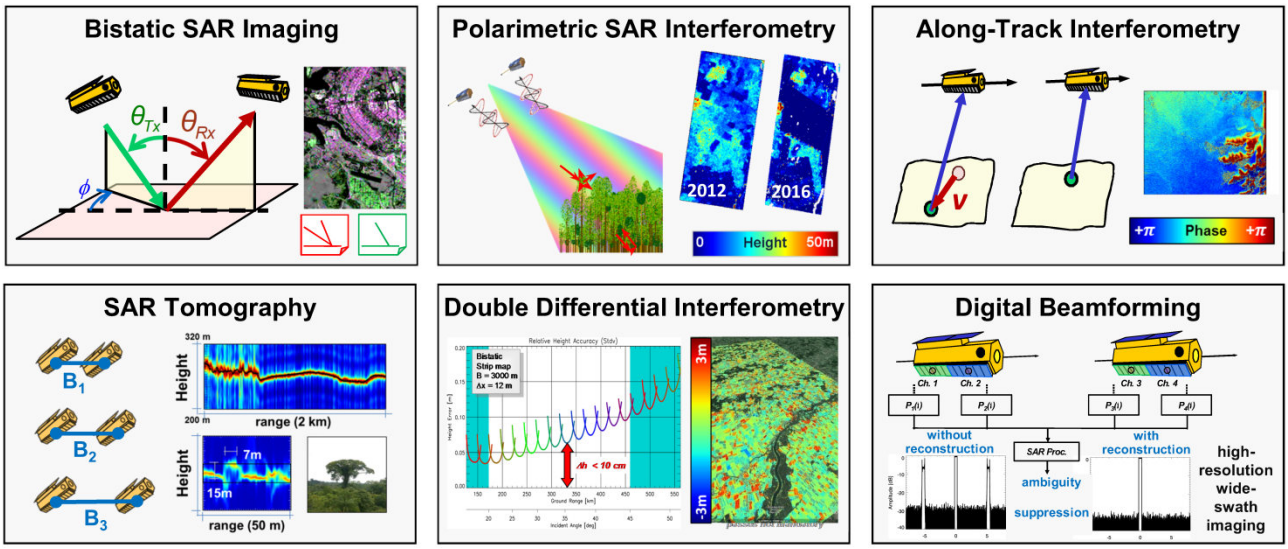

Figure 1.4-3 Examples of secondary objectives of the TanDEM-X mission with respect to the demonstration of new technologies and techniques for the next generation of spaceborne SAR systems

using ICESat laser altimeter heights. After more than four years of data acquisition the processing of the global TanDEM-X DEM was finished in September 2016. It is well within the specifications and in case of the 1 m absolute height error even one order of magnitude better than the required 10 m. Thanks to the continuously adapted acquisition program and dedicated data takes over mountains and deserts, the global DEM is also very complete with only about 0.1% of missing data. Beyond the primary mission objective, TanDEM-X has been used for numerous experiments demonstrating new SAR techniques such as digital beamforming, polarimetric SAR interferometry and along-track interferometry providing two-dimensional surface velocity estimation (see Figure 1.4-3 and Figure 1.4-4). Furthermore, the information of the volume decorrelation of all interferometric data takes has been used to generate a global forest map and to classify different ice facies in Greenland. Despite being well beyond their design lifetime, both satellites are still fully functional and have enough consumables for operation into the 2020s. After completion of the global DEM, it was agreed to continue the TanDEM-X mission as single-pass

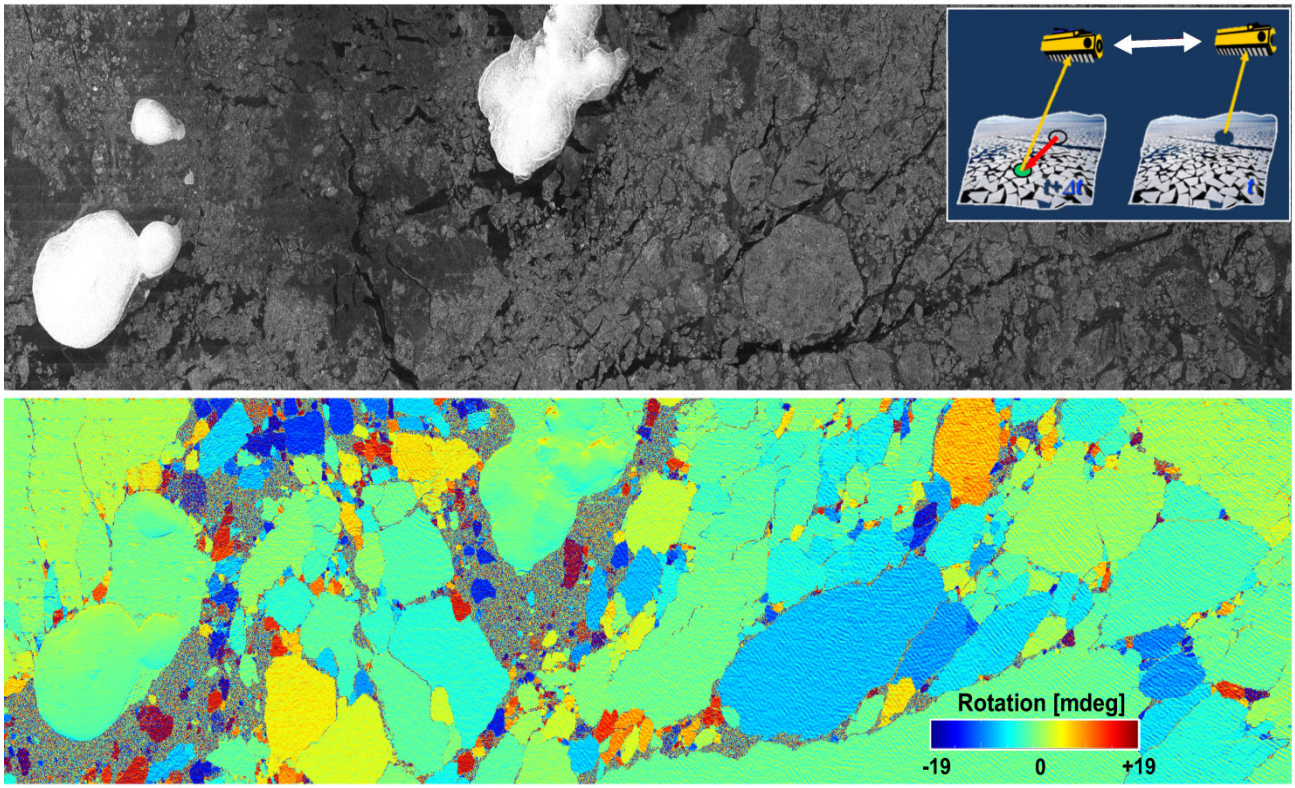

Figure 1.4-4 Demonstration of ice floe rotation measurement by means of along-track interferometry during the science phase of TanDEM-X in 2014. The satellites were operated in wide ScanSAR imaging mode with ca. 70 km (10 seconds) separation in along-track direction, allowing in addition to SAR imaging of polar sea ice (top) not only estimation of drift, but also an extremely precise measurement of the small rotational movements (bottom).

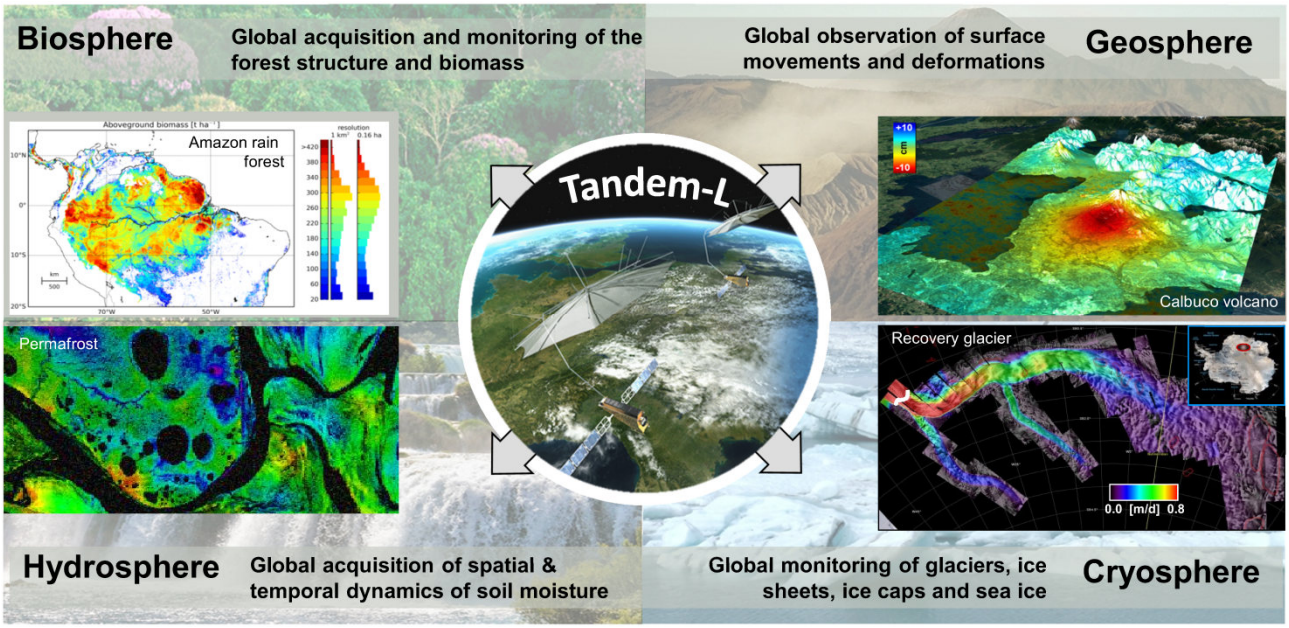

Figure 1.4-5 Tandem-L is a highly innovative mission proposal to monitor dynamic processes in the biosphere, geosphere, hydrosphere and cryosphere with unprecedented accuracy. Besides the scientific component, Tandem-L is distinguished by its high degree of innovation with respect to methodology (e.g., polarimetric SAR interferometry and coherence tomography) and technology (e.g., digital beamforming in combination with a large reflector).

bistatic interferometer, still a unique capability worldwide, and to acquire a global change layer with respect to the TanDEM-X global DEM.

TanDEM-X is also a forerunner for **Tandem-L**, a highly innovative mission for monitoring dynamic processes on the Earth's surface, which has been initiated and proposed by the Institute in 2007 (Section 2.1.3). The combination of digital beamforming techniques with a 15-m diameter deployable reflector antenna enables a weekly global coverage, which is a precondition for observing dynamic processes in the bio-, geo-, hydro- and cryosphere (Figure 1.4-5). The scientific objectives have been developed in the **Helmholtz Alliance** "Remote Sensing and Earth System Dynamics", a joint initiative of eight Helmholtz centers and more than 140 scientific experts from all over the world. In several pre-phase A and phase A studies with NASA/JPL, JAXA and on a national level, the mission concept has been continuously developed and refined. Key mission capabilities are polarimetric SAR interferometry (Pol-InSAR) for measuring forest height, multi-pass coherence tomography for determining the vertical structure of vegetation and ice, and repeat-pass interferometry to retrieve the 3-D deformation with millimeter accuracy. For the space segment, it is assumed that two identical satellites are developed using a 2-ton class satellite bus. The instrument features a digital feed array that illuminates via a large reflector antenna a 350 km wide swath. On receive a narrow high gain beam is digitally generated by combining only a subset of the feed elements, which follows the radar echo across the swath in real time. To avoid gaps at the swath

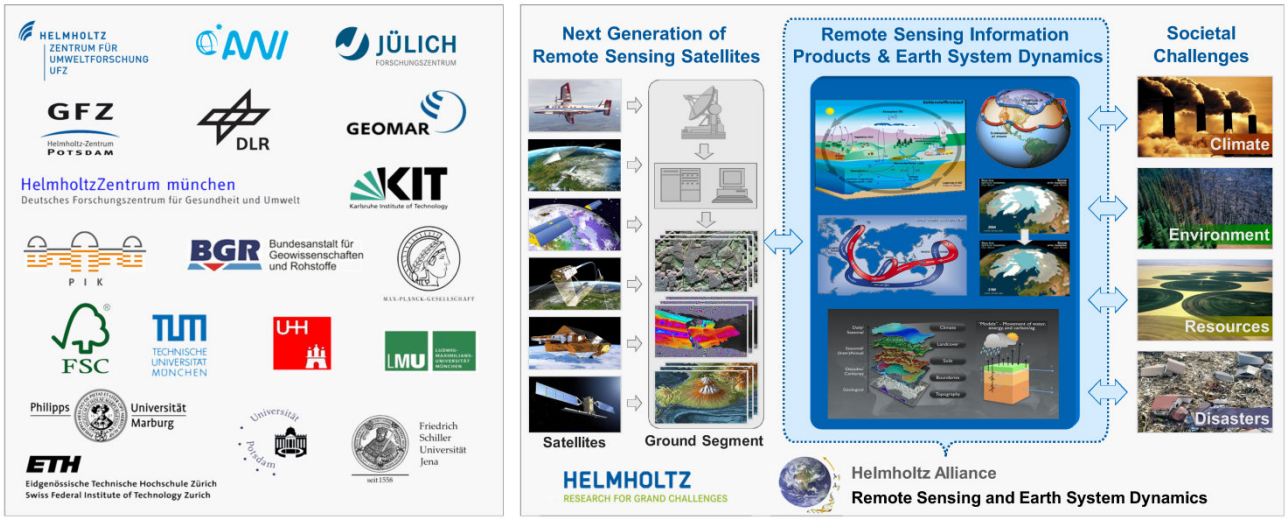

Figure 1.4-6 Main partners of the Helmholtz Alliance "Remote Sensing and Earth System Dynamics" with more than 140 scientists, postdocs and PhD students from eight Helmholtz centers, Max-Planck and Leibniz institutes and other national and international universities, organizations and research institutes (left). One main task of the Helmholtz Alliance has been the development of innovative bio-geophysical information products for the next generation of remote sensing satellites with the goal to address societal challenges of global dimension (right).

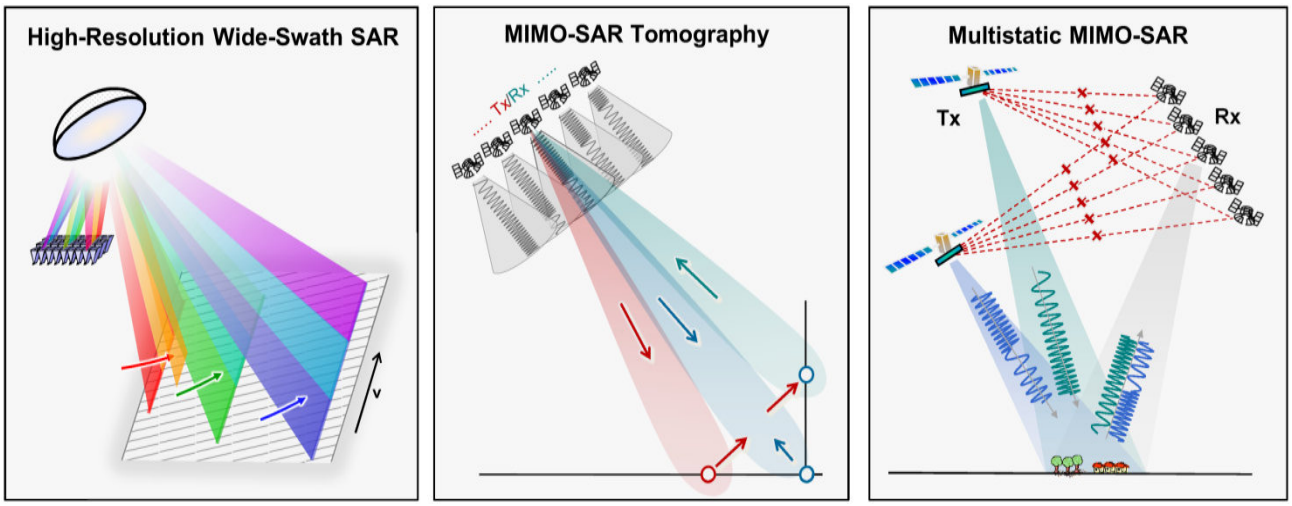

Figure 1.4-7. Innovative SAR system concepts for the next generation of spaceborne SAR systems: Multichannel SAR system with digital beamforming in elevation and azimuth and staggered pulse repetition interval for ultra-wide swath and high azimuth resolution (left), MIMO-SAR tomography with combinations of mono- and bistatic acquisitions for separation of single- and double-bounce scattering (center), and MirrorSAR concept with several receive-only satellites working as simple transponders and two transmit-only radar satellites as an example of an advanced multi-static SAR concept with MIMO operation by means of short-term shift-orthogonal waveforms on transmit (right).

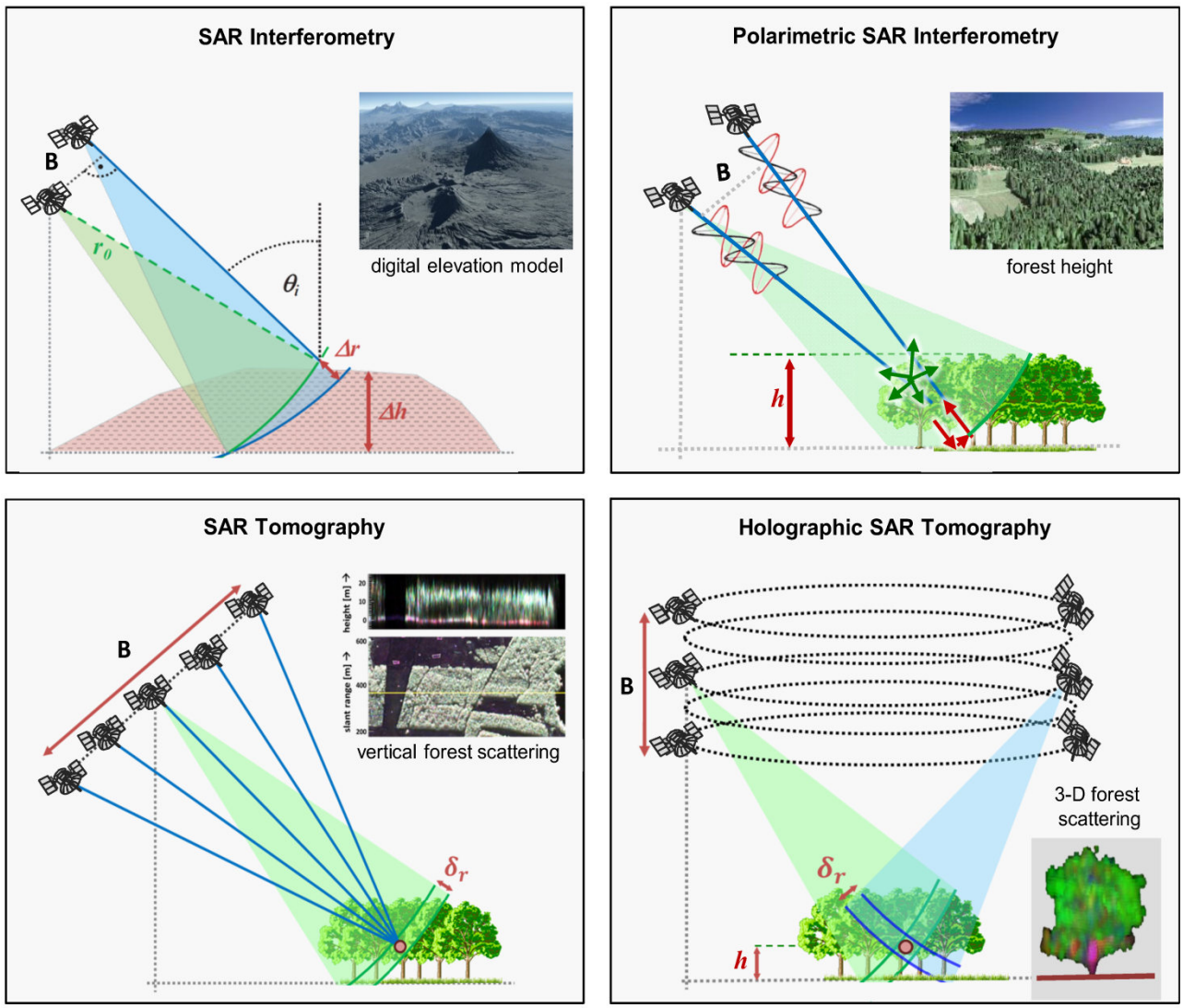

Figure 1.4-8 Based on the bistatic SAR interferometry (top left), TanDEM-X has produced a global DEM of the Earth with unprecedented accuracy. In the last years, the Institute has developed and demonstrated new techniques for multi-baseline SAR imaging like polarimetric SAR interferometry (top right), SAR tomography (bottom left) and holographic SAR tomography (bottom right) which allow expanding the wealth of information products obtained from SAR data.

positions of the transmit pulses the so-called staggered SAR mode has been invented. Continuously varying the PRF results in shifted positions of these gaps that can be interpolated in the azimuth direction resulting in 350 km wide SAR image at 5 to 7 m ground resolution without any gaps. With the Intermediate System Requirements Review (ISRR) the project has successfully completed phase B1 for the mission and ground segment as well as for two competing space segment studies by Airbus Defence and Space and by OHB Space/Hensoldt in the first half of 2018. Tandem-L has been included into the Helmholtz (HGF) roadmap for research infrastructures already in 2011 and has been proposed for inclusion in the roadmap for research infrastructures of the Federal Ministry of Research and Education (BMBF) in 2016. The proposal successfully passed the scientific evaluation by the German Council of Science and Humanities and the final decision by the newly formed German government is expected by end of 2018 or beginning of 2019. Assuming approval later this year, a kick-off into phase B2 seems feasible in the second quarter of 2019, which, according to the latest schedule, would lead to a launch in 2024.

The Institute has been involved in various studies for an X-band follow-on mission that resulted in a recently completed phase A study for a **High-Resolution Wide-Swath (HRWS)** mission. In response to strong user demands for interferometric capabilities the newly developed **MirrorSAR** concept has been proposed and became the baseline for the phase A study of the HRWS mission (Section 2.1.4).

In the last 10 years, the Institute has substantially increased its participation in the European programs for SAR missions, including the Copernicus and Earth Explorer programs. In **ESA's Sentinel-1** and **BIOMASS** projects the Institute is part of the industrial core team and is also responsible for key developments on calibration, end-to-end simulation, as well as interferometric SAR processor prototype (Sections 2.1.7 and 2.1.8). It is also a member of the scientific mission advisory group for BIOMASS.

The Institute has more than 20 years of experience in the analysis and design of **bistatic SAR systems and missions**. In addition to TanDEM-X and Tandem-L, innovative bistatic and multistatic SAR mission concepts like SAOCOM-CS, PICOSAR, SESAME and IRIS have been submitted in the scope of ESA Earth Explorer calls (see Sections 2.2.2 as well as 2.1.6, 2.1.9, 2.1.10 and 2.1.11). SAOCOM-CS, PICOSAR and SESAME are based on receive-only SAR payloads on board small platforms, which fly in formation with an existing main radar satellite as an illuminator. IRIS, on the other hand, is based either on a multistatic SAR concept of transmit and receive satellites or on the MirrorSAR concept and has been investigated for different applications related to high-resolution digital elevation models.

The conceptual design of **new multichannel SAR systems with digital beamforming and MIMO capability** has been a major focus of our research in the context of future spaceborne SAR missions (see Figure 1.4-7 and Section 2.2.1). These innovative mission concepts allow overcoming the fundamental performance limitation of current spaceborne SAR systems in terms of azimuth resolution and imaged swath. Different realizations can be used in order to fulfill the user requirements in the best possible way, such as planar antennas with multi-elevation beams and scan-on-receive, reflector antennas in combination with a digital feed array with digital beamforming, multi-beam imaging with slow PRF variation or azimuth multichannel staggered SAR. Special designed orthogonal waveforms on transmit allow for a MIMO-SAR implementation. Recent examples include advanced multichannel SAR systems which are being considered for the L-band component of the European Copernicus evolution program and for the Sentinel-1 next generation satellites.

New **SAR processing and interferometry algorithms** have been developed in support of the experimental imaging modes of TerraSAR-X/TanDEM-X, of the Sentinel-1 TOPS imaging mode, as well as in preparation for future bistatic SAR missions (see Sections 2.2.2, 2.2.3 and 2.2.4). One main achievement has been the prototype SAR processor for the new staring spotlight operational mode of TerraSAR-X, delivering unparalleled spatial resolution from space. Further new SAR imaging modes have been implemented with TerraSAR-X in order to demonstrate the potential for measuring displacements in azimuth direction, either for 3-D glacier velocity estimation and seismic deformation in the repeat-pass case (2-look TOPS imaging mode) or for 2-D ocean currents and ship velocity measurements (bi-directional SAR imaging mode). Based on the experience gained with the demonstration of the TOPS imaging mode on TerraSAR-X, the first interferometric Sentinel-1A/B TOPS data were processed, analyzed and validated during the commissioning phase of the satellites.

The end-to-end SAR system expertise available at the Institute has been used to implement a very capable and versatile **end-to-end SAR simulator** which encompasses the full complexity of SAR systems and missions up to the generation of higher-level information products (Section 2.2.5). This is an essential task to allow the accurate performance calculation and system optimization for future missions. The developed end-to-end simulator has been used to predict the performance of various SAR missions such as BIOMASS, SAOCOM-CS, HRWS and Tandem-L and is continuously being extended to include new features such as multichannel digital beamforming and bistatic operation with large baselines.

Through European and international projects we could well expand the **radar calibration activities** as well as strengthen our position as a **DLR SAR Calibration Center** (Section 2.2.6 as well as Sections 2.1.7 and 2.1.12). Beyond the outstanding calibration of TerraSAR-X and TanDEM-X, a new generation of remotely controlled high-precision C-band calibration transponders has been developed. Using these transponders and corner reflectors, deployed in our permanent calibration field nearby Oberpfaffenhofen, the overall system calibration for Sentinel-1A/B has been completed, fully complying with the demanding ESA requirements. Furthermore, in response to an open call of the Canadian Space Agency (CSA) for two highly accurate C-band transponders, we succeeded to win the bid in competition with several industry consortia. Both transponders were deployed in Canada in 2017 and have been fully operational since then. With our undisputed role as calibration center for Sentinel-1, with the very successful transponder developments and with further support requests by the Korean Aerospace Research Institute (KARI) for their Kompsat-6 mission, the anticipated role as a DLR SAR Calibration Center is now a reality.

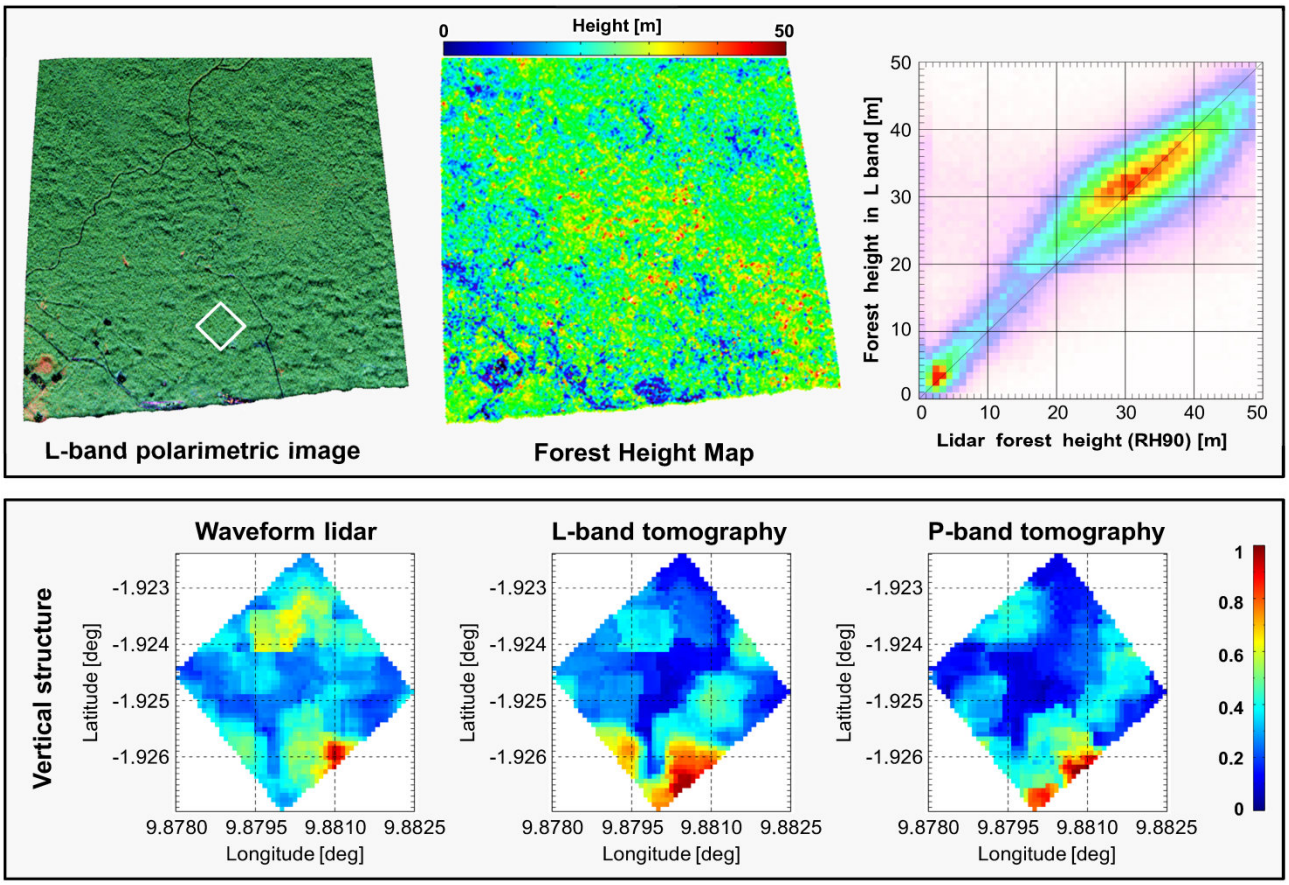

Figure 1.4-9 Forest height and vertical forest structure results from the AfriSAR 2016 campaign. Top: L-band polarimetric image of the Rabi test site (left); forest height map as inverted from L- and P-band tomographic data (middle); correlation between the L-band and lidar-derived forest height across all AfriSAR test sites (right). Bottom: vertical forest structure maps derived from LVIS airborne waveform lidar (left), L-band (middle) and P-band (right) tomographically reconstructed 3-D radar reflectivity measurements over the Smithsonian forest plot in Rabi (indicated by the white rectangle in the polarimetric image).

Polarimetric SAR interferometry (Pol-InSAR) and **SAR Tomography (TomoSAR)** are two powerful SAR remote sensing techniques which allow the extraction of information about natural and man-made objects by evaluating the vertical distribution of the backscattered power, or 3-D reflectivity. In the last seven years, Pol-InSAR evolved from single- to dual- and to multi-baseline configurations, so that more general models could be related to the 3-D reflectivity and used for the inversion of physical parameters in forest, agriculture and ice volumes (Sections 2.2.7 and 2.2.8). Significant advancement has been achieved in forest height estimation (see Figure 1.4-9) which became accurate and stable across different forest types, different terrain conditions, and even in the presence of moderate temporal decorrelation. Pol-InSAR forest height estimation has therefore become an established technique also with respect to future SAR missions like Tandem-L and BIOMASS. For multi-baseline configurations, TomoSAR techniques are unique in estimating the vertical reflectivity profiles. In the last years, the characterization of the performance of the different estimation techniques for natural volumes has advanced with the support of several airborne SAR campaigns. Moreover, algorithms based on coherence tomography were demonstrated with TanDEM-X data (Section 2.2.2) and further adapted to deal with future spaceborne missions, like Tandem-L. Thanks to the F-SAR campaign activities, several innovative information retrieval algorithms have been developed in close collaboration with the Helmholtz Alliance to estimate bio- and geophysical parameters from polarimetric and interferometric SAR data related to applications in the biosphere, cryosphere, geosphere and hydrosphere.

The Institute's activities in the field of **road and maritime traffic monitoring** using air- and spaceborne SAR sensors made significant progress during the past years (Section 2.2.10). For road traffic monitoring a novel multichannel ground moving target indication (GMTI) processor, using a road database and a digital elevation model as auxiliary data, was developed and experimentally verified with the F-SAR sensor. For high-resolution imaging of moving land and maritime vehicles a novel generic inverse SAR (ISAR) processor was developed as well. This ISAR processor does not need any a priori knowledge about the vehicle motion and can be used for linear as well as for circular airborne radar acquisition geometries. For future spaceborne SAR systems with HRWS imaging capability, a novel low PRF GMTI method was developed and verified with F-SAR data. This method allows for the first time simultaneous HRWS SAR imaging and GMTI without changing the system operation mode.

A challenge of particular importance for future low-frequency SAR systems is the dispersive **wave propagation in the ionosphere**, which can lead to interferometric phase errors as well as distortions and defocusing within the SAR image. To minimize such disturbances, the Institute has developed a series of new ionospheric calibration algorithms for fully polarimetric SAR data (Section 2.2.11). As a side-product, important

ionospheric parameters like the total electron content (TEC) and the vertical electron distribution can be estimated with hitherto unknown spatial resolution and accuracy. These calibration algorithms are of crucial importance for the BIOMASS and Tandem-L missions.

As far as the activities related to **antenna design and development** for advanced radar systems are concerned, the Institute has expanded its knowledge and experience by employing novel technologies to improve their performance and to fulfill the requirements posed by the next generation of spaceborne SAR satellites (Section 2.2.12). RF multilayer boards for antenna networks guarantee reliable performance and minimize the influence of production tolerances on the antenna system. The development of metal enclosed radiating antenna elements deals with the topic of dense array antennas with reduced cell size for proper beam forming capabilities. These innovations provide an important contribution to the new generation of airborne and spaceborne SAR antennas. At the same time, the Institute's **Compact Test Range** enhances the accuracy of antenna characterization through the consistent further advancement of measurement techniques and analysis methods (Section 2.2.13). The interrelation between antenna development and characterization is an essential advantage and provides the necessary input to cope with the increasing requirements for precise calibration of modern SAR systems. In this way, the development of new antenna systems such as analog phased array antennas, digital beamforming antennas, or smart and cognitive sensors for future applications becomes much more efficient.

In 2015, the Institute has completed the development and integration of the **new airborne SAR system F-SAR** (Section 2.3.1), and brought it into operation. Its development was triggered by the demand of users and customers for data simultaneously acquired at multiple wavelengths and polarizations, as well as at a much higher spatial resolution. Its current design has the unique ability to acquire fully polarimetric SAR data in five frequency bands (X, C, S, L and P band) with simultaneous recording in multiple frequency bands on four receive channels and is calibrated with very high accuracy. The sensor features single-pass polarimetric interferometric SAR (Pol-InSAR) capabilities at X and S band and a resolution of up to 20 cm both in range and azimuth. The F-SAR modular design, together with a versatile system control, provide the very high level of flexibility and the required degrees of freedom to optimally configure the system for carrying out a diverse set of measurements and experiments.

Since 2015, the F-SAR is fully operational and has been used in various **scientific flight campaigns in Europe, Greenland and Africa**, covering a great variety of research topics (Section 2.3.3). Altogether, a total of 38 different measurement campaigns consisting of 158 flights were carried out, supplemented by 20 calibration and test campaigns with 74 flights, which were undertaken to verify and improve the acquired data quality. Most of the data were acquired in innovative imaging modes: multi-frequency fully polarimetric modes, single-pass polarimetric (along- and across-track) and repeat-pass polarimetric interferometry, tomography, holography and circular SAR (see Figure 1.4-8). The F-SAR measurement activities in recent years show a trend towards large and complex campaigns with many measurement flights, requiring sensor operation in different climate zones of the Earth. One notable measurement campaign was ARCTIC, an expedition towards Greenland's inland ice in spring 2015, where F-SAR collected data in the whole frequency spectrum (X, C, S, L, and P band). Another example of a large measurement campaign was AfriSAR in 2016, which was carried out over the tropical forests of Gabon and focused on the collection of data sets in L and P band, serving as input for the scientific

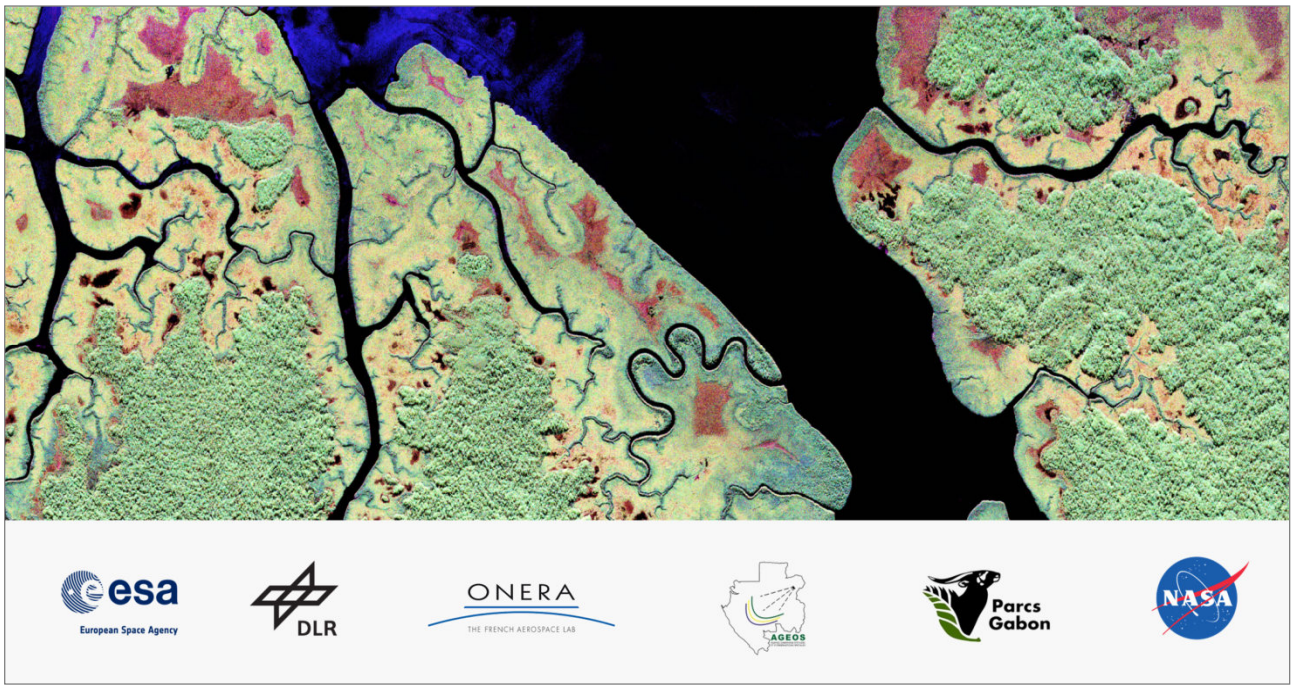

Figure 1.4-10 Polarimetric L-band image (top) acquired with the airborne F-SAR sensor during the AfriSAR campaign in Gabon, 2016. AfriSAR was performed in support of the development of applications for BIOMASS and Tandem-L in cooperation with ESA, ONERA and NASA and local institutions in Gabon (bottom).

community in preparation for the Tandem-L and BIOMASS satellite missions (see Figure 1.4-10). The AfriSAR campaign was organized in close cooperation with ESA and supported by additional flights of ONERA's SETHI SAR sensor, as well as NASA's UAVSAR and LVIS systems. Research based on campaign data acquired by the Institute's F-SAR sensor allowed the development and verification of several **novel signal processing techniques** (Section 2.3.4).

An innovative and very powerful algorithm for the external calibration of multichannel SAR data has been developed to ensure the accurate and comprehensive interferometric and polarimetric calibration of multichannel SAR sensors. The airborne interferometric SAR processing chain has been dramatically extended and improved to support the generation of highly accurate digital elevation models using dual-baseline and dual-frequency SAR interferometry, combining single-pass and large baseline repeat-pass interferometric data. Additionally, new interferometric processing modules, ideally adapted to the processing of tomographic stacks and long-time series, have been established. Also a refined and extended processing chain for circular SAR and holographic SAR data has been implemented, as well as a capable large-scale tomographic processing framework.

Apart from the well-established airborne sensor F-SAR, the Institute has initiated in 2014 the development of a **new airborne SAR system**, the so-called **DBFSAR** (Section 2.3.2). In contrast to F-SAR, DBFSAR is featuring digital beamforming capabilities through a 12-channel X-band front-end and receiver. Its development was primarily motivated by the emergence of various digital beamforming (DBF) techniques for future spaceborne SAR systems and the need for a flexible, airborne experimental platform to provide practical experience and guide the implementation of such missions. In addition, the DBFSAR sensor is intended to address an increasing demand for very high-resolution SAR imagery that exceeds the capabilities of the existing F-SAR system. It is, therefore, designed to acquire data with sub-decimeter resolution using a signal bandwidth of 1.8 GHz. The maiden flight of the DBFSAR system took place in 2016 and demonstrated the basic system functionality; the completion of the entire system is expected for 2019 (see Figure 1.4-11). A further extension of DBFSAR to Ka band and the development of the bistatic L-band system DuoLIM, consisting of two airborne radar systems as a demonstrator for Tandem-L, have been recently initiated (Section 2.3.5).

Building on its end-to-end system expertise, the Institute has supported in the last seven years the German **spaceborne reconnaissance SAR programs** including the operational phase of the SAR-Lupe system and the development phase of the follow-on mission SARah (Sections 2.4.1 to 2.4.7). Governmental spaceborne reconnaissance systems differ significantly from commercial or scientific ones due to the demanding design drivers like the system response time and spatial and radiometric resolution. In order to meet such specific and challenging requirements, comprehensive and experimentally verified simulation tools are absolutely essential for system design, optimization, and operation. During the operational phase of the German reconnaissance system **SAR-Lupe**, a variety of image analysis tools have been implemented by the Institute which are capable of effectively supporting the end user.

For the follow-on mission **SARah** various high-performance mission and SAR system simulators were developed and evaluated as well as a novel and unique end-to-end simulation framework. Primarily, it takes into account the requirements for high spatial resolution and sensitivity and the requirements for a more intuitive and efficient SAR image analysis process. Due to the high-precision modelling of the entire system chain, the simulation concept developed during the reporting period is capable of supporting technical analysis during the design phase, verification of user requirements, as well as the SAR

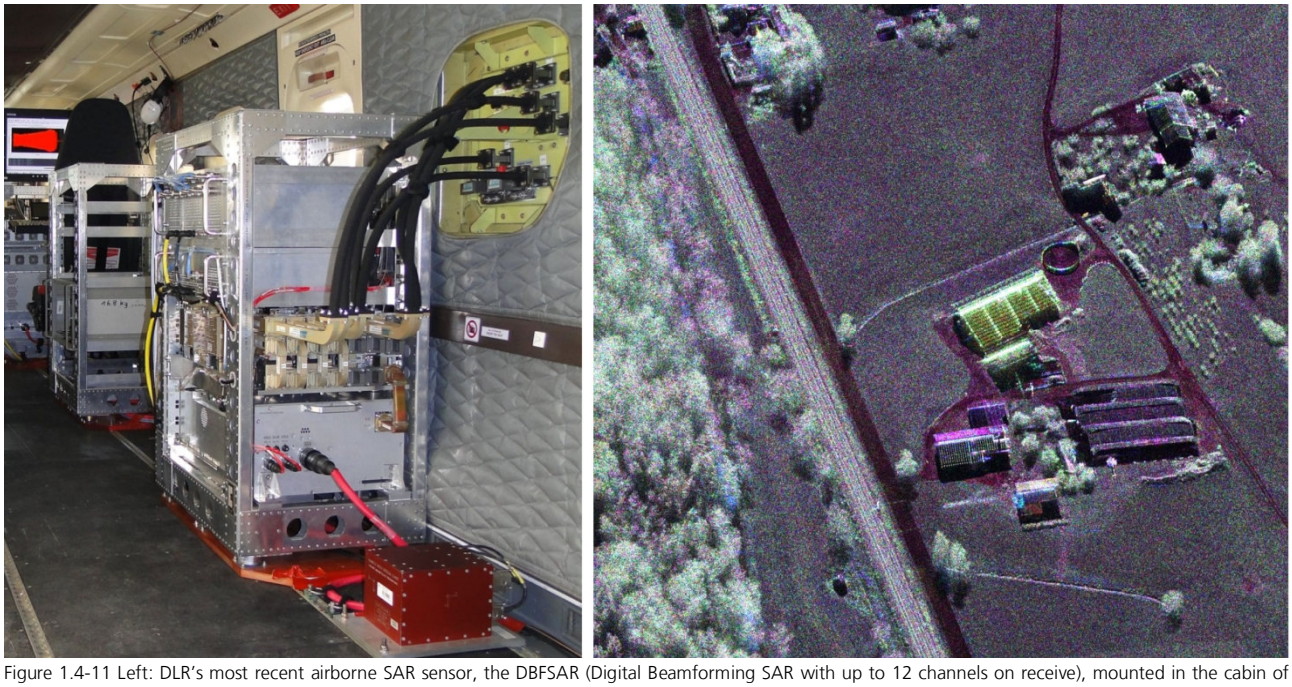

Figure 1.4-11 Left: DLR's most recent airborne SAR sensor, the DBFSAR (Digital Beamforming SAR with up to 12 channels on receive), mounted in the cabin of the DO228-212 research aircraft. Right: polarimetric DBFSAR SAR image; X band, 20 cm × 20 cm resolution, magenta: VV, green: HV, blue: HH polarization.

specific target analysis by the user. The fully generic approach enables the design and analysis of future reconnaissance missions, such as SARah. In the context of the planned SARah follow-on mission **SARah NG**, the Institute is one of the leading contributors to the definition and specification of the mission requirements.

The growing interest of Germany in reconnaissance and security applications raises the importance of research in new **security technologies**. Innovative ground-based solutions, like high-resolution, wide field-of-view and fast imaging microwave sensors are important within this complex field. Hence, a number of high-performance experimental or prototype passive and active imaging sensors have been developed and constructed (Sections 2.4.8, 2.4.9 and 2.4.10). Wide-area surveillance was demonstrated by the LPAS, SUMIRAD and ABOSCA radiometer systems (see Figure 1.4-12), while high-resolution and fully polarimetric imaging capabilities were achieved by the Unirad, Gigarad and TIRAMI-SAR radar systems.

The latest developments encompass a drone based radar system called Dronar and a sensor called Harmony, which is capable of imaging the harmonic behaviour of electrical components. Latest technologies used are, e.g., high-bandwidth digital signal generation, multiple access methods, high-speed sampling, and electronic beam steering. They are accompanied by new and innovative data processing algorithms, like 3-D imaging, physics-based active-passive microwave data integration or advanced image reconstruction from sparsely sampled data. The research spectrum is complemented by research on **metamaterials**, which are used for effectively camouflaging or protecting objects, or for the enhancement of the device performance.

1.5 Benchmarks

The Institute's scientific output has been significantly improved in the last seven years. We increased our key performance indicators like number of journal publications by 92%, number of conference contributions by 11%, doctoral theses by 59%, lectures at universities by 83% and patents by 22%, when compared to the average values achieved in the last evaluation period from 2006 to 2010. We have also performed very well in acquiring third-party funding in open competition, achieving again an increase in the ratio between third-party income and DLR basic funding compared to the previous evaluation period. This is especially remarkable when considering that more than one third of these third-party funds are coming from contracts from industry. The Institute is a much sought-after partner by the space industry in Germany and Europe. In this context we are working as a subcontractor of industry for the ESA satellite missions Sentinel-1C/D and BIOMASS, as well as for the C-band next generation SAR satellite and the L-band SAR system component as a part of the European Copernicus program evolution.

Table 1.5-1 presents a summary of several representative benchmark values and their average values over the three intervals of the Institute's evaluation: from 2000 to 2005, 2006 to 2011 and 2012 to 2017. Despite several demanding large-scale space projects, which require much engineering work, we have been successful in increasing our benchmark values related to the scientific output for all relevant performance indicators. Due to the high qualification of the Institute's researchers at a rather young age, the number of doctoral theses per year has significantly increased in the last few years. Today, we have 25 staff members who are working towards their PhD thesis. A remarkable increase has also been achieved for lectures at universities, whereby three professorships have been assigned in the last ten years and two others are underway. For the next years, we aim at increasing the number of journal publications and the number of lectures at universities to 45 and 12, respectively. Assuming that the number of staff members will remain constant in the next years, the Institute aims at keeping the other scientific benchmarks rather constant in order to ensure sufficient resources for fulfilling the Institute's commitments and responsibilities in the major space projects within the national and European programs.

As far as the finances are concerned, the Institute has increased its third-party income by 31% in the last seven years. On the other hand, the DLR basic funding coming from the program directorates space, aeronautics, traffic monitoring and security increased only by approx. 10% in the same time period. If the salary adjustments and inflation for the Institute's consumables and investments are considered, the DLR basic funding effectively remained constant in the last years. We expect that

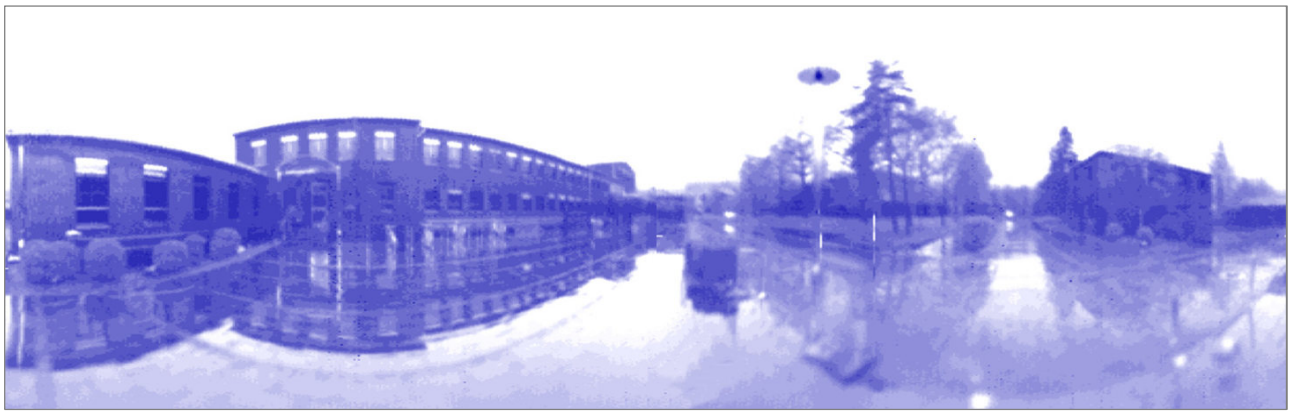

Figure 1.4-12 Panoramic image of the Institute for 360° azimuth angle scanning, acquired with the 90 GHz radiometer system ABOSCA. The image shows the Institute's main building on the left and the main entrance of the Oberpfaffenhofen site on the right. White color indicates cold brightness temperatures (down to 50 K) and dark blue color warm brightness temperatures (up to 300 K).

this situation will improve in the next years, given the most successful Helmholtz evaluation of the DLR space program in 2017, where the spaceborne radar activities were rated truly outstanding within the Earth observation program of DLR. The MoD funding in Table 1.5-1 is fully devoted to the activities within the department Reconnaissance and Security of the Institute and is considered in the benchmark ratio in the last row of this table as third-party income, although these funds are not acquired in open competition. More important than the sole benchmark analysis is the development of the strategic positioning of the Institute. With the missions TerraSAR-X and TanDEM-X, the Institute has been playing a major role in the national radar program. In the next five years, it aims at increasing its participation and contribution to the development of future spaceborne radar missions in the national radar program, at ESA and in the scope of international collaborations. More information about the strategic positioning, personnel, finances and goals of the Institute is provided in the second report of the Institute's evaluation.

1.6 Future Research Activities and Projects

Looking ahead to the next 5 years, the Institute will follow its long-term strategy and continue to initiate, shape and contribute to several large-scale space projects. Table 1.6-1 shows our most important projects. The number of projects since 2006 has considerably increased. By means of the Institute's contributions to the TerraSAR-X, TanDEM-X, PAZ, Sentinel-1A/B, SAR-Lupe and SARah projects, a highly qualified project team has been established. Due to the high degree of innovation in science and technology, the mission proposal Tandem-L represents the most important project for the Institute in the years to come and can be seen as a next milestone in the national radar roadmap after TanDEM-X. The X-band mission proposal HRWS, depending on approval to start the phase B in 2019, would represent another major project with key participation of the Institute. Further, we are also well positioned in all current and future European SAR missions, including Sentinel-1A/B, Sentinel-1C/D, BIOMASS, Sentinel-1 NG and the L-band SAR system in the scope of the EU Copernicus evolution program. Last but not least, we are providing essential contributions to several international missions like PAZ (Hisdesat, Spain), Kompsat-6 (KARI, Korea) and Radarsat Constellation Mission (CSA, Canada).

National Missions and Projects

TerraSAR-X and TanDEM-X are national high-resolution radar satellites launched in 2007 and 2010, respectively. For the TanDEM-X mission, for example, we have contributed with the mission concept including the Helix orbit for formation flying, system engineering, calibration, signal processing algorithms, instrument operation, performance optimization, bistatic radar synchronization, demonstration of new technologies, imaging techniques and applications. Further, we took over the roles of the principal investigator, the lead of the ground segment project at DLR in Oberpfaffenhofen, the mission manager and the science coordinator. TerraSAR-X and TanDEM-X are still fully functional and have sufficient resources available for an extension of the satellites operation by several years. The bistatic operation of the two satellites for DEM and change layer generation is planned until the end of 2019. Due to requirements of the commercial users for higher revisit over specific areas of interest, the close bistatic formation will be probably changed to a pursuit monostatic formation with ca.

	Benchmarks	Average value per year			Increase $\left[\frac{(B-A)}{A}\cdot 100\right]$	Increase $\left[\frac{(C-B)}{B}\cdot 100\right]$
		Average A 2000 – 2005	Average B 2006 – 2010	Average C 2011 – 2017		
Scientific output	**Journal papers**	11.3	15.6	29.9	38%	92%
	Conference contributions	83.5	124	138	49%	11%
	Patents	0.83	1.40	1.71	69%	22%
	Lectures at universities	3.17	5.00	9.14	58%	83%
	Doctoral theses	1.67	2.60	4.14	56%	59%
	Bachelor and Master theses	7.17	13.6	13.9	90%	2%
Finances	**DLR basic funding**	5.2 Mio. €	6.0 Mio. €	6.6 Mio. €	15%	10%
	MoD funding	2.2 Mio. €	2.2 Mio. €	2.4 Mio. €	0%	9%
	Revenues from third-party contracts	2.0 Mio. €	5.2 Mio. €	6.8 Mio. €	160%	31%
	Ratio third-party funding to DLR basic funding	0.81	1.23	1.39	53%	13%

Table 1.5-1 Overview of the Institute's benchmarks from 2000 to 2017

ten seconds along-track separation at the end of 2019. This flight configuration allows parallel operation of both satellites in different imaging modes as well as simultaneous data downlink, so that a higher revisit rate can be achieved. The use of interferometry for high-accurate DEM generation will be, however, restricted to areas with short vegetation or bare soil due to unpredictable atmospheric changes and temporal decorrelation that can occur in this short time due to windy or rainy weather conditions.

Tandem-L is a proposal for a highly innovative SAR mission for climate research and environmental monitoring which was included into the Helmholtz (HGF) roadmap for research infrastructures already in 2011. A formal proposal was submitted in 2016 to the Federal Ministry of Research and Education (BMBF) for the inclusion of Tandem-L in the national roadmap for research infrastructures. The outcome of the evaluation process has been very positive for Tandem-L and a final decision is expected by end of 2018 or beginning of 2019. Tandem-L is the result of three multi-year conceptual and feasibility studies by DLR in close cooperation with the German aerospace industry. The project has successfully passed phase B1 in February 2018. Current activities are focused on predevelopments for the critical instrument technologies: transmit-receive modules and digital electronics. The scientific data exploitation of Tandem-L is being prepared as part of the Helmholtz Alliance "Remote Sensing and Earth System Dynamics", in which already more than 140 scientists from Helmholtz centers (AWI, DLR, FZJ, GEOMAR, GFZ, HMGU, and UFZ), Max-Planck and Leibniz institutes and other national and international universities and research institutes are involved.

Since 2016 the Institute has contributed to the pre-phase A and phase A studies of the HRWS mission proposal. HRWS is an X-band SAR system with imaging spatial resolution as good as 25 cm and includes some innovative technological concepts of the original high-resolution wide-swath (HRWS) SAR system. As for TerraSAR-X, the requirements for HRWS are mainly driven by commercial applications. Due to the requirements for the generation of a very-high resolution DEM with a relative height error (standard deviation) of 1 m and a posting of 4 m, the Institute has proposed the new MirrorSAR concept with 3 receive-only satellites as an add-on to the HRWS satellite, so that the mission requirements can be achieved in a cost-effective way. HRWS has successfully concluded the phase A study with the Preliminary Requirements Review (PRR) in July 2018. Once approved, it is planned to enter phase B in 2019.

The project RSE is fully funded by the German Ministry of Defense (BMVg) and encompasses the activities of the Institute related to security and reconnaissance. It includes the technical support, engineering and mission analysis for SAR-Lupe, SARah and its follow-on system, as well as the active and passive microwave sensor developments for security-related applications. A decision for implementation of the follow-on SARah system is expected in the next few years.

European Projects

Sentinel-1A and Sentinel-1B are two C-band radar satellites from the European Copernicus program which have been launched in 2014 and 2016, respectively. As member of the industrial core team, the Institute was responsible for the end-to-end system calibration. We also performed independent calibration campaigns during the commissioning phase of both satellites and contributed to the radiometric and interferometric data calibration and validation. Our calibration field is the primary calibration site for the Sentinel-1 mission and we are monitoring the long-term radiometric performance as contribution to the mission performance center. The Institute is participating in the same way in the follow-on missions Sentinel-1C and Sentinel-1D, which are currently under development. Further, we are involved in four industrial consortia in the scope of phase A/B1 studies for C-band and L-band systems as a part of the Copernicus evolution program.

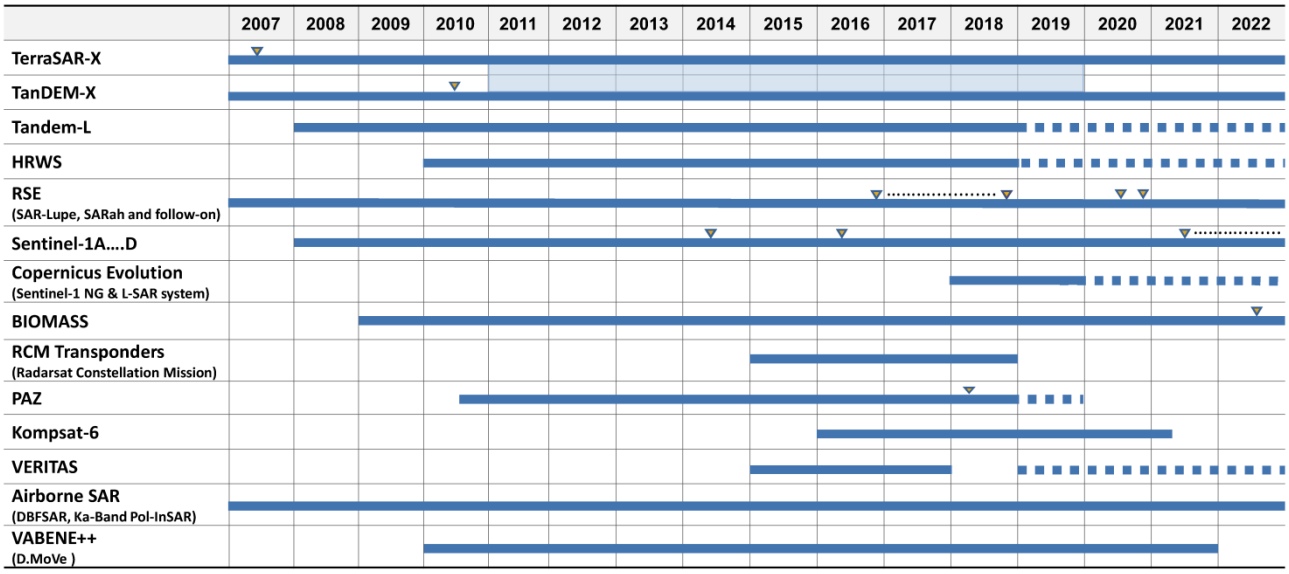

Table 1.6-1 Most important projects in the Institute. Dashed bars show the planned continuation of the respective projects. Satellite launches are indicated by triangles. The close formation flight of TerraSAR-X and TanDEM-X is planned until the end of 2019, afterwards it is planned to operate the satellites in pursuit monostatic imaging mode with 70-km separation in along-track direction.

BIOMASS, an ESA Earth Explorer mission, is a fully polarimetric P-band SAR satellite with a planned launch date in 2022. The Institute is a member of the industrial core team and is responsible for the development of the end-to-end simulator and the SAR processor prototype. It is also involved in several science studies for information retrieval and correction of ionospheric effects, and is a member of the ESA mission advisory group.
The Institute has also contributed to the Spanish PAZ satellite with the delivery of the SAR related software modules for instrument operations and calibration. The PAZ satellite is a TerraSAR-X based satellite which has been launched in February 2018 and is being operated in the same orbit as TerraSAR-X and TanDEM-X by Hisdesat, Spain. It is planned to jointly exploit PAZ, TerraSAR-X and TanDEM-X data with respect to scientific applications which profit from a shorter revisit time.

International Projects

Two highly sophisticated C-band transponders have been developed by the Institute for the Canadian Space Agency which were successfully commissioned in 2017. These transponders have been designed for the calibration of the upcoming Radarsat Constellation Mission (RCM), but are already being used for Radarsat-2. Since 2015, the Institute has also been supporting the Korean Aerospace Research Institute (KARI) Kompsat-6 project, a high resolution X-band mission, with the development of a TOPS prototype algorithm. It is also planned to perform a calibration campaign during the commissioning phase in 2020. In the scope of the NASA/JPL mission proposal VERITAS (Venus Emissivity, Radio Science, InSAR, Topography, And Spectroscopy), the Institute has supported the proposal submitted in 2016 to the NASA's Discovery program with the interferometric SAR processing algorithms, performance estimation and end-to-end simulation. VERITAS has the goal to investigate the origin and evolution of a planet most like Earth. It is planned to resubmit the VERITAS proposal to the next Discovery call in 2019. The Institute is also supporting the L-band series of satellites of JAXA as a principal investigator, a member of Carbon & Kyoto science team and in several calibration and validation activities.

DLR Internal Projects and Research Programs

DLR has four main programmatic areas: Space, Aeronautics, Energy and Transportation, which are complemented by two further cross-sectional programmatic fields: Digitalization and Security. The Institute contributes to all of these programmatic fields with its main research themes: Earth observation, satellite based reconnaissance, microwave sensors for traffic monitoring, aeronautics and security-related applications.
Table 1.6-2 shows the correspondence between DLR's programmatic areas, the research themes of the Institute and the allocation of basic funding resources. For each of the DLR programmatic fields, research programs as well as internal projects are defined. While the Institute can propose research programs according to its own strategic goals, DLR internal projects are elaborated in coordination with the DLR program directorate and several other DLR institutes. The approval of the resources for its research programs is on a yearly basis, while the internal project resources are approved for the respective whole project duration. Examples of topics of our research programs are new SAR concepts and missions, signal processing, airborne SAR, information retrieval and applications, calibration, propagation and signatures. The research programs are closely interconnected with the project activities. As a matter of fact, most of the current large-scale projects of the Institute have started as research programs with typical durations of two to five years. The long-term aspect and the need for establishing a roadmap for the research activities have become clear and are discussed in the second report for the 2018 Institute's evaluation. As of today, the Institute has more than 70% of its resources allocated to DLR projects, external projects and third-party contracts. Due to the success in the approval of the new mid-term and long-term projects, it is expected that this percentage will be maintained in the next five years.
F-SAR is the new airborne SAR system of DLR that became fully operational in 2015. It includes polarimetric operation in five frequencies (P, L, C, S and X band). A Ka-band subsystem is now being developed which includes a fully polarimetric and interferometric imaging mode. First test flights are planned for 2019. More than 50 internal and external flight campaigns have already been executed in the last years including three major campaigns in Greenland (2015), Gabon (2016) and Canada (2018). The F-SAR system is also being upgraded to allow the operation with digital beamforming on receive (DBFSAR). After early successful test flights in 2016, the new DBFSAR system is expected to enter the fully operational phase by the end of 2019. The DBFSAR also incorporates an antenna with six receive-only channels dedicated for road traffic monitoring (DLR internal project VABENE++). A project proposal (D.MoVe) for road infrastructure monitoring using the F-SAR system has been submitted to the Transportation program directorate. The DLR projects Counter-UAS, Diabolo and ITEM-FK (as well as the former projects Mephisto, FaUSST and FFT-2) are performed with BMVg funds as part of the program directorate aeronautics and deal with unmanned aerial systems and agile missiles. Several disciplines like surveillance, aerodynamics, flight control, material sciences, actuation, radar and infrared sensors and signatures are represented. The contributions of the Institute focus on investigations concerning radar signatures, radar detection probabilities and radome microwave transmissivity.
Since 2018, DLR has established the programmatic field digitalization. It is a cross-sectional activity with contributions coming from all other programmatic fields of DLR. The Institute is contributing to this new programmatic field with 12.5% of the DLR basic funding in projects related to big data (large-scale information products derived for example from TanDEM-X data) and a cluster-based implementation of the airborne SAR processor. Further, we also contribute to cybersecurity and to a light-weight radar sensor to be installed in High-Altitude Pseudo Satellites (HAPS) as part of the DLR project Global Connectivity.
With the projects EMS-II and KABUL the Institute is contributing to the programmatic field Security with research topics related to maritime security and drone monitoring.

The Future

At the beginning of the 21st century, our society is facing challenges of global dimension: climate change, sustainable development, scarcity of resources, food security, megacities, mobility and a world-changing security situation. Up-to-date geospatial information is essential, for example, to detect changes in the environment, to understand climate change, to monitor the sustainable use of natural resources, to support precision farming, or to provide information in real time for disaster relief forces in crisis areas. Spaceborne SAR plays a vital role in this task because it is the only sensor technology that is able to provide global, high-resolution imaging during day and night and independent from weather conditions. It provides essential contributions for a wide spectrum of applications such as 2-D, 3-D, and 4-D (space-time) mapping, environmental and infrastructure monitoring, retrieval of physical parameters of land, ocean and ice surfaces, hazard and disaster monitoring as well as reconnaissance and security related applications.

In light of this unique capability of SAR systems and the user requirements for high-resolution and timely geospatial information with global access and coverage, a vision for spaceborne SAR can be formulated. A space-based sensor web consisting of a radar observatory with a constellation of satellites will provide a view of our planet like we are used to see with Google Earth, but with high-resolution images and relevant geospatial information being updated every few minutes.

The way towards this vision requires many key developments in terms of innovative radar concepts, imaging techniques and technologies for which we have established a strategy and a roadmap since many years. This roadmap includes several missions which represent major milestones in this development (see Figure 1.6-1). Looking to the future on this roadmap, digital beamforming is an example of an enabling technology. One main constraint in the design of SAR systems is posed by the minimum antenna area required for suppressing the azimuth and range ambiguities. Due to this constraint it is only possible to achieve either high resolution (i.e., short antenna size in flight direction or azimuth) or wide swath (i.e. short antenna size in elevation or across-track). By means of a multichannel SAR system and associated digital antenna beamforming, this fundamental limitation of SAR systems can be overcome. In particular, the mission proposal Tandem-L is able to interferometrically image the whole Earth´s surface up to twice a week using a digital feed array with 32 channels in combination with a large reflector antenna of 15-meter diameter. This leads to an increase of the imaging capability by two orders of magnitude when compared to the TerraSAR-X and TanDEM-X satellites. By including digital beamforming in azimuth with several multichannel receivers, the imaging capacity can be further increased by another order of magnitude. A fully polarimetric SAR system with 400 km swath and one meter resolution becomes feasible. Besides digital beamforming, further technologies and techniques are being developed in order to design a radar system concept to fulfill specific user requirements in a most effective way: MIMO-SAR, multistatic SAR, MEO-SAR and GEO-SAR.

The Institute has also been directing its efforts towards the advancement of innovative approaches for accurate system calibration of the above mentioned advanced multichannel SAR concepts, in order to ensure improved image quality and information product reliability. Next, digital beamforming and multistatic radars can be designed for a fully software-defined operation, so that an adaptive and cognitive sensing becomes possible. As machine learning and artificial intelligence is being

DLR Programmatic Areas	Institute's Research Programs	Basic Funding	Examples of Internal and External Projects
Space	Earth Observation	47.0%	TerraSAR-X, TanDEM-X, Tandem-L, HRWS, Sentinel-1, BIOMASS, PAZ, NewSpace SAR, F-SAR and DBFSAR, Copernicus Program Evolution (C and L band), Kompsat-6
	Reconnaissance and Security	19.7%	Satellite-based Reconnaissance and Security (RSE), SAR-Lupe, SARah and follow-on mission
Aeronautics	Radar Signatures and Metamaterials	9.8%	Diabolo, ITEM-FK, Counter UAS
Digitalization	Big Data, Cybersecurity, SAR on board HAPS	12.5%	Large-scale Information Products, Cluster-based Airborne SAR Processing, Cybersecurity, HAPS
Transportation	Road Traffic and Infrastructure Monitoring	5.6%	VABENE++
Security	Maritime Security and Drone Monitoring	5.4%	EMS-II, KABUL
Energy	Reduction of Primary Energy Consumption of Buildings	–	GTOM

Table 1.6-2 Resource allocation in the Institute for the research programs in the programmatic areas of DLR. The topics "Reconnaissance and Security" and "Radar Signatures and Metamaterials" are funded by the Ministry of Defense (BMVg). The DLR basic funding totals 70.5% and the BMVg basic funding 29.5%. The program area Energy is fully funded by a third-party project. The DLR basic funding represents approximately 42% of the Institute's budget, the remaining 58% are third-party income.

extensively used to improve information retrieval, a feedback loop can be established with a software-defined radar, which is able to cognitively adapt its imaging mode to optimize the information retrieval.

We have also established a roadmap for key developments for information retrieval and innovative applications. In a general sense, the inversion of geo-biophysical parameters from SAR data is a non-trivial task due to the complex and multifaceted interaction of the electromagnetic waves with the imaged surface and volume scatterers. Model-based algorithms are required to allow a reliable and robust information retrieval. The success of such techniques increases with the amount of observables and information content available in the data. This increase in the information content can be achieved by several means including the use of time series, space diversity in the observation geometry (interferometry, tomography, holography and multistatic), multichannel data acquisition (polarimetry, multi-frequency) and signal bandwidth (geometric resolution) as well as a combination of those. However, each application poses a specific requirement on the sensor characteristics and observation scenario. The forward modeling, followed by an inversion and regularization, is a key procedure to help defining and optimizing the sensor characteristics and observation scenario for each application. We have been working on several innovative approaches like polarimetric SAR interferometry and tomography which allow for the retrieval of new information products for applications in the cryosphere, geosphere, hydrosphere and biosphere. Tandem-L foresees the generation of several high-level information products as part of the operational data processing. Last but not least, data fusion with different sensor types, often based on machine learning and artificial intelligence, can be explored towards the use of complementary information in the multi-dimensional data space.

In some respect, the vision of a SAR sensor web with a constellation of satellites is not too far away. The successful Sentinel-1 satellite series is an important milestone and the implementation of Tandem-L and multistatic SAR missions will represent further major steps towards this vision. The Institute is committed to increase its role in the development of future microwave satellites for Earth observation and aims at expanding its expertise and leadership in strategically important projects and research areas. Together with its cooperation partners in DLR, industry and science, the Institute will play a key role in the realization of this vision.

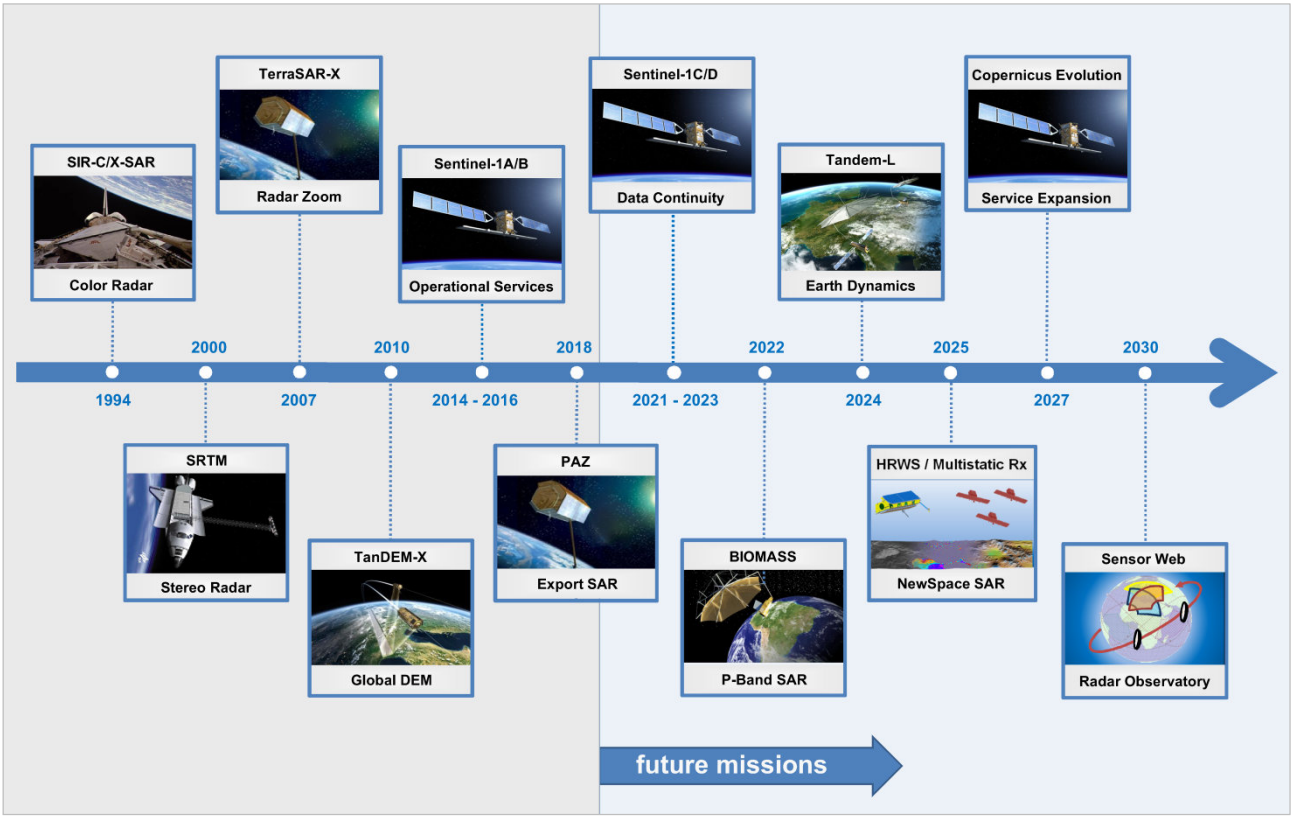

Figure 1.6-1 Roadmap with contributions of the Institute towards the vision of a radar sensor web: a radar observatory for continuous observation of Earth's dynamic processes. SIR-C/X-SAR and SRTM were NASA missions in collaboration with DLR and ASI. TerraSAR-X and TanDEM-X are national missions being operated since 2007 and 2010, respectively. Tandem-L is a mission proposal which was submitted for inclusion in the roadmap of national large-scale infrastructures. Sentinel-1, BIOMASS and the Copernicus evolution missions are part of the European Earth observation program. PAZ is a TerraSAR-X like satellite which has been developed for Hisdesat in Spain. Multistatic HRWS is an X-band mission proposal within the national space program.

2 Research and Project Results

2.1 Spaceborne SAR Missions

2.2 Microwaves Systems and Techniques

2.3 Airborne SAR

2.4 Reconnaissance and Security

2.1 Spaceborne SAR Missions

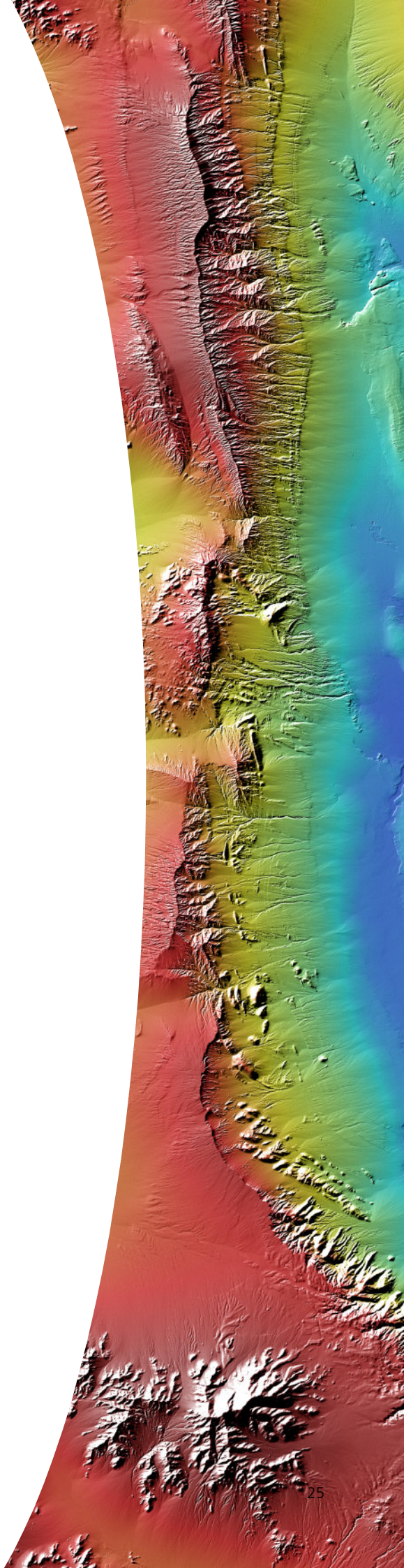

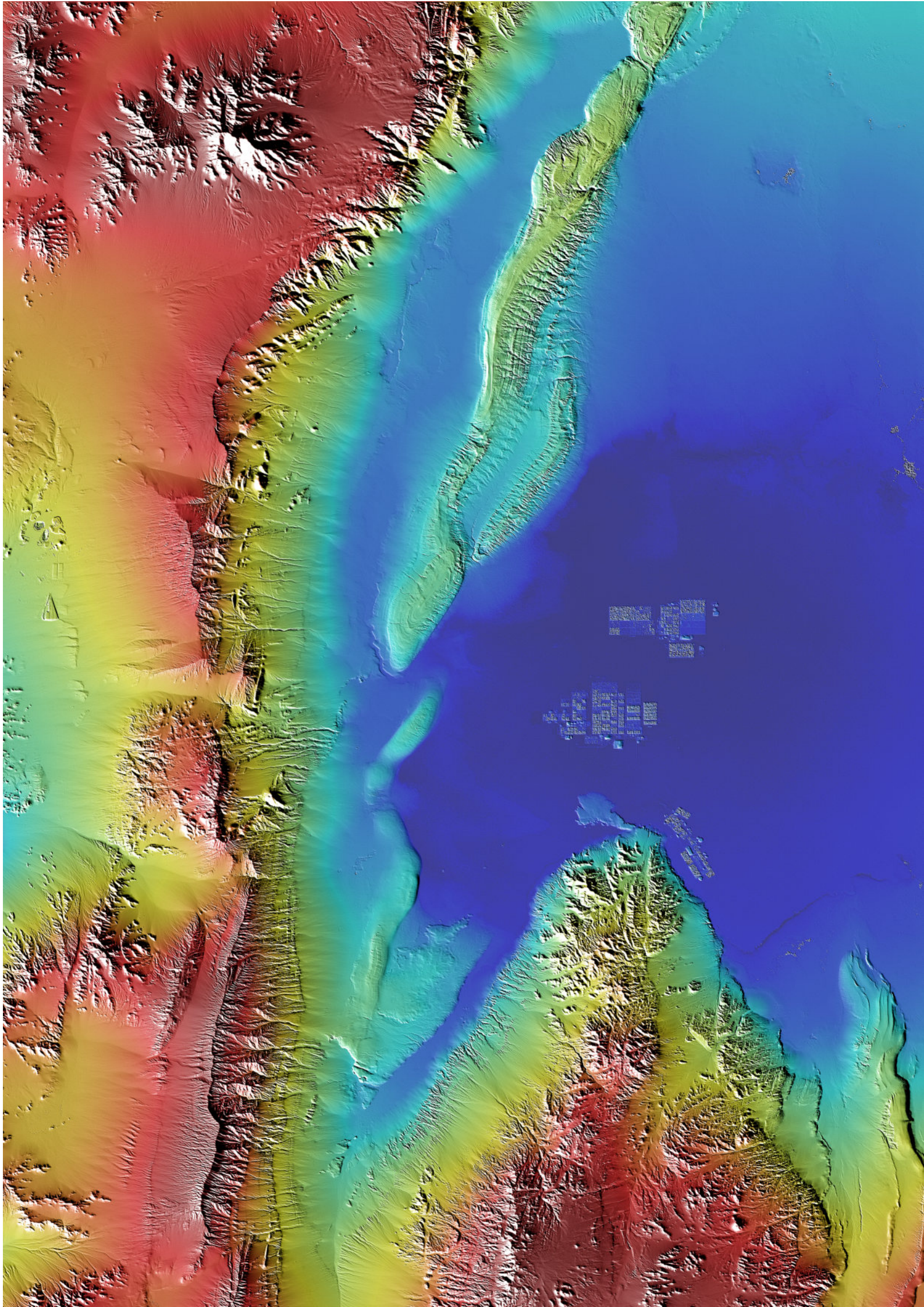

2.1 Spaceborne SAR Missions

Over the last decades, the Microwaves and Radar Institute has built up an unparalleled end-to-end expertise in spaceborne SAR missions, and has become a world leading SAR competence center. The highlight of this reporting period is the successful implementation of the TanDEM-X mission. It demonstrates the Institute's capabilities in the development of innovative mission concepts in response to demanding mission objectives, in leading the project realization facing a number of challenges, and in directing and monitoring the global generation process, from data acquisition through to the final digital elevation model (DEM). The global TanDEM-X DEM is of outstanding quality and exceeds all its specifications, in case of the absolute height error even by one order of magnitude. TanDEM-X is also a precursor for Tandem-L, a pioneering mission for climate and environmental research. Tandem-L is built on a very strong science case developed in a joint effort by eight Helmholtz centers and an international team of more than 100 scientists. Aiming at the observation of dynamic processes in the bio-, geo-, hydro- and cryosphere, this mission requires a novel SAR instrument concept based on digital beamforming in combination with a large reflector antenna. A swath width of up to 350 km enables weekly global coverage as a precondition to observe Earth's system dynamics. Beyond TanDEM-X and Tandem-L, the Institute is making key contributions to the national X-band follow-on mission HRWS, and is involved in all ESA SAR programs. As a member of the industrial core team, we are working on the Sentinel-1 and BIOMASS projects. Furthermore, we have led and been involved in various Earth Explorer proposals. In these proposals, further innovative concepts based on small platforms carrying receive-only SAR payloads and flying in formation with 'illuminators of opportunity', such as, Sentinel-1 have been investigated for different applications – from the measurement of ocean currents to DEM generation, observations in the cryosphere or, in the case of ESA's initiative for a companion to follow the Argentinian SAOCOM, the determination of forest biomass. We are convinced that distributed SAR systems and MIMO techniques will play an important role in future Earth observation missions. With small, distributed platforms, NewSpace approaches will result in considerable cost reduction and will provide a major impulse for next generation spaceborne SAR missions.

2.1.1 TerraSAR-X

The first German radar satellite TerraSAR-X was launched from the Russian Baikonur Cosmodrome in Kazakhstan on June 15, 2007. Three years later, the space segment was expanded by the almost identical TanDEM-X satellite, which has been flying in close formation with TerraSAR-X since October 2010. The two satellites serve two missions: they acquire high-resolution X-band SAR images for the TerraSAR-X mission and operate as a bistatic radar interferometer for the TanDEM-X mission (see Section 2.1.2).

In operation for more than 11 years, TerraSAR-X has achieved remarkable results. Despite a satellite age well beyond the nominal 5.5-year life-time, no significant technical flaws have been encountered. The objective of providing high-quality SAR products in spotlight, stripmap, and ScanSAR imaging modes with various polarizations has been met without any restrictions, and the image quality is just as good as it was at the beginning of the mission. The reasons for the outstanding long-term performance are the excellent construction of the satellite systems, the innovative concept for highly accurate calibration of the radar instrument, and the design of the ground segment tuned to the mission that is able to exploit all of the capabilities of the satellite bus and the radar instrument.

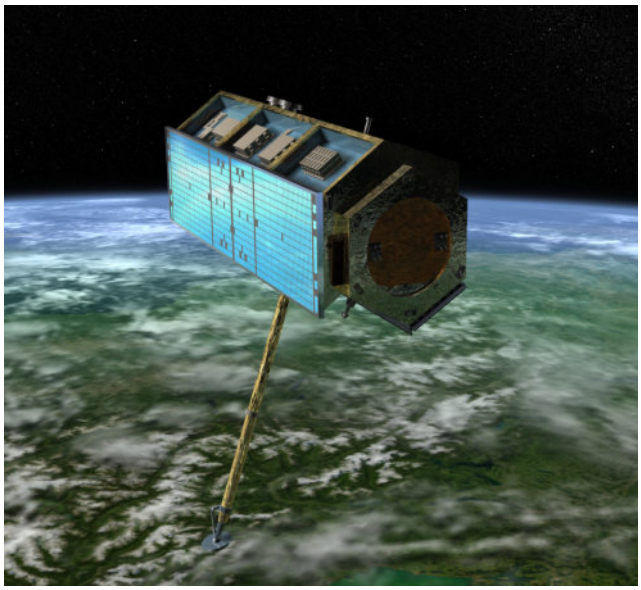

Figure 2.1-1 Artist's impression of the TerraSAR-X satellite in nominal right-looking attitude. The solar array faces towards the Sun, and the X-band radar antenna is mounted on the lower right panel. The deployable boom carries the X-band downlink antenna.

Figure 2.1-2 TerraSAR-X image of the north-western part of Ingolstadt and the Audi car factory acquired on January 11, 2018 in staring spotlight mode. The image covers an area of 5.4 km x 3.2 km at a range and azimuth resolution of 0.75 m and 0.21 m, respectively. The color coding is based on the local image statistics. After more than 11 years in orbit, TerraSAR-X continues to generate high-resolution SAR images of outstanding quality and without any degradation.

The Institute has been a key player in the TerraSAR-X project from its outset. It was involved in the SAR system design; special features are, for example, the dual-receive split antenna that enables experimental fully polarimetric acquisitions and along-track interferometry, total zero Doppler steering, algorithms for ScanSAR and spotlight processing, Pseudo Noise (PN) gating, and algorithms for calibration, as well as several experiments for the demonstration of new techniques and technologies. Our responsibilities included SAR system engineering, performance prediction and control, end-to-end system calibration, as well as the development of processing algorithms for spotlight and ScanSAR modes. As part of the ground segment, the so-called Instrument Operations and Calibration Segment including software modules for instrument operations, SAR system calibration and verification has been developed and maintained, in addition to SAR calibration targets. It is a central part of the ground segment required for the smooth operation of the high-performance SAR instruments on both satellites. SAR experts at the Institute have been involved in the development and testing of the radar instrument and still lead the instrument operations in the control room at the German Space Operations Center.

New Imaging Modes

This early involvement in the satellite development and the flexible design of TerraSAR-X made it possible to carry out sophisticated experiments on the space hardware from the very start of the mission. A most prominent example is the in-orbit demonstration of the Terrain Observation by Progressive Scan (TOPS) mode for ESA's Sentinel-1 project, conducted just a few weeks after the launch of TerraSAR-X. TOPS mode, which – like the ScanSAR mode – acquires data in several sub-swaths, also performs an azimuth steering (backward to forward steering, reversed compared to spotlight mode) to overcome ScanSAR performance degradations caused by the scalloping effect. Early demonstrations also included a wider ScanSAR mode as well as experiments to increase the azimuth resolution in spotlight, referred to as staring spotlight. In staring spotlight, the rotation center of the beam is fixed in the center of the scene, and the azimuth steering angles are increased to ±2.2° compared to ±0.375° in the standard sliding spotlight mode. Whereas grating lobes in the sliding spotlight are 20 dB below the desired steering direction, they become equally high at the extreme steering angles in the staring spotlight mode.

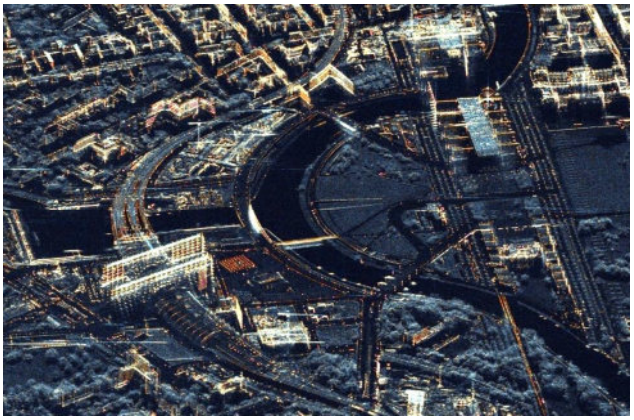

Figure 2.1-3 Staring spotlight acquisition over the political center of Berlin, Germany. Very fine details such as the corners of the main station's steel construction or lightning rods become clearly visible at a resolution of 1 m in ground range and 0.21 m in azimuth. The image is multilooked to 1 m x 1 m and artificially color-coded.

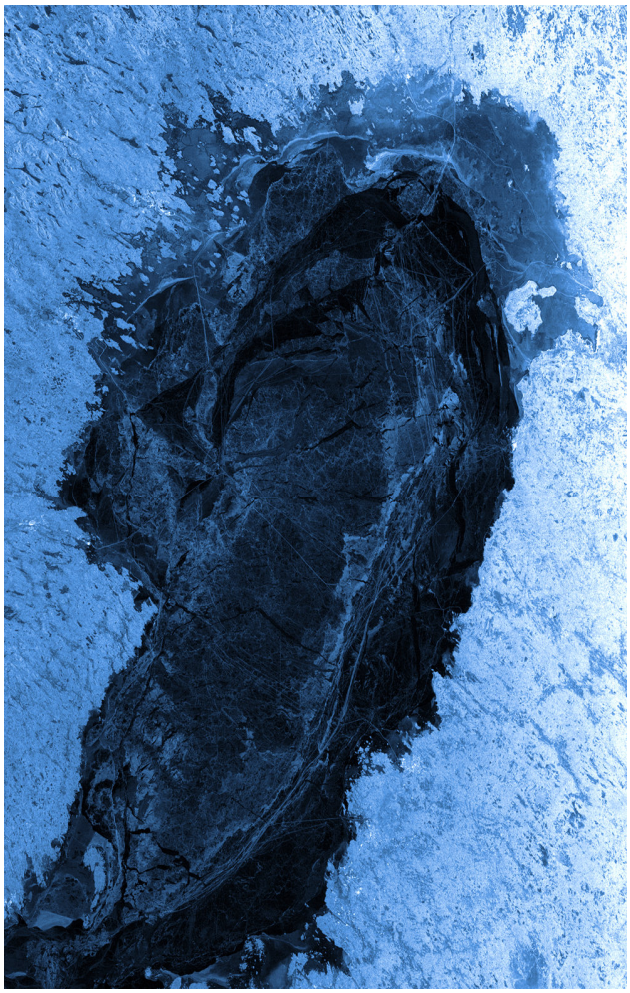

Figure 2.1-4 Wide ScanSAR image of the Gulf of Bothnia acquired on March 6, 2018. At a resolution of ~40 m the image extends over 315 km in azimuth at a swath width of 240 km and is composed of six subswaths. The sea is still frozen and the linear tracks are most likely from ice breakers.

The resulting azimuth ambiguities have been controlled through optimized PRF settings and scene size reductions [J-129], [J-135], [J-58]. Steering angles of ±2.2° are still not the ultimate limit. With the new wrapped staring spotlight mode, the azimuth steering capability of phased array SAR antennas can be further increased to achieve improved azimuth geometric and/or radiometric resolution. It extends the steering to directions with very low signal contribution. Point and extended targets in experimental TerraSAR-X acquisitions were evaluated up to ±4.4° steering, i.e., gains of up to 45 dB below the grating lobes. For TerraSAR-X it was found that an extension of up to about ±3.9° improves the image quality although the cost-benefit ratio decreases with increasing steering angles [J-62].

Both the wide ScanSAR and staring spotlight imaging modes generated highly interesting new products. For this reason, it was decided to implement them as new operational modes in the running mission with the satellites in orbit. The operational wide ScanSAR mode features a swath width of up to 260 km at resolutions of approximately 40 m. Both new modes were well received by the scientific and commercial users.

While investigating the staring spotlight mode the BiDirectional (BiDi) SAR imaging mode was invented and demonstrated with TerraSAR-X [J-166]. The term bidirectional refers to simultaneous imaging in two directions by a single antenna into one receiving channel. The BiDi imaging is based on an azimuth pattern with two steered lobes that point in different directions, an increased PRF, and a separation of the simultaneously received images in the Doppler spectral domain. Figure 2.1-5 (left) shows the BiDi acquisition geometry for simultaneous forward and backward acquisitions. The squint angles for the forward- and backward-looking antenna beams have opposite signs. The same target area is recorded twice as the sensor flies by with an along-track separation in the range of seconds between the two illuminations.

The unique acquisition geometry available in the TanDEM-X

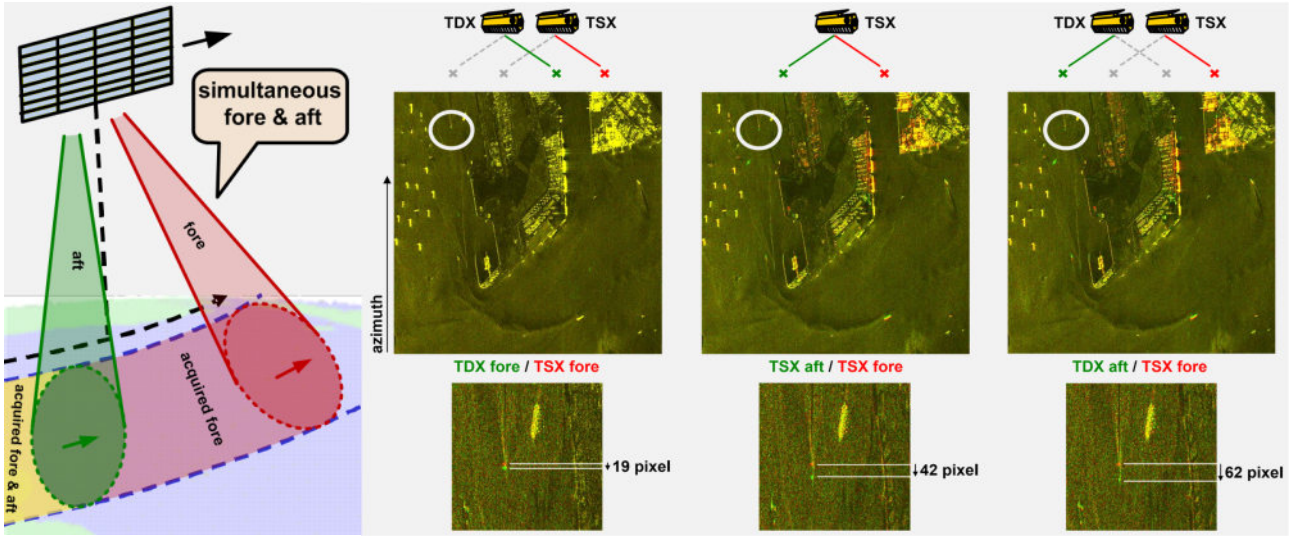

Figure 2.1-5 BiDirectional (BiDi) acquisition geometry example with simultaneous fore and aft acquisitions. In the BiDi-SAR examples on the right, the images of the forward and backward beam are color-coded in red and green, respectively. If no changes occur, the sum image appears yellow. These images are color composites of different combinations of TerraSAR-X and TanDEM-X fore (red) and aft (green) images acquired in BiDi mode over Singapore during the TanDEM-X pursuit monostatic commissioning phase. The azimuth direction is on the vertical axis. The time lag between the fore and the aft image is 2.6 s, 5.9 s and 8.5 s in the left, center and right images, respectively. The lower zoom images around the white circles show a ship moving fast in the opposite azimuth direction. From the distance between the positions in the two images and the corresponding time lag, the ship velocity was estimated to about 6.1 m/s.

pursuit monostatic commissioning phase allowed for BiDi acquisitions with two satellites flying with an along-track separation of 20 km, which corresponds to a time separation of 2.6 s.

The left radar image in Figure 2.1-5 shows the color composite of the TerraSAR-X fore image in red and the TanDEM-X fore image in green. Due to the same azimuth acquisition angle of +2.2°, the backscatter in both images is almost identical and the yellow color prevails. The white circle represents a ship that is moving fast into the opposite azimuth direction (visible from the wake). The smaller image on the bottom zooms into this ship. The velocity of the ship was estimated to be about 6.1 m/s simply by counting the pixels between its position in the TerraSAR-X fore and TanDEM-X fore images.

The image at the top center compares the TerraSAR-X fore and aft images taken at a squint angle of ±2.2° and a time separation of 5.9 s. The difference in the ship position is 42 pixels. The right column images finally compare the TerraSAR-X fore and TanDEM-X aft images at an 8.5-s separation. The backscatter dependence on the azimuth acquisition angle is clearly visible in the right and middle images. Note the striking degree of similarity between the two different images, which is due to the identical angle difference of 4.4°. For comparison, no pronounced backscatter differences can be observed in the left image, demonstrating that the backscatter difference is a pure effect of the aspect angle and not induced by a residual across-track baseline between TerraSAR-X and TanDEM-X.

Radiometric Performance

The radiometric performance has been monitored for the entire mission duration, i.e., more than 11 years for TerraSAR-X and eight years for TanDEM-X. The measurements and extended analyses performed as part of the long-term system monitoring show an outstanding stability of the instrument performance. No trends or degradation have been observed, and all parameters show a stable behavior since the launch of the respective satellites. Moreover, radar cross section measurements of corner reflectors in Figure 2.1-6 confirm an excellent radiometric stability of 0.15 dB over a period of 11 years. Furthermore, this high stability means that the absolute radiometric accuracy derived by the calibration campaign conducted in 2010 is still valid for both satellites.

Never before have two independent spaceborne SAR systems been as accurately calibrated and, consequently, matched to each other. Not only the radiometric performance is outstanding; the geolocation accuracy is also setting benchmarks reaching decimeter accuracies (without reference points). All calibration requirements have been achieved, and most of them even exceeded (see Table 2.1-1). TerraSAR-X and TanDEM-X continue to be perfect twins.

A decade of successful TerraSAR-X operation has proven that the basic design of the overall system – consisting of the space and ground segments – is both robust and flexible enough to meet changing needs and to fulfill the requirements of the scientific and commercial communities during such a long period of time. The flexible design makes it possible to conduct unique experiments and has been successfully used to demonstrate new modes that, in the case of the wide ScanSAR and staring spotlight modes, have even become operational with the satellites already in orbit. Radar performance and calibration of the individual satellites are still well within specifications, and no indication of degradation is noticeable – a fact that is remarkably reflected in the consistently excellent quality of the SAR products. From today's point of view, the satellites and the ground segment operate without restrictions, and the consumables – specifically the propellant and the battery capacity – allow for approximately five more years of satellite operation.

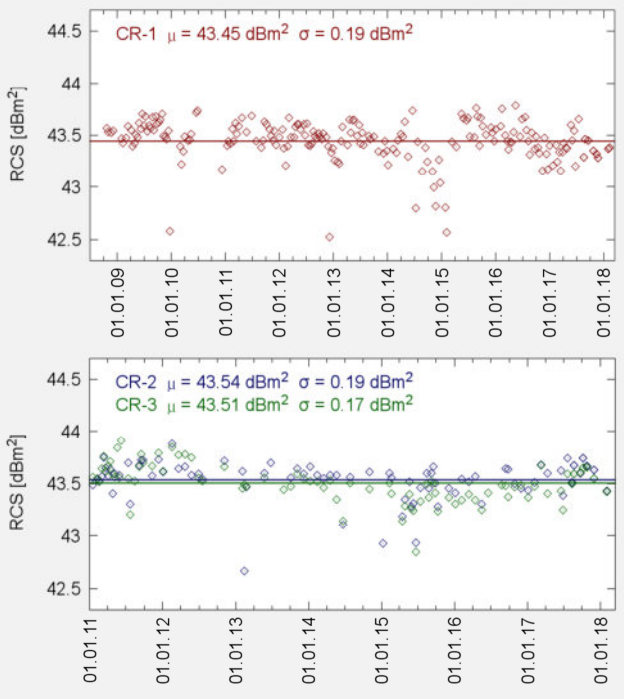

Figure 2.1-6 Radar cross section (RCS) of permanently-installed corner reflectors derived from SAR images acquired by TerraSAR-X (top) and TanDEM-X (bottom) over their elapsed lifetime. Standard deviations below 0.2 dBm² confirm the outstanding absolute calibration and long-term stability of both SAR systems.

Calibration procedure	Goal	TSX	TDX
Internal calibration			
Amplitude	0.25 dB	<0.1 dB	<0.1 dB
Phase	1.0 deg	<1.0 deg	<1.0 deg
TRM setting characterization			
Amplitude	-	<0.2 dB	<0.2 dB
Phase	-	<2 deg	<2 deg
Antenna model verification			
Pattern shape	±0.2 dB	±0.2 dB	±0.2 dB
Beam-to-beam gain offset	±0.2 dB	±0.2 dB	±0.2 dB
Radiometric calibration			
Radiometric stability	0.5 dB	<0.15dB	<0.15dB
Relative accuracy	0.68 dB	0.18 dB	0.17 dB
Absolute accuracy	1.1 dB	<0.34dB	<0.33dB

Table 2.1-1 Radiometric performance parameters for TerraSAR-X (TSX) and TanDEM-X (TDX)

2.1.2 TanDEM-X

TanDEM-X (TerraSAR-X add-on for Digital Elevation Measurements) was invented by the Institute in 2003 and proposed jointly with Airbus Defence and Space in response to a call for the next German remote sensing mission [NJ-9], [NJ-12], [B-8], [IC-99], [IC-184]. From the very beginning, the Institute took the responsibility of the Principal Investigator role and led the overall mission design and ground segment development, including the definition of the orbit geometry, the planning of the bistatic acquisitions on a data take level, the end-to-end calibration of the interferometric system, as well as the definition of mosaicking algorithms and the monitoring and control of the final DEM performance [J-31], [J-162], [J-165], [IC-73].

TerraSAR-X and its almost identical twin TanDEM-X are the first bistatic SAR formation in space enabling single-pass SAR interferometry with flexible selection of baselines and acquisition geometries [IC-164]. The primary mission objective is the generation of a global and consistent digital elevation model (DEM) with unprecedented accuracy (see Table 2.1-2) [J-144], [IC-36], [IC-70], [IC-100], [IC-101], [IC-102], [IC-103], [IC-138], [IC-147], [IC-165]. Since October 2010, the two satellites have been flying at an altitude of 514 km in a so-called Helix formation at typical distances between 120 m and 500 m, as presented in Figure 2.1-7. Images have been nominally acquired in bistatic configuration, where one satellite transmits and both simultaneously receive the backscattered signal from the Earth's surface. This enables the acquisition of highly accurate interferograms, which are not impacted by temporal and atmospheric decorrelation. A dedicated acquisition strategy has been developed and optimized throughout the years, in order to achieve the desired performance homogenously on a global scale.

Beyond the primary mission goal of generating the global DEM, TanDEM-X supports applications based on along-track interferometry (ATI) and the demonstration and application of new SAR techniques, with a focus on multistatic SAR, polarimetric SAR interferometry, digital beamforming and super resolution [J-13], [J-43], [NJ-13], [IC-37], [IC-74], [IC-112], [RC-180], [RC-238], [RC-623].

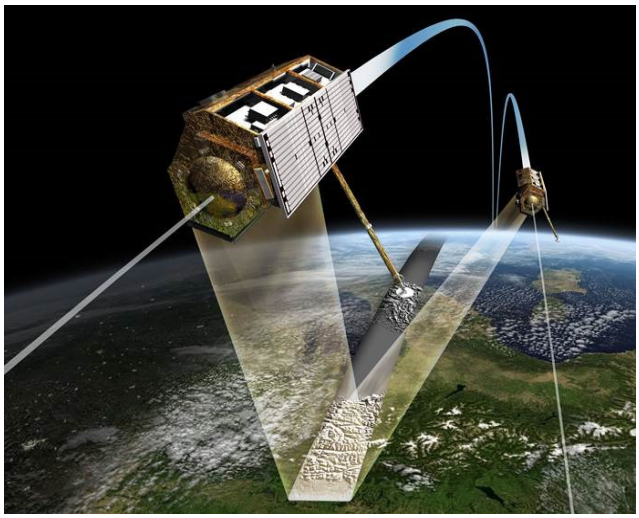

Figure 2.1-7 Artist's impression of TerraSAR-X and TanDEM-X satellites flying in close formation

Global DEM Specification

The global TanDEM-X DEM has been defined to meet or exceed the specifications presented in Table 2.1-2. The height values are referred to the WGS84 ellipsoid and the coverage must reach at least 97% of all land masses, i.e., at most 3% of all DEM pixels over land-covered areas (water bodies excluded) might be flagged as void or invalid (e.g., due to acquisition gaps, low signal quality, shadow or layover effects). All heights shall represent the reflective surface in X band, i.e., the global DEM is a surface model.

Parameter	Definition	Requirement
Relative vertical accuracy	90% linear point-to-point error in 1° x 1° cell	2 m (slope < 20%) 4 m (slope > 20%)
Absolute vertical accuracy	90% linear error (global)	10 m
Spatial resolution	Independent pixels	12 m (0.4 arc sec)

Table 2.1-2 Specification of the TanDEM-X Digital Elevation Model (DEM)

Interferometric Calibration

Data for the global DEM are collected in 30-km-wide stripmap mode. In a fully-automated first processing step, the data are processed into so-called Raw DEMs, covering an area of 30 km x 50 km. Each Raw DEM already needs to be as close as possible to its real height to allow for accurate geocoding and to facilitate the second processing step, in which blocks of the different scenes are calibrated against their neighbors and against ICESat reference heights.

The interferometric calibration includes three different steps: the calibration of the baseline between both satellites, the adjustment of internal delays to allow a radargrammetric determination of the coarse absolute height of the Raw DEM, and finally the correction of phase offsets to adjust the precise absolute height of the DEM in the order of a few meters [J-147], [J-184], [IC-174].

Precise knowledge of the baseline between the two satellites is of vital importance for deriving highly accurate DEMs. The required accuracy in baseline determination is in the order of 1 mm, which corresponds to a vertical offset of about 1 m. Coarse baseline determination is performed by a double differential evaluation of GPS carrier phase measurements. However, the relative satellite positions derived from GPS measurements are biased, mainly due to uncompensated offsets from the SAR antenna phase centers, which results in offsets of several millimeters. To achieve precise baseline calibration, globally distributed flat test sites with a known topographic height have been repeatedly acquired since the beginning of the mission. In this way, initial offsets can be estimated and corrected, making it possible to monitor the baseline stability over time [NJ-15], [RC-574]. The long-term evolution of the radial and along-track components of the baseline bias from 2010 up to 2014 is shown in Figure 2.1-9; the measurements show a standard deviation of 1.31 mm.

The interferometric measurement utilizes the phase difference of

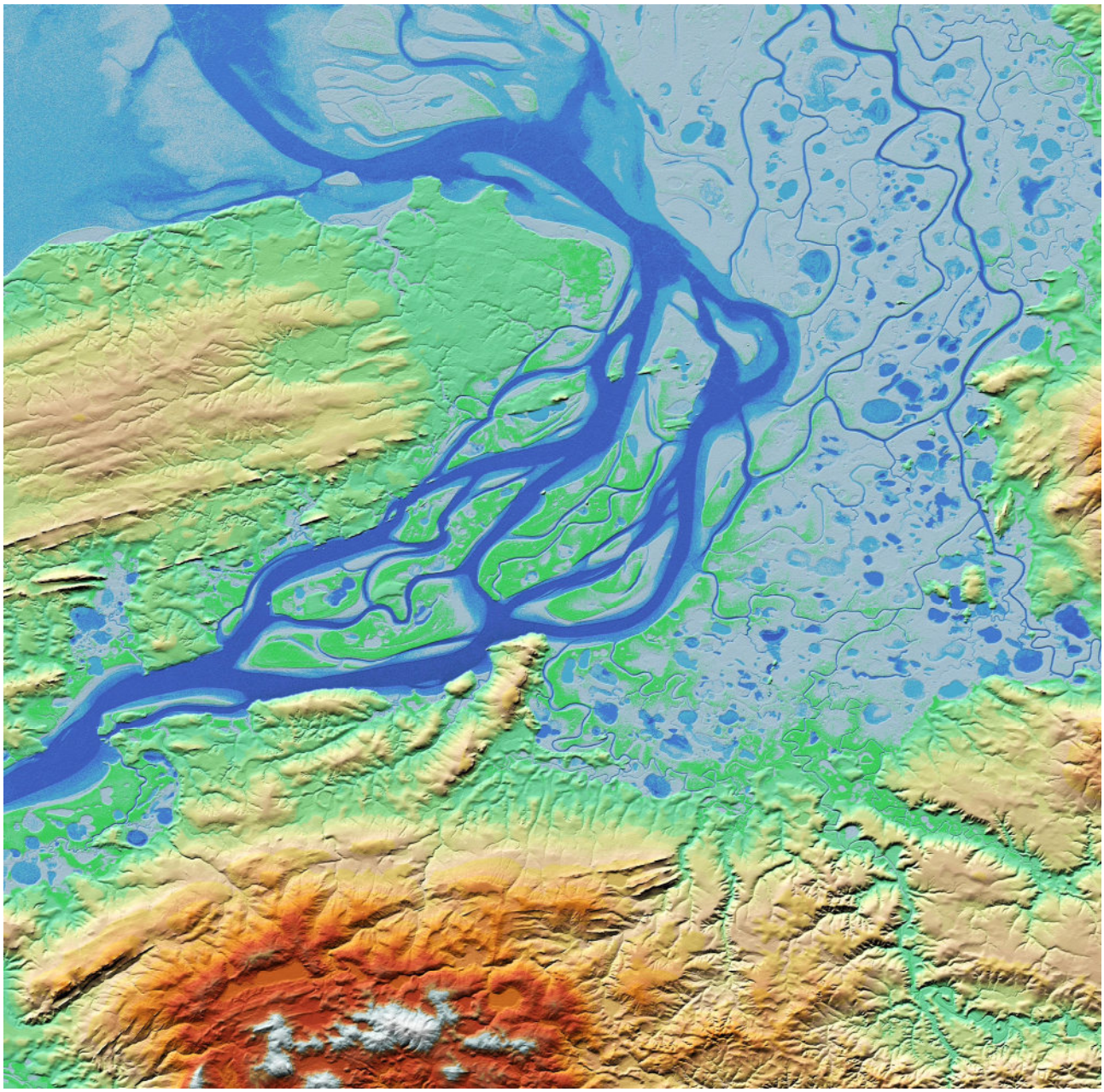

Figure 2.1-8 TanDEM-X DEM covering the area between 73° and 74° north and 86° and 88° east in Russia. The completely frozen river Pjasina meanders into the Kara Sea. The height in this scene varies between 0 m and 280 m.

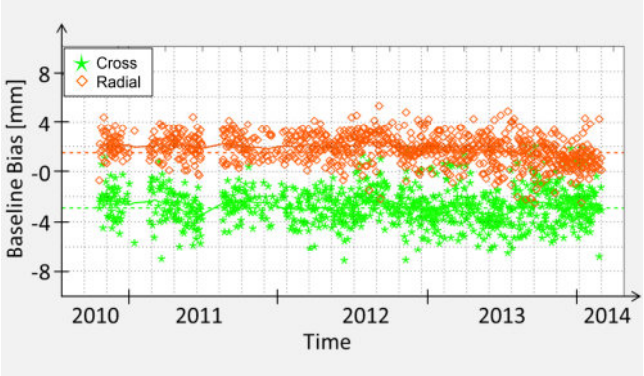

Figure 2.1-9 Long-term evolution of the baseline bias: radial and across-track components in red and green, respectively. Baseline calibration at millimeter accuracies is a precondition for achieving the global DEM specifications.

the acquired SAR data between both satellites. This phase is ambiguous by the wavelength, and thus the correct ambiguity band needs to be resolved. This can be achieved by radargrammetric height determination, which exploits the unambiguous radar signal travel times. For this, a highly precise delay calibration is required to compensate differential delays in the instruments, which can vary depending on radar parameters. Detailed investigations revealed that these delays change with the used synchronization horn antenna, the receiver gain setting, the employed bandwidth, the transmitting satellite, and the position in the orbit [RC-586].
The final adjustment is performed by calibrating the phase offset between both acquisitions based on a comparison with reference data (SRTM and ICESat). This phase offset depends on the transmitting satellite, precise synchronization, and

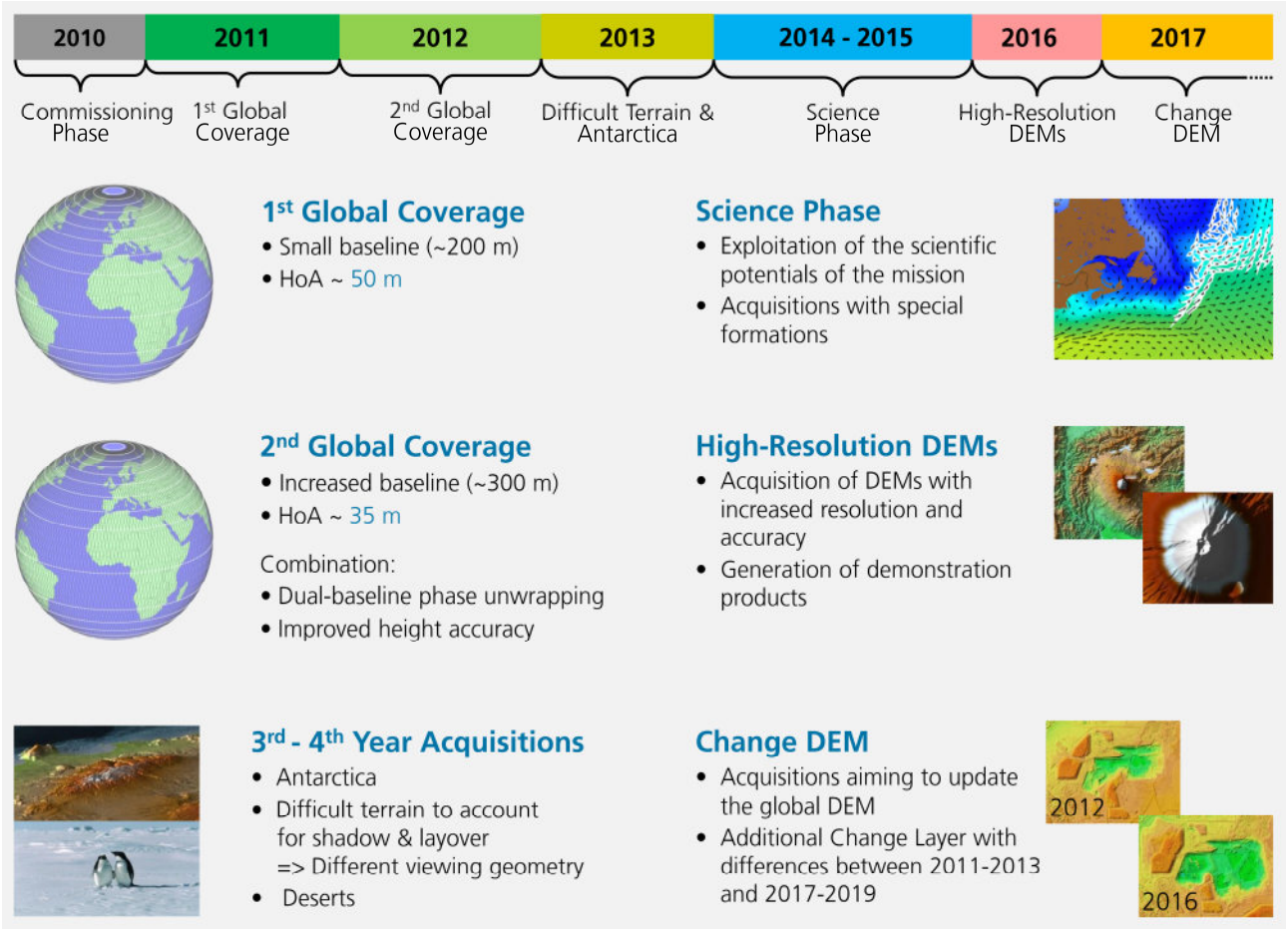

Figure 2.1-10 Mission phases of the TanDEM-X mission. The acquisition of data for the global Change DEM started in 2017 and will last until 2019.

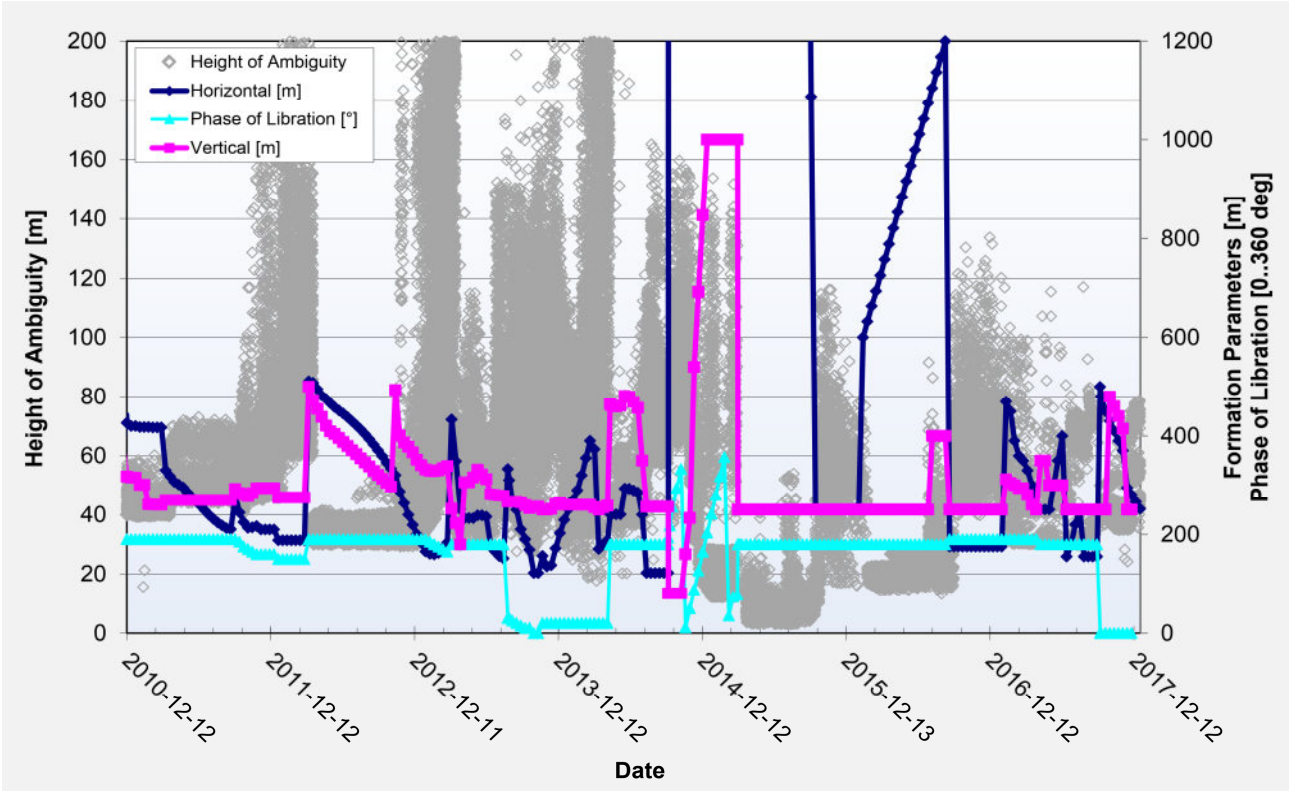

Figure 2.1-11 Evolution of the flight formation parameters over the mission time and corresponding height of ambiguity (gray diamonds). The vertical baseline is shown in pink, the horizontal one in blue, and the phase of libration in cyan.

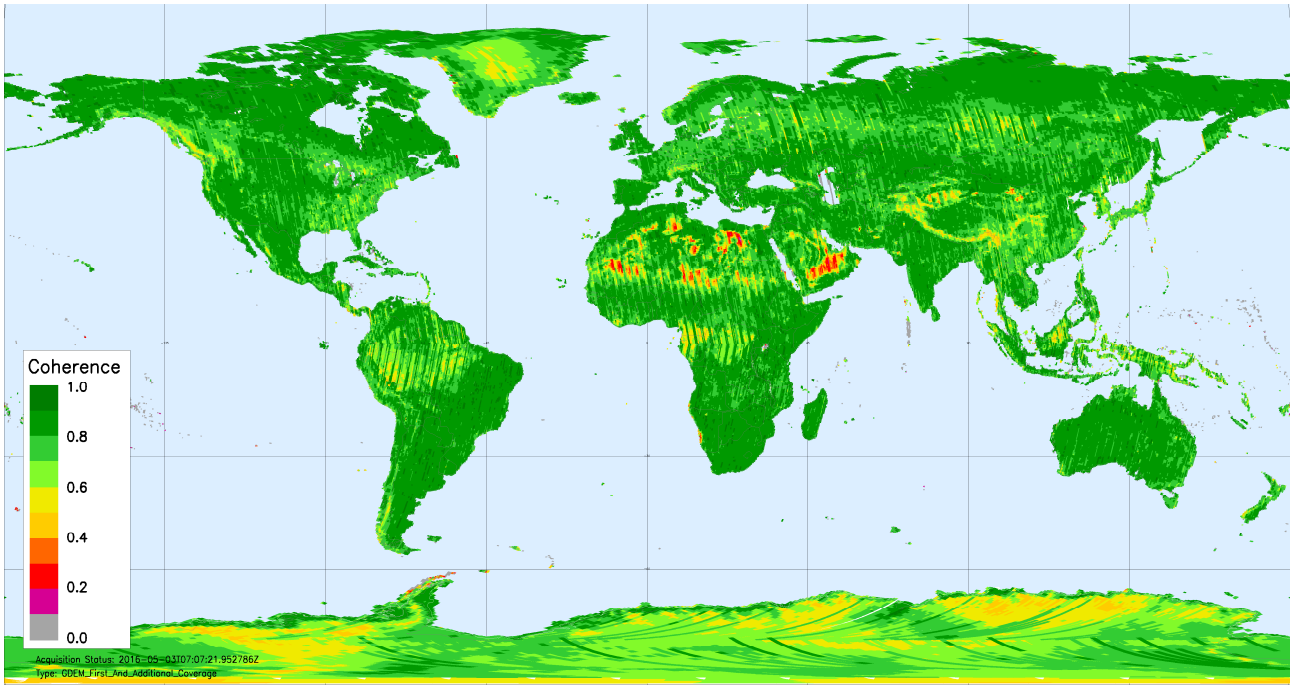

Figure 2.1-12 Global interferometric coherence estimated from the acquisitions of the first TanDEM-X coverage. A coherence of at least 0.6 is required for satisfactory DEM quality.

start-stop time determination [J-125], [IC-186], [RC-448]. Despite the single-pass interferometry, slightly different propagation directions through the troposphere cause small path delay differences that have to be corrected as well. Finally, the calibration of the interferometric system has reached such an accuracy level, that more than 90% of all so-called Raw DEMs are within ±10 m of the reference DEM derived from SRTM/ICESat data already before the final calibration step using ICESat data as reference heights.

Interferometric Coherence

The interferometric coherence of the acquired data has been monitored throughout the entire mission and has served as a trigger parameter for optimizing the global acquisition strategy [J-137]. The global coherence map is shown in Figure 2.1-12. The interferometric coherence represents the normalized correlation coefficient between the pair of interferometric acquisitions, quantifies the amount of noise affecting the interferogram, and is the key parameter for assessing its quality. It comprises all decorrelation sources such as signal-to-noise ratio, quantization, ambiguities, baseline decorrelation, volume decorrelation and temporal decorrelation [J-96], [J-187].

Challenges for DEM Acquisitions

Several error contributions may affect the quality of an interferometric SAR (InSAR) DEM [RC-592]. They depend on both the particular land cover and terrain characteristics of the area under illumination and the specific acquisition geometry used for the data take. In detail:

High-relief terrain: SAR acquisitions over steep and irregular surfaces are often affected by geometric distortions such as shadow and layover. In most cases, a re-acquisition of the affected area from a different observation geometry mitigates such effects.

Forested areas: Over vegetated areas the presence of multiple scatterers at different heights within a single resolution cell causes volume decorrelation. Optimized acquisitions using smaller baselines reduce these effects [J-60], [J-153].

Snow and ice: Similarly to vegetated areas, dry snow/ice-covered regions are also characterized by volume scattering, which leads to volume decorrelation and contributes to a degradation of the interferometric performance.

Sandy deserts: The quality of SAR surveys over sandy regions is strongly affected by the weak backscattered returns, which are caused by a strong absorption of the radar pulses. Again, the use of steeper incidence angles results in an increased backscatter and, consequently, a higher signal-to-noise ratio [J-61], [RC-399].

Phase unwrapping errors: These are the most prominent errors in interferometric DEM processing. In cases where regions of different heights are separated by regions of incoherent data, or if the interferometric phases show significant jumps in the order of the height of ambiguity (i.e., the height corresponding to a full 2π phase change in the interferogram), a correct unwrapping is not possible without additional information. To achieve robust phase unwrapping two TanDEM-X acquisitions with different baselines have been systematically combined.

Data Acquisition Strategy and Optimization

The acquisition strategy to generate the global DEM has been driven by the product specification for the relative height accuracy, which is in turn directly related to the height of ambiguity. Hence, the latter needs to, on the one hand, be sufficiently small to ensure the specification fulfillment on global scale, and on the other it must be large enough to guarantee a robust phase unwrapping process [NJ-13], [RC-596], [R-72].

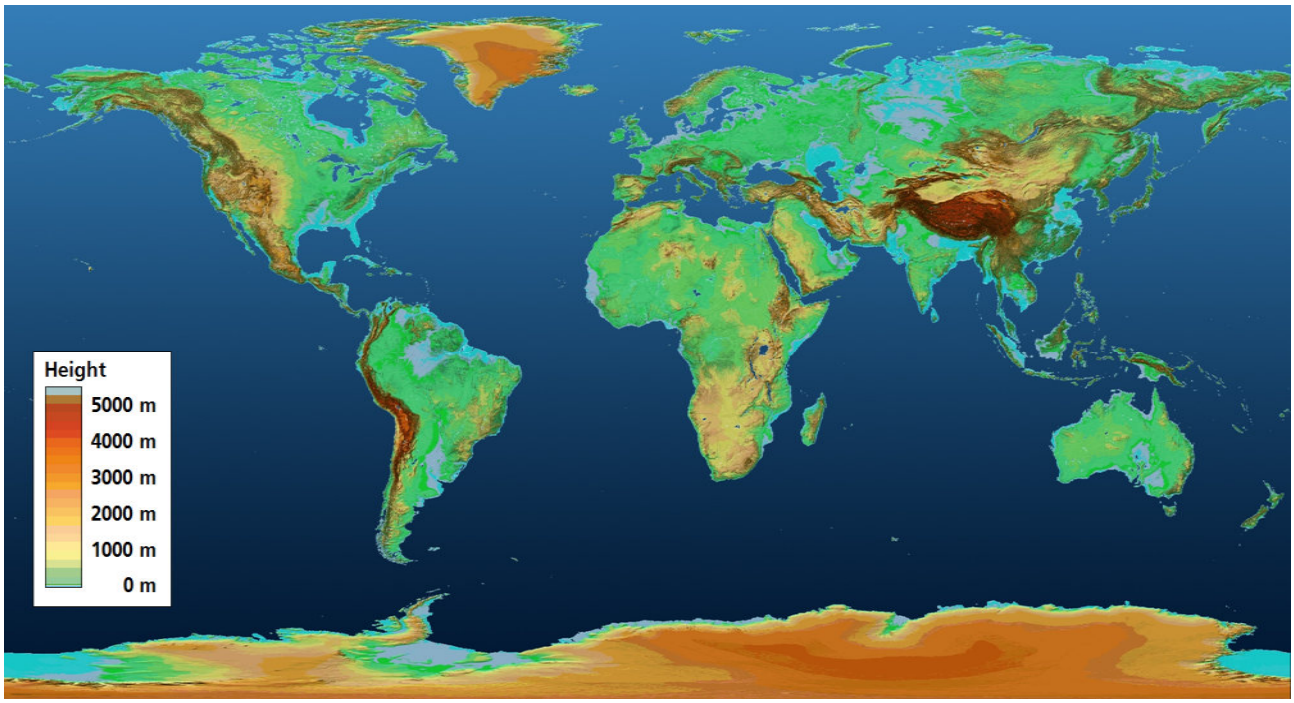

Figure 2.1-13 The global TanDEM-X DEM, which has been available for scientific and commercial applications since September 2016.

Nominal DEM acquisitions were performed in right-looking observation mode in ascending/descending orbits over the Northern and Southern hemisphere, respectively. In order to prevent the satellites from irradiating and potentially damaging each other, the so-called *exclusion zones* have been defined, which constrain the portions of the orbit in which the individual satellites can be active or passive for bistatic data takes.

In the first year of operation – from December 2010 to March 2012 – a global acquisition of the Earth's landmasses excluding Antarctica was carried out (see Figure 2.1-10). According to the acquisition strategy, the orbit formation was properly set in order to keep a height of ambiguity of about 50 m for all different incidence angles and latitudes. The Helix formation has been continuously reconfigured (see Figure 2.1-11).

To allow reliable phase unwrapping, additional acquisitions were performed over densely forested areas (e.g., over the Amazon rainforest in Brazil or the tropical forest in South East Asia) and over mountainous regions. For this reason, acquisitions with a height of ambiguity typically larger than 60 m, hence requiring smaller baselines, were commanded. Such acquisitions were performed starting in October 2011 [IC-173], [IC-202], [IC-203].

The acquisitions of the second global coverage started in April 2012 and lasted until April 2013 [IC-139], [IC-163], [IC-166], [IC-167], [IC-168], [RC-554], [RC-585], [RC-637]. The target height of ambiguity was reduced from 50 m to 35 m. The decrease by a factor of 0.7 was found to be optimal to combine the two acquisitions for the exploitation of multi-baseline phase unwrapping algorithms and for the overall improvement of the relative height accuracy [IC-106], [IC-131], [RC-454], [RC-460], [RC-464], [RC-465]. The two global coverages were performed using swath positions shifted against each other by half of the swath width to reduce the impact of SNR degradation at the swath edges, resulting in nearly constant height performance over the whole access range [IC-136], [IC-137]. In addition, the quantization rates have also been fine-tuned to optimize the trade-off between SAR performance and data volume [RC-506]. Continuous performance analysis and monitoring during the first two years suggested the need to perform further acquisitions with optimized imaging geometry over critical areas [IC-175], [RC-622]. Referring to the global coherence map of the first year shown in Figure 2.1-12, one can notice reduced coherence values over forested area, as well as over snow- and ice-covered regions, deserts and mountainous areas [IC-160]. Moreover, as described above, dedicated data acquisition strategies have been applied to improve the performance over sandy deserts (by acquiring data with steeper incidence angles) and over mountainous regions (with ascending and descending orbit acquisitions) [J-61].

To complete the global DEM generation, Antarctica has also been acquired twice: during the austral winter – between May and July 2013 – and again during the same months in 2014. This made it possible to achieve a stable performance, as no significant snow melt occurred. The central part of Antarctica (over a radius of 1300 km from the South Pole) cannot be seen in the nominal right-looking imaging mode due to the retrograde polar orbits of TerraSAR-X and TanDEM-X. For this reason, left-looking observations using shallower incidence angles above 50° were required [RC-236].

DEM Calibration and Mosaicking

The scene-based processing uses no external reference data for height calibration or phase unwrapping. It relies solely on the excellent synchronization, baseline accuracy, and delay and phase calibration of the TanDEM-X system for DEM geocoding [RC-233].

The small remaining offsets and tilts for a single data take are in the range of a few meters (most of them are even below 2 m). These residual errors are estimated and compensated for in the final processing step using a small selected subset of ICESat

points for calibrating and adjusting single DEM scenes. Finally, an optimized logic is applied to fuse them into the final mosaicked product. Dedicated calibration and mosaicking strategies have been developed in cooperation with the Earth Observation Center at DLR, where experts of our Institute played a key role in the definition of the operational algorithms.

Global DEM Performance

The global TanDEM-X DEM is partitioned into more than 19,000 geocells covering 1° x 1° in latitude and longitude. Each geocell contains the DEM as well as various layers that provide the user with additional information, such as the height error map (HEM), the mosaic of the mean amplitude (AMP), a water indication mask (WAM) and a coverage mask (COV).

The performance presented in this section is assessed separately for three different classes of DEM geocells according to the dominant land cover type: *forest* geocells, characterized by more than 60% of forest coverage; *ice* geocells, with more than 60% of ice or snow coverage; and *generic* geocells, i.e., all other geocells. The first two types are strongly affected by volume decorrelation [RC-330].

Absolute height accuracy: The absolute vertical accuracy represents the uncertainty in the height of a point with respect to the WGS84 ellipsoid caused by uncorrected, slow-changing systematic errors. The evaluation of the final TanDEM-X DEM performance is based on the difference between TanDEM-X and ICESat points not used in the DEM calibration. On a global scale, the performance in terms of absolute vertical accuracy has been evaluated using the best 1000 ICESat validation points per DEM geocell, characterized by the lowest spatial variance, and thus tending towards moderate-relief terrain. The prioritization of flat regions in the evaluation does not compromise the validity of the proposed method, as the main error sources are the remaining tilts and low-varying trends, which affect the entire geocell. The results confirm the outstanding capabilities of the system, with an overall absolute height accuracy at a 90% confidence level of just 3.49 m, which is well below the 10 m mission specification [IC-67] (see Table 2.1-2). Excluding highly vegetated and snow/ice-covered regions characterized by radar wave penetration phenomena, and consequently strongly affected by volume decorrelation, it improves to 0.88 m (for *generic* geocells only). The geocell-based absolute height accuracy at 90% confidence level is depicted in Figure 2.1-14 (top). The effects of penetration are clearly visible over ice-covered and forested areas, where offsets between TanDEM-X and ICESat in the order of several meters are detected.

Relative height accuracy: The relative height accuracy – or point-to-point vertical accuracy – describes the precision of the local height differences and only accounts for random errors [J-192]. The relative height accuracy for each input observation can be directly estimated from the interferometric coherence and the number of looks by assuming a zero-mean Gaussian distribution [J-105]. For each geocell of the mosaicked TanDEM-X DEM, the estimation of the linear point-to-point confidence level for the specified height accuracy is derived from the height error map (HEM) – separately for flat (predominant slope lower than 20%) and steep terrain (predominant slope higher than 20%)

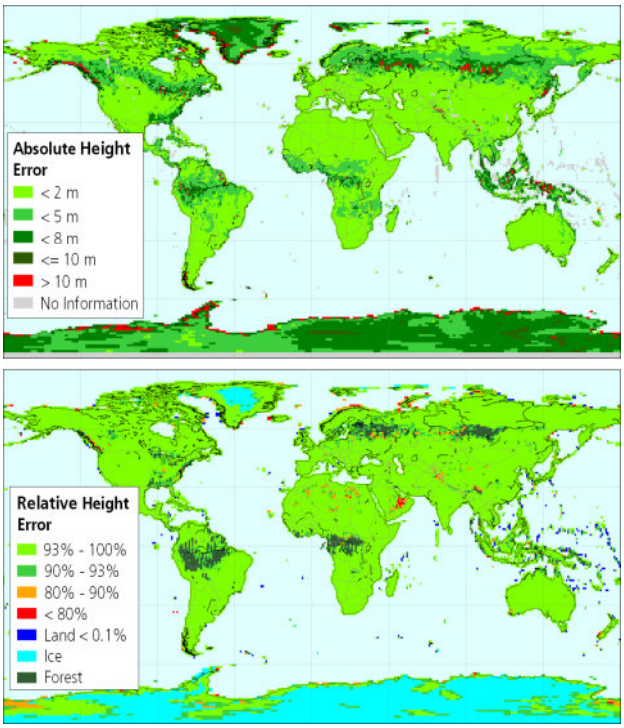

Figure 2.1-14 Geocell-based global DEM performance in terms of absolute height accuracy (top) and relative height accuracy (bottom)

[J-84], [RC-116], [RC-374].

An overview of the relative height accuracy of the final TanDEM-X DEM per geocell is shown in Figure 2.1-14 (bottom). Geocells in dark green and turquoise have an estimated confidence level below 90% and are either dominated by forest or mostly covered by snow or ice. Such geocells are affected by volume decorrelation phenomena, which artificially degrade the interferometric coherence. For this reason, they are disclaimed from the validation process. The same disclaimer is applied to geocells characterized by a large presence of water bodies (land below 0.1% in blue). The mission specification at 90% confidence level (2 m and 4 m for flat and steep terrain, respectively) is met on a global scale for 97.76% of all geocells not disclaimed due to volume decorrelation effects [RC-20].

Voids: Of the total TanDEM-X dataset, voids over land account for only 0.107% of the entire data set [R-126]. In other words, the data coverage is currently better than 99.89% [RC-75]. Figure 2.1-15 shows a comparison of the data coverage for both the unedited SRTM Version 1.0 and the TanDEM-X DEM in the Sahara desert, centered at 29.3°N, 2.5°W. Invalid data are depicted in black. In this example, the original SRTM data have a coverage of less than 75% whereas TanDEM-X has full (100%) data coverage.

The generation of the global DEM, which is the primary mission objective, was successfully completed in September 2016. The data quality and coverage are outstanding [J-31], [B-4], [RC-61], [RC-62], [RC-103], [RC-228]. DEM performance specifications have all been met or exceeded. In the case of the absolute height accuracy, the final result is one order of magnitude better than the 10 m requirement, as summarized in Table 2.1-3. The TanDEM-X interferometric data contain much more than the surface topography [RC-101]. For example, the global coherence data that have been primarily used to monitor and control

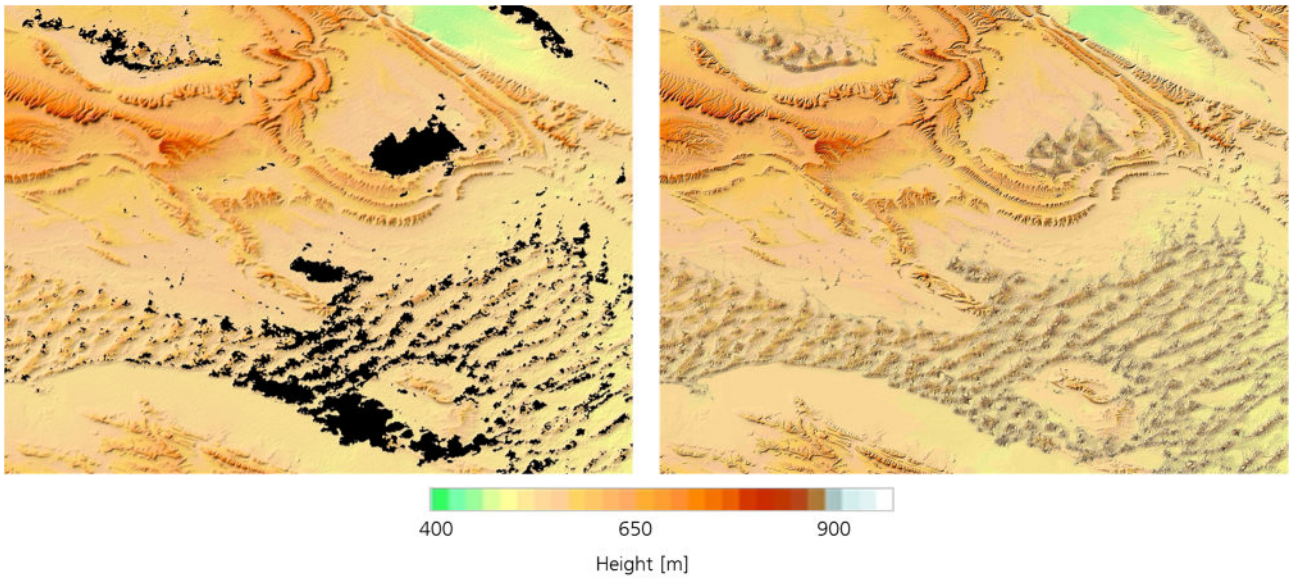

Figure 2.1-15 Comparison of voids between SRTM unedited version 1.0 (left) and TanDEM-X (right) DEMs in the Sahara Desert at 29.3°N, 2.5°W, where black represents invalid data.

the data acquisition contain interesting information on the surface cover that can be used to discriminate vegetated from non-vegetated areas, or to classify ice sheets, as described in the following section.

The Global TanDEM-X Forest/Non-Forest Map

Forests cover about 30% of the Earth's landmasses, play an essential role in many of our planet's dynamic processes, and are of extreme importance for all living species, preservation of biodiversity and healthy ecosystems. However, the rate at which severe loss and degradation of forests is occurring is alarming. Generating an up-to-date map of the global forest areas was therefore the main motivation for the TanDEM-X Forest/Non-Forest map [RC-63].

The used data set comprises all TanDEM-X images acquired for the generation of the global DEM between 2011 and 2016. To limit the computational load, quicklook data characterized by a ground resolution of 50 m x 50 m have been used to generate the global product. In the classification process, several observables systematically provided in the TanDEM-X quicklook data have been exploited, such as the bistatic coherence, the calibrated amplitude, and the digital elevation information. The amount of volume decorrelation can be directly derived from the interferometric coherence and has been used as main indicator for the identification of vegetated areas. It quantifies the amount of decorrelation due to multiple scattering within a volume, which typically occurs in presence of vegetation [J-60].

A machine-learning classification method based on fuzzy clustering was developed to generate the global Forest/Non-Forest map, [RC-64], [RC-76], [RC-102], [RC-156], [RC-157], [RC-158], [RC-224], [RC-279]. It was applied to the volume decorrelation derived from TanDEM-X scenes extending over 30 km x 50 km. The output is the so-called weighted membership matrix, which describes a pixel's probability of belonging to either the 'Forest' or the 'Non-Forest' classes. The final binary information is then obtained by properly thresholding such a matrix.

In the next step, all available acquisitions from the TanDEM-X global data set are properly combined and mosaicked. Typically, at least two (over mountainous terrain, forests, and sandy desert regions up to 10) coverages are available; overall, more than 500,000 bistatic scenes have been considered. The weighted membership matrix is used as input data for the mosaicking process in each scene. For each pixel on the ground, all available independent observations are combined by taking into account the reliability of each input measurement. Other information available at scene level, such as layover and shadow layers, the

Statistics	Generic geocells	Ice geocells	Forest geocells	All geocells
Number of geocells	12,257	3019	4113	19,389
Landmass [million km²]	96.68	14.31	33.22	144.21
Accumulated number of validation points (millions)	10.20	2.71	2.58	15.49
Mean height deviation of validation points [m]	0.04	-2.83	0.57	-0.37
Accumulated absolute height accuracy of 10 m (linear error)	99.84%	98.42%	99.17%	99.48%
Accumulated absolute height accuracy with 90% linear error [m]	**0.88**	**6.37**	**2.33**	**3.49**

Table 2.1-3 Summary of the absolute height accuracy, evaluated using the best 1000 ICESat validation points per DEM geocell. The achieved performance is provided for generic, ice, forest and all geocells.

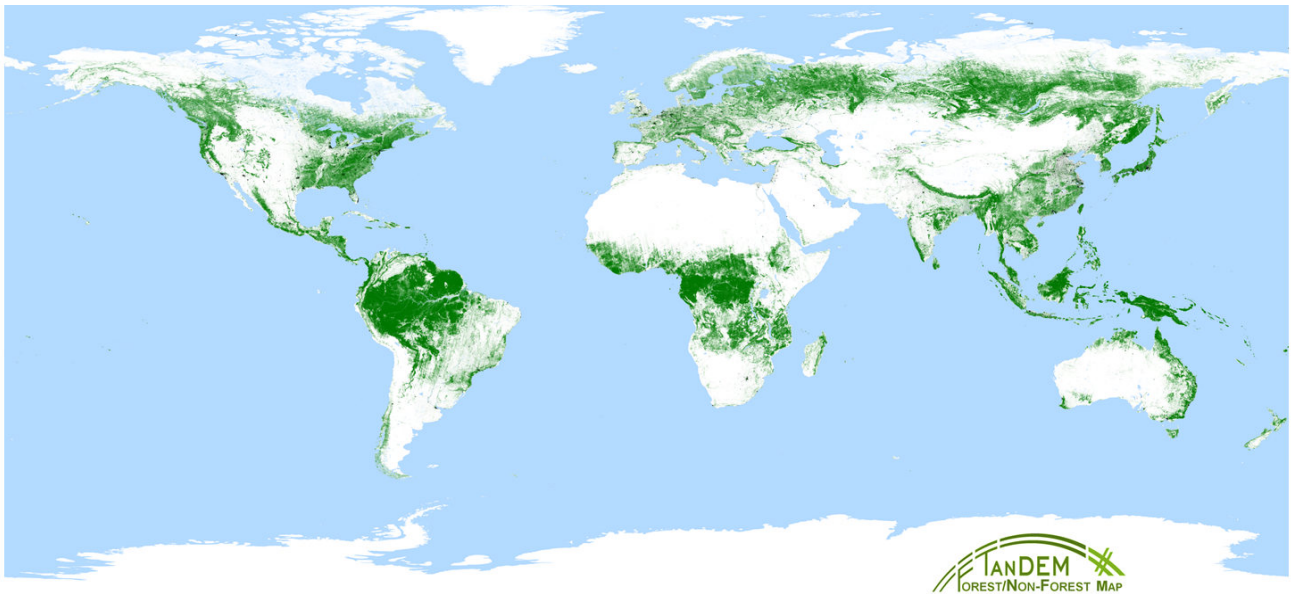

Figure 2.1-16 TanDEM-X Forest/Non-Forest map (green: forest, white: non-forest, light blue: water)

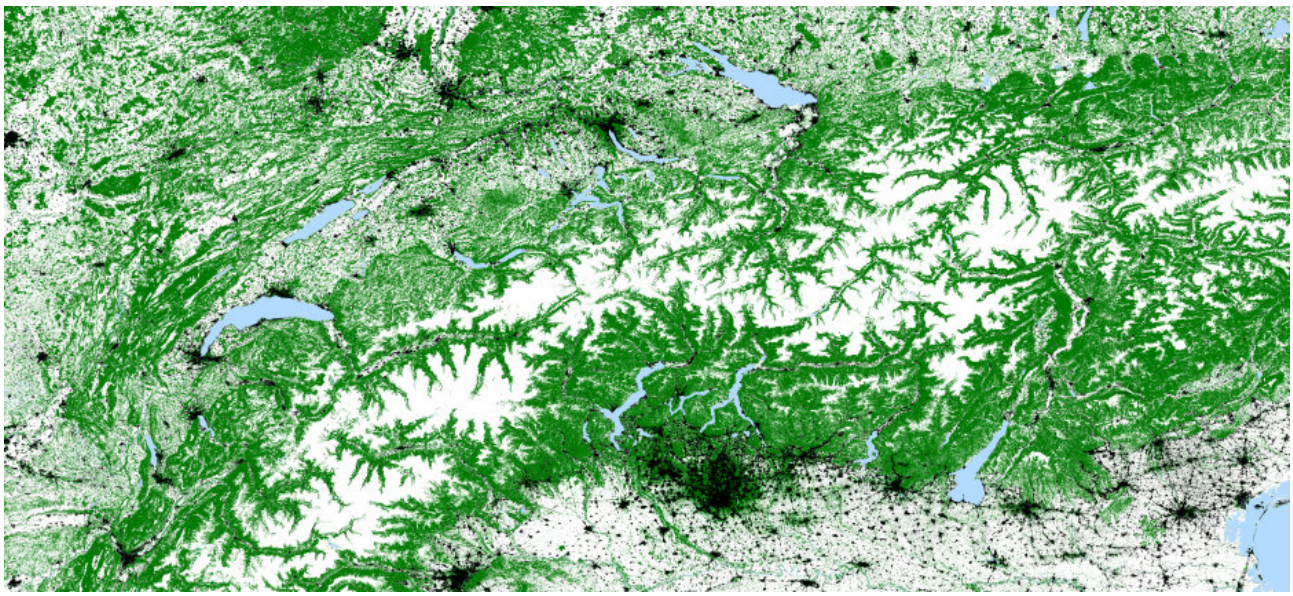

Figure 2.1-17 Zoom in on the Alps of the Global TanDEM-X Forest/Non-Forest map (green: forest, white: non-forest); urban areas (depicted in black) were identified using the TanDEM-X Global Urban Footprint (GUF) from DLR-DFD, while water bodies (light blue) were masked using the ESA CCI Land Cover Map.

local incidence angle and the height of ambiguity are also exploited in the mosaicking process.

Finally, additional annotation layers are utilized or directly generated to filter out water bodies, cities, deserts, and geographic regions above the altitude of the tree line, where no tall vegetation can grow. For example, a global map of the tree line boundary altitude has been derived by combining information from the TanDEM-X global DEM and the GlobCover classification map provided by the European Space Agency.

The global TanDEM-X Forest/Non-Forest map is presented in Figure 2.1-16, and a zoom-in of the final product over the Alps in Figure 2.1-17.

The validation of the global product represents a challenging task that is still ongoing, since it requires reliable external reference data. The performance observed from a first analysis over dedicated test sites is very promising [RC-21], and the obtained classification accuracy ranges between 85% and 93%.

As mentioned before, the global TanDEM-X Forest/Non-Forest map has been produced at the quicklook resolution of 50 m x 50 m. High-resolution forest classification maps from TanDEM-X data are being produced at an independent sampling of 12 m x 12 m using standard boxcar multilooking, which is also applied in the operational DEM processing chain. They can be exploited on a local scale to further improve the classification detail and accuracy, making a regular monitoring of forests possible. Furthermore, advanced processing techniques, based, for example, on the use of non-local filters, are being investigated as well [RC-69]. They allow a significant de-noising and simultaneous detail preservation of the classified images, especially over agricultural areas.

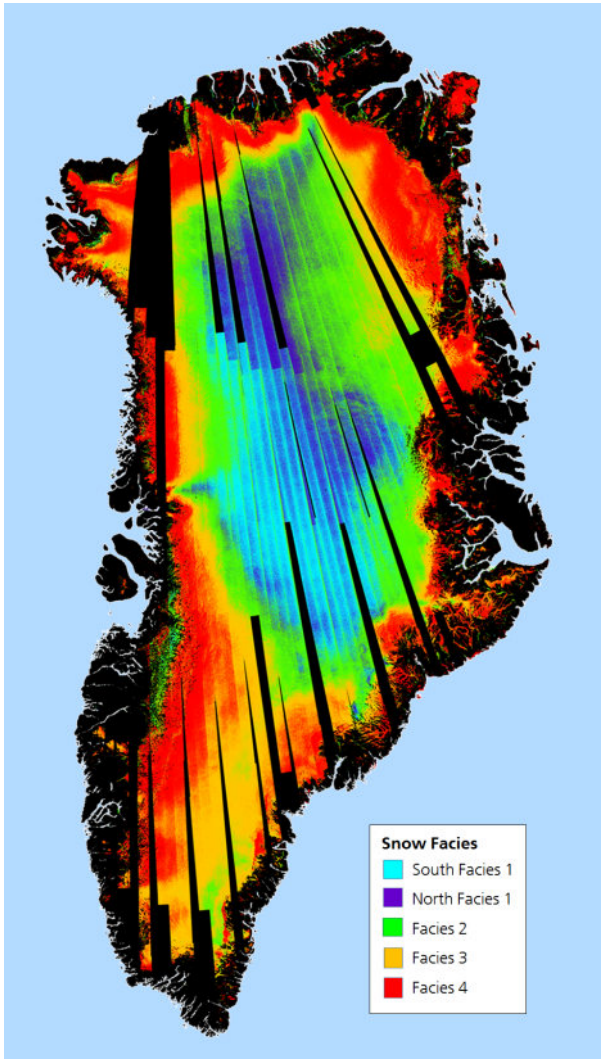

Figure 2.1-18 Classification map of different snow facies over the Greenland ice sheet derived from TanDEM-X interferometric data. Facies 1 is mostly dominated by the presence of dry snow while melt phenomena increase towards the outer facies, mostly characterized by the presence of percolating features and wet snow.

Greenland Ice Sheet Classification

TanDEM-X data also enable the discrimination of additional land cover classes, such as permanent snow and ice-covered regions, man-made structures, water bodies or agricultural areas [RC-40], [RC-42], [RC-309], [RC-425]. As an example, Figure 2.1-18 shows a classification map of different snow facies over the Greenland ice sheet. It was derived from TanDEM-X data acquired during the winter of 2011 by combining both backscatter information and volume decorrelation in an unsupervised k-means fuzzy clustering algorithm [RC-199], [RC-200]. Each facies is characterized by different snow characteristics, such as the density, grain size, and microstructure of firn [J-32], [RC-308].
In the future, these activities will be expanded, and TanDEM-X data will be combined with other sensors to improve the ability to see and follow dynamic changes in the land cover at a larger scale and over a wider time span [RC-201]. Investigations on the use of Sentinel-1 data to detect hot spots of deforestation activities, which can then be monitored in high resolution by TanDEM-X, are the first step in that direction [RC-60].

TanDEM-X Digital Beamforming Experiments

From the very first ideas for a DEM generation mission, it became clear that a bistatic SAR interferometer featuring a multitude of modes in combination with adjustable baseline configurations is the perfect test bed for advanced radar techniques. One very interesting example is the demonstration of the capabilities of future distributed SAR satellite systems.
Classical single-channel SAR systems have limited capabilities when it comes to the imaging of a wide swath with high azimuth resolution, since they are constrained by contradicting PRF requirements. Indeed, wide swaths require low PRF values, whereas the broad Doppler spectrum, an inherent property of images with high azimuth resolution, calls for high PRF values to satisfy the Nyquist criterion. The utilization of multiple phase centers in azimuth offers the possibility to reduce the PRF, and therefore to acquire a wide swath with high azimuth resolution.

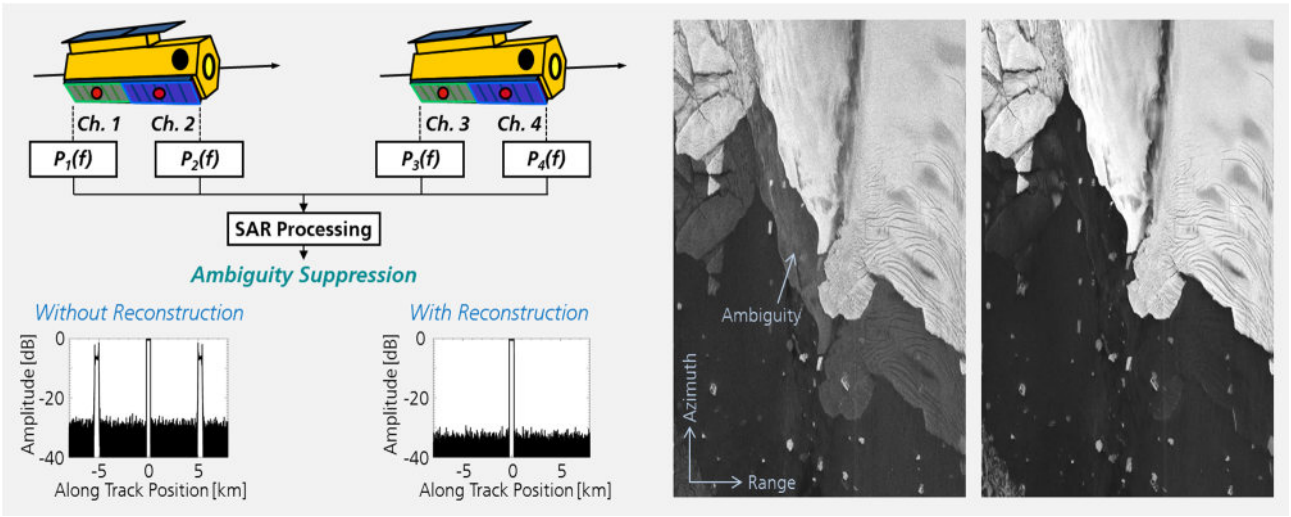

Figure 2.1-19 Left: Schematic overview of ambiguity suppression by means of digital beamforming, which enables high-resolution wide-swath imaging. Right: Comparison of a low PRF TerraSAR-X image (left SAR image) and the image reconstructed from four azimuth channels with two channels each on TerraSAR-X and TanDEM-X, both operated in DRA mode (right SAR image). The azimuth resolution of the reconstructed image is improved by a factor of two. Additionally, the ambiguities are significantly reduced, which is clearly visible at the land-sea transition comparing the left and the right SAR image.

TerraSAR-X and TanDEM-X each provide two azimuth phase centers in the so-called dual-receive antenna (DRA) mode. During nominal operations, the receive signals of the fore and aft halves of the antenna are added using a hybrid coupler and recorded as the sum channel. In the DRA mode, the signal on the difference port of the hybrid coupler is also recorded using the redundant receiver chain. The application of a calibration and reconstruction algorithm enables the separation of the signals of the fore and aft antenna halves.

A first demonstration of azimuth ambiguity suppression using single satellite TerraSAR-X DRA mode data [J-160] was followed by a second one with both TerraSAR-X and TanDEM-X in a multistatic configuration [RC-151], [RC-152]. When operated in DRA mode, this provides up to four phase centers on two satellites, as depicted in Figure 2.1-19 (left). The multistatic character of the experiment is extremely interesting since constellations or swarms of several small and cost-effective satellites are a promising option for future high-resolution wide-swath SAR imaging. The flexibility of the TerraSAR-X and TanDEM-X system in terms of orbit geometries and instrument commanding offers the unique possibility to demonstrate new techniques such as the multichannel SAR signal reconstruction with actual spaceborne data.

Dedicated data takes in stripmap mode were acquired over the coastline of Antarctica for the experiment. One of the most significant performance parameters, which has to be analyzed for a multichannel system, is the azimuth ambiguity-to-signal ratio. The commanding was thus adjusted to PRFs lower than nominal in order to provoke azimuth ambiguities in the single-channel SAR data. The actual scene in Figure 2.1-19 (right) was chosen to contain a high contrast region, i.e., a land-sea transition, where azimuth ambiguities are easily recognized.

To highlight the azimuth ambiguity suppression capabilities, the sum channel image of TerraSAR-X is compared with the reconstructed image based on four channels of both satellites as shown in Figure 2.1-19 (right). The image on the left is the standard TerraSAR-X SAR image showing strong ambiguities in the water area. The right image is processed to an azimuth resolution improved by a factor of two. In addition, the azimuth ambiguities in the water near land are clearly reduced in the right image [RC-38]. These results are regarded as an important step towards the vision of distributed SAR systems.

TanDEM-X Science Coordination

The Institute has the role of the TanDEM-X Principal Investigator and is also coordinating the international science team. Since 2010 the coordination of the international science team and the data take planning has been one of the major tasks, and has substantially contributed to the dissemination of the mission data. Six special announcements of opportunity (AO) have been launched for data take requests and over 1500 proposals have been received from 1140 science investigators worldwide. The majority of the proposals have been received from German scientists, confirming the national needs for the acquired TanDEM-X data.

A great success was the high demand for the TanDEM-X 12 m DEMs, with approximately 900 proposals and over 17,000 data products (geocells). The top three application spheres are geosphere, cryosphere and hydrosphere (see Figure 2.1-20) with a regional focus on Europe, Asia, all mountainous areas and the polar regions (Greenland and Antarctica), as shown in Figure 2.1-21. Proposal submissions are accepted at any time through the general announcement of opportunity. The 90 m DEM product will be made available to the science community without the need to submit a proposal. Upon simple registration, it will be possible to download the data globally via an FTP server. Currently, a dedicated observation plan is acquiring data for the next global DEM generation. Two main products will be available after the global acquisition: one new global 12 m DEM change layer and an updated TanDEM-X 12 m DEM. Dedicated future AOs are planned for the exploitation of the 30 m DEM and the Change DEM.

One additional task for the science coordination is to guarantee the exchange and feedback from the scientists that have used the data. The scientific results of the principal investigators have been presented in regular coordinated sessions at conferences (EUSAR and IGARSS 2011-2018) and the bi-annually organised TanDEM-X science team meetings at DLR.

There has been great participation in the science team meetings (2006, 2008, 2011, 2013 and 2016), with approximately 200 to 300 scientists presenting their results in oral or poster presentations. Selected applications have been posted as web blogs on the DLR portal.

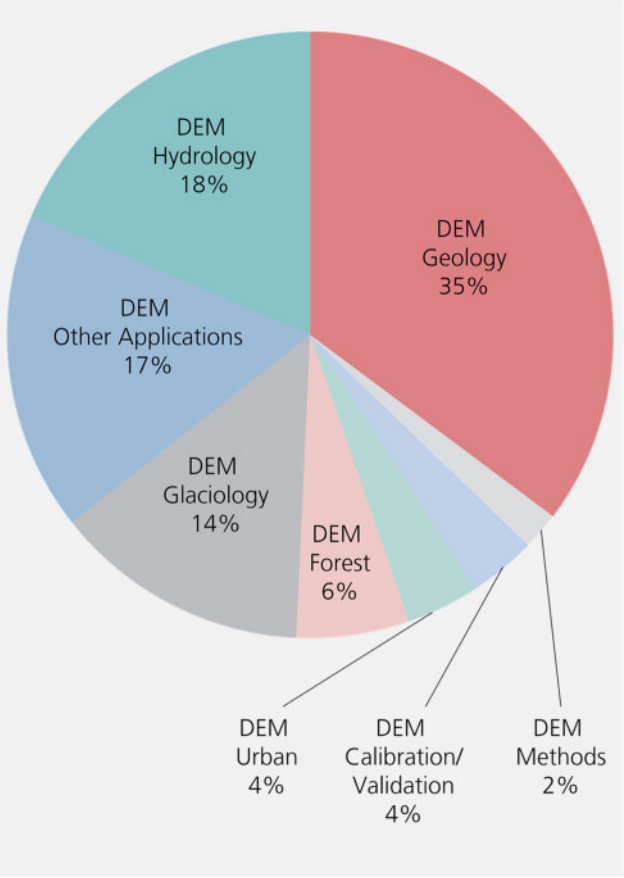

Figure 2.1-20 TanDEM-X DEM proposal submission statistics for the application spheres

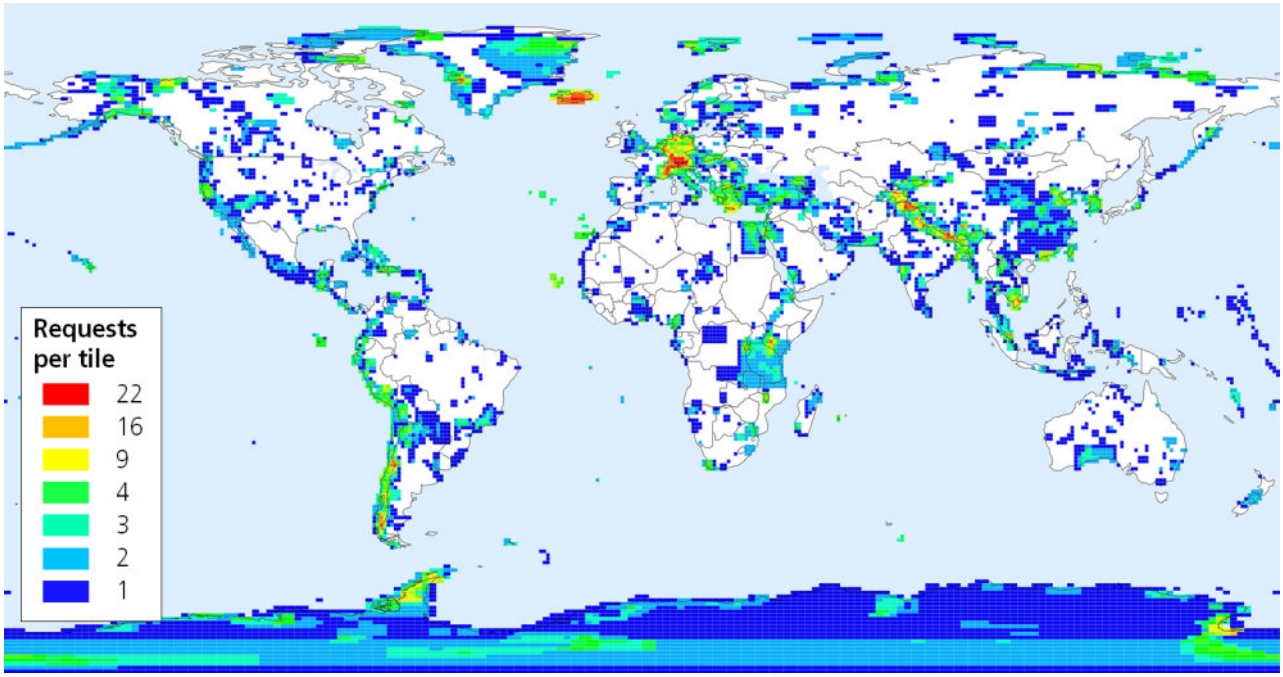

Figure 2.1-21 Global distribution of the TanDEM-X data requests for the digital elevation model in 12 m posting

Outlook

Despite being well beyond their design lifetime, both satellites are still fully functional and have enough consumables for operation into the 2020s. After completion of the global DEM, it was agreed to continue the TanDEM-X mission as single-pass bistatic interferometer, still a unique capability worldwide.

The quality of the global DEM generated by TanDEM-X is outstanding. A comparison between the DEM of the Shuttle Radar Topography Mission (SRTM) from the year 2000 and TanDEM-X (2013) in Figure 2.1-22 clearly shows the improvement in the horizontal resolution and height accuracy.

Most interesting in this example are the height changes that occurred in the time span of 13 years. In order to acquire topographic changes on a global scale and with high accuracy, a new bistatic acquisition plan has been developed taking into account the various lessons learned from the first global DEM acquisitions. According to the current plan, data for this global change layer will be acquired until the end of 2019, and it is expected that the product becomes available about one year later. This update of the global DEM of TanDEM-X is also considered a first step into future missions dedicated to the observation of dynamic processes on the Earth's surface.

TanDEM-X is an impressive demonstration of the Institute's outstanding end-to-end expertise in radar remote sensing. It is also the result of a long-term programmatic focus in Germany's national space program. This mission encompasses scientific and technological excellence in numerous aspects, including the first demonstration of a bistatic (distributed) SAR satellite system in space and the first close formation flight for an operational space application. Furthermore, TanDEM-X makes an important contribution to the conception and design of future SAR missions.

The most prominent example is Tandem-L, a mission to monitor dynamic processes on the Earth's surface with unprecedented accuracy, and which is described in the following section.

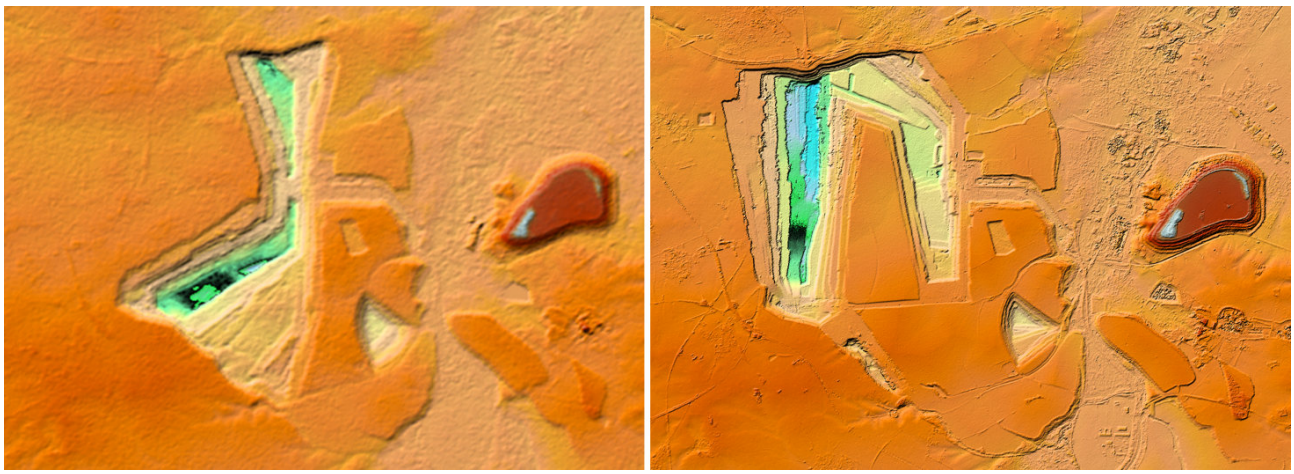

Figure 2.1-22 DEM of the evolution of the Garzweiler mine in Germany as seen by SRTM in 2000 (left) and TanDEM-X in 2011 (right)

2.1.3 Tandem-L

Tandem-L is a proposal for an innovative L-band SAR mission [J-97], [RC-43], [RC-44], [RC-86], [RC-281] for the systematic observation of dynamic processes on the Earth's surface with hitherto unparalleled quality and resolution. Due to the novel imaging techniques and the vast recording capacity of up to 8 terabytes/day, it will provide vital information for addressing pressing scientific questions in the biosphere, geosphere, cryosphere and hydrosphere, and will make an essential contribution to better understand the Earth system and its dynamics.

The Tandem-L mission concept is based on the use of two SAR satellites operating in L band with variable formation flight configurations and is distinguished by its high degree of innovation. Examples are polarimetric SAR interferometry (Pol-InSAR) for measuring forest height; multi-pass coherence tomography for determining the vertical structure of vegetation and ice; the utilization of the latest digital beamforming techniques in combination with a large deployable reflector for increasing the swath width and imaging resolution; and the formation flight of two cooperative radar satellites with adjustable baselines for single-pass interferometry.

The Tandem-L mission proposal was initiated by the Institute in 2007. Since then, we have been the driving force in its development, covering all aspects from the definition of the

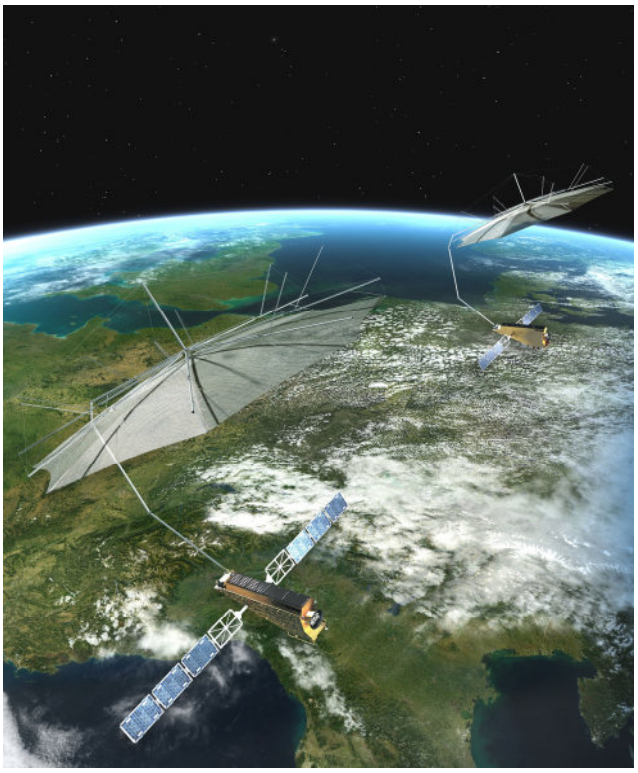

Figure 2.1-23 Artist's impression of the Tandem-L satellite twins flying in close formation

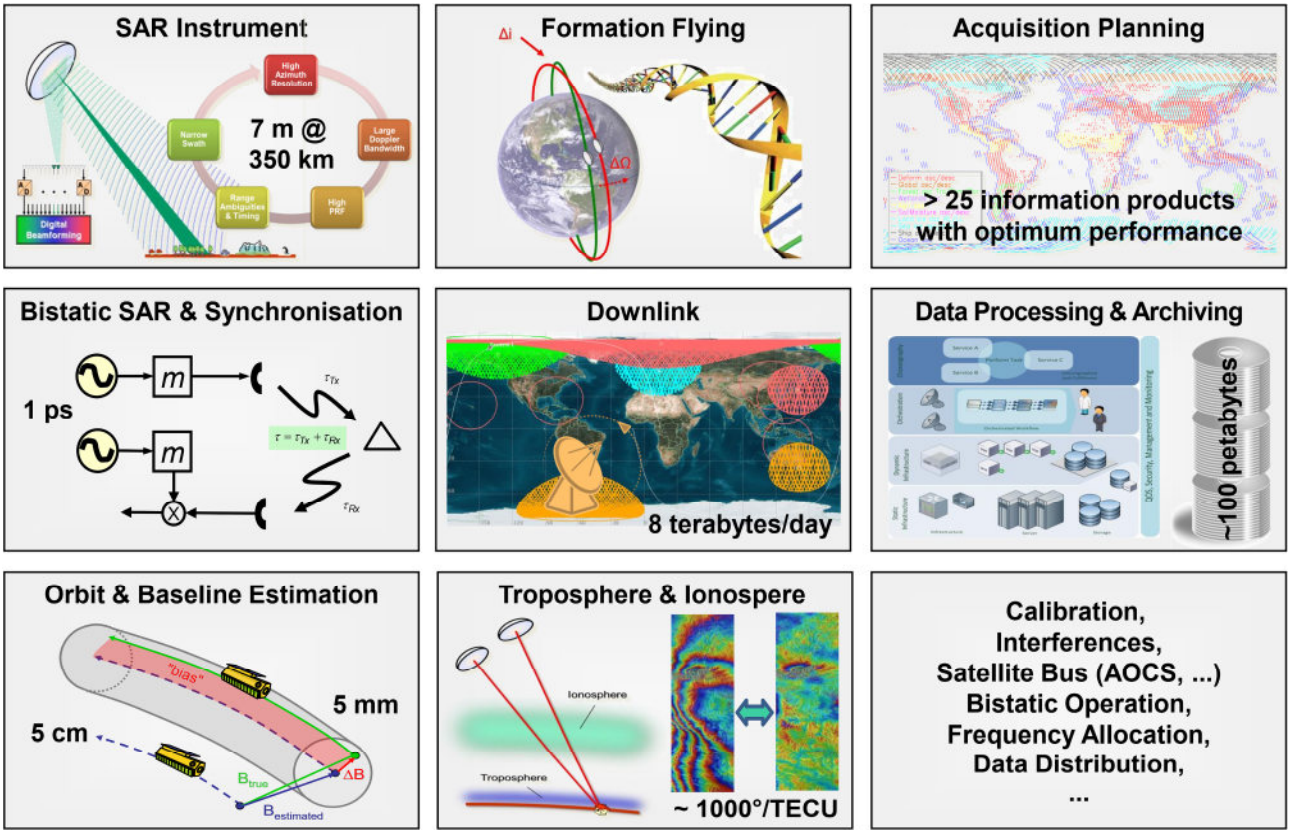

Figure 2.1-24 Tandem-L is based on two L-band SAR satellites flying in close formation and operating as a bistatic SAR interferometer. While key capabilities such as close formation flight, synchronization and precise baseline determination have been successfully demonstrated with TanDEM-X, this innovative concept brings with it new challenges. The most important elements are the advanced instrument featuring digital beamforming in combination with a 15 m deployable reflector, the generation of a consistent systematic observation plan for 25 information products, the processing and dissemination of roughly 100 petabytes of data, or the estimation and correction of propagation effects.

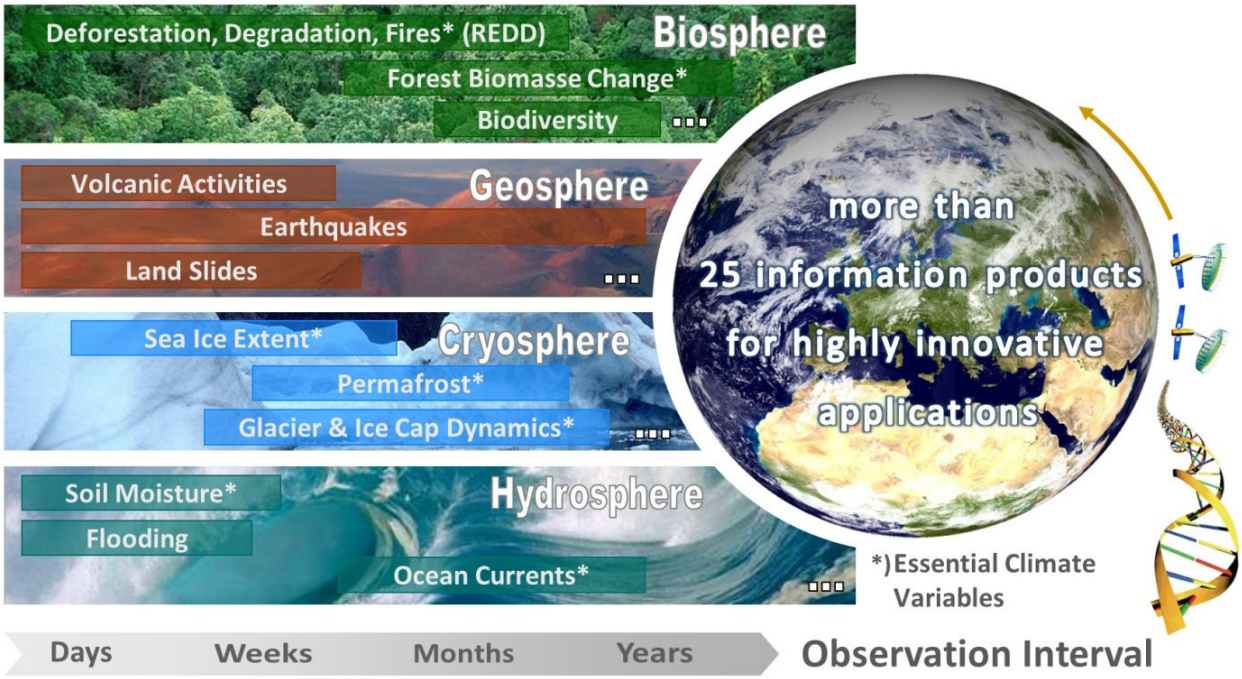

Figure 2.1-25 Tandem-L provides a unique observatory to monitor dynamic processes in the bio-, geo-, cryo-, and hydrosphere. A highly innovative instrument technology enables short observation intervals, as are required for the systematic monitoring of the Earth system and its dynamics.

science requirements and mission objectives, the mission, spacecraft, SAR instrument and calibration concepts, through to the definition of suitable flight formations, the optimization of a feasible observation concept, as well as the prediction of the higher-level product and overall mission performance. The Institute has also led the pre-phase A, phase A and phase B1 studies with a team of more than 80 scientists in close cooperation with the German aerospace industry. Phase B1 was successfully concluded with an Intermediate System Requirements Review in early 2018. It involved the various DLR teams in charge of the mission, ground and user segment, as well as Airbus Defence and Space and OHB/Hensoldt, who performed competitive space segment studies.

Mission Objectives

The Earth system is constantly changing, and dynamic processes occur in different spheres and at different time scales. Tandem-L is an innovative satellite mission for the global observation of these dynamic processes on the Earth's surface with unprecedented quality and resolution. Figure 2.1-25 shows a number of selected examples to illustrate the spectrum of observation intervals needed to analyze important dynamic processes in the different Earth spheres. Tandem-L has been designed to observe a wide range of processes at adequate time intervals. Owing to its novel imaging techniques and its great acquisition capacity, Tandem-L will deliver urgently-required information for finding solutions to pressing scientific questions in the domain of the bio-, geo-, cryo- and hydrosphere. In this way, Tandem-L will significantly contribute to obtaining a better understanding of the Earth system and its dynamics.
Important mission goals are the global measurement of forest biomass and its variation in time for a better understanding of the carbon cycle; the systematic monitoring of deformations of the Earth's surface on a millimeter scale for the investigation of earthquakes and risk analysis; the quantification of glacier motion and melting processes in the polar regions; the fine scale measurement of variations in the near-surface soil moisture, as well as observations of the dynamics of ocean surfaces and ice drift. Tandem-L will simultaneously measure seven essential climate variables in a single satellite mission.
The following list summarizes, for each sphere of the Earth system, three key scientific questions that Tandem-L will address, and for which it is designed to provide answers.

Biosphere

How large is the amount of biomass stored in the Earth's forests, and what is its spatial distribution, considered in various scales of resolution?

How do the biomass and the structure of forests change over time? Where and to what extent are these changes taking place? Where are the hotspots of anthropogenic deforestation?

How do climate change and anthropogenic disturbance impact the structure and stability of forests? Where does disturbance occur, and how quickly is it spreading?

Geosphere

Is it possible to measure the build-up of stress along plate boundaries (at scales >> 1000 km²) and to improve the forecast model for a particular earthquake?

Where is the fault zone of an earthquake located and how big is it? How much energy is accumulated prior to an earthquake, and how much of it is released during the earthquake and the subsequent phase of relaxation? Is it possible to use

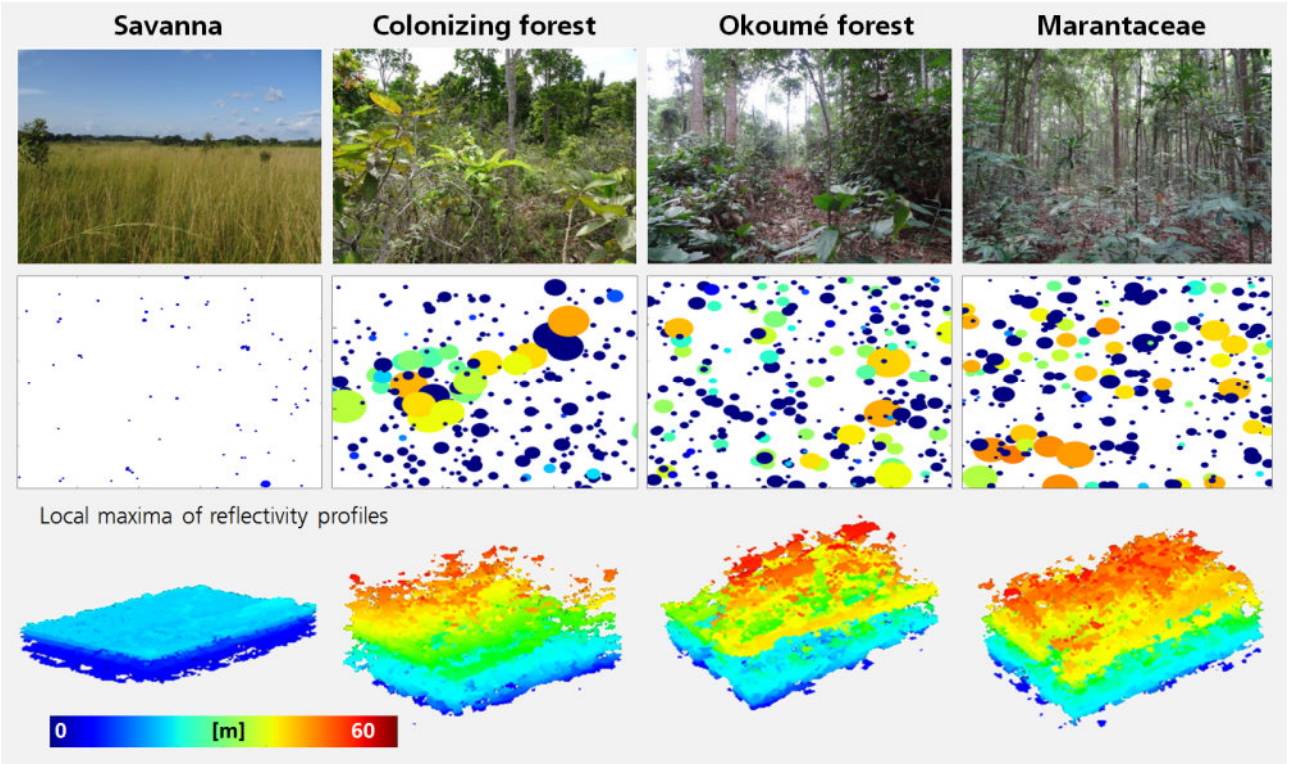

Figure 2.1-26 Different types of forests and savanna (top) compared in terms of their height profiles. The tree heights of exemplary scenes for each forest type are estimated and shown in the middle. The size of a circle represents the size of the crown while the color indicates the height of the tree. The local maximum height of the scene is given in the form of reflectivity profiles (bottom).

measurements of surface deformation to predict threats in volcanic regions? How are volcanoes connected to their environment?

Cryosphere

What is the impact of climate change on glaciers and ice caps? Which mechanisms cause this change, and how can they be better assessed?

Which processes drive current mass depletion in the major ice sheets? How can the uncertainties in determining mass changes be reduced?

How is global climate change altering sea ice drift and the deformation patterns in the Arctic and Antarctic? What methods can we use to improve the modelling of internal forces and to obtain better sea ice forecasts?

Hydrosphere

How do the spatial and temporal dynamics of soil moisture contribute to soil and plant transpiration? How does this affect the exchange of water and energy between the soil and the atmosphere? How do soil moisture patterns influence the formation of new ground water, surface run-off and soil water storage in moderately large river basins?

How strong is the link between spatiotemporal changes in soil moisture and changes in the regional climate (and weather)?

The data provided by Tandem-L will answer these and many other questions. To accomplish this, the data will first be consolidated as highly aggregated information products.

Mission Products

The Tandem-L mission will acquire global radar images in short repeat cycles (up to twice per week) in order to provide answers to the manifold scientific questions detailed above. A systematic global data acquisition schedule optimally meets the various scientific requirements while leveraging synergies, such as using a single radar image in several higher-level information products to the largest extent possible. To this end, the overall system is designed to allow the satellites to record up to 8 terabytes of raw radar data per day and to download this data via a Ka-band datalink to a global network of ground stations.

The Tandem-L mission will generate a broad range of SAR and higher-level products. SAR products contain raw data or image data from monostatic or bistatic acquisitions. Beyond the commonly known complex and detected products, the SAR product portfolio also contains stacks of repeat-pass monostatic or bistatic acquisitions.

A unique feature and major challenge of the Tandem-L mission is the systematic generation of 12 higher-level products, including forest height, structure and biomass, various surface deformation and displacement products, as well as digital elevation models. Mature algorithms are already available for these higher-level products. Additional products for applications in the hydro- and cryosphere are expected to be developed by the scientific community in the course of the mission. The acquisition of adequate SAR data for these applications is already covered in the observation concept. All applications and products are summarized in Table 2.1-4.

To facilitate the development of additional products, users will be able to use a so-called processing and exploitation platform

	Application		Mission Product	Resolution	Accuracy
Biosphere	Upper canopy height & Height change		Forest height & forest height change	50 m (global) 30 m (local)	10% or 2 m for heights <20 m
	Forest structure & change		3-D forest structure & change	50 m (global) 30 m (local)	20% or 20 t/ha for biomass <100 t/ha
	Above ground biomass & change		Forest biomass & change	100 m (global) 50 m (local)	20% or 20 t/ha for biomass <100 t/ha
	Agricultural products		SAR products	40 m @ 16 looks	-
Geosphere	Global strain rate map		3-D deformation rate maps	50 m	Vertical/East: 1 mm/year North: 10 mm/year
	Large-scale deformation		3-D deformation rate maps	50 m	Vertical/East: 1 mm/year North: 10 mm/year
	Earthquakes		LOS displacement maps	50 m	10 mm @ distances of 10 km
	Volcanoes	Long-term volcanic deformation	LOS deformation rate maps	50 m	-
			3-D deformation rate maps	50 m	Vertical/East: 1 mm/year North: 10 mm/year
		Volcanic activity	LOS displacement maps	10 m	10 mm @ distances of 10 km
	Small-scale deformation	Landslides	LOS displacement maps	10 m	10 mm @ distances of 10 km
			LOS deformation rate maps	50 m	-
		Urban subsidence	PSI deformation database	-	1 mm/year
Global	Digital elevation model (bare surface)		Digital terrain model	12 m	5 m (slopes ≤ 20%), 10 m (slopes > 20%)
	Digital elevation model (forest)		Digital terrain model Digital surface model	50 m 50 m	5 m (slopes ≤ 20%), 10 m (slopes > 20%) 10% of the forest height or 2 m for heights < 20 m
	Digital elevation model (ice, snow, dry sand)		SAR products	10 m	-
Hydrosphere	Soil moisture & soil moisture change		SAR products	20 m	-
	Coastal area change Ocean currents Wave height & wind speed velocity		SAR products	20 MHz (range) 7 m (azimuth)	-
Cryosphere	Glacier velocity & ice elevation change Land ice structure Grounding line position Sea ice type, extent and concentration Regional permafrost extent		SAR products	10 m	-

Table 2.1-4 Overview of Tandem-L applications, corresponding mission products, and associated resolution and accuracy

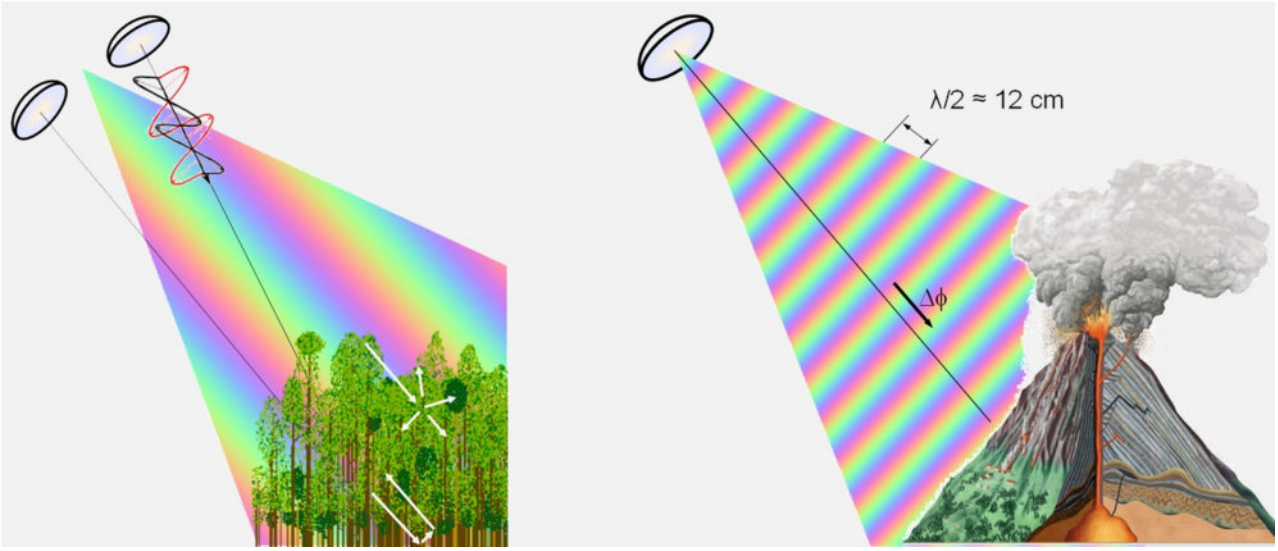

Figure 2.1-27 The two basic measurement modes of Tandem-L. Left: The 3-D structure mode employs polarimetric SAR interferometry and coherence tomography to measure tree heights and vertical vegetation profiles. The individual contributions from ground and canopy can be separated via their polarimetric signatures, and the corresponding heights can be measured by across-track interferometry and multi-baseline tomography. Right: The deformation mode employs repeat-pass interferometry to measure surface deformations with millimetric accuracy.

to apply individual, user-defined algorithms to generate higher-level information products at local and regional scales.
SAR products will be free of charge for all users, while higher-level information products such as forest biomass, deformation maps and digital elevation models will only be free of charge for scientific users.

Mission Concept

The Tandem-L mission concept relies on a systematic data acquisition strategy using two cooperating L-band SAR satellites flying in close formation. A sun-synchronous orbit at an altitude of 745 km (at the equator) and a repeat cycle of 16 days has been selected. This orbit ensures full global coverage in the quad-polarized mode providing a swath width of 175 km. Since the single- and dual-polarized modes provide a doubled swath width of 350 km, each point on the Earth can be mapped with at least two incident angles from both ascending and descending passes. The satellite system will be operated in the following basic measurement modes:
The **3-D structure mode** is especially designed for the three-dimensional surveying and tomographic imaging of volume scatterers, such as vegetation, ice, snow, and dry soil/sand. This mode uses both satellites to collect fully polarimetric and interferometric SAR data with adjustable across-track baselines (Figure 2.1-27, left). The simultaneous data acquisition with two satellites makes it possible to minimize errors from temporal decorrelation and atmospheric disturbances. This enables the generation of vertical structure information with unprecedented resolution and accuracy. The 3-D structure mode optimally fulfills the requirements of a large number of scientific applications pertaining to the biosphere, hydrosphere and cryosphere. The basis of the 3-D structure mode is the combination of polarimetric SAR interferometry (Pol-InSAR) with multiple baseline SAR coherence tomography. Tandem-L will be the first radar mission that can provide recurrent 3-D structure measurements with high spatial and temporal resolution on a global scale. The repeated tomographic observations will provide a unique data set for the scientific monitoring of internal structure dynamics in vegetation, soil and ice. A further important application is the simultaneous generation of both a digital surface and a digital terrain model, thereby complementing and updating the digital elevation data acquired by TanDEM-X.
The **deformation mode** employs repeat-pass interferometry to systematically monitor small and large-scale shifts on the Earth's surface with accuracies down to centimeters or even millimeters (Figure 2.1-27, right). An innovative ultra-wide swath SAR imaging mode with 350 km across-track coverage and a hitherto unparalleled azimuth resolution of 7 m will support the generation of consistent image stacks for large contiguous areas with frequent updates. This provides a solid data set to mitigate temporal decorrelation as well as tropospheric and ionospheric propagation errors. 3-D motion vectors are derived by combining data acquired from ascending and descending orbits with different incident angles, as well as in right- and left-looking configurations. Important applications served by the deformation mode are the large-scale monitoring of tectonic shifts at plate boundaries, the regular observation of volcanoes, the surveillance of urban subsidence, and systematic surveys of potential landslide areas.
The Tandem-L acquisition plan foresees a systematic variation of the across-track baselines to optimize forest height and vegetation profile measurements in the 3-D structure mode. To provide accurate tree heights and vertical structure profiles in the tropical forests, up to six acquisitions with vertical wavenumbers ranging from 0.05 rad/m up to 0.6 rad/m are planned for each season. Assuming an orbital altitude of 745 km and incident angles ranging from 30° to 40° in the bistatic quad-pol mode, this corresponds to horizontal baselines between 0.8 km and 19.9 km in the Helix formation with no radial orbit separation at the equator. An elegant technique to provide this

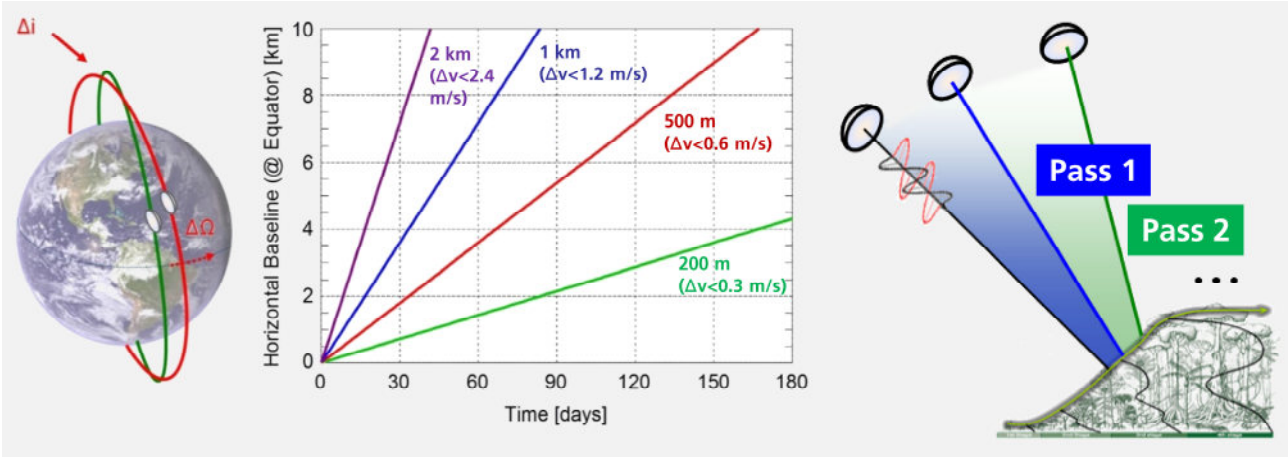

Figure 2.1-28 A systematic variation of the equatorial across-track baselines can be achieved by using orbits with slightly different inclinations. The inclination offset Δi causes a relative drift of the ascending nodes. The drift rate depends linearly on the inclination offset, whose adjustment requires a certain amount of fuel (Δv). Polarimetric SAR tomography makes it possible to derive the vertical profile of the forest canopies on a global scale.

wide range of across-track baselines exploits the naturally occurring differential secular variations of the right ascension of the ascending nodes in response to slightly different inclinations. Figure 2.1-28 illustrates the evolution of the horizontal baselines at the equator for different inclination offsets. The range of baselines adjusted for the 3-D structure mode provides also adequate geometries for DEM acquisitions with homogenous global height performance.

A challenge for Tandem-L is the adjustment of large across-track baselines at higher latitudes for the observation of temperate and boreal forests, and the measurement of vertical ice structure in polar regions. One opportunity to tackle this challenge is the use of a large eccentricity offset to provide a sufficient radial orbit separation at high latitudes, although a significant amount of fuel will be required to compensate the resulting motion of libration for longer time periods. Another opportunity is the use of the so-called pursuit monostatic mode, in which the satellites fly at along-track distances of several hundred kilometers. The time offset due to this along-track distance and the corresponding rotation of the Earth provides sufficiently large baselines at high latitudes. Furthermore, as the satellites acquire data independently in monostatic mode, the effective baseline doubles compared to bistatic data takes. During specific mission phases, the two satellites can also be used in a constellation mode. For this, one satellite is transferred in along-track direction by several thousand kilometers in order to reach the same ground track shifted by an integer number of days. The resulting two-satellite constellation can then effectively shorten the revisit times by a factor of two. This is of great advantage for those applications that require frequent interferometric observations or short average access times. Furthermore, the Tandem-L satellites can operate in both right- and left-looking mode without any limitations.

Satellite System

For the space segment it is assumed that two identical satellites are developed using a 2-ton class satellite bus. The satellites will be designed for a lifetime of 10 years, with all consumables supporting a mission extension to 12 years. Both bistatic and independent monostatic operation will be adopted in dedicated mission phases. For bistatic measurements, a bidirectional RF link is foreseen that can provide, a posteriori (i.e., on ground), a highly accurate mutual time and phase referencing with accuracies in the order of a few picoseconds and a few degrees in L band, respectively (heritage from TanDEM-X).

The relative position between the satellites will moreover be determined by double differential dual-frequency GNSS measurements. This approach, which has been used operationally during the TanDEM-X mission, can provide precise estimates of the 3-D baseline vector between the two satellites with accuracies below one centimeter.

Consolidated concepts for the Tandem-L spacecraft have been developed in the competitive phase B1 studies by Airbus Defence and Space and OHB/Hensoldt (see Figure 2.1-29).

SAR Instrument Innovations

The Tandem-L science requirements are met through an advanced instrument with capabilities beyond that of any known SAR sensor. Its key feature is the combination of a large deployable reflector antenna with a digital feed array [IC-46], [RC-25], [RC-132]. This allows a flexible beam shaping on transmit for optimum illumination of up to 350 km swath width. On receive, employing beamforming in the digital domain, multiple beams follow the radar echo while it traverses the swath. This is done by digitizing the echo signal received by each antenna element, yielding multiple digital data streams that are filtered (processed) on board the satellite.

The achievable SAR performance excels that of any current SAR system. In addition, Tandem-L is capable of fully polarimetric operation, thus adding a new dimensionality to conventional SAR performance. The fact that the entire beamforming is done in the digital domain gives access to a huge variety of digital filtering techniques, which can be applied using the available hardware [J-183], [IC-12], [RC-153], [RC-255]. For example, frequency dispersive filters, time varying impulse responses, angular nulling filters, or data compression (pre-summing) may

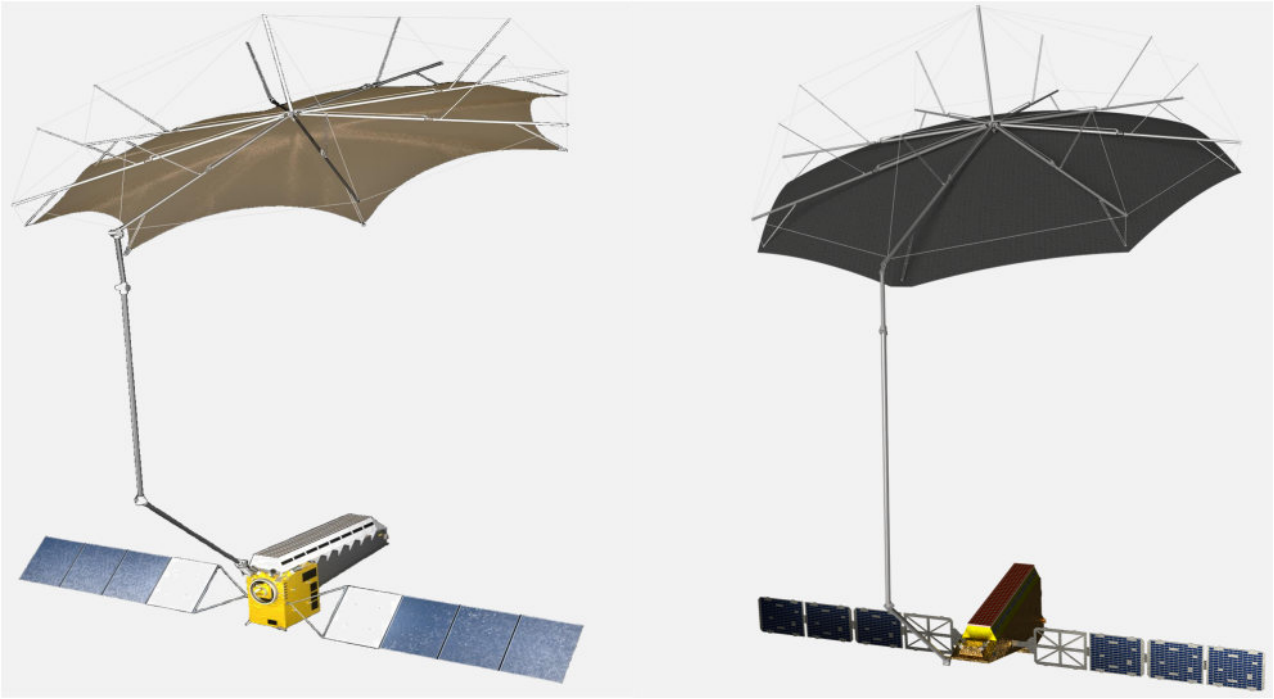

Figure 2.1-29 Phase B1 status of the Tandem-L spacecraft concepts: OHB/Hensoldt (left), Airbus Defence and Space (right)

Parameter	Value	Comments
Orbit height	745 km (@Equator)	231 orbits in 16-day repeat cycle
Orbital tube	500 m (3σ)	tube diameter, refers to master satellite
Horizontal baselines	800 m … 20 km	variable horizontal baselines for bistatic mode in close formation
Radial baselines	0 - 600 m	radial baselines are mainly for passive safety in close formation (Helix concept)
Local time	6 h / 18 h	dawn/dusk
Inclination	98.4°	Sun-synchronous orbit
Revisit time	16 days	the 350-km wide-swath mode enables up to 4 global data acquisitions from different viewing directions every 16 days
Frequency	L band	available frequency band: 1215 … 1300 MHz
Range bandwidth	84 MHz, 40 + 5 MHz, 20 + 5 MHz	split bandwidth modes for ionospheric corrections
Azimuth resolution	7 m	for swath widths up to 350 km (single/dual-pol.) for swath widths up to 175 km (quad-pol.)
Polarization	single/dual/quad	
Downlink capacity	~ 8 terabytes/day	via global network of Ka-band ground receiving stations
Look direction	right & left	nominal: right-looking, left-looking by horizontal/yaw satellite rotation
Reflector diameter	15 m	deployable reflector
Mission lifetime	10 years	consumables for 12 years

Table 2.1-5 Key parameters of the Tandem-L mission

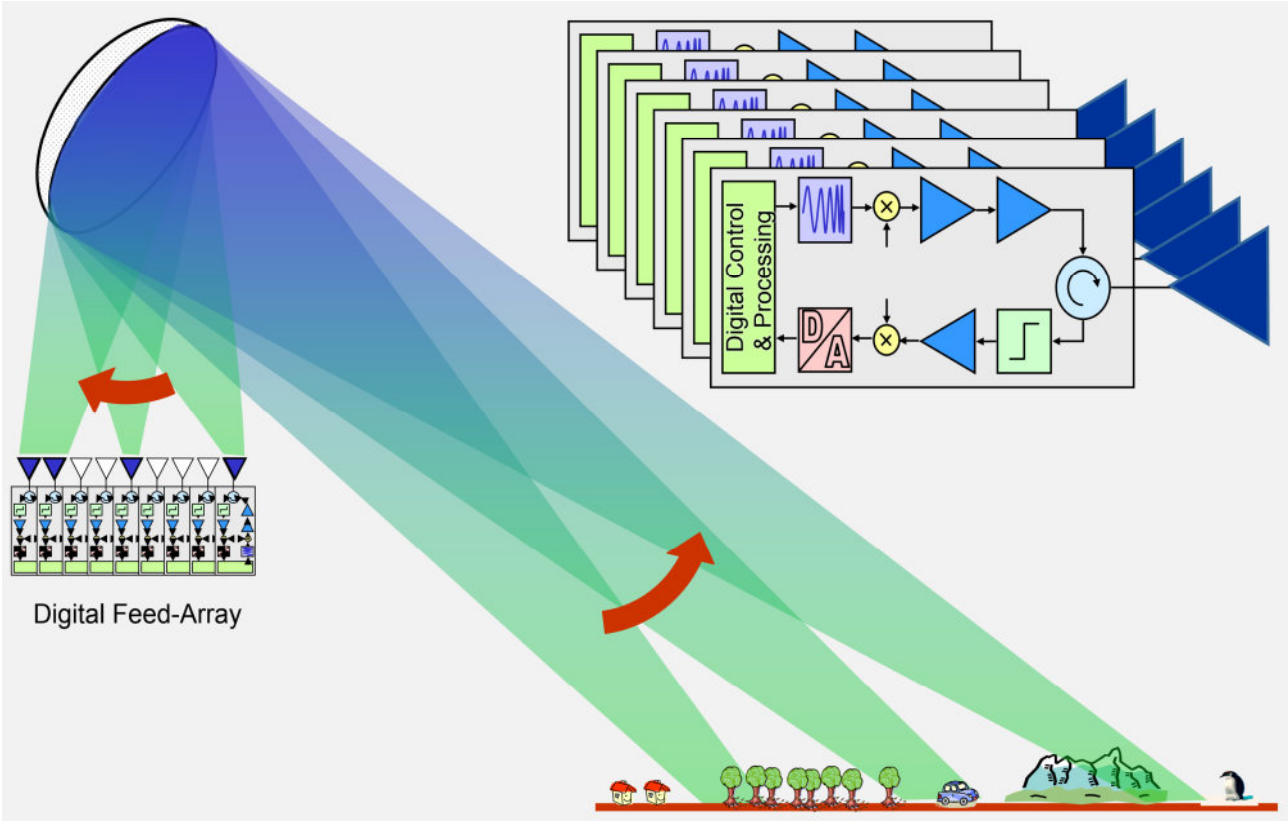

Figure 2.1-30 Scan-On-Receive operation principle where the entire swath is illuminated with all elevation feed elements active, while on receive a narrow high gain beam follows the pulse on ground. To cover a 350 km swath width at a sufficiently high PRF, pulses have to be transmitted in between, leading to blind ranges. At a constant PRF, these blind ranges result in images showing gaps at fixed swath positions. To close these gaps, the Institute developed the staggered SAR mode – a combination of continuous PRI variation and on-board interpolation of gaps (see Figure 2.1-31).

be applied on board. The SAR image generation (processing) is performed on the ground. Mastering the instrument design options and trades is a challenge, but the (digital) instrument offers all control capabilities necessary for optimization. This represents a quantum leap in SAR instrument evolution.

Wide Swath Imaging

The acquisition of very wide swaths with sufficient sensitivity requires large antennas to be deployed in space. Representing the state of the art for communication satellites, large mesh reflectors are now being considered for spaceborne SAR missions [PhD-19]. In contrast to direct radiating planar array antennas, a reflector is illuminated by an array of feed elements, which in turn deflects the electromagnetic wave towards the Earth's surface. A peculiarity of such array-fed reflector antennas is that each feed element receives echo signals from an essentially non-overlapping angular domain. A reflector is shown in Figure 2.1-30, where the feed array is almost horizontally aligned. A wide swath is illuminated by all elements simultaneously transmitting the chirp signal. On receive, a narrow high gain beam is generated by adopting only a small subset of feed elements in concordance with the direction of the echo signal. By this, the receive beam is scanned across the swath from near to far range. This scanning operation, referred to as SCan-On-REceive (SCORE), can be efficiently implemented by means of digital feed array hardware.

On receive, the individual antenna feed signals are routed separately for horizontal and vertical polarization through individual transmit-receive modules and then digitized in the corresponding digital beamforming unit. Typically, a beam for a specific direction is generated by combining the output signals of three to seven of the 32 elevation elements. This combination is performed in field programmable gate array (FPGA) units using complex weights, read from look-up tables.

Staggered SAR

Staggered SAR is an innovative concept developed at the Institute, which is based on the continuous variation of the pulse repetition interval (PRI) [J-36], [J-112], [J-140], [J-141], [PhD-10], [RC-444], [RC-444], [RC-542], [RC-634], [RC-635]. Digital beamforming on receive allows simultaneous imaging of multiple sub-swaths through multiple elevation beams, but 'blind ranges' are present between adjacent sub-swaths, as the radar cannot receive while it is transmitting (Figure 2.1-31, left panel). If the PRI is continuously varied, the position of the blind ranges will be different for each transmitted pulse (Figure 2.1-31, right panel). A method has been developed to select the PRIs of the sequence such that two consecutive samples in the azimuth direction are never missed [J-140], [J-141], [PhD-10]. In this way, if the signal is averagely oversampled in azimuth, it is possible to accurately interpolate the data on a uniform grid and obtain a high resolution SAR image over a wide continuous swath.

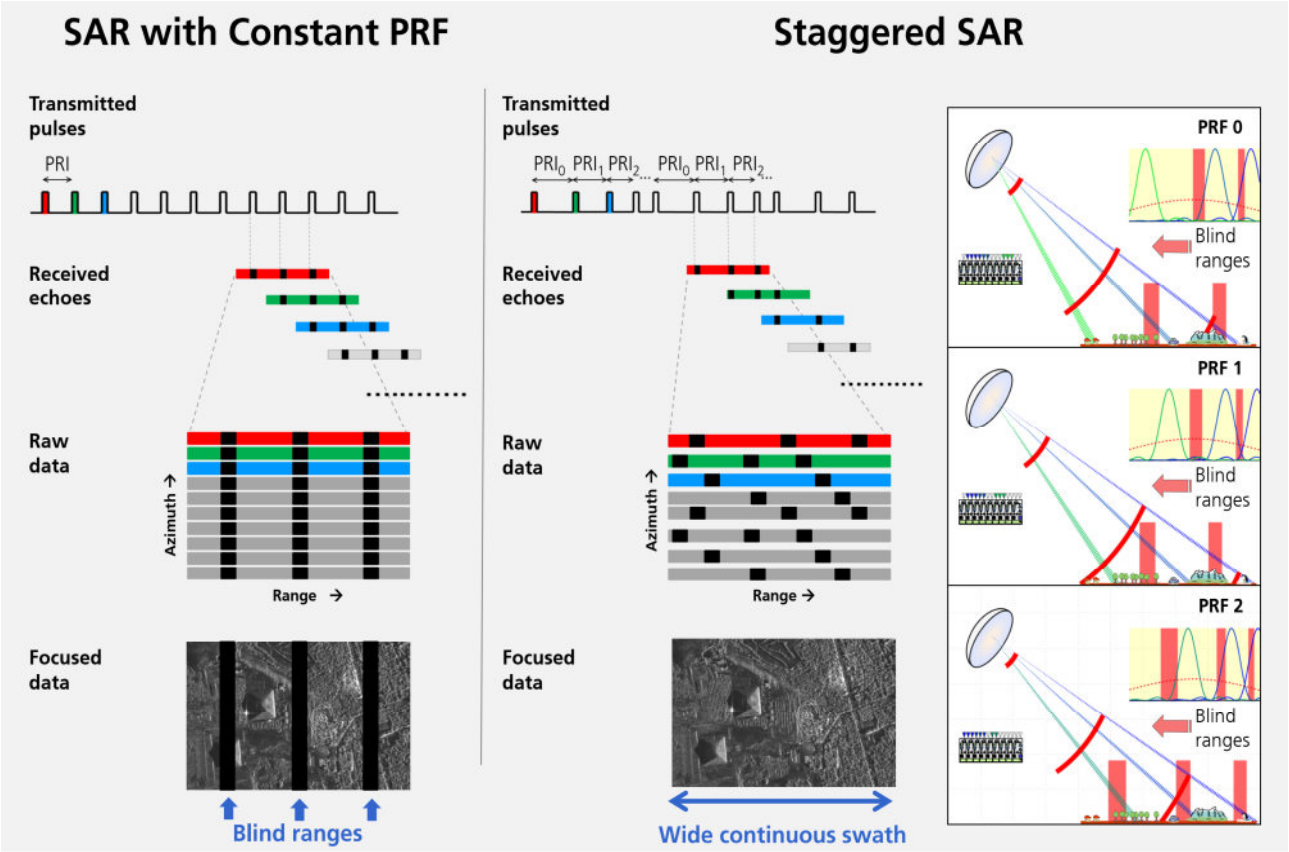

Figure 2.1-31 Transmitted pulses and corresponding received echoes (same colors as the transmitted pulses) with blind ranges (samples in black, where the echo cannot be recorded, as the radar is transmitting) (top). Raw data obtained by arranging the received echoes side by side (middle). Focused data for a SAR with constant PRI showing gaps at blind ranges (bottom left) and a gap-free image for a staggered SAR (bottom right).

The oversampling in azimuth determines the increase of the data volume to be downlinked, which can, however, be significantly reduced by filtering and decimating the data on board [J-72], [PhD-10], [RC-328], [RC-367], [RC-446], [RC-447]. If optimized sequences of PRIs are used, and data are resampled using best linear unbiased (BLU) interpolation, it can be shown that the aforementioned system is able to image an up to 350 km wide continuous swath with noise equivalent sigma zero and ambiguity performance shown in Figure 2.1-32 [J-36], [J-37], [PhD-10], [RC-222], [RC-327], [RC-329], [RC-445].

SAR Performance

The generation of the mission products in Table 2.1-4 requires the acquisition of high-quality SAR data. Key performance parameters are summarized in Table 2.1-6. The instruments can operate in single-, dual-, and quad-pol modes at range bandwidths of 20, 40 or 84 MHz. Split bandwidth acquisitions with 20 + 5 MHz and 40 + 5 MHz allow ionospheric corrections. At an azimuth resolution of 7 m, the swath width is 350 km and 175 km in single-/dual- and quad-pol modes, respectively. The noise equivalent sigma zero (NESZ) shall be below -25 dB in single/dual, and -28 dB in quad-pol for the most demanding 84 MHz bandwidth mode. The total ambiguity-to-signal ratio (ASR) shall be lower than -25 dB (-22 dB for cross-pol). As an example, Figure 2.1-32 shows the NESZ and ASR for the different polarization channels of the 84 MHz quad-pol mode.

System Calibration

Calibrating a SAR system based on a large deployable reflector fed by a digital feed array employing digital beamforming also requires new concepts [R-36], [RC-197], [RC-198], [RC-307], [P-4]. Examples are continuous pointing monitoring and calibration [RC-37], real-time (on-board) corrections of transmit/receive module phase drifts [R-100], interferometric (phase and baseline) calibration, and compact reference targets [RC-210], [P-9], [J-82], [R-120].

Well-controlled and well-known antenna pointing is one of the most critical issues for systems with large deployable reflectors and is even more critical for the highly sensitive narrow SCORE beams. As described above, the Tandem-L SAR instruments combine antenna elements in elevation with complex weights to generate several digitally-formed antenna beams, which are simultaneously recorded. Depending on the acquisition mode, not all receiving channels are always in use, for example because the associated receive beam would be located outside the swath. These idle times can be used to additionally generate and record a notch pattern for quasi-continuous pointing determination [RC-56].

Up to now elevation pointing measurements have been performed over homogeneously distributed targets like the Amazon rainforest. For quasi continuous measurements this technique has to be extended to any target. Section 2.2.6 presents exemplary results obtained with TerraSAR-X over an

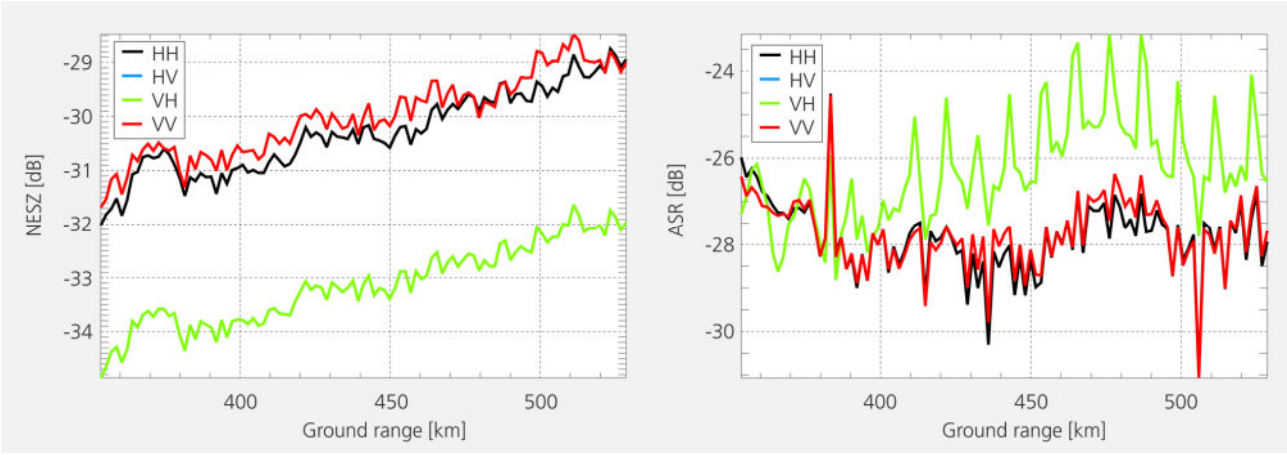

Figure 2.1-32 Exemplary performance plots showing the NESZ (top left) and ASR (top right) for the most demanding 84 MHz quad-pol mode. Black, red and green curves represent the NESZ and ASR for HH, VV and VH polarizations, respectively. The HV polarization plotted in blue is identical and overplotted by VH polarization and therefore not visible.

Polarization	Bandwidth	Azimuth Resolution	Swath Width	NESZ	ASR
Single/Dual	20 + 5 MHz	7 m	350 km	< -30 dB	< -25 dB
Quad	20 + 5 MHz	7 m	175 km	< -32 dB	< -25 dB*
Single/Dual	40 + 5 MHz	7 m	350 km	< -28 dB	< -25 dB
Quad	40 + 5 MHz	7 m	175 km	< -30 dB	< -25 dB*
Single/Dual	84 MHz	7 m	350 km	< -25 dB	< -25 dB
Quad	84 MHz	7 m	175 km	< -28 dB	< -25 dB*

Table 2.1-6 Key parameters and performance figures for the Tandem-L SAR system. *) ASR for cross-pol channels shall be below -22 dB.

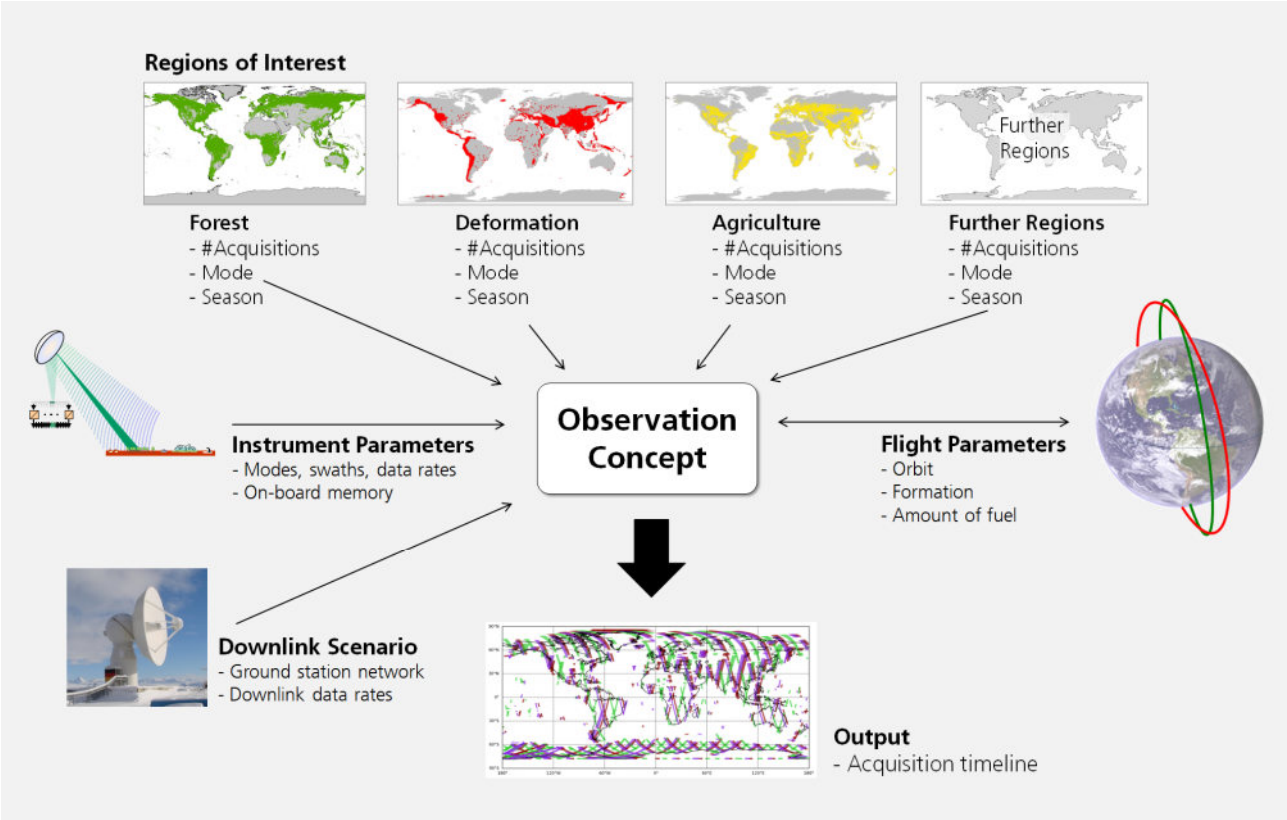

Figure 2.1-33 Schematic representation of elements to be considered in the development of the Tandem-L observation concept

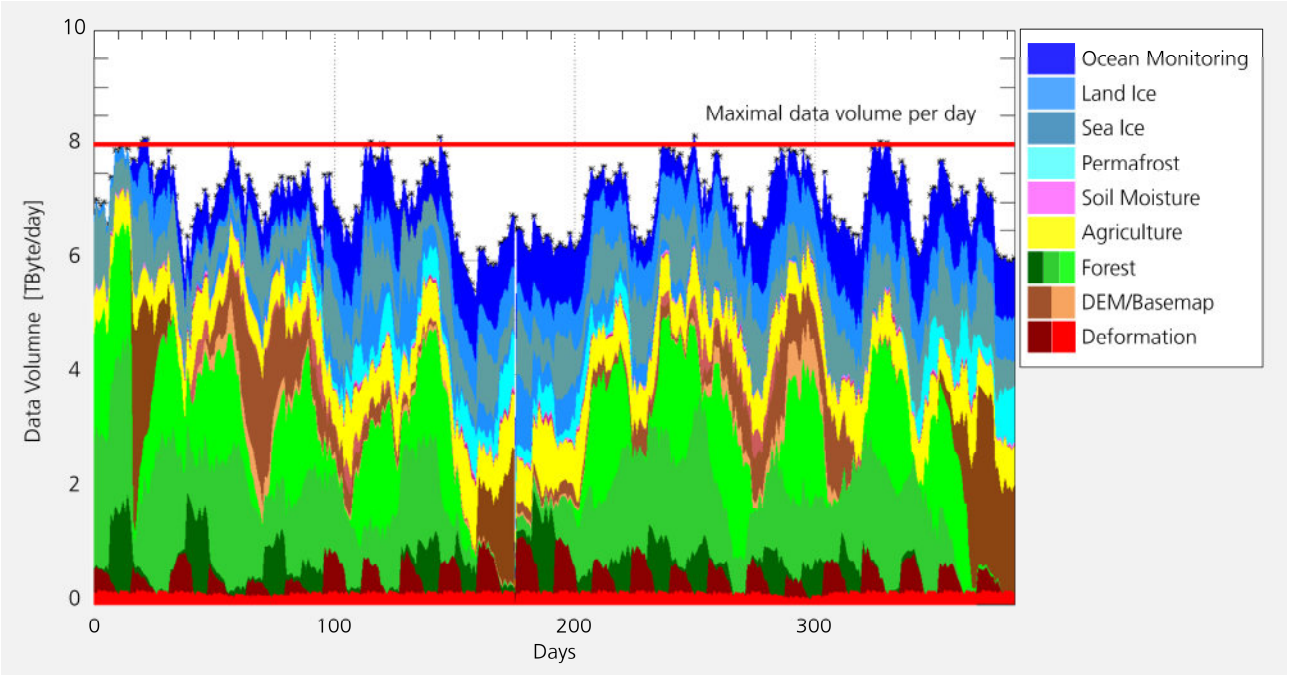

Figure 2.1-34 Daily data volume for the close formation phases. Colors indicate the different applications as described in the box in the upper right. Up to 8 terabytes/day can be downlinked to the mission baseline network of five ground stations.

inhomogeneous area in China. Subtracting the image acquired with regular beams from the one collected using notch beams, and evaluating the difference in amplitude and phase allows pointing determination at millidegree accuracies. Thus, for areas with sufficient SNR, it is possible to conduct repetitive pointing measurements to track deformations in the antenna structure.

Observation Concept

Tandem-L combines unprecedented imaging capabilities with equally ambitious observation requirements. For this reason, the development and optimization of an observation concept has been in the focus of the project from the very beginning. Figure 2.1-33 presents this process showing the inputs and constraints and the output results. Starting points for the various applications in the different spheres are the regions of interest (ROI), e.g., forested areas, areas prone to seismic or volcanic activities, ice- and snow-covered regions, etc. Depending on the higher-level information products, SAR data must be acquired over these ROIs in specific modes at certain baseline geometries. Most higher-level products require several acquisitions or even long time series – so-called stacks – with the two satellites operating either in close formation, constellation, or pursuit monostatic configuration.

A sequence of mission phases focusing on different applications is established in the first step. Examples for these phases are the close formation for tomographic observations of tropical and temperate forests, the pursuit monostatic configuration for achieving large baselines at higher latitudes, or the left-looking configuration for acquiring areas in Antarctica not covered in right-looking mode. In general, the focus is never on a single application: for example, surface deformation measurements and DEM generation are being served in parallel. Beyond the application requirements, the definition of the flight configurations also aims at minimizing the fuel consumption. Once the mission phases have been defined, timelines are generated at single acquisition level in an optimization process that accounts for the required SAR and configuration mode for certain applications. This process accounts for the available on-board resources (mass memory, instrument duty cycles, etc.) and the downlink capacity of the ground station network. One result is the daily data volume acquired, as shown in Figure 2.1-34 for the close formation phases.

Higher-Level Product Performance

The Tandem-L mission will generate a broad range of well-specified higher-level information products. To achieve these specifications, adequate SAR data have to be acquired and the higher-level product performance predicted applying representative simulations. The performance is evaluated using tools based on performance models, SAR instrument performance parameters, and acquisition timelines. The performance is analyzed on a global scale. As an example, Figure 2.1-35 shows the predicted deformation rate accuracy, which is well within the required 1 mm/year for East-West and up-down and 10 mm/year for North-South components.

HGF-Alliance Remote Sensing and Dynamics of the Earth System

Led by the Institute, the scientific data exploitation from Tandem-L is being prepared as part of the Helmholtz Alliance Remote Sensing and Earth System Dynamics (EDA). The main goal of the EDA Alliance, initiated in 2012 by the impulse and networking fund of the Helmholtz Association, was to establish

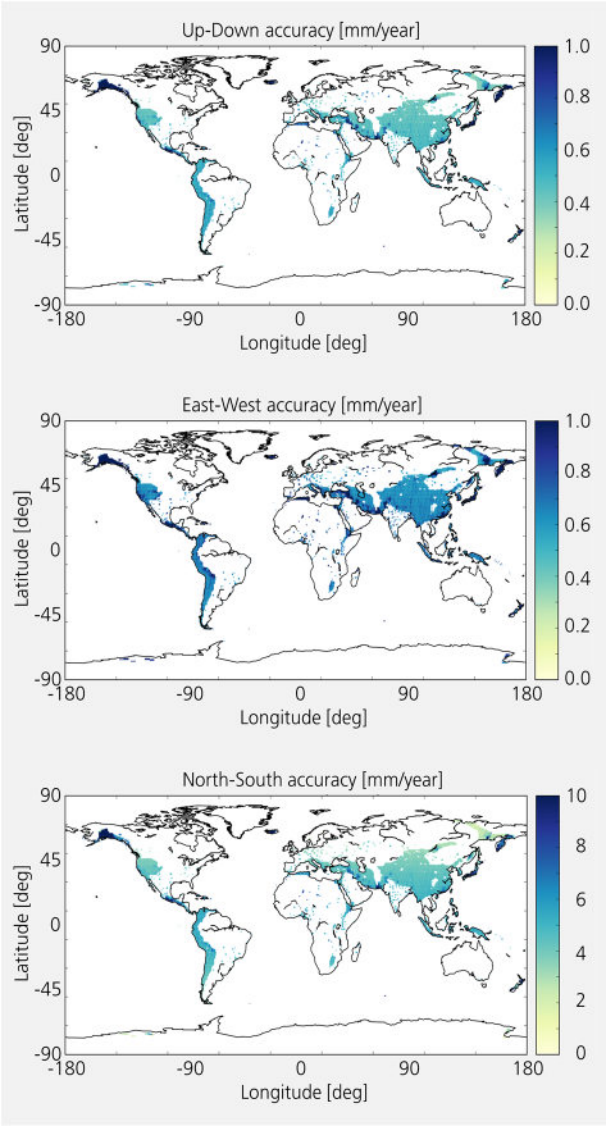

Figure 2.1-35 Tandem-L mission performance for large-scale deformation. The performance is shown as the achievable accuracy in the 3-D deformation rate expressed in mm/year for the three components: up-down (top), East-West (middle), and North-South (bottom).

links between the dynamic processes of Earth systems and Earth observation.

Due to Germany's leading competence in radar remote sensing the focus was set on data and products provided by Tandem-L. The use of such data and products generated at high spatial and temporal resolutions on global scales in environmental science models will revolutionize today's understanding of dynamic Earth systems.

Up to 140 scientists from eight Helmholtz Centers, two Max Planck and one Leibniz institutes, as well as eight universities, one federal institute and two international organizations worked together in the fields of bio-, geo-, hydro- and cryosphere research until the end of 2017.

The activities mainly focused on the following four central tasks:

- Biosphere: Global forest structure and biomass dynamics are evaluated for forest and biodiversity monitoring and the quantification of the global carbon cycle.
- Geosphere: The ability to measure topographic variations with millimeter accuracy is explored to improve our understanding of earthquake, volcano and landslide processes.
- Hydrosphere: The quantification of soil moisture and its variations at a high spatial resolution is assessed with respect to hydrological models and the global water cycle.
- Cryosphere: The estimation of melting and change processes in snow, ice, sea ice and permafrost is assessed in terms of global climate change.

Many outstanding scientific results regarding these key topics have been achieved over the past years by the Helmholtz Alliance EDA. These results are reflected in over 150 reviewed and partly awarded publications to date. The Helmholtz Alliance EDA has been able to link the expertise of radar remote sensing specialists with that of natural scientists and modelers in an internationally unique way. For the participating research institutes, this offered the unique opportunity to combine interdisciplinary know-how and train a new generation of young scientists. In addition, it enabled the intensification of cooperation between the research facilities of the Helmholtz programs Earth and Environment, as well as Space, so that the Helmholtz Alliance EDA is now an important interface between these two programs.

The activities in the Alliance are also integrated in other major research programs of the Helmholtz Association, such as TERENO, ACROSS and MOSES. In addition, members of the Alliance are involved in a number of international technical and scientific committees (e.g., BIOMASS Mission Advisory Group, Sentinel-1 Mission Advisory Group, CEOS SAR Calibration Subgroup, IEEE GRSS Instrumentation and Future Technologies, etc.). With these participations, the Alliance was able to gain valuable input for the research program, as well as to internationally promote its research activities.

Figure 2.1-36 shows the Traunstein mega plot – a large permanent forest research plot of 25 ha that was established as an activity of the EDA Alliance. With 30,000 measured trees, this new super test site is highly valuable as a permanent reference for remote sensing, as well as for understanding large-scale forest structure. Radar and lidar campaigns have been conducted in addition to the full forest inventory. Since 2017, this research plot is part of the global Smithsonian Tropical Forest Institute Network (ForestGEO). The full data set for this test site is available to the scientific community.

Implementation Plan

Tandem-L was included in the Helmholtz (HGF) roadmap for research infrastructures in 2011, and was proposed for inclusion in the roadmap for Research Infrastructures (FIS) of the German Federal Ministry of Research and Education (BMBF) in 2016. Leading responsible institutions for the FIS application are six Helmholtz centers in the research field Earth and Environment (AWI, FZJ, GEOMAR, GFZ, HMGU and UFZ) and DLR in the HGF research field Aeronautics, Space and Transport. The FIS proposal successfully passed the scientific evaluation by the German

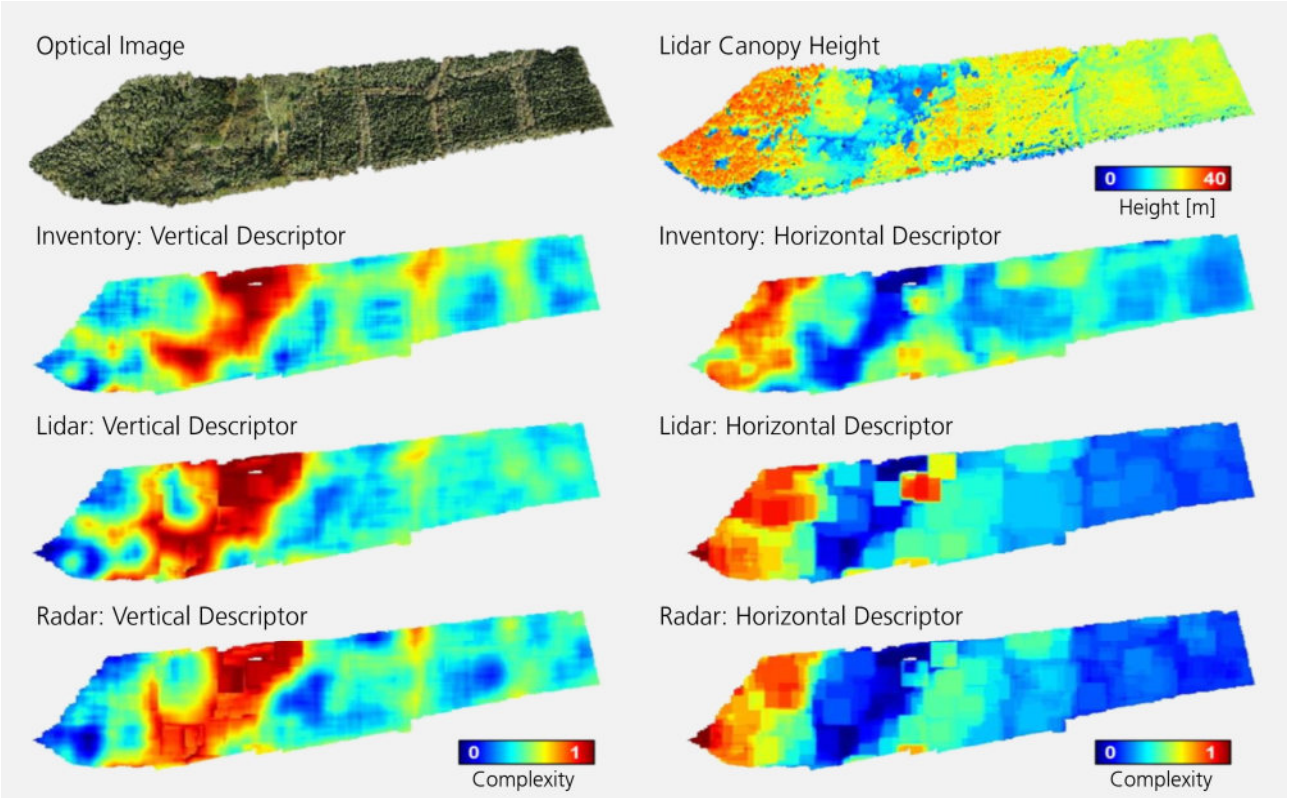

Figure 2.1-36 Traunstein mega plot. Top: optical image (left) and lidar derived canopy height map (right). Horizontal (on the right) and vertical (on the left) structure maps scaled from 0 (low complexity) to 1 (high complexity) derived from the inventory data (second row), lidar measurements (third row) and radar measurements (fourth row).

Council of Science and Humanities, and the final decision by the newly-formed German government is expected for autumn 2018. Assuming approval later this year, a kick-off into phase B2 seems feasible in the second quarter of 2019, which according to the latest schedule would lead to a launch in 2024. With a design lifetime of 10 years and possible extension (additional consumables), mission operations will last until 2036, while data evaluation will continue for several years.

Uniqueness and Programmatic Role of Tandem-L

Germany placed itself at the forefront of international, high-resolution radar remote sensing through the successful implementation of the satellite missions TerraSAR-X and TanDEM-X. Not only does Tandem-L possess the potential to secure this hard-earned position of leadership in the long term; the sheer breadth of the mission objectives as a vital contribution to climate research and environmental monitoring, and the inclusion of new scientific applications, make it equally capable of substantially increasing national and international visibility. Due to the unique set of data products, the mission will be a milestone in remote sensing, and the revolutionary techniques and technologies will form the basis for future generations of satellite SAR systems. The Tandem-L mission will open the door to a future global remote sensing system for the continuous observation of the Earth's surface, as currently exists for weather prediction, in which a network of geostationary satellites is used.

2.1.4 High-Resolution Wide-Swath SAR

TerraSAR-X and TanDEM-X have been implemented in a public private partnership between DLR and Airbus Defence and Space. The agreement foresees that the revenues of the commercial exploitation shall be used to fund an X-band follow-on mission. Therefore, under the lead of Airbus Defence and Space several studies have been performed in the last decade. Until 2012, a 600 MHz system called TerraSAR-X2 was investigated up to

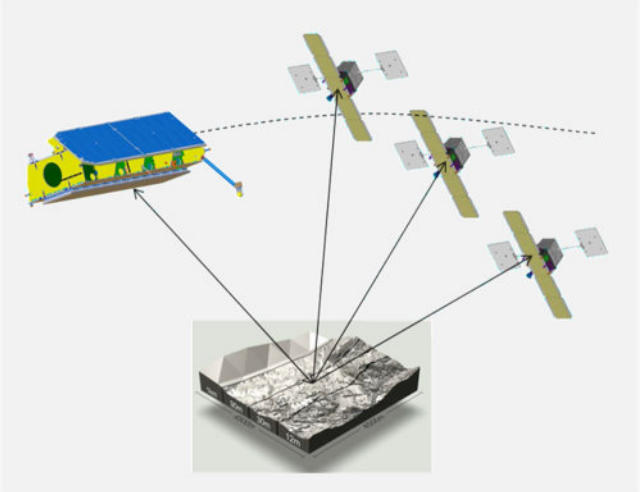

Figure 2.1-37 MirrorSAR concept as the current baseline for the HRWS mission

phase A. In parallel, the extension of the frequency band allocated for Earth observation from 600 MHz to 1200 MHz was initiated and finally approved by ITU.
In the long-term evolution of the radar line in the German space program, a so-called High-Resolution Wide-Swath (HRWS) mission was planned for the early 2020s. To prepare for such a mission, technological pre-developments were initiated by the DLR Space Administration in 2006. ESA also became interested and launched similar activities. In 2016, influenced by all these developments, it was decided to directly proceed with the HRWS mission, and the DLR Space Administration launched a phase 0 / phase A study.
The Institute was involved in most of these activities and always pushed for a full-fledged digital beamforming system featuring SCan-On-REceive (SCORE) techniques in combination with multiple azimuth phase centers (MAPS) to achieve a wide swath at a high resolution. In the phase 0 study it became clear that such a system is not affordable within the budgetary constraints. Hence, the system was de-scoped giving up SCORE and only retaining MAPS. Furthermore, the key feature of planar arrays, the electronic beam steering in azimuth and partially in elevation, was replaced by so-called Controlled Momentum Gyroscopes (CMG) that provide a high mechanical agility instead. Taking advantage of the high available bandwidth, a frequency scanning functionality was proposed. Exploiting the frequency dispersivity of the antenna, beam steering in elevation can be achieved that allows for a swath width of up to 200 km. At the end of phase 0, the mission definition review came to the conclusion that interferometric capabilities should be added to enhance this concept.
Just in time, the Institute invented and patented the MirrorSAR concept, a new multistatic approach for robust single-pass interferometry and generation of digital elevation models. Compared to previously published bi- and multistatic SAR systems, the receiver satellites are considerably simplified, as their main functionality is reduced to a kind of microwave mirror (or space transponder) which routes the radar echoes towards the transmitter. The forwarded radar signals are then coherently demodulated within the transmitter by using the same oscillator that had been used for radar pulse generation. The main benefits of the MirrorSAR concept are in general:

1. the considerable simplification of the hardware and thermal design of the receiver satellites, which lowers their mass, size and power demand,
2. the reduction of system losses due to the lack of circulators and switches,
3. the decreased peak power demands which reduce the complexity of the high-power amplifier and its associated power supply electronics in the transmitter satellite,
4. the opportunity for bistatic SAR synchronization without a dedicated synchronization link, and
5. the opportunity for efficient multi-satellite data compression which lowers the downlink requirements and reduces the mission operation costs.

The companion satellites are exclusively designed to receive the radar signals reflected from the Earth's surface and are only used for interferometric acquisitions. In addition, the MirrorSAR principle eliminates the need for units for demodulation, digitization, storage and downlinking of the radar data by the companion satellites. Instead, these processing stages are carried out by the main satellite, which receives the ground-reflected radar signals of the companion satellites via a phase-preserving radio link. In other words, the companion satellites work in a similar way to transponders that relay the ground-backscattered radar signal to the main satellite. Since at least three companions are deployed, multiple interferometric images with different baselines can be acquired simultaneously from the same area. The combination of multiple baselines during DEM processing is essential for robust phase unwrapping to enhance the accuracy of the final product.
The HRWS project has successfully completed the phase A study. Full implementation is currently under discussion between DLR Space Administration, Airbus Defence and Space, and governmental authorities.

2.1.5 PAZ

On February 22, 2018 the first Spanish Earth observation satellite PAZ was successfully launched on board a Falcon 9 rocket.

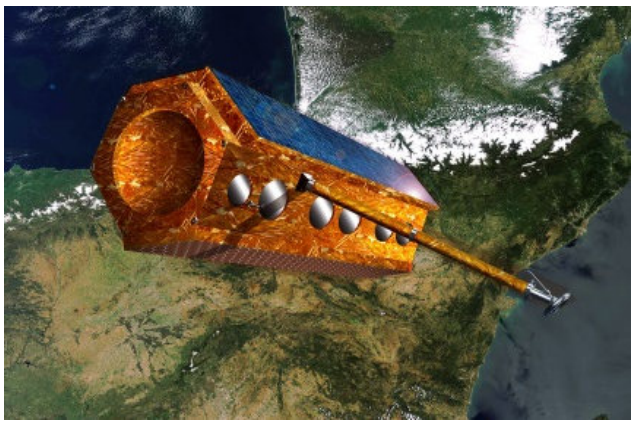

Figure 2.1-38 Artist's view of the PAZ satellite in orbit since February 22, 2018. Clearly visible are the microstrip patch radiators of the SAR antenna (lower surface), otherwise PAZ is a copy of TerraSAR-X.

Figure 2.1-39 High-resolution spotlight image of DLR Oberpfaffenhofen acquired by PAZ on May 11, 2018 (© HISDESAT)

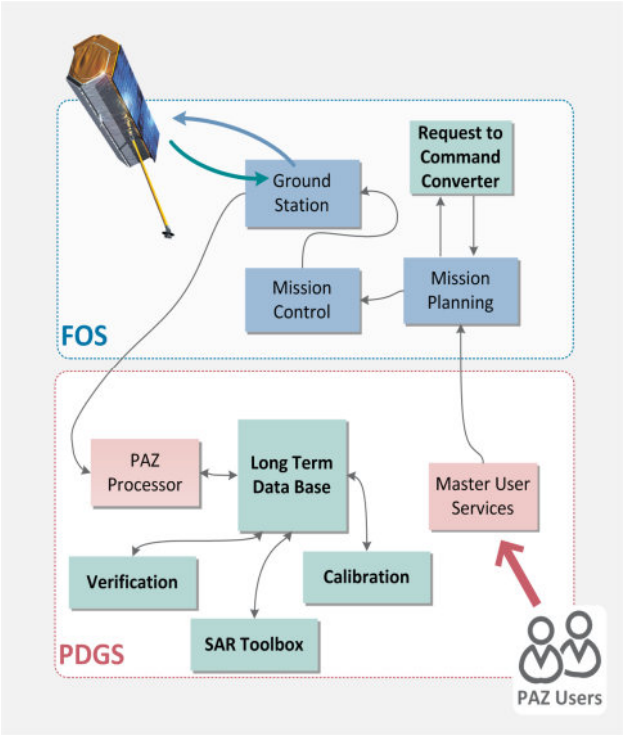

Figure 2.1-40 Institute's software (in green) and its major interfacing systems embedded in the PAZ ground segment

Following a commissioning phase of 6 months, the PAZ satellite has a lifetime of five-and-a-half years. The primary mission goal is to provide X-band imaging capacity to both civil and military users with applications ranging from defense and security observations, through to cartography and disaster monitoring.
The satellite is based on SAR technology initially developed for the German TerraSAR-X and TanDEM-X satellites, hence making it the third satellite in this family. One significant difference of PAZ is the antenna front-end, which is again an active phased array antenna, but built up of microstrip patch radiators instead of slotted wave guides. PAZ has been placed on the same orbit as its German counterparts. Its product portfolio is also similar to that of the TerraSAR-X satellite, i.e., ranging from about 1 m resolution for spotlight mode with a scene size of 10 km x 10 km to about 18 m resolution for ScanSAR mode with ground range extension of 100 km. Therefore, using the TerraSAR-X and PAZ satellites, an external user may obtain comparable images, but with an improved repeat cycle of 4 or 7 days compared to the 11 days of TerraSAR-X.
The owner of the PAZ satellite is the Spanish company HISDESAT, while the National Institute of Aerospace Technology (INTA) – the Spanish equivalent of DLR – implemented the ground segment and is responsible for operating the mission. Since the 90s, there has been a long-standing cooperation between INTA and the Microwaves and Radar Institute, whose extensive knowledge and experience in the SAR payload operation and calibration, and in the overall mission management made it an excellent partner for INTA.
The Institute has developed essential parts of the joint TerraSAR-X and TanDEM-X ground segment (GS) that are logically bound together in the so-called Instrument Operations and Calibration Segment (IOCS). Building on that, IOCS software for autonomous data take command generation is now also part of the Flight Operations Segment (FOS) of the PAZ GS, and is tightly linked to their mission planning system.
Another software suite developed by the Institute and consisting of calibration and verification tools has been incorporated in the PAZ Payload and Data Ground Segment (PDGS). It supports the overall calibration of the SAR system including the antenna pattern generation. Other software of this suite enables the monitoring of the in-orbit SAR system operation on a data take to data take basis, but also on a long-term scale in order to identify degradation trends and anomalies.
Beyond the technical cooperation, a joint scientific exploitation is foreseen using PAZ in constellation with the TerraSAR-X/ TanDEM-X formation to increase the imaging capacity and to allow shorter interferometric repeats.

2.1.6 PICOSAR

The launch of Sentinel-1A in 2014 triggered a wide range of scientific and radar mission-related developments and proposals. Motivated by this opportunity and a DLR internal call for small satellite missions, the Institute conceived the Passive Interferometric Ocean Currents Observation Synthetic Aperture Radar (PICOSAR) mission concept [RC-471], [B-6] as an extension to the Sentinel-1 mission consisting of two small, low-cost and low-power spacecraft, each carrying a passive, receive-only SAR payload. The original Sentinel-1 mission is enhanced by the addition of a unique along-track interferometer optimized for ocean surface current measurements. The concept was aimed at filling major gaps in the observation and subsequent understanding of oceans. In particular, PICOSAR would allow direct global measurements of ocean surface velocities with unprecedented accuracies, opening the possibility of studying mesoscale and, most notably, sub-mesoscale processes. Sub-mesoscale phenomena, with scales in the 10 to 70 km range, are responsible for vertical mixing key processes that play an important role in climatic processes (e.g., vertical transport of CO_2) as well as the transport of nutrients necessary to sustain marine ecosystems. In addition, PICOSAR would provide improved observations of the global sea state (significant wave height, wave spectra) and surface winds.
As illustrated in the top plot in Figure 2.1-41, the PICOSAR interferometer, consisting of two compact receive-only C-band radar satellites, flies at a safe distance to a Sentinel-1 radar satellite, which serves as a transmitter of opportunity. The bottom plot of Figure 2.1-41 shows the demonstration of cross-platform ATI over sea surfaces with the TanDEM-X satellites. From an along-track interferometry point of view, the distance to the Sentinel-1 satellite was uncritical, and could be in a range from 25 to 100 km, or even more. The along-track baseline between the PICOSAR satellites is the outcome from an optimized trade-off between interferometric intrinsic sensitivity and temporal decorrelation (see Figure 2.1-42). A separation of 100 m is near the optimum for high wind conditions and yields satisfactory performance in all cases. Global coverage is mandatory, and thus PICOSAR acquisitions were tied to the

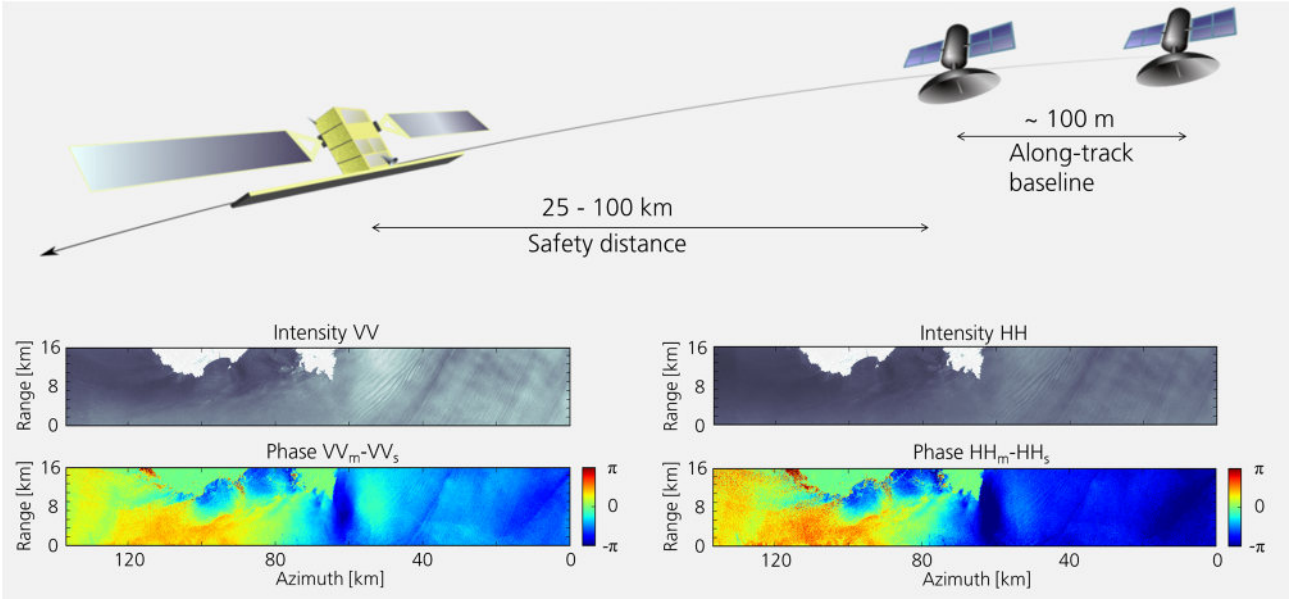

Figure 2.1-41 Illustration of the PICOSAR formation following the Sentinel-1 satellite at a safe distance (top); demonstration of ATI over sea in dual-pol mode close to the Gulf of Roses with TanDEM-X (bottom). V and H stand for vertical and horizontal polarizations, while m and s for master and slave.

operating modes of Sentinel-1, i.e., PICOSAR operates while Sentinel-1 operates in wave mode (WM), where 20 x 20 km^2 vignettes are acquired every 100 km, alternating at 23° and 36° incidence angles. The across-track separation between the PICOSAR satellites should remain within 20% of the along-track separation. This small distance required the use of a Helix concept for safe formation flying. The close formation required autonomous formation flying capabilities and therefore a mutual exchange of precise GPS data (via sync link). The required autonomous formation flying capabilities (< 1 cm along-track and < 1 mm line-of-sight relative position knowledge, 0.1° attitude control accuracy, 0.01° attitude knowledge) have been demonstrated by the PRISMA mission.

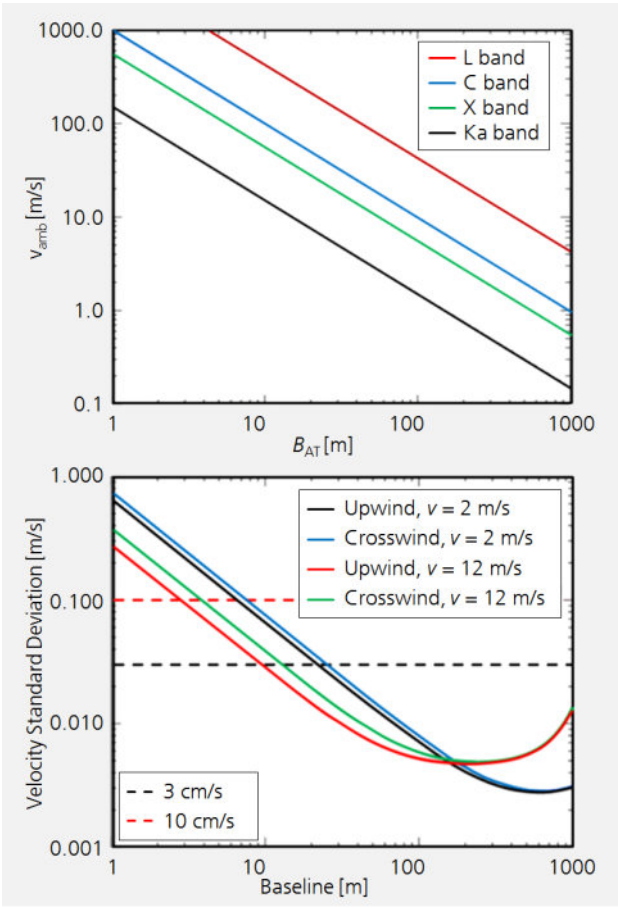

Figure 2.1-42 Unambiguous velocity margin as a function of along-track baseline at L, C, X and Ka band (top); RMS surface velocity error as a function of baseline (bottom)

Since the PICOSAR instrument was only passive, it was possible to tailor it to a very low-power and low-weight design consisting of a 2.0 - 2.5 m reflector antenna with two feeds (for the two required incidence angles). The resulting mass and power budget was 35 kg and 50 W (continuous), respectively. With operations connected to the Sentinel-1 WM operations, the average data volume per day would not exceed 800 Gbits.

In addition to the scientific goals of PICOSAR, the mission would have also served as a technology demonstrator for several novel technologies, i.e., multistatic SAR (consolidating TanDEM-X experience and taking a first step towards multistatic configurations) and autonomous formation flying (a very tight formation is required that can only be achieved by implementing automated formation control). Despite the solid science perspectives of the concept, PICOSAR was not selected for implementation, mainly due to budget constraints.

2.1.7 Sentinel-1

In the framework of ESA's Copernicus program, as member of the industrial core team of Sentinel-1A/B, the Institute developed the overall system calibration and validation concept for the radar instruments [RC-532], [R-323], [R-354], [R-355], [R-380], [R-463]. Novel methods, which were developed for the active phased array SAR instruments on TerraSAR-X [RC-628], [J-180], [J-149], [RC-472], [J-147], [RC-344], [J-155], [J-44], [RC-657] and TanDEM-X [IC-243], [J-184], [IC-173], [J-173], [RC-636],

Figure 2.1-43 Sentinel-1, ESA's C-band satellite as part of the Copernicus Program (left); DLR's remote controlled corner reflector (center) and transponder (right) deployed and operated for Sentinel-1

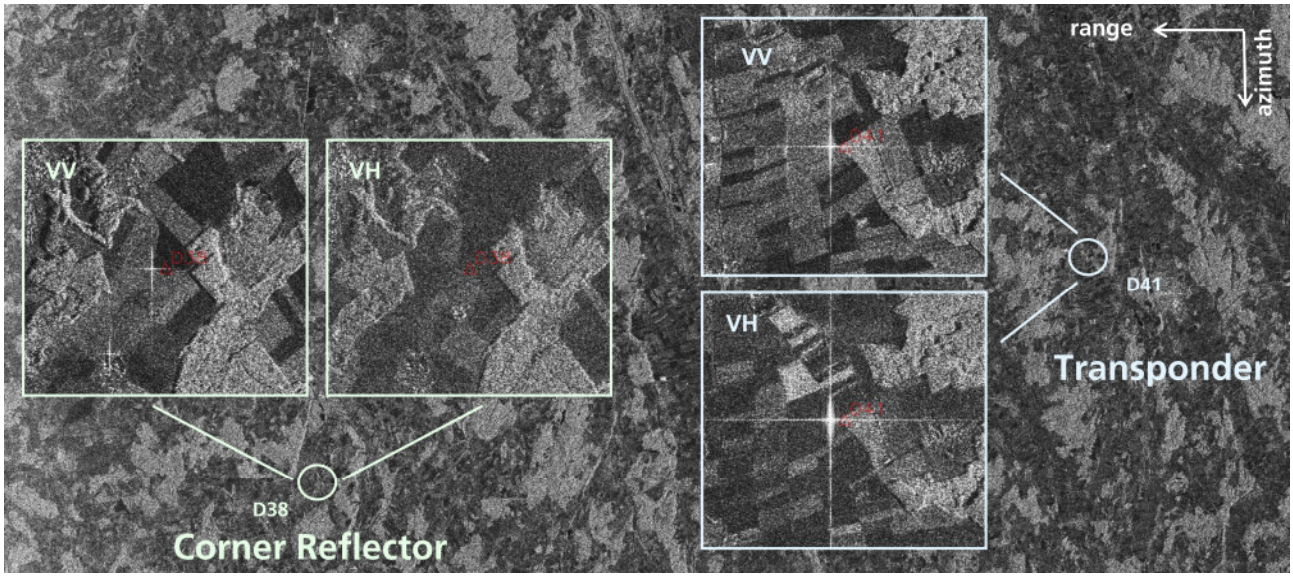

Figure 2.1-44 Sentinel-1 SAR image over the DLR calibration site in stripmap mode for the co-polar channel VV. The regions around the deployed reference targets are zoomed into and also show the cross-polarization channel VH. While the corner reflector is only visible in the VV image, the DLR Kalibri transponder re-transmits both polarization signals simultaneously.

[RC-700], [RC-702] were the starting point for the Sentinel-1 calibration developments. The major challenge of calibrating Sentinel-1 is achieving an absolute radiometric accuracy of 1 dB (3σ) for all operation modes. Such accuracy in the order of laboratory equipment had never been required before for a spaceborne SAR system. Furthermore, the Interferometric and the Extra Wide Swath modes (IW and EW) are realized by Terrain Observation by Progressive Scan (TOPS-SAR) [J-75], i.e., by an azimuth-sweeped ScanSAR operation to overcome the systematic performance variations in standard ScanSAR data, known as scalloping. Also featuring dual-polarization, Sentinel-1 is based on a multitude of different antenna beams realized by means of an active phased-array antenna. Furthermore, in order to achieve a short revisit time, the mission is based on a two-satellite constellation, in which both satellites are operated in monostatic mode and fly in the same sun-synchronous orbit plane with a 180° orbital phasing difference. Consistent high product quality can only be ensured if the radiometric matching of the two SAR systems can be achieved at the level of the required absolute radiometric accuracy.

Key elements of the overall calibration concept are a precise antenna model [RC-360] providing the numerous beam patterns for radiometric corrections and the so-called internal calibration [RC-443], a set of sophisticated procedures for monitoring gain and phase drifts in the instrument electronics, including the transmit-receive modules of the antenna. Due to the specific design and artefacts that occurred only after the hardware integration, this internal calibration on the first Sentinel-1 satellite became highly complex, hence requiring the evaluation of a series of calibration signals. For external calibration the Institute developed a new generation of reference targets, the so-called "Kalibri" transponders, featuring a radar cross section accuracy of 0.2 dB [RC-388], [RC-185], [RC-210], [R-355], [RC-581], [RC-589], [J-154], [J-82], [P-9], [RC-110], [RC-246], [RC-247], [RC-431], [RC-313], [RC-420], [RC-668]. Together with remote-controlled corner reflectors, these targets have been providing the absolute reference since the launch of Sentinel-1A in 2014 (see Section 2.2.6). Under direct ESA contracts independent commissioning phases of Sentinel-1A (S-1A) in 2014 [J-70], [RC-319], [RC-436], [IC-132], [R-293]–[R-297], [R-323] and of Sentinel-1B (S-1B) in 2016 [J-34], [IC-66], [RC-216], [RC-219], [R-119], [R-121], [R-122] were performed.

It confirmed the outstanding instrument stability and absolute radiometric accuracy within the required 1 dB (3σ) limit, and an outstanding phase stability for differential SAR interferometry based on the TOPS imaging mode. The Institute continues to support ESA in the subsequent development of Sentinel-1C/D [R-48], [R-50], [R-51], [R-52], [R-54], [R-56] as well as with long-term calibration monitoring for Sentinel-1A/B [RC-68], [RC-214], [RC-316], [RC-317], [R-110], [R-112], [R-221], [R-47], [R-111].

Internal Calibration

Temperature drifts and internal hardware characteristics influence the radar signal path causing gain and phase fluctuations during data acquisition. These changes in the signal path appear due to thermal effects, degradation, or extreme conditions in space. In order to monitor and compensate for them, the instrument hosts a complex internal calibration facility, which is based on the acquisition of different types of internal calibration measurements, leakage suppression algorithms, and the application of the Pulse-Coded Calibration (PCC) method [RC-443]. The instrument drift was analyzed during the commissioning phases of Sentinel-1A and Sentinel-1B to confirm the instrument stability over time. It is derived by the compression and evaluation of calibration pulses acquired periodically and interleaved with the imaging radar data. Exemplarily, Figure 2.1-45 shows the instrument drift of Sentinel-1B in amplitude and phase for a long IW data take with a duration of 25 min. While the front-end temperatures (see top plot) increase in all panels by about 20° C during SAR imaging operation, the Sentinel-1B instrument drifts only about 0.25 dB in amplitude and about 18° in phase (bottom plot). As the instrument drift shown in Figure 2.1-45 is almost linear, we obtain a theoretical drift of 0.01 dB in amplitude and 0.6 deg in phase per minute, respectively. This demonstrates the high stability of the Sentinel-1B instrument over long data takes without any compensation. In fact, the measured drifts are compensated during SAR processing, and the remaining residual variations are less than 0.1 dB in amplitude and a few degrees in phase.

Antenna Model Verification

The antenna model is a key element for accurate calibration. In addition to pointing determination, the antenna model is mainly used for generating the reference antenna patterns for radiometric corrections in the SAR processor as well as for predicting the relative gain between different beams. Compensating these gain offsets, only one absolute calibration factor has to be derived which is valid for all beams and modes. This strategy, developed by the Institute and described in [R-323], [R-354], [R-355], [R-380], [RC-532], reduces the calibration effort during the commissioning phase considerably and was successfully applied to TerraSAR-X and TanDEM-X [RC-628], [IC-243]. A precondition is the precise validation of the antenna model on ground and a subsequent in-flight verification, which is performed for azimuth patterns by means of ground receivers or receiver units of transponders, and for elevation patterns by acquisitions over the Amazon rainforest. One example of azimuth patterns measured and verified in flight is shown in Figure 2.1-46. The figure depicts all measurements recorded during an overpass of Sentinel-1B in stripmap operation. The top graph shows the measured patterns (in blue, yellow and red) as well as the calculated reference patterns (black line). At the bottom of this figure, the difference between the reference pattern and the measured patterns is shown in the same respective colors. The averaged difference is shown in black. The deviation within the 3-dB beam width between measured and modeled transmit patterns is less than 0.035 dB (1σ) for all stripmap beams verified in flight. This result confirms the high

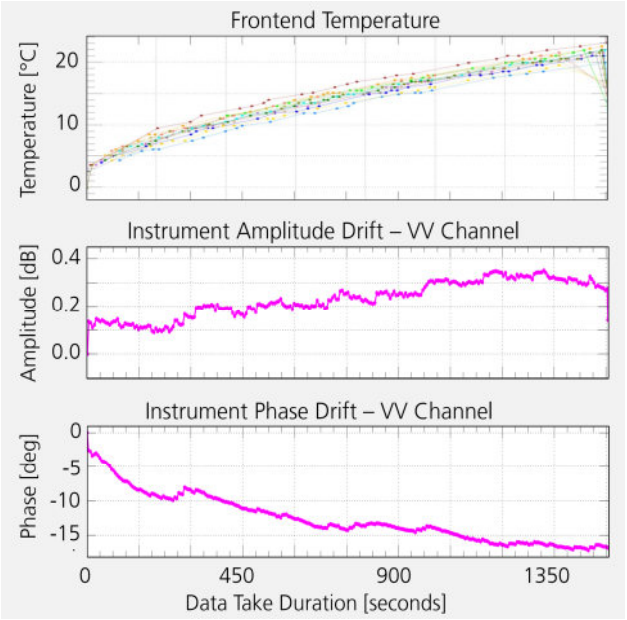

Figure 2.1-45 Sentinel-1B front-end temperature drift (top plot, each color indicates one of the 14 tiles); instrument drift in amplitude and in phase (middle and bottom plot) of the co-polar channel (VV) for a 25 min long IW data take acquired during the commissioning phase on May 17, 2016.

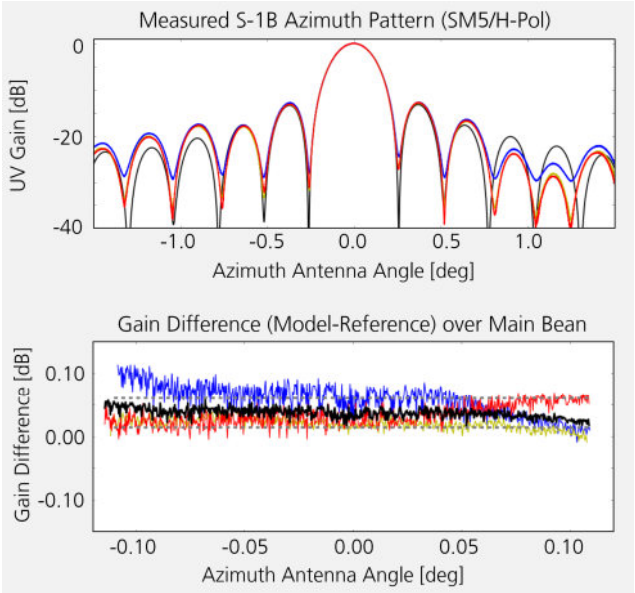

Figure 2.1-46 Sentinel-1B azimuth patterns for stripmap beam 5 (SM5) measured on June 29, 2016 normalized to the maximum of the main beam. Top: measured patterns versus azimuth angle in blue, red and green, and the reference pattern in black. Bottom: zoom into the main lobe area, deviation between the average of all measurements and the reference pattern in black.

accuracy of both the antenna model in azimuth direction and the method of verifying the azimuth patterns in flight by means of ground receivers. For the TOPS modes (IW and EW) of Sentinel-1, where the azimuth beams are steered from aft to fore, the method explained previously needs to be extended to consider the pattern compression due to steering. The approach to reconstruct the compressed azimuth pattern from the antenna model was first introduced by the Institute [J-149] and takes into account the following:

- accurate knowledge of the imaging geometry (i.e., between the satellite and the transponder position on the Earth's surface),
- the antenna excitation coefficients,
- precise knowledge of the right sequence of steered azimuth beams and scanned elevation beams, and
- the correct time synchronization of the data.

The complexity of analyzing transponder recordings increases with the number of azimuth beams. Sentinel-1 uses a very fine granularity in azimuth steering, with a total of around 800 steered azimuth beams per burst. Practically, each pulse is commanded with a different azimuth beam. EW mode employs five subswaths in elevation, i.e., the TOPS azimuth pattern for this mode is not only composed of more than 4000 azimuth beams, but each package of 800 patterns per burst is also weighted with the gain of the elevation pattern for the corresponding subswath. Hence, thousands of different patterns construct the complicated overall TOPS azimuth pattern measured by the transponder. A prerequisite for the antenna pattern verification is the correct time synchronization between the signal received by the transponder and the position and attitude of the satellite. Figure 2.1-47 shows the comparison of a measured Sentinel-1A TOPS azimuth pattern in EW mode with the reconstructed pattern using the antenna model.

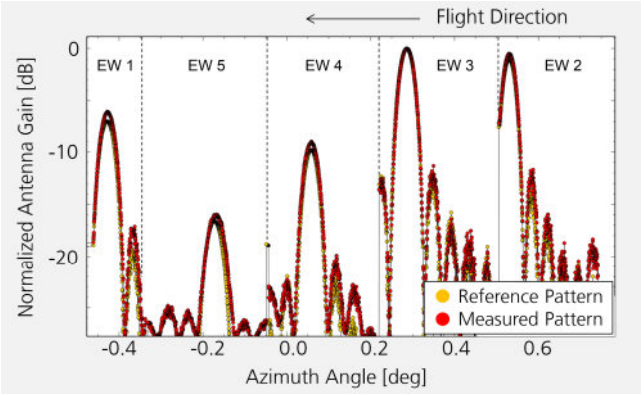

Figure 2.1-47 Comparison of TOPS azimuth patterns of the EW mode. Red: measurement executed on August 2, 2014, yellow: pattern reconstructed by means of the antenna model for Sentinel-1A

Radiometric Calibration and Cross-Check between Sentinel-1A and Sentinel-1B

Once the internal calibration and antenna pattern correction (shape and beam-to-beam gain offset) are performed, the image information is transformed into maps of RCS or backscattering coefficient by applying the absolute calibration factor which is annotated in the SAR data products. In order to determine this key factor, the Sentinel-1A and Sentinel-1B system were measured against the DLR reference targets featuring precisely known RCS, see Section 2.2.6.
Figure 2.1-48 shows how accurately Sentinel-1A and Sentinel-1B have been absolutely calibrated by the Institute and consequently been matched to each other. This cross-check is focused on the IW mode, which is the main SAR operation mode and currently the best calibrated one for both systems. Concentrating on the absolute calibration factor derived for all polarization channels, no significant dependencies across the entire IW swath can be observed. There is neither a dependency from beam to beam – i.e., from sub-swath to sub-swath – nor overlook angle across the sub-swath, i.e., within one beam.

The remaining standard deviation of the measurements is a measure for the absolute radiometric accuracy. For the IW mode absolute radiometric accuracies of 0.38 dB for Sentinel-1A and 0.36 dB for Sentinel-1B have been achieved. Hence, this radiometric cross-check between Sentinel-1A and Sentinel-1B for the IW mode shows how accurately the systems can be adjusted, and demonstrates the compatibility of both SAR systems providing an almost identical absolute radiometric accuracy, ensuring high image quality. In other words, the user will not be able to distinguish between Sentinel-1A and Sentinel-1B calibrated SAR images.

Interferometric Verification

The Institute has also been deeply involved in the interferometric verification of the IW mode of Sentinel-1.
As its name indicates, the mode was conceived to provide interferometric SAR products to the SAR community, similar to

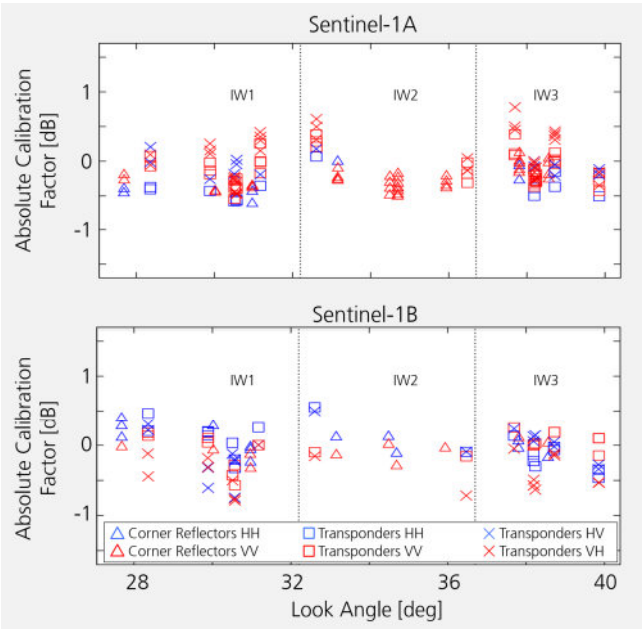

Figure 2.1-48 Absolute calibration factor derived from point targets for the IW mode (triangles: corner reflectors, squares: co-pol transponders) and distinguished between transmit polarization (blue: H on transmit, red: V on transmit). Top for Sentinel-1A; bottom for Sentinel-1B.

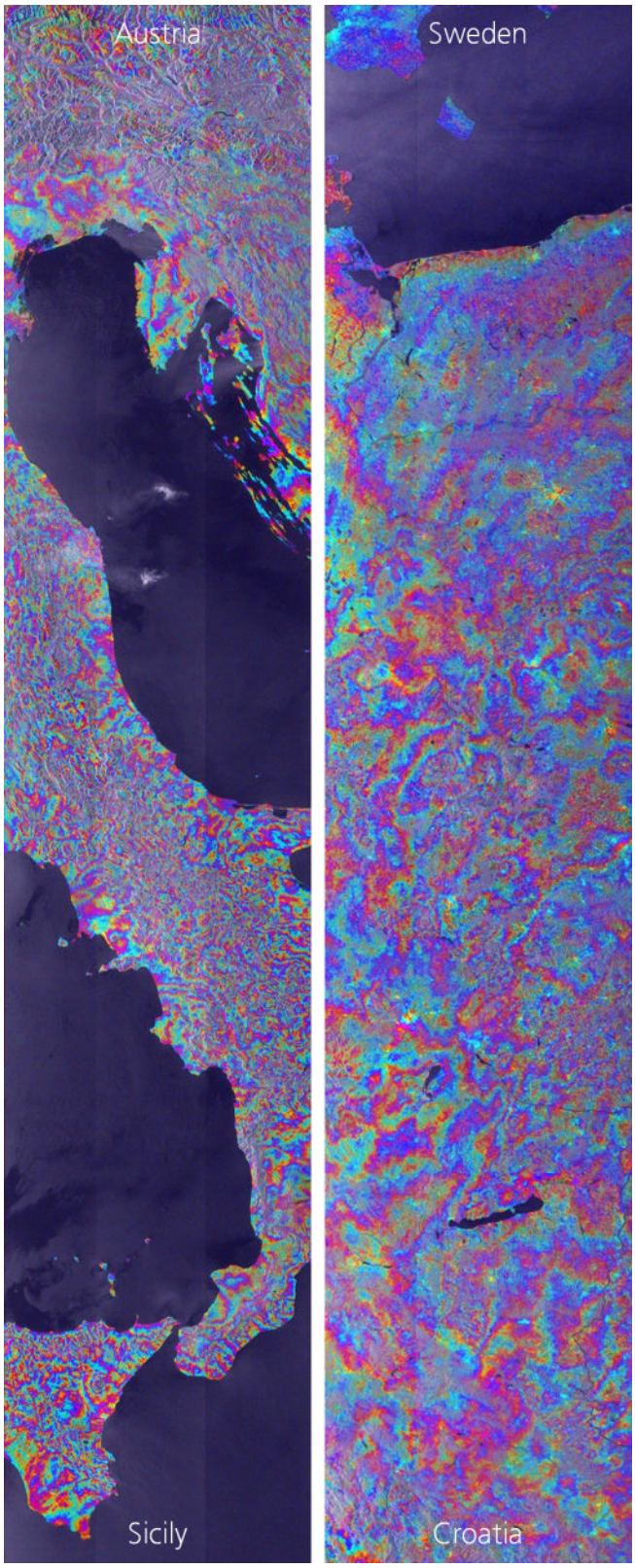

Figure 2.1-49 Sentinel-1 interferograms. Left: one of the first Sentinel-1A repeat-pass interferograms over Italy processed at the Institute. The image shows the DEM-flattened phase with overlaid reflectivity, extending from Sicily to the Austrian Alps. Right: one of the first interferograms between Sentinel-1A and Sentinel-1B with a 6-day repeat pass. The image shows the DEM-flattened phase with overlaid reflectivity. The acquisition extends from Croatia to southern Sweden. In both cases, the phase variations that can be observed are related to the delay introduced in the signal when travelling through the lower troposphere.

previous ESA missions such as ENVISAT and ERS-1/2.

Due to its particularities, the processing of interferometric products is not straightforward and needs to be done carefully, as explained in Section 2.2.4. During the commissioning phase, the Institute successfully processed the first Sentinel-1 interferograms, hence demonstrating the feasibility of generating InSAR products with Sentinel-1 and consolidating the interferometric processing chain proposed by the Institute [J-190], which is currently the baseline approach by the SAR community to process IW products interferometrically [J-75]. Figure 2.1-49 (left) shows one of the first Sentinel-1A interferograms computed during the commissioning phase by the Institute. The two data takes were acquired over Italy in 2014 on August 9 and August 21, and have a length of 1200 km and an IW swath width of 250 km. Figure 2.1-49 (right) shows one of the first interferograms between Sentinel-1A and Sentinel-1B acquired on June 13 and June 19, 2016, respectively, with a length of 1400 km. Since the phase has been DEM-flattened, all the phase artefacts that can be observed in the two interferograms are due to tropospheric effects.

No phase jumps between bursts or sub-swaths were detected when performing the interferometric verification activities, hence confirming the good instrument performance of both units, as well as the accurate interferometric processing. In addition, during the commissioning phase of Sentinel-1A the Institute discovered that azimuth spectral decorrelation was occurring for long data takes due to the loose orbit eccentricity control – a previously unknown issue affecting burst modes [J-103], [RC-303]. As a consequence, the orbit eccentricity control was tightened, hence improving the quality of the Sentinel-1 interferograms. Additional verification, research and promotion activities related to Sentinel-1 interferometry have been carried out in the last four years, especially in the frame of the INSARAP study [R-211], [R-212], [R-248], [R-276], [R-277], [R-278], but also as support for the Sentinel-1A and Sentinel-1B commissioning phases. These activities have resulted in a number of journal and conference publications [J-40], [J-29], [J-68], [J-102], [IC-26], [IC-28], [IC-61], [IC-91], [IC-92], [RC-46], [RC-50], [RC-163], [RC-301], [RC-302].

2.1.8 BIOMASS

BIOMASS, selected as the 7th ESA Earth Explorer mission, is scheduled to be launched in 2022 and is currently undergoing phase C (i.e., detailed design phase). The primary mission objectives of BIOMASS are to determine the distribution of above-ground forest biomass, and to measure annual changes in above-ground forest biomass stocks globally. Secondary mission objectives are the mapping of ice sheets and their subsurface structure, glacier flow, and geological features in arid regions. To achieve these objectives, BIOMASS is implemented by means of a reflector-based P-band synthetic aperture fully polarimetric radar (see Figure 2.1-50) operating at 435 MHz with a bandwidth of 6 MHz in a 3 to 4 days repeat-pass interferometric mode, and has an expected mission lifetime of 5 years.

As the first spaceborne mission to operate in P band, BIOMASS is facing a number of scientific and technological challenges. The Institute has been actively involved in BIOMASS from the very beginning contributing significantly in mastering these challenges. It has already been part of the international team of scientists submitting the original BIOMASS proposal in response to ESA's 7th Earth Explorer call back in 2005, and has since supported BIOMASS with critical scientific and technical contributions, as well as with unique airborne campaigns through all mission and selection phases. It has participated in the BIOMASS Mission Advisory Group since 2006.

The Institute has played a leading role in the scientific activities of BIOMASS since the beginning, and is responsible for the definition, generation and validation of the forest height product. In the context of BIOMASS, forest height is obtained by means of model-based inversion of (three) Polarimetric Interferometric Synthetic Aperture Radar (Pol-InSAR) acquisitions performed during the main mission phase in a 3 - 4 days repeat-pass interferometric mode. Accordingly, multi-baseline inversion schemes optimised with respect to the P-band scattering characteristics, able to deal with the presence of temporal decorrelation and performing under the constraints imposed by the limited BIOMASS bandwidth have been developed. The inversion methodology has been continuously improved over the last years so that, today, forest height is by far the most mature and developed product of BIOMASS, well understood in terms of performance and limitations.

The development of the BIOMASS Pol-InSAR inversion algorithm was strongly supported by a number of dedicated airborne experiments in boreal (BioSAR 2), temperate (TempoSAR) and tropical (AfriSAR) forests. Figure 2.1-51 shows the forest height map obtained from the inversion of P-band Pol-InSAR data acquired in the framework of the AfriSAR campaign in February 2017 over the Rabi test site in Gabon. The site is covered by a mixture of disturbed and natural upland and wet forest stands with a mean tree height of about 35 m.

Of the same critical importance for BIOMASS, and at the same time unique in terms of innovation, are the Institute's contributions to the polarimetric and ionospheric calibration of the BIOMASS data. One important step was to understand

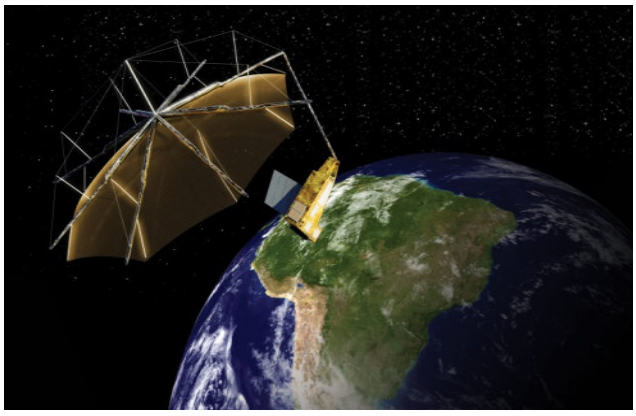

Figure 2.1-50 Artist's impression of the BIOMASS satellite with the characteristic reflector antenna

that the very accurate Faraday rotation estimates possible in P band when converted to total electron content (TEC) – using the geometry defined by the SAR line of sight (LOS) and Earth's geomagnetic field – can be used to compensate for a wide range of ionospheric distortions in SAR images.

This opened the door for accurate ionospheric calibration even on single BIOMASS images. Figure 2.1-52 shows an interferometric example of such a correction by means of ALOS PalSAR acquisitions performed close to Fairbanks, Alaska. The polarimetric Pauli RGB composite of the master is shown on the left; next to it is the coherence of the interferogram formed with a second (slave) image acquired 46 days later without ionospheric correction. The next image is a differential TEC map derived from Faraday Rotation estimates of each image. The image on the right shows the interferometric coherence map after ionospheric correction using the differential TEC map.

A second critical breakthrough was achieved with the separation of ionospheric-induced distortion (Faraday rotation) from system-induced distortion (i.e., polarimetric cross-talk) based on the frequency dependency of the Faraday rotation across the system bandwidth. This is essential to perform polarimetric system calibration in the presence of residual Faraday rotation distortions as well as to obtain unbiased Faraday rotation estimates.

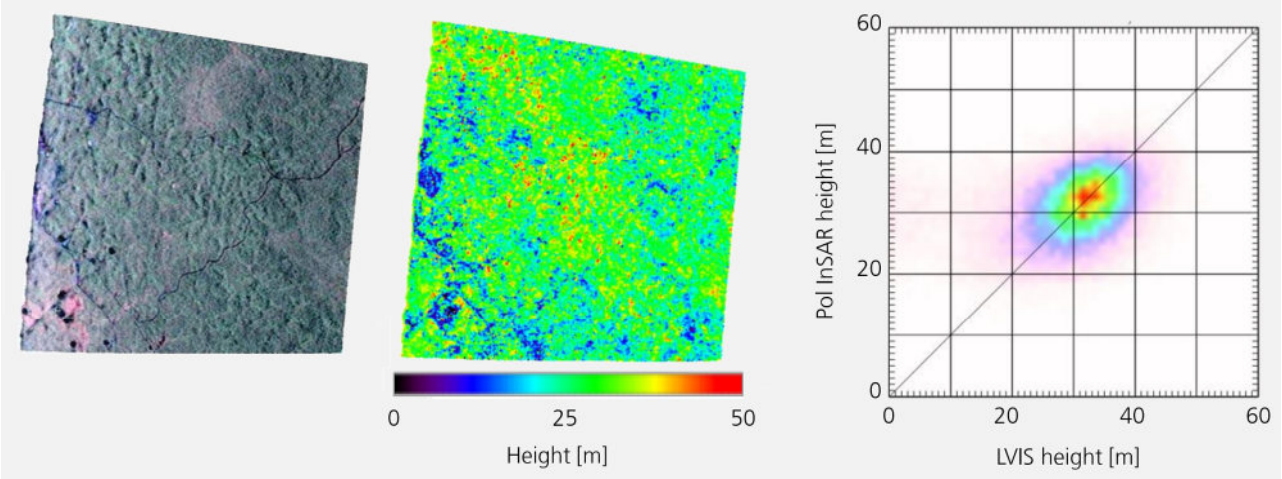

Figure 2.1-51 Polarimetric Pauli RGB composite of the Rabi test site in Gabon (left), forest height map obtained from the inversion of P-band Pol-InSAR data (middle), and validation plot of the Pol-InSAR derived heights against wide beam lidar airborne derived heights (right). The data were acquired by DLR's F-SAR in the framework of the AfriSAR campaign in February 2016.

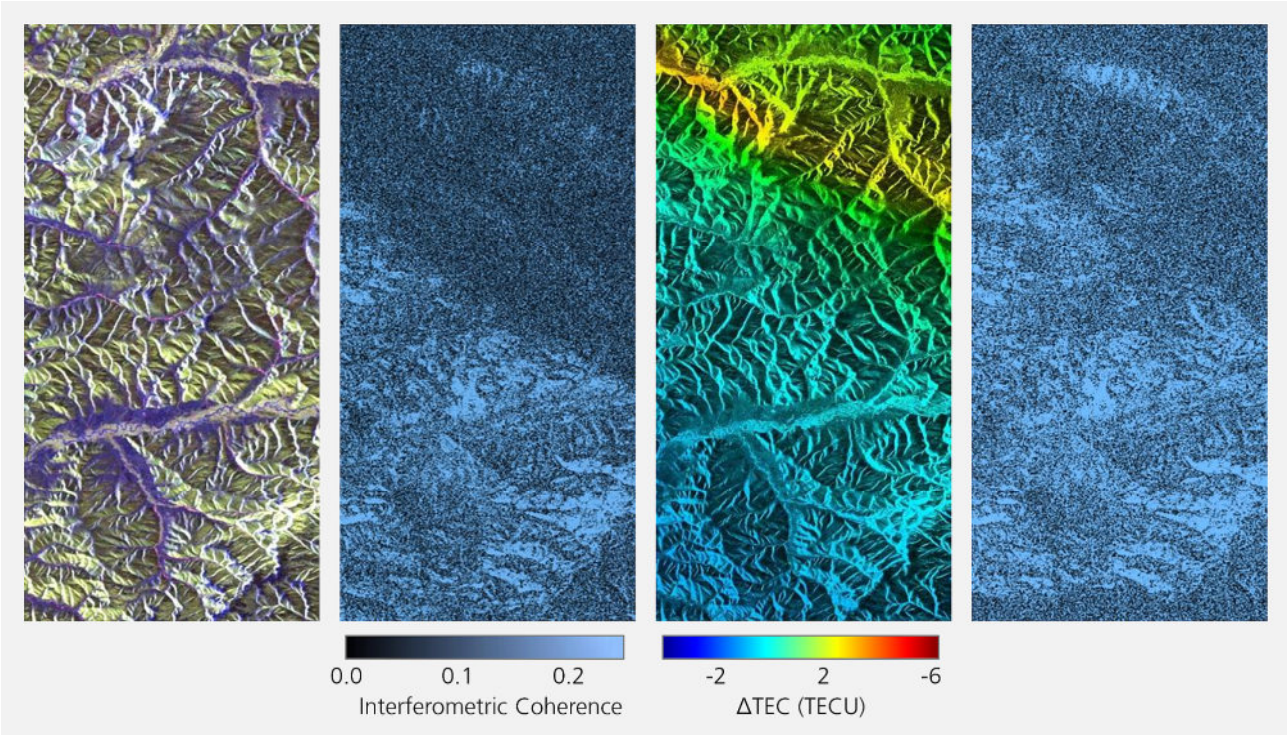

Figure 2.1-52 From left to right: i) polarimetric Pauli RGB composite of the Fairbanks scene acquired by ALOS PalSAR on April 1, 2007; ii) interferometric coherence map scaled from 0 (black) to 1 (blue) without ionospheric correction (the slave image is acquired 46 days later); iii) differential TEC map in TECU (superimposed on the amplitude image of the site) derived from differential Faraday Rotation estimates; iv) interferometric coherence map after ionospheric correction using the differential TEC map.

With the selection of BIOMASS at the User Consultation Meeting in Graz, Austria in spring 2013, BIOMASS entered into its implementation phase and the Institute increased its involvement. In parallel to the science and calibration activities, it became part of the industrial core team and is responsible for the following key developments:

1. The BIOMASS End-to-End Performance Simulator Front End (BEEPS-FE) – a complete end-to-end chain of modules representing the space segment. The simulator includes modules for scene generation, geometry, ionosphere, instrument simulation, platform and on-board data generation as well as a performance assessment module, and allows the simulation of the complete process and flow from a simulated scene to Level 0 (i.e., raw data). The BEEPS-FE will go beyond the sensitivity analysis, and will help to consolidate our understanding of the main BIOMASS error sources (especially instrument-related or environmental errors, including ionospheric disturbances and RFIs), and allow for the quantification of their impact on the mission performance.
2. The Ground Processor Prototype (GPP) that processes BIOMASS Level 0 data to Level 1a/1b (i.e., calibrated single look complex SLC data, see example in Figure 2.1-52). The GPP consists of the Level 1 Processor Prototype and the External Calibration Module and implements the radiometric, polarimetric and ionospheric calibration corrections. The GPP will be used by ESA to support the development and validation of the operational processor to be implemented within the Payload Data Ground Segment, to support the assessment of the instrument performance, and to consolidate the processing algorithms during on-ground and in-orbit tests.
3. The Institute is further responsible for the development, implementation and verification of the prototype processor for the operational forest height product in the frame of the BIOMASS Level-2 Implementation Study. Activities include research, development, test and prototyping of the algorithm, as well as the algorithm performance assessment procedure.

These three activities are strongly interconnected and serve multiple purposes within the BIOMASS mission framework, as they support the development and verification of the space segment, the development of the ground segment, and the commissioning and exploitation of the BIOMASS mission.

2.1.9 SESAME

SESAME (SEntinel-1 SAR companion Multistatic Explorer) was a passive SAR satellite mission proposed by the Institute in response to the ESA's 9th Earth-Explorer call. SESAME was intended to extend the capabilities of Sentinel-1 by adding a pair of close formation-flying, receive-only spacecraft in order to enable single-pass interferometric observations, as illustrated in Figure 2.1-53.

The SESAME mission was dedicated to the observation of land surface topography, topographic change and bio-geophysical parameters in order to advance the scientific understanding and modelling of dynamic processes of the geosphere and biosphere. The observations focused on processes associated with distinct temporal changes in the shape and elevation of land

surfaces and ice bodies, as well as forest height and biomass. Available topographic databases with (near) global coverage lack the ability to capture and quantify key features required to study dynamic processes that shape and transform land surfaces, ice bodies and vegetation cover. The SESAME mission was aiming to fill this critical gap by providing repeat acquisitions of precise, spatially-detailed elevation data over land surfaces, including ice covered areas and forests.

The primary SESAME objectives responded directly to specific challenges posed by ESA's Earth Observation Science Strategy for Cryosphere, Solid Earth and Land Surface, exploiting the single-pass interferometric SAR capability of the mission. In addition to single-pass interferometric acquisitions, the geometric diversity resulting from the proposed configuration would allow for the retrieval of the 3-D deformation vectors including an improved North-South component by means of differential interferometric SAR.

SESAME's system concept was based on two receive-only C-band radar satellites flying in close formation relative to each other and at an along-track distance of roughly 200 km with respect to Sentinel-1C or Sentinel-1D, which were to be used as transmitters. Formation flying provided the opportunity to dynamically reconfigure the baseline geometry according to the specific observational requirements.

The use of Sentinel-1 as illuminator had a number of advantages, such as its very high orbit duty cycle and the systematic acquisition plan. However, it also imposed several constraints, for example the standard use of TOPS in the Interferometric Wide Swath (IW) mode.

The first consequence was thus the need to follow the azimuth scanning performed during TOPS acquisitions. The baseline operating concept was to acquire only one of the three sub-swaths of Sentinel-1's IW mode. Access to the different sub-swaths would be provided in successive passes through attitude steering of the spacecraft. In addition to allowing the use of fixed beams, this relaxes the data volumes making them manageable by the proposed small platform concept at the cost of requiring several Sentinel-1 repeat cycles to provide global coverage.

The preliminary acquisition timeline for one year included one northern polar phase and one southern polar phase and two non-polar phases providing acquisitions over most regions of interest, dedicated primarily to boreal forests and solid earth,

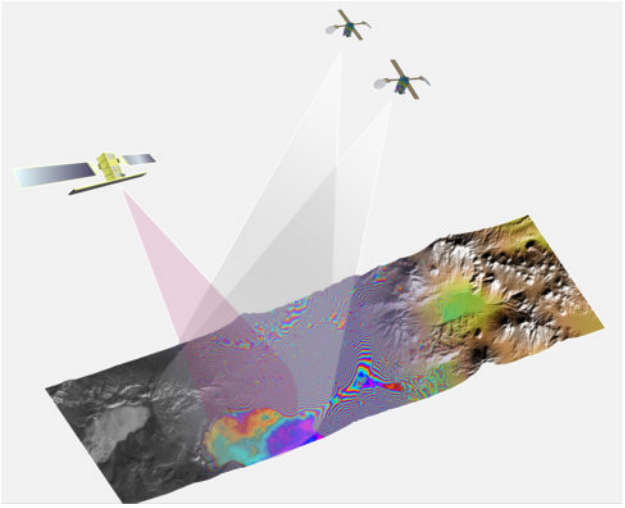

Figure 2.1-53 Artist's impression of SESAME system concept

compliant with the orbit duty cycle and data throughput capabilities of the system.

The main driver for the mission design was the repeated generation of digital elevation models (DEMs), or in the case of forest canopies of digital surface models (DSM), by means of single-pass SAR interferometry. The expected height accuracies ranged from a few decimeters up to 1 or 2 meters for DEM postings from 200 to 50 m, respectively. Figure 2.1-54 shows the relative height error (200 m product), both on global (left) and polar (right, North Pole map), scales. The average height error over the global scale for a single acquisition was about 1.1 m.

In addition to comprehensive time series of DEMs or DSMs, SESAME would provide stacks of bistatic SAR images, yielding a third independent line-of-sight component for the estimation of 3-D deformations. Current SAR missions typically only provide two InSAR observation geometries corresponding to the ascending and descending tracks. As a result, there is a gap in the observation of the North-South component of solid earth deformations, which SESAME aimed to fill. The final performance computed over a mission duration of 5 years, and the combination of the ascending and descending passes of Sentinel-1 and SESAME showed a very high accuracy in the estimate of the deformation vector down to less than 1 mm/year for the up-down and East-West direction and comparable, in the order of a few mm/year, for the North-South motion retrieval.

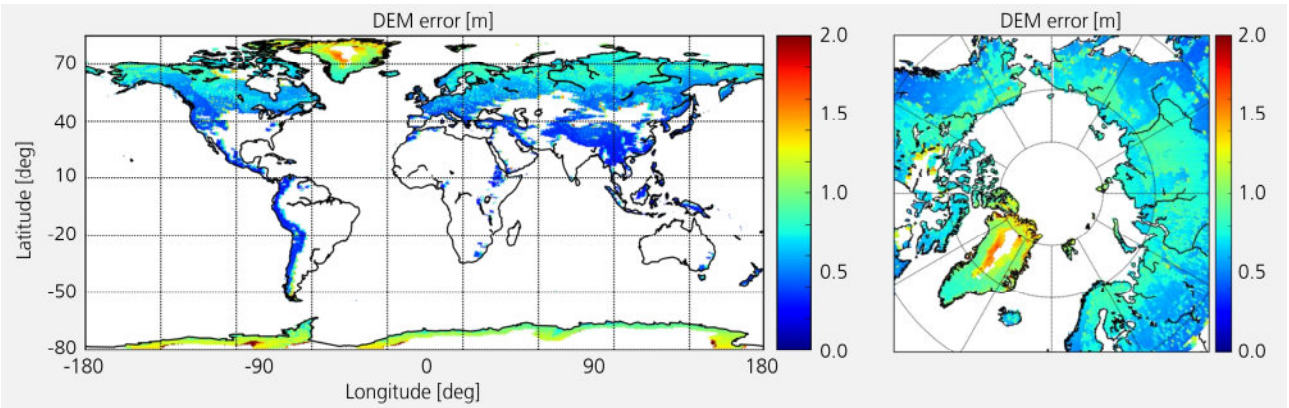

Figure 2.1-54 SESAME global (left) and North Pole (right) performance expressed as relative height error (68% point-to-point confidence interval) for a posting of 200 m

2.1.10 IRIS

A proposal for a new science mission has been submitted by the Institute in response to ESA's 10th Earth Explorer call (EE-10). The overarching goal of Interferometric Radar for (the observation of) Ice, glaciers and permafrost dynamicS (IRIS) is to contribute to the deeper understanding of dynamic processes in the cryosphere and to provide highly precise input data to model, quantify and predict processes and interactions within the different elements of the cryosphere and with other Earth sphere compartments. IRIS will provide very accurate high-resolution measurements of topography, mass balance and structural changes in the cryosphere, including permafrost areas, glaciers, land and sea ice, while at the same time contributing to the measurement of volume change processes in the geosphere including volcanic, landslide and seismic regions. In addition, IRIS will generate a global digital elevation model (DEM) of about one order of magnitude better than the current reference provided by TanDEM-X.

The main goal of the mission is the measurement of the static and dynamic component of the cryosphere with decimetric accuracy and metric resolution. The primary objectives of the mission are served by the system's capability to deliver multi-temporal series of very accurate estimates of surface topography. The primary mission objectives focus on: a) the monitoring of the degradation of permafrost regions by means of seasonal DEM acquisitions and estimates of temporal mass changes, b) the measurement of sea ice topography, including the estimation of snow and ice freeboard, and the characterisation of leads, polynyas and ridges, and c) the mass balance of Alpine and outlet glaciers, ice caps and ice sheets. The secondary mission objectives include relevant parameters of the geosphere, such as the monitoring of the topography and volume changes of volcanoes; the on-demand monitoring of large displacements and mass changes associated with geo-hazards including landslides, rockfalls and seismic events; the global mapping of coastal lines; and the estimation of forest height change.

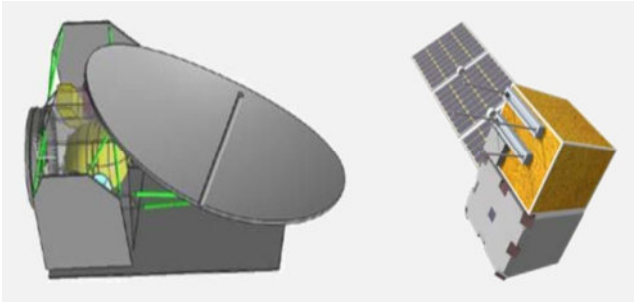

Figure 2.1-55 Candidate platforms suggested by OHB for the MirrorSAR IRIS implementation. The left platform contains a fully active Ka-band instrument fitted with a rigid reflector antenna. The right platform in the 100 kg class contains a passive Ka-band instrument (deployed antenna not depicted in the figure).

The IRIS space segment is composed of a cross-platform Ka-band SAR interferometer with at least two spacecraft flying in an adjustable formation capable of dynamically suiting the scientific observation needs. Figure 2.1-55 shows two potential platforms suggested by one of the industrial partners for the IRIS implementation. The use of multistatic across-track SAR interferometry at 35.75 GHz allows for the measurement of static and dynamic topography avoiding systematic artefacts caused by the penetration of the radar waves in semi-transparent media at lower frequencies. Moreover, Ka band allows for the implementation of a reasonably-sized distributed system within the allocated budget for the EE-10 envelope, avoiding compromises in performance arising from inadequately small antennas.

IRIS will deliver Ka-band SAR imaging with about 3 m² geometric resolution over a dual swath of about 25 km with two or three simultaneous baselines of a few hundred meters. With a duty cycle of about 6 minutes per orbit, the previous values make it possible to generate two surface models per year over the cryosphere, a yearly global DEM, as well as a selected number of acquisitions over volcanic and forest areas of interest. Figure 2.1-56 shows the preliminary performance assessment for the two IRIS sub-swaths. All things considered, IRIS will fill critical observation gaps of the current Copernicus and Earth Explorer

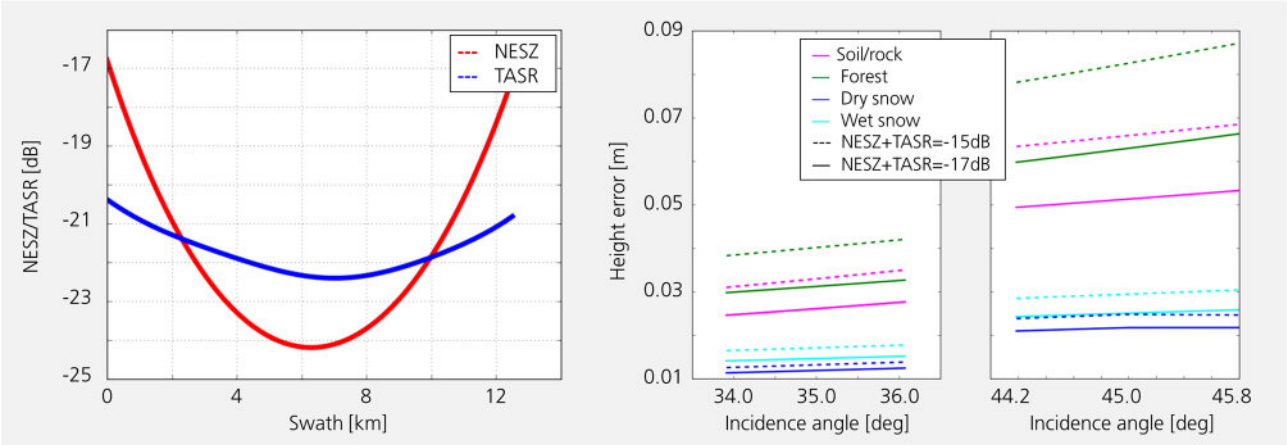

Figure 2.1-56 Noise equivalent sigma zero (NESZ) and total ambiguity-to-signal ratio (TASR) for the far range IRIS sub-swath at around 45° incidence angle. Further pattern optimisation is expected to homogenize the sensitivity values around -19/20 dB (left). Relative height error (point to point) for IRIS interferograms computed for four representative terrain types (magenta for soil/rock, green for forest, blue for dry snow, cyan for wet snow), two NESZ+TASR combinations (solid -17 dB, dashed -15 dB), posting of 100×100 m², and a perpendicular baseline of 400 m (right).

missions (e.g., Sentinel, BIOMASS, Cryosat) by providing frequency diversity and enhanced spatial resolution, while at the same time offering the Earth Observation community and future ESA missions (e.g., Aeolus, EarthCARE) a global topographic reference of unprecedented accuracy, which will certainly improve the quality and interpretation of an immense volume of past, present, and future scientific data. A decision for the implementation of phases A to B1 of three parallel Explorer missions is expected by the end of September 2018.

2.1.11 SAOCOM-CS

In 2013, the Argentinian Comisión Nacional de Actividades Espaciales (CONAE) offered ESA the free launch of a small satellite together with SAOCOM-1b. SAOCOM (Satelite Argentino de Observación Con Microondas) is Argentina's constellation of two fully polarimetric L-band SARs (1a and 1b) flying on the COSMO-SkyMed orbit, and intended for long-term monitoring and emergency management applications. Based on past Earth Explorer proposals, and in cooperation with CONAE, ESA initiated studies on the feasibility of a passive receive-only add-on satellite to allow for dual-pol single-pass L-band InSAR observations enabling bistatic radiometric measurements with variable bistatic angles, single-pass interferometry and correlative tomography.

The Institute supported ESA in the conception of the SAOCOM-CS mission with a preliminary study (pre-phase A) involving mission design and feasibility. In particular, we contributed to the definition of the scientific objectives of the mission, the design of the required baselines, formation flying aspects for the different phases of the mission, as well as other technical aspects such as processing and synchronisation strategies. We participated in the SAOCOM-CS expert group meetings during the project lifetime, contributing to system, mission, and scientific aspects.

During the phase A-B1 activities of the SAOCOM-CS mission, the Institute was involved in two main activities: i) the assessment of the radiometric, interferometric and tomographic performance of SAOCOM-CS in a global manner resulting in the derivation of instrument, calibration, and ground segment requirements for the mission, and ii) the definition of the ground segment architecture and algorithms. In particular, the Institute focused on the definition of bistatic SAR focusing and tomographic kernels, as well as a preliminary bistatic calibration concept including time and phase synchronisation approaches based on AutoSync (see Section 2.2.2).

Some results achieved during this phase are presented in Figure 2.1-57. Phase B1 was closed with no identification of showstoppers for mission implementation. We further supported ESA during phase B2 in two major activities: i) the development of a SAOCOM-CS Performance Verification Simulator to support the instrument prime contractor Airbus Defence and Space (CASA) in instrument development and to assess in-flight performance during the commissioning phase of the mission including support to both CASA and the Agency concerning the bistatic calibration and synchronisation aspects, and ii) the development of a generic bistatic end-to-end (E2E) simulator to support the development and consolidation of processing and calibration algorithms, as well as for assessing mission performance.

The SAOCOM-CS scenario was intended as a specific use case of the bistatic E2E simulator. The mission was discarded for full implementation at the end of phase B2.

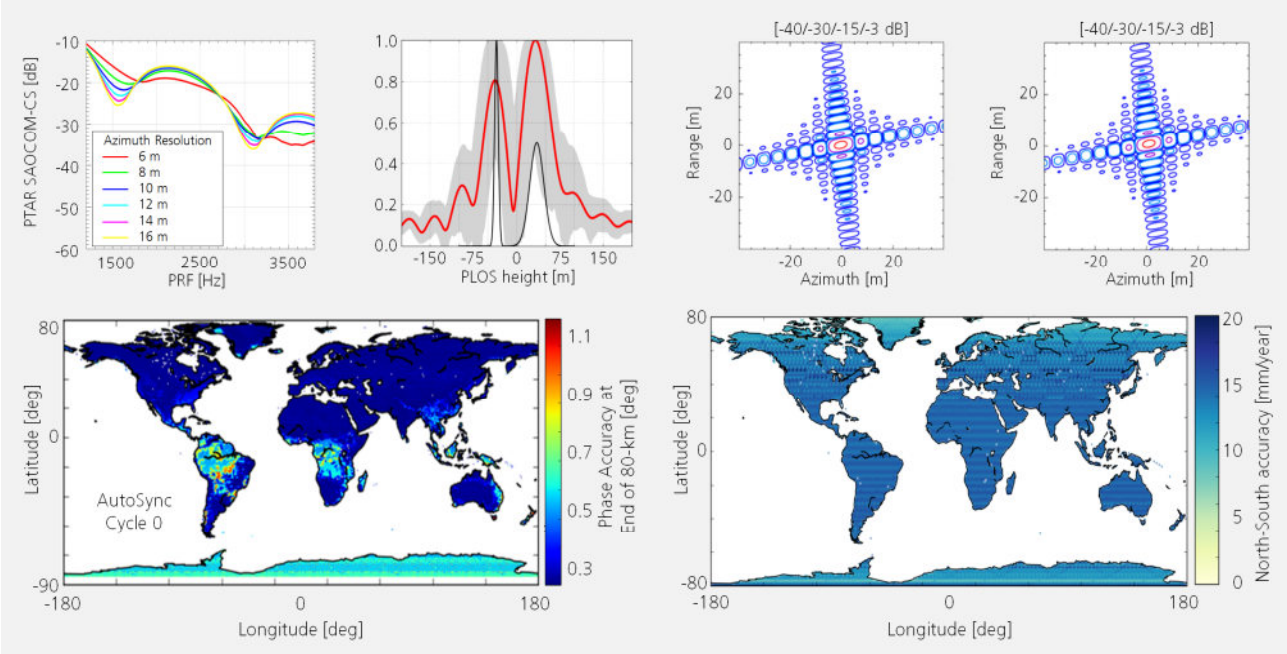

Figure 2.1-57 Results achieved by the Institute during the studies conducted for ESA in the phase A/B1 study of the SAOCOM-CS mission. Top left: Bistatic PTAR as a function of the operational PRF for the optimization of the PRF of the acquisition. Left, top right: Tomographic performance examples used for the derivation of baseline calibration requirements. Bottom left: AutoSync performance for the small baselines of the tomographic cycle for the assessment of the suggested synchronisation approach. Top right: Impulse responses of the suggested bistatic processing kernel for the bistatic forward-looking phase (250 km along-track baseline). Bottom right: Accuracy in the measurement of the North-South deformation component.

2.1.12 KOMPSAT-6

The Institute has been involved in several activities in the frame of the KOMPSAT-6 mission of the Korea Aerospace Research Institute (KARI), which is scheduled for launch in 2020. The KOMPSAT-6 mission will consist of a multimode SAR satellite operating in X band with a nominal azimuth resolution of 2 m in stripmap mode, a spotlight mode with 0.5 m resolution, and also supporting ScanSAR and TOPS modes with an azimuth resolution of 20 m. Figure 2.1-58 shows a model of the KOMPSAT-6 satellite. The payload and bus are being partly manufactured by Airbus Defence and Space; hence the similarities between its design with the TerraSAR-X satellite.

In 2012, in preparation for KARI's KOMPSAT-6 RFP, the Institute provided technical consultancy on the topics of SAR performance, SAR processing and SAR system calibration [R-369], [R-412], [R-416]. The consultancy was mainly based on the Institute's heritage from the TerraSAR-X mission.

In a second study conducted between 2015 and 2017, the Institute provided technical support for the implementation of the algorithms developed at the Institute to process data acquired in the TOPS mode, the so-called Baseband Azimuth Scaling (BAS). In the frame of this study, simulated TOPS data were provided in addition to support regarding the computation of the TOPS timeline and the interferometric processing of TOPS data (see the activities related to Sentinel-1 and TOPS interferometry in Sections 2.1.7 and 2.2.4, respectively).

Figure 2.1-59 shows an example of one of the simulated scenes, consisting of point targets over a clutter background, provided to KARI in the frame of the study.

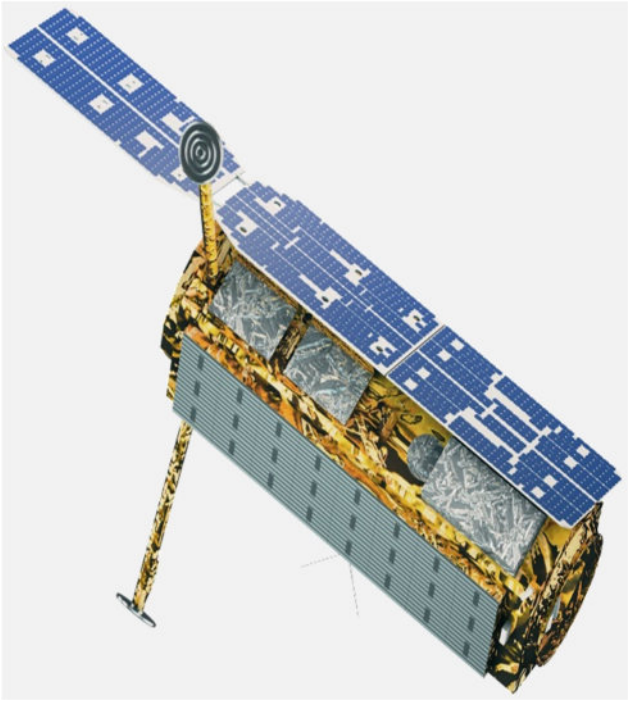

Figure 2.1-58 The KOMPSAT-6 satellite

In the next step, the Institute will support KARI in the calibration of the KOMPSAT-6 SAR system [R-416]. Starting in mid-2019, several analysis tools and the alignment tool will be adapted to the KOMPSAT-6 characteristics. Then, the DLR calibration site [J-30], [RC-305], [RC-306] will be prepared for a comprehensive calibration campaign during the commissioning phase in 2020.

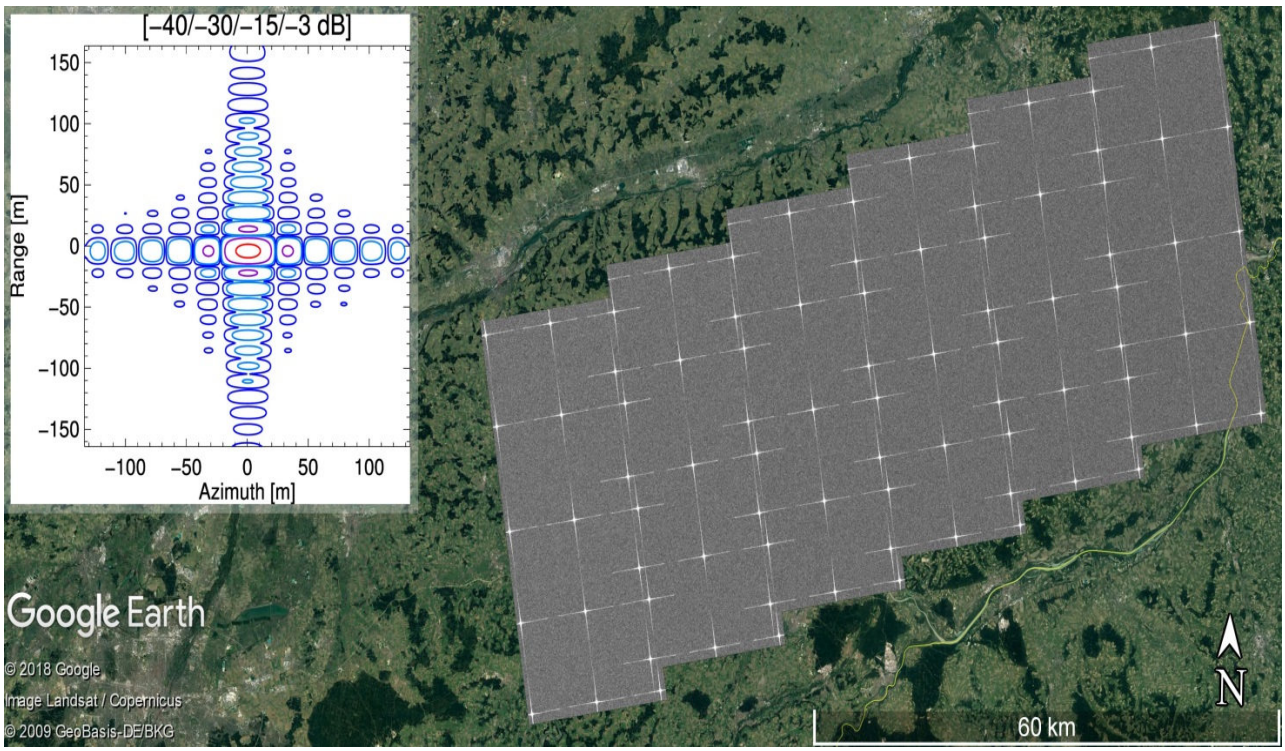

Figure 2.1-59 Simulated TOPS acquisition with the KOMPSAT-6 timing processed with the TAXI processor and geocoded. The KOMPSAT-6 mode has an azimuth resolution of 20 m and a swath coverage of 100 km using six sub-swaths. The simulated data consist of a set of ideal point targets over a clutter background, including only two bursts per sub-swath, resulting in an azimuth extension of about 40 km for each sub-swath. The contour plot of the impulse response function for one of the simulated point targets is shown on the top left.

2.1.13 RADARSAT Constellation Mission Transponder

In October 2014 the Canadian Space Agency (CSA) issued a request for proposal for two C-band transponders for the upcoming RADARSAT Constellation Mission (RCM). The Institute prepared an offer based on the complete in-house developments for the Kalibri transponders (see Section 2.2.6) and won against Canadian industrial competitors.
Over the last decades, the Institute has developed and built highly accurate transponders in various frequency bands including X, C, and L band for different SAR missions. The focus on the latest transponder development Kalibri was placed on radiometric accuracy and autonomous, long-term operation throughout the entire SAR mission lifetime [RC-388], [RC-185], [RC-480], [RC-581], [RC-668], [R-283], [MaT-17], [MaT-53], [MaT-6]. To fulfil the specific CSA requirements and the demanding environmental conditions in the Montreal region several adaptations had to be implemented, such as:

- an improved temperature control system for operation at temperatures ranging from -30° C to +30° C (storage temperature: down to -40° C),
- adjustable radar cross sections (RCS) and receive levels,
- a look angle extension up to 85° in elevation with an absolute alignment accuracy of +/-0.5°,
- a more user-friendly graphical user interface and additional operational modes like the stand-by mode or manual orientation of the positioner.

Furthermore, a multitude of Canadian standards had to be observed, starting from a flame-resistant housing, a warning system in case of manual operation, through to the (TÜV-like) Canadian certification of the whole transponder system. Finally, maintenance and short response times were realized by monitoring all relevant components remotely via internet from Oberpfaffenhofen at a distance of more than 6000 km.
The RCM transponder consists of an indoor control unit and an outdoor unit which is designed for all-season autonomous outdoor operations, see Figure 2.1-60 (top) [R-26], [R-34], [R-35], [R-39]–[R-46], [R-55], [R-57], [R-58], [R-81]–[R-89], [R-98], [R-124], [R-139]–[R-179], [R-201]–[R-204], [R-213], [R-214], [R-215], [R-225]–[R-231].
For this purpose the transponder's transmitting and receiving antennas together with the RF circuitry are embedded in a temperature stabilized housing. Since a transponder is used as a calibration standard, the transponder must itself be accurately characterized, calibrated and monitored during operation. This is achieved by internal and external transponder calibration, comparable to the calibration process of a SAR instrument.
A radar cross section of 64 dBm² was measured with an absolute radiometric accuracy of only 0.2 dB for both RCM transponders. This radiometric accuracy was achieved by different measurement set-ups and a comparative study of all the results [J-154], [RC-313], [RC-420], [RC-431], [RC-589], [MaT-45]. Beyond that, the novel, so-called 3 transponder method for accurate transponder RCS calibration has been developed and patented [J-82], [RC-110], [RC-246], [RC-247], [P-9].

Figure 2.1-60 Installation of the C-band transponder system developed by the Institute for the Canadian Radarsat Constellation Mission featuring RCS of 64 dBm² at an absolute accuracy of 0.2 dB, RCS stability below 0.1 dB, and remote control (top). RCM transponder at CSA headquarters near Montreal, Canada (bottom).

An outstanding radiometric stability of below 0.1 dB has been achieved by implementing an internal calibration loop. Furthermore, the FPGA-based receiver chain allows for coherent recording of radar pulses at full bandwidth and for measuring the azimuth antenna patterns during an overpass of the satellite. As the polarizations of the receive and transmit antennas are independently adjustable [RC-111], [RC-210], [R-284], the RCM transponder is also well suited for calibrating fully polarimetric SAR systems like RCM.
The RCM transponders are remotely aligned towards the satellite by a two-axis positioner. The transponder configuration for satellite overpasses and the corresponding data acquisitions are conducted in an automated fashion and can be conveniently scheduled and monitored by a web interface.
Upon the on-site installation in Canada, the commissioning was completed in 2017 using Sentinel-1. Both units have since been in operation without any significant problems. The successful completion of this contract is a milestone in the Institute's hardware development.

2.1.14 VERITAS

The Venus Emissivity, Radio science, InSAR, Topography, And Spectroscopy (VERITAS) mission investigates the origin and evolution of a planet most similar to Earth. Venus is the second closest planet to the Sun and shows a few peculiarities. It takes Venus 243 Earth days to rotate once around its axis, and 224 Earth days to orbit the Sun. As such, one day on Venus is almost as long as a Venus year. Further, Venus rotates backwards (retrograde rotation, i.e., the Sun rises in the West). Venus' evolution clearly diverged from Earth's. Only by understanding our twin planet can we know how unique Earth's evolution may be, and thus predict how terrestrial planets elsewhere may become habitable.

VERITAS determines how and when Venus diverged from Earth by addressing a series of focused, hypothesis-driven questions. Are tesserae remnants of an earlier, wetter past? Is there evidence for a past tectonic or cratered surface beneath the plains? How and when did Venus resurface? What are the sources and rates of present day volcanism?

The VERITAS [RC-80] mission was one of five missions selected by NASA for a phase A study among several proposals for future planetary missions. Led by the Jet Propulsion Laboratory (JPL), phase A was conducted together with Italian Space Agency (ASI), the German Aerospace Center (DLR) as well as Lockheed-Martin as an industrial partner.

The main focus of the Institute was on VISAR, the X-band (7.9 GHz) single-pass Venus Interferometric Synthetic Aperture Radar with two antennas separated by 3 meters. The imaged 14 km swath allows the acquisition of data for a global DEM of Venus within two years. One of the main challenges is the low data transmission rate to Earth, which requires on-board data focusing and interferogram generation in order to reduce the data volume. The Microwaves and Radar Institute, leading the phase A from the DLR side, was responsible for the on-board data processing and compression (see Figure 2.1-61) and SAR performance computation. Furthermore, an end-to-end simulator software was used to test the complete chain starting from the raw data generation up to the focused SAR images and interferograms. In addition, the Remote Sensing Technology Institute (DLR) participated and shared the task of the on-ground data processing and DEM generation/calibration.

A DLR team participated in a NASA review of the VERITAS mission proposal at JPL in November 2016. Regrettably, the VERITAS mission was not selected for realisation beyond phase A. Nevertheless, the cooperation between the DLR and JPL technical expert teams demonstrated the excellence of both institutions and the capability of joint mission proposals. A VERITAS Explorer Mission is currently being proposed for NASA's New Frontiers Program.

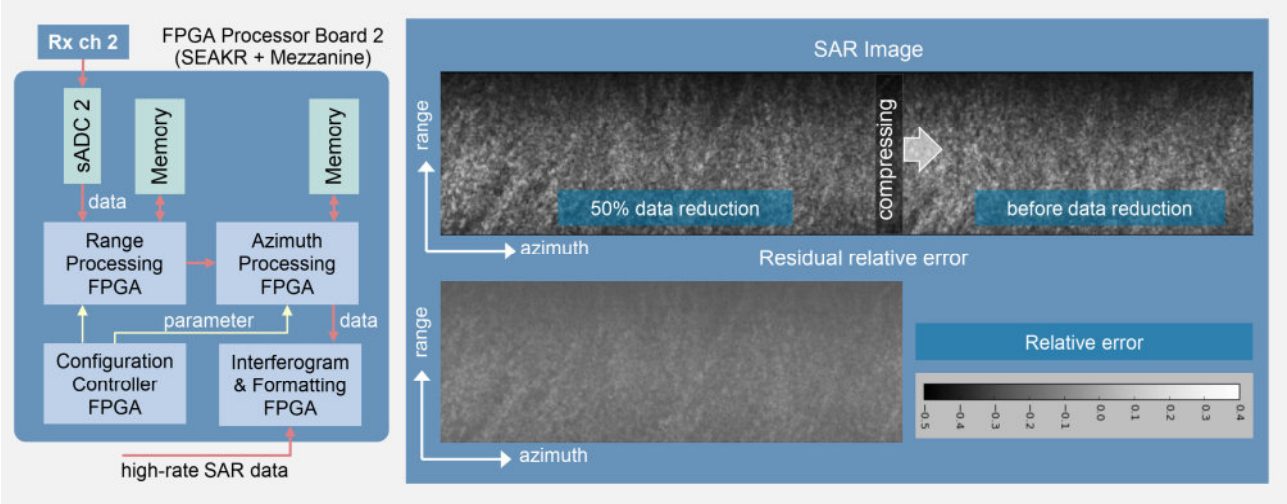

Figure 2.1-61 On-board data compression is crucial for VERITAS because of the limitations of the data link to Earth. Therefore, the image data compression is implemented in hardware (left). DLR tested image data compression algorithms on exemplary SAR images. The evaluated residual error (right) shows that compression of up to 50% of the original data volume seems feasible with acceptable impact on the radiometric accuracy.

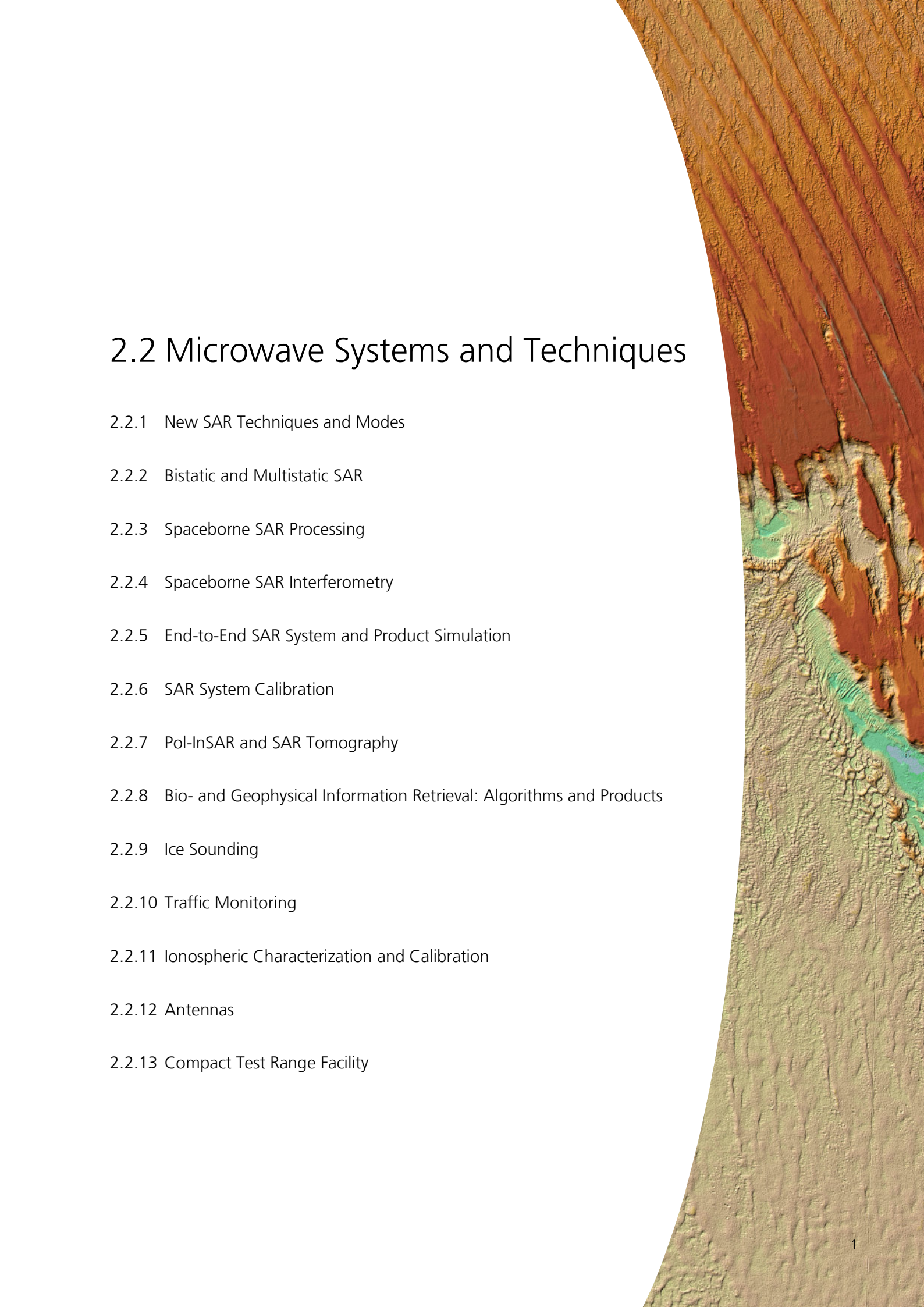

2.2 Microwave Systems and Techniques

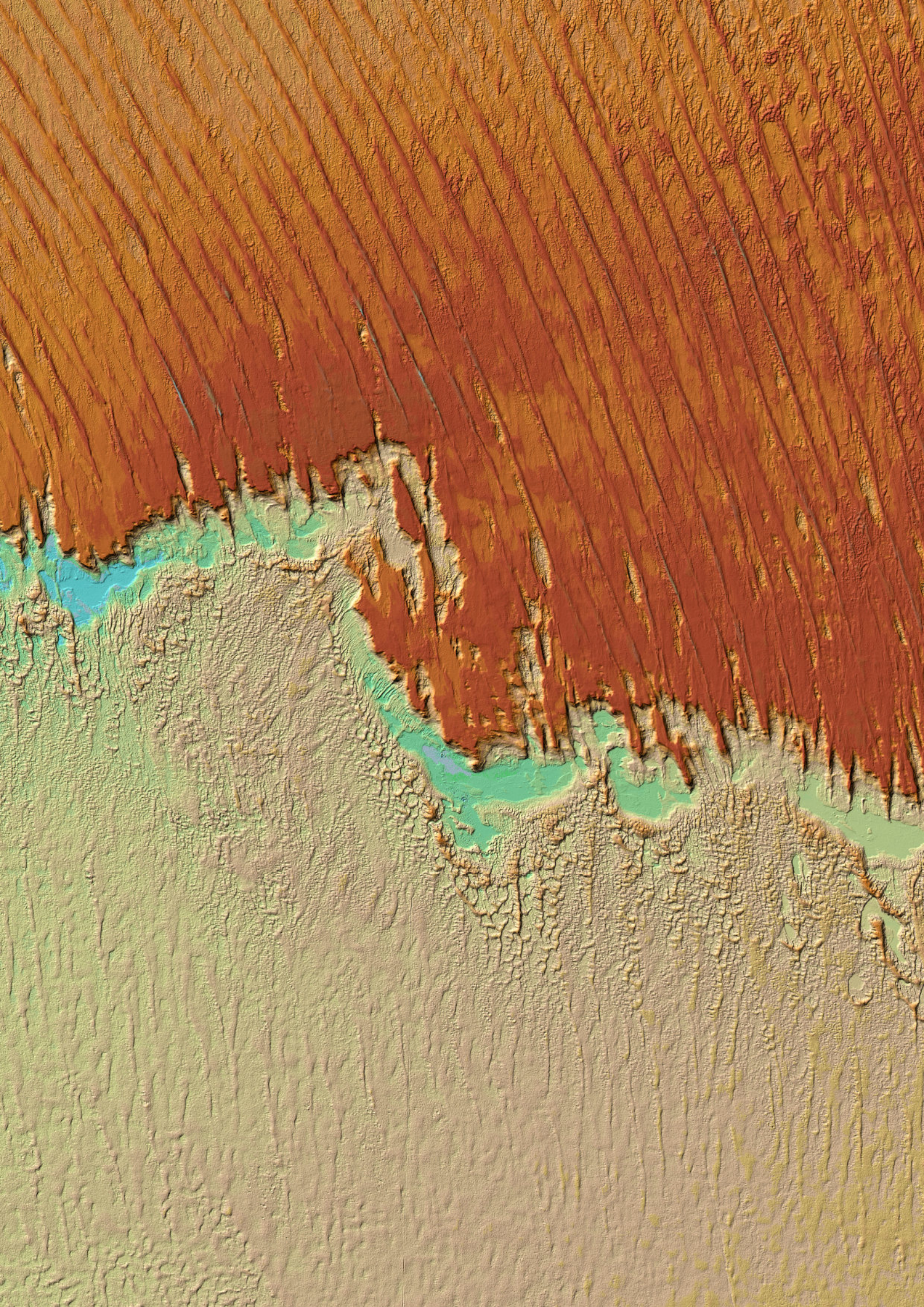

2.2 Microwave Systems and Techniques

The Institute looks back to a long history of research activities in the field of microwave remote sensing, and has now taken the international leadership in the development of cutting-edge SAR systems and applications. Many of the radar concepts invented at the Institute one decade ago have gestated, grown and matured to the point where they are indispensable for the implementation of current and future SAR missions. This is evident from TanDEM-X and Tandem-L, which would have been inconceivable without the prior developments on bi- and multistatic SAR, digital beamforming and information retrieval. The current reporting period is again characterized by a series of unique achievements that will shape the future of radar remote sensing. An outstanding example is the development of a new generation of digital radar systems that exceeds the mapping capabilities of state-of-the-art SAR satellites by two orders of magnitude, thus keeping pace with increasing user demands. Research on bi- and multistatic SAR has likewise led to exciting innovations, including the data-based synchronization technique AutoSync and the fractionated space transponder concept MirrorSAR, which is already an integral part of the multistatic HRWS mission proposal. Major achievements were also made in the areas of spaceborne SAR processing and interferometry. Examples are a new staring spotlight mode for TerraSAR-X that provides an azimuth resolution down to 14 cm, the world-wide first demonstration of TOPS interferometry with both TerraSAR-X and Sentinel-1, and a novel bidirectional SAR imaging mode to measure along-track movements with hitherto unprecedented accuracy. An innovative multichannel technique to measure the beam-pointing in reflector-based SAR systems and a new algorithm for correcting ionospheric propagation errors were developed for the calibration of future low-frequency SAR systems. Furthermore, considerable progress has been made in the area of polarimetric SAR interferometry and tomography; an important example is the retrieval of forest height, which evolved from an experimental algorithm to a highly accurate operational information product as required for Tandem-L. Further highlights are the experimental results for the retrieval of 3-D forest structure, crop phenology, and the internal structure of glaciers and ice sheets. In the field of traffic monitoring, a novel ground moving target indication (GMTI) processor with an incorporated road database has been developed and experimentally verified to serve future real-time applications. Last but not least, basic research on new SAR systems and applications has been complemented by a number of innovative antenna developments and measurements within the Institute's Compact Test Range, as required for the demonstration of novel radar techniques in various frequency bands and sensor configurations.

2.2.1 New SAR Techniques and Modes

Limitations of Conventional SAR Systems

Synthetic Aperture Radar is currently a well-established remote sensing technique that can provide high-resolution radar images of the Earth's surface regardless of weather conditions and sunlight [J-167]. SAR images of the Earth are now acquired on a regular basis by an increasing number of satellites and form the basis for a wide range of remote sensing applications and services. While the performance of spaceborne SAR systems has significantly evolved over the past decades, their imaging capabilities are still rather limited. Figure 2.2-1 shows a performance comparison of two state-of-the-art SAR systems visualizing their limitations in terms of resolution and coverage. As a representative example, Sentinel-1 can acquire SAR images with an azimuth resolution of 20 m and a swath width of 250 km using its standard interferometric wide-swath (IW) mode. In stripmap mode, the resolution can be improved to 5 m, but only at the cost of narrowing the swath to 80 km. This example demonstrates that current SAR technology is not capable of obtaining both a high resolution (e.g., 1 m) and a wide swath (e.g., 500 km) simultaneously.

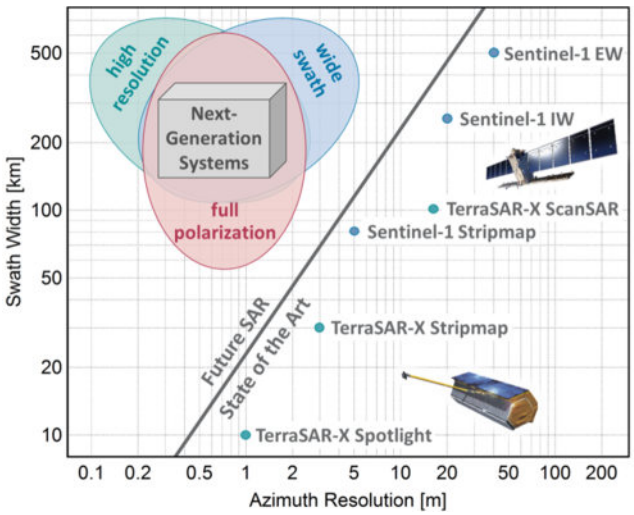

Figure 2.2-1 The imaging capabilities of current spaceborne SAR systems and missions are limited such that they can either achieve a high azimuth resolution or map a wide swath, but not both at the same time as exemplified by the various imaging modes of TerraSAR-X and Sentinel-1. This fundamental limitation can be overcome by employing radar instrument architectures with multiple transmit and/or receive channels in combination with innovative SAR operating modes.

Multichannel SAR Systems

To overcome this fundamental limitation, the last years have seen intense national and international research activities towards new SAR system designs and architectures that employ not only one, but multiple digital channels in their receiver chain. These multichannel instrument architectures mark a paradigm shift in the design of SAR systems, and the Institute has shaped this future from the very beginning with numerous key innovations and strategic developments that are well documented by a multitude of peer-reviewed journal publications and patents [J-36], [J-37], [J-72], [J-90], [J-94], [J-112], [J-114], [J-124], [J-140], [J-141], [J-156], [J-157], [J-158], [J-160], [J-161], [J-176], [J-183], [J-199], [P-3], [P-5], [P-6], [P-8], [P-14], [P-18], [P-20], [P-21], [P-22]. The proposed SAR techniques, modes and system concepts are well suited to improve the imaging performance of future SAR systems by one or even two orders of magnitude if expressed in terms of acquired image pixels per second [IC-12], [IC-69], [IC-187], [RC-153]. The extended mapping capabilities of this new generation of multichannel SAR systems go hand in hand with the increasing demands of the scientific and user community, and thus provide a suitable means to cost-efficiently serve future Earth observation applications [J-97], [J-167].

Figure 2.2-2 illustrates a representative subset of the multichannel SAR system concepts that were either invented by the Institute or to which it made major contributions. An early example is the High-Resolution Wide-Swath SAR, also known as HRWS. This system employs a large receiving antenna that is divided into multiple subapertures, each connected to an individual receiver channel. Multiple subapertures in elevation are used to steer – in real time – a narrow elevation beam in synchrony with the direction of the arriving radar wavefront. This scan-on-receive technique is well suited to enhance the sensitivity and radiometric resolution without compromising the swath width [J-114], [IC-69], [RC-227], [RC-335], [RC-336]. Moreover, multiple subapertures in azimuth sample the arriving wavefront at a set of mutually-displaced along-track positions. These additional azimuth samples allow for the imaging of a wider Doppler spectrum without rising azimuth ambiguities, thereby improving the azimuth resolution. To process the multichannel SAR data, a dedicated reconstruction algorithm has been developed at the Institute and experimentally verified using both the Institute's airborne radar and the split antenna of TerraSAR-X [J-157], [J-161], [J-176], [J-199], [IC-217], [RC-663], [RC-666]. This algorithm has been extended to wide-swath ground moving target indication [J-156], [RC-347] (see also Section 2.2.10), and a new technique to periodically shift the phase center of the transmit antenna has been developed and patented to further improve the imaging performance [P-18]. Extensive investigations were also carried out with regard to error analysis and the calibration of multichannel SAR systems [J-164], [J-186], [IC-135], [RC-52], [RC-81], [RC-82], [RC-84], [RC-85], [RC-310], [RC-463], [RC-500], [RC-501].

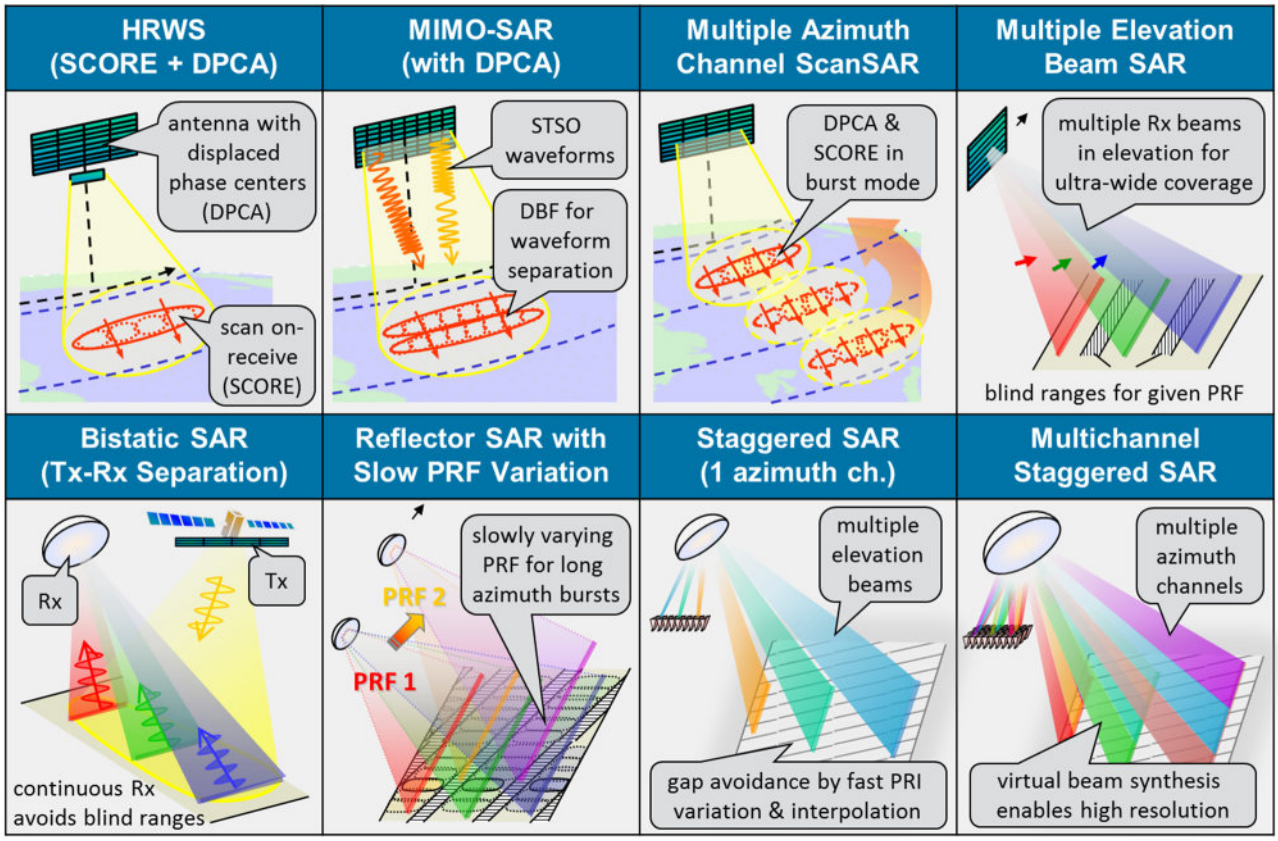

Figure 2.2-2 The Institute has developed and patented a wide range of highly innovative radar concepts and techniques that form the basis of a new generation of SAR sensors and missions with tremendously increased imaging capabilities. The main text provides a more detailed explanation of each individual system concept.

MIMO SAR

While the HRWS system with its multichannel stripmap mode is well suited for improving the azimuth resolution to one meter or even better, it is inappropriate for wide swath mapping, as a rather long antenna in the order of 15 m and beyond will be required for swath widths larger than 150 km. A possible solution to extend the swath consists in the use of two transmitters at the same time, as illustrated in Figure 2.2-2 at the top of the second column. Such a Multiple-Input Multiple-Output (MIMO) SAR offers the opportunity to double the swath width while keeping the overall antenna length constant [J-94], [J-124], [P-21]. For this, two mutually Short-Term Shift-Orthogonal (STSO) waveforms are simultaneously transmitted from the antenna's trailing and leading edges, and the corresponding radar echoes are then separated by digital beamforming on receive in elevation [J-124], [J-160], [IC-185], [IC-187], [RC-429], [RC-430], [RC-523], [RC-553], [RC-639], [RC-652], [RC-653], [PhD-31], [P-22]. Figure 2.2-3 illustrates the deterministic relation between time, angle of arrival and instantaneous frequency of the radar echoes for a distributed scatterer scenario that is simultaneously illuminated by a chirp and its cyclically shifted copy. As the radar echoes from the two waveforms never occupy the same cell of the 3-D information cube, they can be separated by an appropriate space-time-frequency processing as described in [J-124].

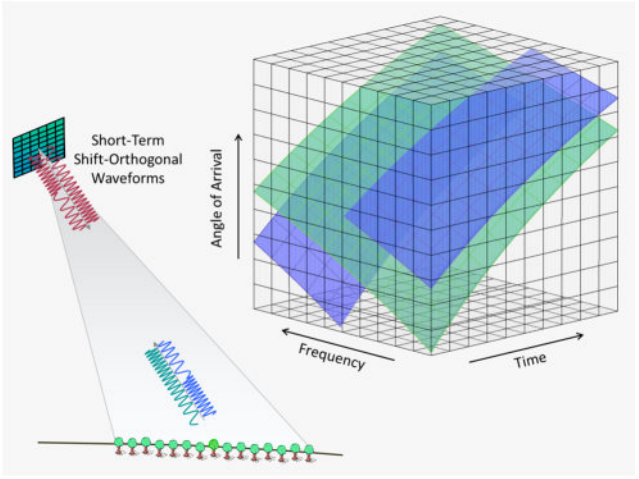

Figure 2.2-3 Information cube for a MIMO SAR that illuminates a wide scene composed of distributed scatterers by two mutually short-term shift-orthogonal waveforms. As their radar echoes fill different portions of the information cube, they can be separated by a time-variant frequency-selective digital beamforming technique (cf. [J-124]).

Multichannel ScanSAR

Another opportunity to extend the swath width of a SAR system with multiple azimuth channels is an operation in ScanSAR mode as illustrated in Figure 2.2-2 on the top of the third column. Such a concept has been intensively studied in close cooperation between the Institute and Airbus DS in the frame of several ESA studies as a potential successor to the current generation of Sentinel-1 satellites [RC-8], [RC-52], [RC-81], [RC-82], [RC-83], [RC-84], [RC-85], [IC-135], [RC-227], [RC-310], [RC-335], [RC-336], [RC-463], [RC-500], [RC-501]. The goal is to map a 400 km wide swath at a resolution of 5 m. The multichannel ScanSAR system needs a broad Doppler spectrum sampled by a large number of azimuth apertures for the imaging of a wide swath with high azimuth resolution. Hence, each subswath will be characterized by a considerable variation of the Doppler centroids. The associated squint angle variations, which increase for longer wavelengths, may in turn cause new challenges for SAR data interpretation due to the continuously changing line-of-sight vectors [RC-366]. In addition, adjacent points on the ground will be imaged by widely separated bursts that collect radar echoes propagated through different portions of the ionosphere [RC-153], [IC-12]. This will become a challenge for low-frequency SAR systems, which require excessive multilooking over large areas for the correction of ionospheric propagation errors [RC-182].

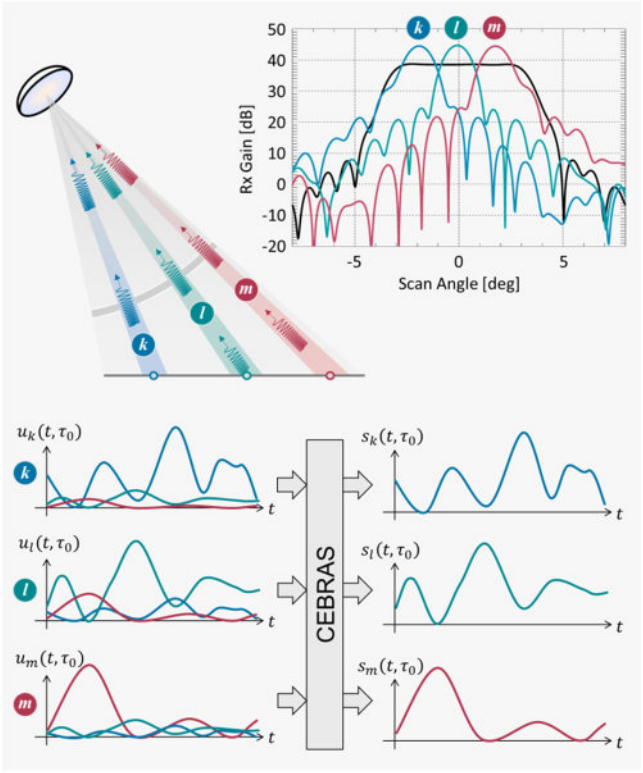

Figure 2.2-4 CEBRAS is a new hybrid space-ground beamforming technique to suppress range ambiguities in spaceborne SAR systems with multiple elevation beams. First, conventional scan-on-receive is performed in real time on board the satellite by employing a set of dispersive elevation beams that maximize the collected signal energy for each transmitted pulse. The corresponding radar signals are then downlinked to the ground, where they are range compressed. The residual range ambiguities are removed for each range bin by jointly processing all received signals from the different beams. This exploits the fact that the useful signal for one beam is the ambiguity for another beam. The suggested two-stage approach has the advantage that a robust range ambiguity suppression can be performed on ground without tremendously increasing the on-board processing demands or the data downlink volume. As described in [IC-81], the ground processing may involve adaptive nulling and/or blind source separation techniques to account for satellite attitude and instrument phase errors, residual calibration errors, as well as azimuth- and range-variant topography changes.

SAR with Multiple Elevation Beams

To avoid these issues and to simplify the spacecraft design, a number of alternative SAR instrument architectures and

operation modes have been developed at the Institute [J-36], [J-90], [J-97], [J-140], [J-141], [J-158], [J-183], [IC-12], [IC-81], [IC-187], [RC-25], [RC-83], [RC-132], [RC-153], [RC-184], [RC-255], [RC-281], [RC-444], [RC-445], [RC-451], [RC-452], [RC-542], [RC-573], [RC-634], [RC-635], [RC-659], [RC-676], [P-3], [P-5], [P-6], [P-8], [PhD-3], [PhD-10], [PhD-19]. A feature common to all these innovative concepts is the use of multiple elevation beams, which, at each point in time, acquire the scattered radar echoes from not only one, but multiple transmit pulses. This is illustrated on the upper right of Figure 2.2-2.

The multiple elevation beam technique is well suited to increase the coverage without having to resort to an excessive number of bursts, but also faces two key challenges. The first is related to range ambiguity suppression, as the simultaneously arriving radar echoes from different transmit pulses have to be mutually separated. Hence, a sufficiently high antenna is required that is capable of forming narrow elevation beams as required for a low range-ambiguity-to-signal ratio. In turn, the demand for narrow elevation beams favors the use of deployable reflector antennas that are lightweight and can be efficiently stored in the launcher, while providing a large aperture in space. If necessary, the requirements for the receiving antenna could also be relaxed by employing a new hybrid technique that combines the real-time beam steering in elevation on-board the satellite with an integrated multichannel SAR processing on the ground. Figure 2.2-4 illustrates the basic idea of this promising technique, which has been named Cross Elevation Beam Range Ambiguity Suppression (CEBRAS). A distinctive feature of CEBRAS is its ability to significantly improve the range ambiguity suppression a posteriori in the ground processor without the need for a detailed knowledge of the antenna patterns at the time of SAR data acquisition [IC-81].

The second challenge of a multiple elevation beam SAR is related to the emergence of blind ranges, as a spaceborne radar cannot transmit and receive at the same time. Due to the constant PRF, these blind ranges are then visible as gaps in the wide image swath. One possibility to avoid such gaps is a spatial separation of the transmit and receive antennas on two distinct spacecraft, as illustrated in Figure 2.2-2 on the lower left [IC-12]. As the transmitter and receiver can now operate at the same time, blind ranges are avoided and it is even possible to use a frequency-modulated continuous-wave (FMCW) transmit signal that decreases the peak power and simplifies the spacecraft design. The drawback of this approach is that a separate satellite is required for scene illumination, but such a fractionated system may nevertheless become cost-efficient in the case that two or more receiver satellites are needed for interferometric or even tomographic applications [IC-11].

SAR with Slow PRF Variation

Another way of avoiding range gaps is illustrated in Figure 2.2-2, at the bottom of the second column. Here, the pulse repetition frequency is slowly varied such that the blind ranges gradually migrate across the wide swath [RC-153], [IC-12]. As a result, valid SAR data can be acquired for each range. This advantage comes, however, at the cost of a discontinuous synthetic aperture. As illustrated in Figure 2.2-5, each point on the ground is mapped by a burst of contiguous SAR pulses resembling the data structure of a classical ScanSAR mode. The gaps between the bursts are, however, very short, as all swaths are imaged simultaneously as a result of the multichannel data acquisition with multiple elevation beams. The shortened gaps enable an improved azimuth resolution

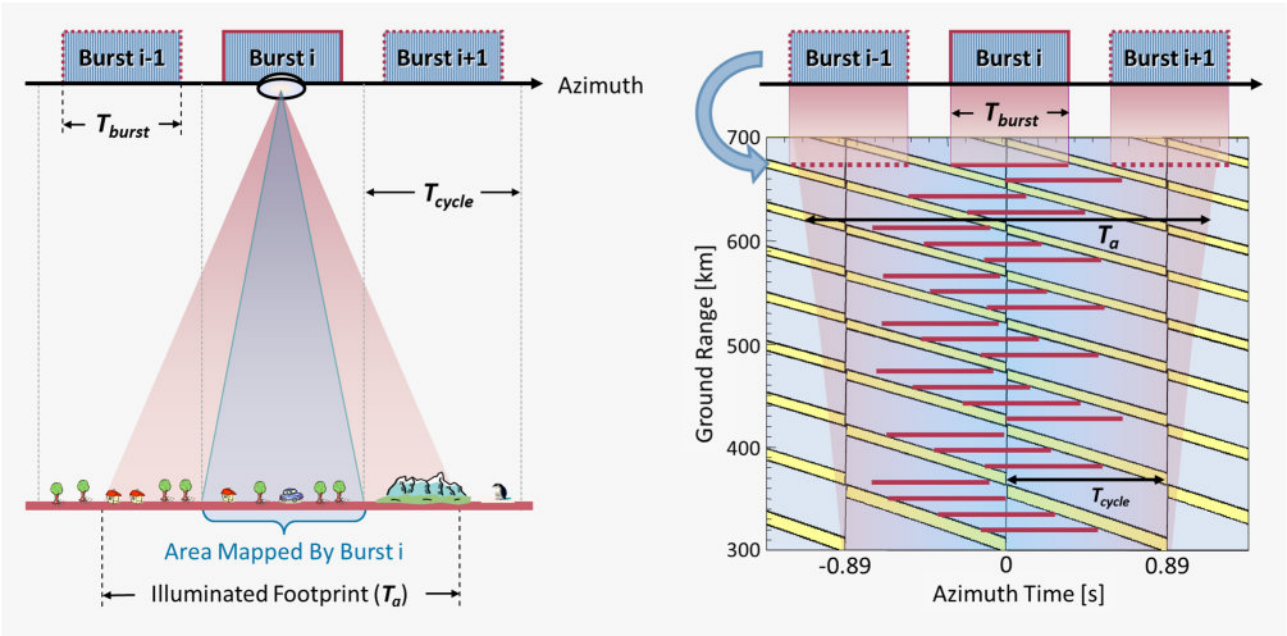

Figure 2.2-5 Illustration of a wide swath SAR mode with slow PRF variation. The left figure shows for a given range bin the periodic interruption of the synthetic aperture due to the transmit events. Each burst of valid SAR data has a duration of T_{burst} and the bursts are periodically repeated with cycle time T_{cycle}. The yellow stripes in the right figure show how the position of the gaps varies over a 400 km wide swath where the PRF is periodically increased from 5000 to 5145 Hz within a cycle time of T_{cycle} = 0.89 s. These parameters are suitable for a C-band SAR system that maps a 400 km wide swath with an azimuth resolution of 5 m using a compact planar antenna with an aperture area of 3 x 3 m² [RC-153]. The red horizontal bars indicate for a given set of ground range positions the bursts from which a target at an azimuth time of t_a = 0 s is imaged.

without increasing the illuminated Doppler spectrum. Moreover, squint angle variations are reduced in comparison to ScanSAR, which favors a more homogeneous imaging geometry with less line-of-sight variations and their associated difficulties for image interpretation [RC-366].
As an example, a C-band SAR system that maps a 400 km wide swath with an azimuth resolution of 5 m has been suggested in [RC-153]. Such a powerful system can be realized using a rather compact planar antenna with an aperture area in the order of 3 m x 3 m. A peculiarity of this mode is that additional azimuth looks with coarser resolution can be formed for each range, as indicated by the red dotted lines in Figure 2.2-5. The additional information may then be used for several purposes, such as interferometric multilooking, improved radiometric resolution, or even multisquint observations for the measurement of along-track movements. Slow PRF variation is currently being considered in several ESA studies as one of the most promising techniques for imaging ultra-wide swaths in a fully polarimetric mode, as the antenna area can be kept at a reasonable size [IC-12].

Staggered SAR

An alternative to the slow PRF variation is a SAR mode where the pulse repetition interval (PRI) is rapidly varied according to a periodically repeated sequence of non-uniform PRIs. This mode, which has been denoted as staggered SAR [J141], enables a gapless stripmap-like SAR imaging with wide swath coverage (see also Section 2.1.3). As illustrated in Figure 2.2-6, this is possible by choosing the non-uniform PRI sequence such that the range gap is shifted from pulse-to-pulse by one full gap length. Hence, the radar echoes from two consecutive pulses are never lost at the same range. Assuming a sufficiently high average pulse repetition frequency, the non-uniformly sampled raw data can then be interpolated to a uniform grid and further processed as in a conventional SAR. For this purpose, a dedicated technique known as best linear unbiased (BLU) interpolation has been developed at the Institute and verified with experimental data from TerraSAR-X and F-SAR [J-140], [J-141], [PhD-10], [J-36].
An inherent challenge of staggered SAR is that a high average PRF is required, which raises both the vulnerability to range ambiguities and the amount of data to be transferred to the ground. To cope with the first challenge, an increased antenna height is needed, which can be provided by a large deployable reflector as suggested for Tandem-L (see Section 2.1.3). Moreover, a dedicated real-time on-board data reduction technique has been developed to cope with the second challenge [J-72], [RC-328], [RC-367], [RC-446], [RC-447].

Multichannel Staggered SAR

While the staggered SAR concept is well suited to image a wide swath (e.g., 400 km) with an azimuth resolution in the order of 5 m, it fails when a higher azimuth resolution, in the order of 1 m, is requested. This is due to the fact that a very short antenna would be needed to illuminate the corresponding Doppler spectrum. Here, the associated increase of the PRF poses a severe challenge to the suppression of range ambiguities, which becomes even more demanding if a system with full polarization is requested. Such challenges can be avoided by using a longer antenna with multiple azimuth

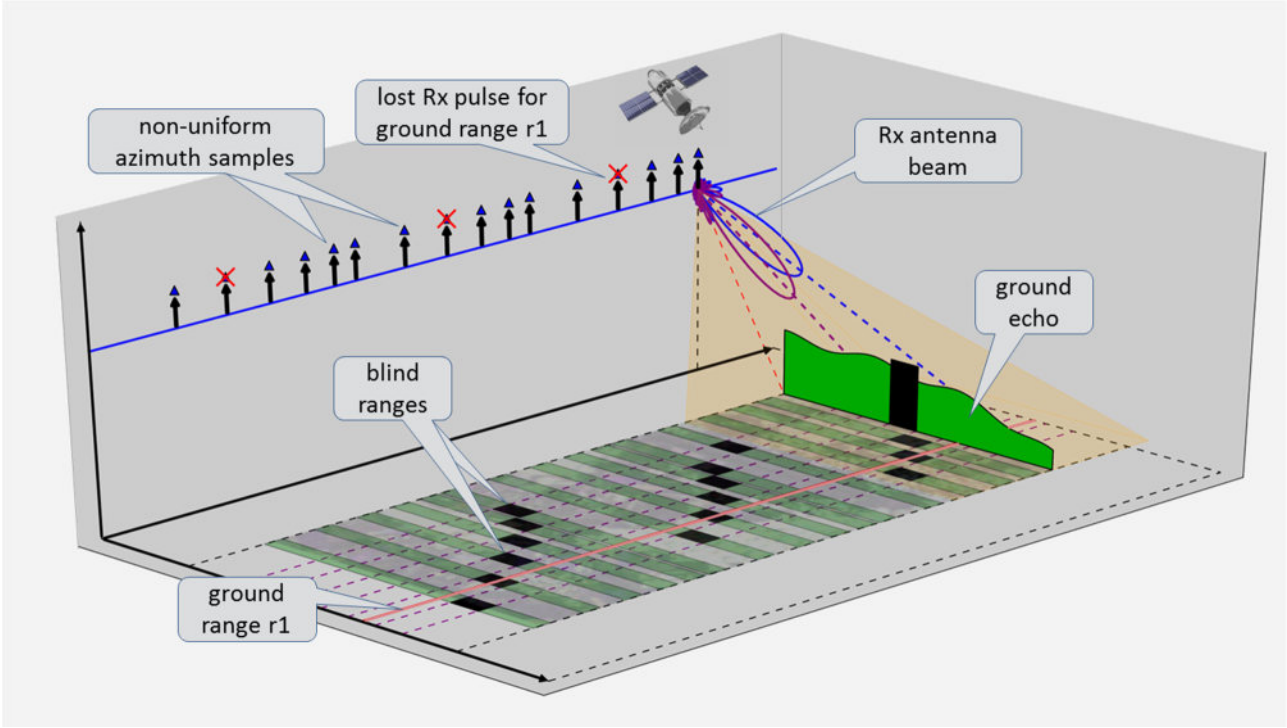

Figure 2.2-6 Illustration of staggered SAR where the blind ranges migrate rapidly across the wide swath (see also Figure 2.1-31 in Section 2.1.3). The non-uniform PRI is chosen such that the lost range bins from two successive transmit pulses cover distinct range positions. As a result, the synthetic aperture contains for each range bin only short gaps and a uniformly sampled SAR signal can be recovered by linear interpolation [J-140], [J-141].

channels, as illustrated on the lower right of Figure 2.2-2. Here, each azimuth beam covers a narrow Doppler spectrum. A broad Doppler spectrum is then obtained by combining the data from multiple azimuth beams.

This combination can be easily performed in the azimuth frequency domain by using a constrained beamformer that maximizes the antenna gain for each desired Doppler frequency, while suppressing the signals arriving from ambiguous Doppler frequencies [J-183], [PhD-19]. However, this technique requires a set of uniformly sampled SAR signals, which are not available if PRI staggering is used to map a wide swath without gaps. To cope with this challenge, a new technique denoted as Virtual Beam Synthesis (VBS) has been developed and patented by the Institute [RC-53], [RC-184], [A-P3], [PhD-2], building up on the idea of varying the effective phase center of a reflector antenna by adjusting the feed excitation [J-79]. VBS presents itself as a digital beamforming technique over multiple received signal echoes and it is called "virtual" because no actual antenna beam can be associated to this method. It is only through VBS that staggered SAR can achieve very fine azimuth resolution. To illustrate the capability of this new technique, Figure 2.2-7 shows a performance example for a highly advanced L-band SAR system capable of imaging a 400 km wide swath with 2 m azimuth resolution in full polarization. Compared to the extended wide-swath (EW) mode of Sentinel-1, the imaging capacity is increased by a factor of 160, when expressed in terms of the number of acquired SAR image pixels per second. The factor of 160 results from a factor of 20 in azimuth resolution, a factor of 4 in range resolution, and a factor of 2 for the two additional polarization channels. Moreover, if compared to Sentinel-1, the imaging performance in terms of noise equivalent sigma zero (NESZ), azimuth ambiguities (AASR) and range ambiguities (RASR) is significantly improved, as required for SAR imaging in L band, which has to cope with a higher dynamic range if compared to a C-band radar.

Ground-Based MIMO Radar Demonstrator

A modular ground-based MIMO radar demonstrator has been developed at the Institute [RC209], [RC-382], [RC-522], [RC-606], [RC-624] to experimentally verify the functionality and demonstrate the performance of the various new SAR techniques, modes and system concepts. The MIMO demonstrator is equipped with 8 coherent receive channels and 4 coherent transmit channels, each capable of radiating an independent radar signal created by an arbitrary waveform generator (AWG). Thanks to its flexibility and reconfigurability, it has been used for a number of experiments. Examples are the demonstration of a new MIMO-SAR quad-pol mode, where two orthogonal polarizations are transmitted at the same time using mutually short-term shift-orthogonal waveforms [RC-209],

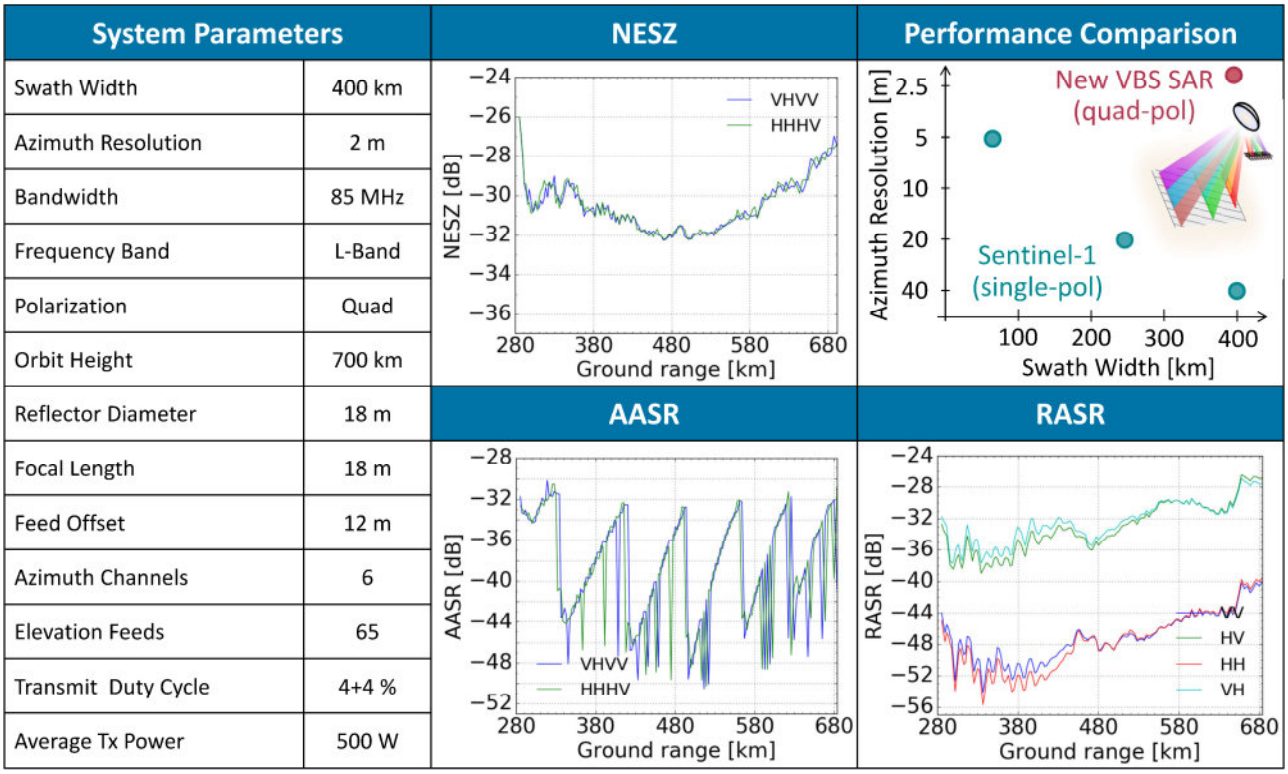

Figure 2.2-7 Performance example of a reflector SAR system that employs the multichannel staggered PRI mode in combination with the new Virtual Beam Synthesis (VBS) technique. The highly advanced SAR instrument is capable of imaging a 400 km wide swath with an azimuth resolution of 2 m and a range resolution better than 5 m in full polarization. Compared to the extended wide-swath (EW) mode of Sentinel-1, this corresponds to an increase of the imaging performance by more than two orders of magnitude, when expressed in terms of the number of SAR image pixels acquired per second. This unprecedented performance becomes possible by employing a reflector with a diameter of 18 m that is illuminated with 6 azimuth and 65 elevation feeds, each connected to an individual Rx channel. As shown on the right, such a system can achieve an excellent SAR performance where the noise-equivalent sigma zero (NESZ) is always better than -26 dB (typically below -28 dB), the azimuth ambiguity-to-signal ratio (AASR) is always better than -30 dB and the range ambiguity-to-signal ratio (RASR) is always better than -26 dB (typically below -30 dB) for the most critical cross-pol channels.

[RC-429], the demonstration of scan-on-receive with both planar and reflector-based antennas, and the demonstration of a new tomographic imaging mode – referred to as MIMO-SAR tomography – which allows for the separation between different scattering mechanisms by exploiting beam diversity on transmit and receive [RC-154], [RC-207].

As a representative example, we describe the experimental verification of the new VBS technique introduced in the previous section. This proof of concept was performed in X band using a reflector antenna illuminated by a digital feed with 8 azimuth channels. As the short range requires simultaneous radar signal transmission and echo reception, a separate horn antenna was used to transmit the radar pulses. As shown in Figure 2.2-8, the imaged scene consists of one corner reflector used for calibration in addition to a formation of four corner reflectors and a metal wire fence. The antennas were mounted on a 6-m mast and carried by a railcar. A detailed description of the complete experiment – including aspects such as the multichannel calibration, signal and image processing, as well as error assessment – can be found in [PhD-3]. At this point, only two exemplary results are shown on the upper left and right of Figure 2.2-8, where the image of a conventional uniformly sampled SAR acquisition is compared to the reconstructed image acquired with the multichannel staggered SAR mode and processed by the VBS technique. The results are nearly identical, and closer evaluation indicates that the magnitude-squared difference between the reconstruction and the reference is below -30 dB [PhD-3].

Outlook

This section provided a brief overview of the new SAR modes and multichannel instrument architectures that the Institute has developed over the last seven years. These unique developments will improve the performance of future SAR systems by one to two orders of magnitude, thus meeting the constantly increasing requirements of users and applications.

However, the advancement of synthetic aperture radar does not stop here, and the Institute's current research activities show several trends for the future. One such development are SAR systems in a Medium Earth Orbit (MEO), where the high altitude enables large-scale observations with very short revisit cycles, as required for applications like soil moisture mapping or sea ice monitoring [IC-47]. Such systems will greatly benefit from the large aperture provided by deployable reflectors in combination with the advanced digital beamforming techniques developed at the Institute.

Another promising development are distributed SAR systems, where the scene is observed by multiple radar satellites flying in close formation. The coherent combination of the radar echoes received by such a sparse aperture is well suited to suppress ambiguities, and thus enables the use of smaller antennas [RC-38], [RC-151], [RC-152], [RC-160], [RC-161]. In the mid-term, this will lead to reconfigurable SAR systems that use formations of small low-cost satellites to serve demanding tasks like high-resolution wide-swath SAR imaging in concert with single-pass interferometry or even tomography [RC-153]. Such

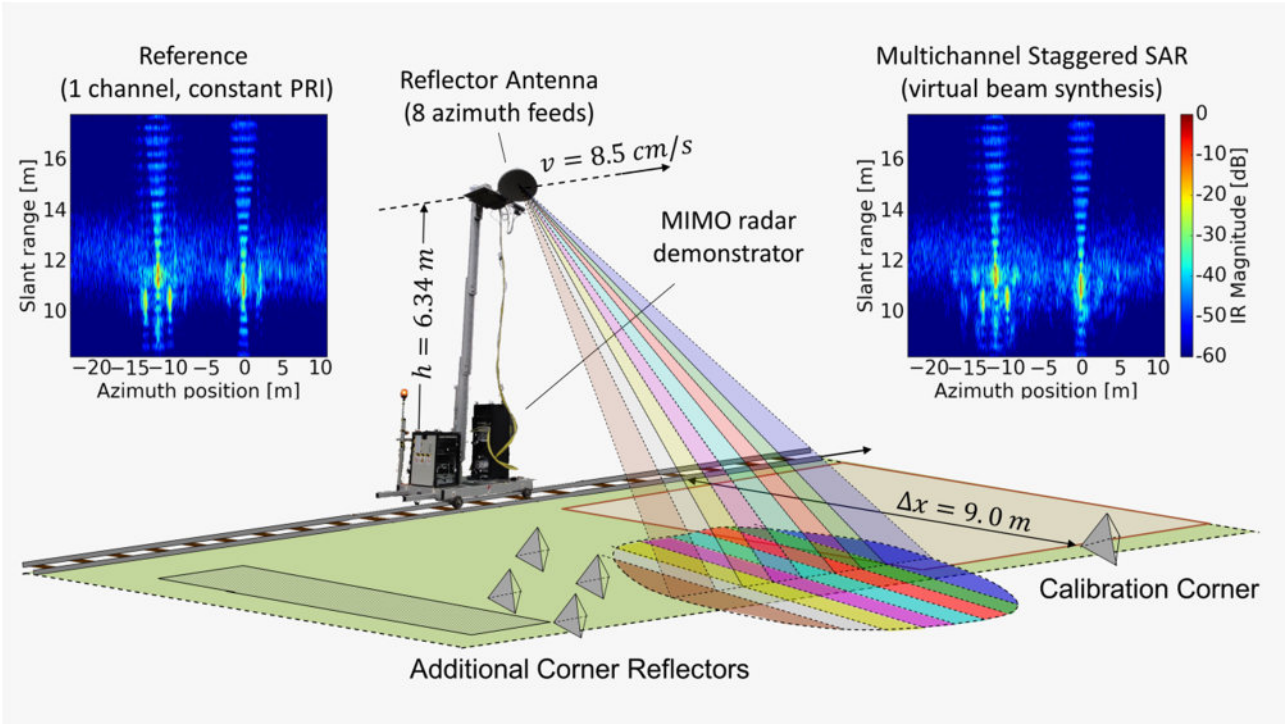

Figure 2.2-8 Demonstration of multichannel staggered SAR with the Institute's ground-based MIMO radar demonstrator. A reflector antenna with 8 azimuth channels was mounted on a 6 m long boom and slowly carried by a railcar along straight tracks. The upper left image shows a single-channel SAR image obtained using a highly uniform PRF in combination with a single broad reference beam, while the upper right image shows the multichannel staggered SAR reconstruction using the new VBS technique. The results are nearly identical, and a detailed quantitative analysis in the vicinity of the isolated calibration corner reflector indicated that the magnitude-squared difference between the reference and the reconstructed image is below -30 dB [PhD-3].

developments may be further supported by new fractionated SAR concepts like MirrorSAR (see also Section 2.2.2), where the receiver satellites are radically simplified by reducing their functionality to a mere space transponder [IC-11]. Since the receivers need neither a full radar receiver nor on-board data storage and downlink, they can be deployed on very small platforms such as those currently being developed by several manufacturers in the NewSpace context. MirrorSAR may be combined with multiple transmitters that radiate different waveforms to separate their radar echoes. This not only enables a further increase in SAR imaging performance, but also paves the way for new applications like MIMO-SAR tomography [RC-154]. The transmitted waveforms of such a MIMO SAR may even be adjusted in real time based on the information collected by the recorded radar echoes. Such an adaptive radar system can then be regarded as a first step towards a cognitive SAR, which directs its available resources to those parameters and areas that provide maximum information gain analogous to the selective attention mechanisms of the human visual system with its saccadic eye movements. These examples show the rich and interesting future that awaits the development of new SAR systems.

2.2.2 Bistatic and Multistatic SAR

Bistatic and multistatic SAR systems offer a number of unique opportunities that will increase the capability, reliability and flexibility of future SAR missions when compared to traditional monostatic sensors. The separation of the transmitter and receiver satellites enables unique observation geometries, where the ground can be imaged from multiple angles at the same time. This information gain increases with the number of receivers, and the associated satellite formations can, moreover, be reconfigured and fine-tuned to dynamically optimize the system sensitivity both radiometrically and interferometrically to the intended measurement. These features make bistatic and multistatic SAR systems unique for a number of Earth observation applications. Examples are topographic mapping, enhanced scene classification, observation of ice mass and volume changes, vegetation structure characterization and 3-D deformation monitoring. The Institute looks back to almost 20 years of experience in the design and analysis of bistatic SAR systems and missions. Over these years, an unparalleled know-how has been built up, accompanied by unique bistatic experiments in various air-to-air, space-to-air and space-to-space configurations, as summarized on the left of Figure 2.2-9. In the last decade, the focus was on the design, implementation and operation of TanDEM-X, followed by the ongoing development of Tandem-L (see Sections 2.1.2 and 2.1.3). Additional highlights were the preparation and submission of the Earth Explorer mission proposals PICOSAR, SESAME and IRIS together with the performance and algorithmic analyses for ESA's SAOCOM-CS mission (see Chapter 2.1). The right part of Figure 2.2-9 illustrates ongoing bistatic activities, including the development of the airborne system DuoLIM in preparation for Tandem-L (see Section 2.3.5) and the elaboration of various proposals for future bistatic and multistatic SAR missions.
The following paragraphs summarize the analyses, experiments and research conducted at the Institute in the frame of the aforementioned activities. The results demonstrate the great potential of bistatic SAR for future Earth observation missions.

TanDEM-X, Tandem-L and Earth Explorer Proposals

In addition to its operational stripmap mode, the TanDEM-X formation has also been operated over the past years in experimental bistatic high-resolution (spotlight, both sliding and staring) and wide-swath (ScanSAR and TOPS) modes. Direct applications of these modes include the measurement of high-resolution topographic maps or fast motions (i.e., within the several seconds of the synthetic aperture). The ability to operate bistatically in the basic imaging modes of the instrument has been used in combination with the BiDirectional (BiDi) mode [J-166] to acquire a number of experimental data takes. In particular, this mode allows the simulation of (stereoscopic) spaceborne geometries with moderate bistatic angles, providing sensitivity to roughness, which can be further translated into physical parameters of the scene. Figure 2.2-10 shows an example of a bistatic BiDi acquisition over Tromsø, Norway, with the results from the aft and fore beams shown on the bottom in the left and right columns, respectively. The image pairs are

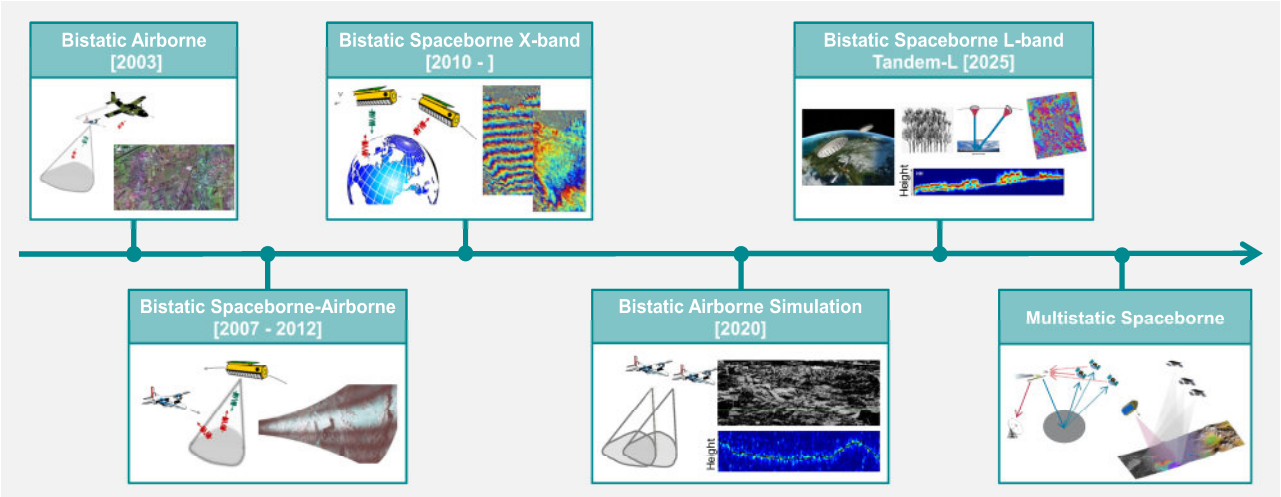

Figure 2.2-9 Schematic illustration of the evolution from bistatic experiments to current and future bistatic and multistatic SAR missions proposed by the Institute

zooms close to the coast, where differences in the reflectivity (top), coherence (mid), and interferometric phase (bottom) of the ocean surface become apparent – even at this moderate observation angle difference of 4.4° – providing sensitivity to the estimation of the wind speed in the scene.

A key feature of many spaceborne bistatic and multistatic SAR systems is the availability of one or several single-pass interferometric channels, providing the geometric flexibility for tuning the baseline to the observation needs. In particular, bistatic SAR offers the possibility of adjusting the along-track baseline to the expected motion in the scene – i.e., shorter baselines support the estimation of faster motions and vice versa. Examples of the use of TanDEM-X in maritime security and ship monitoring were already shown at early stages of the TanDEM-X mission [J-42]. Later, experimental bistatic BiDi TanDEM-X data takes have been used to estimate the 2-D velocity components induced by ocean currents, as shown in the bottom interferograms of Figure 2.2-10, and further discussed in Section 2.2.4. The PICOSAR mission proposal (cf. Section 2.1.6) elaborated at the Institute relies on the use of bistatic (i.e., cross-platform) along-track interferometry for the global measurement of ocean surface velocities.

Analogously, increasing the across-track baselines yields the potential of deriving very accurate topographic maps. Note that larger baselines provide enhanced interferometric sensitivity, which results in less noisy measurements despite the smaller averaging factor,. The ability to alter the bistatic formation to the specific observation needs has been extensively used in bistatic mission studies over the past years. In particular, the proposals prepared for the Earth Explorer 9 and 10 calls – SESAME and IRIS – showed the possibility of achieving global topographic maps with decimetric accuracy and metric posting by using large across-track interferometric baselines (cf. Sections 2.1.9 and 2.1.10).

However, the advantages of bistatic SAR interferometry are not limited to single-pass acquisitions. In particular, bistatic SAR systems are perfectly suited to deliver 3-D deformation measurements in repeat-pass scenarios [RC-51]. The availability of very large along-track baselines – in the order of hundreds of kilometers – provides enough angular diversity in the line of sight for a stable inversion of all three deformation components, while allowing for a reduction of the tropospheric noise due to the spatial correlation of the propagation signature, as illustrated in the left image of Figure 2.2-11. The right plot in Figure 2.2-11 shows that an effective squint angle of 10 degrees (i.e., along-track baseline of about 250 km) allows for the retrieval of East-West and North-South components of the deformation with similar accuracy. This concept and the associated performance analyses were developed at the Institute during the preparation of the SESAME Earth Explorer proposal. The concept has then been introduced to SAOCOM-CS for the definition of a deformation phase, and is also included as a dedicated feature of the SESAME mission proposal (cf. Sections 2.1.9 and 2.1.11).

Following the line of utilizing flexible observation geometries, bistatic and multistatic SAR appear to be predestined for imaging semi-transparent media such as forests, agriculture, dry soil or ice by means of SAR tomography (cf. Section 2.2.7).

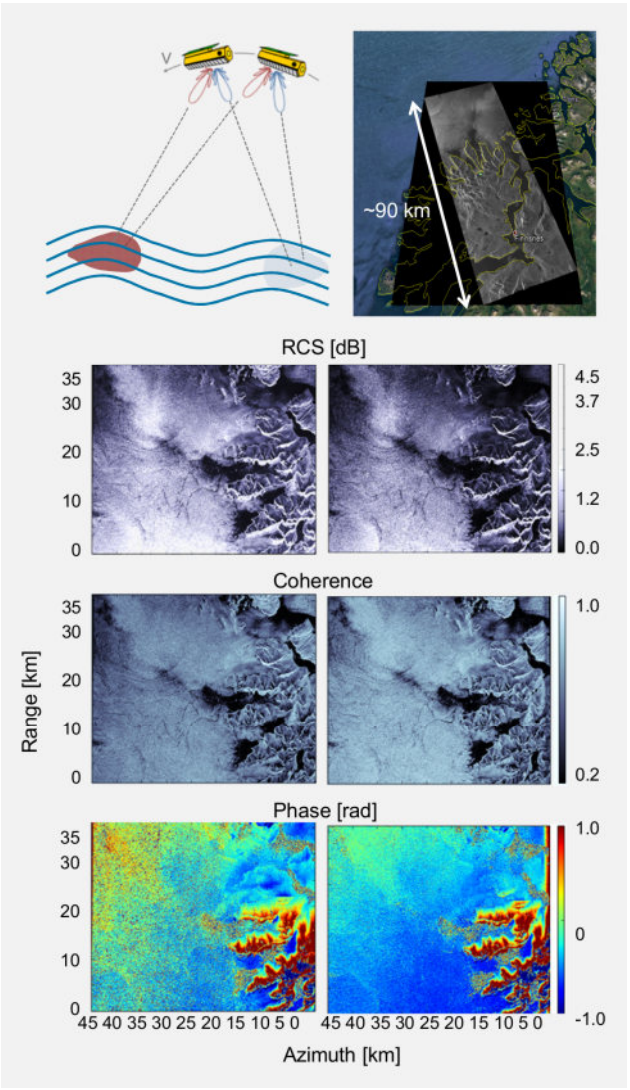

Figure 2.2-10 Top: schematic view of the bistatic BiDi acquisition mode and a geocoded bistatic BiDi SAR amplitude image over Tromsø, Norway. Bottom: zooms of the aft (left) and fore (right) beams close to the coast, in which the ocean presents distinct radiometric (top) and coherence (mid) signatures, even at the moderate squint angle difference of 4.4°. Along-track interferometric pairs for the aft and fore channels (bottom) can be used to estimate 2-D ocean surface velocity maps (see also Sections 2.1.1 and 2.2.4).

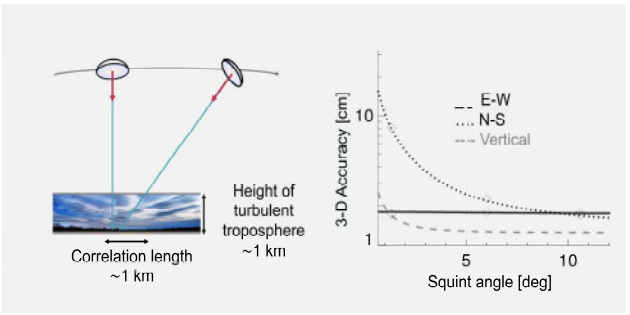

Figure 2.2-11 Example of the use of bistatic SAR to estimate all three components of the deformation vector with similar accuracy. The left image shows the angular diversity provided by bistatic SAR configurations with large along-track baselines, but still correlated atmospheric disturbances. The plot shows the predicted accuracy in the retrieval of the three components of the deformation vector (i.e., vertical, North-South, East-West) versus the effective squint angle provided by the bistatic formation.

Coherence-based SAR tomography uses single-pass complex interferograms – typically acquired with a bistatic formation – as inputs for the construction of a tomographic aperture. The across-track baseline of the bistatic pair is varied within subsequent passes to cover the extent of the tomographic aperture with appropriate sampling, as illustrated in Figure 2.2-12. The figure also shows one of the first demonstrations of coherence-based tomography from TanDEM-X data acquired over the Swedish boreal forest during the science phase of the mission.

As discussed in Section 2.1.3, coherence-based tomography is the basic technique to measure forest structure in Tandem-L [J-97] and one of the main reasons why Tandem-L is implemented as a bistatic system. Many of the results obtained during the development of the Tandem-L observation concept, in particular the baseline formation strategy, were also used by the Institute to support the definition of ESA's SAOCOM-CS mission (cf. Section 2.1.11).

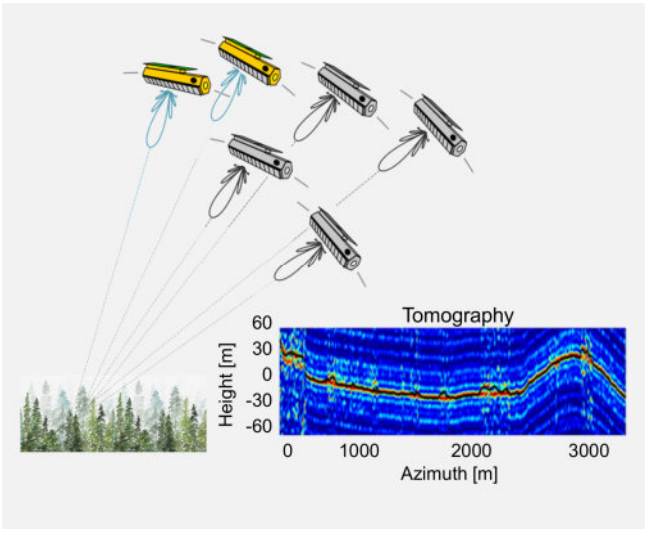

Figure 2.2-12 The flexibility in the variation of the baseline provided by bistatic SAR enables the use of coherence-based tomographic techniques. The figure illustrates the effective spatial sampling positions of the tomographic aperture (left) and one of the first coherence-based tomograms obtained from TanDEM-X data acquired over the Swedish boreal forest (bottom right).

Fractionated and NewSpace SAR Concepts

Multistatic SAR missions with three or more receiver satellites will open the door to a new dimension of radar remote sensing. One example is multi-baseline cross-track interferometry for the generation of high-resolution digital elevation models with decimeter-level height accuracy. A second example is single-pass tomography for the three-dimensional imaging of volume scatterers that are semitransparent to microwaves. Further examples are multiangular backscatter measurements for speckle reduction and improved scene characterization, super resolution in range and azimuth, 3-D velocity measurements of moving objects, or even 4-D monitoring of internal structure changes in semitransparent scatterers such as vegetation, ice and dry soil.

Despite these manifold opportunities, only one bistatic SAR system has been deployed in space. The main reasons for this imbalance between opportunities and investment are the complexities and costs associated with bi- and multistatic SAR systems. Important cost drivers are the duplication of hardware for the reception, storage and downlink of radar data, the increased launch mass and volume for the deployment of multiple satellites, the additional hardware for accurate phase synchronization, and the need for a high downlink capacity to transfer the radar data from multiple satellites to the ground. To address these challenges, the Institute has developed the innovative SAR system concept MirrorSAR, which has the potential to significantly reduce the complexity and costs of future bi- and multistatic SAR missions [IC-11].

MirrorSAR is a fractionated radar concept in which scene illumination and spatial sampling of the scattered radar wavefront are performed by separate platforms. At the same time, MirrorSAR aims to radically simplify the receiver satellites. This is achieved by reducing their main functionality to a transponder-like routing of the radar echoes from the passive receivers to the active transmitter(s), as illustrated by the red arrows in Figure 2.2-13. In the transmitter, the forwarded radar signals are coherently demodulated, which makes a bidirectional phase synchronization link unnecessary, and it becomes even possible to combine the radar echoes from multiple satellites for data compression. Since the receiving

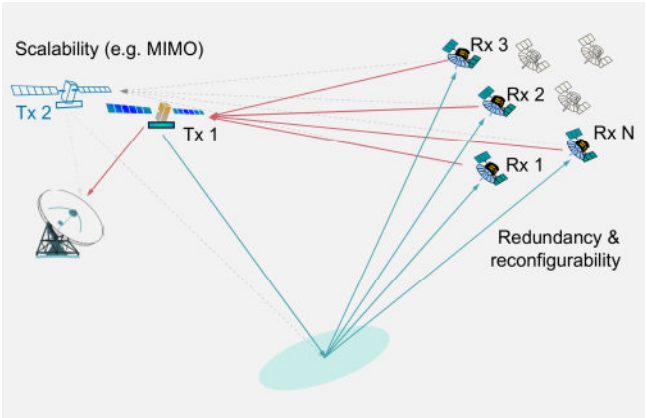

Figure 2.2-13 Illustration of the MirrorSAR concept. A wide scene is illuminated by one or multiple transmitter (Tx) satellites. The scattered waves are spatially sampled by multiple receivers (Rx) that route their received radar echoes to the transmitter. The transmitter coherently demodulates and combines the forwarded signals before the relevant information is transferred to the ground. The forwarding of the Rx signal by a phase-preserving modulation avoids the need for a dedicated synchronization link.

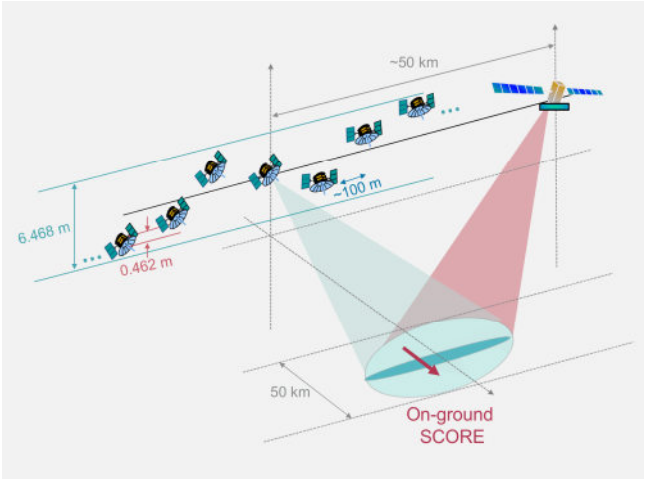

Figure 2.2-14 Illumination geometry for the floating swarm configuration with receive-only satellites

satellites act as mere microwave mirrors, they require neither fully equipped radar receivers nor expensive data storage and downlink systems. This radical simplification will in turn reduce their mass, power, accommodation and control demands, supporting the use of small low-cost platforms, as already proposed for the multistatic extension of the HRWS mission or the Earth Explorer proposal IRIS (cf. Sections 2.1.4 and 2.1.9).

The applications of multistatic SAR systems discussed so far are based on the combination of multiple SAR images – each acquired by a different platform. A further opportunity arises from combining the multistatic radar echoes on a raw data level, as it enables the suppression of range and azimuth ambiguities, and thus the use of a smaller antenna for each receiver. First steps towards such a distributed aperture concept have already been realized, both on an experimental level [RC-151], [RC-152] and on a system design level [RC-160], [RC-161].

Among them, the Floating Swarm is the first concept to describe and combine the positions of the swarm satellites in the vertical or radial dimension – for example, the formation of a common swarm elevation antenna – as illustrated in the X-band formation example shown in Figure 2.2-14. The receiver swarm follows the illuminating satellite by approximately 50 km in along track at an orbit height of 514 km. A 50 km ground swath is acquired at 45° incidence angle with 1.1 m geometric resolution. The along-track positioning of the receiver satellites requires a relative separation in the order of 100 m, and a relative positioning accuracy in radial direction in the decimeter range. From the 20 real receiver satellites, an equivalent antenna with an elevation height of ~6.5 m and a spacing of 0.462 m is synthesized by processing on ground.

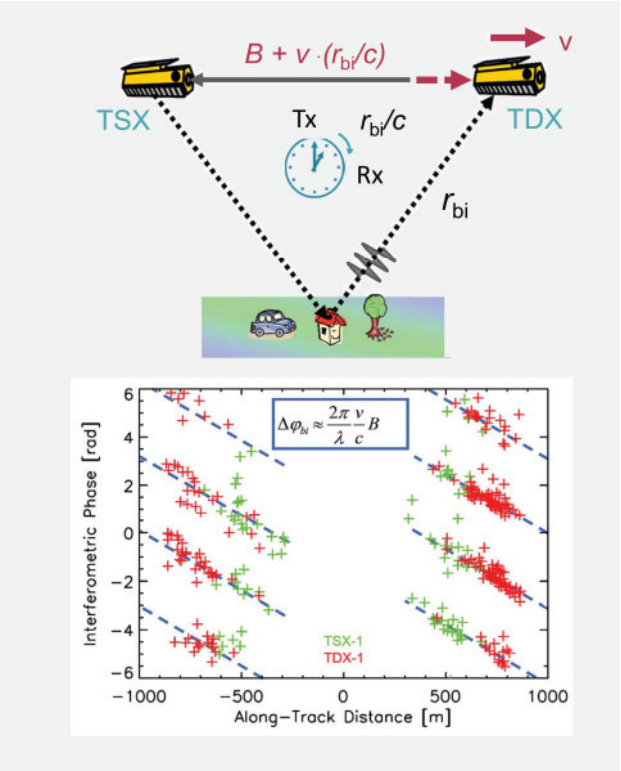

Figure 2.2-15 Top: bistatic SAR data acquisition as seen from an Earth-centered, Earth-fixed (ECEF) reference frame, where the scene is stationary and the satellites are in motion. Bottom: TanDEM-X interferometric phase offsets as a function of the along-track displacement. The relativistic prediction (dashed blue lines) agrees well with the measurements (crosses).

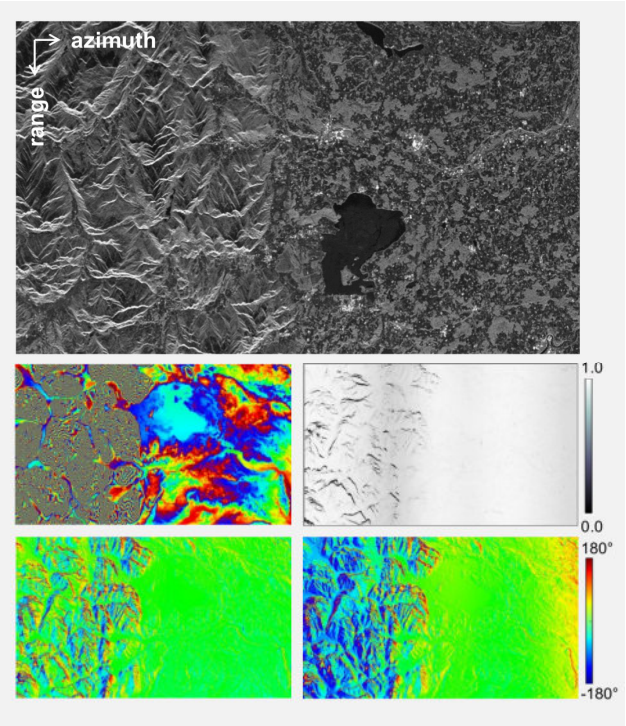

Figure 2.2-16 Example of a SAOCOM-CS simulation showing the feasibility of clock recovery using AutoSync. The input ALOS-2 reflectivity image over Wallerfing, Germany (top), the decorrelation introduced by clock errors (mid right), the interferometric fringes after ellipsoid removal (mid left), and the interferometric phase after DEM fringes removal with (bottom left) and without (bottom right) AutoSync. The blue and yellow colors at the edges of the lower right interferogram are caused by uncompensated clock errors.

Bistatic Synchronization

The identification of relativistic effects in the TanDEM-X interferometric observations contributed to the accurate calibration of the system and the achievement of the mission objectives in terms of the absolute height error [J-125], [RC-586]. In the beginning, these effects led to unexpected and latitude-dependent height offsets up to several tens of meters and were later explained by the relativity of simultaneity; as bistatic SAR processing and synchronization are performed in different reference frames, they are no longer associated with the same time. Figure 2.2-15 (top) illustrates the radar data acquisition and exchange of synchronization pulses in an Earth-centered, Earth-fixed (ECEF) reference frame, as used for SAR processing. Since the satellites move at high speeds in this frame, the signal from the synchronization link has to travel a longer path, as would have been the case in a reference frame moving with the satellites. This difference is indicated by the dashed red arrow. The plot on the bottom shows the good agreement between the relativistic prediction of the interferometric phase and the observed phase offsets, which were derived from the TanDEM-X height offsets.

Another processing aspect that has been extensively studied in the frame of current mission proposals is data-based synchronization, referred to as AutoSync [PhD-28]. In particular, AutoSync was the key element in the performance investigation conducted for ESA in the frame of the SAOCOM-CS mission

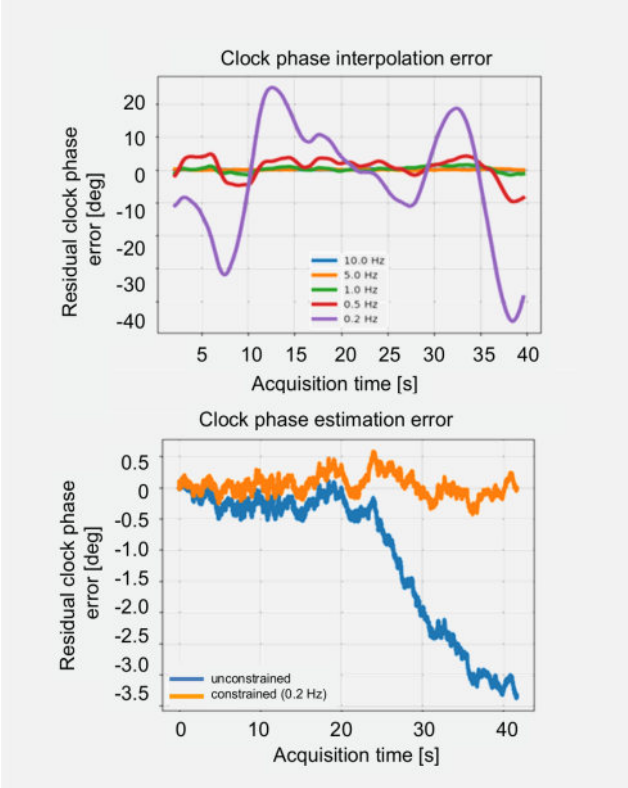

Figure 2.2-17 Example showing the feasibility of using AutoSync for effectively reducing the rate of exchange of synchronization pulses in Tandem-L. Top: realizations of clock phase interpolation errors for different synchronization frequencies. Bottom: realizations of residual clock phase estimates after AutoSync for constrained (orange) and unconstrained (blue) integration.

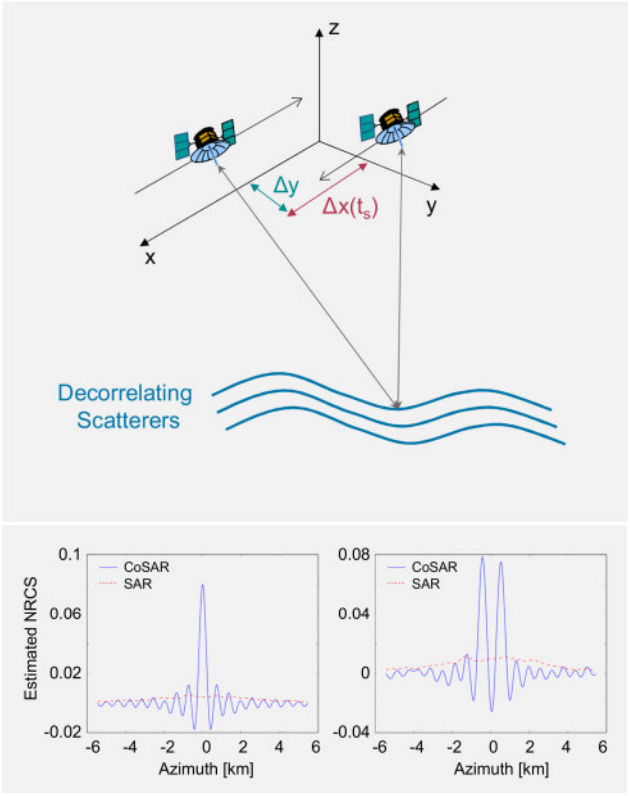

Figure 2.2-18 Summary of CoSAR observation geometry and imaging characteristics. Top: schematic view of the CoSAR imaging principle. Bottom: CoSAR simulation for one (left) and two (right) rapidly decorrelating targets. The red dashed curves compare the defocusing of a conventional SAR [J-59].

(Section 2.1.11), and it was central to the calibration concept suggested by the Institute [RC-205]. The feasibility of on-ground data synchronization in the absence of a dedicated synchronization link was shown. This assessment was further demonstrated using the End-to-End (E2E) tool developed at the Institute for ESA (see Section 2.2.5), which contains a clock recovery module based on AutoSync [RC-427].

Figure 2.2-16 gives an example of a SAOCOM-CS simulation based on ALOS-2 data over Wallerfing, Germany. The figure shows the input reflectivity (top), the coherence loss introduced by the clock (mid right), the resulting interferogram after ellipsoid removal (mid left), and the interferograms after DEM fringes removal with (bottom left) and without (bottom right) clock synchronization using AutoSync.

The use of AutoSync has also been studied in the context of the Tandem-L mission as a possible means to reduce the required exchange rate of synchronization pulses. Simulations conducted using Sentinel-1 data show that the exchange rate of the synchronization pulses can be lowered by about one order of magnitude (e.g., from 2 Hz to 0.2 Hz) by simply constraining the AutoSync integration step to the data available from the synchronization link. Figure 2.2-17 shows this by a realization of the expected clock phase interpolation error for different values of the synchronization pulse exchange rate (top) and two realizations of the AutoSync estimation error (bottom) using a constrained (orange) and unconstrained (blue) integration.

Correlating SAR (CoSAR)

Correlating SAR (CoSAR) is a novel radar imaging concept for observing the statistical properties of rapidly decorrelating surfaces such as oceans at hectametric scales [J-59], [RC-203], [RC-204], [RC-505]. Though not necessarily a bistatic concept, CoSAR shares many similarities with bistatic radars in terms of system and imaging characteristics. As illustrated on the top of Figure 2.2-18, a CoSAR system consists of two radars that move relative to each other in the along-track (i.e., azimuth or cross-range) direction. This unconventional imaging geometry enables the measurement of the spatial autocorrelation function of the scattered signals by evaluating the quasi-simultaneously received radar echoes as a function of the along-track distance. By virtue of the Van Cittert–Zernike theorem, the autocorrelation function can then be further processed to obtain several unique parameters of rapidly decorrelating scenes, including the normalized radar cross section, Doppler velocities and surface topography. As a possible implementation in space, a CoSAR mission concept consisting of two geosynchronous radar satellites flying at the opposite sides of a quasi-circular trajectory [RC-396] has been developed at the Institute. The plots on the bottom of Figure 2.2-18 show simulation results for one (left) and two (right) targets that demonstrate CoSAR's ability to rapidly image decorrelating targets at a resolution of a few hundred meters.

2.2.3 Spaceborne SAR Processing

Ultra-High-Resolution Staring-Spotlight Imaging

The new capabilities of existing and future SAR sensors have motivated the investigation of new operating modes and processing concepts capable of enhancing the information content of SAR data. A clear example is provided by the ultra-high-resolution staring-spotlight (ST) mode of the TerraSAR-X satellite, which was first investigated based on a set of experiments performed at the Institute [J-129], [J-135]. The staring spotlight mode steers the antenna beam electronically within ±2.2°, which goes far beyond the ±0.75° span of the standard high-resolution sliding spotlight (HS) mode. Thanks to this larger angular span, an azimuth resolution of 16 cm without spectral weighting can be achieved, in comparison to the 1 m of the HS mode. However, using the nominal TerraSAR-X processing chain resulted in a severely degraded impulse response, which was mainly caused by the following effects: the hyperbolic approximation of the range cell migration during the SAR focusing operation, the motion of the satellite during the transmission/reception of the chirp signal (intra-pulse effect), the delay introduced by the troposphere, and the defocusing due to topography mismatch. Thanks to the experiments performed with TerraSAR-X staring spotlight data, it was possible to investigate the effects and develop new and efficient solutions to compensate for them, as reported in [J-135], [J-106], [RC-615], [RC-419]. Figure 2.2-19 presents the block diagram of the proposed processing chain for high-resolution spotlight data, with the new processing steps highlighted in red. The Sub-Aperture Topography- and Aperture-dependent algorithm (SATA) and the Post-processing Algorithm for Squint and Topography Accommodation (PASTA) are efficient Fourier-based algorithms to accommodate the space-variant topography variations within the scene. These two approaches are based on the Institute's heritage in the development of advanced motion compensation algorithms for airborne SAR, whose applicability was extended to the spaceborne case [J-106], [RC-419], [RC-613]. Figure 2.2-20 shows the contour plot of the interpolated impulse response function of a corner reflector before and after applying the suggested corrections, where the improvement is evident. Figure 2.2-21 shows the portion of an ST image over DLR's site in Oberpfaffenhofen, including a comparison with the HS mode for the same multilooked resolution. After the successful consolidation of the new processing algorithm, the staring spotlight mode was integrated operationally as part of the TerraSAR-X ground segment, an activity performed together with the Remote Sensing Technology Institute (IMF) and the German Remote Sensing Data Center (DFD) [J-129], [J-58].

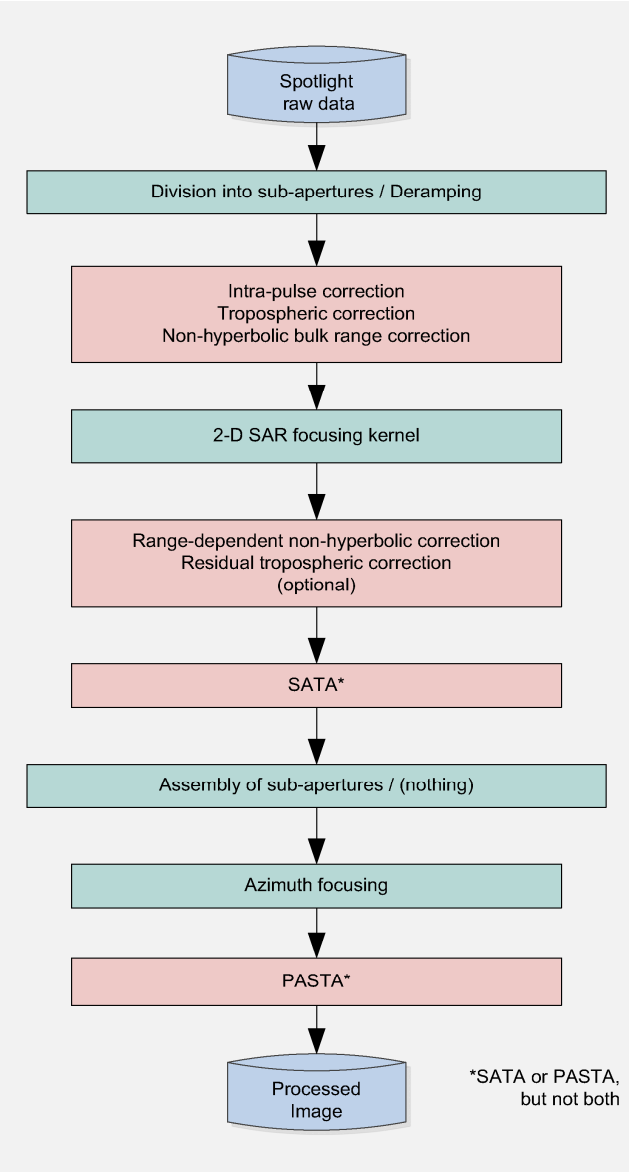

Figure 2.2-19 Proposed processing chain for ultra-high-resolution spotlight data. SATA stands for Sub-Aperture Topography- and aperture-dependent Algorithm, and PASTA for post-processing algorithm for squint and topography accommodation. The new processing steps are highlighted in red.

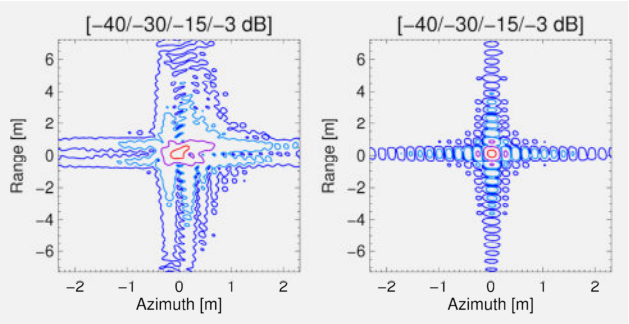

Figure 2.2-20 Contour plots of the interpolated impulse response function of a corner reflector after processing with the conventional TerraSAR-X processing chain (left) and with the proposed processing chain for the staring spotlight mode (right). The nominal resolution in the range and azimuth dimensions is only achieved in the second case. The contour levels are indicated above the images.

Wrapped Staring Spotlight Mode

Wrapped staring spotlight [J-62], [P-2] is a new imaging concept to increase the azimuth steering capability of phased array SAR antennas in order to improve the azimuth and/or radiometric resolution. For this, the steering is extended to directions with very low signal contribution. It was investigated whether

steering directions with small antenna gain could improve the SAR image quality. Point and extended targets in experimental TerraSAR-X acquisitions were evaluated up to ±4.4° steering – i.e., with gains up to 45 dB below the grating lobes.

One of the innovations developed in the frame of these investigations is the wrapped commanding of steering angles. Figure 2.2-22 shows the antenna lobes pointing into the desired steering directions in green, and the undesired grating lobes in red. The available on-board look-up table for steering angles can be directly used up to ±2.2°. Beyond that, larger steering angles are obtained without the need for additional on-board stored azimuth patterns by re-accessing the available angles and performing the extraction of the desired steering directions later during the SAR focusing operation.

Figure 2.2-23 shows corner reflector measurements obtained with the wrapped staring spotlight mode. The azimuth resolution steadily improves to 0.14 m by increasing the processed bandwidths up to 68 kHz. For comparison, the staring spotlight mode of TerraSAR-X exploits only 38 kHz. Two statistical approaches were developed to improve the radiometric performance [J-62]: the space invariant Look-Normalized Pattern Compensation (LNPC) and the space variant Ω-weighting. Figure 2.2-24 shows highly zoomed TerraSAR-X images over Easter Island in staring and wrapped mode. In the wrapped mode, the contrast for man-made targets is improved by up to 20%. For extended targets, the radiometric resolution is improved from 2.3 dB to 2.0 dB, and the equivalent number of looks (ENL) is improved from 2 looks to 4 looks [J-62].

Figure 2.2-21 TerraSAR-X spotlight images acquired over Oberpfaffenhofen, Germany. The images are excerpts from larger images and show an area of 1000 m x 500 m. The upper image was acquired in nominal high-resolution sliding spotlight (HS) mode, while the lower image was captured in the new ultra-high-resolution staring spotlight (ST) mode. Both images were multilooked to the same resolution of 1 m × 1 m. The improvement in speckle reduction due to the larger multilook factor is evident for the new ST mode.

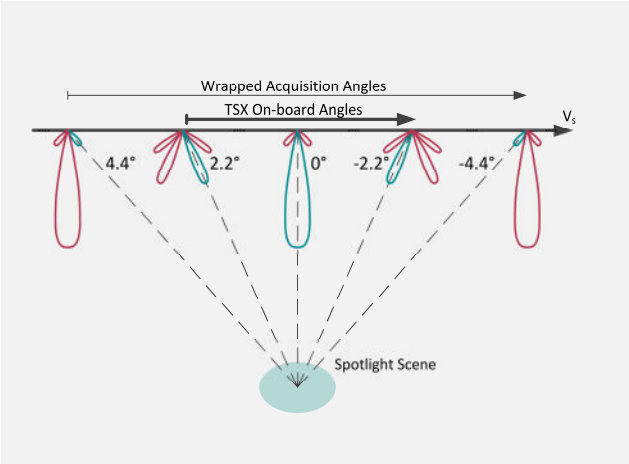

Figure 2.2-22 Desired steering lobes (green) and undesired grating lobes (red). The steering angles stored in the on-board look-up table of TerraSAR-X cover a range up to ±2.2°. Steering angles beyond this range are obtained by re-accessing the available steering angles.

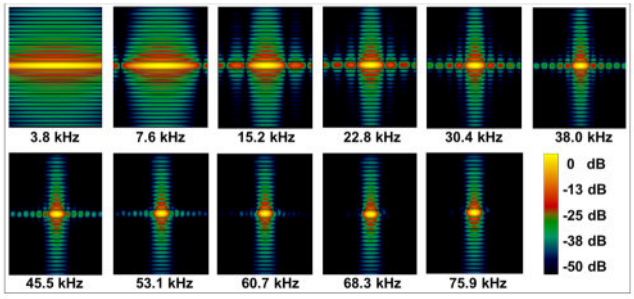

Figure 2.2-23 Corner reflector measurements in a TerraSAR-X wrapped staring spotlight image for a systematic increase of the processed Doppler bandwidth. Note the improvements in azimuth resolution and sidelobe suppression (azimuth is in the horizontal direction).

Bistatic SAR Imaging Kernels

To support bistatic mission concepts with large along-track separations (over 50 km) between transmitter and receiver, it was also necessary to develop new processing algorithms. In the frame of the SESAME and SAOCOM-CS mission analysis studies (see Sections 2.1.9 and 2.1.11, respectively) several efficient Fourier-based bistatic processing algorithms have been investigated and proposed, which can handle extreme geometries with large bistatic squint angles (> 20°). Figure 2.2-25 shows the block diagrams of the proposed focusing algorithms based on a numerical omega-k kernel [RC-181]. All phase functions and interpolations are performed based on numerical computations, i.e., no analytical formulas are used to perform the range-variant processing. The solution on the right in Figure 2.2-25, where the Stolt mapping is based on the singular value decomposition (SVD), is more accurate and can also handle spaceborne forward-looking geometries. The derivation of these algorithms was supported by a tool developed at the Institute capable of evaluating the performance of Fourier-based focusing kernels without having to explicitly implement them [J-136], [RC-418]. The proposed methodology is convenient for situations such as very high-resolution spaceborne SAR or bistatic imaging, where the assumption of a hyperbolic range history does not hold anymore, and, hence, a compact analytic expression of the point target spectrum is not available. Thanks to its computation effort, which is several orders of magnitude less than that of a time-domain simulation followed by the true processing, it can be further exploited for various mission

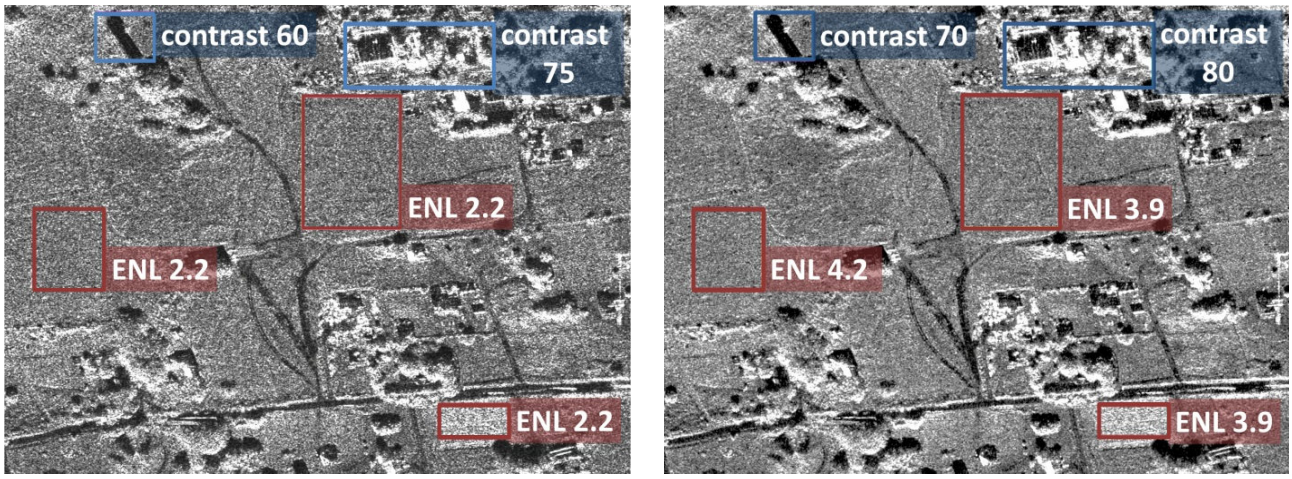

Figure 2.2-24 TerraSAR-X images acquired in staring (left) and wrapped (right) spotlight mode. The statistical evaluations for homogeneous areas (red) show a duplication in terms of effective number of looks (ENL) and an increase in image contrast of 15% for regions with man-made targets (blue).

scenarios to evaluate the most suitable processing kernel in terms of efficiency and accuracy.

Reconstruction of Coherent Pairs

The TanDEM-X formation is a cooperative bistatic SAR system with a synchronization link between the transmitter and the receiver. The information extracted from the exchanged pulses is used for the phase synchronization between the local oscillators in both satellites, as well as for the computation of the bistatic replica. This synchronization link creates periodic gaps in the SAR raw data that degrade the image quality after the SAR focusing operation. In order to overcome this issue, and due to the fact that a pair of coherent data is available from the interferometric acquisition with two satellites, a method that exploits the common information part in one image to reconstruct the other image and vice versa has been developed [J-101], [RC-517], [RC-609], [RC-610]. The proposed approach consists of three main steps: the first one accounts for the differences in the observation geometry between master and slave acquisitions – that is, it interpolates the available master data to the slave geometry and limits the interpolated result to the common range bandwidth. The second step is a calibration to deal with differences between the systems, e.g., antenna pattern compensation. The third and last step is an autofocus used to account for all possible inaccuracies introduced in the previous two steps, guaranteeing both amplitude and phase continuity. The proposed method outperforms spectral estimators operating on a single SAR image, which can only properly recover data from point-like targets. Figure 2.2-27 shows the azimuth impulse response of a target before (black) and after (red) reconstruction. A considerable sidelobe reduction can be observed with the proposed method, i.e., the missing data have been properly recovered. Figure 2.2-26 shows an example of real TanDEM-X bistatic data acquired over a vegetated area in Indonesia, which is rather homogenous. The data correspond to a dual polarization acquisition with a PRF per channel of approximately 2500 Hz and a processed azimuth bandwidth of roughly 1100 Hz. The SAR acquisition was periodically interrupted due to the synchronization link with

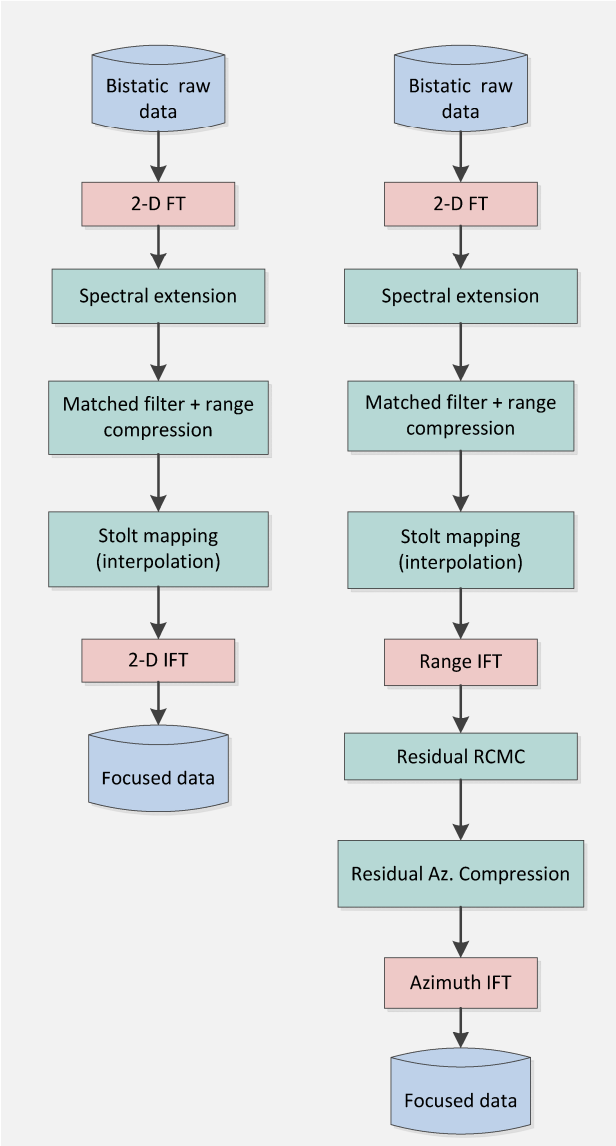

Figure 2.2-25 Block diagrams of the proposed focusing algorithms for large along-track bistatic configurations based on a numerical omega-k kernel. FT/IFT stands for Fourier transform/inverse Fourier transform, and RCMC for range cell migration correction.

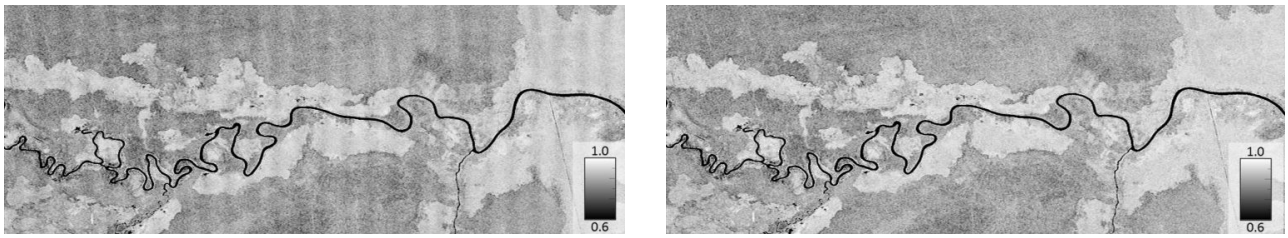

Figure 2.2-26 Example of TanDEM-X bistatic coherence over a vegetated area. The image on the left shows the loss of coherence in the nominal interferogram, where periodically missing data due to bistatic synchronization lead to an undesired modulation of the coherence along azimuth (horizontal direction in the image). The image on the right shows the coherence obtained after applying the newly developed reconstruction method.

a frequency of 5 Hz, and 5 pulses were exchanged during each synchronization event. The degradation caused by the periodic data loss can be appreciated in the interferometric coherence shown on the left of Figure 2.2-26, where a modulation along the azimuth direction is clearly seen due to the small dynamic range. The figure on the right shows the coherence after applying the developed reconstruction method. In this case, the modulation is no longer present, demonstrating the successful reconstruction over distributed scatters.

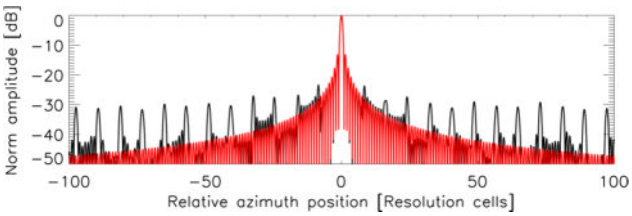

Figure 2.2-27 Interpolation of bistatic SAR data with gaps due to interleaved periodic synchronization pulses: the azimuth impulse response of a target obtained from the gapped data (black) and obtained from the reconstructed data (red).

2.2.4 Spaceborne SAR Interferometry

During the last six years, a large number of interferometric experiments have been performed and evaluated with both the TerraSAR-X satellite and the TanDEM-X formation. The following subsections present the most relevant examples.

TOPS Interferometry

In the frame of ESA studies, and in preparation for the Sentinel-1 mission (see Section 2.1.7), the TerraSAR-X satellite was commanded to operate in the experimental TOPS mode in order to acquire data in a repeat-pass configuration to perform a set of interferometric investigations. Due to the particularities of the TOPS mode, interferometric processing is not straightforward, and the investigations resulted in the proposal of a new interferometric processing chain for TOPS (and, in general, for burst modes), which is depicted in Figure 2.2-28 [J-190], [J-75]. A very good azimuth coregistration performance for TerraSAR-X and Sentinel-1 data – in the order of 1 cm (about 0.001 azimuth samples) – is required to avoid phase discontinuities between bursts after the mosaicking operation. Such performance can be achieved by exploiting the burst overlap areas – a technique named Enhanced Spectral Diversity (ESD) [J-190] – which is based on the spectral diversity technique developed at the Institute in the late 90s. The ESD approach, combined with a geometric-based coregistration, ensures the retrieval of accurate TOPS interferograms and is currently used as baseline by the SAR community to process Sentinel-1 interferometric data for land applications, such as earthquakes, volcanoes, landslides, time series and glaciers. Figure 2.1-49 in Section 2.1.7 shows an example of a Sentinel-1 TOPS interferogram over Italy obtained with the proposed processing chain. Also in the frame of TOPS interferometry, a new technique has been developed to improve the coregistration performance when working with image stacks and to mitigate the effects of temporal decorrelation when exploiting ESD [J-40], [RC-78], [RC-226].

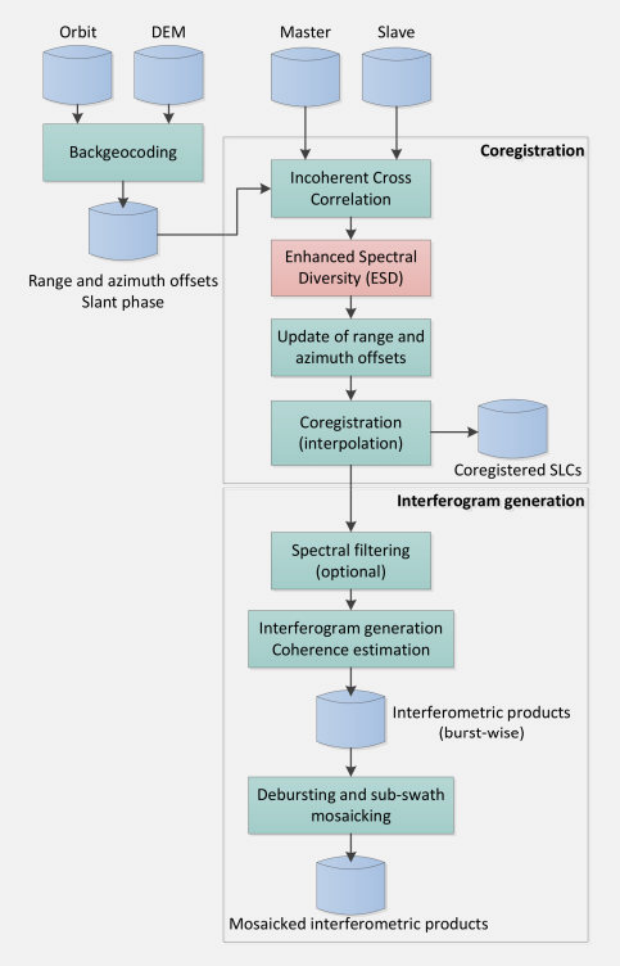

Figure 2.2-28 Proposed interferometric processing chain for burst modes, i.e., TOPS and ScanSAR. The incoherent cross-correlation and Enhanced Spectral Diversity (ESD) are used to estimate a constant offset in range and azimuth for the complete scene. The computation of the geometric offsets based on the orbits and an external DEM ensures a very good relative coregistration accuracy, while ESD is used to achieve the stringent centimetric-level coregistration requirement for burst modes.

Experimental TerraSAR-X 2-Look Burst-Mode Interferometry

The TOPS and ScanSAR modes allow to retrieve a very good estimate of the azimuthal motion in the scene by exploiting the overlap areas between bursts, as already explained in the previous section. However, in the case of conventional 1-look burst modes like Sentinel-1, the extent of the overlap areas is less than 5% of the total azimuth coverage, hence becoming insufficient for most non-stationary scenarios. The solution to this problem is the exploitation of 2-look wide-swath burst modes. With this acquisition strategy, each point on the ground is observed under two different squint angles (or Doppler centroids), thus making it possible to achieve continuous coverage for the retrieval of the azimuthal motion by exploiting this angular diversity. Several experiments have been conducted with the TerraSAR-X satellite in the 2-look TOPS and ScanSAR modes over non-stationary scenes to demonstrate the applicability of such modes [RC-302], [RC-182], [IC-35], [IC-68]. Figure 2.2-30 shows an example of the 2-look TOPS mode over the Petermann glacier in Greenland with two repeat-pass acquisitions separated by 11 days. Figure 2.2-30 (middle) shows the original differential interferogram, where the azimuth phase discontinuities between bursts due to the motion of the glacier can be clearly observed. Additionaly, it is clear that these discontinuities are space variant. By exploiting the two looks, the azimuthal motion can be estimated pixelwise in an accurate manner. A further advantage of the 2-look modes is that they allow the retrieval of the azimuthal motion with a better accuracy than that allowed by the azimuth resolution, hence improving the sensitivity to the North-South direction, which is usually the direction to which spaceborne SAR missions with near-polar orbits are less sensitive.

Interferometric Bidirectional SAR

The angular diversity of the 2-look TOPS mode allows a better sensitivity to the azimuthal motion, but such sensitivity is constrained due to the need of acquiring multiple sub-swaths. The bidirectional SAR mode [J-166], though constrained to a single swath, offers the possibility to increase the azimuth sensitivity. This mode exploits the fact that, with the proper electrical steering in phased array antennas, an antenna diagram with two equal main beams can be achieved, whose separation depends on the distance between the antenna elements, and which for TerraSAR-X results in a separation of 4.4°. The mode clearly requires a PRF about a factor of two larger than for a nominal acquisition in order to properly sample the fore and aft beams so that they can easily be Doppler filtered during SAR processing. With this large angular separation, the sensitivity to the along-track motions is two orders of magnitude better than when using conventional cross-correlation techniques, whose performance is limited by the azimuth resolution [IC-68], [RC-302], [IC-35]. Figure 2.2-31 shows an example of an 11-day repeat-pass bidirectional SAR interferogram over the Petermann glacier, where the sum and difference of the fore and aft interferograms include the information related to the across- and along-track motion in the scene, respectively. In the difference interferogram, a phase fringe corresponds to 20 cm of motion in the azimuth dimension.

The bidirectional interferometric mode can also be exploited to measure the ocean surface velocity by using the TanDEM-X formation in bistatic mode [RC-397]. For this particular experiment, the bistatic acquisitions were performed in a mission phase where at some particular latitudes the interferometric baseline was suitable for along-track interferometry of the ocean surface – namely a small across-track baseline and an along-track baseline of about 100 m. The radial and azimuth velocity components can be measured by combining the fore and aft beams. Figure 2.2-29 shows the retrieved 2-D velocity field over the Kara Sea, in the Russian Arctic. The acquisition took place on September 13, 2013, and is 210 km long and 26 km wide. It is assumed that most of the estimated velocity field is caused by wind-wave driven geophysical biases. Under this assumption, Figure 2.2-29 shows the direction and relative strength of this bias, which seems geophysically consistent with wind-driven waves moving predominantly in the positive azimuth direction, which are discontinued on the left (i.e., North-West) side of Novaya Zemlya.

The two bidirectional InSAR experiments described above demonstrate the potential of multiple squinted beams for the accurate retrieval of the along-track component of the motion in the scene, whether for land or ocean applications. Similar modes are currently being explored in the frame of future mission concepts.

Persistent Scatterer Interferometry

The so-called persistent scatterer interferometry (PSI) exploits image stacks in order to mitigate atmospheric artefacts and overcome the limited knowledge of the topography to retrieve a more accurate measurement of the deformation time series. In the last years, the Institute has developed a flexible PSI chain, which has been used to perform several investigations [J-64], [IC-26], [IC-28], [IC-61], [IC-91], [IC-92], [RC-46], [RC-50], [RC-163], [RC-301], [RC-302], [RC-474], [RC-507]. This PSI chain was especially relevant in the frame of the ESA InSARap project in order to evaluate the PSI interferometric performance

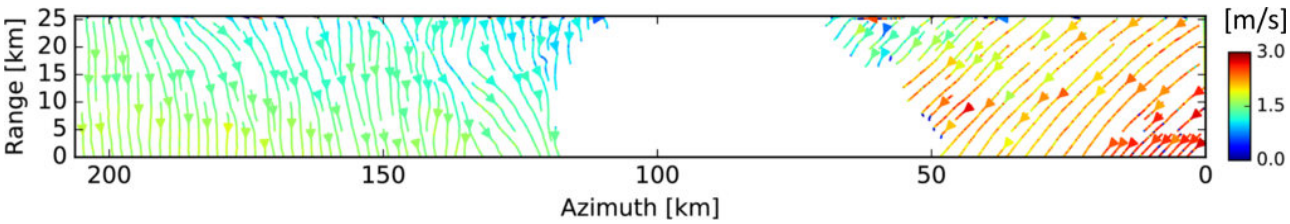

Figure 2.2-29 Effective 2-D velocity field measured with TanDEM-X in the experimental bidirectional InSAR mode. The land area corresponding to Novaya Zemlya island has been masked out.

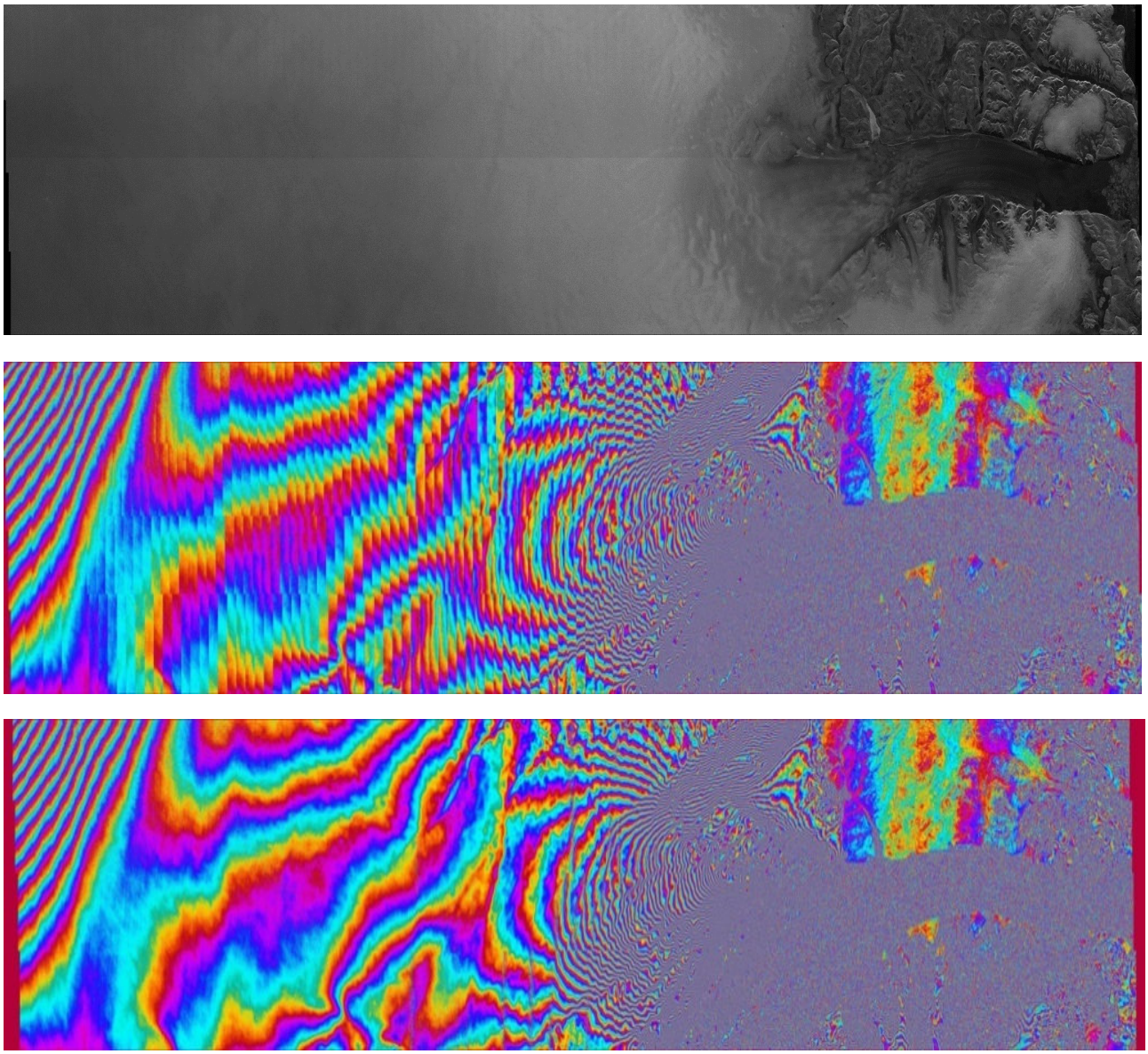

Figure 2.2-30 TerraSAR-X TOPS interferogram over the Petermann glacier, Greenland. Top: reflectivity image. Middle: original differential interferogram following removal of the topographic component. The phase discontinuities between bursts are due to the azimuthal motion of the Petermann glacier. Bottom: corrected differential interferogram following removal of the azimuthal component of the motion by exploiting the 2 looks.

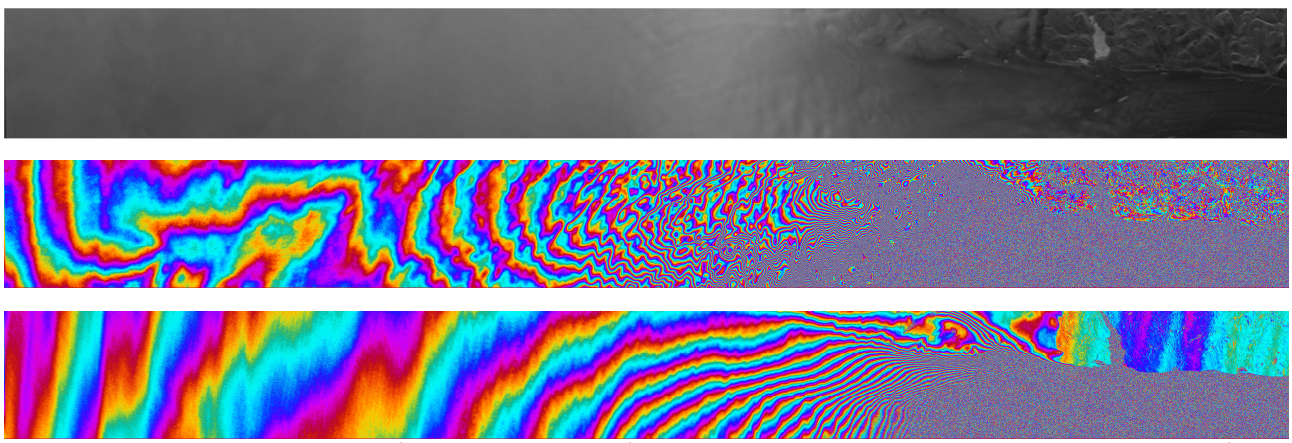

Figure 2.2-31 Bidirectional repeat-pass SAR interferograms with a time lag of 11 days over the Petermann glacier, Greenland. From top to bottom: reflectivity image, sum interferogram (sensitive to across-track motion) and difference interferogram (sensitive to along-track motion). In the latter case, the horizontal gradient agrees with the expected glacier flow.

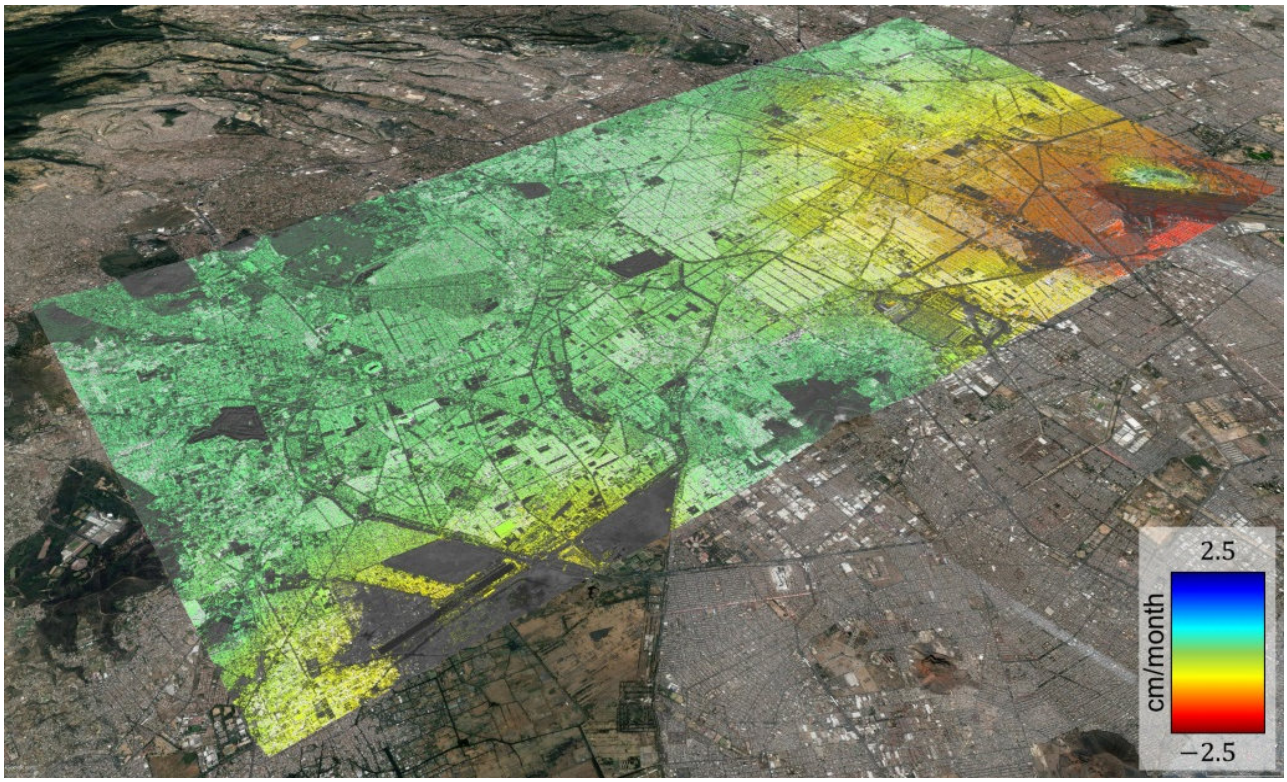

Figure 2.2-32 Estimated mean deformation velocity map over Mexico City, showing the well-known subsidence pattern due to ground water extraction and soil compaction. A mean density of 23,000 persistent scatterers per square kilometer is obtained thanks to the fine resolution of the TerraSAR-X stripmap mode.

for the Sentinel-1 satellite. The resulting deformation time series were validated with in-situ measurements (see Figure 2.2-65 in Section 2.2.8). The existing PSI chain was updated to allow the efficient processing of a large number of persistent scatterers (PS) [J-64]. Figure 2.2-32 shows the estimated mean deformation velocity map over Mexico City retrieved with a stack of 36 TerraSAR-X images acquired in stripmap mode between October 2009 and January 2012. Approximately 5.7 million valid PSs were detected and processed in a scene size of 11 km x 22 km, which results in a density of 23,000 persistent scatterers per square kilometer. The well-known subsidence pattern occurs due to ground water extraction and soil compaction.

Large Baseline Experiments with TanDEM-X

The standard TanDEM-X DEM product has a relative vertical accuracy for flat to moderate terrain of about 2 m. By increasing the spatial baseline between the satellites, this accuracy can be improved at the expense of volume decorrelation and a higher phase fringe frequency. Hence, in order to fully profit from the increased theoretical height sensitivity, sophisticated algorithms for the interferometric processing need to be considered. In this context, the Institute has developed a novel dual-baseline region-growing algorithm for the phase unwrapping of large-baseline interferograms [J-28], [RC-177], [RC-178], [RC-296]. Figure 2.2-33 shows the comparison between the standard and the experimental TanDEM-X DEM south of the city of Kaufbeuren, Germany. The standard DEM has a grid with a 12 m posting and consists of an average of four DEMs acquired over different passes. The experimental DEM was generated for a grid with 6 m posting with data from two passes acquired during the mission science phase. The two experimental interferograms were taken with large baselines, and heights of ambiguity of 14 m and 9 m; hence, they are able to deliver topographic measurements of low and non-vegetated areas with a higher quality than the standard TanDEM-X DEM product, as shown in the example.

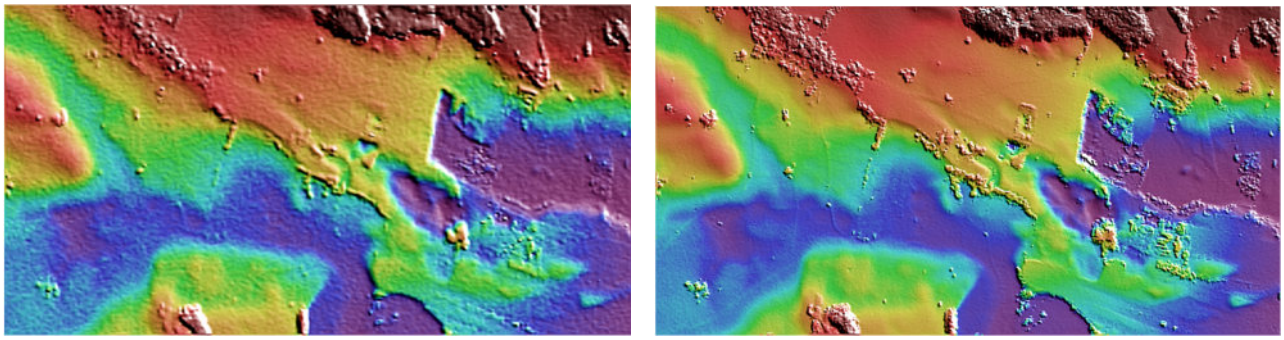

Figure 2.2-33 Zoom of the DEMs over an area south of Kaufbeuren, Germany. Left: standard TanDEM-X DEM obtained with four passes. Right: dual-baseline DEM computed with two large-baseline interferograms. The latter clearly has a much better relative accuracy.

2.2.5 End-to-End SAR System and Product Simulation

Observation needs in terms of availability, accuracy, and revisit times are becoming increasingly stringent with the growth of the community of SAR users. As a direct consequence, future Earth and planetary observation missions will consist of increasingly complex systems and operate under challenging atmospheric and environmental conditions. To better understand the influence of the instrument, platform, propagation and environment on mission performance, the Institute has developed configurable End-to-End (E2E) SAR simulation tools which can be tailored to different systems. In addition to their usefulness in assessing overall mission performance in complex simulation scenarios, E2E simulators are also valuable and powerful tools for the development and testing of on-board and on-ground processing and calibration algorithms.

Figure 2.2-34 shows the block diagram of a generic E2E simulation chain composed of i) a raw data simulator capable of including L1 (e.g., intensity images, interferograms) or L2 (e.g., volume or polarimetric structure) characteristics into the simulated raw data while incorporating instrument and environment information, ii) a prototype processor responsible for the processing of the simulated raw data according to the available on-ground information (e.g., orbits, pointing); and iii) a performance assessment module, which automatically evaluates the performance of the simulated system. Examples of various missions, systems and imaging modes, which have been simulated with the E2E developed tools, are discussed in the following subsections.

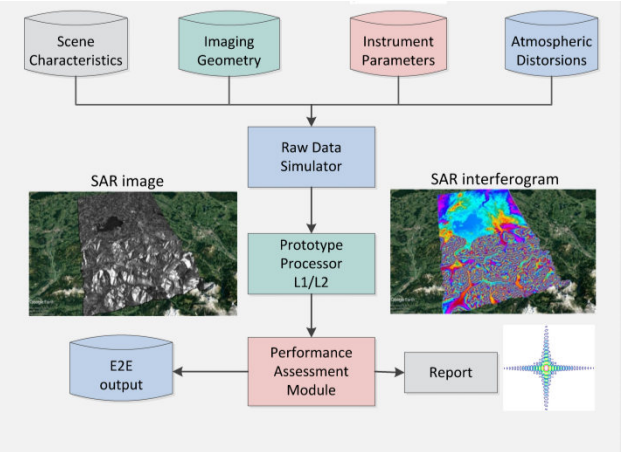

Figure 2.2-34 Generic block diagram of an E2E SAR simulation tool composed of a raw data simulator, a prototype processor, and a performance assessment module. Inputs to the simulator characterize the scene, the instrument, the platform, the atmospheric propagation and the environment.

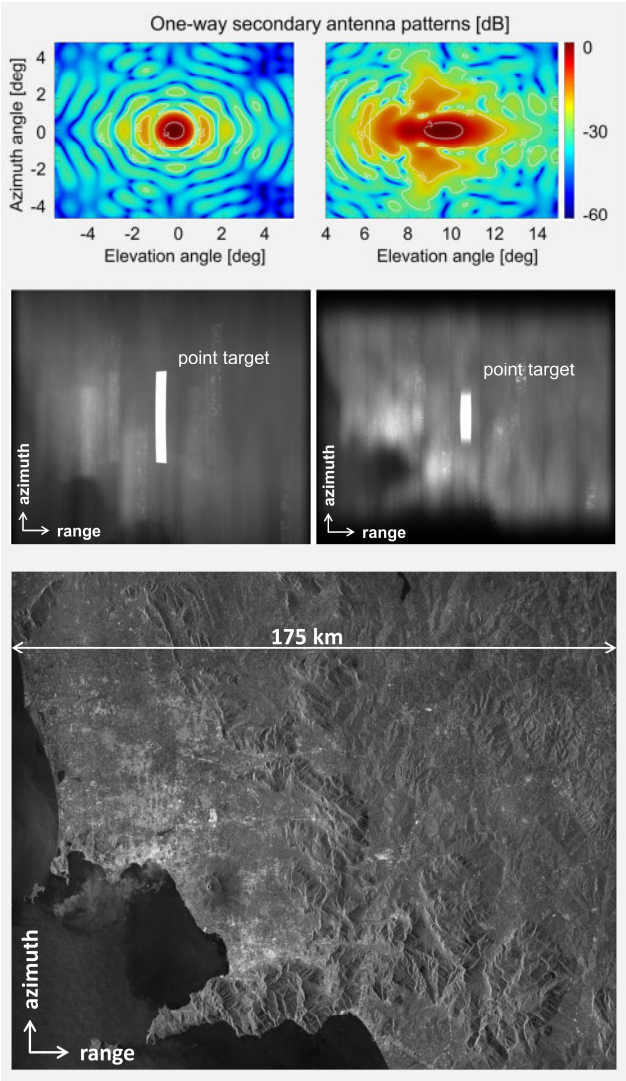

Figure 2.2-35 Tandem-L end-to-end simulation using a reference Sentinel-1 image. Top: secondary antenna patterns of the center (left) and edge (right) feed elements. Reference raw data (mid left) and Tandem-L simulated raw data including antenna patterns and beamforming (mid right). Bottom: simulated Tandem-L image after on-board azimuth filtering and on-ground processing conducted with TAXI.

Tandem-L End-to-End Simulator

A Tandem-L (cf. Section 2.1.3) end-to-end simulator to understand the impact of the instrument and observation concept on the mission product quality was developed at the Institute as part of the phase B1 activities. Integrated into the Institute's TanDEM-X interferometric processor (TAXI), and making use of its geometric functions, the Tandem-L simulator mimics the reflector antenna patterns, the multichannel front-end architecture, the staggered SAR mode, the on-board processing stages including digital beamforming (e.g. SCORE), the azimuth filtering (interpolation, resampling and data reduction), and the simulation of azimuth ambiguities. Figure 2.2-35 shows an example of the simulation, using as reference a Sentinel-1 image over the Gulf of Naples. The figure shows the secondary reflector antenna patterns of the central and edge feed antenna elements, the amplitude of the reference raw data set (i.e., including neither the antenna patterns nor SCORE), the raw data after applying the antenna patterns and SCORE, and the resulting image after on-board azimuth filtering and processing with TAXI.

End-to-End Simulators for ESA

The Institute has developed, and continues to develop, a number of end-to-end simulators for the assessment of the

performance of current and future SAR missions for ESA. This activity started with BEES (BIOMASS End-to-End Simulator), an L2 simulator for the BIOMASS Explorer mission (cf. Section 2.1.8). BEES incorporates a polarimetric and tomographic forward model for the simulation of BIOMASS scenes, a reverse interferometric stage, an ionospheric simulation module, and a prototype L2 processor. It was used during phase B1 to characterize the L2 performance in terms of biomass retrieval biases and variances, according to the error sources of the instrument, platform and environment, as well as with respect to the biomass estimation algorithms [RC-670].

The Institute is currently developing an upgrade of BEES called C-BEEPS (Complete BIOMASS End-to-End Performance Simulator). C-BEEPS is a tomographic and polarimetrically consistent L1 end-to-end simulator conceived for the B2/C/D/E phases of the BIOMASS project. The tool, considered as a crucial component for the mission performance optimization, is being developed for ESA by the Institute in the industrial core team under contract of the mission prime Airbus UK. It will support the design of different system aspects and the performance assessment of the L1 products of the mission. The main components of C-BEEPS are being developed as part of two independent projects: i) the raw data simulator and performance assessment modules (BEEPS), and ii) an L1 Ground Processor Prototype (GPP) including ionospheric and external calibration functionalities.

With respect to BEES, C-BEEPS represents an improvement in terms of simulation fidelity and performance, ensuring direct representability of instrument, environment, calibration, and ground-segment aspects. Figure 2.2-36 gives an example of a BIOMASS simulation over Lopé, Gabon. The figure shows a geocoded interferogram for a baseline of 350 m computed with a preliminary version of C-BEEPS.

As part of the activities conducted for ESA during the phase B2 of SAOCOM-CS, the Institute has also implemented a bistatic end-to-end simulator. This simulator – which will also be used in the study of future companion SAR missions in C band – features exact bistatic geometry, tomographic and interferometric capabilities, as well as a dedicated AutoSync clock synchronization step [IC-33] (see results in Section 2.2.2).

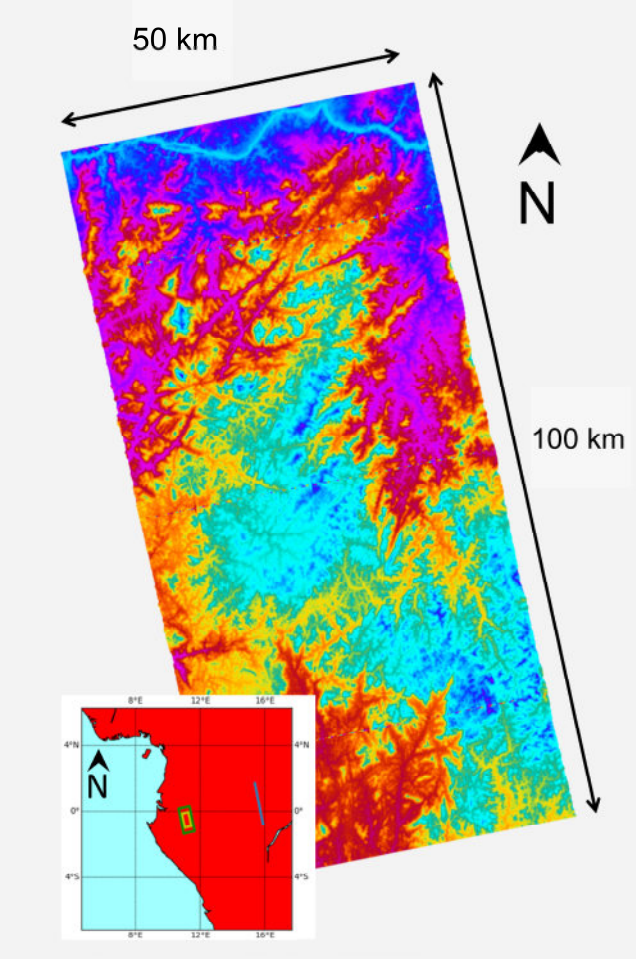

Figure 2.2-36 Example of a BIOMASS end-to-end simulation, computed with a preliminary version of C-BEEPS showing a geocoded interferogram over Lopé, Gabon (baseline of 350 m, temporal and volume decorrelation excluded).

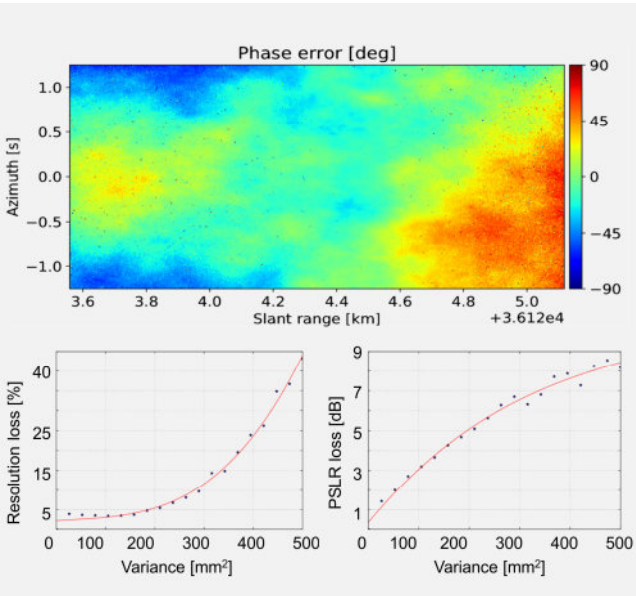

Figure 2.2-37 Example of a GEO SAR simulation including the effect of the atmospheric propagation. Top: atmospheric screen resulting from a GEO SAR simulation using a time-variant model. Bottom: azimuth impulse response degradation experienced by an L-band GEO SAR with 300 s integration time as a function of increasing tropospheric variance.

High-Orbit SAR End-to-End Simulation

High-orbit (e.g., MEO or GEO) SAR systems offer an excellent opportunity to achieve continental coverage and daily revisits with a single spacecraft. Changes in radar wave propagation, progressive decorrelation of targets in the scene, and time-variant instrument effects are expected to play a major role in the performance of these systems due to the typically long integration times, which range from tens of seconds to several hours. In order to support accurate simulations of future high-orbit SAR systems, the Institute has developed a space-variant reverse backprojection kernel [J-21] integrated into the E2E simulator. Figure 2.2-37 (top) shows an atmospheric phase screen simulated on a Sentinel-1 reflectivity image and mapped to a GEO SAR survey using a time-variant model incorporated on the reverse backprojection kernel. The bottom curves show the impulse response degradation of an L-band GEO SAR with 300 s integration time for increasing values of tropospheric power variations [J-22].

2.2.6 SAR System Calibration

Calibration of spaceborne SAR systems is an essential task to establish the relationship between radar measurements and geophysical parameters. This includes the geolocation of the SAR image, its backscattering characteristics (in amplitude and phase), and polarimetric information. Keeping up with the growing demand for accurate SAR data products on the one hand, and the growing complexity of innovative spaceborne SAR systems (with a multitude of different imaging beams and novel operation modes like TOPS [RC-449], sliding spotlight, etc.) on the other, requires sophisticated concepts, precise algorithms and adequate facilities in order to efficiently calibrate such complex spaceborne SAR systems.

DLR SAR Calibration Center

In calibration projects for ERS, X-SAR/SIR-C, ENVISAT/ASAR, TerraSAR-X [RC-628], TanDEM-X [IC-243], [RC-700], [RC-702], [RC-705] and Sentinel-1A [J-70] and -1B [J-34], the Institute has built up more than 25 years of expertise in end-to-end SAR system calibration – including extended field campaigns – and has proven its ability to manage highly complex and large projects. Efficient strategies [R-415], [R-416], [RC-532], [R-223], innovative methods [P-9], [P-4], [J-149], [J-147], [PhD-4], [PhD-12], [PhD-18] and accurate reference targets as shown in Figure 2.2-39 have been developed [RC-388], [J-154], [J-82], [RC-313], [RC-210]. Based on our unique experience, a suite of analysis and evaluation tools, the DLR calibration site (shown in Figure 2.2-38) featuring a series of calibration targets (transponders and corner reflectors of various sizes), and supported by a well-equipped laboratory [J-30], [RC-305], [RC-306], a decision was made to establish the DLR SAR calibration center. Beyond TerraSAR-X and TanDEM-X, the DLR SAR Calibration Center has been supporting ESA's Sentinel-1A/B mission since 2014 (see Section 2.1.7). These missions enabled the achievement of a set of accuracies for the different calibration methods and techniques, which are summarized in Table 2.2-1, and which can be considered as benchmarks. Furthermore, we recently established an agreement with the Korean Aerospace Research Institute (KARI) to perform independent calibration measurements on KOMPSAT-6 (see Section 2.1.12) after its launch in 2020. To be well prepared, particularly for upcoming SAR missions focusing on longer wavelengths in L or even P band – such as Tandem-L [J-97], [RC-36] or ESA's BIOMASS mission – novel concepts and innovative methods are currently being developed and presented in the following [RC-37], [RC-56], [RC-57], [RC-197], [RC-198], [RC-307], [R-36], [R-37], [R-100], [R-120], [MaT-10], [MaT-23], [MaT-28], [InT-6].

Calibration Method	Accuracy
Estimation of Instrument Drift	
Amplitude / Phase	< 0.1 dB / < 1 deg
TRM Characterization PN-Gating / PCC Technique	
Amplitude / Phase Setting	< 0.2 dB / < 2 deg
Geometric Calibration	
Azimuth / Range	< 10 cm / < 10 cm
Pointing Determination	
Azimuth / Elevation	2 mdeg / 2 mdeg
In-Orbit Antenna Model Verification	
Amplitude Accuracy	< 0.2 dB
Channel Imbalance Determination	
Amplitude / Phase	< 0.4 dB / < 3 deg
Radiometric Calibration	
Radiometric Stability	0.2 dB
Absolute Radiometric Accuracy	0.3 dB

Table 2.2-1 Calibration methods developed by the DLR SAR Calibration Center and achieved accuracies

Challenges and Strategy for the Calibration of Future Low-Frequency SAR Systems

Upcoming spaceborne SAR missions operating at longer wavelengths require comparably large antenna structures. In case of Tandem-L, a large deployable reflector (LDR) antenna, combined with an innovative feed system enabling digital beamforming techniques, is designed to realize a high-performance SAR sensor in L band without the need for a huge planar antenna array in space. ESA's BIOMASS mission, the first spaceborne P-band mission, is also based on a large offset reflector antenna. The use of large deployable reflector antenna technology in turn leads to new challenges for the calibration of future spaceborne SAR systems.

A key element is the so-called antenna model approach, which has been successfully developed and applied in the TerraSAR-X [RC-628], TanDEM-X [IC-243] and Sentinel-1A/B [J-70], [J-34] satellites, and which has to be expanded to cope with the special features of Tandem-L and BIOMASS. Furthermore, new concepts to realize compact ground-based calibration targets are currently under investigation and will be developed in the frame of an internal DLR project [R-120]. At lower frequencies, propagation through the ionosphere causes additional perturbations that must be corrected, e.g., by using parameters provided by global navigation satellite systems.

Antenna Model Approach

Compared to planar SAR antennas, the antenna model for a system comprising a reflector antenna combined with digital beamforming requires some adjustments and enhancements (see Figure 2.2-40). Due to the large dimensions of the Tandem-L spacecraft, especially the size of the boom and LDR assembly, on-ground characterization of the fully assembled system is no longer feasible.

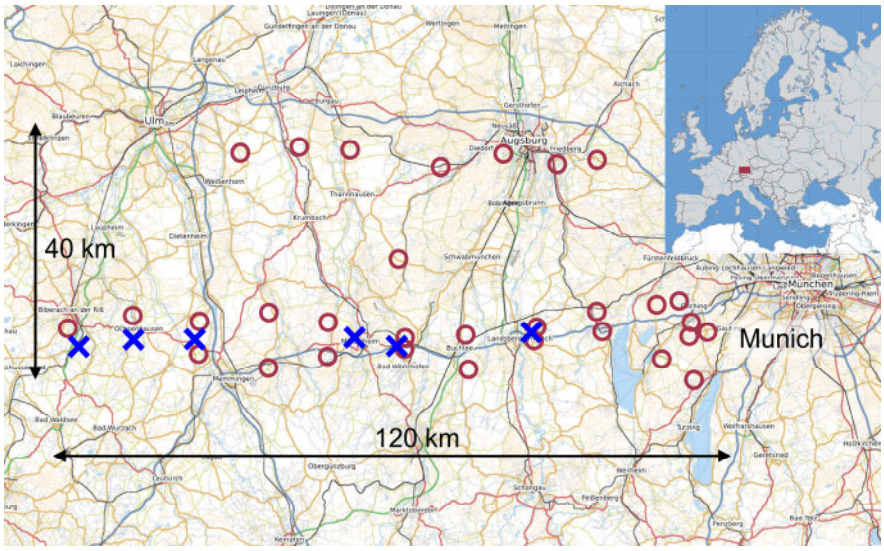

Figure 2.2-38 The DLR calibration site consists of 37 target positions with 20 permanently installed corner reflectors. The six newly installed remote-controlled targets are shown in blue (Map: © OpenStreetMap).

Figure 2.2-39 "Kalibri" C-band transponder developed for Sentinel-1

Nevertheless, the primary near-field antenna patterns of the feed elements – embedded in an array structure directly on the satellite bus – must still be carefully characterized on ground before launch. The measurements of these primary antenna patterns will be used as input for a dedicated electromagnetic field simulation, together with the known geometry of the LDR and boom assembly in order to retrieve the secondary embedded far-field antenna patterns of the whole array-fed reflector antenna system.

The antenna model for Tandem-L will actually comprise two modules: a physical antenna module for electromagnetic field simulations of the secondary antenna patterns mentioned above and a digital beamforming module for calculating digitally formed antenna beams using dedicated DBF algorithms.

The first module will be used to calculate separate physical far-field antenna patterns for each radiating element and both polarizations. This requires time-consuming simulations. Then, the second digital beamforming module employs the known weighting coefficients, which are applied to the pre-calculated secondary antenna patterns during data acquisition to generate the final digitally formed antenna beam patterns required for SAR focusing. Both modules are currently being developed by the Institute.

Antenna Pointing Determination

The large physical dimensions of the antenna system lead to another challenge – thermal effects and mechanical forces can lead to small deformations in the antenna structure. While the effect of these small deformations seems to be negligible for the overall antenna pattern, it has to be considered for the antenna pointing [RC-37], [RC-56]. The time scale for these deformations can last from minutes (temperature changes over one orbit) to months (seasons). Repeated measurements of the antenna pointing are thus necessary to meet the performance requirements.

The antenna pointing in azimuth direction can be estimated from the Doppler centroid of a processed SAR image and

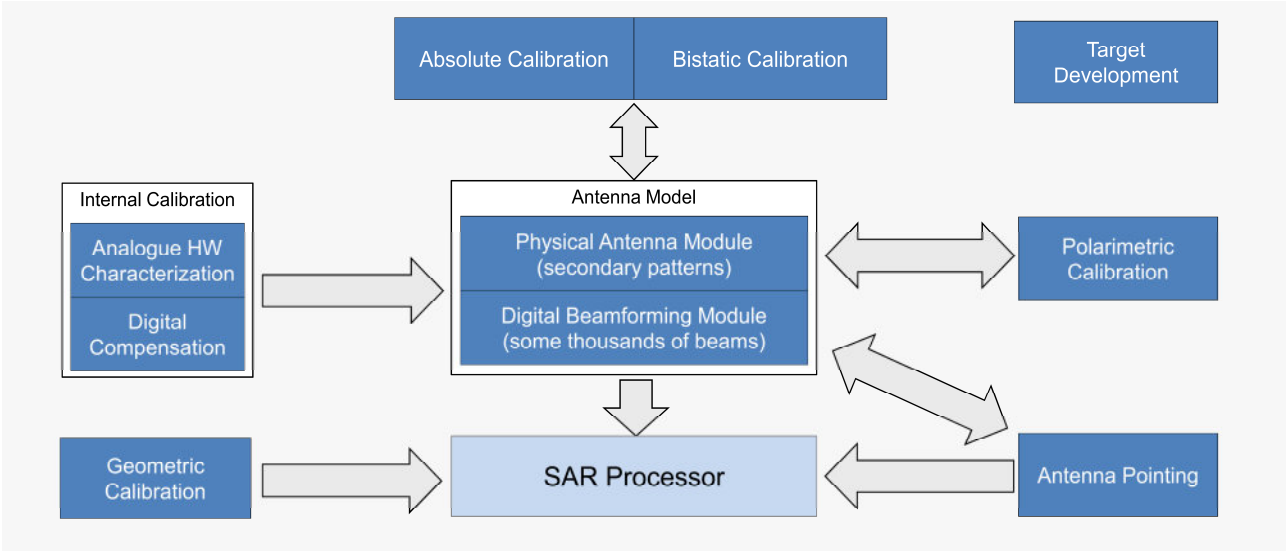

Figure 2.2-40 The calibration of Tandem-L will be based on an elaborated antenna model

compared to the expected pointing. Homogeneous distributed targets such as the Amazon rainforest are frequently used to determine the antenna pointing in elevation. By commanding notch patterns to the phased array feed, the resulting steep groove can easily be detected after SAR focusing to determine the elevation pointing (cf. Figure 2.2-41). Unfortunately, the spread of these distributed targets is not wide enough to sufficiently trace pointing changes around the orbit. Additional calibration targets are thus required. For this purpose, inhomogeneously distributed targets may be employed by combining notch and regular antenna patterns: data from regular patterns are used to smooth variations in the reflected power, which would disturb measurements using only notch beams. This is done by normalizing the complex signal from the notch beam using a simultaneously acquired regular acquisition. Thus, for areas with sufficient SNR, repetitive pointing measurements become feasible to track changes in the antenna structure [RC-37], [RC-56].

The proposed pointing determination technique has been successfully demonstrated thanks to the flexible SAR instrument of TerraSAR-X. For this purpose, the beam switching mode was utilized. In this mode, the receive antenna pattern is toggled for each radar pulse. This feature was used to simulate the acquisition of two images – one with the regular beam and the other with the notch beam. The two acquired and coregistered level-1 images are shown in Figure 2.2-41. The notch is visible in the brighter edges compared to the swath center. Additionally, many range ambiguities appear due to the non-optimized antenna pattern for the used timing (doubled PRF to acquire two images).

The extraction of phase information from only one of the acquired images would not be meaningful, since the unknown phase of the target is dominant. The difference image is shown in Figure 2.2-42 in amplitude and phase. In this plot, the antenna pattern notch is more visible and the phase image clearly shows the location of the notch. The quality of the measurement becomes even more obvious when calculating the range profile, i.e., averaging in azimuth as shown in Figure 2.2-43. A steep null of several tens of dB can be found in the power profile and the 180-degree phase shift is also at the expected location in the phase profile.

The shown range profiles result from a relatively short data take of only 57.6 km, and with a setup of the radar instrument that produces many ambiguities. The performance of an optimized DBF SAR system is expected to be even superior. Nevertheless, the presented results already allow for an elevation pointing determination down to an accuracy of only a few tens of millidegrees.

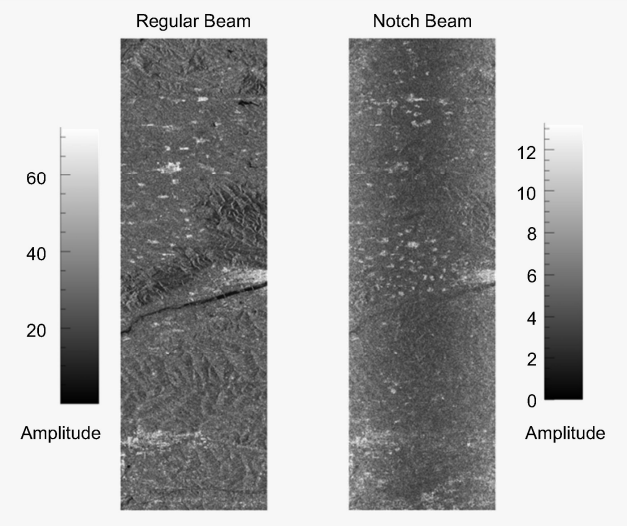

Figure 2.2-41 Image amplitudes over a non-homogeneous area in China using the TerraSAR-X beam switching mode to acquire images using a regular (left) and notch beam (right) simultaneously.

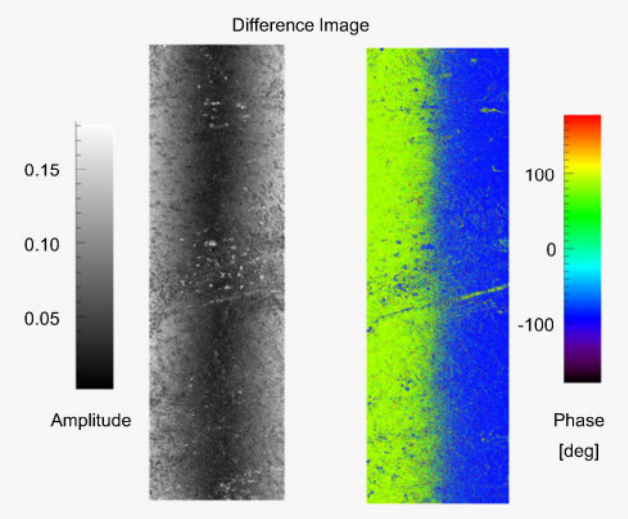

Figure 2.2-42 Difference image in amplitude (left) and phase (right) from the same scene as shown inFigure 2.2-41.

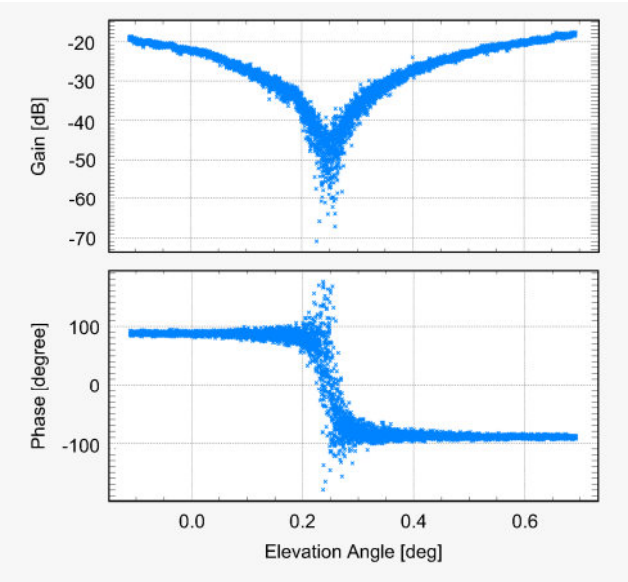

Figure 2.2-43 The range profiles as derived from the difference image shown in Figure 2.2-42. Top: amplitude, bottom: phase difference in degrees.

Next Generation Calibration Transponders

In view of future SAR missions, the Institute has identified the following key aspects to be addressed by new calibration hardware, all of which are covered within the DLR internal project "Kalibri Next Generation" [R-120]:

- support of low frequencies, i.e., L band for the Tandem-L mission [J-30], [RC-305], [RC-306] and P band for BIOMASS,

- processing of high bandwidths (up to 1.2 GHz) at X band, as envisaged for HRWS (see Chapter 2.1.4), and

- fully polarimetric capabilities as foreseen by Tandem-L and BIOMASS.

In addition to these additional demands, DLR's next-generation transponder systems will inherit the successful concept of the "Kalibri" C-band transponders [RC-388], [RC-185], [RC-480], [RC-581], [R-283], [MaT-17], [MaT-53], [MaT-6], [RC-313], [RC-589], which were developed for ESA's Sentinel-1 mission (see Section 2.1.7) and adapted for the Canadian Radar Constellation Mission on behalf of the Canadian Space Agency (CSA), see Section 2.1.13. "Kalibri" is designed for all-season autonomous outdoor operation. It is remotely aligned towards the satellite by a two-axis positioner. This in-house developed transponder is based on a two-antenna design ensuring a small time delay between reception and re-transmission of the radar signal. It features a modular setup for easy adaptation to other frequency bands, such as X band.
The transponder's transmit and receive antennas are embedded in a temperature-stabilized housing together with the RF analog circuit. The superior radiometric stability of below 0.1 dB is maintained by an internal calibration loop. An FPGA-based subsystem allows for a digital recording of radar chirps. The configuration of satellite overpasses and the corresponding data acquisitions are conducted in an automated fashion and can be conveniently scheduled and monitored by a web interface. Towards upcoming missions, this concept will be adapted to X-, L- and P-band frequencies and enhanced by dual-polarization capabilities to allow for fully polarimetric measurements. This requires new antenna concepts currently being investigated by the Institute.
Antennas suitable for SAR calibration transponders have to fulfill a multitude of electrical and environmental requirements. The most important are:

- relatively broad main lobe region maintaining an axial symmetry and stable gain over the desired bandwidth,

- low sidelobe ratio,

- high cross-polarization isolation,

- dual-polarization capabilities,

- compact and lightweight design and

- robust structure for long-term, all-season operation.

The fulfillment of the above electrical demands in a compact design suitable for DLR's remotely controlled transponder concept is a main challenge. Extensive in-house R&D resulted in an innovative antenna design based on a choked Gaussian horn antenna which was named VeGA (German for "Verkürzte Gauß Antenne") [MaT-10], [MaT-23], [MaT-28], [InT-6]. Simulations of VeGA (see Figure 2.2-44) predict a smooth gain pattern with a nominal gain of about 15 dBi while maintaining a cross-polarization isolation better than 30 dB.

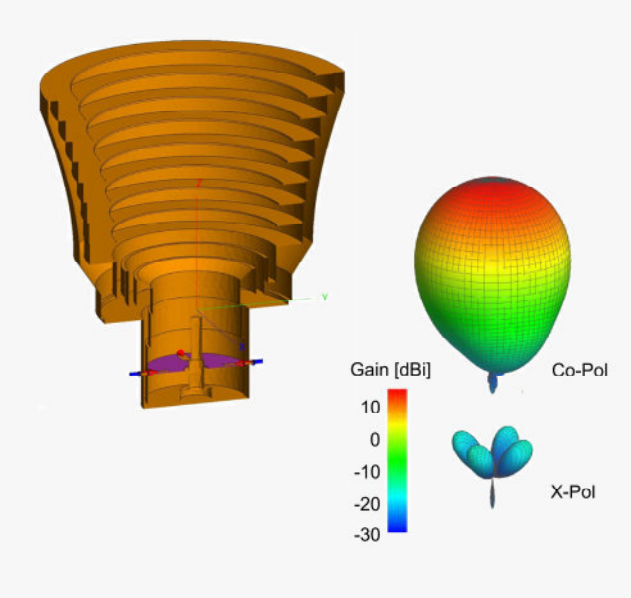

Figure 2.2-44 Cross-section of the VeGA antenna (short Gauß antenna) and simulated gain pattern for co- and cross-polarization

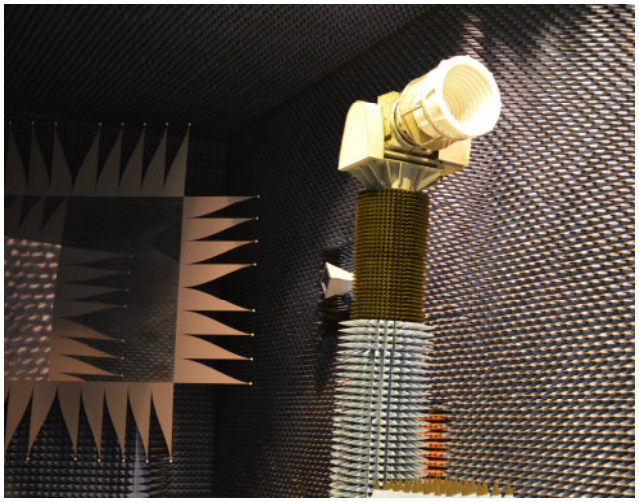

Figure 2.2-45 Printed VeGA antenna (short Gauß antenna) mounted on a positioner in DLR's Compact Test Range

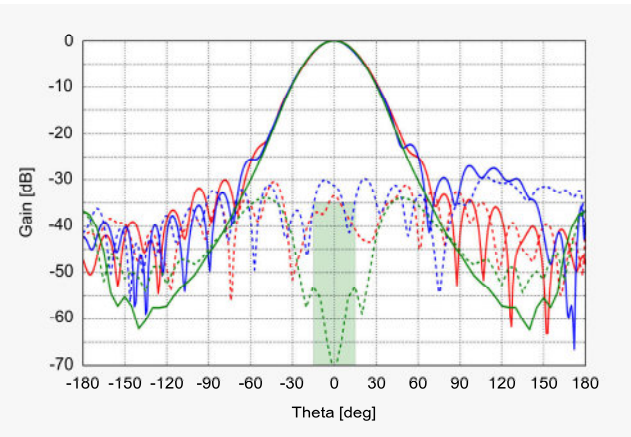

Figure 2.2-46 Measured (blue and red) and simulated gain (green) of the printed VeGA antenna as a function of the angle θ (vertical plane), normalized to the maximum gain. Solid lines denote the co-polarization component, dashed lines the cross-polarization. For the measurements, the results from both orthogonal channels (Port-B1B3 and Port-B2B4) of the antenna are shown [MaT-10], [MaT-23], [MaT-28], [InT-6].

A compact and light prototype antenna was manufactured at C band and L band using 3-D printing. The compact VeGA horn antenna is more than 3 times smaller and 10 times lighter than the currently used transponder antennas at the same frequency range. The performance of both antennas was already proven by measurements at DLR's Compact Test Range facility (cf. Figure 2.2-45 and Figure 2.2-46). With our DLR SAR Calibration Center and the continuing effort on developing new calibration techniques, targets and evaluation tools, the Institute is well prepared for the challenges of the next generation of SAR missions.

2.2.7 Pol-InSAR and SAR Tomography

Polarimetric SAR Interferometry (Pol-InSAR) is today an established SAR remote sensing discipline that explores the polarimetric diversity of interferometric measurements for the generation of novel quantitative and qualitative information products. In the last decade, Pol-InSAR processing techniques and inversion algorithms have undergone a remarkable development, especially with respect to the estimation of the structural parameters of volume scatterers such as vegetation structure, snow depth and ice layering. Such products have the potential to revolutionize the way ecosystem changes are addressed today, as they not only enable comprehensive monitoring of critical ecosystems, but are also of high relevance for the initialization of ecological and climate process models.

In the last seven years, Pol-InSAR has evolved from single- to multi-baseline and tomographic configurations, raising its potential to a new level. Multi-baseline configurations make it possible to create observation spaces with sufficient dimensionality to resolve even complex 3-D scattering processes. In addition, the complementarity of the information content makes the combination of polarimetric and baseline (i.e., angular) diversity unique, enhancing the sensitivity to the dielectric and geometric properties of the scatterers.

The extension of single- to dual- and multi-baseline Pol-InSAR enabled the use of more general inversion models while improving their robustness and conditioning. As a result, forest height inversion became accurate and stable, even in the presence of moderate temporal decorrelation, in difficult terrain conditions, and across a wide range of forest structure types. This development was also essential with respect to future SAR missions like BIOMASS and Tandem-L, where forest height estimates by means of Pol-InSAR are important inputes for deriving direct and/or intermediate products.

Figure 2.2-47 shows two forest height maps obtained from the inversion of L- (left) and P-band (right) Pol-InSAR data acquired in the framework of the AfriSAR campaign in February 2016 over the Pongara National Park. The site is home to some of the tallest mangrove forests in the world, towering up to 60 meters. The validation plots at the bottom of Figure 2.2-47 demonstrate the remarkable performance in terms of absolute height estimation and cross-correlation between the two frequencies. In addition to forest height, the availability of more than one spatial baseline dramatically improved the estimation performance of the underlying ground. Figure 2.2-48 compares

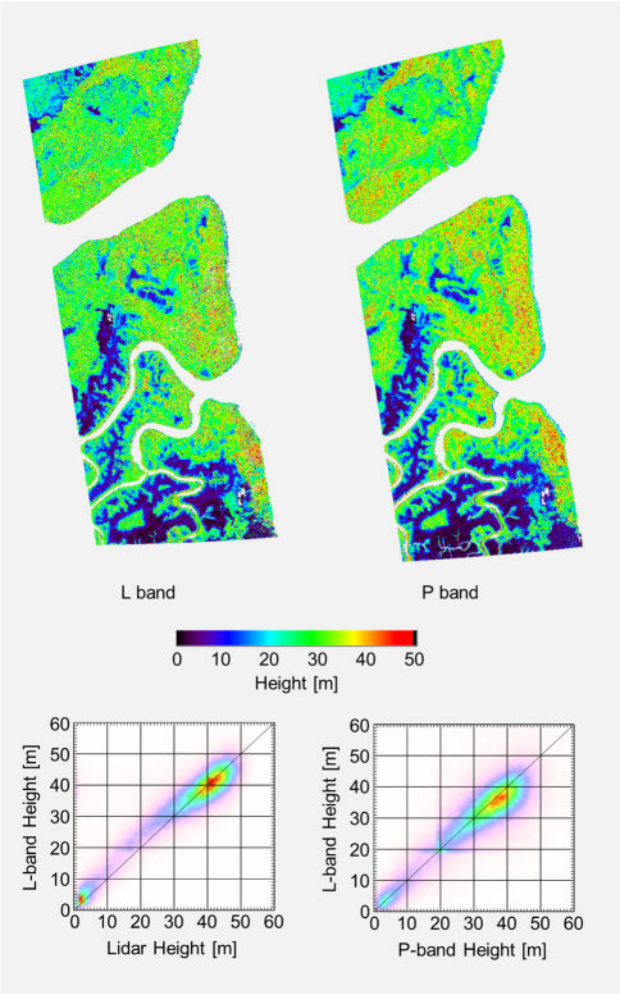

Figure 2.2-47 Forest height maps as inverted from L- (top left) and P-band (top right) Pol-InSAR data. The correlation between the L-band and lidar-derived forest height is shown on the bottom left; the correlation between L- and P-band height estimates on the bottom right. All data sets have been acquired in the framework of the AfriSAR campaign in February 2016 over the Pongara National Park in Gabon.

underlying ground terrain maps derived from L- and P-band Pol-InSAR data, acquired in the framework of the same AfriSAR campaign over the Lopé National Park, with the ones derived from full waveform airborne lidar data. This site is challenging as it is covered by a variety of tropical forest stands with heights often exceeding 50 m, and a hilly terrain, with local slopes steeper than 20°. The histograms of the estimation errors with respect to the lidar digital terrain model (DTM) indicate an accuracy of 3 to 5 m.

The availability of multiple data takes acquired with slightly different incidence angles along spatially displaced tracks or orbits finally allows the reconstruction of the 3-D radar reflectivity by means of Synthetic Aperture Radar Tomography (TomoSAR) techniques. Although a number of TomoSAR reconstruction algorithms have been developed and demonstrated over the years, their performance in the case of volume scatterers remains sub-optimal. Conventional Fourier beamforming algorithms allow an accurate radiometric reconstruction, but acceptable vertical resolutions require a comparatively large number of acquisitions. On the other hand,

super-resolution algorithms such as the Capon spectral estimator achieve a higher vertical resolution with a smaller number of acquisitions, but at the cost of a degradation or even loss of radiometric accuracy.

It is important to realize that the reconstructed 3-D reflectivity is a radar quantity that depends not only on the 3-D distribution of the scatterers in the scene and on their dielectric properties, but also on the radar frequency, polarization and incidence (or look) angle [IC-126]. This is shown in Figure 2.2-49 where an L-band reflectivity profile – i.e., a slice of the 3-D reflectivity along a forest transect in the Traunstein site – is shown at different polarizations: HH on top, HV in the middle and VV at the bottom. Seen from left to right the transect crosses mature stands (with heights up to 35 m), a bare field, a transition stand and finally younger stands (with heights of about 30 and 15 m, respectively). The relative contrast between ground and canopy scatterers changes with polarization. The relative ground power is consistently lower in HV than in HH or VV, and higher in HH than in VV as a result of dihedral scattering contributions.

Similarly, changing the radar frequency changes the effective scatterers [IC-25], [IC-89], [RC-286]. Lower frequencies are more sensitive to larger (i.e., in the order of the wavelength) vegetation elements. At the same time, the lower attenuation of the canopy increases the visibility of lower vegetation layers and of the ground. In contrast, the sensitivity to smaller vegetation elements increases with increasing frequency while the stronger canopy attenuation reduces the visibility of the ground. This frequency dependency can be seen in Figure 2.2-50, where for the same forest transect as in Figure 2.2-49, the reflectivity profiles at P, L, S, and X band are shown. At P band, even in the HV polarization, the dominant scatterer is the underlying ground. At L band, the ground and canopy contributions appear more balanced, while at X band the canopy layer becomes dominant. The S-band profiles appear very similar to the X-band ones. This is, however, not representative as Traunstein was covered by snow at the time of the S-band acquisitions.

Until the development of single-pass tomographic configurations – i.e., satellite formations that will be able to acquire all tomographic images at the same time – the acquisition of tomographic data sets will be affected by changes of the reflectivity occurring within the time period between the individual acquisitions.

The concept of coherence-based SAR tomography was developed to reduce the disturbance induced by temporal decorrelation, which constrains the implementation of tomographic techniques in conventional repeat-pass SAR configurations. It relies on a single-pass interferometer that provides a set of single-pass interferometric acquisitions with different spatial baselines in a repeat-pass mode. For the reconstruction of the 3-D radar reflectivity, conventional spectral estimation algorithms need to be adapted to the reduced set of single-pass coherences instead of the full acquisition covariance matrix [RC-508]. In this way, high frequency decorrelation effects, such as wind induced decorrelation, can be mostly compensated for. However, the problem of a possible change in reflectivity during the time required to perform all single-pass interferometric acquisitions remains.

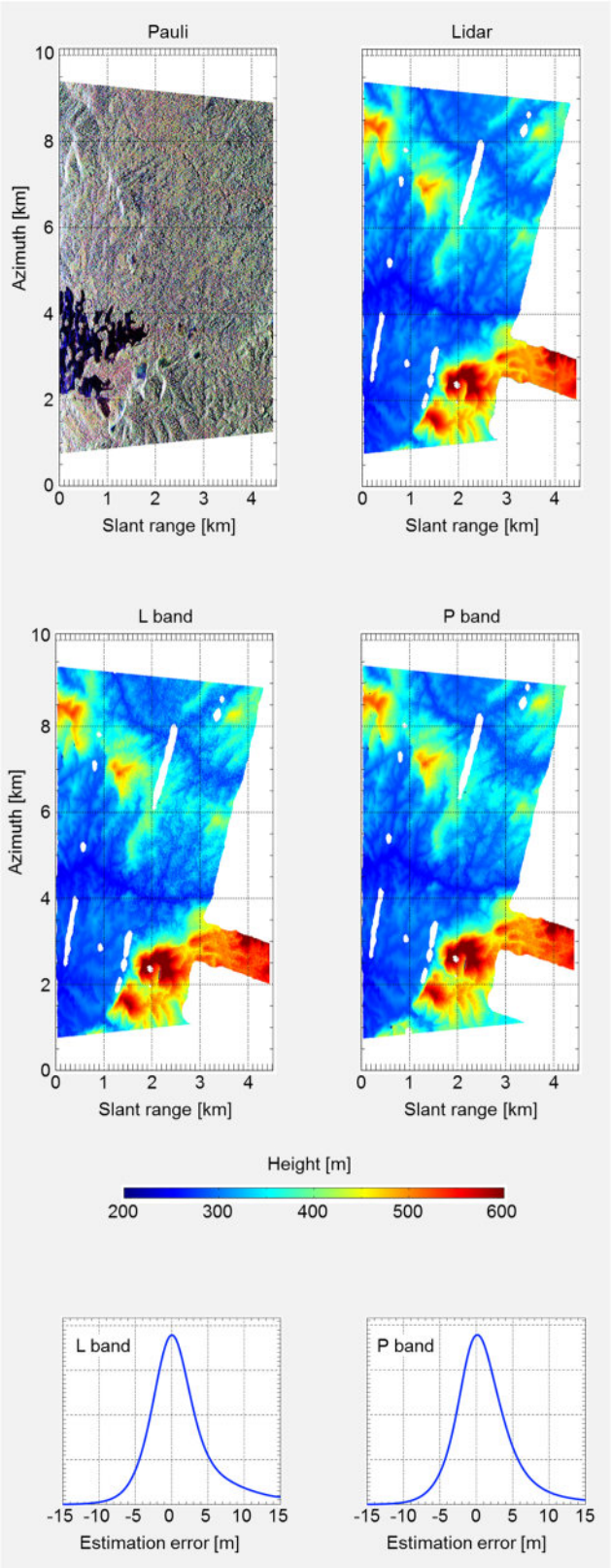

Figure 2.2-48 Underlying ground terrain maps of the Lopé National Park in Gabon derived from L- (middle left) and P-band (middle right) Pol-InSAR data and full waveform airborne lidar data (top right). The polarimetric Pauli RGB composite image at P band is shown on the top left. The histogram of the difference between L-band and lidar estimates is shown on the bottom left; the difference between P-band and lidar estimates is shown on the bottom right. The data sets were acquired in the framework of the AfriSAR campaign in February 2016.

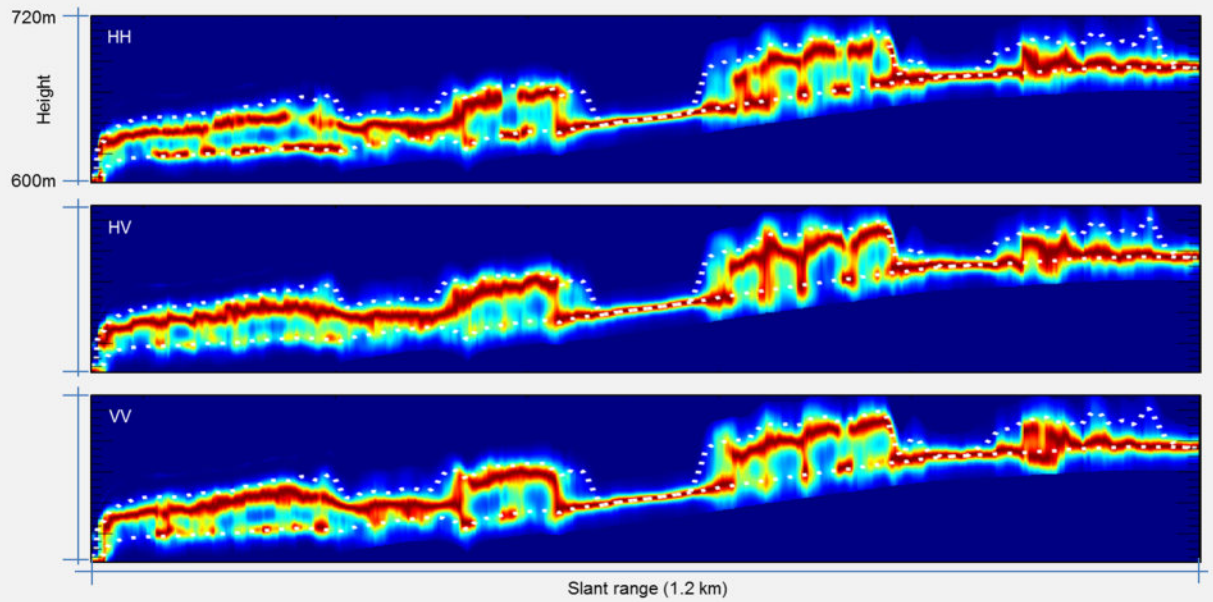

Figure 2.2-49 L-band reflectivity profile along a forest transect in the Traunstein site shown at different polarizations: HH on top, HV in the middle and VV at the bottom. The white dotted lines indicate the lidar-derived ground topography and the forest top height. The data were acquired in the framework of the TempoSAR 2012 campaign.

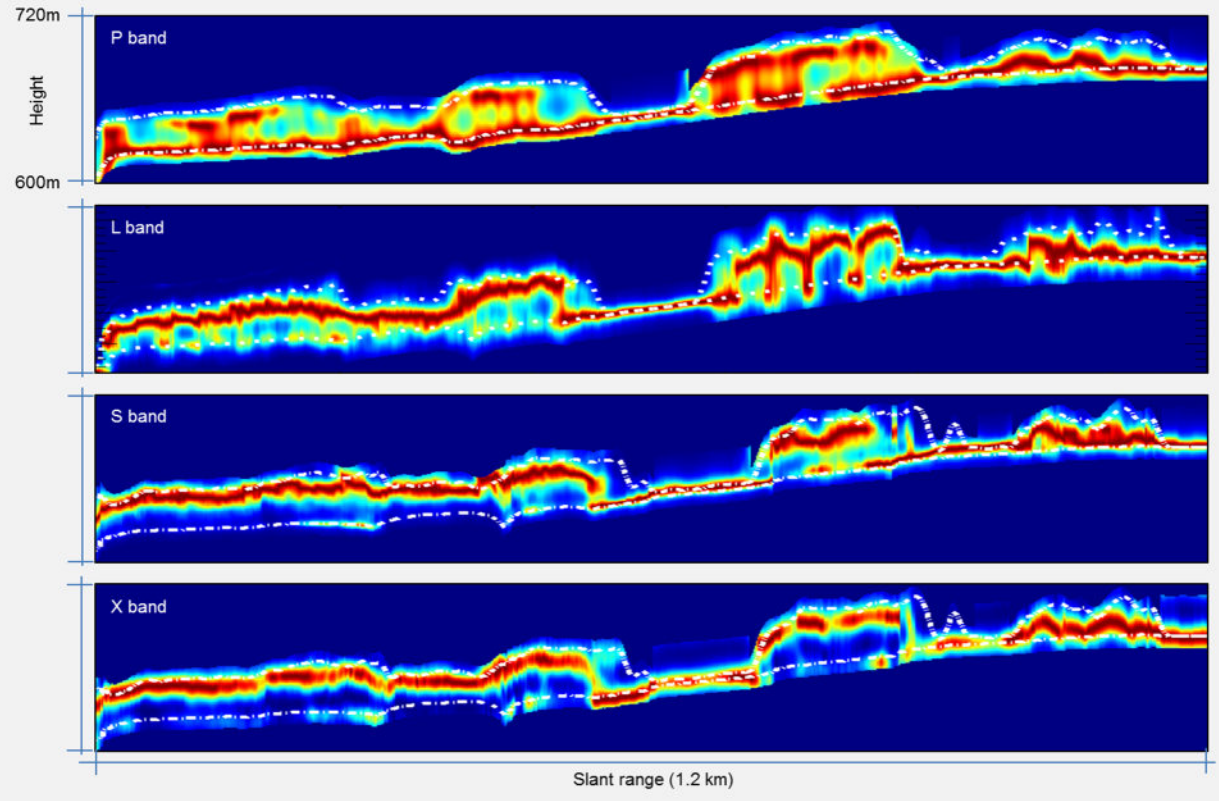

Figure 2.2-50 Reflectivity profile along a forest transect in the Traunstein site at different frequencies. The white dotted lines indicate the lidar-derived ground topography and forest top height. The datasets were acquired in the framework of different F-SAR campaigns between 2012 (L band) and 2016 (S band).

Coherence-based SAR tomography is especially important at higher frequencies where even small temporal baselines may introduce large temporal decorrelation. A first demonstration was performed by means of multi-baseline TanDEM-X bistatic [RC-509] and pursuit monostatic acquisitions [IC-16].

Figure 2.2-51 shows an example of Capon TanDEM-X profiles reconstructed by using 5 TanDEM-X acquisitions over the Tapajos site located in the Amazon basin. The Capon profile obtained from conventional repeat-pass tomographic processing is shown on the top, and the profile obtained by using the single-pass coherence-based implementation can be seen on the bottom. While the conventional profile is strongly affected by temporal decorrelation, the improvement in the coherence-based profile is evident, especially for the forest stands at the left. The achieved quality now enables the detection of large emerging trees, as shown in the lower section of Figure 2.2-51.

It is worth noting here that the tomographic reconstruction of the S- and X-band profiles in Figure 2.2-50 was also performed by means of coherence-based SAR tomography using the respective single-pass XTI modes of F-SAR.

Finally, when implementing TomoSAR techniques in the framework of spaceborne missions, the vertical resolution and ambiguity suppression of the imaging process are limited by the rather low number of datasets that can be acquired within a time interval that is acceptable in the context of the scene (i.e., reflectivity) stationarity. The use of compressive sensing (CS) techniques makes it possible to cope with the limited number of acquisitions and provides the highest resolution under the relevant TomoSAR conditions [J-145]. However, as an intrinsic consequence of super-resolution, the radiometric accuracy is compromised. A direct comparison of a wavelet-based CS against a Fourier and a Capon tomographic reconstruction from five L-band acquisitions along a transect in Traunstein is shown in Figure 2.2-52. The improvement in resolution with CS is remarkable, making it possible to distinguish scattering contributions that are just a few meters apart within the forest canopy.

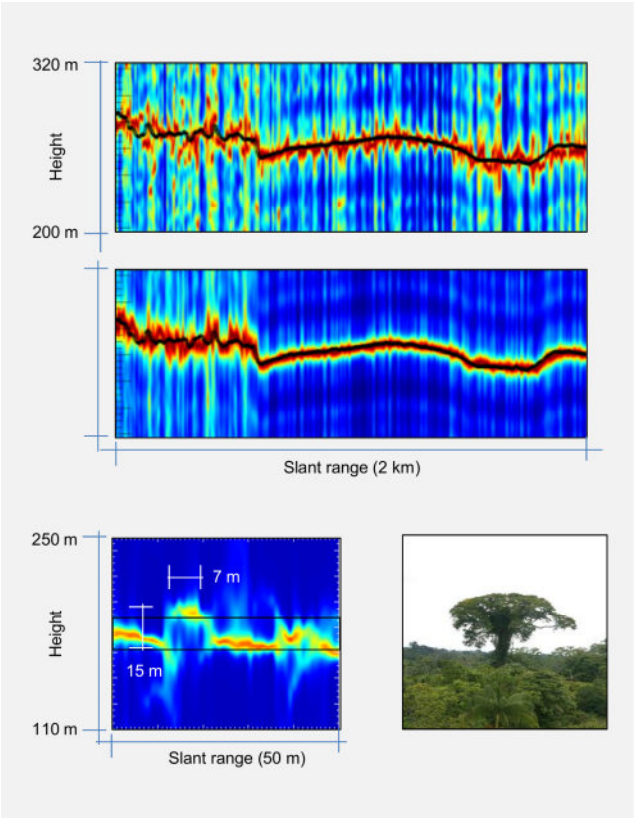

Figure 2.2-51 Reflectivity profile from TanDEM-X acquisitions using a conventional Capon reconstruction (top) and single-pass coherence-based reconstruction (middle) over the Tapajos super test site in Brazil. The reflectivity signature of a single large emerging tree is shown on the bottom.

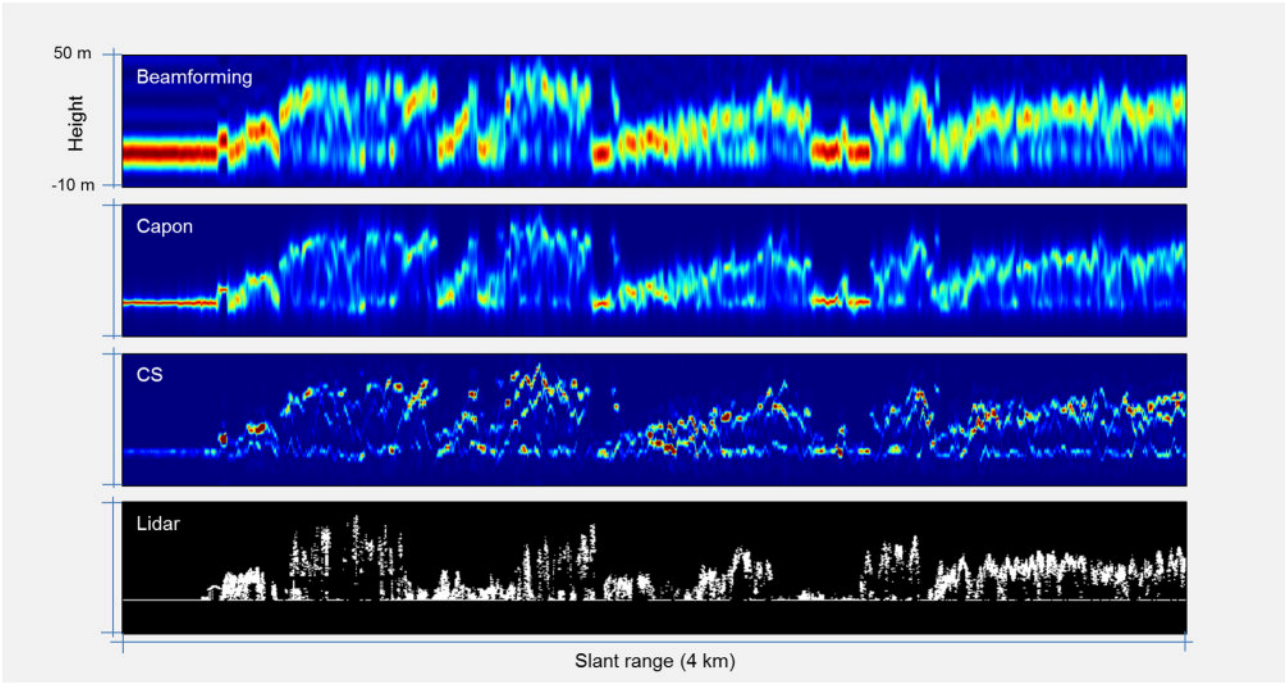

Figure 2.2-52 Comparison of different tomographic reconstruction algorithms for the same forest transect in the Traunstein site in L band: Fourier beamforming (top), Capon spectral estimator (second from top) and compressive sensing (third from top). A lidar profile of the same transect is shown on the bottom. The data set has been acquired in the framework of the TempoSAR 2012 campaign.

2.2.8 Bio- and Geophysical Information Retrieval: Algorithms and Products

Over the past seven years, the qualitative and quantitative characterization of natural volume scatterers using multi-parameter SAR measurements has experienced an impressive development initiated by the advancement of multi-baseline Pol-InSAR and tomographic techniques. The Institute has not only maintained its leading role in the development of new information products from multi-parameter SAR data – established with the invention and evolution of Pol-InSAR – but has also successfully expanded its leading expertise to new domains. This development process was maintained by the interaction of new science perspectives with technological advances that meshed together harmonically.

The availability of new air- and spaceborne data sets acquired in the framework of pioneering and trendsetting air- and spaceborne experiments, together with the development of new – or the optimization of existing – processing and inversion algorithms, allowed a new quality in 3-D and 4-D processing. A fundamental challenge was (and still is) the physical interpretation of the reconstructed 3-D and 4-D radar reflectivity. Its frequency and polarization dependency, combined with the concurrent sensitivity to geometric and dielectric properties, makes a direct interpretation ambiguous and non-trivial, further, the lack of suitable 3-D reference data complicates the interpretation even more. Accordingly, this task can only be attempted in close cooperation with national and international experts and institutions with competence in the exploration and modelling of the Earth's different ecosystems. In addition to the already established cooperation partners, the Helmholtz Alliance Remote Sensing and Earth System Dynamics offered a unique pool of expertise in bio-, geo-, hydro- and cryosphere research that was indispensable for the physical interpretation of the multidimensional radar reflectivity measurements.

The next step after the physical understanding of the data is the development of the inversion methodology. This step refers not only to the design of suitable models and the definition of effective algorithms for inversion, but also to the validation and evaluation of the estimates. A close cooperation with bio-, geo-, hydro- and cryospheric researchers or institutions is indispensable here as well – not only for the definition of relevant physical parameters and products, but also for the design and implementation of validation campaigns and the assessment of the achieved results.

Finally, the new products and retrieval algorithms developed play a main role within the framework of actual and future spaceborne missions. On the one hand, they allow ongoing and planned missions such as BIOMASS and Tandem-L to reach (and maybe even exceed) their ambitious mission objectives, while, on the other hand, they are incorporated into the mission and operation design of future missions.

Forest Applications

Forest parameter retrieval is by far the most developed amongst all application fields. This is motivated by the rising awareness of large-scale quantitative forest monitoring for understanding and quantifying the role of forests in the context of climate change and sustainable management of natural resources.

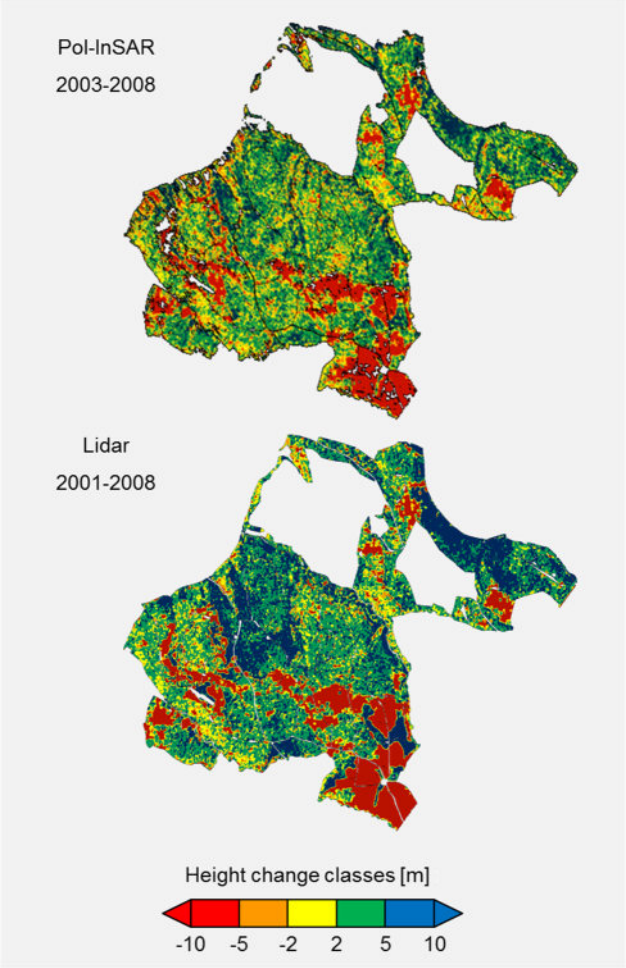

Figure 2.2-53 Forest height change maps of the Traunstein forest as derived from Pol-InSAR forest height measurements at L band between 2003 and 2008 (top) and from lidar forest heights between 2001 and 2008 (bottom) in five height change classes.

Forest height was the first quantitative product derived from single- and multi-baseline polarimetric interferometric SAR (Pol-InSAR) data that reached operational status in the early years of this decade. Since 2015, the focus was on forest height dynamics. A significant result was the demonstration of forest height change estimation using Pol-InSAR data systematically collected since 2003. An example is illustrated in Figure 2.2-53, where the maps show changes in forest height between 2003 and 2008 in the Traunstein test site in southern Germany [RC-234]. The top shows the change map derived from Pol-InSAR measurements, while the bottom shows the corresponding map derived from airborne lidar measurements acquired in the same years. The sensitive ecological value of these maps becomes clearer when forest height change is plotted against forest height as shown in Figure 2.2-54. The results on the top and bottom were derived from Pol-InSAR and lidar measurements, respectively. The two figures directly reveal growth rates and can be used to describe forest productivity at stand as well as forest level.

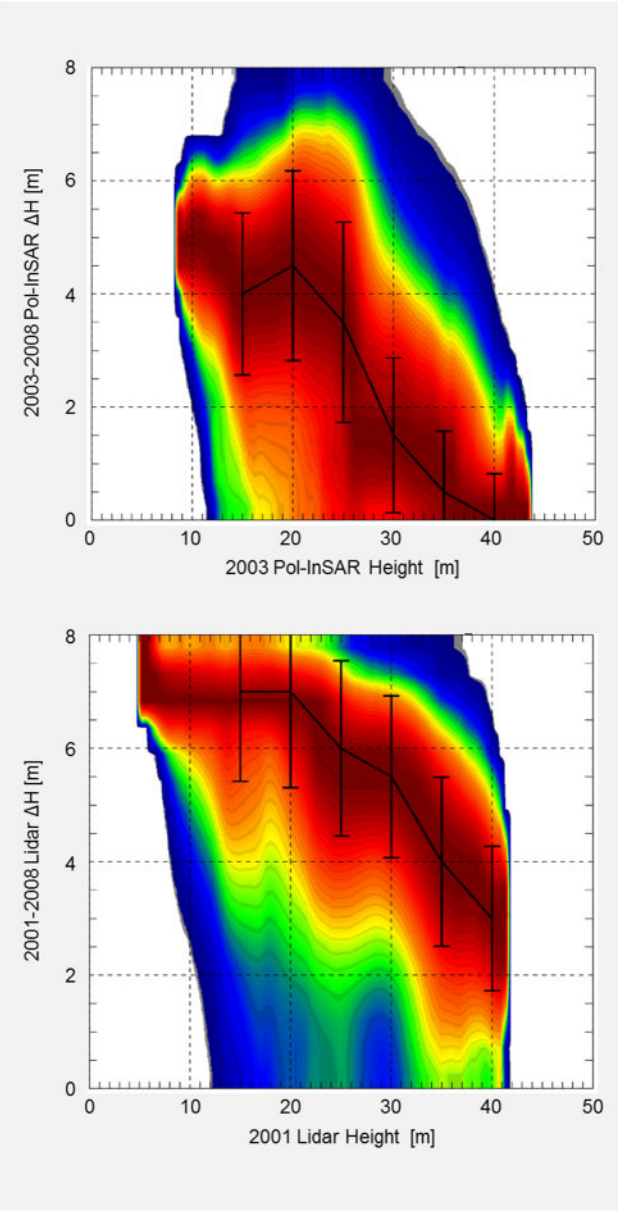

Figure 2.2-54 Forest height change ΔH vs. forest height for the change maps shown in Figure 2.2-53: Pol-InSAR-estimated change between 2003 and 2008 (top) and lidar-estimated change between 2001 and 2008 (bottom).

However, the most striking developments have been achieved with respect to forest structure. In the framework of the forest activities within the Helmholtz Alliance Remote Sensing and Earth System Dynamics, forest structure has been recognized as the element that allows the connection of modern aspects of forest ecology – far beyond forest biomass and productivity – to radar remote sensing. On the one hand, 3-D forest structure reflects the state of the forest and its evolution, while on the other hand, it may be derived from 3-D radar reflectivity measurements.

The evolution and refinement of coherent multi-baseline (tomographic) processing techniques dramatically increased the quality of the reconstructed 3-D radar reflectivity. This provided a deeper insight into the 3-D scattering processes at different polarizations and frequencies, as well as into the opportunities arising from this new measurement technique to monitor and investigate 3-D forest structure. Figure 2.2-55 compares vertical profiles at P and L band with lidar waveforms over three different ground inventory plots within the Lopé National Park in Gabon [IC-25]. The data were acquired in 2016 during the AfriSAR campaign. For each inventory plot, 8 profiles are extracted from the full 3-D data sets. These profiles, which are separated by 10 m, are superimposed in Figure 2.2-55 and give an impression of the structure variability. The first plot (left column) is very homogeneous. While the lidar waveforms have only a distinct maximum close to the top canopy height at ~40 m due to the high attenuation, the L- and P-band profiles reveal scattering contributions close to the ground. In the second plot (middle column), most lidar waveforms have a pronounced maximum around 30 m, accompanied by weaker contributions at lower heights. The L- and P-band profiles behave similarly. However, the contributions closer to the tree tops are less pronounced at P than at L band. Finally, the third plot (right column) appears highly heterogeneous. In the lidar waveforms, the strongest contributions are located between 20 and 40 m. At P band, the main contributions are distributed within a narrower height range. At L band these contributions are more pronounced than at P band and reveal stronger contributions closer to the ground that are "invisible" at P band.

In order to interpret the 3-D radar reflectivity in relation to physical forest structure and to create a common framework for field inventory and remote sensing data, a new concept was developed based on the fact that horizontal and vertical forest structure measures are complementary. Accordingly, forest

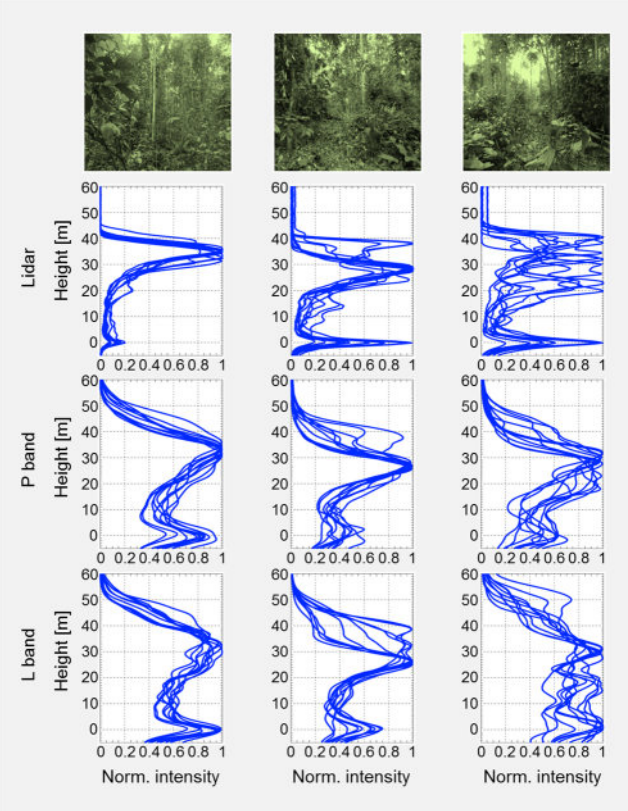

Figure 2.2-55 Reflectivity profiles reconstructed by SAR tomography at P and L band compared to lidar waveforms for three ground inventory plots within the Lopé National Park in Gabon. Eight profiles separated by 10 m have been extracted for each inventory plot from the full 3-D data sets. The data were acquired in the framework of the AfriSAR campaign in February 2016.

reflectivity structure was addressed in terms of a horizontal (e.g., stand density index) and a vertical (e.g., tree height heterogeneity) descriptor that allow the definition of a 2-D plane where stands can be projected according to their structure complexity (see Figure 2.2-56) [RC-70]. The concept of classifying forest types by means of horizontal and vertical structure descriptors has been adapted to the reconstructed 3-D radar signature by establishing the adequate descriptors and developing the appropriate processing methodology [J-7], [J-110], [J-111]. The new approach proved to be able to describe and distinguish a variety of temperate and tropical forest structural types [RC-70]. The same concept has been used to demonstrate the ability of horizontal and vertical structure indices derived from 3-D radar reflectivity to detect anthropogenic or natural changes in forest structure [J-7]. Figure 2.2-57 shows on the top a color composite of a polarimetric radar image of the forest of Traunstein, and below on the bottom, the vertical structure indices derived from 3-D radar reflectivity measurements performed in 2008 (left) and 2012 (right). The increase of the vertical structure index reflects the increase in forest structure complexity following the thinning of many mature stands in Traunstein.

A special case are forest applications developed in the context of the TanDEM-X mission. Differently than expected, TanDEM-X data became significant and unique for a range of

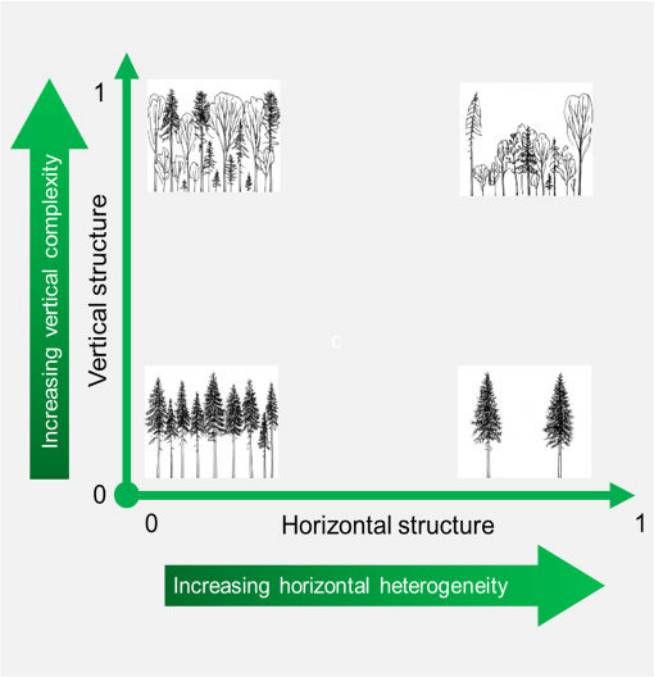

Figure 2.2-56 Forest structure classification plane on which forest stands can be projected according to their horizontal structure heterogeneity (by means of stand density index) and vertical structure complexity (by means of tree height heterogeneity).

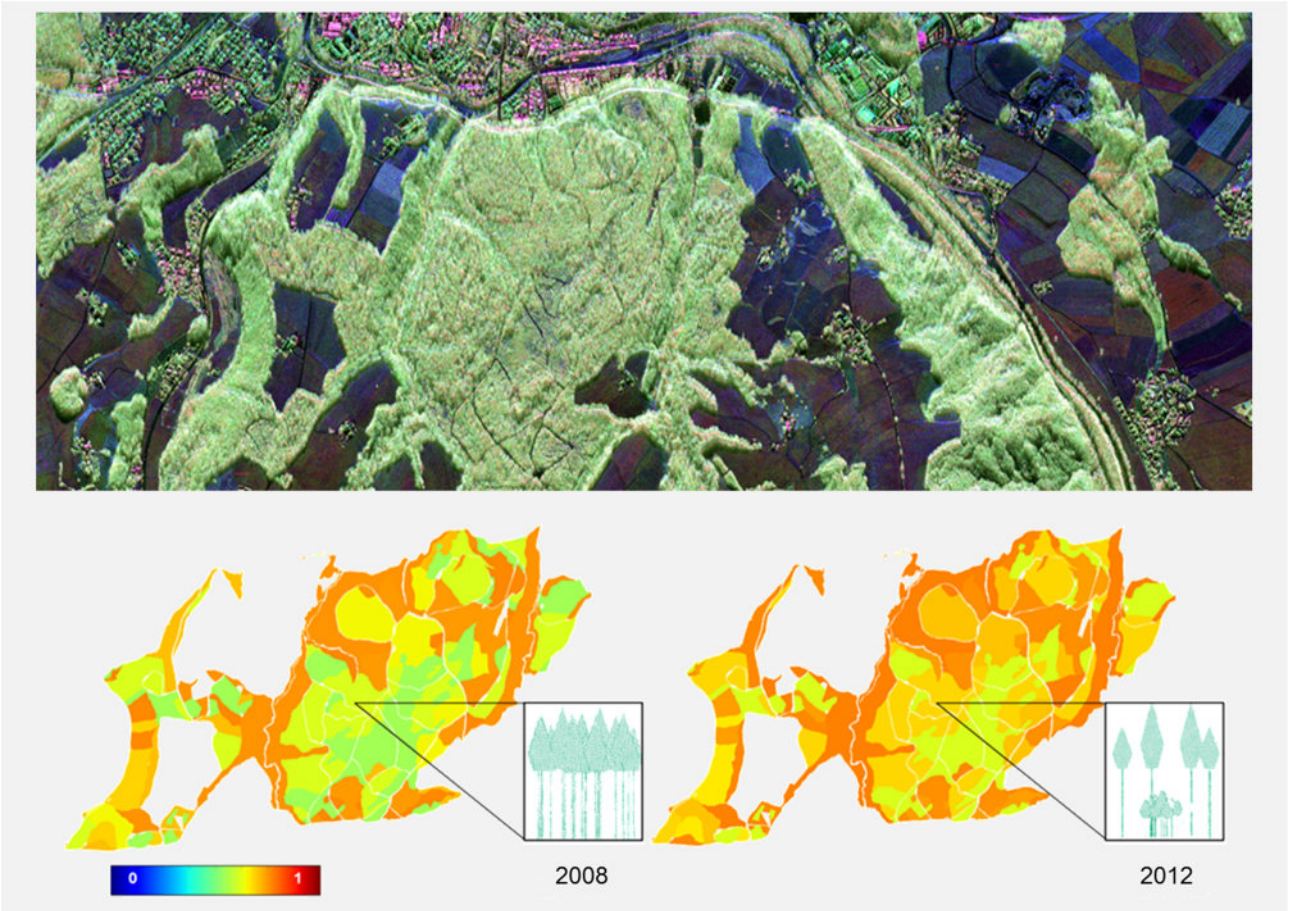

Figure 2.2-57 Top: Polarimetric Pauli RGB composite image at L band of the Traunstein test site. Bottom: Vertical structure indices derived from 3-D radar reflectivity measurements performed in 2008 (left) and 2012 (right) over the Traunstein test site. The increase of the complexity of the forest following the thinning of many mature stands, as illustrated by the insets, is reflected by a higher vertical structure index derived from the tomographic SAR data.

forest applications. While the high attenuation rates at X band limit the penetration capability into vegetation, this is partially compensated by the high spatial resolution and the absence of temporal decorrelation in TanDEM-X. Therefore, the sensitivity of the interferometric coherence to vertical forest structure proved to be valuable for a number of forest applications [J-71], [J-126].

Forest height inversion has been implemented and validated in two fashions: i) in terms of dual-polarimetric TanDEM-X data sets (usually HH and VV) without requiring any a priori information and ii) in terms of single-polarimetric TanDEM-X data sets, this time requiring the availability of an external DTM. While the first approach requires the "visibility of the ground", and is therefore limited by the penetration capability at X band, the second one performs even when the X band does not penetrate all the way down to the underlying ground. Figure 2.2-58 shows four forest height maps obtained from four different TanDEM-X data takes acquired on August 25, 2011, December 13, 2011, December 24, 2011 and January 4, 2012 over the Mawas test site located in Central Kalimantan, Indonesia. The site is covered by riverine and mainly tropical peat swamp forest disturbed by strong logging activities back in the 90s.

The agreement with the height maps from data acquired in the wet season (i.e., December and January) and their accuracy indicate a very good inversion performance. The underestimation of forest heights obtained from the data acquired at the end of the dry season (i.e., August) by about 3 m is primarily due to the dried-out tree tops, making them transparent for the electromagnetic waves, even at X band [J-126].

Agriculture Applications

The estimation of agricultural crop characteristics is essential for the assessment of crop phenology, especially during the growing and developing phases. This is important, as the knowledge of the phenology stage defines the crop water requirements and allows the forecast of potential yields. In this context, the perspective is to estimate crop characteristics from SAR measurements (alone or combined with optical remote sensing measurements) for the initialization of simulation

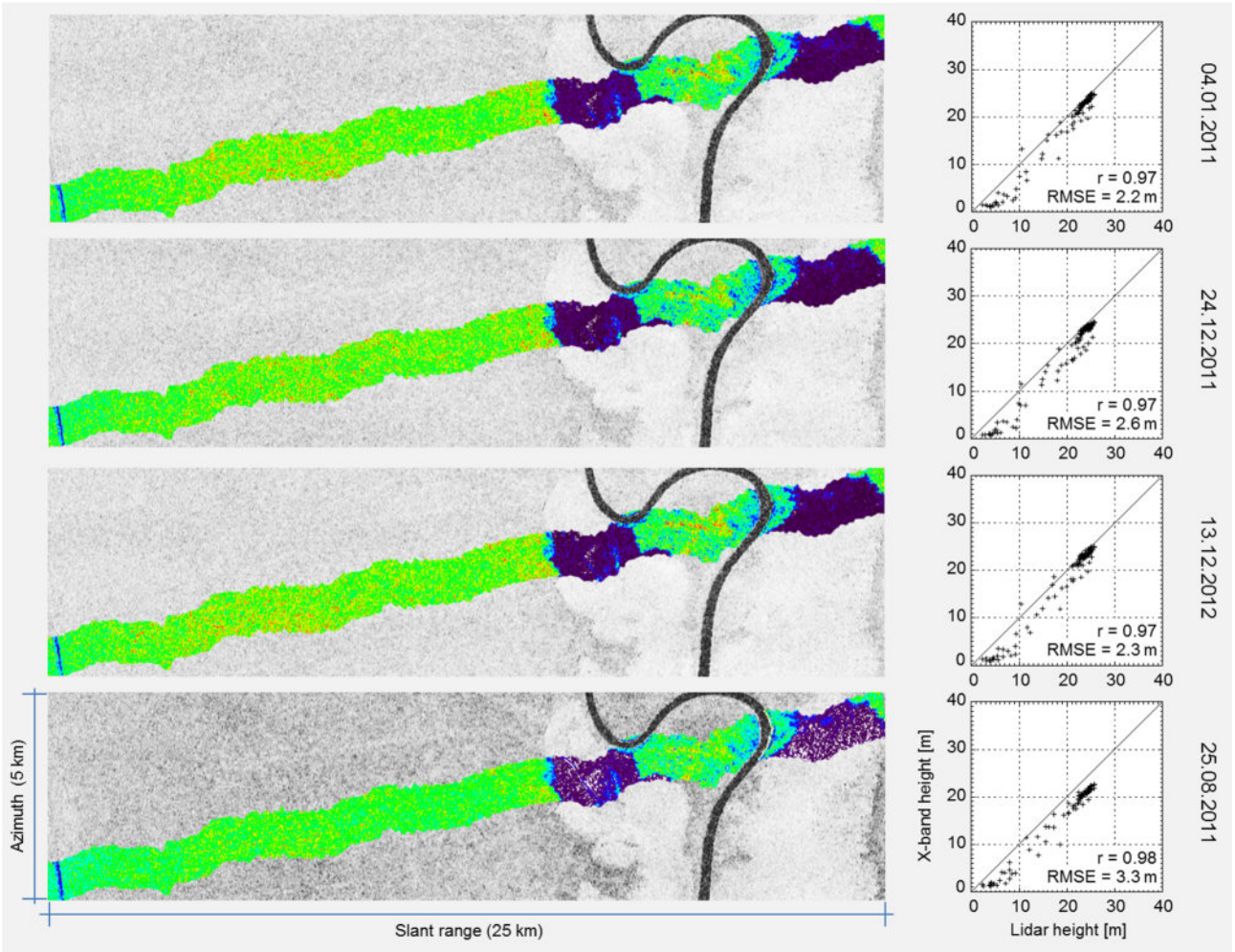

Figure 2.2-58 Forest height maps derived from four TanDEM-X acquisitions superimposed on the associated interferometric coherence images (left) and validation plots against lidar forest height measurements (right). The TanDEM-X scenes were acquired on December 13, 2011 (top); December 24, 2011 (second from top); January 4, 2012 (third from top) and August 25, 2011 (bottom) over the Mawas test site located in Central Kalimantan, Indonesia. The first three data sets were acquired in the wet season, while the last one in the dry season.

models that can predict the development and yield of crops as a function of management practices and environmental conditions. Indeed, in the last years it has been possible to make great strides toward the estimation of agricultural crop characteristics from multi-parameter SAR data [J-26], [J-159].

The first important result was the development of a dedicated polarimetric change detection algorithm based on the decomposition of the covariance matrices in two different data acquisitions, revealing the information related to the relative change (i.e., the increase or decrease of backscattering power at each possible polarization state). Multi-baseline Pol-InSAR techniques, together with a deeper understanding of the inherent ambiguity ruling the separation of ground and volume scattering contributions (in terms of covariance matrices), further enables the physical interpretation of these changes and an estimation of the (polarimetric) covariance matrices for distinct ground scattering contributions. This is a breakthrough, as it allows the separation of canonical ground (i.e., surface and dihedral) scattering contributions and opens the door for the unambiguous estimation of soil and vegetation dielectrics and their moisture content [J-17], [J-27], [IC-22], [RC-35].

Figure 2.2-59 shows the polarimetric entropy and the mean alpha angle of the ground scattering component under a corn field at X, C and L band. While the field is almost bare on the first date, the plants reach 0.6 m on June 12 and 1.7 m on July 3. The entropy of the isolated ground component remains below 0.6, confirming the presence of only two deterministic (i.e., non-depolarizing) scattering mechanisms. The alpha angle indicates an increasing dihedral contribution with plant growth, especially at X and C band.

Finally, the first multi-baseline multi-frequency SAR data time series experiments, acquired over the duration of the most important crop development cycles, and supported by detailed in situ measurements, provided the next boost in understanding the complex interaction of electromagnetic waves with agricultural vegetation. The tomographically reconstructed 3-D radar reflectivity in different polarizations and frequencies enables to resolve scattering contributions occurring at different (crop) heights and to relate their temporal evolution to changes in crop phenology. This knowledge facilitates distinguishing changes in plant geometry (as the alignment of stalks and leaves) from dielectric changes (as the drying or the water redistribution within the plants) [RC-35], [RC-270], [RC-147].

Such an impressive example is shown in Figure 2.2-60. A radar reflectivity profile along a transect that crosses a corn and a wheat field is shown on the top at C and on the bottom at L band. The profiles on the left were acquired on July 3 and the ones on the right 3 weeks later on July 24. Looking at the corn field on July 3, the dominant scattering contribution at C band is on the lower part of the plants, while at L band there is almost no vegetation effect. Three weeks later, there is a significant scattering contribution from the vegetation layer at both frequencies as a result of the water content redistribution within the plants. In these three weeks the wheat field dried out from a vegetation water content of 60% to 27%. At L band there is almost no sensitivity, while at C band the drying process is indicated by a lower located dominant scattering contribution.

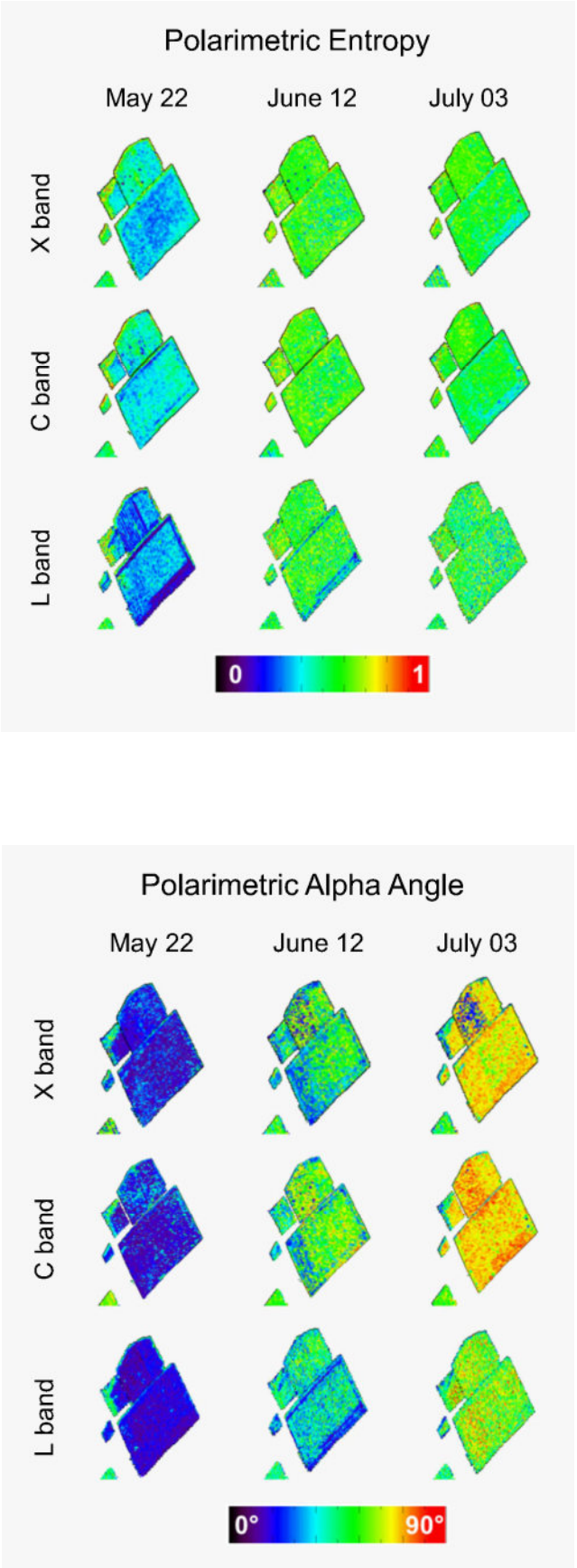

Figure 2.2-59 Polarimetric entropy (top) and mean alpha angle (bottom) maps of the ground scattering component under a corn field at X, C and L band for three different dates associated to three different development stages.

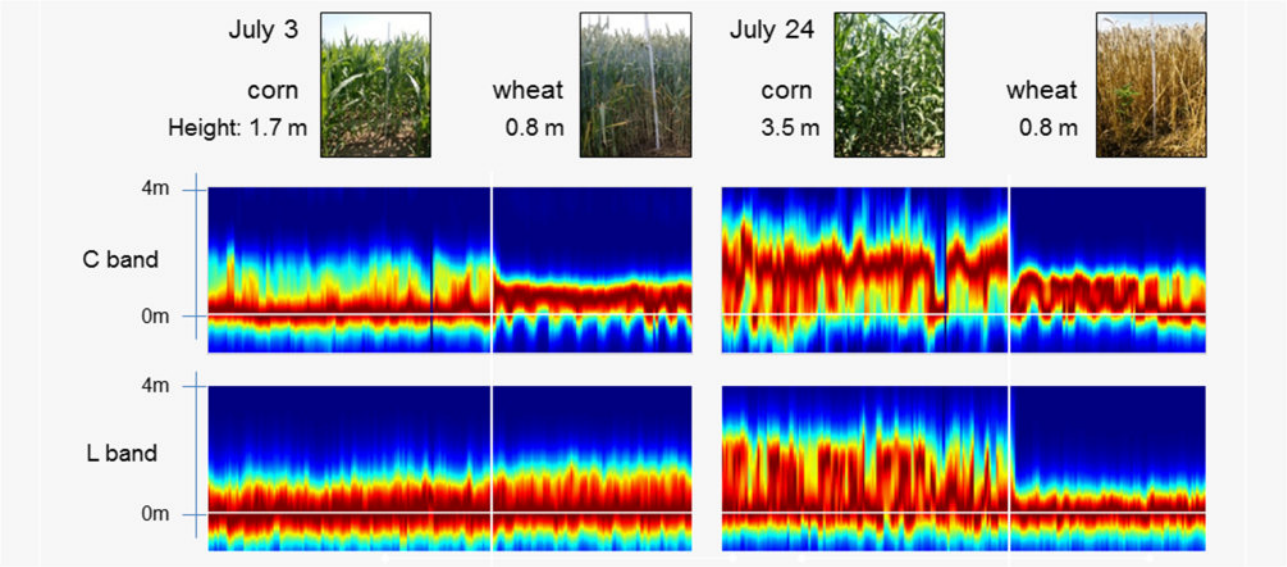

Figure 2.2-60 Reflectivity profiles along a transect that crosses a corn and a wheat field for two dates: July 3 on the left and July 24 on the right. The profiles are shown for C band on the top and L band on the bottom (both at HH polarization). In the time between the two acquisitions the corn grew from 1.7 m up to 3.5 m while the wheat dried out from a vegetation water content of 60% to 27%. The horizontal white line indicates the location of the underlying ground. The vertical white line indicates the location of the field border. The datasets have been acquired in the framework of the CROPEX 2014 campaign.

Snow and Ice Applications

The subsurface structure of snow and ice bodies is one of the critical unknowns for assessing their current condition and temporal change. The ability of microwaves to penetrate into or even through snow and ice layers and their sensitivity to geometric and dielectric characteristics make SAR configurations a unique tool for snow, firn and ice monitoring. In the last years, the evolution of snow and ice applications have undergone significant development. The first was initiated by advances in understanding the interaction of polarized electromagnetic waves with the micro-structure of snow, firn and ice volumes. Triggered by new laboratory results indicating the anisotropic structure of snow and ice, the experimental demonstration by means of polarimetric SAR measurements of dielectric anisotropy in snow and firn as a result of temperature gradient metamorphism was an important result [J-65], [J-66], [J-132].

This aspect, together with a better description of the internal structure of snow and firn layers provided by field measurements, was essential for interpreting the scattering signature at different frequencies and for the development of new retrieval algorithms. Firn and ice layers are composed of ice grains. At higher frequencies, scattering occurs on single ice grains. Lower frequencies with wavelengths larger than the grain size are not affected by single ice grains but are sensitive to grain density and orientation variations in the layer. Snow and ice packs consist of layers with different ages, densities, crystal types, and grain size. The recrystallization and sintering lead to increasing or decreasing densities, anisotropies and increasing ice grain sizes, which causes changes in the microwave propagation speed, the reflection, and the scattering properties of the snow pack. Conventional polarimetric scattering and decomposition models have been reviewed and improved on the basis of this new understanding [J-65]. Multilayer snow, firn and ice models have been developed and validated including the anisotropy (i.e., orientation distribution) and density of the ice grains, as well as enclosed ice lenses as they develop by the refreezing of melt water [J-65]. Using these new models it was possible to estimate (and validate) the thickness and structural anisotropy of snow and firn layers by means of polarimetric phase differences at different frequencies in Alpine and Polar glaciers and ice sheets [RC-168], [J-66]. At the same time, the separation of different glacier zones and the estimation of the equilibrium and firn line – i.e., the transition between the individual ice zones and their annual variation – have been demonstrated with fully polarimetric SAR data [RC-168]. Figure 2.2-62 shows a 200 km transect acquired at L band during the ARCTIC15 airborne campaign starting on the left with Greenland's west coast at an altitude of 300 m and ending on the right in the inner part of the ice sheet at an altitude of 2100 m. The high values of polarimetric HH-VV phase difference in the accumulation zone indicate the presence of a thick layer of anisotropic firn, while almost no phase difference is observed over the ablation zone where firn is absent. The clear decrease of the phase difference values in the transition between the two zones is related to the rapid decrease of firn with altitude. The red line indicates the equilibrium line, at about 1700 m, which ideally separates the ablation from the accumulation (firn) zone.

The second important development step was facilitated by a number of multi-baseline or tomographic Pol-InSAR data sets acquired in the frame of airborne experiments on Alpine and Polar glaciers. The tomographic reconstruction of the 3-D radar reflectivity at different polarizations and frequencies critically improved the understanding of the penetration and of the 3-D scattering processes occurring in firn and ice sheets. Accordingly, the access to the 3-D reflectivity enables the separation of scattering at the snow-ice interface from subsurface scattering occurring in the underlying ice volume and to detect air, water and/or firn bodies embedded in the ice volume, as well as surface-like layers at different depths [RC-166]. Figure 2.2-61 shows tomographic reflectivity profiles of a 1 km long transect site in Greenland from data acquired

in the frame of the ARCTIC15 campaign. At L band, the top layer is 1-2 m lower than the reference top layer estimated by GPS as the upper snow layer becomes more and more transparent at lower frequencies. A thin subsurface layer is visible along the whole transect approximately 5 m below the upper surface. At HH, a deeper discontinuous layer at -30 m becomes visible, while at HV a third layer at -10 m can be clearly distinguished. The penetration depth is about 40-50 m. At P band a similar picture is obtained, but it is more blurred as a result of the increased volume decorrelation due to the deeper penetration. Scattering contributions become visible down to 60 m.

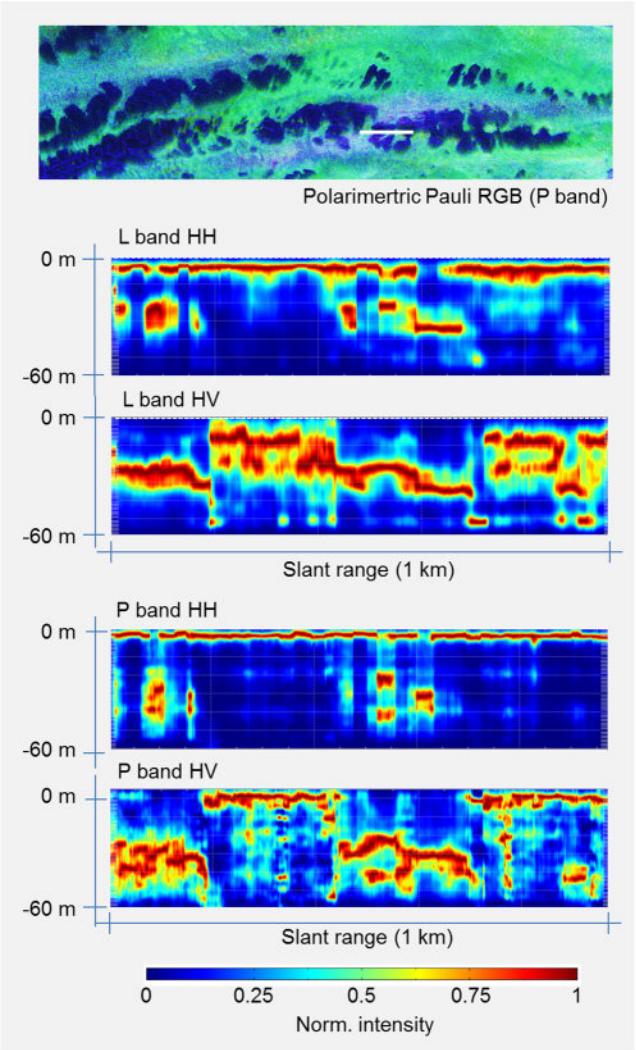

Figure 2.2-61 Reflectivity profile along a 1 km long transect in the K-transect site in Greenland. From top to bottom: at L band in HH and HV, and at P band in HH and HV polarizations. The location of the transect is indicated by the white line segment on the polarimetric Pauli RGB at P band shown on the top.

Geosphere

One of the most successful SAR applications in the geosphere is interferometry. Its main two products are the generation of DEMs with metric accuracy and resolution, as demonstrated by the TanDEM-X mission (see Section 2.1.2), and the retrieval of deformation with sub-centimetric precision and metric resolution by means of differential interferometry (see Section 2.2.4). The latter encompasses a wide range of applications, especially focused on the risk management of geohazards like earthquakes (occurring mainly due to tectonic strain), volcanoes, landslides, inactive mines or coastal subsidence and floods. The monitoring of urban scenarios for hazard prevention in the presence of subsidence due to ground water extraction or construction is also extensively exploited, since the high spatial resolution of SAR allows for the monitoring of single buildings. As an example of geohazard monitoring activities at the Institute, Figure 2.2-64 shows the deformation measured with two Sentinel-1A acquisitions after the eruption of the Calbuco volcano in Chile on April 22, 2015. The data were interferometrically processed and calibrated at the Institute, and subsequently provided to scientists of the German Research Centre for Geosciences (GFZ), who used the data to improve the modelling of the source and in this way increase

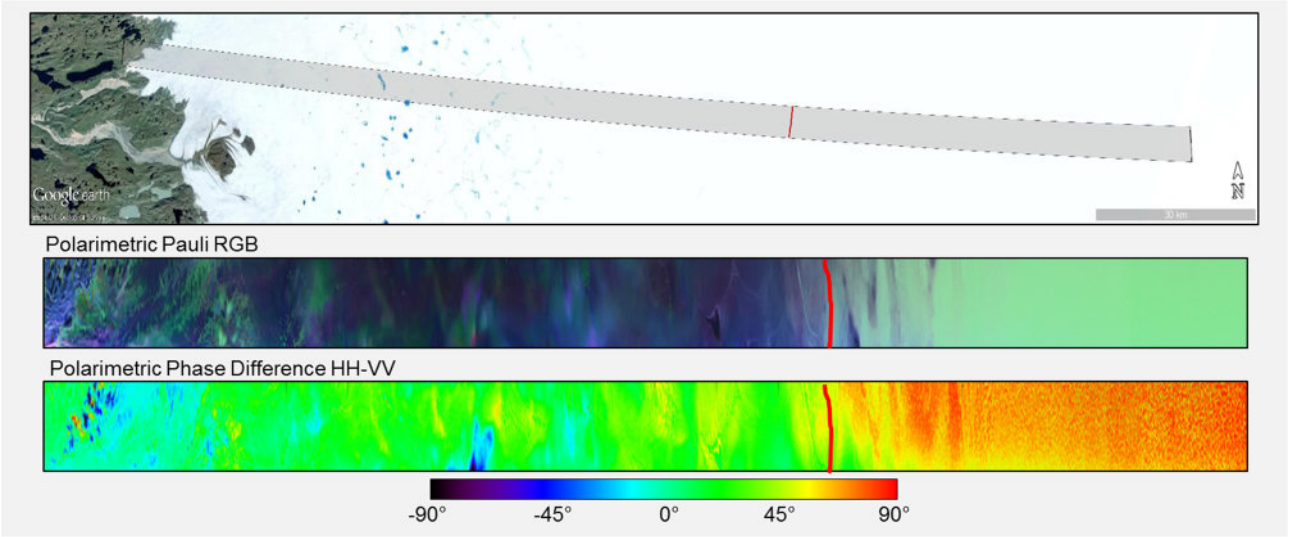

Figure 2.2-62 Quad-polarimetric transect acquired at L band during the ARCTIC15 campaign with a length of 200 km starting on Greenland's west coast at an altitude of 300 m (left) and reaching through to the inner part of the ice sheet at an altitude of 2100 m (right). The red line indicates the equilibrium line, located at an altitude of about 1700 m, which separates the ablation from the accumulation (firn) zone. The polarimetric Pauli RGB composite image is shown in the middle. The polarimetric HH-VV phase difference is shown on the bottom.

understanding of the underlying processes that triggered the eruption of the volcano [J-29]. Another example of geohazard risk management is presented in Figure 2.2-63. The image shows the co-seismic deformation measured with two Sentinel-1A and Sentinel-1B interferograms of the M 6.2 (4 km depth) earthquake that hit central Italy on August 24, 2016. In this particular case, thanks to the availability of the two Sentinel-1 units – which reduces the revisit time to only six days – the east-west/vertical inversion could be computed just three days after the event, hence providing further relevant information for modelling and risk management. Two further seismic events took place in central Italy on October 26 and October 30, and were likewise monitored by the Sentinel-1 constellation. The data processed at the Institute were provided to the National Institute of Geophysics and Volcanology (INGV) as part of a cooperation in the frame of the InSARap study of the European Space Agency [IC-26], [IC-28].

As presented in Section 2.2.4, the PSI technique exploits image stacks to retrieve the time series of the deformation, and is being intensively exploited for both urban and risk management. Figure 2.2-65 shows an example of the mean deformation velocity map retrieved over the Campi Flegrei caldera, Italy, by exploiting a stack of 105 Sentinel-1A and Sentinel-1B images acquired between April 2015 and November 2017. For this particular run, two Sentinel-1 sub-swaths were processed, with a total coverage of 170 km × 150 km. This example also shows the potential of differential interferometry combined with wide swath acquisitions for deformation

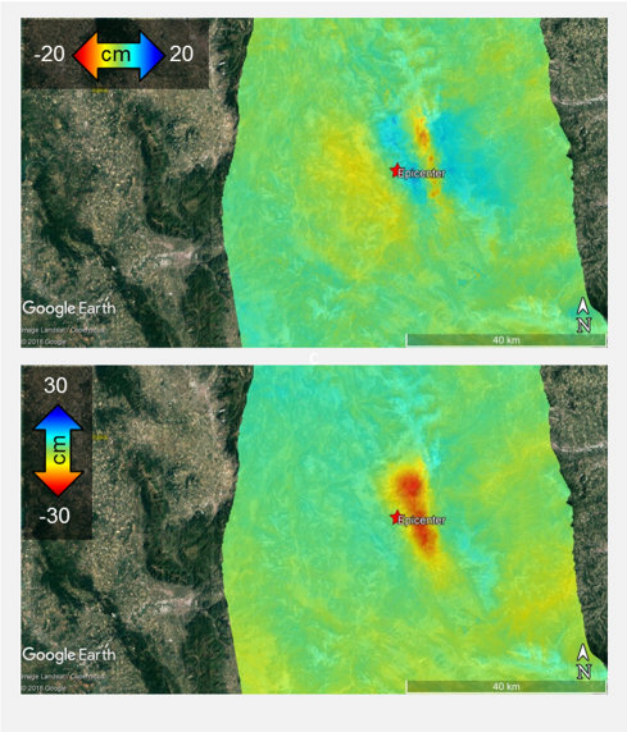

Figure 2.2-63 Co-seismic deformation due to the earthquake that hit central Italy on August 24, 2016. Horizontal (top) and vertical (bottom) deformations estimated from two Sentinel-1A and Sentinel-1B 6-day repeat-pass ascending/descending interferograms. The vertical displacement was larger than 30 cm in some areas.

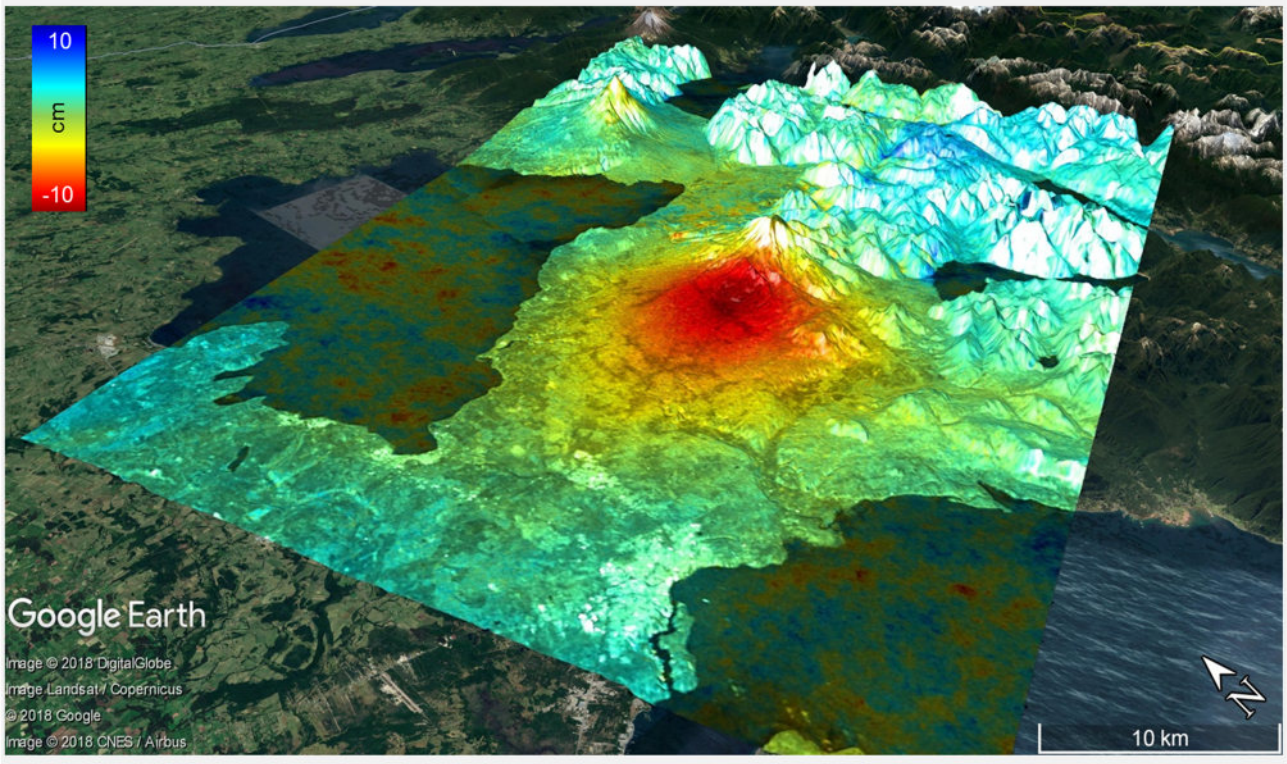

Figure 2.2-64 Artistic view of the deflation measured with two Sentinel-1A acquisitions after the eruption of the Calbuco volcano on April 22, 2015 in Chile. The interferogram was processed and calibrated at the Institute. The two Sentinel-1 passes were acquired on April 14 and April 26 in an ascending configuration. The deflation of the volcano after the eruption can be clearly observed, reaching a maximum of 10 cm in the line-of-sight direction. These data were used in cooperation with the German Research Centre for Geosciences to improve the modelling of the source and to better understand the underlying processes that triggered the eruption.

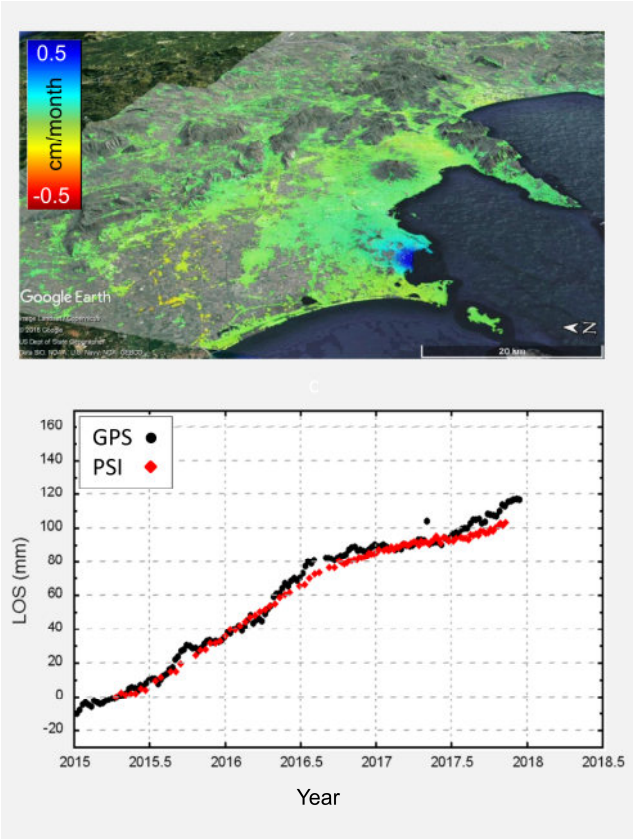

Figure 2.2-65 Mean deformation velocity map obtained via PSI processing of 105 Sentinel-1A and Sentinel-1B images acquired between April 2015 and November 2017 over Italy in descending configuration. The uplift at the Campi Flegrei caldera can be clearly observed (bluish area close to the sea). The plot on the bottom shows the good agreement between the retrieved time series deformation (dotted red) and the cGPS measurements (dotted black) at the ACAE monitoring station. The analyses were performed in cooperation with the National Institute of Geophysics and Volcanology (INGV), Vesuvius Observatory, who provided the comparison with the cGPS measurements.

monitoring. The uplift measured at the caldera (bluish area close to the sea) can be clearly observed and agrees well with in situ geodetic measurements performed with continuous GPS (cGPS) and leveling.

By combining the measurements obtained in ascending and descending configurations, the east-west and vertical motions were also retrieved and validated. Similar to the previous example, the presented results were obtained in the frame of the InSARap study with ESA. With these measurements, geophysicists can improve the modelling of the source under the caldera to allow a better monitoring and risk assessment.

2.2.9 Ice Sounding

In 2011, following previous studies on spaceborne systems, the Institute initiated a new activity on airborne ice sounding with digital beamforming, including algorithm development for surface clutter suppression for high-altitude ice sounding radars. Depending on the flight altitude and the characteristics of the ice sheet, each range bin of the signal received by an ice sounder may be composed of returns from the ice surface, internal layers and the bed. Provided that the ice sounder has multiple receiving channels in the across-track direction, it is possible to suppress unwanted off-nadir echoes and/or focus those contributions at their original across-track positions, therefore allowing for a 3-D SAR imaging mode.
Data from the POLARIS P-band system, built by the Technical University of Denmark (DTU) under contract with ESA, were analyzed in the frame of a funded ESA study. In February 2011, POLARIS was operated with four antenna phase centers in cross track to acquire data at the Jutulstraumen outlet glacier in Antarctica. The investigation concerned the suitability and performance of the following algorithms adapted to the purpose of surface clutter suppression: traditional beamforming, nulling and optimum beamforming for clutter angles derived from a digital elevation model, and data-adaptive minimum-variance distortionless-response (MVDR) beamforming. The optimum and the MVDR beamformer proved to be robust against noise scaling, which originated from the large separation of the across-track apertures. Due to noise scaling, the simple nulling approach proved insufficient for a considerable range of depth values, whereas simple beamforming did not remove the clutter to the same extent

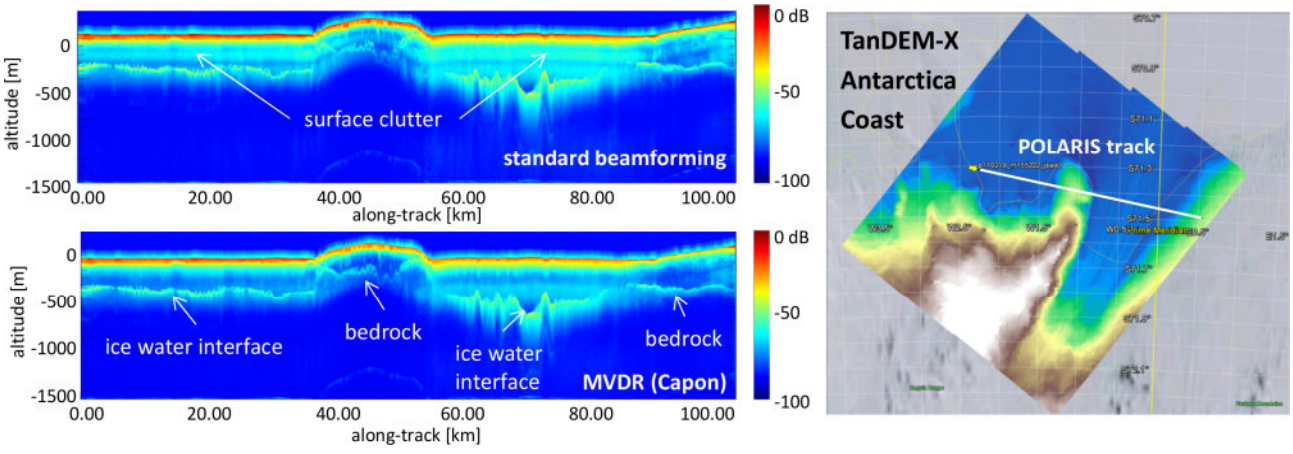

Figure 2.2-66 First results of digital beamforming for radio echo sounding showing improvement in ice surface clutter suppression when MVDR (bottom left) is compared to standard beamforming (top left). The data were acquired in 2011 at P band (435 MHz) by ESA's POLARIS sensor at Jutulstraumen glacier, Antarctica, along a linear flight track as indicated by the white line in the TanDEM-X DEM shown on the right. The faint yellow contour marks the continent border.

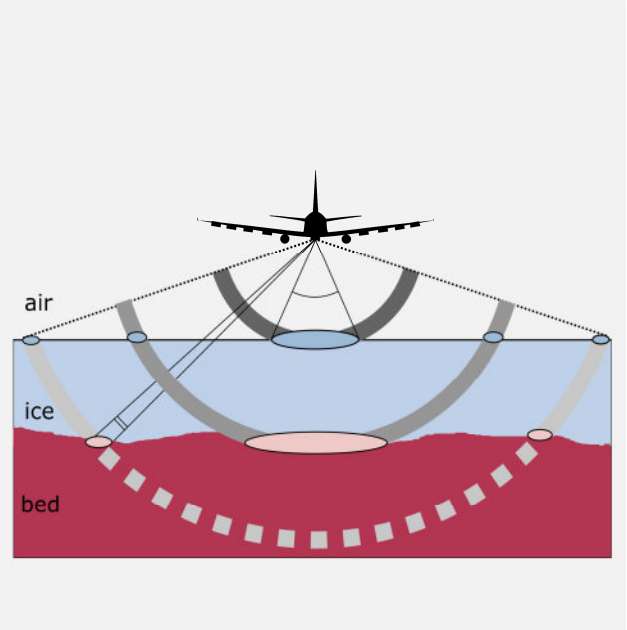

Figure 2.2-67 Across-track geometry of ice sounding radar operation with multiaperture antenna systems

as the other approaches (see Figure 2.2-66) [RC525], [B-IC130].
The analyses have also been extended towards analyzing the feasibility of clutter suppression for a P-band spaceborne sensor operating with a multiple receive antenna aperture. A minimal spaceborne sounder system with three receive apertures has been investigated, each with dimensions of 4 m x 4 m and separated by 4 m. It has been shown that clutter suppression is feasible for a symmetric geometry with negligible across-track slope of the ice surface. However, a fourth aperture adds stability to the reconstruction and should be considered, while separations larger than the aperture size affect certain reconstruction methods for specific depth and should be avoided.
The across-track arrangement of antenna elements also allows the 2-D retrieval of ice bed topography and the measurement of the internal layers' slopes in cross track (cf. Figure 2.2-67). The question was whether techniques used in SAR tomography can be adapted and extended to become beneficial in this case. Thus, the Institute established a cooperation with the Kansas University Center for the Remote Sensing of Ice Sheets (CReSIS) and received data acquired with the Multichannel Coherent Radar Depth Sounder (MCoRDS) in Greenland at VHF frequencies (150 MHz) with up to 16 antenna phase centers.
The physical dimensions of the aircraft limit the achievable electrical length of the across-track baseline. This fact presents a challenge for conventional beamforming, as its resolution is inversely proportional to the available baseline. We investigated the use of MVDR and, for the first time, also sparse signal reconstruction approaches, implemented using the M-FOCUSS algorithm (MMV Multiple-Measurement-Vectors FOCal Underdetermined System Solver). The algorithm seeks to solve the tomographic inverse problem by putting a sparsity restraint on the unknown signal in across-track direction. The algorithm additionally imposes smoothness of the unknown signal in azimuth, thereby achieving additional robustness against noise [RC24], [RC131]. As compared to MVDR, the use of M-FOCUSS offers better denoising, which improves the contrast of SAR tomograms of the ice sheet as demonstrated in Figure 2.2-68. If provided with an optimal sparsifying dictionary, it also leads to a better resolution of the ice sheet features in across track, thus ensuring a better quality of the inputs needed for the modelling of the ice sheet mass balance (such as across-track orientation of the internal layers and the bed). It also allows for improved detection of the bed under low SNR conditions, which usually happens at great depths or for outlet glaciers.
The advantage of sparse reconstruction lies in its ability to work under various ranges of sampling geometries as well as with a limited number of receive channels. The latter is critical in ice sounding applications, as it is prohibitively hard to design airborne sensors with large across-track apertures in the VHF range.

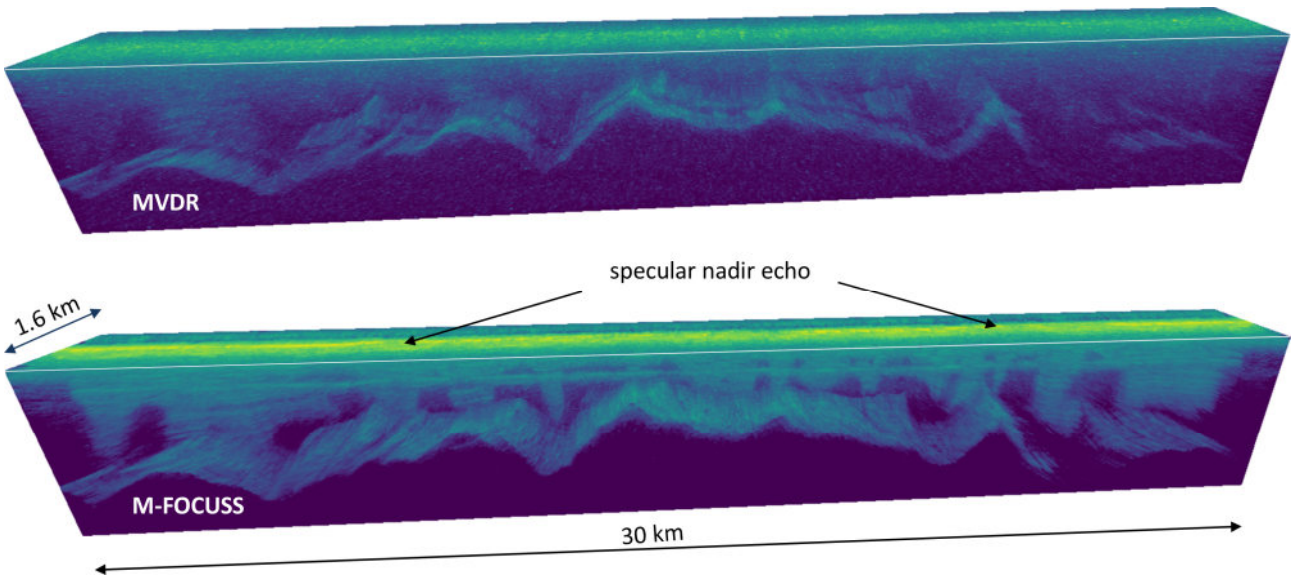

Figure 2.2-68 Qualitative comparison of MCoRDS data processed with state-of-the-art MVDR (top) and a newly developed M-FOCUSS approach based on compressive sensing. Processing with M-FOCUSS improves contrast, spatial resolution and SNR.

2.2.10 Traffic Monitoring

The Institute's activities in the field of road and maritime traffic monitoring have evolved during the past years. The Institute has been involved in DLR projects and also in several third-party funded studies related to air- and spaceborne traffic monitoring. For radar-based traffic monitoring, multiple receiving antennas arranged in along-track direction are needed in general. With multiple antennas, the scene on ground is seen from the same point in space at slightly different times. This is the key for detecting slowly moving vehicles embedded in a strong clutter environment, and for accurately estimating their geographical positions, velocities and moving directions.

Airborne Traffic Monitoring

The DLR projects VABENE and VABENE++ are related to traffic management in the occurrence of large scale events and disasters. Herefore, a novel a priori knowledge-based multichannel ground moving target indication (GMTI) processor with an incorporated OpenStreetMap road database and digital elevation model (DEM) was developed [J-175], [RC-550], [RC-98]. The processor uses space-time adaptive processing (STAP) for clutter suppression, as well as a novel error model which makes it possible to reduce the number of false detections [J-1]. The training data needed for effective clutter suppression are selected automatically. One further advantage of the developed processor, compared to state-of-the-art processors, is that only small sections around the roads need to be processed instead of the full data set. This reduces the required computation power, and hence the processing time significantly, and opens the door for real-time capability [RC-183]. A traffic monitoring result obtained with four-channel F-SAR data is shown in Figure 2.2-69.
The investigations carried out in the VABENE project resulted, among others, in a comprehensive book chapter on "Multi-Channel SAR for Ground Moving Target Indication" which is published in [B-7].

In addition, in VABENE++ the capabilities for using consumer mobile phone LTE equipment to transmit traffic data and high-resolution radar images from DLR's research aircraft DO 228 to the ground were successfully demonstrated [RC-312], [IC-38]. The acquired experience was exchanged with experts from Airbus Helicopters in Donauwörth who are interested in integrating such capabilities on their platform. Furthermore, a new high-gain X-band antenna with 6 receiving channels was developed. This antenna will further improve the traffic monitoring performance and will even enable future investigations on novel multichannel algorithms.

Maritime Moving Target Indication and Imaging

Since 2016, the Institute has been involved in the DLR project EMS II. The objective of this project is to acquire and use multichannel F-SAR and DBFSAR/VSAR airborne radar data to investigate and demonstrate new methods and applications for maritime security. A novel generalized inverse SAR (ISAR) processor has been developed in this context [RC-6], [R-61] (cf. Figure 2.2-70). This processor is able to generate high-resolution ISAR image sequences and high-resolution range profile sequences of moving ships, regardless of whether the data were acquired during linear, circular or arbitrary flight tracks of the radar platform (cf. Figure 2.2-71). The images and range profiles can be used for ship classification and recognition purposes. One ISAR imaging result obtained from a circular flight track with the antenna pointing to the outside of the circle is shown in Figure 2.2-72. The ISAR processor was evaluated with real fully polarimetric F-SAR data, simultaneously acquired in X and L band during a two-day North Sea flight campaign near Cuxhaven. As ground truth, automatic identification system (AIS) data transmitted from the ships were provided. In addition, the Bad Bramstedt BP24 ship, operated by the German federal police, carried out some maneuvers with different velocities. During each circular flight track with the antenna pointing to the circle center, the police ship was observed for approximately 7 minutes by the radar. Thanks to the acquired unique data pool, it will be possible to investigate novel imaging and

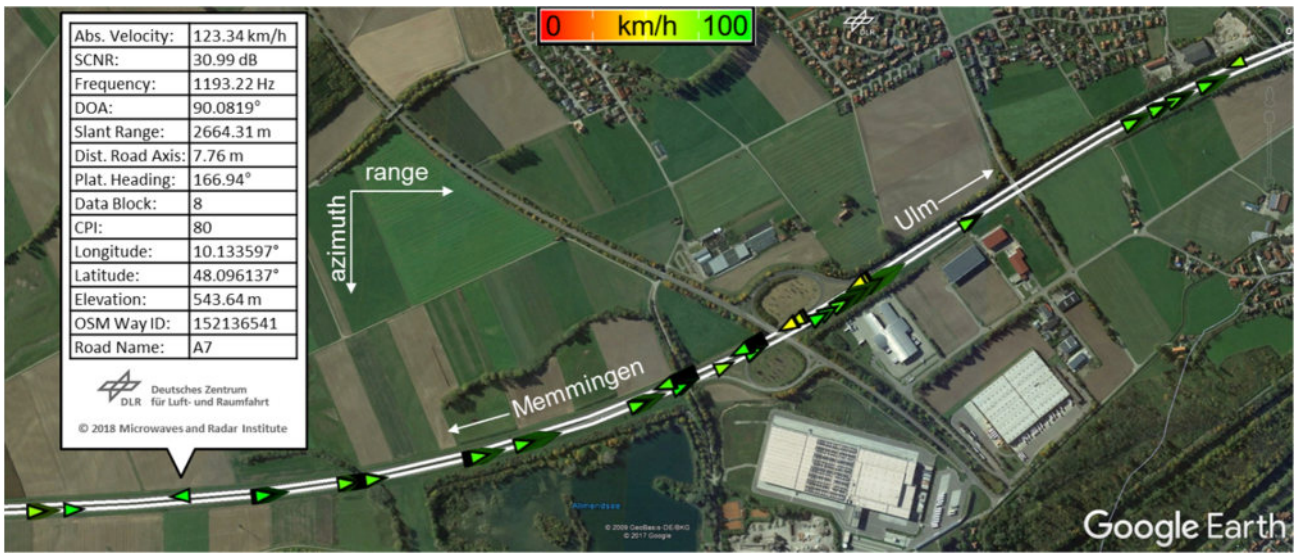

Figure 2.2-69 Traffic monitoring result obtained from the novel a priori knowledge-based multichannel GMTI processor. The automatically detected vehicles are shown as color-coded triangles, and the autobahn A7 road axes are shown in white. Each vehicle was detected several times and observed for a few seconds.

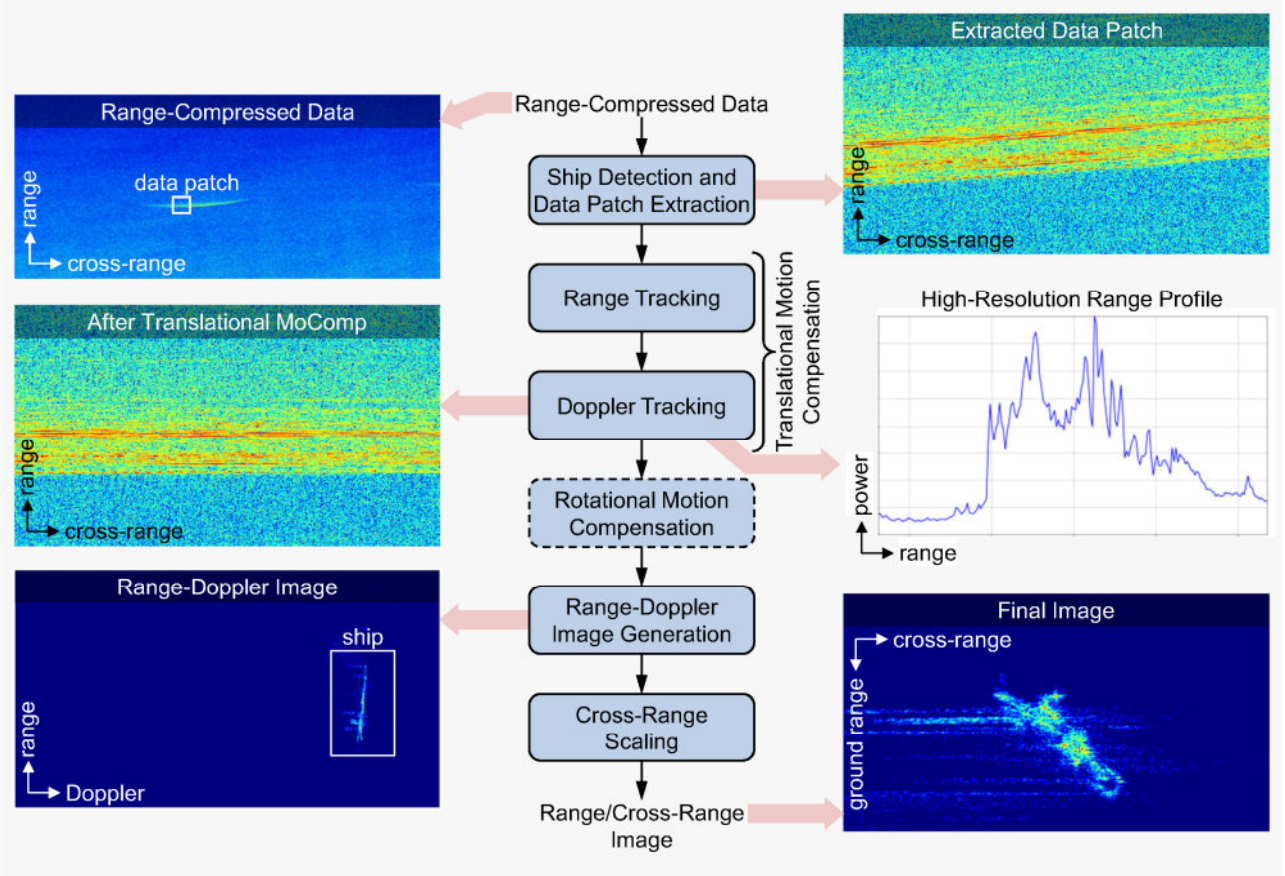

Figure 2.2-70 Simplified block diagram of the novel ISAR processor which generates a high-resolution ISAR image sequence of moving land and maritime vehicles, regardless of whether the data were acquired during linear, circular or arbitrary radar platform flight tracks.

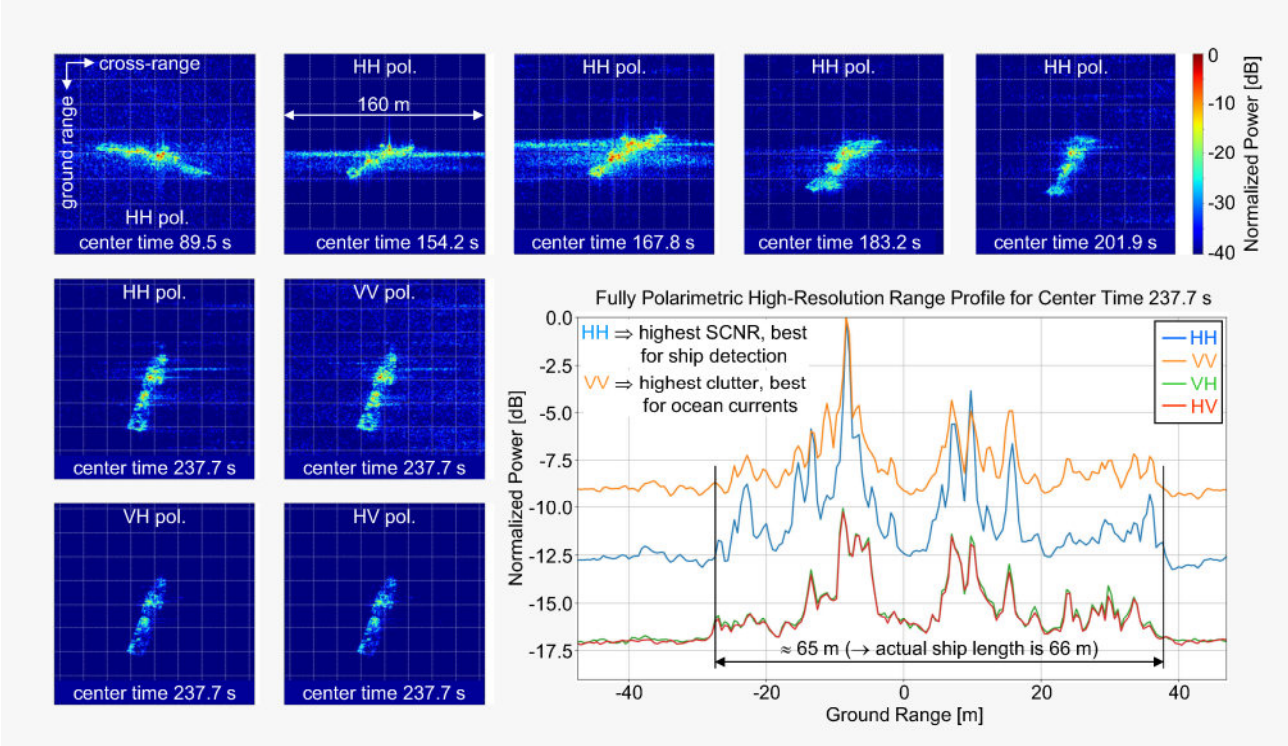

Figure 2.2-71 Automatically obtained X-band ISAR image sequence of the Bad Bramstedt police ship (top and left) and the fully polarimetric high-resolution range profile (bottom right) corresponding to the images labelled with a center time of 237.7 s. The radar data were acquired during a circular F-SAR flight at 5600 m altitude. The coherent integration time per ISAR image was set to 1.7 s.

tracking algorithms, as well as ocean surface clutter models needed for constant false alarm rate (CFAR) ship detection in the future. One goal of the EMS II project is for the full ship processing chain including detection, tracking, ISAR imaging and AIS data fusion to run on the on-board processing hardware developed in VABENE and VABENE++. A dual-channel AIS receiver was additionally integrated into one of the DBFSAR/VSAR racks for AIS data fusion.

Future Systems

Different Ka-band spaceborne system concepts with a clear focus on moving target indication applications were proposed and investigated within the "Multichannel Ka-band SAR for moving target indication" study, funded by the European Space Agency (ESA). In the frame of this study, a comprehensive moving target performance estimator was also developed and verified with Monte Carlo simulations. One advantage of the short Ka-band wavelengths is that a very good GMTI performance can be achieved from space, even with comparatively small along-track antenna separations. The drawback is that rather high pulse repetition frequencies (PRFs) beyond 10 kHz are needed for classical GMTI processing. This requirement would result in a significantly decreased swath width in the order of 10 km. A completely novel GMTI processing scheme was proposed to overcome this problem.

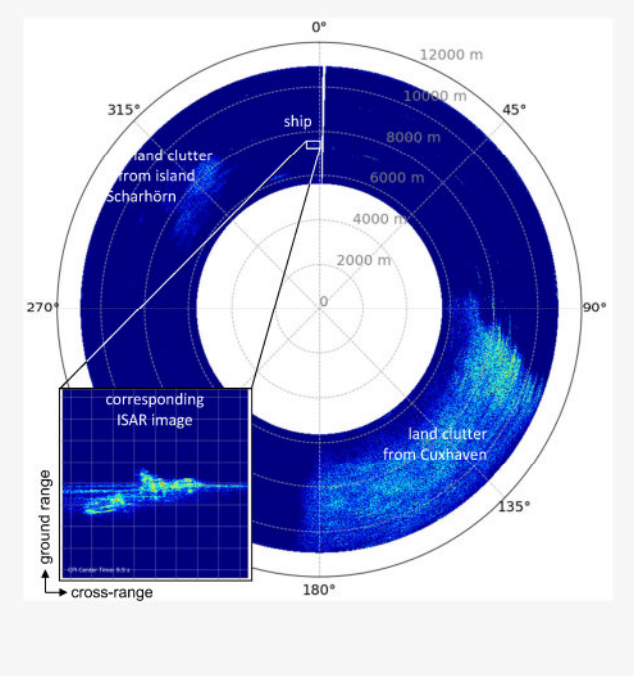

Figure 2.2-72 Polar plot of range-compressed X-band data showing an annulus acquired near Cuxhaven, Germany. The data contain several ships as well as land clutter from the town Cuxhaven (bottom right) and Scharhörn island (top left). One of the detected ships is highlighted and its corresponding ISAR image is shown on the bottom left.

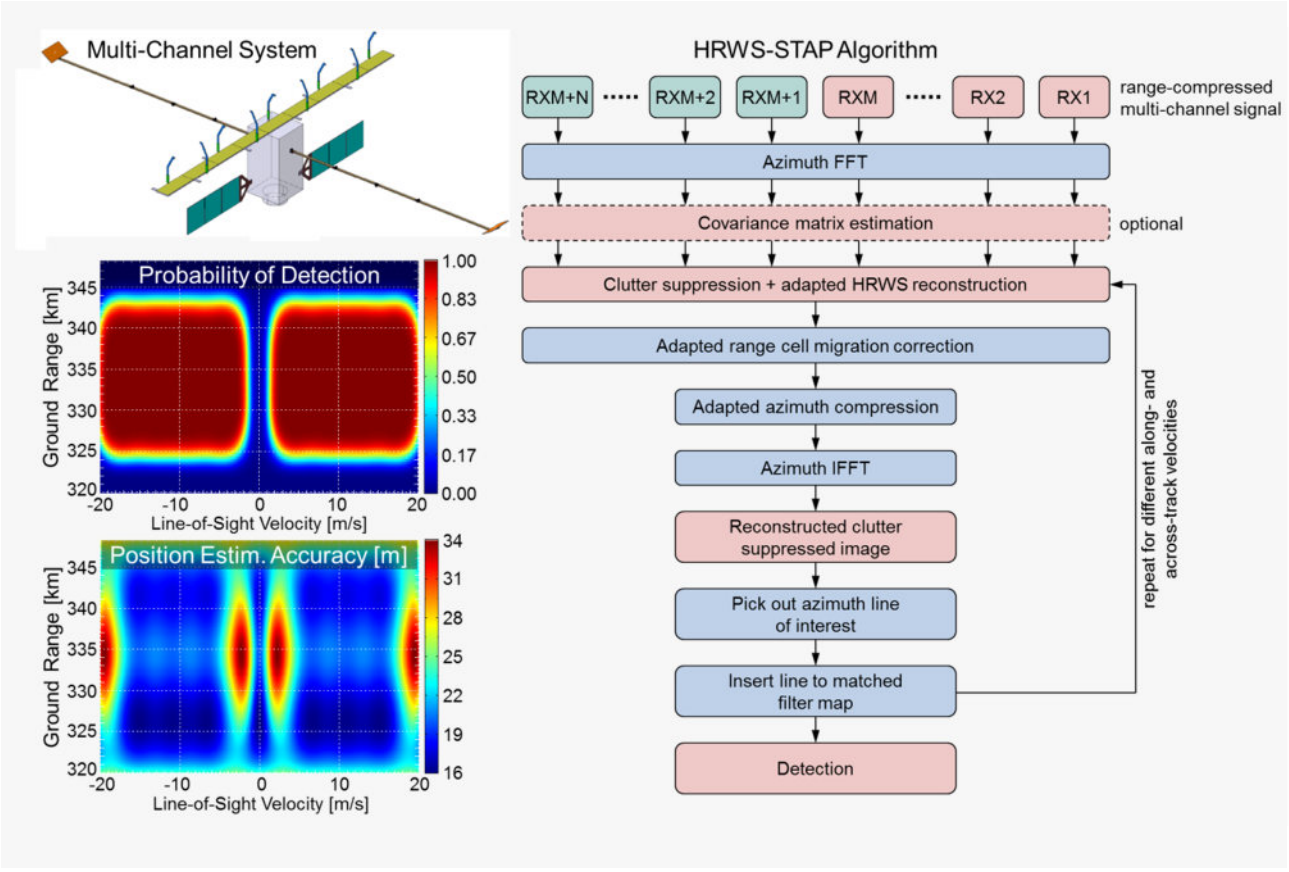

Figure 2.2-73 The structure of a novel low PRF algorithm with incorporated space-time adaptive processing is shown on the right. This algorithm can, for instance, be used for the proposed multichannel Ka-band system depicted on the top left. HRWS across-track interferometry (XTI) and GMTI can be carried out simultaneously without changing the system operation mode and the PRF. The achievable GMTI performance for a particular scenario is also shown (bottom left).

Several novel low PRF GMTI algorithms were developed and verified with comprehensive Monte Carlo simulations [J-77] and real multichannel F-SAR data [RC-99]. These novel algorithms make it possible to decrease the PRF significantly. Simultaneous High-Resolution Wide-Swath (HRWS) SAR imaging and GMTI is enabled without changing the system operation mode and the PRF.

An exemplary multichannel Ka-band system investigated in the study is shown in Figure 2.2-73. The proposed HRWS-GMTI ideas finally resulted in a patent, which the Institute holds together with Airbus Defence and Space [P-1].

In 2015, the Institute was involved in a third-party study funded by Airbus Defence and Space Ottobrunn. The task was to investigate the SAR imaging and GMTI performances of different low-power and low-weight radar configurations that fit on their Zephyr platform. This slowly flying high-altitude pseudo satellite (HAPS) platform is operated in the stratosphere and powered by solar cells. The design driver in the study was the very limited available transmit power. Eventually, it turned out that with a well-designed radar and operation mode – even with a low peak transmit power in the order of 50 W – a swath width of 25 km can be imaged with a reasonable quality from an altitude of 20 km [R-131]. With a sufficiently long antenna, integrated for instance in the fuselage of the HAPS, maritime moving target indication (MMTI) with swath widths of up to 100 km is possible [RC-5].

2.2.11 Ionospheric Characterization and Calibration

The increasing importance of spaceborne SAR missions operating at lower frequencies entails the development of effective and robust ionospheric calibration algorithms. However, the intensified ionospheric impact and demanding requirements on radiometric accuracy, resolution and geolocation, combined with complex instrument modes such as ScanSAR or TOPS make the development of suitable calibration schemes a challenge. A better understanding of the ionospheric impact on SAR data has to be established to address this challenge.

In the last decade, the calibration of ionospheric SAR data was boosted with the launch of the Advanced Land Observing Satellite (ALOS) in 2006 and its enhanced successor ALOS-II in 2014. Both sensors provided polarimetric and/or interferometric SAR data systematically, globally and across the whole solar cycle for the first time. Indeed, the datasets collected by ALOS and ALOS-II provided a unique database for the investigation of a wide range of ionospheric effects. As an active member of JAXA's Calibration and Validation group, the Institute was involved in the calibration of both missions from the very beginning, playing an integral role and expanding its competence in ionospheric calibration of SAR data.

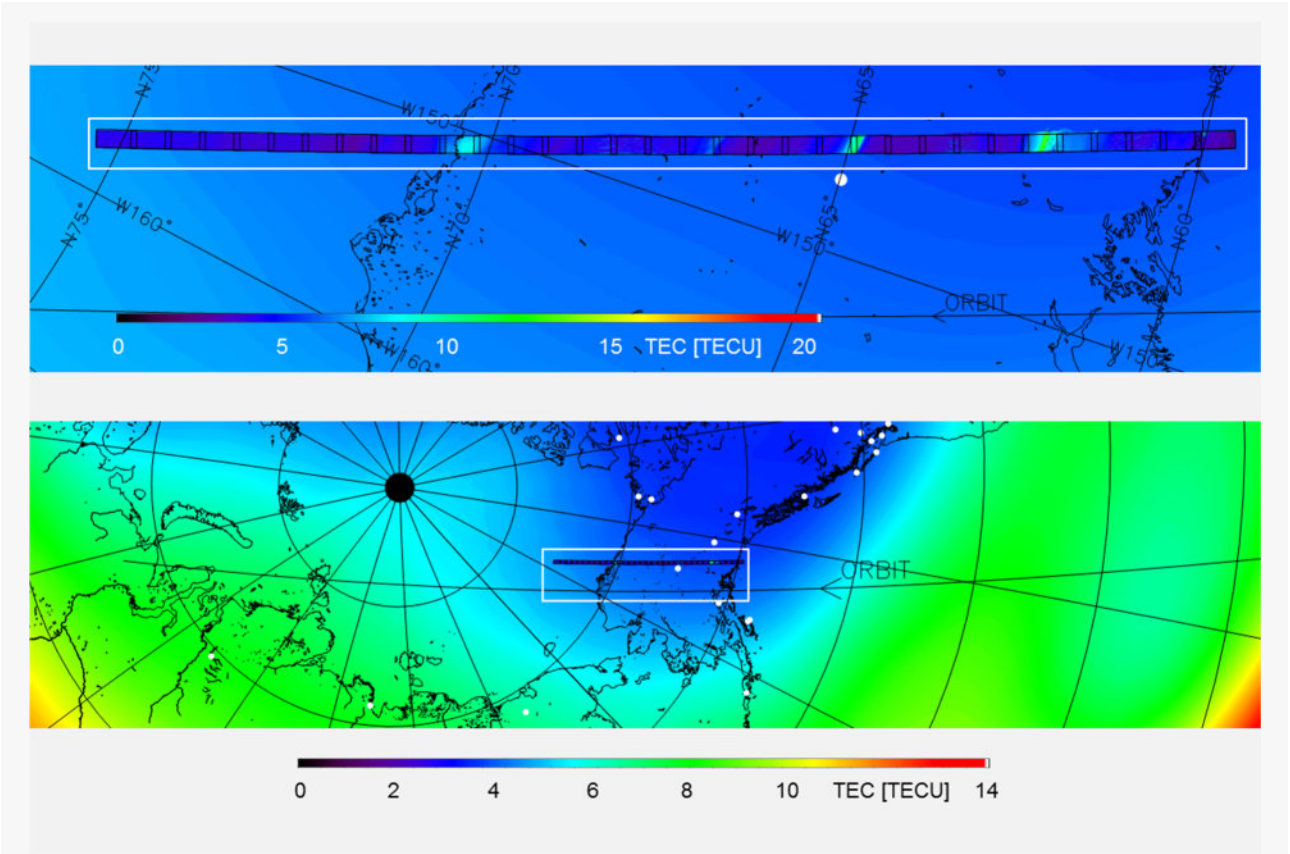

Figure 2.2-74 Top: TEC estimates derived from 33 consecutive quad-polarimetric ALOS-PalSAR images along a 3600 km transect from the Pacific to the Arctic Ocean across Alaska superimposed on TEC estimates from the global GNSS network performed at the same time. Bottom: zoom out of the map section shown on top (indicated by the white rectangle). The white dots indicate the location of the GPS stations used for the generation of the GNSS TEC map.

At the same time, the Institute benefited from the cooperation with national and international experts on ionospheric modelling and ionospheric GNSS measurements. The access to unique experimental ionospheric data sets was essential for a more accurate parameterization of the 3-D ionospheric structure in SAR calibration algorithms. This made the development of generic schemes for the calibration of polarimetric and/or interferometric data sets with an improved performance in terms of accuracy and/or stability possible. This is essential for the success of future missions such as BIOMASS and Tandem-L, which significantly depend on how well the distortions caused by the ionosphere can be finally compensated. The development of ionospheric expertise with respect to SAR data over the last seven years is one of the Institute's success stories. During this time, the Institute has become a leading international authority in the field of ionospheric SAR calibration.

Parallel to the development of advanced ionospheric calibration algorithms, the progress in understanding the interconnections between ionospheric and SAR image parameters triggered a paradigm shift: instead of looking at the ionosphere only as a "disturbing" medium, the potential of SAR configurations to characterize the ionosphere and estimate important ionospheric parameters with unprecedented accuracy and on spatial scales that where impossible before, was recognized. The Institute was one of the pioneers in this direction, advancing the estimation of ionospheric parameters from SAR data.

A first important result in this context was the ability to map the lateral distribution of the total electron content (TEC) by converting Faraday rotation estimates from quad-polarimetric SAR data. The high spatial resolution of SAR enables the mapping of the lateral TEC distribution at the same scale continuously along thousands of kilometers, while the conventional GNSS derived global TEC maps fail to capture TEC structure at sub-kilometer scale.

Figure 2.2-74 compares a GNSS TEC map (background) to TEC estimates derived from 33 consecutive quad-polarimetric ALOS-PalSAR images along a 2000 km transect from the Pacific to the Arctic Ocean across Alaska acquired on April 1, 2007. The ionospheric fluctuations – a result of an interplanetary magnetic field direction reversal – appeared just before the SAR acquisition. The SAR-derived TEC maps clearly show four TEC surge crests at a distance of about 250 km from each other. The GNSS derived map reproduces only a biased large-scale TEC trend as a result of the low density of GPS receivers in that area.

Even more impressive is the potential arising from the variation of individual ionospheric distortions along the synthetic aperture. Accordingly, the variation of the acquisition geometry along azimuth provides an important framework for analyzing and characterizing the spatial variability of the ionosphere at a single image basis. Figure 2.2-75 shows a slice through a 3-D reconstruction of the electron density obtained from the variation of Faraday rotation across the synthetic aperture of a single quad-polarimetric ALOS-PalSAR scene acquired over Alaska on April 1, 2007. The red dashed line indicates the electron density profile measured by HAARP (High Frequency Active Auroral Research Program) at the same time as the ALOS acquisition. The surprisingly good agreement indicates the potential of SAR configurations to revolutionize ionospheric

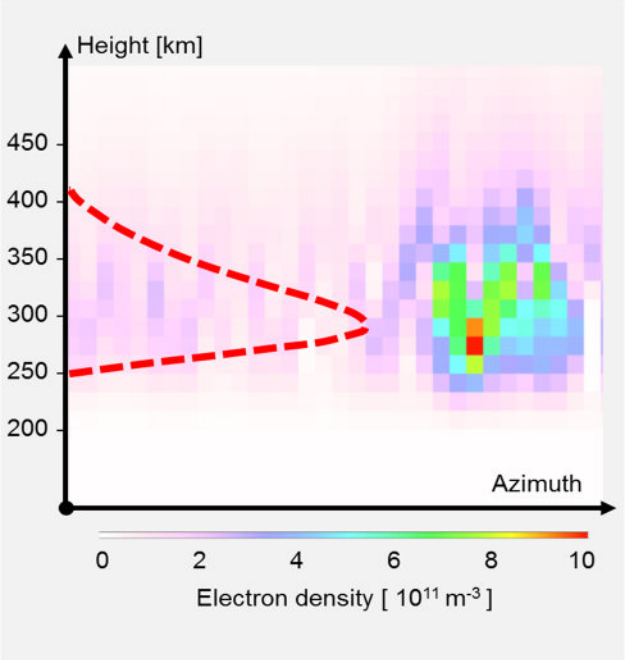

Figure 2.2-75 Slice through the 3-D electron density reconstruction from the variation of Faraday rotation across the synthetic aperture of a single quad-polarimetric ALOS-PalSAR scene acquired over Alaska on April 1, 2007. The red line indicates the electron density profile measured by HAARP (High Frequency Active Auroral Research Program) in the region at the same time as the ALOS acquisition.

research, and motivates the design of a future SAR mission dedicated to the exploration of the ionosphere.

2.2.12 Antennas

Today's requirements in radar system design and data performance are extremely challenging. All components in the system chain must be optimized in order to guarantee the data quality necessary to support state-of-the-art and future innovative SAR information products. Demanding requirements on amplitude and phase calibration, antenna beam pointing, cross-pol isolation, and long-term stability over a large frequency range lead to the development of new antenna concepts, simulation tools and measurement techniques.

Antenna Development

The Institute's activities in antenna development and characterization cover a wide range of technologies and microwave frequencies. To deal with all topics in antenna design, simulation tools as well as outstanding measurement capabilities are available for the entire development loop. This includes modelling, assembling, analyzing, and optimizing; thus, all topics related to antenna development, installation and operational aspects are covered. The comparison and validation of simulated and measured data in the Compact Test Range (CTR, see Section 2.2.13) enhances the development efficiency and gathers specific experience in antenna modeling and manufacturing processes.

Various antenna technologies and radiating structures are employed to support the Institute's airborne radar system F-SAR

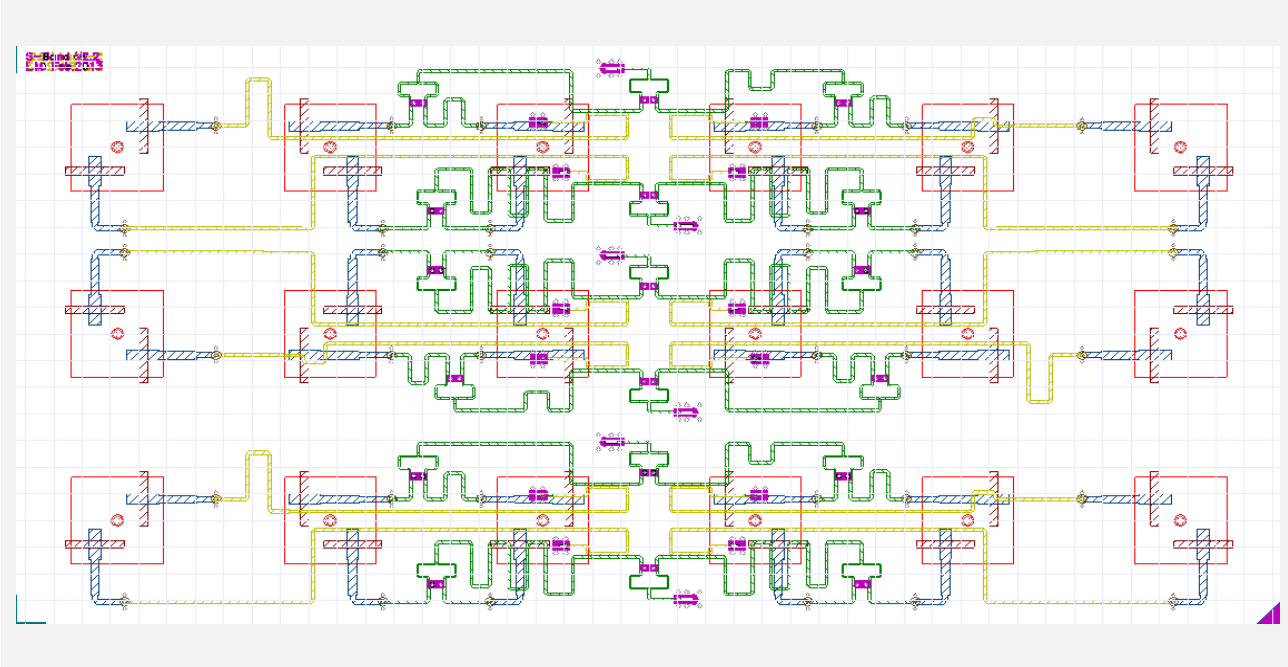

Figure 2.2-76 Layout of an S-band antenna with 300 MHz bandwidth, composed of 11 copper layers

(Section 2.3.1) and follow-up systems like DBFSAR, as well as enhancements in frequency range and interferometric capabilities. The mounting structures, necessary to equip the airplane with the antenna system, are included into the design and development chain and are considered from the very beginning, including the requirements for airworthiness certification. The antenna is thus modelled in its operational environment (cf. Figure 2.2-76 and Figure 2.2-77). One challenge in the development of a prototype antenna for airborne SAR is the combination of structural, mechanical, aerodynamic and electromagnetic aspects to achieve the best system performance and safety. A dedicated software suite is employed in order to cope with these challenging requirements. Modelling with validated parameters generates improved inputs to produce more realistic and reliable simulation results. This design procedure, including the characterization in the Compact Test Range and, if needed, a redesign, provides continuously higher efficiency in antenna development [RC-278].
Beyond the airborne SAR activities, the antenna developments encompass several projects at the Institute. Some highlights in antenna design are presented in the following section.

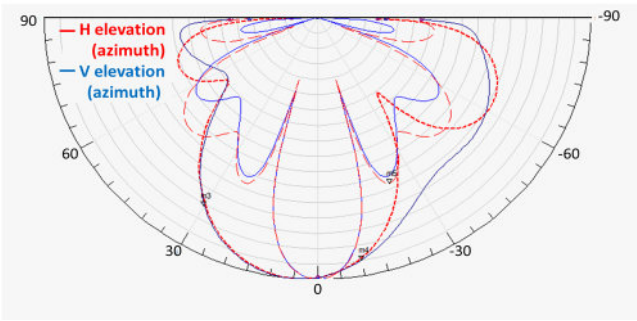

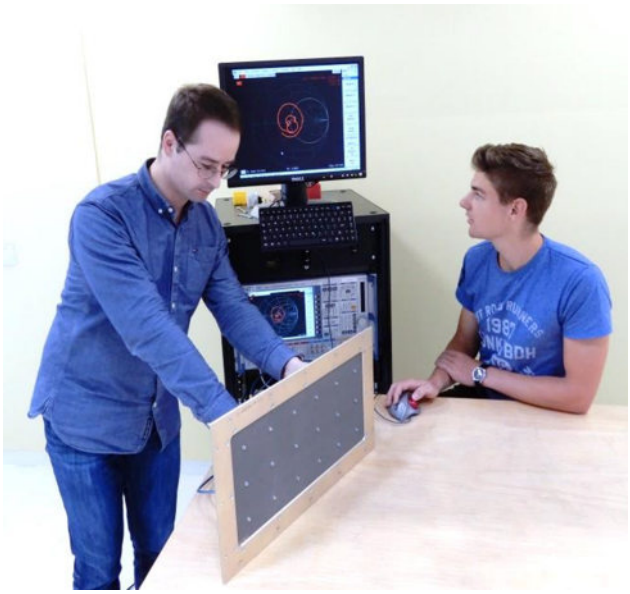

Figure 2.2-77 Top: elevation and azimuth patterns for H and V polarization in one diagram. The wider elevation patterns are pointing to 5 degrees off-nadir direction and show equally shaped patterns between -10 and 40 degrees. The narrower azimuth patterns are also in good accordance within the main beam area. Bottom: S-band antenna with 300 MHz bandwidth.

L-Band Antenna of the F-SAR

A new antenna with four selectable main beam positions in elevation was designed to support airborne L-band SAR data acquisitions (cf. Figure 2.2-78). Mounted on the right-hand side of the airplane's cabin, the elevation beam can be steered to incident angles of 25, 30, 35, and 40 degrees. The antenna beam pointing is switchable from one flight track to the next. Like most antennas for the airborne SAR, it provides dual polarization. To perform the electrical beam steering, the 24 double-stacked patch elements are combined in four rows with six elements per row. The azimuth network is part of the radiating structure, whereas the elevation beam steering

network is housed in a separate box. The separation of the elevation network is necessary due to the high pulse power of 1 kW. High power connectors, matched microstrip layout and proper thermal design are challenging aspects, especially for long data takes at high altitudes. The antenna provides a bandwidth of 150 MHz at 1325 MHz center frequency and has been fully operational since 2014 as part of the F-SAR system.

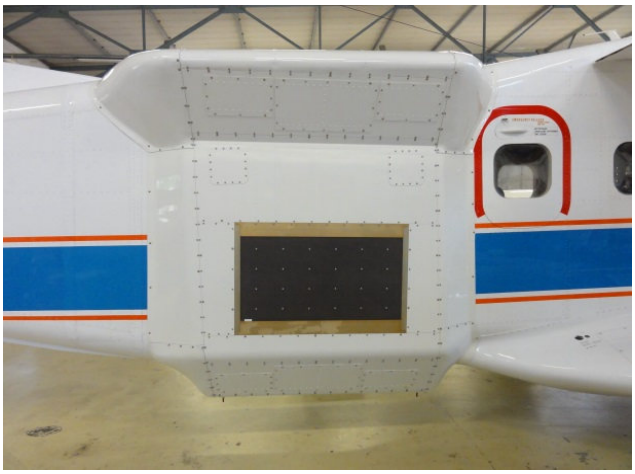

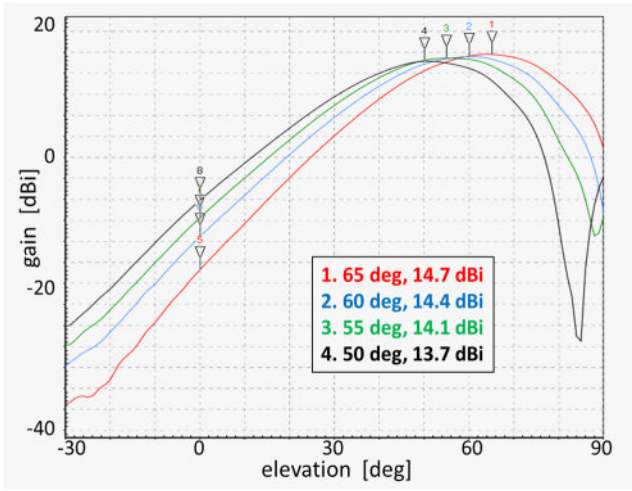

Figure 2.2-78 Top: L-band antenna mounted within the antenna carrier. Bottom: principal elevation cuts of the H-pol pattern. The four elevation cuts show the gain as a function of the off-nadir angle after beam steering to the annotated angles.

P-Band Antenna of the F-SAR

Most airborne SAR antennas are based on microstrip patch elements using different techniques to enhance bandwidth and radiation performance. To deal with the long wavelength in P band, and in view of the space limitations of the aircraft cabin, a new and innovative radiating element with reduced size was developed to generate a physically small but dense array antenna. The final array cell size was only 0.4 λ. A large number of array elements is used to control the radiation pattern of the bottom-mounted antenna outside of the desired swath in both the nadir and opposite swath directions. Dense arrays are in general adversely affected by high mutual coupling between adjacent elements. The new design gives the freedom to handle each radiating element as an individual radiator, with only minor degradation from mutual coupling [RC-278]. A dedicated beamshaping is applied for the off-nadir main beam, which points to an angle of 42° (cf. Figure 2.2-79). The antenna can additionally be used in a sounder mode. By replacing the elevation power divider, the P-band antenna also supports DBF activities with a dedicated transmit pattern and five receiving channels. Operating at a center frequency of 435 MHz, the antenna was successfully used during the AFRISAR campaign [RC-155] in preparation for ESA's BIOMASS mission and for ice and glacier applications over Greenland.

X-Band DBF Antenna Modules for Airborne SAR

A new generation of flexibly usable wideband antenna modules has been developed to support airborne X-band SAR applications related to the demonstration of digital beamforming (DBF) and ground moving target indication (GMTI). Each of the 100 mm x 25 mm antenna modules consists of 4 dual-polarized stacked patch elements and an integrated network, combining the radiating elements to two SMP connectors. In view of the main application, the module is referred to as a digital beamforming receive antenna module (DBFRAM). The antenna has a 2 GHz bandwidth at 9.6 GHz

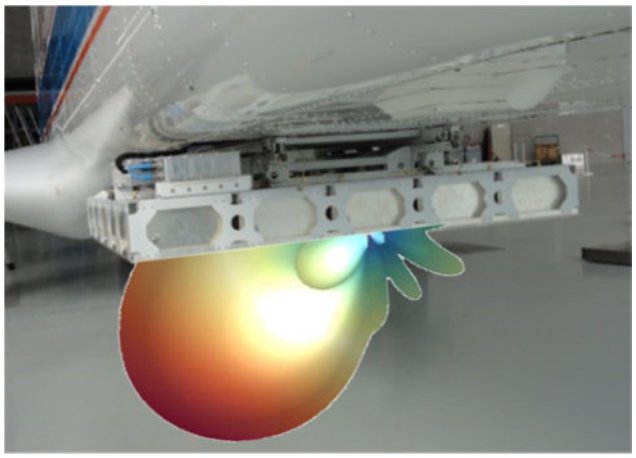

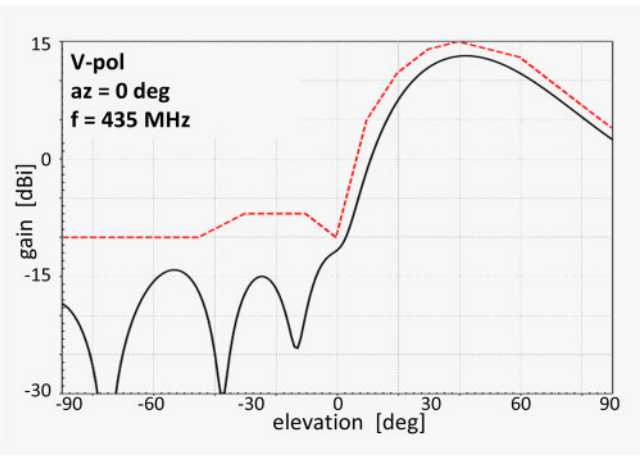

Figure 2.2-79 Left: P-band antenna mounted under the airplane DO 228 with a three-dimensional overlay of its pattern. Right: principal cut through the V-pol pattern, where the red dashed line shows a mask indicating the required pattern shape. The antenna has a bandwidth of 50 MHz at a center frequency of 435 MHz and the cross-polar isolation is below -25 dB.

center frequency and represents a suitable subarray to configure large antenna groups. The Institute has built about 300 DBFRAM modules to be used in different antenna setups [RC-54].
A representative example of an antenna array composed of multiple DBFRAM modules is the V-SAR antenna for GMTI applications. This complex antenna configuration is used to detect moving targets and estimate their velocity and direction of motion either over land or sea (cf. Section 2.2.10). As shown in Figure 2.2-80, a 1.3 m long antenna box houses three individual antenna setups. A long dedicated transmit antenna generates a narrow azimuth beam. Six receiving antennas were placed next to each other in flight direction for GMTI operation. The third antenna in the frame is a dual-polarized imaging antenna, capable of operating in transmit and receive mode. The GMTI antenna houses 80 DBFRAM modules in total. The DBFRAM modules will also be used to form the receiving antenna in a dedicated antenna case for the new DBFSAR system. The flexibility of the modules enables a huge variety of possible configurations to investigate new and innovative DBF modes for SAR applications.

Figure 2.2-80 Individual DBFRAM modules assembled to an antenna array (top) and V-SAR box (middle). The V-SAR box accommodates three antennas, each formed out of a large number of DBFRAM modules to serve both GMTI and SAR imaging modes. The zoom on the bottom shows one subarray of the GMTI receiving antenna together with its attached power combiner network where all conductive structures are visible.

Overview of Ongoing Antenna Developments

A current project at the Institute is the development of a new airborne Ka-band polarimetric SAR interferometer for the exploration of ice and glaciers. This development asks for a special antenna design paired with an innovative antenna mounting structure. In total, two transmit antennas and four receiving antennas will be used to form a single-pass interferometer with multiple baselines. As the center frequency is approximately 36 GHz, the physical length for each baseline has to be known with submillimeter accuracy. This becomes a challenging aspect, especially if one takes into account that the antenna structure will be mounted underneath the airplane. Considering the required accuracy, the change in size of common materials due to the expected temperature variations will be in the same order of magnitude. Similar considerations apply to the waveguides and coaxial wires connecting the radar system inside the cabin to the antennas on the outside.
For enhanced system performance, slotted waveguide antennas have been developed to guarantee a high efficiency. However, it was not possible to achieve all mechanical and electrical requirements with conventional manufacturing methods. As a solution, the complex mechanical structures inside the waveguides were printed in plastic material and treated with copper to generate a conductive surface (cf. Figure 2.2-81). Now, the roadmap for the Ka-band antenna development foresees a full 3-D printed design in one piece, including all components of the feeding network.
In addition to the manifold antenna developments (see Table 2.2-2), the Institute is capable of simulating electrically large field and wave-propagation problems with special software suites. Examples are the full wave analysis of a 5 m trihedral corner reflector over ground, used for AFRISAR calibration [IC-6], [IC-120], and a 3-D full wave analysis of the Compact Test Range [MaT-15], [RC-45].

Figure 2.2-81 Ka-band slotted waveguide antenna prototype out of 3-D printed plastic metalized with copper

Frequency Band / Description	Center Frequency [GHz]	Band-width [MHz]	Pol.	Peak Power [kW]	Quantity [+ spare]	Line of Sight, Special Properties	Technology
P	0.425	50	H, V	1	1	sidelooking, nadir, DBF	cavity
L	1.325	150	H, V	1	1	sidelooking, 4 positions	patch
S	3.25	300	H, V	2	2 [1]	sidelooking	patch
C	5.3	500	H, V	2	1 [1]	sidelooking	patch
X	9.6	800	H, V	2	3 [1]	sidelooking	patch
DBFRAM	9.6	2000	H, V	0.5	300	DBF	patch
DBF Tx	9.6	2000	single	3	2 + 2	equal pattern	horn
V-SAR	9.6	1800	H, V	1	1	GMTI	DBFRAM
DBF Rx	9.6	1800	H, V	0.5	1	DBF	DBFRAM
Ka	36	1000	H, V	1	6	sidelooking	slotted waveguide
DuoLim	1.325	150	H, V	1	3 [1]	sidelooking, 4 positions	cavity
IoSiS Tx	9.6	4000	single	4	1	boresight	corrugated horn
IoSiS Rx	9.6	4000	single	1	1	offset parabolic	horn antenna
CTR RCS Feed	4.8 – 8.0	3200	dual	0.1	2	CTR feed	quad ridge horn
CTR RCS Feed	26-38	12,000	dual	0.1	2	CTR feed	quad ridge horn

Table 2.2-2 Overview of the antenna developments at the Institute. The antennas are developed for the airborne SAR system, the IoSiS radar for imaging of satellites (cf. Section 2.4.9), or for the Compact Test Range.

2.2.13 Compact Test Range Facility

The Compact Test Range (CTR) is the heart of our TechLab, where all hardware developments and measurement facilities are concentrated at the Institute. It is fully equipped to conduct antenna radiation measurements and radar cross section (RCS) characterization. It offers excellent measurement precision in both amplitude and phase, well above that of "standard" free-space antenna ranges at microwave frequencies. Latest improvements are the spherical wave expansion technique to reduce measurement noise from angular quantization and the enhanced antenna analysis option provided by the cutout area of interest around the antenna elements. The CTR is not only a key measurement facility for all internal antenna developments, but is also increasingly requested by external customers. It delivers unique processing and data analysis capabilities to an antenna designer.

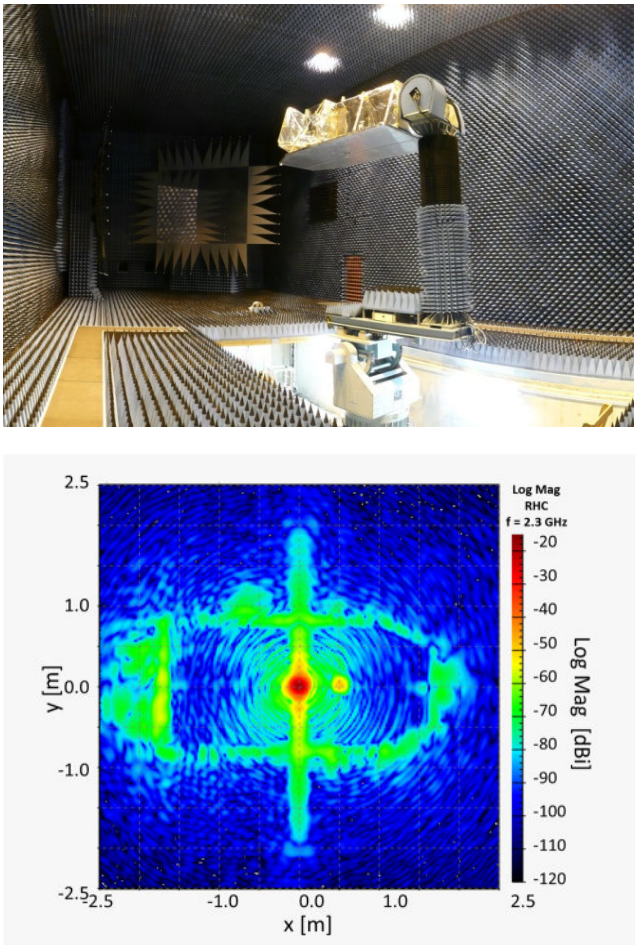

Figure 2.2-82 Mock-up of the PRISMA satellite under test in the CTR (top) and measured near-field projection (bottom). The contour of the satellite's solar panel is clearly visible, including a small hole for the sun tracker, appearing as a light yellow dot right from the active antenna element at the center.

Far-Field to Near-Field Transformation

The CTR software provides the ability to transform the measured far-field data into a near-field characteristic. This is possible thanks to the outstanding stability of the measurement system under long-term spherical measurements. The ability to derive the near-field characteristic is extremely useful for detailed antenna analyses, where all features from the antenna and the installation structure become visible. As an example, Figure 2.2-82 shows a mockup of the Italian PRISMA satellite during S-band measurements. The primary goal was to optimize the command link coverage. All dimensions and structural parts of the satellite appear in the near-field transformation. This illustrates not only that the close-by structural elements influence the antenna, but that the whole supporting

structure has to be optimized for proper antenna performance. The far-field to near-field transformation technique is also used to analyze antennas during optimization routines. Unexpected behavior of test objects is often driven by manufacturing failures or structural elements of the mounting device. If the devices are part of the antenna structure, like in the F-SAR antenna carrier, the near-field transformation gives helpful information about the field distribution inside and outside of the active antenna elements.

Hybrid Characterization of Electromagnetic Large Problems

The antenna characterization capabilities at the Institute are enhanced by the use of "hybrid characterization methods". A hybrid characterization merges measurement results with simulation data to obtain a reliable and validated solution. By this, it may overcome the limitations in measurement, mainly due to extreme test object size, and, at the same time, proves the simulation results by dedicated comparison of measurement results and simulation data.

However, devices under test sometimes exceed the limits of the facility – either in size, weight or availability. It is state of the art to scale down devices under test and to increase the measurement frequency to perform characterization tasks on scaled objects. But this method fails in the case of dielectric materials. If parts of an antenna are made of dielectric materials, the whole setup will not produce authentic results.

The Institute's Compact Test Range offers hybrid characterization capability, where critical parts of the device under test are measured and the results act as a source to carry out simulations of the entire structure. The necessary interface between measurement and simulation tools is available in the CTR data processing software. It is based on the coefficients of the spherical wave expansion method, and the results are fed into the simulation software, representing the electrical behavior of the antenna element as a bundle of spherical wave expansion weighted coefficients.

The hybrid characterization was successfully demonstrated In the EU project "HEXAFLY" (cf. Figure 2.2-83, Figure 2.2-84, and Figure 2.2-85). The objective is the coverage of the telecommand and telemetry link budget for different antennas at certain positions on a flight model for hypersonic flight tests.

With a length slightly greater than 4 m, the CTR cannot cover the full dimensions of the flight model. Additionally, the required mounting structure would have distorted the measurement even if the dimension of the quiet zone was able to cover the size of the flight model. To characterize the antenna patterns on the HEXAFLY flight model, one antenna element was characterized separately and measured for the case where it was mounted on a small structural section. Both results were compared to a full simulation of the same configuration. Once the antenna element was simulated, the measured excitation coefficients of the antenna were used to feed a further simulation. This approach was used to validate the hybrid method.

All further characterizations were performed on the entire 3-D CAD model of the HEXAFLY flight model by standalone simulations and measured excitation coefficients [RC-45].

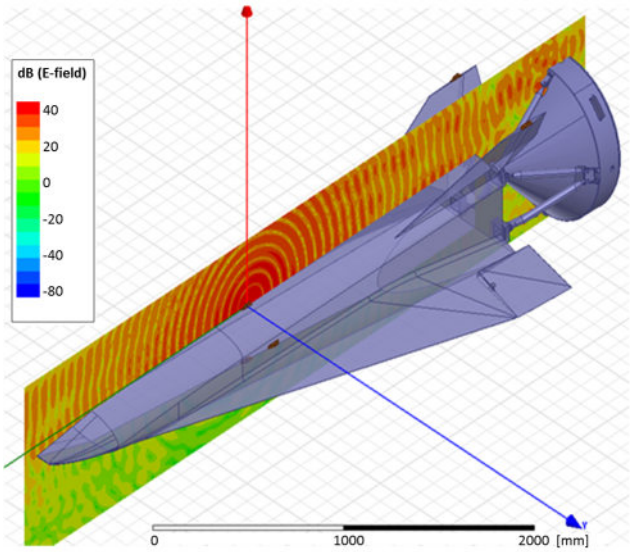

Figure 2.2-83 Principal cut through E-field distribution originating from the telemetry antenna mounted on the body of the hypersonic demonstrator HEXAFLY, based on simulation data.

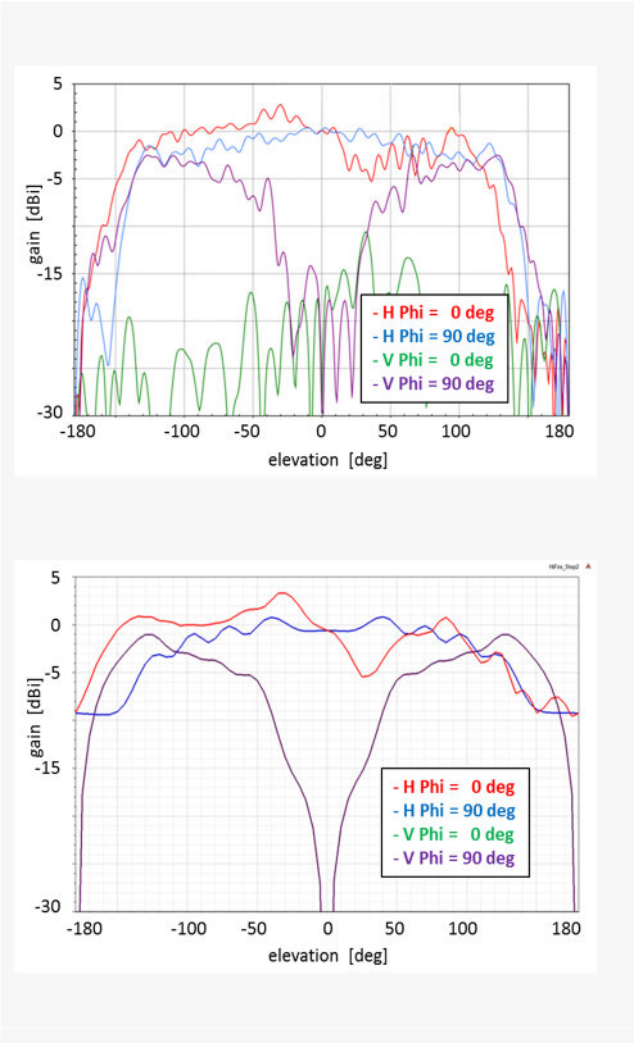

Figure 2.2-84 Top: measured data of the telemetry antenna mounted on top of the fin in two polarizations for both principal cuts. Bottom: comparison with simulation results. Despite the different boundary conditions, the results are comparable in amplitude and shape.

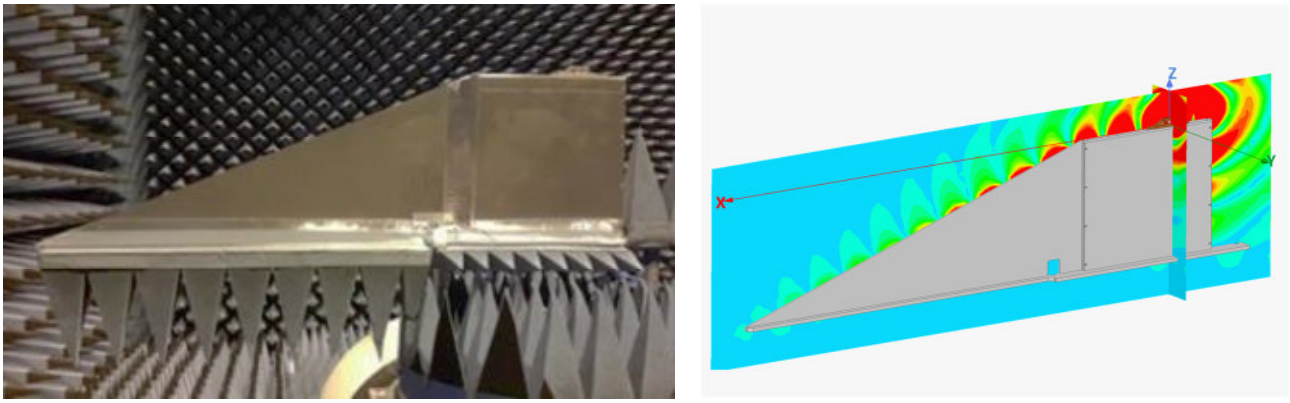

Figure 2.2-85 For validation purposes, the telemetry antenna was measured on an isolated model of the HEXAFLY fin and compared with simulation results.

The hybrid characterization has multiple advantages. It is a fast and reliable method for investigating large antenna problems in limited time, it is comparable to measurement results, and it includes validation methods. To enhance the reliability, we were able to solve most of the electromagnetic problems with two independent software suites and different solver technologies.

The Institute's Compact Test Range is an outstanding measurement facility for highly accurate antenna and RCS characterization. Moreover, it provides unique opportunities for the development of new measurement and antenna analysis methods. Advanced methods are introduced, tested and validated in close collaboration with the software developer.

Continuous enhancement of measurement accuracy, especially at higher frequency ranges, is driven by internal and external needs. The latest improvements on the feed support structure reduce, for example, mechanical oscillations from the building floor, and a new air conditioning system supports constant temperature during long-term measurements. The close connection between antenna development and characterization gives strong inputs in both directions, enhancing antenna development and supporting the Compact Test Range with simulation and modelling capabilities.

2.3 Airborne SAR

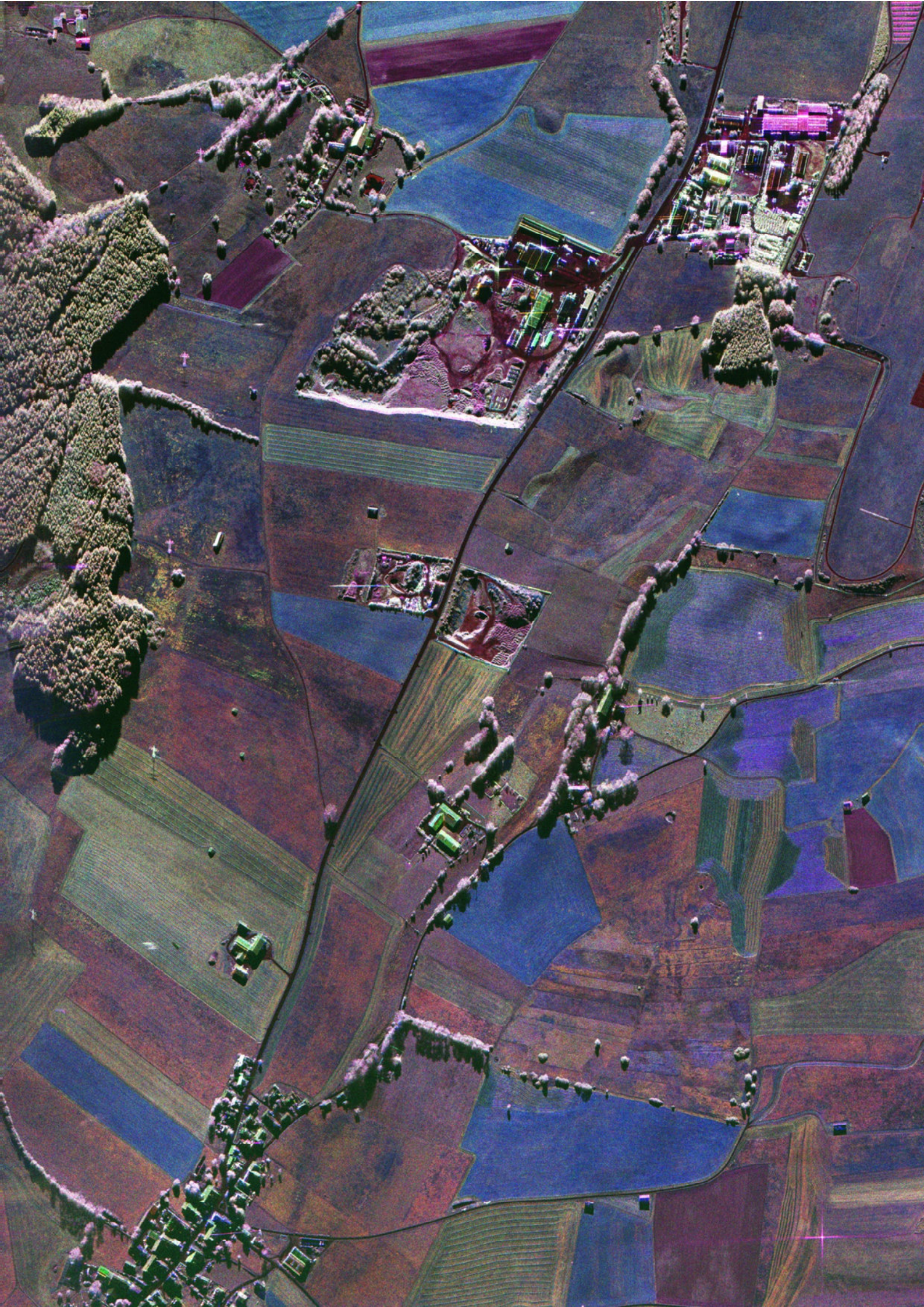

2.3 Airborne SAR

Airborne SAR technology has been a central research area at the Institute for more than three decades. The Institute designs, builds and operates cutting-edge airborne SAR sensors, which are continuously pushing the state of the art in modern SAR imaging. The availability of such an airborne testbed plays a very important role in the preparation of upcoming spaceborne SAR missions (e.g. BIOMASS) and in the design of innovative future missions (Tandem-L, HRWS). The current operational system – the F-SAR sensor – can be considered one of the most advanced airborne SAR sensors in the world. It has several unique features, such as the capability to simultaneously acquire fully polarimetric SAR data in up to four frequency bands and to operate in innovative imaging modes such as polarimetric SAR interferometry, tomography and holography. In addition, it offers two single-pass polarimetric interferometers, a very high spatial resolution, and generally exhibits excellent data and calibration quality. The next-generation sensor DBFSAR, which is currently under development, adds multi-channel digital beamforming modes and boosts the spatial resolution to the sub-decimeter scale. In addition to sensor development, the Institute organizes and conducts extensive airborne SAR campaigns on a regular basis. The data acquired, processed and delivered as part of these campaigns are the basis for innovative research at DLR and various institutions around the world.

2.3.1 The Advanced Airborne SAR Sensor F-SAR

Airborne SAR technology, the operation of airborne SAR instruments and the development of new applications based on polarimetry, interferometry and tomography have a long tradition at the Institute. Thirty-five years ago, in 1983, these developments began with the airborne Experimental Synthetic Aperture Radar, E-SAR, which was intended as a technology testbed to establish expertise in SAR system design, signal processing and image analysis. In the years that followed, the E-SAR instrument was used in a large number of scientific flight campaigns. It was continuously upgraded and improved until its decommissioning in 2009.
In the meantime, the Institute had initiated the development of a new, more advanced airborne SAR instrument, named F-SAR. This system is fully operational since 2015.

F-SAR Instrument Overview

F-SAR has the unique ability to acquire fully polarimetric SAR data in five frequency bands – X, C, S, L and P band – with simultaneous acquisition in multiple frequency bands on four recording channels. The sensor features single-pass polarimetric interferometric SAR (Pol-InSAR) capabilities in X and S band. Moreover, repeat-pass Pol-InSAR is a measurement mode available in all bands.

F-SAR is DLR's current airborne testbed for SAR technology and remote sensing applications and, as such, is primarily intended to support and prepare future satellite SAR missions. The motivation for the development of the instrument was the high demand for SAR data acquired simultaneously at different wavelengths and polarizations, as well as an increasing demand for very high spatial resolution.
The F-SAR sensor consists of modules that use modern hardware and commercial off-the-shelf components. For the purpose of experiments and operational data acquisition campaigns, the system is installed on board DLR's Dornier DO228-212 research aircraft.
The attainable range resolution is determined by the transmitted signal bandwidth and is, in practice, related to the wavelength. While the signal bandwidth in P band is limited to 50 MHz by hardware components and ITU regulations, a step-frequency approach is used to achieve up to 760 MHz of effective signal bandwidth in X band, corresponding to a very high spatial resolution of up to 25 cm [J-169]. A summary of F-SAR's general technical parameters can be found in Table 2.3-1.
All antennas of F-SAR point to the right of the aircraft. Figure 2.3-1 shows the instrument as it is installed on DLR's DO228-212 research aircraft. The radar hardware comprises a sensor control and several data acquisition subsystems, to

	X	C	S	L	P
Radar frequency [GHz]	9.60	5.30	3.25	1.325	0.435
Bandwidth [MHz]	760	384	300	150	50
PRF [kHz]	5	5	5	10	10
Transmit power [kW]	2.50	2.20	2.20	0.90	0.90
Duty cycle [%]	5	5	5	10	10
Range resolution [m]	0.25	0.5	0.67	1.35	4.0
Azimuth resolution [m]	0.2	0.3	0.35	0.4	1.5
Flight altitude range	From 2000 ft above ground level to 22,000 ft above mean sea level				
Off-nadir angle range	Nominal from 25° to 60°; extended from 20° to 65°				
Ground range coverage	From 600 m to 6 km depending on flight altitude				
Operational endurance	Between 2.5 h and 5 h depending on system configuration				
Sampling	8 bit real; 1 GHz/500 MHz selectable; maximum number of samples 64 k per line; 4 recording channels				
Data rates	Up to 190 Mbyte/s (per rec. channel)				

Table 2.3-1 F-SAR instrument key technical parameters. The system is currently being extended for operation in Ka band. The X- and S-band subsystems can both operate in single-pass polarimetric interferometric mode.

which individual RF modules are connected in a modular fashion (see Figure 2.3-2).

The modular design, in combination with a versatile system control, provide a very high level of flexibility and the degrees of freedom to configure the system optimally for conducting a diverse set of measurements and experiments. The design also makes the system easy to extend in order to accommodate additional frequency bands or specific measurement equipment.

The F-SAR sensor features a high-precision timing unit, which is able to ensure a long-term frequency stability of the system of $3 \cdot 10^{-7}$ per year and a timing jitter below 15 ps during data acquisition. The range delay and the range gate are freely selectable in multiples of 32 ns. Multi-band pulse transmission and recording can be configured in various ways, including both sequential and simultaneous pulse sequences, as well as half- and full-baseline single-pass interferometric modes. The receive bandwidth and the associated analogue input filters can be toggled between 50, 100, 200 and 400 MHz.

A further important component of F-SAR is the very high-precision navigation and positioning unit, which is based on real-time differential GPS coupled with a high-end inertial measurement unit (IMU). It achieves an offline positioning accuracy of approximately 2 cm, which is essential for accurate repeat-pass interferometric measurements. The navigation subsystem also provides feedback to the pilots guiding them to fly along pre-defined flight tracks with very small deviations of only 2-3 m given favorable weather conditions.

A special F-SAR antenna carrier was developed and certified airworthy. It is mounted behind the aircraft's right wing and carries up to seven planar dual-polarization array antennas: three for X band, one for C band, two for S band and one for L band. The P-band antenna is mounted under the front section of the cabin, as shown in Figure 2.3-3.

The antenna carrier allows the antenna configuration to be changed or different antennas to be mounted with only minimal effort in terms of airworthiness certification. In its nominal configuration, the carrier provides three fully polarimetric single-pass interferometers: across track (XTI) in S band and X band, and along track (ATI) in X band. The nominal baselines are approximately 1.60 m (XTI) and approximately 85 cm (ATI).

Operational F-SAR Instrument Configurations

The Dornier DO228-212 aircraft has a maximum payload of about 1400 kg. The flight endurance attainable for acquisition campaigns is variable and depends primarily on the weight of the equipment installed. By virtue of its modular design, the F-SAR sensor can be adapted to the particular campaign

Configuration	X	C	S	L	P	Endurance
F-SAR X-C-S-L	9.600	5.300	3.250	1.325	---	3.75 – 4.25 h
F-SAR P	---	---	---	---	0.435	4.0 – 4.5 h
F-SAR L	---	---	---	1.325	---	4.25 – 4.75 h
F-SAR L-P	---	---	---	1.325	0.435	3.5 – 4.0 h
TERENO	Combination of F-SAR L + PLMR-2 + Thermal Camera					4.0 – 4.5 h

Table 2.3-2 F-SAR instrument configurations, the center frequencies in GHz, as well as the corresponding endurance. The special TERENO configuration was implemented for the Helmholtz project TERENO and combines F-SAR L-band, an L-band radiometer and a thermal camera for soil moisture mapping.

Figure 2.3-1 DLR's DO228-212 D-CFFU research aircraft with the F-SAR installed on board. Left: side view of the aircraft with the X-, C-, S- and L-band antennas at the rear of the aircraft and the P-band antenna under the aircraft body. Right: a view inside the aircraft cabin during the operation of F-SAR.

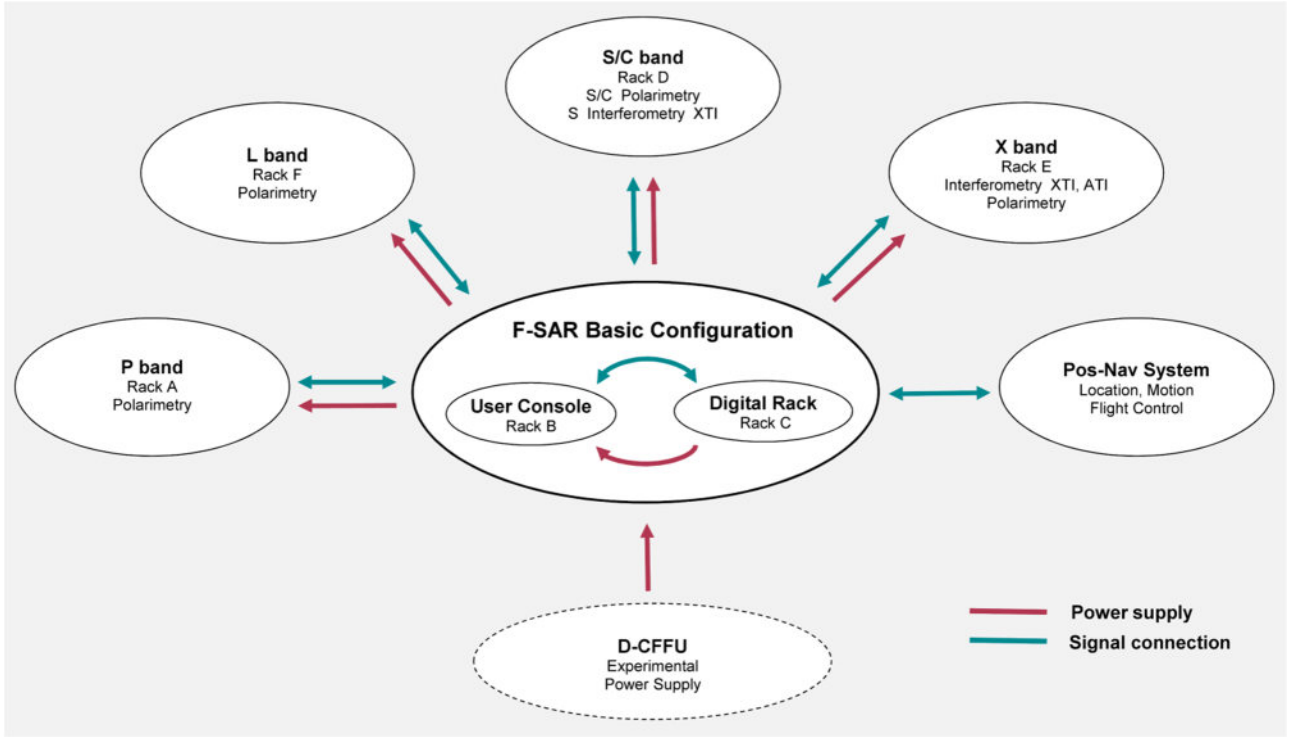

Figure 2.3-2 The modular system concept underlying F-SAR for polarimetric/interferometric multi-frequency operation in X, C, S, L, and P band. By design, the system is easily expandable and can be adapted to various mission scenarios.

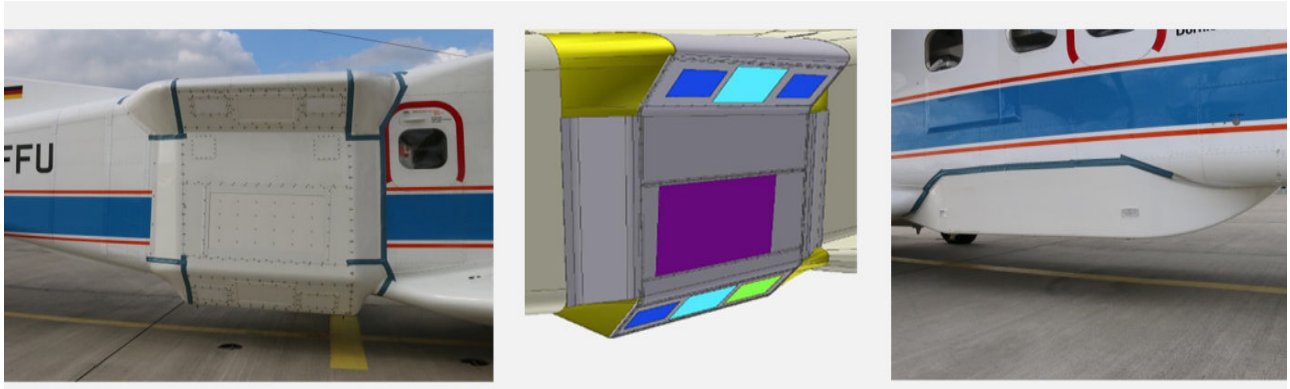

Figure 2.3-3 Left: the F-SAR antenna carrier, installed on DLR's DO228-212 research aircraft. Middle: schematic drawing of the F-SAR antenna carrier with the nominal antenna configuration: 3 X-band (blue), 2 S-band (light-blue), C-band (light-green) and L-band (purple) antennas. Right: the P-band antenna, mounted under the aircraft's body.

requirements, while maximizing performance. At the time of writing, five specific F-SAR instrument configurations have been certified airworthy and used for measurement campaigns. These configurations are listed in Table 2.3-2. Further configurations will be implemented as the need arises.

F-SAR X-C-S-L is the most intensively used configuration. It supports simultaneous data acquisition in the X-C-L or X-S-L modes in a single pass (see Figure 2.3-4). By design, C and S bands cannot be acquired simultaneously in a single pass.

The X-C-S-L configuration is unique in that it offers simultaneous single-pass polarimetric interferometry in X and S band, as well as polarimetric and repeat-pass interferometric measurement modes in all bands. Optionally, a second antenna for single-pass across-track interferometry for a single polarization (either H or V) in C band is currently being integrated.

F-SAR's L-P configuration is especially useful for forestry applications, for example to measure biomass, and uses auxiliary data products such as TanDEM-X DEMs as external inputs for interferometric processing. Operational L-P measurement modes include the innovative tomographic and holographic imaging techniques, as well as repeat-pass polarimetric interferometry. All of these imaging techniques have been developed and validated at the Institute on the basis of airborne SAR data collected by the Institute's airborne SAR sensors.

F-SAR Instrument Performance

Nowadays, environmental monitoring and climate research place stringent precision and stability requirements on measurements taken by modern SAR instruments. Meeting these requirements requires regular overflights of a calibration test site to monitor system stability, precise internal instrument calibration, and accurate on-ground antenna pattern characterization. All of these tasks are driven by and provide essential inputs to a highly sophisticated SAR processing facility and calibration procedure.

The Institute maintains a test site for external SAR instrument calibration at the former military airfield of Kaufbeuren in the South of Germany. A total of 14 conventional trihedral and

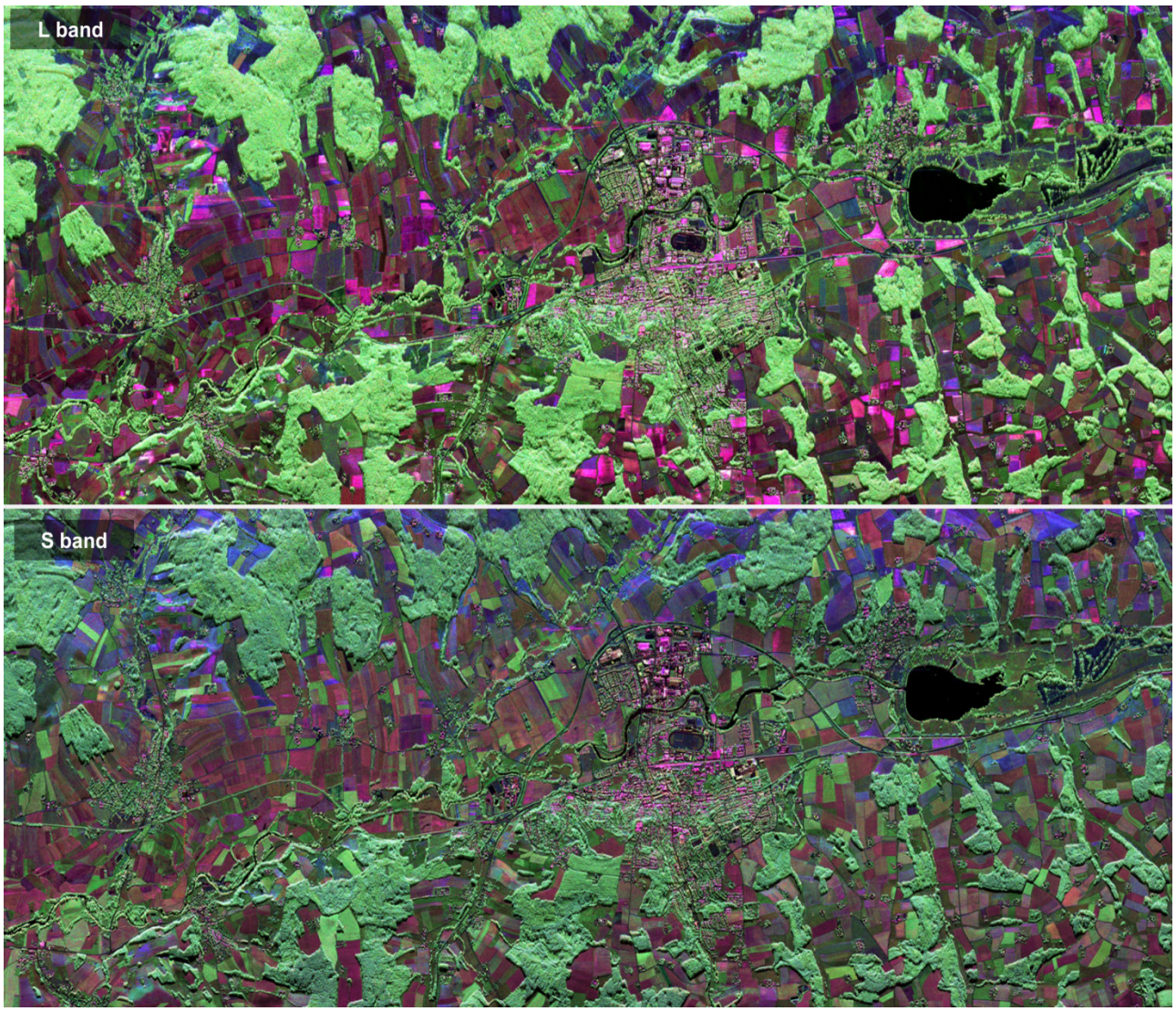

Figure 2.3-4 F-SAR fully polarimetric simultaneous dual-band image acquisition of the test site Simbach in Southern Germany. The colors correspond to the basic polarimetric scattering contributions (blue = surface scattering, red = double bounce scattering, green = volume scattering).

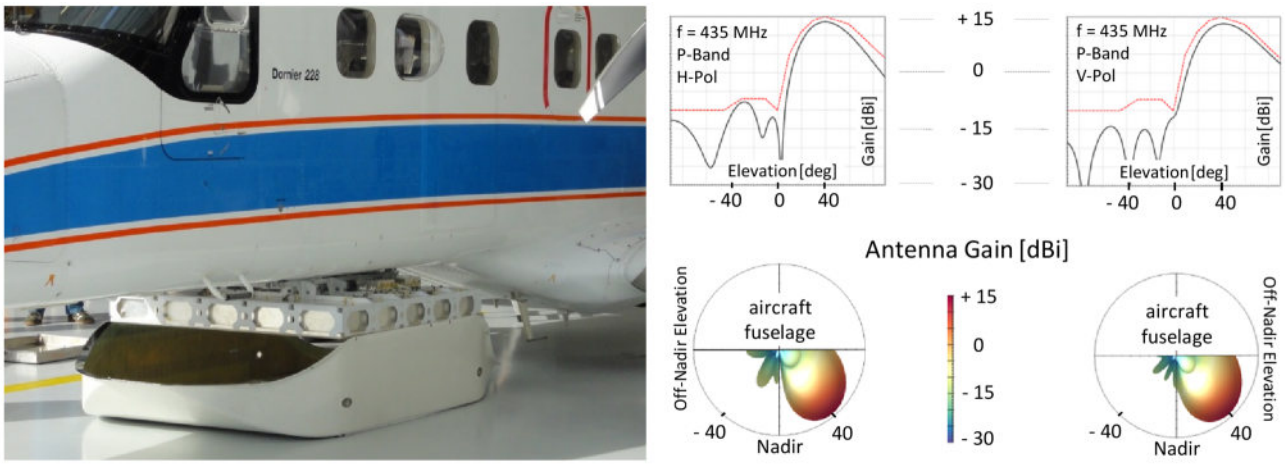

Figure 2.3-5 The F-SAR P-band antenna. Left: photo of the antenna before mounting the wind shield. Right: beam pattern optimized to similar shaped H and V patterns in the desired swath and canceling out nadir, as well as opposite swath illumination, as measured in the DLR Compact Test Range facility.

dihedral corner reflectors of sizes ranging from 90 cm to 250 cm leg length are deployed at this site. The standard look direction is to the North for all reflectors, and the targets cover an off-nadir angle range between approximately 25° to 60°. The site is used for all F-SAR frequency bands, to some extent even for P band.

The system performance parameters – which are verified each time F-SAR is installed on board the aircraft and before regular data collection is performed – include point target range and azimuth position and resolution, radar cross section (radiometric calibration), accurate polarimetric/interferometric inter-channel phase differences, as well as antenna mount angles and lever arms.

As an input to the radar data calibration process, the complete complex transfer function of every SAR antenna is characterized with high precision and in 3D, i.e., as a function of squint, elevation and over the entire sensor bandwidth. These antenna measurements are carried out at the Compact Test Range (CTR) of the Institute, where all relevant environmental effects, due to for example the antenna carrier and wind shield, are taken into account [RC-588]. As an example, Figure 2.3-5 illustrates the P-band antenna characteristics at the center frequency and in both, horizontal and vertical polarizations.

For the purpose of internal calibration, radar signal replicas are recorded in the laboratory and during each F-SAR measurement flight. Each replica recording characterizes the signal distortions as they propagate through the sensor, such as non-ideal transmission characteristics in the transmitter and in the receiver chains. In addition to compensating for these distortions, the analysis of replica recordings also serves to monitor instrument stability.

A summary of the typical F-SAR instrument performance is given in Table 2.3-3, while Figure 2.3-4 serves to illustrate the excellent imaging capabilities and high calibration accuracy of the F-SAR system.

2.3.2 The Airborne Digital Beamforming Sensor DBFSAR

One of the challenges in the design of future spaceborne SAR systems is to achieve an optimal performance/cost tradeoff while enabling large-scale imaging with short revisit intervals. Digital beamforming is a technology that can be used to overcome the limitations imposed by constraints involving the antenna size and signal timing in traditional spaceborne SAR systems. This trade-off prevents the SAR sensor from attaining both a high azimuth resolution and a large swath width.

	Rg position error		**Az position error**		**RCS error**		**HH/VV phase diff.**		**NESZ**
	μ_{rg}	σ_{rg}	μ_{az}	σ_{az}	**μ**	**σ**	**μ**	**σ**	**(25°/45°/60°)**
RF	**[m]**	**[m]**	**[m]**	**[m]**	**[dB]**	**[dB]**	**[°]**	**[°]**	**[dB]**
X	-0.005	0.045	0.013	0.052	-0.152	0.275	1.09	4.12	-32/-34/-28
C	-0.005	0.045	0.013	0.052	0.058	0.396	0.581	1.36	-33/-40/-27
S	0.007	0.051	0.034	0.062	-0.133	0.338	0.254	2.08	-28/-34/-30
L	0.008	0.048	-0.024	0.035	0.125	0.184	1.07	1.67	-40/-46/-42
P	-0.064	0.095	-0.016	0.078	-0.139	0.268	0.188	2.98	-44/-46/-46

Table 2.3-3 Summary of the F-SAR instrument performance, as determined on the basis of raw data collected in 2016. The last column gives noise equivalent sigma zero (NESZ) levels obtained from the cross-polarization channel coherence.

As described in more detail in Section 2.2.1, digital beamforming is thus a key technology for future satellite missions, as it enables a great amount of flexibility in the sensor imaging mode as well as new approaches to sensor calibration, interference removal and ambiguity suppression. Airborne SAR sensors with digital beamforming capabilities are essential tools in the preparation for such missions, as they allow the necessary technology and data processing strategies to be experimentally established before being implemented on a satellite.
The existing F-SAR system provides only two simultaneous receive channels per frequency band, and is consequently not suitable for demonstrating digital beamforming techniques. For this reason, in 2014 the Institute initiated the development of a new airborne SAR system – the so-called DBFSAR – with digital beamforming capabilities. Its development was motivated primarily by the emergence of various digital beamforming (DBF) techniques for future spaceborne SAR systems and the need for a flexible, airborne experimental platform to provide practical experience and guide the implementation of such missions.
In addition, the DBFSAR sensor is intended to address an increasing demand for very high-resolution SAR imagery that exceeds the capabilities of the existing F-SAR system.
The DBFSAR system comprises three principal components:

- Digital subsystem: the digital backend includes data sampling and recording hardware for 12 receive channels, each with a 2 GHz bandwidth, the instrument control components and a user console for the flight operator. It can drive one or several RF radar frontends, including the existing F-SAR frontends.

- X-band subsystem: a new multi-channel radar frontend that contains all RF components, including the X-band high power amplifier. It features 12 simultaneous receive and 4 sequential transmit channels.

- DBF antennas: the DBF antenna configurations use a dedicated carrier, which supports 4 single polarization X-band transmit antennas, aligned horizontally or vertically to form wide or narrow beams, and 12 receive antennas that can be arranged in various spatial configurations.

As in the case of F-SAR, DBFSAR adopts a modular system layout. The design is easily expandable by additional hardware components that implement specific measurement techniques. The modularity of both sensors will allow F-SAR and DBFSAR to be merged into a single system in the near future. Many system settings of DBFSAR can be programmed virtually without constraint, leading to an enormous flexibility with regard to possible experiments and new imaging modes.

The Digital Subsystem

All of the components for the central system control and in-flight operation are integrated in the digital rack, as shown in Figure 2.3-8. This rack includes the radar display, navigation display, console, and components for 12-channel data acquisition and near-real-time on-board processing. The system control and data acquisition units can, by design, drive both the new digital beamforming X-band subsystem of DBFSAR (via Ethernet) and the existing, older F-SAR RF racks (via CAN bus). The entire radar can be controlled by a single operator. The data acquisition unit (DR2 in Figure 2.3-8) consists of 12 8-bit analogue-to-digital converters (ADC), each with a 4 GHz sampling rate and integrated FPGAs for on-board data preprocessing. An inter-channel synchronization of the receive windows to within 15 ps is achieved; the precision of the range delay is better than 80 ps.
The radar raw data are recorded with a maximum of 3 GB/s on 12 SSD drives, which can be accessed over a 10 Gbit/s Ethernet interface for data transfer. For on-board processing, the data streams of all ADCs can be fed to 3 high-performance CPUs.
The high-precision timing unit (DR3 in Figure 2.3-8, shown in Figure 2.3-6) is used to generate the reference frequencies (DBFSAR: 100 MHz, F-SAR: 50 MHz). The ADC clock's function is to trigger the radar synchronization and generate the time stamps that provide a link between navigation and raw data. The timing unit is based on a rubidium atomic clock, which can be synchronized with the GPS time of the navigation system, and achieves a frequency stability of better than $5 \cdot 10^{-12}$ per year. Timing jitter is negligible and, in fact, too small to be measured.
The radar control unit (DR5 in Figure 2.3-8) is used to run and

Figure 2.3-6 The high-precision DBFSAR timing unit featuring a GPS synchronized rubidium atomic clock with a frequency stability better than $5 \cdot 10^{-12}$ per year.

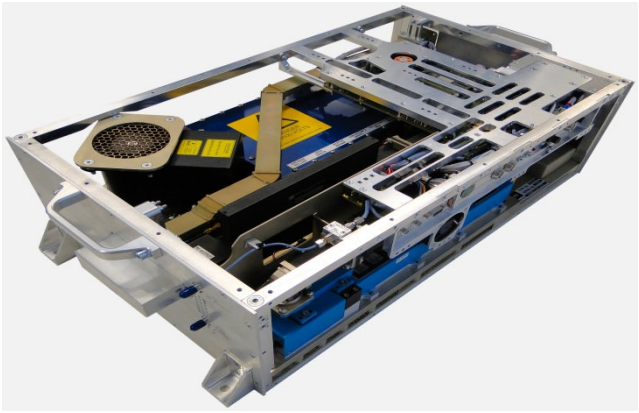

Figure 2.3-7 DBFSAR's X-band travelling wave tube amplifier (8.6-10.4 GHz, +65 dBm peak power, 10% RF duty cycle, 10 kHz PRF, 40 µs maximum pulse length).

monitor radar instrument operation. It includes a 20" display and a rugged keyboard – both certified for airworthiness. The control computer runs the new DBFSAR control software or an adapted version of the F-SAR control software on top of the Linux operating system. A dedicated 10 Gbit/s Ethernet interface is provided to connect an additional GPU module for enhanced real-time processing.

The DBF X-band Subsystem

The X-band frontend integrates transmitter, signal generation and the 12-channel receiver of the radar. The transmitter/receiver bandwidth lies in the 8.6 to 10.4 GHz range, and the pulse modulation is freely programmable.
The X-band subsystem is controlled in real-time via Ethernet, transmit and receive triggers, and a system clock. All oscillators are strictly coupled with the 100 MHz system reference. Trigger and system reference signals are generated in the digital subsystem. The X-band subsystem can be connected to 12 receive and 4 transmit antennas, where the former are operated simultaneously and the latter sequentially.
An air-cooled, wide-band travelling wave tube (TWTA) is used as the high-power amplifier (X1 in Figure 2.3-8, shown in Figure 2.3-7). It achieves a peak transmit power of around 2 kW with a high maximum duty cycle of 10%. The antenna switching matrix (X2 in Figure 2.3-8) is a high-power transmit matrix based on wave-guide technology and includes 12 integrated LNAs and bandpass filters on the receive side. The transmit power can be switched to either the transmit ports or onto a dummy load. Each LNA input can be connected to a calibration signal through a coupler, fast switches and a power divider. This internal calibration loop can be used to ensure an amplitude stability of 0.1 dB, a phase stability of 5° and a delay calibration of better than 5 ps. The signal generator (X3 in Figure 2.3-8) contains a chirp generator with up-conversion and the network for control- and reference signal distribution. It is an arbitrary waveform generator (AWG) that can create transmit signals of up to 1.8 GHz bandwidth. The waveform is freely programmable up to a maximum duration of 250 ms. It is possible to register up to 8 waveforms, which can either be transmitted sequentially or stitched together to form a single waveform. Generating FMCW signals is also possible.
The 12-channel down converter (X4 in Figure 2.3-8) supports a frequency range of 8.6 to 10.4 GHz on input and involves a demodulation to a range between 20 and 1820 MHz using a single-sideband downconverter. With the integrated actuators, the receive gain can be varied synchronously within a dynamic range of 63 dB, either from pulse to pulse or even within a pulse. The conversion frequency and phase can be freely programmed through the oscillator. Possibilities for step-frequency operation and the use of external oscillators are also implemented.

The DBF Antenna Configuration

The DBFSAR antenna system consists of four single-polar horn antennas in transmit and 12 DBF receive antennas in microstrip-

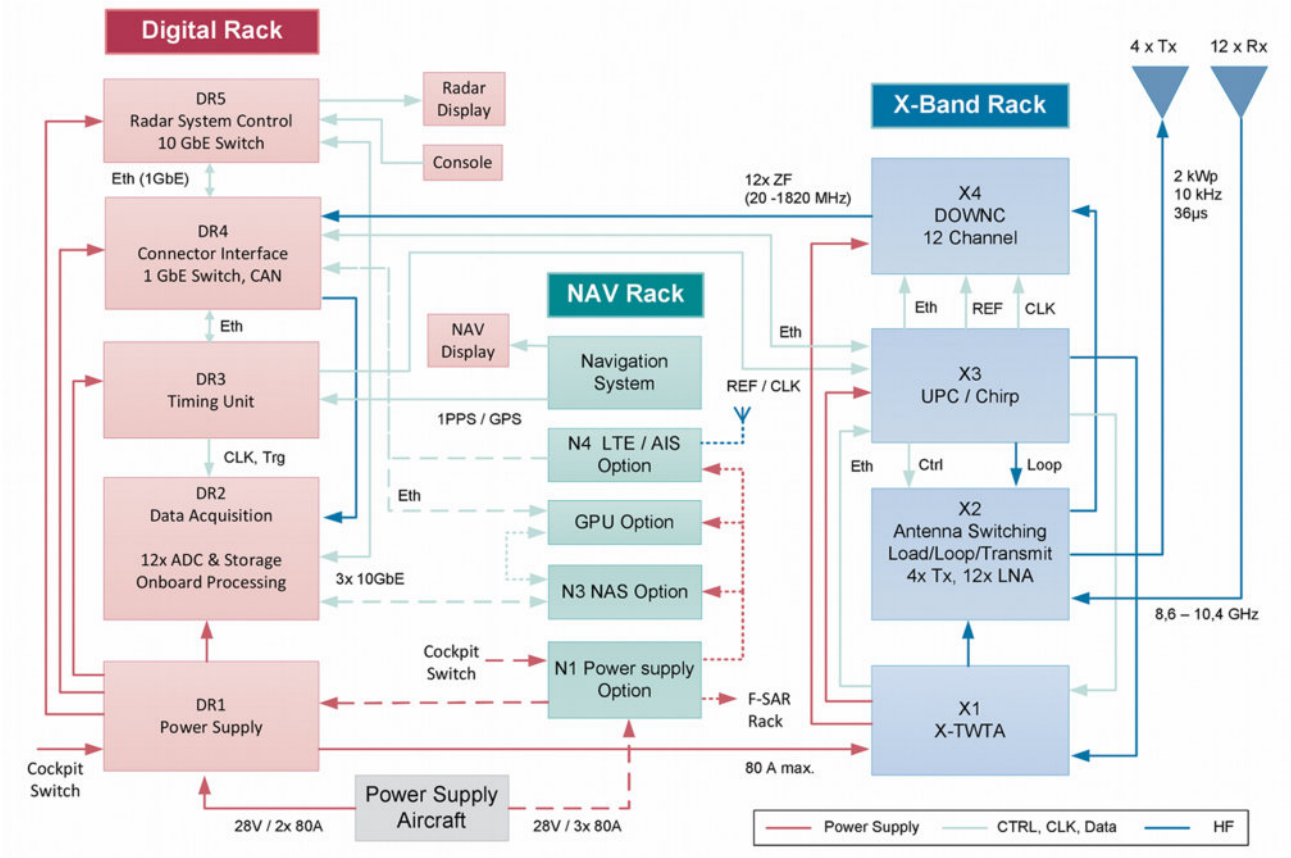

Figure 2.3-8 DBFSAR block diagram. Up to 4 transmit and 12 receive channels in X band can be implemented to demonstrate new digital beamforming techniques.

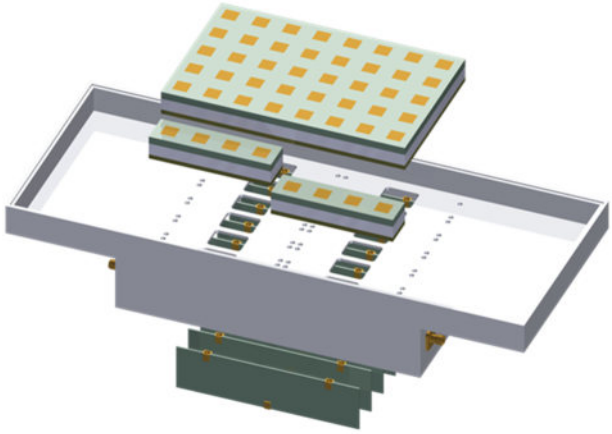

Figure 2.3-9 Schematic drawing of the DBFSAR receive array. The individual 1 x 4 receive modules can be placed and combined in various ways to obtain different DBF configurations.

Figure 2.3-10 The DBFSAR racks mounted in the aircraft cabin during the maiden flight. The 6 waveguide connectors to the outside antenna configuration are visible on the right.

patch technology. The transmit antennas are designed for a high average power and all antennas feature a high bandwidth of 2 GHz around the 9.5 GHz center frequency to fully support the DBFSAR system requirements. On transmit, the 3 dB beamwidth is about 30° in both azimuth and elevation; an alternative pair of antennas to generate a narrower 16° beam in azimuth is foreseen. The receive antennas are based on DBF modules containing 1 x 4 individual patches, denoted as Digital Beam Forming Receiving Antenna Module (DBFRAM). These modules are highly efficient (> 75%) and use constant amplitude and phase tapering to minimize the noise figure.

A maximum of 12 receive channels, each using DBFRAM modules, are combined to form a DBF receive array, illustrated in Figure 2.3-9. This array allows pointing angles in the range of ±15°, corresponding to the illumination footprint of the transmit antennas.

A flexible antenna backplane allows for various spatial arrangements of DBFRAM modules in along- or across-track configuration, or even a combination of both. In addition, pairs of DBFRAM modules may be combined to yield 1 x 8 or 2 x 4 subarrays in the full DBF configuration. In general, individual DBFRAM modules may be mounted either horizontally or vertically on the antenna backplane.

Mounting a large number of antennas on the body of an aircraft – as is required for digital beamforming – requires a dedicated antenna carrier. A carrier of this kind is currently being developed for DLR's DO228-212 (D-CFFU) aircraft. It will face towards the right from the lower middle section of the

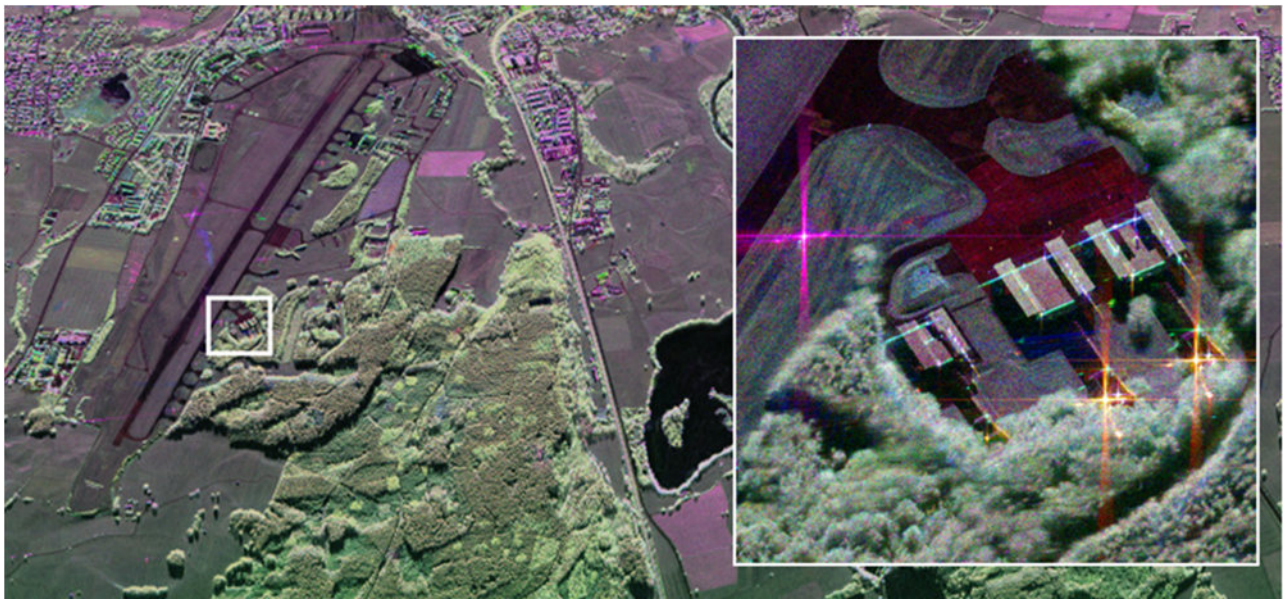

Figure 2.3-11 First fully calibrated DBFSAR image acquired over the F-SAR/DBFSAR calibration test site in Kaufbeuren (HH=blue, VV=red, HV=green). The inset zoom into a small part of the scene illustrates the high-resolution capabilities of DBFSAR.

aircraft fuselage and will mount the antennas with 45° mechanical tilt in elevation. This arrangement minimizes multi-path effects due to interactions with the aircraft body and helps to provide an optimal illumination of the important incidence angle range between 30° and 60°.
The DBFSAR antenna carrier is scheduled for testing in 2019. The first flight tests of the new radar instrument, described in detail in the following section, used the existing F-SAR antenna carrier together with the F-SAR antennas. These trials were therefore limited to simplified DBF modes with three polarimetric receive channels and bandwidths no higher than 800 MHz. Additional flight tests using DBFSAR antenna configurations will follow in 2019.

Maiden Flight and First Results

The maiden flight of the DBFSAR system took place on November 29, 2016 over the calibration test site Kaufbeuren in Southern Germany. For this flight, the three F-SAR X-band antennas were mounted in an interferometric across-track/along-track configuration. All F-SAR antennas are dual-polarimetric, such that it was possible to demonstrate the simultaneous acquisition of 6 channels with 800 MHz bandwidth.
The first flights were an unprecedented success, and data in various imaging modes were collected and processed. Figure 2.3-11 depicts an image of the full approximately 3-km-wide swath. The data set shown is fully calibrated and was processed with a resolution of 19 cm x 10 cm in range and azimuth, respectively. A zoom into a small area containing a trihedral corner reflector and several strong target responses is shown on the right side of the figure.
These results were achieved without any auto-focusing techniques – with motion compensation based solely on the navigation data provided by the GPS/IMU subsystem of the instrument. The theoretical spatial resolution was reached – as confirmed by analysis of the responses of radar reflectors in the scene – and an excellent phase and amplitude calibration of the system could similarly be verified [RC-54].
Additional flights that included the first interferometric configurations were performed in April 2017 over the Lake Starnberg area in Germany. These flights were mainly used to evaluate interferometric imaging modes and to test system stability and geolocation accuracy over longer image strips. Figure 2.3-12 shows an overview of the test site. Several image strips were successfully processed and geo-coded.
Also shown in Figure 2.3-12 is the differential across-track phase in both half- and full-baseline mode. The depicted phase corresponds to the difference in height relative to the topographic height of the TanDEM-X DEM. Apart from resolution effects, no distorting phase trends are visible, indicating that the interferometer has a high calibration accuracy. Similar results were obtained for the along-track interferometer. Further tests using the full bandwidth of 1.8 GHz and 12 receive channels, and employing real digital beamforming modes, will be conducted in 2019.

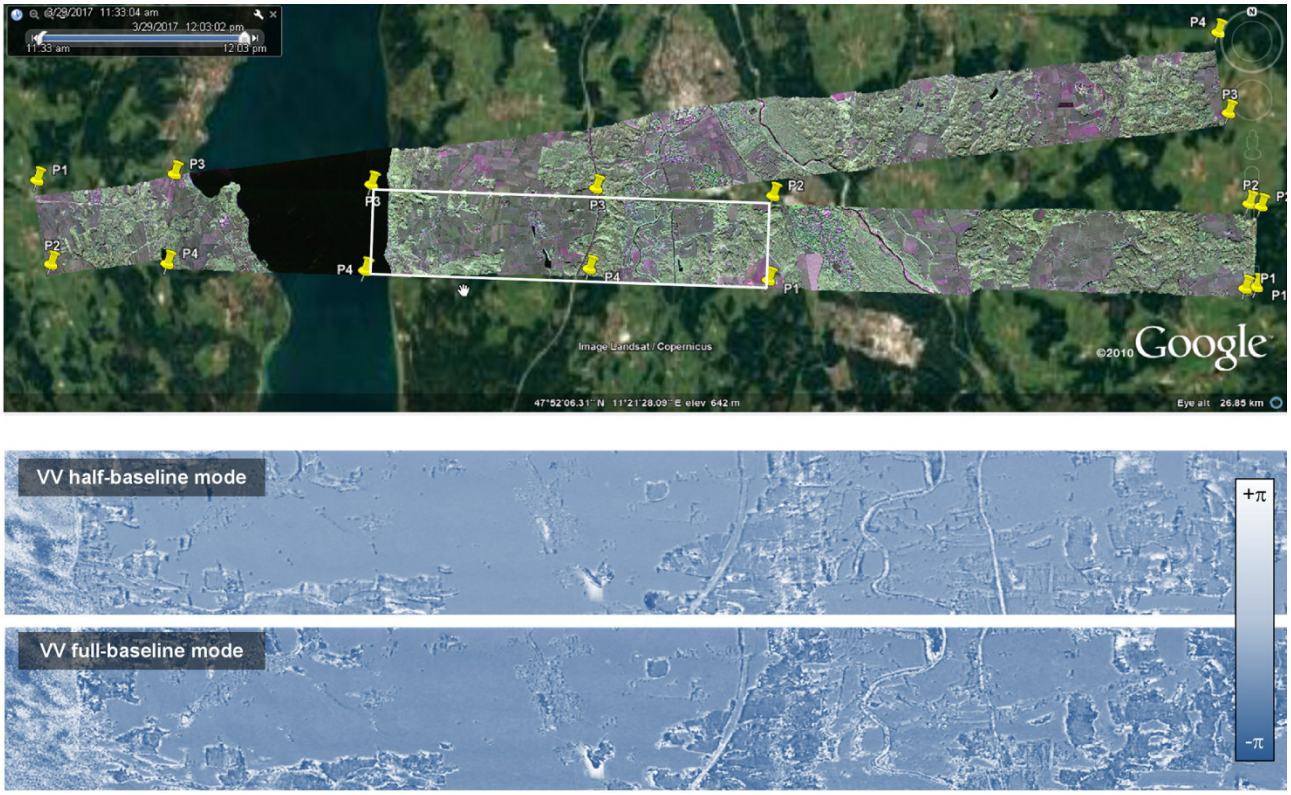

Figure 2.3-12 Top: overlapping DBFSAR acquisitions in the region of Lake Starnberg in Germany. The images represent geo-coded polarimetric data. This flight was used to evaluate interferometric imaging modes and to test system stability and the geolocation accuracy over longer image strips. Bottom: DBFSAR interferometric measurements in simultaneous half- and full-baseline mode, showing residual phase as measured relative to a TanDEM-X digital elevation model. The absence of visible phase trends indicates the high calibration accuracy of the associated interferometer.

2.3.3 Major F-SAR Campaigns

Between 2011 and 2015, the F-SAR system became fully operational and sufficiently mature for campaigns covering a great variety of research topics. A total of 38 different measurement campaigns consisting of 158 flights and more than a thousand polarimetric, multi-frequency SAR data acquisitions were carried out, leading to more than 60 TB of raw data and 400 TB of image data. In addition, 20 calibration and test campaigns with 74 flights were undertaken to verify and improve the quality of the acquired campaign data, mostly carried out over DLR's calibration site at the airport of Kaufbeuren, located approximately 80 km south-west of Munich.

Most of the data were acquired in new, innovative imaging modes: multi-frequency fully polarimetric modes, single-pass polarimetric (along- and across-track) and repeat-pass polarimetric interferometry, tomography, holography and circular SAR. Some data sets were also acquired in pseudo 4-channel, real 2-channel, as well as in P-band sounder modes for research on SAR information extraction and processing algorithms.

The F-SAR measurement activities conducted in recent years show a trend towards larger and more complex campaigns with many measurement flights in various ecosystems and climate zones (see Figure 2.3-13). One of the most challenging measurement campaigns was ARCTIC, an expedition to Greenland's inland ice in spring 2015, where F-SAR collected data across the entire frequency spectrum (X, C, S, L, and P band) over test sites, for many of which complementary data are available from other scientific organizations. The campaign also featured a stop-over in Iceland to collect data for analyzing young volcanic geology in support of NASA/JPL's VERITAS mission proposal. The second large measurement campaign was AfriSAR in 2016, which was carried out over the tropical forests of Gabon and focused on the collection of data sets in L and P band as input for the scientific community in preparation for the Tandem-L and BIOMASS satellite missions. The AfriSAR campaign was organized in close cooperation with ESA and supported by additional flights of ONERA's SETHI sensor, as well as NASA's UAVSAR and LVIS systems. Both campaigns, ARCTIC and AfriSAR, involved in situ activities by DLR staff and external partners to carry out additional measurements on ground and to support the precise calibration of the sensors on site.

Numerous other measurement campaigns took place in and around Germany, covering test sites for research regarding soil moisture (SOIMEX), agriculture (CROPEX), high-precision DEM generation over tidal flats (TOPSAR), military purposes (SWISAR, DALOEX, ATRSAR), long-term temporal change and tomography in forestry (TMPSAR, FOREST, SARTOM), traffic monitoring and disaster response (VABENE), archaeology (ARCHEO), and glaciology of temperate alpine glaciers (ICESAR).

As an interesting overall development, multi-temporal information has started to play an increasingly important role in recent F-SAR campaigns. Short revisit times of 15 to 20 minutes were planned and achieved with pass-to-pass data combinations (VABENE). Time delays of several hours to days were accomplished by combining data acquired in repeated flights on the same or the next day (DALOEX). Weekly flights were carried out for research into agricultural applications (CROPEX), while forestry also involved much longer time intervals with yearly repetitions (TMPSAR).

The following sections describe some of the particularly interesting F-SAR campaign highlights of recent years in more detail.

Agriculture and Soil Moisture (CROPEX, SOIMEX)

SAR imagery of agricultural areas shows strong changes in the backscatter properties during crop growth and as bio- and geophysical properties vary. This highly important research topic is of great potential with regard to future applications such as the optimization of irrigation or in monitoring plantations. Satellites may eventually be used for operational data collection, but airborne SAR data are essential to research and develop models and algorithms.

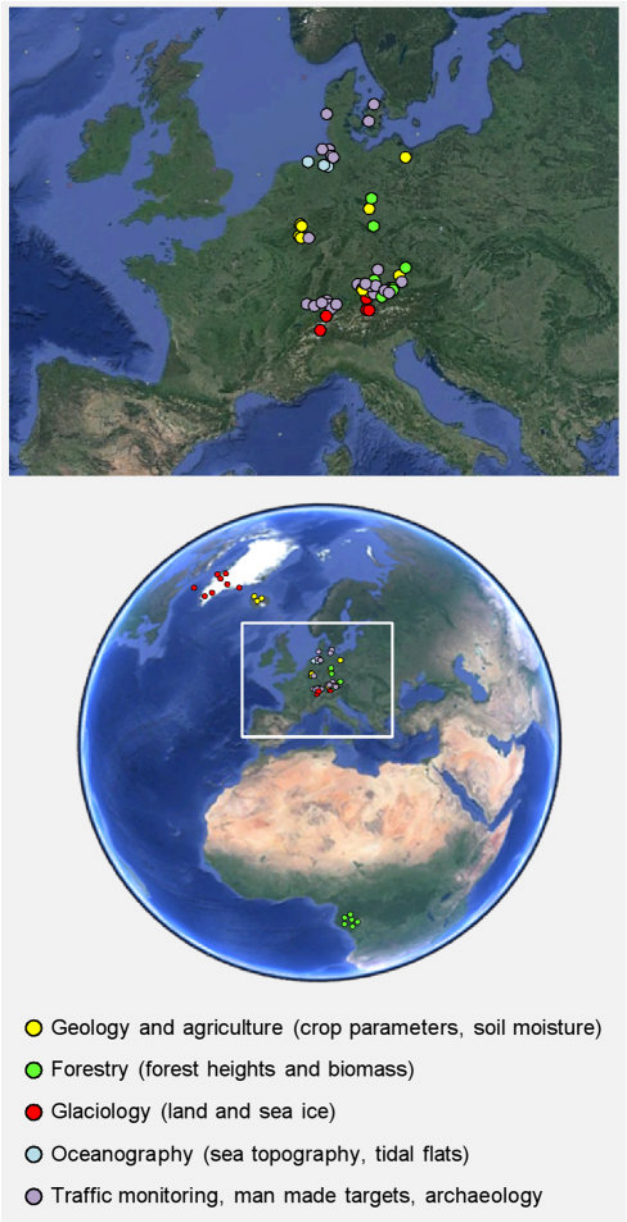

Figure 2.3-13 Test sites of airborne F-SAR campaigns between 2011 and 2017.

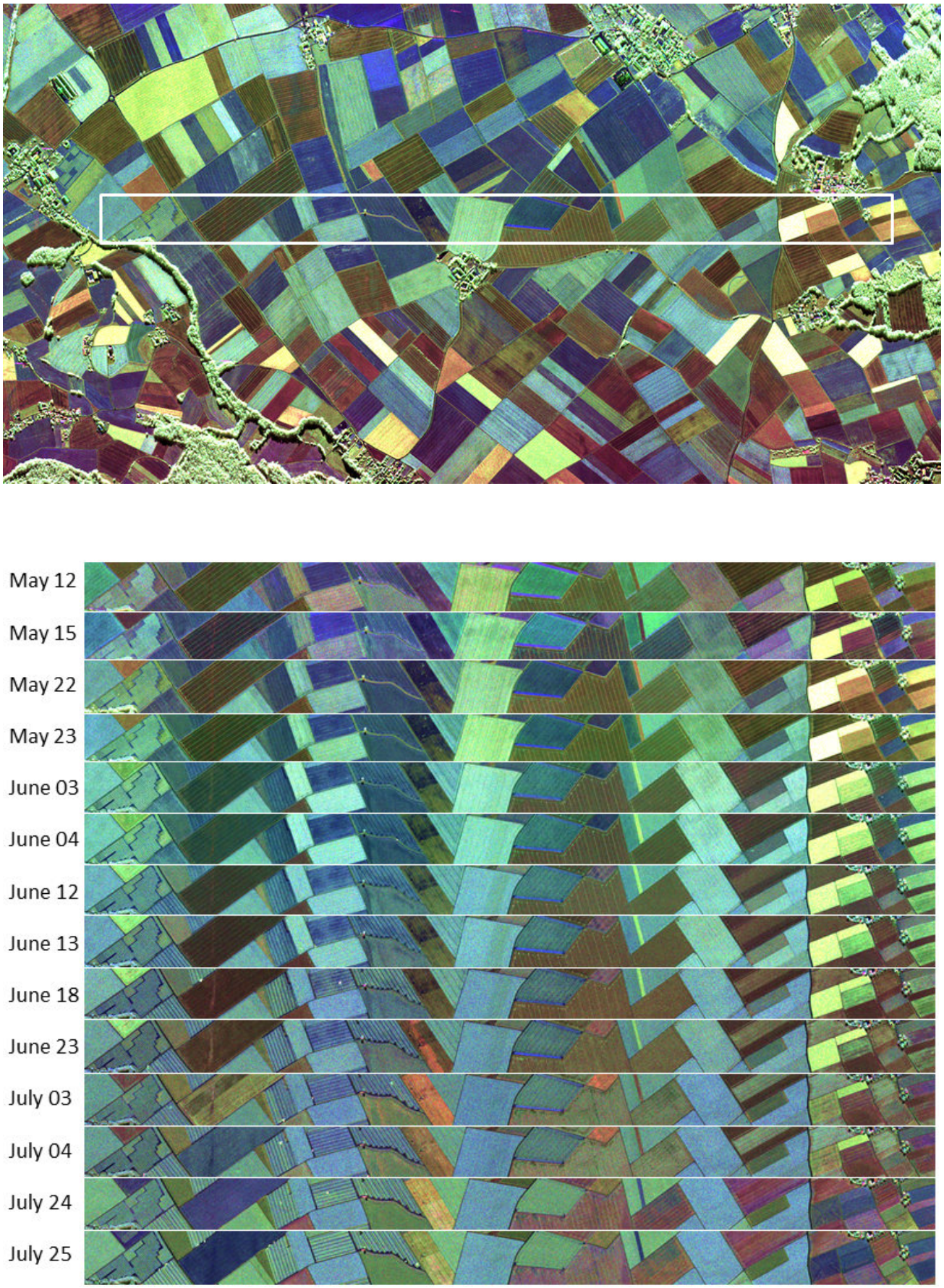

Figure 2.3-14 Time series of fully polarimetric C-band data at the CROPEX agricultural test site near Wallerfing, Germany. The time series depicted illustrates the diversity of agricultural crops in this region, as well as their temporal variability over the growth period between May and July 2014.

As part of the CROPEX project, between 2013 and 2015, SAR data were acquired at regular intervals over the very heterogeneously structured agricultural area of Wallerfing near Deggendorf, Germany. The flight activities in 2014 were especially intensive, with almost weekly flights covering the entire growth period. During this period, 15 separate flights provided polarimetric interferometric and tomographic data in X, C, and L bands (see Figure 2.3-14), which were used to determine properties such as vegetation height, soil moisture, or the temporally variable appearance of individual plant species. The aircraft measurement campaign was accompanied by extensive field measurements to obtain ground truth to support the scientific exploitation of the data [PhD-1].

The SOIMEX project, which took place between 2012 and 2015, was concerned with soil moisture measurements at several designated German test sites characterized by variations in geology and morphology. This campaign used a DigiTHERM thermal camera and a PLMR-2 radiometer installed on the aircraft alongside the F-SAR instrument to allow data collection for improved estimation of soil moisture using a combination of active and passive microwave sensing techniques. The flights were mainly carried out in the early morning and late evening hours, when the influence of solar radiation on the passive measurements is negligible. The thermal camera and the radiometer were provided by the Forschungszentrum Jülich – the principal project partner. SOIMEX is part of the TERENO program of the Helmholtz association, which acquires long-term ground and atmospheric data at various representative test sites across Germany to advance research into the interactions between soil and the atmosphere and the impact of climate change on these interactions.

One of the goals of SOIMEX was to demonstrate that robust and accurate soil moisture estimation from SAR data is feasible, irrespective of the angle of incidence in the SAR data. This research objective was achieved, as verified by comparison with long-term measuring stations for weather and soil data set up in the individual test sites. In the course of this work, a SAR data mosaic was generated in which the borders of the individual scenes are virtually invisible, which is an indication of the outstanding radiometric calibration of the data (see Figure 2.3-15). The results of soil moisture estimation under vegetation were published in [J-57].

High-Precision DEMs (TOPSAR)

Changes in the topography of the Wadden Sea pose a major problem for shipping in the tidal flats along the German North Sea coast. Within a year, safe fairways can shift, so changes must be recorded and maps need to be corrected promptly. This task is currently accomplished with a regular schedule of flights with airborne laser scanners (ALS). However, ALS is only able to provide a narrow swath, which makes the data acquisition process very time- and cost-intensive. The aim of the TOPSAR project in 2012 and 2013 was to determine whether multi-frequency airborne interferometric SAR can produce elevation models of mudflat areas of a sufficiently high quality to complement, and potentially replace, future ALS measurements at much lower operational costs (see Figure 2.3-16).

For this purpose, the tidal flats in the Juist and Jade Bight test areas were imaged at X and S band in seven flights. A new innovative imaging mode, using a combination of single-pass and repeat-pass interferometric measurements, was

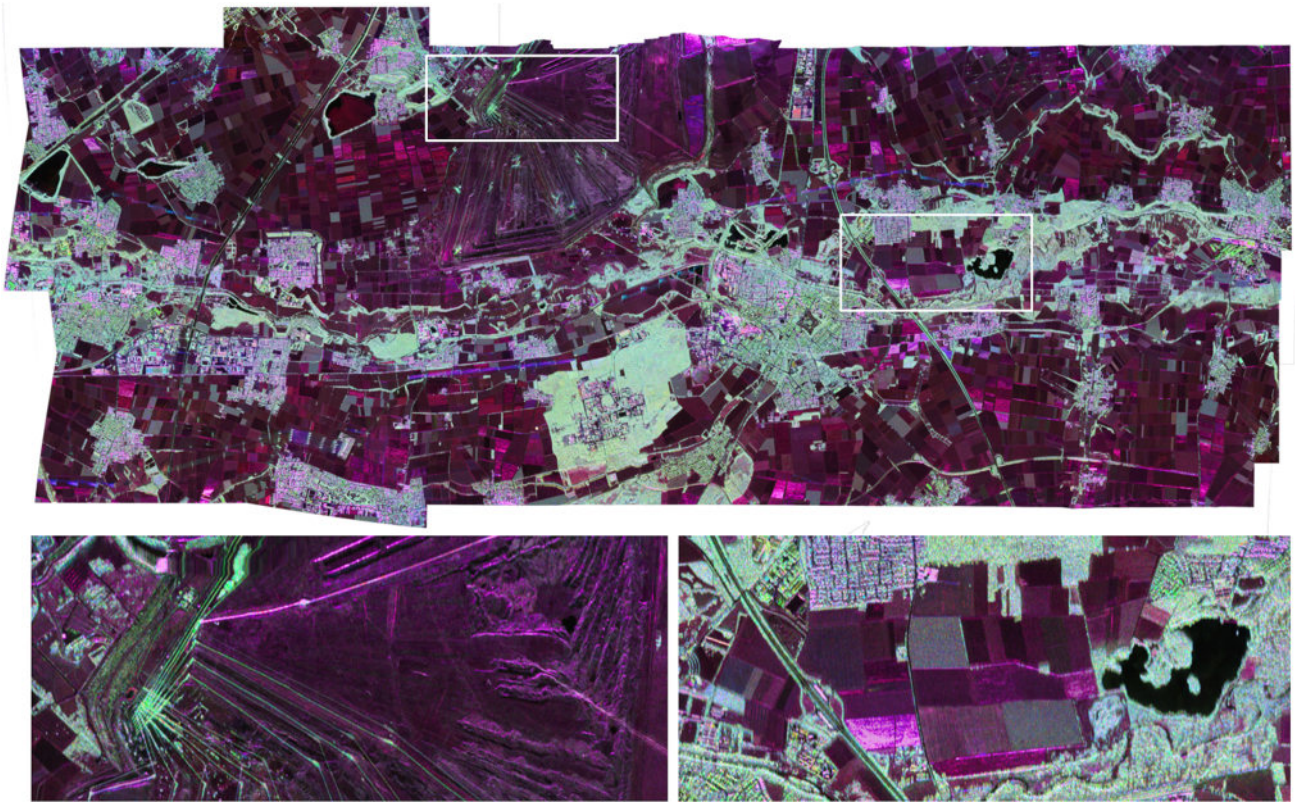

Figure 2.3-15 A mosaic of 11 separate polarimetric L-band SAR images acquired near Jülich, Germany. The large, open brown coal pit Inden is clearly visible close to the center in the upper half of the mosaic. The imagery of the different acquisitions combines seamlessly due to the accurate radiometric calibration.

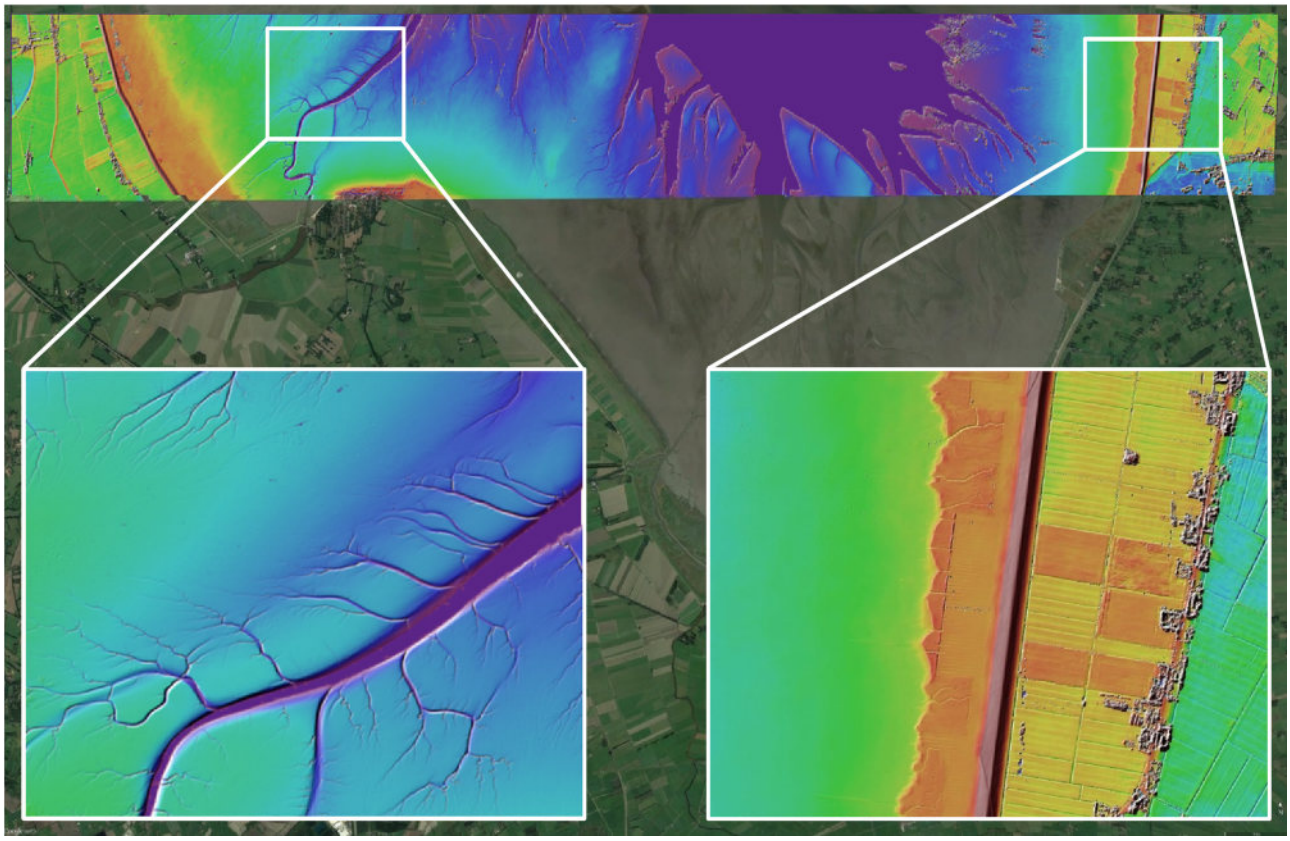

Figure 2.3-16 A very high-precision DEM of tidal flats in the Jade Bight area (German Wadden Sea) obtained from interferometric SAR measurements. The dam is the highest object in the image while the lowest visible parts are drains of the Jadebusen, which is flooded twice a day. The purple parts contain invalid data due to open water. A vertical DEM accuracy of about 10 cm was reached [PhD-7].

employed to significantly improve the attainable height accuracy. To ensure data quality, 15 radar reflectors were installed in the Juist and Jade Bight areas, and ground profiles were measured using differential GNSS to obtain centimeter accuracy. A special challenge in the later processing of the SAR data was the very low level of backscatter in parts of the moist tidal flats. A special radar configuration was developed to optimize the SNR in these regions (see also Section 2.3.4).

Land and Sea Ice (ARCTIC)

An important development field in SAR research concerns the investigation of snow and ice by means of polarimetry, interferometry and tomography. The highlight in ice research at the Institute in recent years was the ARCTIC measurement campaign – an expedition to Greenland in spring 2015. ARCTIC was dedicated to SAR measurements of the diverse types of arctic land and sea ice. The campaign was unique in that F-SAR was used to acquire SAR data at four different wavelengths (X, C, S, and L band), of which up to three could be recorded simultaneously. In addition, dedicated P-band acquisitions were performed over specific test sites to supplement the multi-frequency acquisitions at shorter wavelengths.

In order to ensure a highly accurate sensor calibration, several radar reflectors were installed in the area around Kangerlussuaq and F-SAR calibration data were acquired and evaluated throughout the campaign, especially after every modification of the F-SAR sensor. In addition, radar reflectors were deployed in the individual test areas on the ice shield and ground penetrating radar measurements, as well as probe measurements of the near-surface snow and ice stratifications were carried out. To accomplish these *in situ* activities, a ground team had to be flown to each test site with an additional transport aircraft equipped with skis. They then had to carry out all of the on-ground activities within a few hours, including the GNSS positioning of the radar reflectors to centimeter accuracy. Wooden mounts for the corner reflectors were fixed deep in the hard packed snow in the correct orientation, the corner reflectors were placed on them and their positions were measured by differential GNSS with centimeter accuracy. In addition, ground-based radar and snow probe measurements were carried out (see Figure 2.3-18).

The ARCTIC campaign involved a total of 24 flights over 11 test sites that were carried out within one month with the F-SAR sensor installed on-board DLR's DO228-212. A part of the campaign was performed for the Danish Ministry of Defence Acquisition and Logistics Organization (DALO). The spectrum of test sites for which data were acquired ranges from areas at the highest point of the ice sheet, where new snow is deposited and where thaw events are extremely rare even in summer, over areas where even horizontal ice motion takes place but crevasses or water inclusions are absent, to areas at the edge of the ice sheet with an abundance of crevasses and a low altitude that implies annual thaw events in summer.

In East Greenland, the campaign included the fast-flowing Helheim glacier (see Figure 2.3-19) as well as the so-called Lost

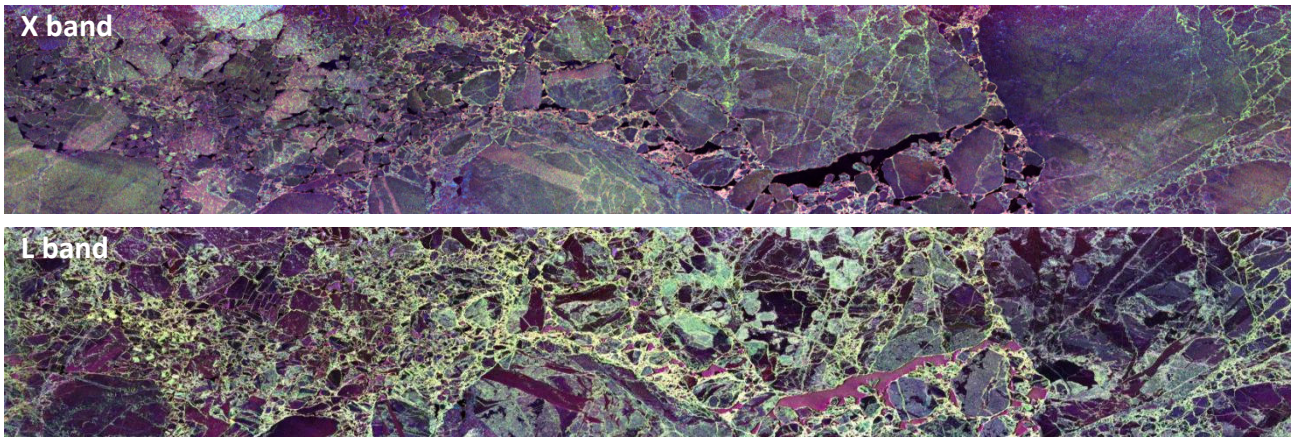

Figure 2.3-17 Arctic Ocean in the Davis Strait south of Disco Bay: simultaneously taken SAR images in X-band (above) and L-band (below) displayed in Pauli decomposition. Longer wavelengths penetrate the ice deeper than short wavelength, providing enhanced sea ice classification possibilities.

Squadron, an area in which a squadron of World War II bombers is now hidden under the ice. In addition, two very long data sets were acquired. The first was a 100-km-long strip of sea ice recorded off the west coast of Greenland (see Figure 2.3-17). The second was a 230-km-strip covering the ice sheet from the edge of the ice near Kangerlussuaq, reaching far inland to show the enormous diversity and variability in the radar signature of land ice in a single data set (see Figure 2.2-62). Various new and innovative imaging methods were used to provide data to support the different and complex scientific objectives of this campaign: single-pass polarimetric interferometry in X and S bands, step-frequency data acquisitions in X band to provide the highest possible spatial resolutions, circular flights for tomography and holography in L and P bands, stripmap mode tomography in different frequencies, as well as recordings in sounder mode in P band.

Figure 2.3-18 Unpacking the equipment for a short five-hour stay on Greenland's ice shield. Everything had to be prepared at the basecamp in Kangerlussuaq to the greatest possible extent. The extreme polar cold was a challenge for the electronic equipment and the staff.

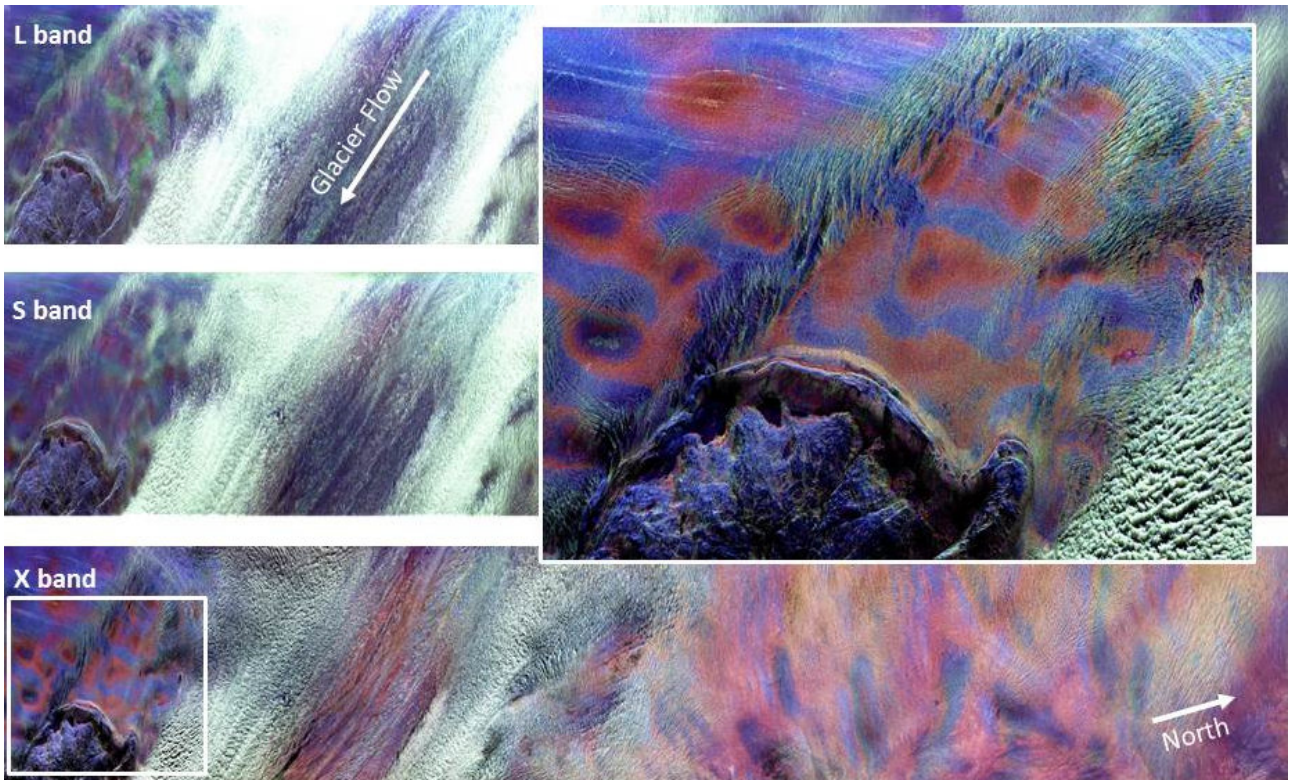

Figure 2.3-19 The Helheim glacier in Greenland, simultaneously imaged by F-SAR in L, S and X bands, all in fully polarimetric mode. In X band, differential path delays between the polarizations are seen to cause changing polarimetric signatures depending on penetration depth (see zoom at the upper right).

Forestry (TEMPOSAR, AfriSAR)

For many years, the Institute has actively pursued forestry research. Polarimetric SAR interferometry and, increasingly, long-wavelength SAR tomography in the L and P bands have been successfully used to estimate various forest parameters, such as forest height and structure, underlying topography, and forest biomass. The latter parameter is of particular importance in the modelling of climate change, as it is directly related to the local capacity to store carbon.

Future satellite SAR missions, such as Tandem-L and BIOMASS, are being designed to collect this information globally and, in the case of Tandem-L, with a high revisit rate. The Institute's airborne campaigns represent an important preparatory step for these satellite missions, as the scientific community receives data long before the launch of the satellites such that algorithms and evaluation procedures can be tested and refined.

The TEMPOSAR project entails the monitoring of a managed temperate forest near Traunstein, Germany, that undergoes a change in structure and composition as a result of a different forest management. In addition, a part of the test site has been reforested following severe storm damages due to cyclone *Kyrill* in 2007. The regrowth of the damaged areas as well as the changes in forest structure have been monitored for over a decade: first using the Institute's E-SAR, and later the F-SAR sensor. In recent years, the data collection over the site has been extended from purely polarimetric interferometric acquisitions to fully polarimetric tomographic measurements (see Section 2.2.8).

In 2016, next to Traunstein, a large research plot was established as a new super test site in a highly diverse structured forest. This mega-plot is highly valuable as a permanent reference for remote sensing as well as for understanding the large scale forest structure. Accordingly, the area is regularly covered by F-SAR acquisitions and in situ monitored by the Technical University of Munich. Since 2017 the site is part of the Smithsonian Forest Global Earth Observatory (ForestGEO). The full data sets for this test site are available to the scientific community.

The AfriSAR campaign focused on collecting and evaluating polarimetric interferometric and tomographic SAR data acquired in L and P bands over various types of tropical rainforest in Gabon, Africa, to prepare for ESA's BIOMASS and Germany's Tandem-L satellite missions (see Figure 2.3-20). The campaign was commissioned by ESA, and entailed data collection with ONERA's SETHI SAR sensor during the dry season in July 2015, as well as acquisitions with the Institute's F-SAR sensor over the same test sites during the rainy season in February 2016. In addition, NASA carried out independent measurements with its full-waveform Lidar LVIS and its UAVSAR radar system in February 2016. To support the scientific exploitation of the SAR data, extensive ground truth was collected by project partners.

During the campaign, the Institute's F-SAR sensor acquired a comprehensive data set comprising 15 flights over six different test sites (see example in Figure 2.3-21 and Figure 2.2-55). In addition to multi-baseline tomographic imaging with parallel flight paths, separate acquisitions used an experimental imaging mode based on a concentric multi-circular sensor track with changing heights. Dedicated system calibration flights were carried out over the Kaufbeuren calibration field before and after the campaign.

Furthermore, a very large trihedral radar reflector with an edge length of 5 m was deployed at the Nkok test area in Gabon and was used to verify the excellent system stability of the F-SAR instrument and the very high calibration quality of the acquired SAR data throughout the campaign (see Figure 2.3-22).

Figure 2.3-20 The AfriSAR team together with ESA's project coordinator in front of DLR's DO228-212 research aircraft at Libreville airport in Gabon. The radar antenna carrier is clearly visible on the side of the aircraft behind the wing.

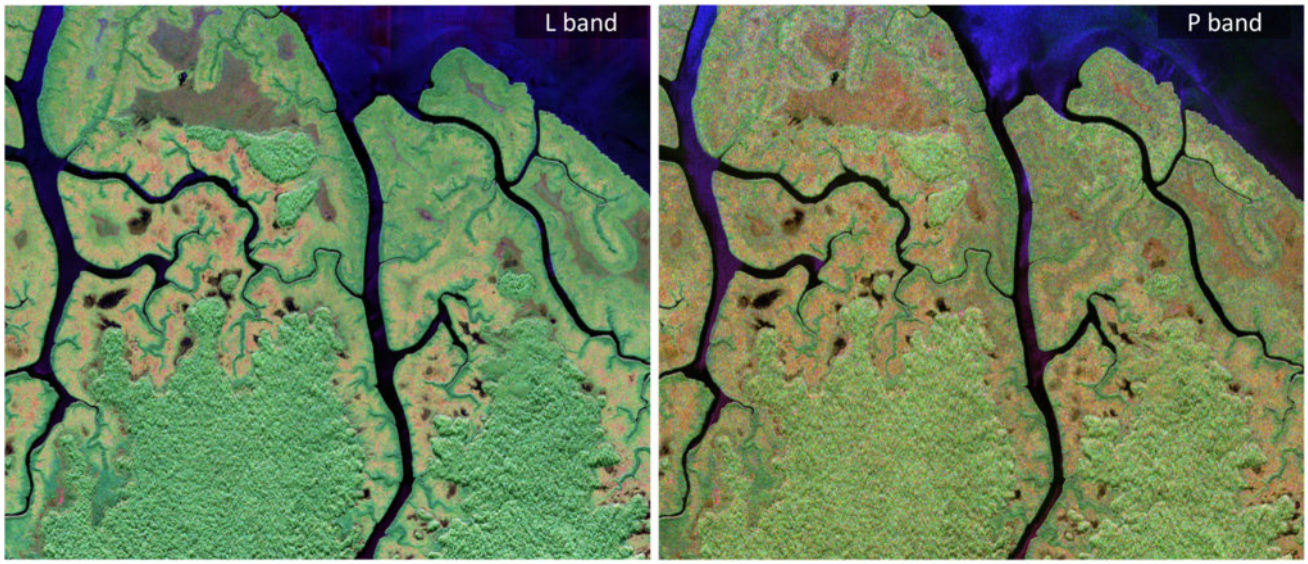

Figure 2.3-21 The Pongara national park south of Libreville, Gabon, with mangrove forest and rain forest, simultaneously imaged by F-SAR in L and P bands in fully polarimetric mode. While the P-band images are intended for research in preparation of ESA's BIOMASS mission, the L-band data are of great interest in the development of Tandem-L applications. The stronger penetration depths of P band can be observed in the rain forest areas. While in L band most of the backscatter originates from undirected reflections in the crowns of the trees – coloring the rain forest areas in a strong green – there is a substantial portion of double bounce scattering at the ground and stems of the trees in P band which turns the color into a reddish green. In the much lower mangrove forests (upper part of the image), both L and P bands create a large amount of their backscatter due to double bounce scattering with the flooded forest floor/ground surface, thus appearing red in the images. The scientific exploitation of the data is aided by the fact that full-waveform laser scanning data acquired by NASA's LVIS-sensor over this test site is also available.

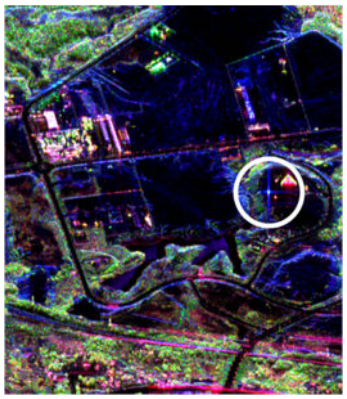

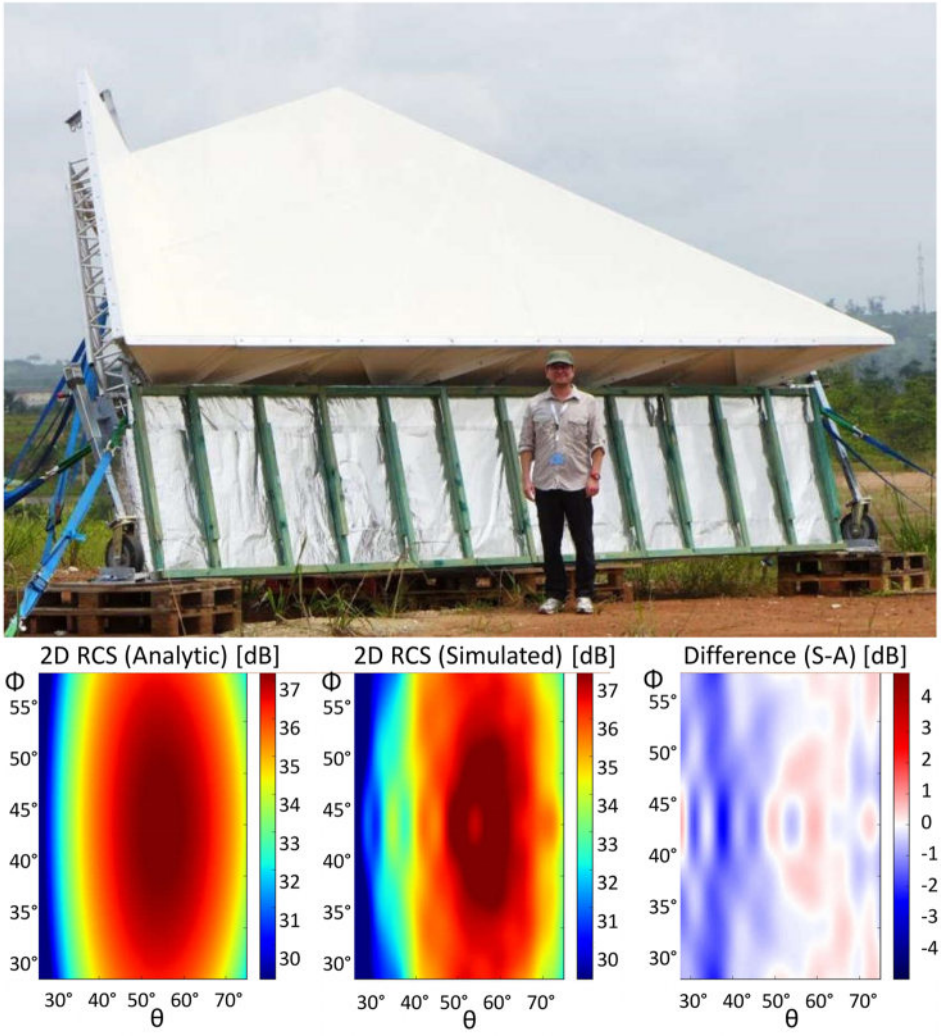

Figure 2.3-22 To enable the high-quality calibration of F-SAR's P-band data – acquired with a wavelength of 67 cm – a very large corner reflector with 5 m edge length was installed on the calibration site in Nkok, Gabon. A metallic shield was placed below the reflector's lower plate to dampen possible plate-ground reflections, which would otherwise degrade the response of the corner reflector. Even with this very large reflector and the precautions taken, the backscattered intensity of the reflector cannot be adequately modelled by the well-known analytic geometrical optics approach. A detailed simulation of the electromagnetic (EM) behavior of the trihedral reflector was therefore undertaken, and the results were found to faithfully reproduce the real behavior of the reflector in the F-SAR data. This detailed EM simulation deviates by up to 2 dB from the predictions of the geometrical optics approach (right plot).

2.3.4 Processing Algorithms

Research based on campaign data acquired by the Institute's F-SAR sensor allowed the development and verification of several novel applications and signal processing techniques for SAR systems. Techniques such as polarimetric SAR interferometry, differential SAR interferometry and SAR tomography have almost become routine for modern airborne SAR sensors. But for these applications to be successfully applied or even feasible, a robust and modular processing framework must be in place to provide the flexibility required to serve different user needs and application requirements. The Institute has further developed and operationalized its airborne interferometric processing chain, which currently ensures precise SAR data calibration, supports SAR image formation for the new DBFSAR sensor data at maximal resolution, and supports the automated segmented processing of very long data acquisitions. On the functional level, further important developments have been conducted in recent years, as described in the following.

A new and very powerful **algorithm for external calibration of multi-channel SAR data** has been developed to ensure the accurate and comprehensive interferometric and polarimetric calibration of multi-channel SAR sensors. It is fundamentally different from state-of-the-art approaches using focused SAR data in that it is based on the analysis of range compressed data [RC-32]. The approach developed is suited, and even essential, for the characterization and calibration of future multi-channel spaceborne SAR systems with digital beamforming and/or multiple azimuth phase centers. First analyses in this direction are taking place in the context of ESA's ongoing Calibration and Data Reduction study [RC-81].

The airborne **interferometric SAR processing chain** has been considerably extended and improved. In particular, a new interferometric processing module, ideally adapted to the processing of tomographic stacks and long time series, has been established. The robustness of the new processing approach stems from considering all possible interferometric combinations when estimating residual baseline errors and tomographic SAR phase offsets.

A refined and extended **processing chain for circular SAR** and holographic SAR data has been established (see Figure 2.3-28); it integrates the fast factorized backpropagation algorithm, supports 3-D tomographic focusing, and includes the accurate radiometric calibration of the outputs [PhD-8].

Different polarimetric SAR speckle filters were designed and integrated into a **robust incoherent change detection framework** [RC-146], [IC-79] (see Figure 2.3-23). The concept has been successfully applied in the context of internal DLR projects, but also for external contracts with the Danish Defence Acquisition and Logistics Organization (DALO).

To meet the demand for extremely accurate and high-resolution digital elevation models, a new **processing chain for dual-baseline, dual-frequency SAR interferometry** has been established. The approach combines single-pass and large baseline repeat-pass interferometric data. The processing chain includes newly developed algorithms for robust dual-frequency phase unwrapping, baseline calibration, estimation and correction of residual motion errors, and data fusion and

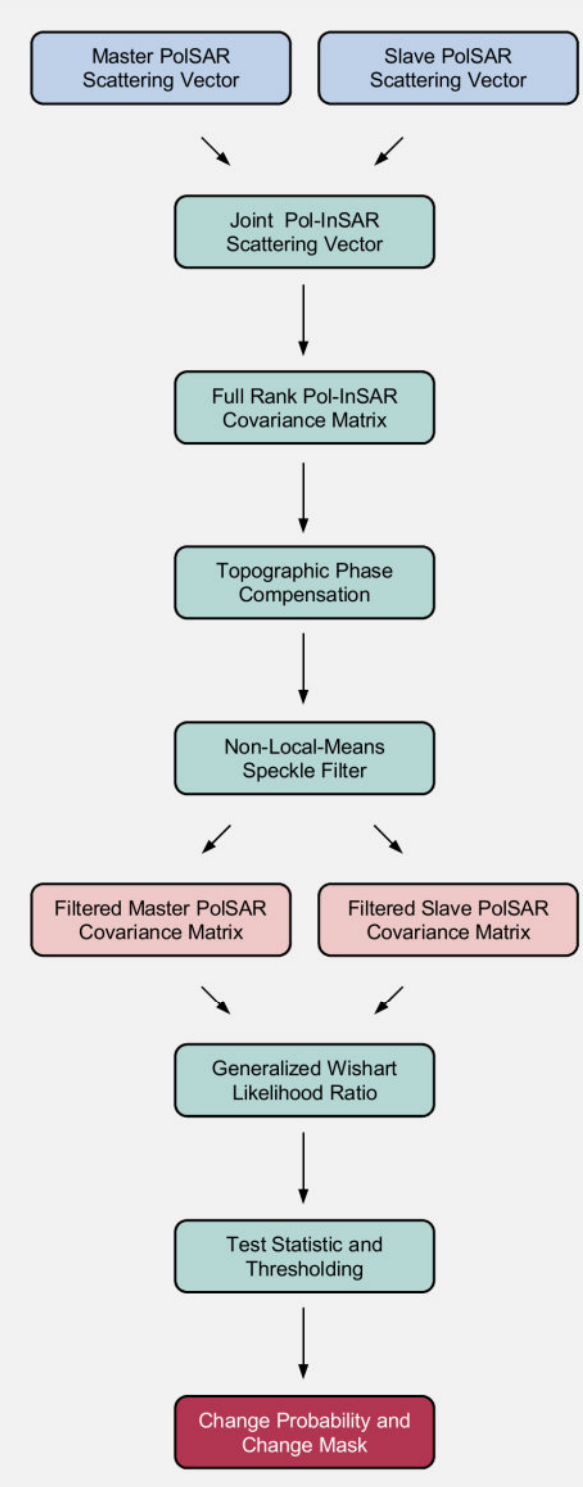

Figure 2.3-23 Data flow in the polarimetric change detection framework, which includes the joint non-local means speckle filtering of the interferometrically co-registered input data.

filtering [PhD-7], [RC-414], [RC-178], [J-28]. In terms of accuracy, the method has been shown to generate DEMs comparable to those produced by airborne laser scanning (ALS) sensors.

A first **prototype of a tomographic scene processor** has been developed and applied to the automated processing of interferometric stacks of polarimetric F-SAR data. The tomographic processing chain is modular and provides numerous

different tomographic focusing approaches (e.g., different types of MVDR, MUSIC, compressive sensing). The tomographic kernel is applied to entire scenes, using multiple CPU cores for parallel processing, and the processor provides tools for visualizing the 3-D results.
In the following, the polarimetric change detection framework, the new external calibration approach, the circular SAR processing and the dual-frequency dual-baseline DEM generation chain are described in more detail.

Polarimetric Speckle Filtering and Change Detection

Applications related to security and disaster monitoring play an important role in SAR remote sensing and, very often, require methods for reliably detecting changes that have taken place in the time separating a given pair of SAR acquisitions. A change detection approach based on polarimetric analysis – including advanced speckle filters – was developed at the Institute and proved to be much more robust against temporal decorrelation than interferometric change detection methods.
The processing pipeline for polarimetric change detection begins with master and co-registered slave data output by the operational interferometric airborne SAR processing chain and then proceeds as follows (see Figure 2.3-23):

- After cross-polar symmetrization, master and slave PolSAR scattering vectors within the region of interest are concatenated to obtain a single 6-element vector in each resolution cell.

- The outer product of these vectors yields singular 6 times 6 covariance matrices. A 4 x 4 spatial presumming then yields full- rank Pol-InSAR covariance matrices.

- The Pol-InSAR covariance matrices are speckle filtered using the non-local means filter [J-104].

- The two 3 x 3 block diagonal matrices of the filtered result are then used as the input polarimetric SAR datasets for change detection.

It should be noted that the joint filtering of master and slave data in the third step is essential, as it ensures that the resolution preserving, spatially adaptive filter operates on master and slave data in precisely the same fashion.
Independently filtering the two data sets using an adaptive filter

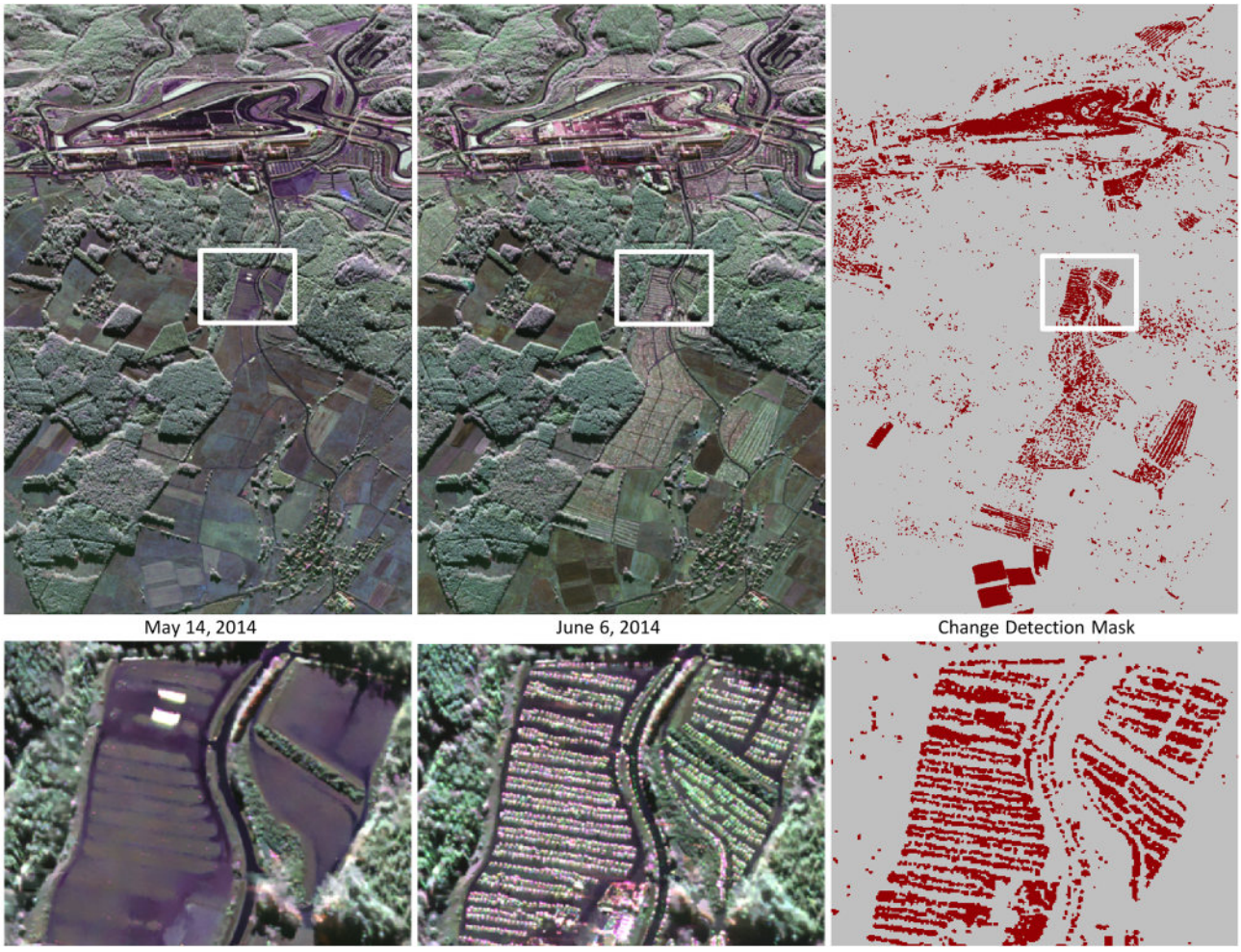

Figure 2.3-24 Polarimetric change detection using a joint polarimetric/interferometric non-local means SAR speckle filter. The results shown are based on two polarimetric F-SAR data sets acquired in X band three weeks prior to and during the Rock-am-Ring Festival in June 2014. The zooms highlight the area of a parking lot/field, which appears empty for the first data take and full of cars on the second. Distributed scattering areas are correctly classified as unchanged. The joint non-local means filter is essential for maintaining the high spatial resolution while achieving an extremely low false-alarm rate.

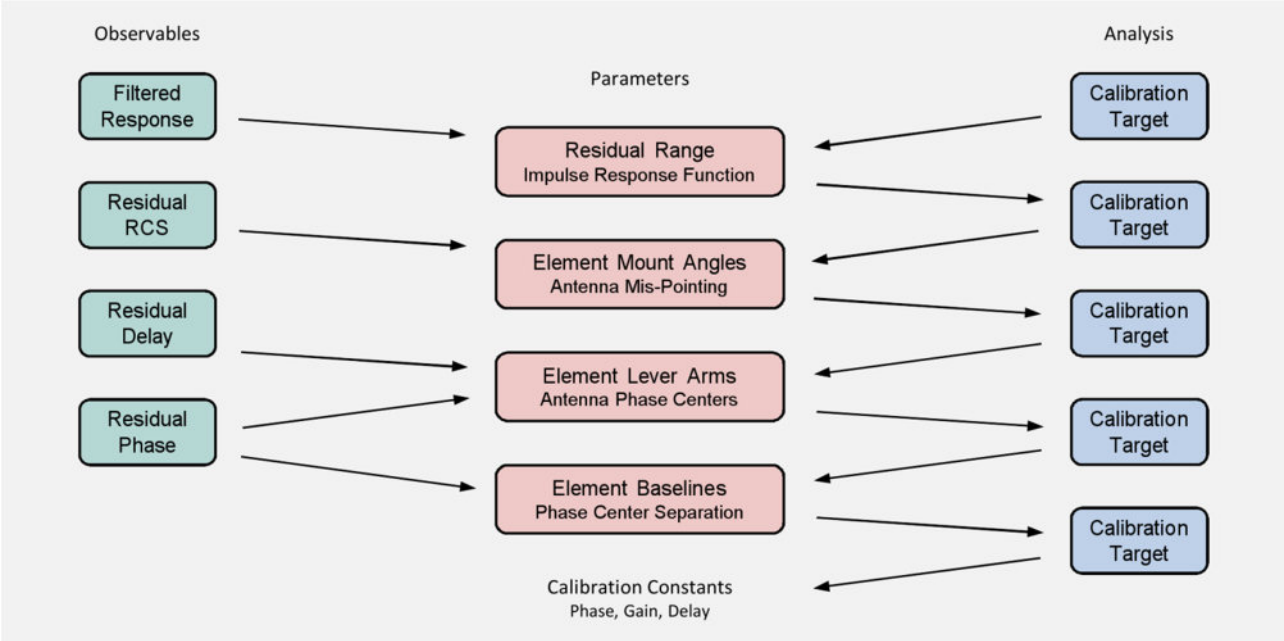

Figure 2.3-25 Sequential calibration of different sensor parameters based on range compressed SAR data containing the response of trihedral reflectors. The approach explicitly includes the precise calibration of antenna mount angles, lever arms and the baselines between antennas in addition to traditional parameters like the internal delay and RCS offsets.

would, by contrast, introduce artefacts near image discontinuities, where inconsistent spatial filtering of master and slave causes discrepancies that are then misinterpreted as temporal change.

The new change detection approach was applied with very promising results to F-SAR data from the DALOEX campaigns as well as to data from flights carried out in the context of the *Rock-am-Ring* festival as part of the VABENE++ project, with a focus on large event monitoring. Figure 2.3-24 shows the detection results based on data from two *Rock-am-Ring* flights that were separated by 21 days, with the later acquisition on the first day of the festival [IC-79].

All of the changes to infrastructure (e.g., the stages, food trucks), parking lots, campgrounds, and even the crowds of people are properly detected by the proposed framework. Regions of natural, distributed scattering (e.g., fields and forest) are, on the other hand, not classified as change, despite the considerable temporal decorrelation.

External Calibration of Multi-Channel SAR Data

Multi-channel SAR instruments – with SAR polarimetry, single-pass interferometry and/or digital beamforming – require the consideration of highly accurate calibration parameters during processing. These parameters are typically derived on the basis of dedicated SAR acquisitions containing reference targets with known properties. Conventional approaches evaluate the radar cross section (RCS), the internal delay errors and inter-channel phase offsets based on the responses of trihedral reflectors in focused SAR imagery.

These approaches are not, however, able to derive corrections for possible antenna mount angles (mispointing) and interferometric baseline errors. A new method has been designed to overcome these shortcomings (see Figure 2.3-25). It is based entirely on the analysis of range-compressed raw data and leverages the pulse-by-pulse analysis of amplitude, phase and delay variations observed within the range histories of reference targets to fully characterize and correct propagation direction dependent calibration issues. In addition, the approach does not depend on prior SAR image focusing in azimuth, which is essential in cases where azimuth beamforming techniques are

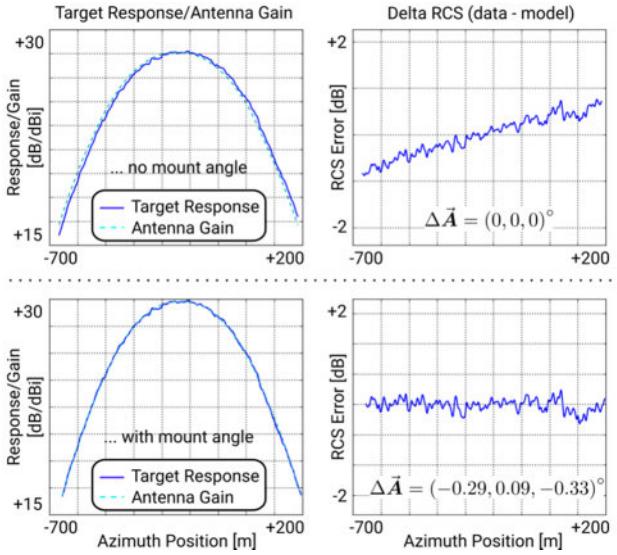

Figure 2.3-26 Impact of the antenna mount angle calibration on the residual RCS errors along azimuth, illustrated by a single 1.5 m trihedral reflector imaged by F-SAR at C band in VV polarization. Left: superposition of the target intensity before antenna pattern correction and the antenna gain.
Right: residual RCS error after antenna pattern compensation. Top: before mount angle calibration. Bottom: after mount angle calibration. The introduction of the mount angle correction ($\Delta\vec{A}$) is seen to remove the RCS error trend (top right) over the illumination time of the target.

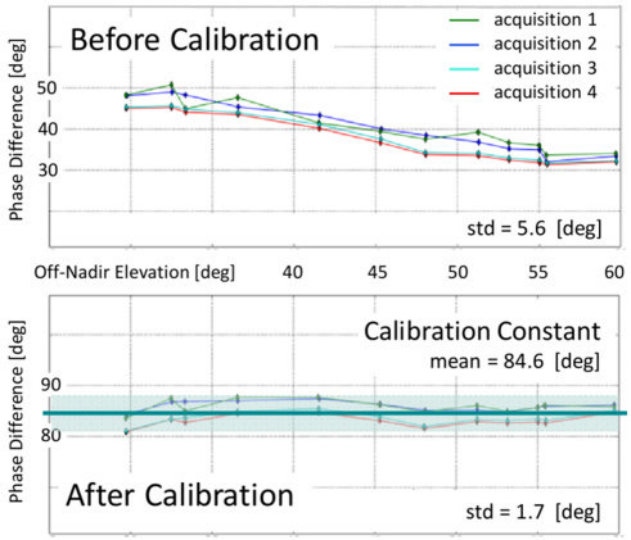

Figure 2.3-27 The HH to VV phase difference measured on focused SAR imagery of trihedral reflectors in four independent, fully polarimetric X-band acquisitions of the F-SAR sensor before and after baseline calibration. A standard deviation of the phase of only 1.7° is achieved.

required, and thus presupposes an accurate calibration of the sensors' antenna array. The method successively estimates a set of calibration parameters for each channel of the multi-channel SAR sensor, and is used prior to routine processing of any F-SAR or DBFSAR image products. The method currently includes estimates of the following parameters [RC-32]: residual correction for the range impulse response function in each channel, a mount angle for each antenna element, a lever arm for each antenna element, the baselines between different antenna elements, and a final complex calibration constant for each channel.

Each parameter estimation is coupled to the process of target analysis, which involves identifying the 2-D extent of the reference target response in a given data channel, compressing the data in range, taking into account internal calibration measurements, and generally correcting for all expected properties of the response.

These corrections account for the known antenna gain, the expected target backscatter intensity, range cell migration and the associated carrier phase variation, as well as free space propagation losses. To provide useable results, the target analysis includes a clutter suppression filter that singles out the direction of arrival corresponding to the target. The filter significantly increases the SNR and is especially important for channels that are undersampled in azimuth.

Corrections for mount angles, lever arms and baselines are model-based and are estimated via robust L1-norm minimization, taking into account all reference targets deployed across the swath in all available calibration data takes. Figure 2.3-26 and Figure 2.3-27 illustrate the estimation and correction of antenna mount angle and baseline calibration parameters.

Circular SAR and SAR Holography

An inherent limitation of the polarimetric interferometric SAR and tomographic SAR imaging modes is their narrow angular range of observation in azimuth. In order to increase the range of azimuth aspect angle measurements, a wider angular synthetic aperture, such as circular, may be used.

The holographic SAR imaging mode is defined as a solution for fully characterizing the 3-D backscattering of the scene of interest over 360°. It is the synergy of holography, tomography and multi-circular SAR acquisitions. In this context, the Institute has continued its research in the field of circular SAR by extending its studies towards the evaluation of multi-circular acquisitions, the first of which was performed in P band in 2011 over a test site in Switzerland [J-134].

The top part of Figure 2.3-28 illustrates the basic imaging geometry and the track distribution for the first fully polarimetric holographic data set acquired in L band over Kaufbeuren, Germany, by the Institute's F-SAR instrument in July 2012.

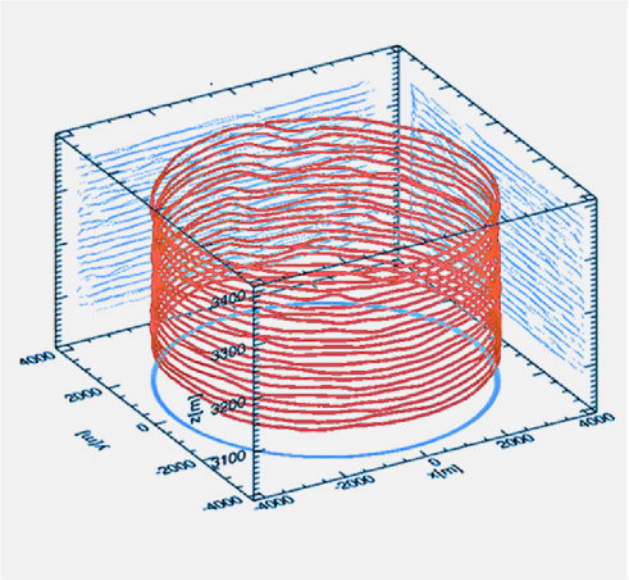

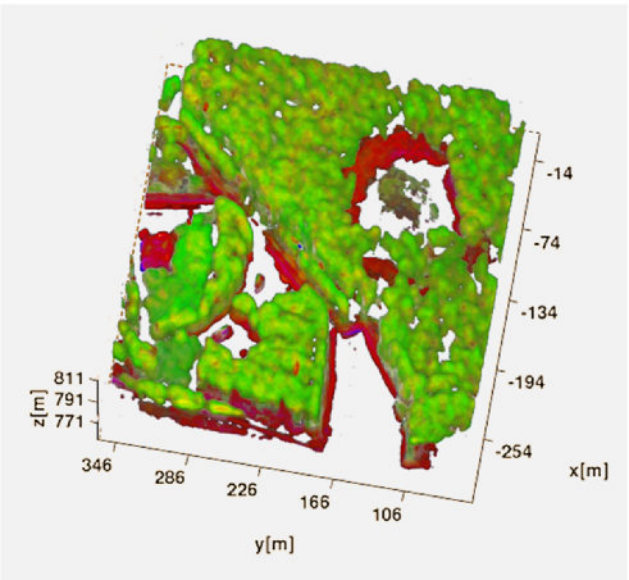

Figure 2.3-28 Top: holographic SAR imaging geometry and the sensor track of the first holographic measurement conducted in L band over Kaufbeuren, Germany, in July 2012. Bottom: first demonstration of polarimetric SAR holography, obtained by incoherent summation of 36 sub-aperture tomograms, each processed independently with compressive sensing. Image representation is in the Pauli basis.

A total of 20 circles – each separated by an altitude of 15 m to give a total vertical baseline span of 285 m – were included in the acquisition. This data set was one of the major inputs for research on the retrieval of 3-D information [PhD-8]. Several different algorithms, such as the 3-D coherent SAR imaging using the fast-factorized backpropagation (FFBP) algorithm, were developed to integrate information over the full 360° in azimuth, as well as a 2-D coherent processing in sub-apertures of, for instance, 10° width with FFBP followed by 3-D tomographic processing based on compressive sensing. The tomograms corresponding to individual sub-apertures may then be added incoherently or they undergo a generalized maximum likelihood ratio test (GMLT) to select the maximum intensity of all sub-apertures and polarizations for each altitude.
The first option maintains the best possible resolution in the horizontal plane, but incurs a high computational burden, since the result must use a very dense horizontal grid (i.e., 6 cm by 6 cm spacing for L band). The second processing option is better suited for the natural media such as forest or ice, which are often anisotropic scatterers, such that there is little to be gained from coherent integration over large apertures. A result obtained via compressive sensing followed by incoherent summation of sub-apertures is shown at the bottom of Figure 2.3-28. The excerpt shows a 300 m by 300 m forested region within the much larger illuminated 2 km-diameter-area. The color coding reveals double-bounce scattering at the tree trunk to ground interface and the random contribution of individual tree canopies in the cross-polarization [J-67].
The analysis of multi-circular acquisitions also supports investigations into the potential of combined tomograms from ascending and descending orbits in future spaceborne SAR missions.

Dual-Baseline Dual-Frequency SAR Interferometry

For airborne SAR sensors, the sensitivity of single-pass interferometric measurements is limited by the physical dimensions of the antenna carrier on the aircraft. It constrains the across-track interferometric baseline to between 1 and 2 m, which implies a relative height accuracy of roughly 0.5 - 1 m, depending on the image SNR. Much better relative accuracies can be achieved in a repeat-pass scenario with large, flexible baselines, which are adapted to the characteristics of the imaged area and the user needs. Until recently, the presence of residual motion errors and the difficulty posed by phase unwrapping have hampered the successful generation of large scale digital elevation models using large-baseline airborne SAR data.
The availability of the F-SAR sensor, which allows simultaneous data acquisition in multiple frequency bands, together with dedicated algorithms for the joint evaluation of dual-baseline and/or dua-frequency data have made it possible to generate very accurate, high-resolution digital elevation models. The generation of DEMs with horizontal and vertical resolutions comparable to those attainable with Airborne Laser Scanning (ALS) has been demonstrated impressively on this basis.
The main algorithmic building blocks of the new robust, dual-frequency, dual-baseline SAR data processing pipeline are depicted in the block diagram in Figure 2.3-29 and can be summarized as follows [PhD-7]:

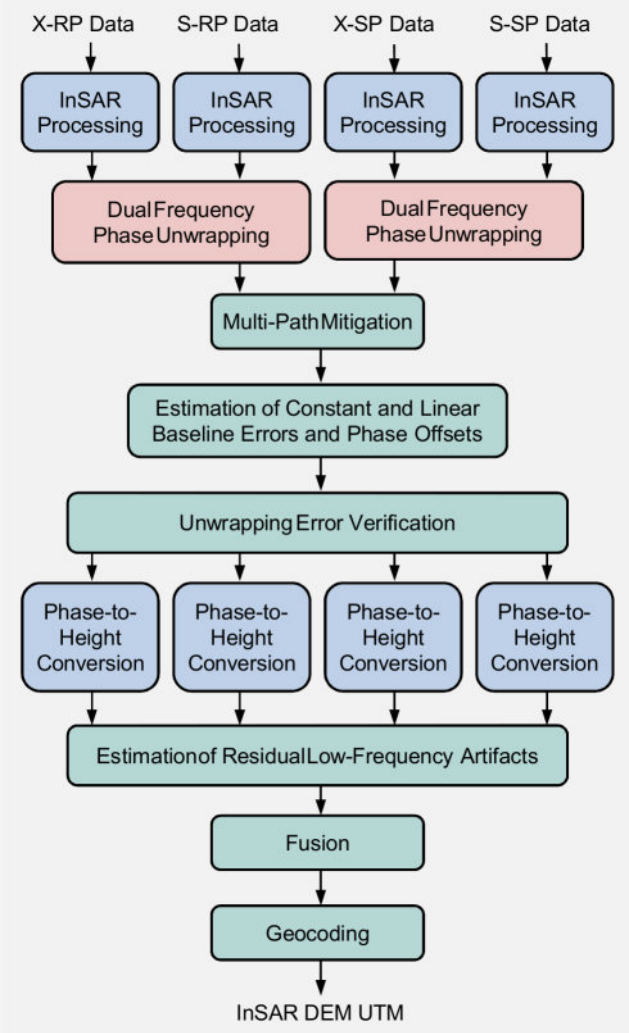

Figure 2.3-29 Processing of dual-frequency (X and S bands) and dual-baseline (single- and repeat-pass) interferometric SAR data for precision DEM generation. The tags X-RP, S-RP, X-SP and S-SP stand for X-band repeat-pass, S-band repeat-pass, X-band single-pass and S-band single-pass, respectively.

- The interferometric phases in different frequency bands (e.g., X and S band) are unwrapped jointly. This ensures consistent results over large areas, even in the presence of regions that are disconnected due to low coherence (e.g., islands surrounded by water). Working independently on single- and repeat-pass data sets is essential in this step.

- Multi-path mitigation may be applied to single-pass interferometric data. The repeat-pass data set is used to identify and quantify the correction for the multi-path phase in the single-pass interferogram.

- Constant and linear baseline errors are estimated for the repeat-pass baseline pairs. The single-pass data are considered unbiased (up to a global phase offset) and are thus used to derive these constant and linear coefficients.

- The dual-baseline data are used to identify and correct residual unwrapping errors, which may be present in the repeat-pass data.

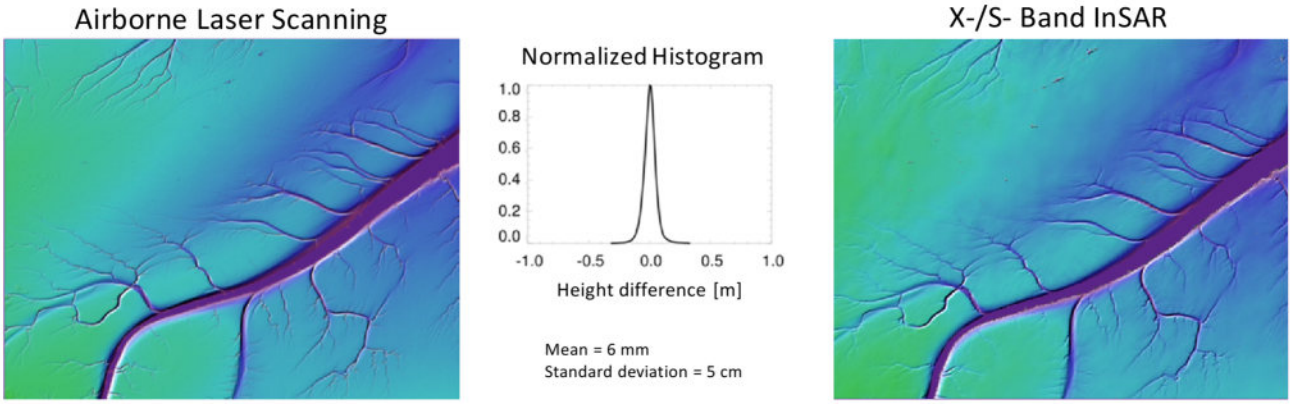

Figure 2.3-30 The evaluation of a digital elevation model of tidal flats obtained via dual-baseline, dual-frequency (DBDF) SAR interferometry (zoom of approx. 2 km by 2 km). The histogram shows the difference with respect to state-of-the-art airborne laser scanning (ALS). The standard deviation and bias between the measurements are approximately 5 cm and 6 mm, respectively.

Phase-to-height conversion is performed independently for each data set. Low-frequency differential artefacts, where the repeat-pass pairs have been affected by, for instance, changing atmospheric conditions, can be corrected using the single-pass information, which is not affected by this type of error.
The four data sets are fused to generate a final DEM. Either maximum likelihood summation is used and/or wavelets employed to achieve better noise reduction and preservation of small scale features.
The approach has been validated in the context of a project in cooperation with the German Federal Institute of Hydrology (BfG), where SAR data were used for mapping the subtle elevation changes of tidal flats in the Jade Bight on the North Sea coast of Germany. The accuracy achieved has been shown to be comparable to that of ALS derived data, both in terms of horizontal spacing (1 m x 1 m) and vertical resolution (better than 0.1 m, see Figure 2.3-30). Since, compared to ALS sensors, airborne SAR can map a considerably larger swath and is much less affected by weather, it is an economical alternative for this application and will be actively pursued in future.

2.3.5 Future Developments

Together, the existing F-SAR and the upcoming DBFSAR sensors are very well suited to address the needs arising in many of the current SAR imaging, technology and remote sensing application trends. Nevertheless, there are certain upcoming imaging technologies that are beyond the scope of these sensors. First of all, recent spaceborne SAR mission concepts confirm a rising interest in wavelengths shorter than X band. Secondly, bistatic imaging has been established by the TanDEM-X formation in X band, but application development for Tandem-L lacks a suitable database. The Institute has therefore recently initiated the development of two additional airborne radar segments to supplement the existing sensor hardware: the so-called "Ka-band Pol-InSAR demonstrator", an interferometric Ka-band radar, and the so-called "DuoLIM" sensor, a bistatic extension to F-SAR in L band.
Further upcoming developments include an airborne MIMO (Multi-In Multi-Out) SAR and a miniaturized lightweight SAR for drones and high-altitude unmanned platforms.

Ka-Band Pol-InSAR demonstrator

The aim of the project "Ka-Band Pol-InSAR demonstrator" is to add an additional Ka-band (~35 GHz, λ~9 mm) subsystem to the airborne SAR system F-SAR/DBFSAR. This frequency band generally allows for the construction of relatively compact SAR sensors. In particular, Ka-band interferometers with very short baselines can still achieve very good phase sensitivity. This is of particular interest for satellite applications where, in certain cases, an entire interferometer can be realized on only one satellite and a tandem formation is not necessary (e.g., PicoSAR study, see [RC-471], [B-6]). The compact dimensions also make it easier to set up multiple transmit and receive branches for advanced imaging modes using digital beamforming or MIMO techniques.
Ka-band interferometers are considered to be very promising for cryosphere applications, especially for tracking ablation processes of glaciers with high accuracy. In addition, Ka-band polarimetry can be used to sense the structure of the upper snow cover and thus provides access to biophysical parameters such as the snow/water equivalent, the snow cover ratio or the snow lines of high mountain glaciers. The combination of Ka-band polarimetry and interferometry (Pol-InSAR) is of particular interest in view of new applications, such as crop biomass estimation. To date, the Institute has carried out several mission and application studies for ESA [IC-2], [RC-671], [R-62]. The timely installation of a corresponding demonstrator is perceived to be of great importance for securing the Institute's technological leadership in the SAR area.
The project "Ka-Band Pol-InSAR demonstrator" is jointly funded by the Institute and the ETH Zurich in Switzerland. The development of the system began in 2017 and is foreseen to be completed in 2020. The sensor is designed to operate polarimetrically and interferometrically (Pol-InSAR) and simultaneously acquire data corresponding to 3 baselines ranging between 20 and 150 cm (see Figure 2.3-31). It will support full- and half-baseline imaging modes, feature a spatial resolution of about 30 cm and image a swath of 2 km for the standard platform altitude of approximately 3 km above ground. Improvements of the spatial resolution are possible and entail the implementation of a suitable wide-band antenna technology at a later stage.

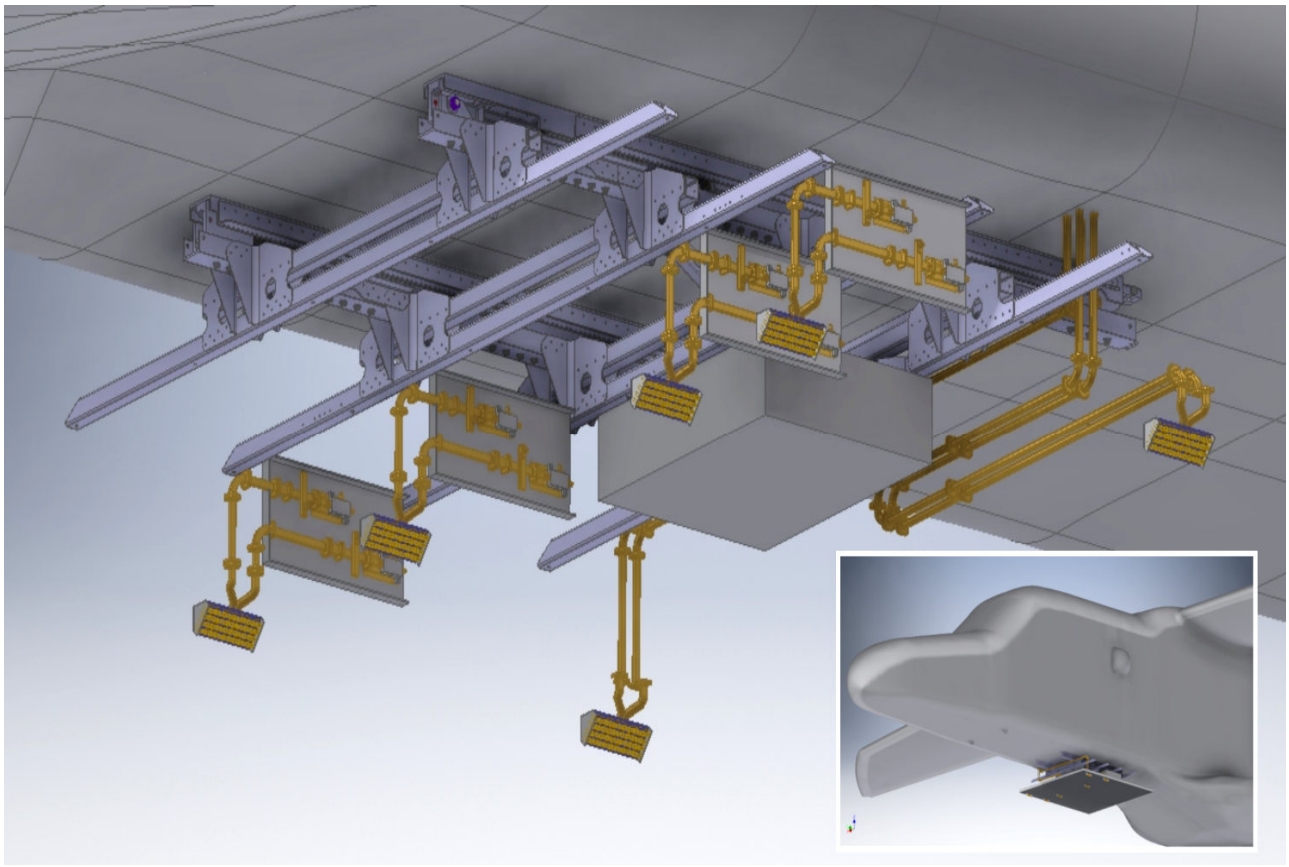

Figure 2.3-31 Technical drawing of the envisioned multi-baseline interferometric Ka-band antenna setup, featuring 4 dual-polarized receive antennas and 2 dual-polarized transmit antennas. The Ka-band antenna carrier will be mounted below the fuselage at the same place of the F-SAR's P-band carrier.

DuoLIM

The second ongoing development, called "DuoLIM" (Duo L-band SAR IMager), was motivated due to the fact that there are currently no sensors – either satellite-supported or airborne – capable of generating Tandem-L-like radar data. The use of a single sensor in repeat-pass mode inevitably yields monostatic imagery with a certain, fixed geometry that may be degraded by strong temporal decorrelation artefacts due to changes that occur in between acquisitions. By contrast, the simultaneous use of two L-band sensors will enable bistatic SAR images acquired in flexible geometries. The availability of such data would boost the Tandem-L product development before mission launch. On the one hand, DuoLIM data will allow researchers to develop robust processing algorithms for the various application scenarios of Tandem-L. On the other hand, it may also be possible to identify novel applications requiring special imaging modes that have not yet been investigated in detail. For this reason, the primary goal of the major investment DuoLIM is to set up an airborne L-band SAR system that can be paired with DLR's existing F-SAR sensor to generate Tandem-L-like data products. For this purpose, the DuoLIM system will be operated at the same time as F-SAR and in bistatic mode (see Figure 2.3-32). The envisioned L-band SAR system includes a digital backend, an L-band high-frequency frontend, bistatic synchronization capabilities, and a high-precision navigation system. Gimbal-mounted antennas will be used in order to realize variable bistatic angles in both elevation and azimuth.

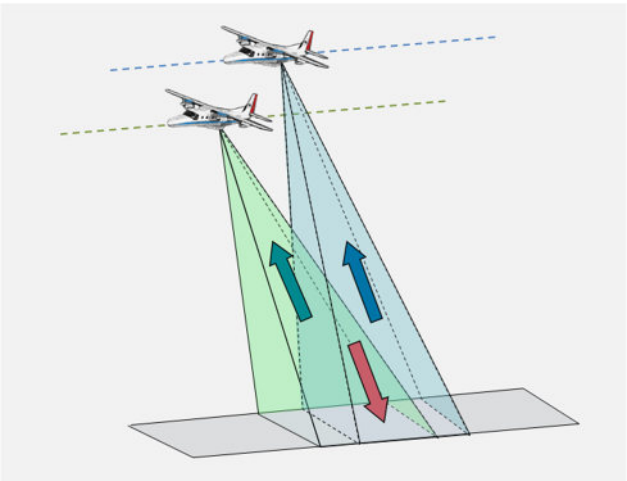

Figure 2.3-32 A sketch illustrating bistatic SAR imaging with two SAR sensors. The flexible DuoLIM system will allow research into Tandem-L-like imaging configurations by using two airborne platforms with varying across-track and along-track separation.

The specification, design and construction of the system are being carried out at the Institute, as such devices are not otherwise commercially available.

The funding of the DuoLIM project was approved by DLR at the end of 2017. The development of the system began in early 2018 and is scheduled to be completed in 2021.

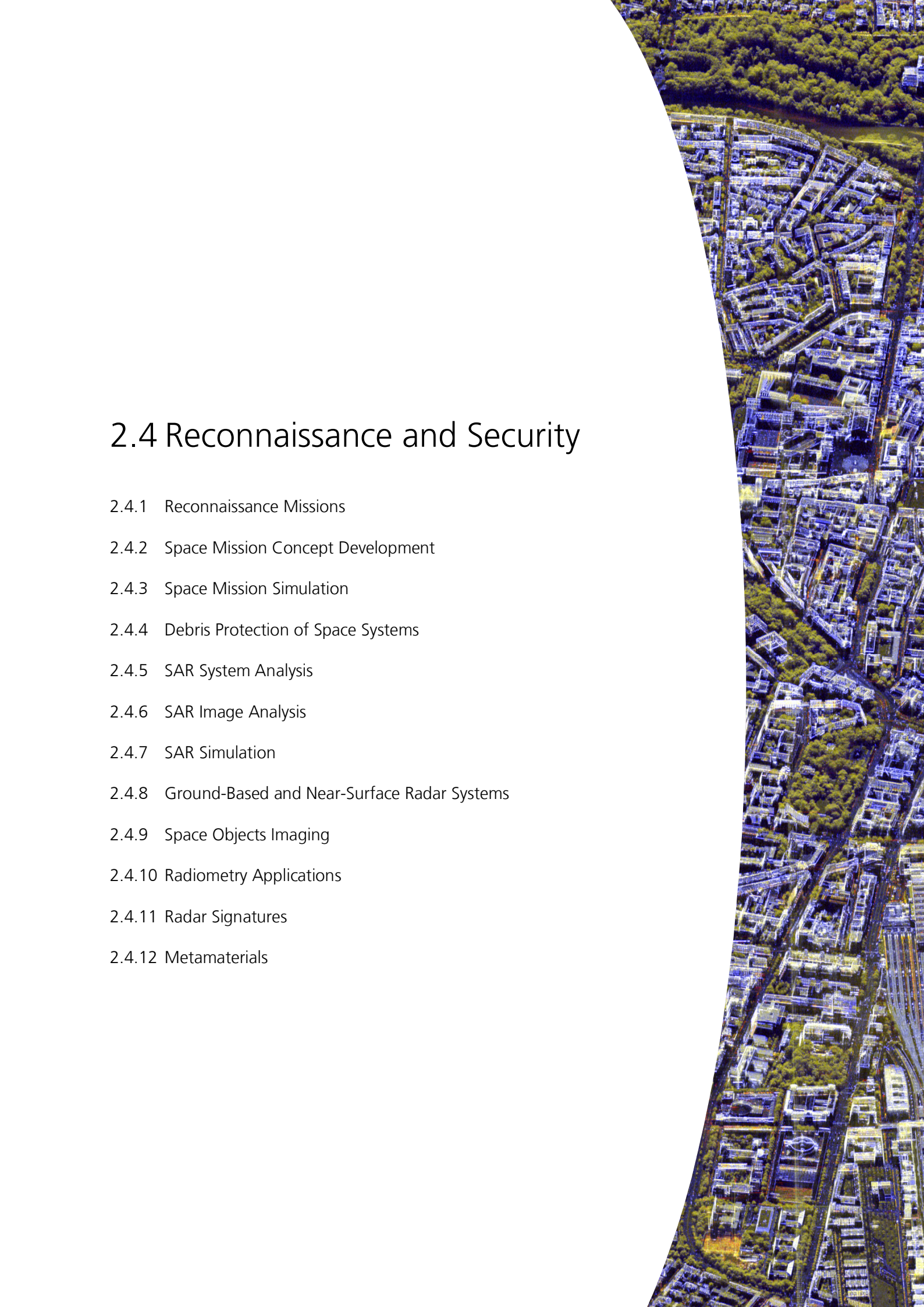

2.4 Reconnaissance and Security

2.4.1 Reconnaissance Missions

2.4.2 Space Mission Concept Development

2.4.3 Space Mission Simulation

2.4.4 Debris Protection of Space Systems

2.4.5 SAR System Analysis

2.4.6 SAR Image Analysis

2.4.7 SAR Simulation

2.4.8 Ground-Based and Near-Surface Radar Systems

2.4.9 Space Objects Imaging

2.4.10 Radiometry Applications

2.4.11 Radar Signatures

2.4.12 Metamaterials

2.4 Reconnaissance and Security

Security research has considerably expanded in the last decade, and has thus become a significant cross-sectional program area at DLR. Connecting the civilian and military domains, security research consistently yields high-potential dual-use technologies for various applications. Against this backdrop, the Microwaves and Radar Institute has been conducting reconnaissance and security research for nearly 30 years. The Institute has specialized on development, analysis and simulation of space-based SAR systems capable of delivering high spatial and radiometric resolution imagery in an efficient and timely manner. The complexity of advanced high-performance satellite systems demands holistic research approaches encompassing all software and hardware system components – such as signal processing tools, state-of-the-art sensors and mission planning software – required to support present and future satellite missions.

The setup of novel ground-based experimental SAR demonstrators, the design of advanced microwave radiometers, and the analysis of electromagnetic interaction with natural materials and metamaterials are carried out in order to support this research field. In addition, a wide range of software tools were developed at the Institute to visualize different types of man-made objects, as well as natural phenomena. The in-house software tools RADIAN and SAREF are instrumental in research on the optimization of information retrieval from SAR images. The Institute's hardware activities have focused on the development and construction of the advanced high-performance radar and radiometer systems Gigarad, TIRAMI-SAR, and SUMIRAD. These are used for various applications, such as ground-based imaging of satellites, landmine detection or enhanced vision. Finally, electromagnetic signature and material research focuses on the theoretical and experimental investigation of novel structural designs and metamaterials for RCS prediction, analysis, and reduction.

2.4.1 Reconnaissance Missions

Today's political, natural, and social environment is changing at a fast pace. In light of this rapidly changing ecosystem, the maintenance of independent reconnaissance capabilities for security purposes has become crucial. Satellite platforms equipped with radar and optical sensors that provide high spatial and radiometric resolution offer the only reliable global source for acquiring this type of information unintrusively and in accordance with international regulations.

The importance of spaceborne reconnaissance is clearly underlined by the increasing number of radar and optical satellite missions launched for security purpose to date. SAR-Lupe, a constellation of five satellites launched between 2006 and 2008, is the first German spaceborne radar reconnaissance system. It is exclusively used for military purposes, whereas other missions like COSMO-SkyMed, Radarsat-2 and TanDEM-X can be considered as systems for dual-use applications. The SAR-Lupe system has been operating for more than 10 years, yielding outstanding performance, and will reach the end of its lifetime in the next few years. For SAR-Lupe, the Institute is responsible for advising end users, providing scientific support in data analysis, and delivering advanced software tools to enhance image products for significantly improved data analysis.

With the purpose of advancing state-of-the-art technologies and addressing new reconnaissance challenges, the follow-on mission SARah is presently under development and will be operational within the next few years (see Figure 2.4-1). The Institute is strongly involved in the SARah mission through multiple tasks. These encompass the basic design with respect to advanced system performance facing the new reconnaissance challenges and the transformation of military user requirements into high-level technical system specifications. Furthermore, the development of new and innovative simulation tools is a key task. Simulation tools are developed for mission planning and more detailed SAR system analysis and synthesis, comprehensive target signature prediction and analysis, target feature enhancement and extraction, as well as optimization of the system chain during development in light of changing user requirements.

The simulation tools developed in the context of SARah are also being extensively used for technical analyses and shadow engineering of industry during the SARah realization phase. As part of future operations, access to mission and image data will enable a reliable evaluation process.
In parallel to SARah activities, collateral research work is being conducted to address SARah's follow-on reconnaissance system SARah NG, which will feature enhanced capabilities and functionalities. Increasing importance is also being placed on data fusion technologies for SAR and optical imagery, in order to enhance the information content and broaden application areas, to consolidate the image analysis process, and to guarantee more intuitive data content. Finally, in order to face the dramatic increase of data volumes, considerable efforts were launched to increase the level of automatization of the image analysis process.

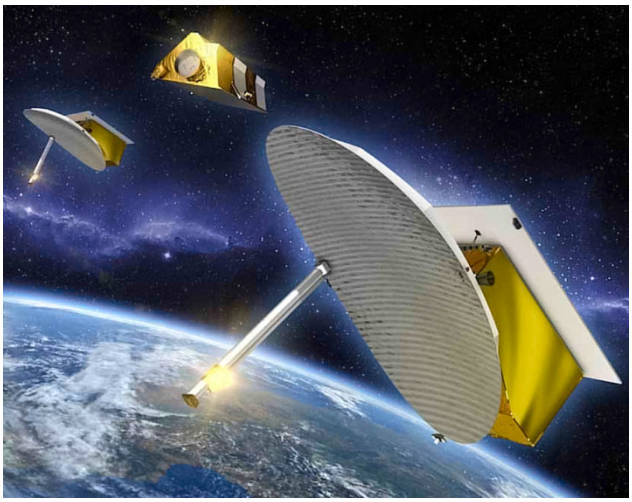

Figure 2.4-1 Artist view of SARah constellation consisting of 3 satellites (courtesy of OHB)

2.4.2 Space Mission Concept Development

The development of innovative space mission concepts for security purposes is a core activity of the reconnaissance activities. Figure 2.4-2 provides an outline of the elements of the mission concept development process. The process comprises the mission planning, mission simulation and mission analysis phases. The mission simulation and planning phases generate the inputs for the mission analysis phase based on preliminary assumptions, such as the number of satellites required or the necessary energy storage capacity of the single satellites. User requirements and environmental constraints are taken into account (Figure 2.4-3) in this phase. Within the mission analysis phase, the generated mission scenario is then investigated using the in-house mission analysis tools, such as the Multi-Satellite Mission Planning (MSMP) software. The results of such analyses lead to the consolidation of several key performance parameters (e.g., system response time, mission response time, image information age), and a basic system concept.

Examples of key performance parameters are:

- System response time: The elapsed time between an image request, e.g., for Earth observation systems, and the delivery of an imagery product to the human analyst.
- Mission response time: The elapsed time between satellite command upload and data download to a ground station.
- Image information age: The elapsed time between the data acquisition and the delivered image product.

These performance parameters can be used to quantify user requirements during the space system design process and as indicators for end customers. The definition of accurate and meaningful performance parameters for space systems is crucial to ensure a common understanding towards the customer, the engineers and the management. The Institute performs all steps of the mission concept development and systems engineering for various dual-use and military studies.

Figure 2.4-2 Elements of the concept development process for a space mission including planning, simulation and analysis.

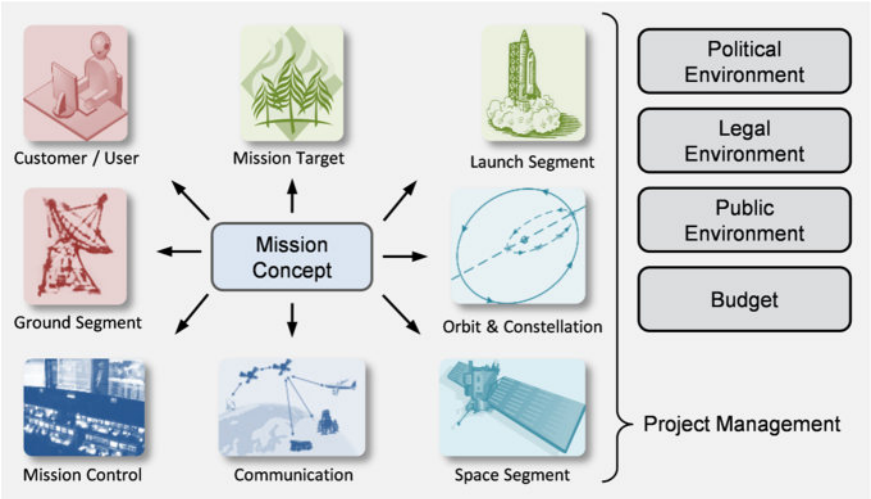

Figure 2.4-3 The space mission architecture must take into account various constraints (e.g., political, legal). Key space system elements are shown in different colors. The space segment components are aquamarine, ground segment components are red and mission planning components blue.

2.4.3 Space Mission Simulation

When planning a new space system or optimizing an existing one, simulating and analyzing the end-to-end mission performance is necessary in order to provide the decision-makers with the information they need to make key decisions on the optimization or creation of a reconnaissance space mission. The Institute offers support to various stakeholders by employing cutting-edge tools for system simulation. The simulation comprises the mission planning segment, the ground segment, the communication segment and the space segment. The end-to-end system-design process of a spaceborne system is conceptually shown in Figure 2.4-4.

The end-to-end system simulator, which has been continuously refined since 2001 at the Institute, enables the design, simulation and evaluation of possible space system configurations and the assessment of essential performance metrics (e.g., number of images, system response time and image information age). All subcomponents of the end-to-end system simulator are seamlessly interlinked and form the space system simulation concept (see Figure 2.4-5).

Herein, the mission planning software is used to obtain an optimized, operational mission plan taking into account the limited resources of the satellite system. Tasks are sent from the ground segment through the communication segment to the space segment. The space segment itself can consist of one or more satellite systems, where each satellite can be divided into bus and payload subsystems. The sensor element of the payload must be able to generate the raw data containing the relevant information. Accordingly, the satellite bus must ensure the correct orientation of the sensor in a fast and precise manner for a given target. Finally, the valuable data are transferred via the communication segment to the ground segment in a secure and fast way. The whole system chain of the system design process ensures the fulfilment of the specific user requirements respecting sensor design, constellation of several satellites, communications strategy, mission plan, and image evaluation on ground.

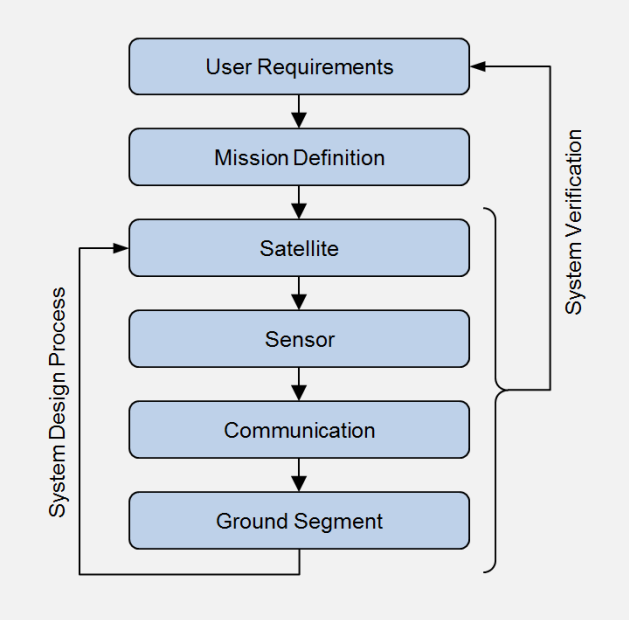

Figure 2.4-4 End-to-end chain for the system design process for a spaceborne remote sensing system

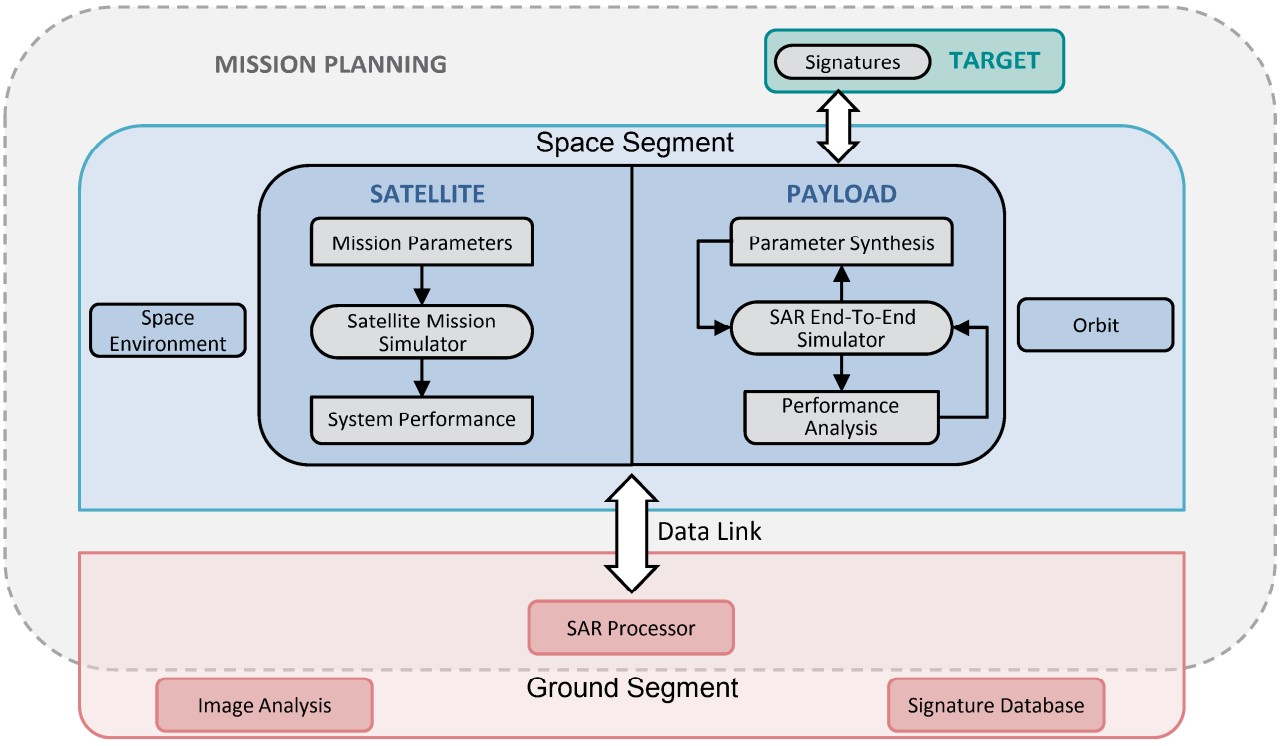

Figure 2.4-5 The top-level space system simulation concept with space and ground segment considering different mission and sensor parameters for satellite mission simulation, SAR end-to-end simulation and signature identification

Simulation Framework

Based on the simulation concept a simulation framework to combine the various simulation tools has been developed for space mission definition. These were developed for detailed system performance estimation of diverse space-based synthetic aperture radar and electro-optical satellite missions.
The primary objective of the simulation framework is the definition of the mission scenario. A consistent and careful definition can reduce the risk of inconsistencies in scenario analysis using different software tools. It is specifically designed to speed up workflows and standardize the visualization and reporting of analysis results.
The secondary objective of the simulation framework is to provide a platform for users, where existing and newly developed software tools can be easily added due to its modular nature.
The framework clearly benefits from its modular concept. Analysis results from one tool can be reused in another tool based on the same scenario. In addition, standardized reports can be generated automatically. It guarantees repeatability of the analysis results by other project participants, and speeds up the analysis workflow.
The simulation framework is conceptually divided into visualization, scenario definition, orbit calculation and analysis modules. The analysis modules can be distinguished in scenario-dependent and scenario-independent tools.
The scenario-independent analysis tools of the simulation framework consist of an area generator, frame converter, baseline calculator, versatile orbit generator, and a two-line element residuals module.
On the other hand, the scenario-dependent analysis tools consist of an interferometric analysis, contact pattern, deorbiting analysis, constellation analysis and monitoring, interference analysis, satellite download conflicts tool, and the MSMP. The MSMP is designed to calculate the system performance of a given set of satellites, ground stations and targets. The main outputs are the key performance parameters, i.e., the amount of images that can be acquired, the system response time and the image information age. The impact of different planning algorithms can be seen in the performance parameters of the satellite system based on the MSMP analysis results.
An example of results from a mission analysis with the simulation framework is shown in Figure 2.4-6. It depicts the coverage of a 24-satellite constellation. Coverage maps are used to analyze the performance of satellite missions for commercial, public and military clients.
Another key application of the simulation framework is the analysis of download conflicts of multi-satellite missions. The download capacity of an Earth observation satellite system tends to be a bottleneck, especially if multiple satellite missions need to share a ground station antenna within the given ground segment infrastructure. It is thus necessary to identify conflicts between different satellites and their download opportunities within the same, or across different, missions.
Furthermore, conflicts in download opportunities of a single satellite to different ground stations must be detected. A conflict is defined as a time interval during which two or more systems, a satellite or a ground station, are in contact with another system without this system being capable of simultaneously handling all assets. The simulation framework offers various algorithms to solve the identified conflicts. The

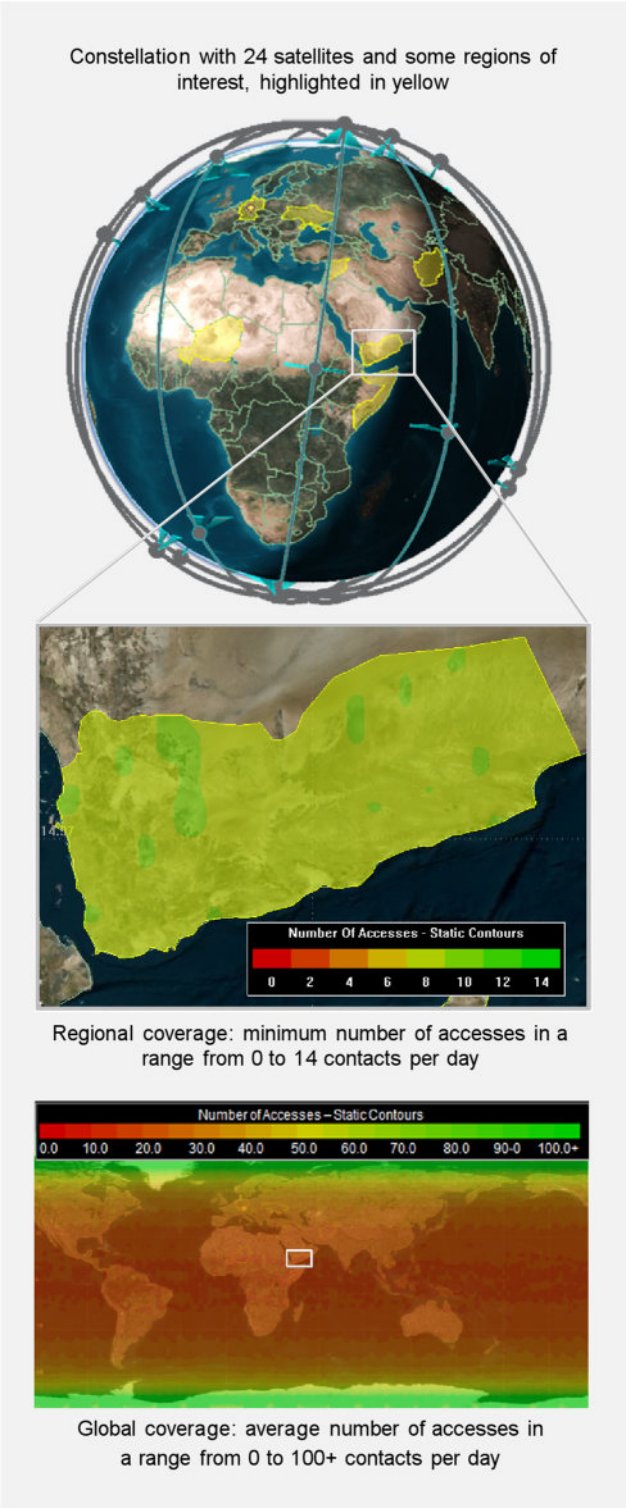

Figure 2.4-6 Global and regional coverage analysis of a constellation of 24 satellites

algorithms consider technical constraints in addition to political ones, e.g., various companies seeking long contact times for their assets in orbit. The simulation framework is capable of optimizing the total download time for the orbit configuration taking the environment and potential conflicts in a cross-system constellation into consideration.

In an ideal case, the net contact time between satellite and ground station – the time in which no conflicts are considered – can be used to download data. The simulation framework algorithms can approximate real world circumstances with procedures such as the first contact approach. In this method, the first satellite, which comes into the access area of the ground station, is allocated the complete contact. The first contact approach can be further subdivided into two algorithms. The first algorithm can use the remaining contact time for other satellites. In this way the time can be used to download data when the contact time is sufficient. The second algorithm only uses the first contact and lapses the rest of the contact time. The performance of the two algorithms is shown in Figure 2.4-7. In this example, the 7-day scenario consists of one ground station and two satellites. The analysis shows the first algorithm achieving the best system performance. With this information, a cost function can be created and additional parameters (e.g., orbit parameter, ground station location) analyzed to find the best system configuration.

In addition to the example detailed above, the simulation framework is able to apply even more complex algorithms. These algorithms may consider multi-transponder configurations, different slew times, data rates, data relay satellites, and system priority levels.

The simulation framework is only one link in the chain of analysis tools required for the analysis of the overall system performance of a space mission. It is generally used in phase 0 studies or trade studies, e.g., whether an existing system should be extended and multiple options are available for additional ground stations.

Regarding the simulation framework context Figure 2.4-8 shows a workflow involving the satellite download conflict calculation and the MSMP tool. In this case, the MSMP is allocated a conflict-free ground station contact list generated by a pre-defined algorithm.

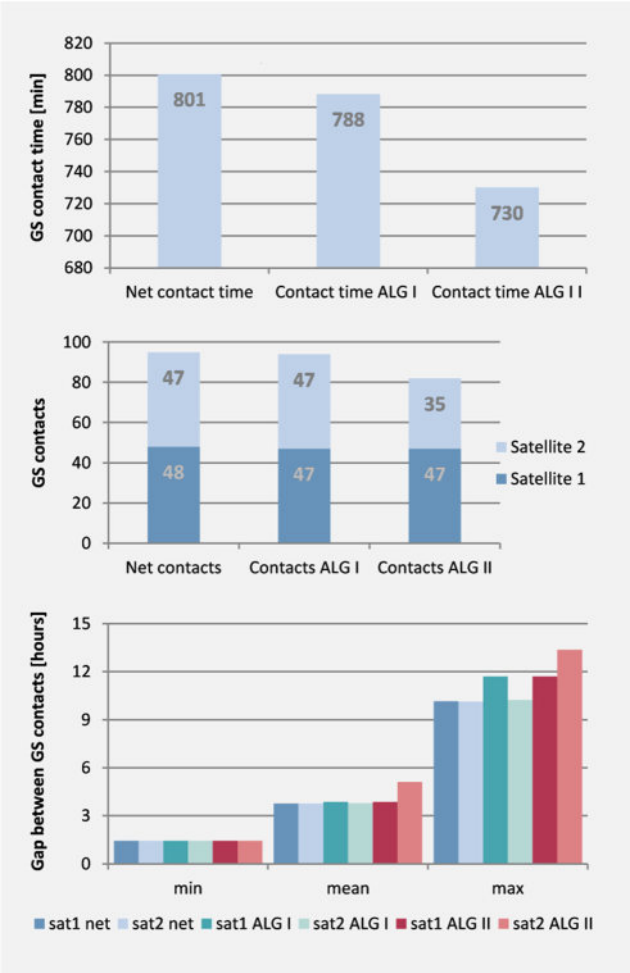

Figure 2.4-7 Comparison of different conflict-resolving algorithms (ALG I and II), leading to different communication times. Algorithm I yields a 58-minute longer contact time, which can be used for additional data download. The maximum gap between the ground station (GS) contacts for satellite 1 is equal to algorithm II, but satellite 2 achieves a 3.1-hour smaller gap compared to algorithm I which leads to a better system performance in terms of image information age (see lower plot, bars on the right).

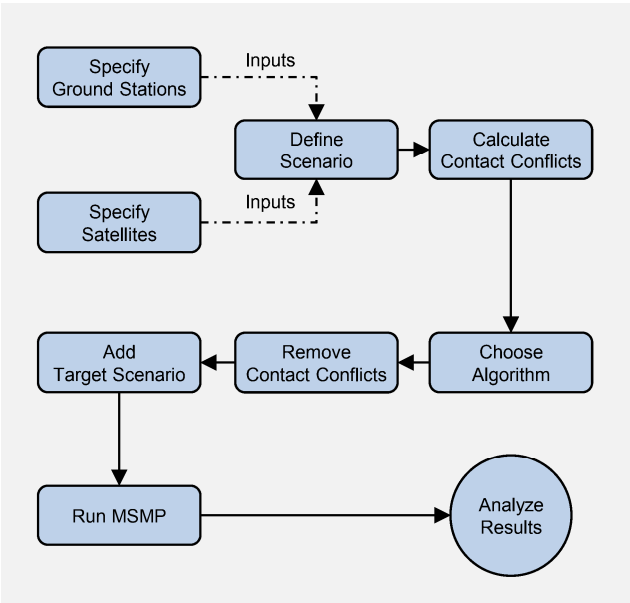

Figure 2.4-8 Workflow of a scenario analysis regarding download conflicts using the Multi Satellite Mission Planning (MSMP) tool

2.4.4 Debris Protection of Space Systems

Space is a harsh environment in terms of temperature, radiation and gravity. In addition, in the vicinity of the Earth space debris poses a significant danger to active satellites. Debris is composed mainly of artificially created objects such as old rocket stages or defunct satellites. According to ESA, there are about 166 million objects in space (see Figure 2.4-9). Space debris appears in different sizes (paint flecks [µm], fragments [mm] - [cm], rocket stages [m], old satellites [m]) and consists of different materials (e.g., aluminum, carbon fiber reinforced plastic (CFRP), fuel). Debris larger than 10 cm can be detected in low Earth orbit by the Space Surveillance Network (SSN). Of the estimated 29,000 objects larger than 10 cm, approximately 18% are defunct satellites, 6% are active satellites and 18%

spent upper rocket stages (see Figure 2.4-10). To counter the threat of a collision with tracked objects, active satellites are able to perform collision avoidance maneuvers. For debris smaller than 1 cm, the space system can be protected by design measures like double or multi-layer Whipple shields. For small particles, those Whipple shields are effective, but since they add to spacecraft volume and increase the weight of the system, they are mostly used for manned space systems.

Foam Debris Protection

The goal of foam debris protection is to develop a small, compact and lightweight design for improved space-debris protection by substituting the honeycomb with a foam structure able to achieve the needed stiffness for the main satellite structure (see Figure 2.4-11). In this context, the Institute established a joint study team with the Fraunhofer Institute for Manufacturing Technology and Advanced Materials and the Chair of Astronautics at the Department of Mechanical Engineering of the Technical University of Munich. The Technical University of Munich provided the facilities for the high-velocity impact tests at 5 km/s.
Different types of substitute foam materials were investigated. The materials under investigation were connected by an adhesive matrix and exhibited different densities and sphere sizes. The first investigated material was ordinary foam bought at a local hardware store. This material already showed an enhanced protection capability. Another material that was tested was aluminum foam with an interior of foam spheres. As a metal foam, this material has no outgassing, eliminating the possibility of subsequent damage to payloads or sensors, such as the optics of a star-tracker. Figure 2.4-11 on the right shows an alternative material buildup with loose spherical aluminum foam filling. Impact results show good protection capabilities, but the overall weight of this structure is too high for space applications. Other material pairings will have to be investigated in the future to reduce the weight and create unique materials for the protection of satellites.

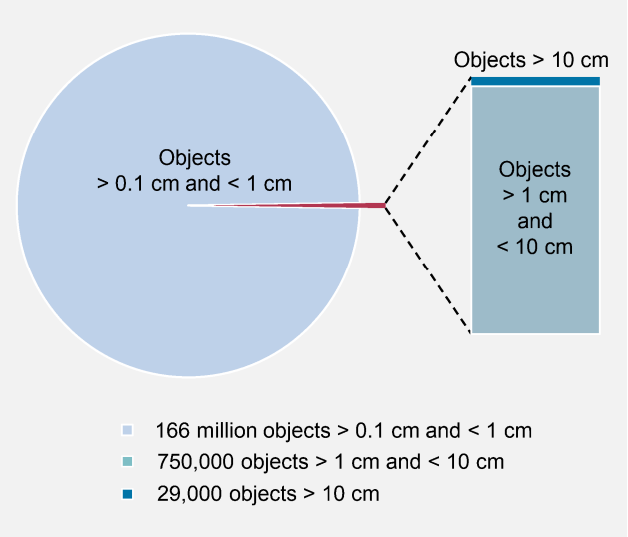

Figure 2.4-9 Debris object size distribution, as estimated by ESA statistical models

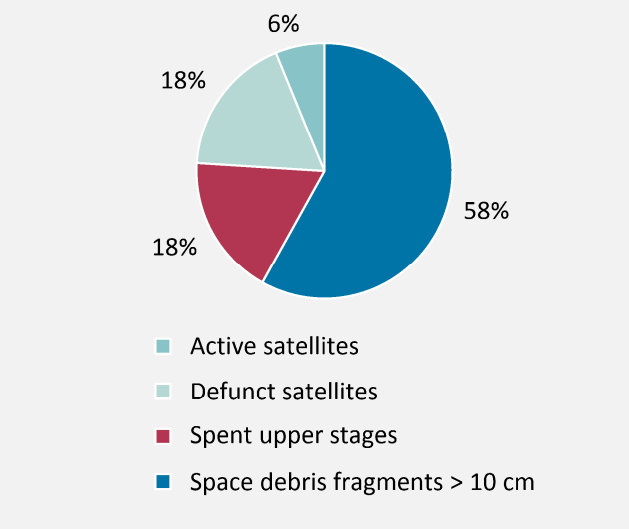

Figure 2.4-10 Type of debris larger than 10 cm, as estimated from Space Surveillance Network observations

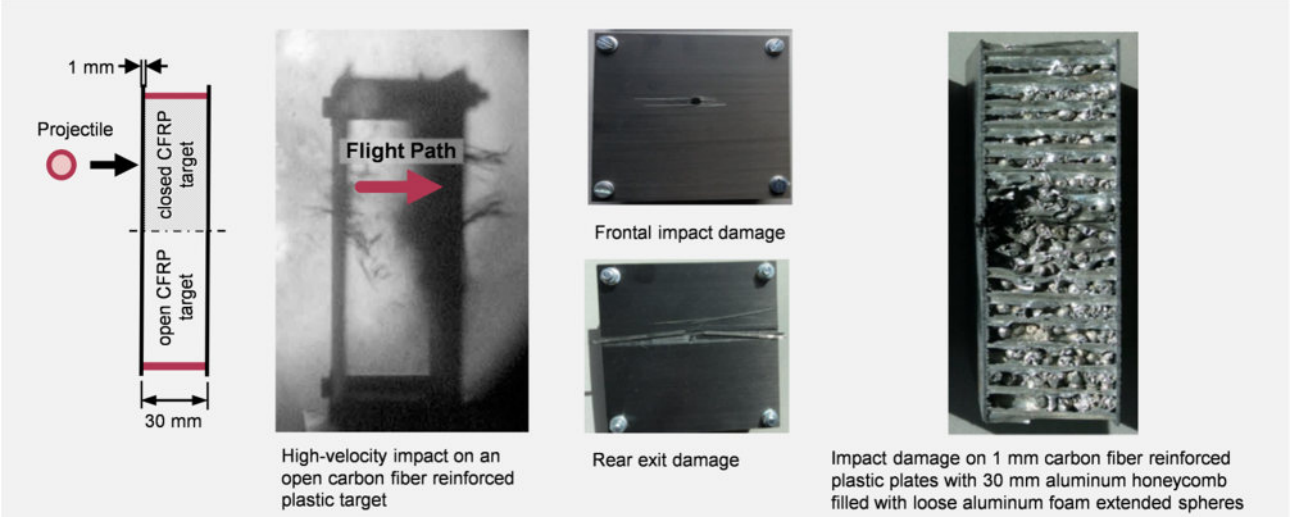

Figure 2.4-11 High-velocity impact on an open and closed carbon fiber reinforced plastic target with front impact and rear side exit holes in the open structure, as well as a side view of the closed structure filled with aluminum honeycomb and loose aluminum foam extended spheres.

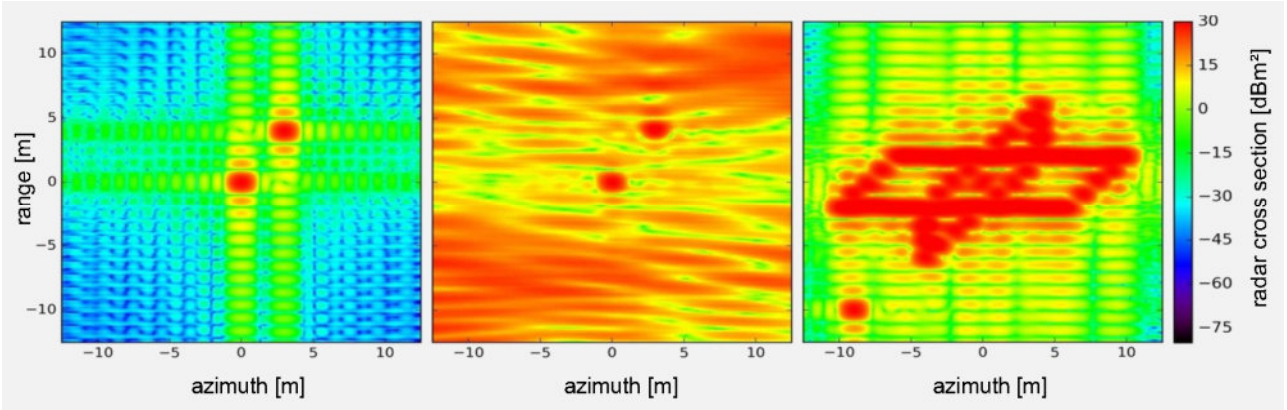

Figure 2.4-12 Simulated SAR images: reference without jamming (left) incoherent chirp jammer with jamming chirps similar to radar signal, transmitted during the entire recording (middle), intelligent spoofing causing constructive overlay (right).

2.4.5 SAR System Analysis

The Institute is involved in the operation of several SAR systems for reconnaissance and security. During the past few years, the number of SAR images exhibiting image degradation due to jamming has grown noticeably. Jamming, that is the disturbance of radar signals and echoes, can occur unintentionally, e.g., caused by an incorrectly configured transmitter, or be fully intentional, as is mostly the case in a military context. Current sensors are usually only equipped with a simple sensitivity-control technology or shutdown switches to avoid damage in the case of high power-signal reception. Simple jammers may just transmit a continuous wideband signal at high power, which leads to a blinding of the sensor. However, the latest developments in sophisticated signal processing and hardware have led to jammers of a new kind. These jammers are able to imitate the signal shape of the expected radar signal. Thus, understanding the exact effects in radar sensors and SAR processing that are caused by jammers is necessary to develop countermeasures for future SAR systems.

A modular simulation framework capable of synthesizing a radar sensor and its respective SAR processing algorithm for the analysis of jamming effects on SAR data at each state was developed. This framework can be equipped with different kinds of jammer modules to investigate their effects. In general, SAR jammer devices may vary signal power, signal shape and signal timing, dependent on the specific SAR system to be jammed.

Several classes of jammers have been defined as a reference for testing SAR systems and countermeasure algorithms or provisions. One of the more sophisticated and intelligent systems would be a jammer that controls signal shape, timing and transmission power based on a priori knowledge of the sensor's flight path. This jamming signal would be a kind of worst-case scenario since it is not distinguishable from the undisturbed radar echo signal.

This, in theory, allows intelligent jammers to insert or remove targets from the recorded scene by constructive or destructive signal overlay. Examples of simulated images, jammed by a signal with controlled shape or timing, are shown in Figure 2.4-12.

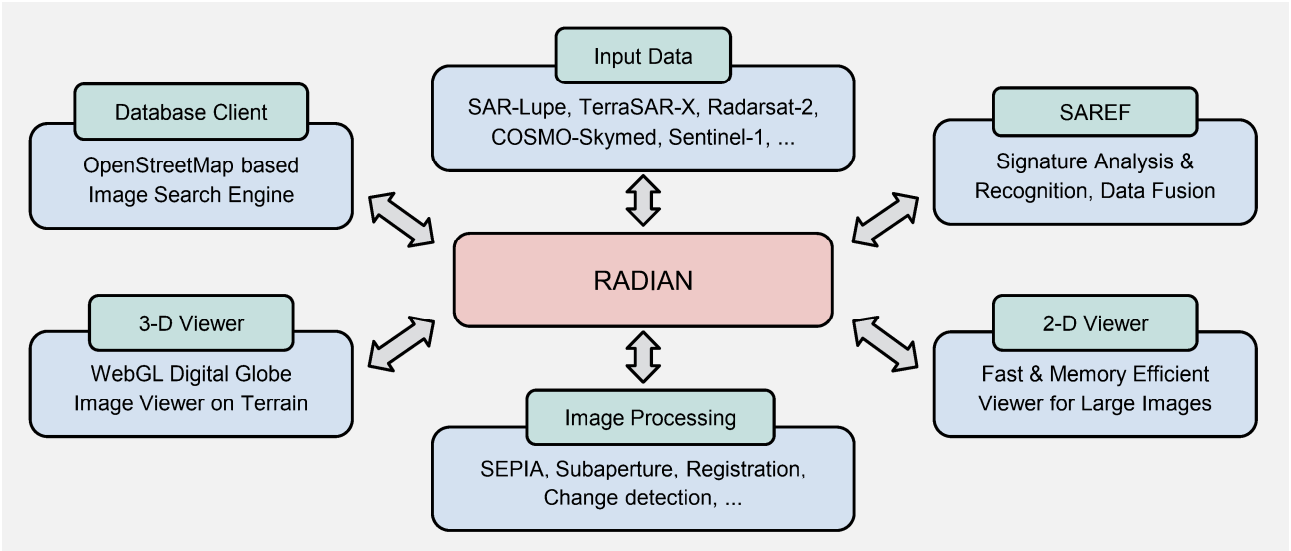

Figure 2.4-13 Components of the RADIAN software package: Available image data can be loaded through a specialized database application. Readers for the data are implemented not only for the most common SAR sensors, but also for optical, map & DEM data.

Current developments on methods for the design of more robust SAR systems against jamming cover approaches in alternative transmit signals, modern antenna technology and flight geometry. These developments and analyses are accompanied by corresponding measurement campaigns.

2.4.6 SAR Image Analysis

With the launch of the first German spaceborne reconnaissance system SAR-Lupe in 2006 the demand for high-level SAR image enhancement techniques increased substantially. The need for expertise in all subsystems of a spaceborne SAR sensor prompted the Institute to develop and realize sophisticated filter and visualization methods.
The security requirements demanded a complete stand-alone in-house implementation, which was the starting point of the RADar Image ANalysis software suite known as RADIAN [R-1]. Its use in the operational image production chain of SAR-Lupe, made it possible to achieve the highest technology readiness level. The following sections describe the basic concept and modules of RADIAN, and illustrate its wide range of outstanding functionality with selected examples for TerraSAR-X data.

RADIAN: A Radar Image Processing Package for Security Applications

The first version of RADIAN was implemented as a command-line tool with a single functionality. It was able to load a SAR-Lupe dataset and process it with an intricate chain of filters to reduce the speckle noise, while maintaining the high spatial resolution of the image. Additionally, the algorithm significantly improved visual signature segmentation by introducing a brownish coloring of the image, which gave it the name SEPIA (see Figure 2.4-14).
In the meantime, the little black box application from version 1.0 has significantly evolved into a software package with a considerable amount of separate modules and a wide range of image processing functionalities [IC-72] in its current release version 2.4, as can be seen in Figure 2.4-13. Especially in the environment of an operational military user segment, numerical robustness and efficiency are crucial factors that require continuous testing. Additionally, image operators have a very limited time frame for analysis; thus, intuitive and simple handling, 1-click solutions and automated product creation are of utmost interest. The enhancement of the interpretability of radar imagery and the colors of products (urban vs. rural scenes) are also very important. Finally, RADIAN can be operated fully offline when using public map or terrain data.
RADIAN's sophisticated database client is able to download available data from a local storage or remote server. The import routines not only support SAR imagery, but also optical, digital elevation model and map data. Public data, like that of Sentinel-1 or OpenStreetMap can be downloaded either online from the web or from local mirror servers (thus ensuring offline operation). The visualization of an image is handled by a highly efficient 2-D viewer application specifically designed for the display of large datasets. Certainly, the main task of

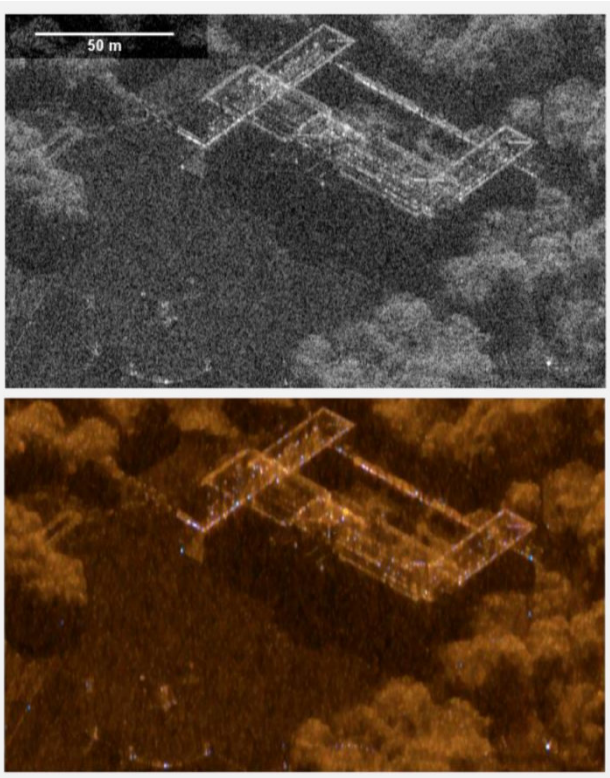

Figure 2.4-14 Single image filtering on a TerraSAR-X image detail of the Royal Palace in Oslo: Original data (top), filtered with SEPIA exhibiting noise and sidelobe reduction with a brownish (sepia) coloring but without loss of resolution (bottom). See also the center of Figure 2.4-15 for a comparison.

RADIAN is to create high-level image products from the data sources. For this, a wide range of image processing functionality is available either for the enhancement of single image data or the accurate registration, preparation and information extraction of series of images.
Finally, RADIAN is not only able to handle 2-D data, but can also handle 3-D data. A 3-D viewer supports visualization and provides the ability to overlay 2-D terrain textures over a digital globe. Additionally, arbitrary CAD models of target objects like airplanes can be inserted into the 3-D environment. In RADIAN, these features are primarily used to embed the self-developed SAR simulator SAREF, enabling users to perform tasks such as signature analysis or pattern recognition directly. These features will be explained in more detail in the next section.

Incoherent and Coherent Change Detection

In addition to the all-weather night-and-day capability of a spaceborne SAR system, its ability to perform change detection is of great value. Given a repeat-pass orbit, e.g., from TerraSAR-X, change detection robustness can be significantly improved by an exploitation of the whole history of earlier images. Thus, the signal-to-noise ratio can be significantly enhanced and the detection of changes improved accordingly. Figure 2.4-15 shows a composite image generated by the fusion of a series of 34 images taken over a 32-month period, each filtered by SEPIA, exploiting the coherence between successive images and highlighting current differences. The single

image detail in Figure 2.4-14 shows how the original data are dominated by a noisy speckle characteristic, reducing contrast, and making detection of objects with lower radar cross section more difficult. Figure 2.4-15 illustrates a significantly enhanced contrast. Due to this coloring, clustering objects of the same temporal and scattering properties – especially from man-made structures – can be easily distinguished from rather rural surroundings. Just as this method improves the visual interpretation, the analysis of a series rather than a pair of images also yields more robustness to automated target detection approaches. More work will be done on applying sophisticated algorithms for multi-temporal despeckling of single SAR images to facilitate automatic change detection.

Automated Change Detection

In recent years, the amount of available SAR image data has exponentially increased as a result of a larger number of satellites and a new generation of SAR sensors capable of acquiring more data. To deal with the increasing amount of data, new methods capable of automatically extracting relevant information are currently being developed. These are based on the expertise in SAR image analysis acquired during the development of RADIAN, and inspired by recent advances in other fields such as computer vision. These new automatic methods should serve as a complement to the traditional strategy based on visual image analysis by human operators. The goal is to inform the image analysts of relevant changes taking place at locations of interest automatically.

The current work focuses on the automatic detection of changes corresponding to the movement of man-made targets, such as ships or airplanes, which are especially relevant for defense and security applications. To simplify the detection of these specific types of targets, map data obtained from OpenStreetMap are used together with the SAR images [RC-72]. The inclusion of map data provides very useful context information, detailing the content of each scene, which helps to delimit the possible locations of these targets. Two examples for the monitoring of both ship and airplane movements are shown in Figure 2.4-16. For each example, a pair of TerraSAR-X images acquired with the staring spotlight imaging mode was used for the change detection. Objects highlighted in green are absent from the scene after the first image acquisition, whereas objects highlighted in red correspond to additions. As it can be seen, changes due to the movement of man-made objects like ships and airplanes can be effectively detected using very high-resolution spaceborne SAR sensors.

In order to obtain these results, a standard incoherent change

Figure 2.4-15 Exploitation of a series of 34 TerraSAR-X images of the Royal Palace in Oslo over 32 months: Color composite of SEPIA-filtered single images and pairwise coherence images. The bluish color indicates persistent scatterers, red shows strong amplitude change, and the greenish yellow color indicates coherency loss (mostly due to vegetation).

detection approach was first applied to detect changed pixels with a strong increase/decrease of backscatter. These changed pixels are then grouped together using a density based clustering algorithm, resulting in clusters corresponding to the changed objects. These objects can then be classified into different categories according to their spatial and radiometric properties, as well as the available prior knowledge about the scene obtained from OpenStreetMap. This classification step can be used to distinguish uninteresting changes (e.g., seasonal effects like snow) from those of interest.
Future work will be focused on improving the accuracy of this automatic change detection, as well as on the automatization of the target recognition using the SAR simulator SAREF (see next section for SAR simulation). The inclusion of SAR simulation will enable a more detailed recognition, e.g., allowing the identification of specific airplane models by using their corresponding 3-D CAD models.

2.4.7 SAR Simulation

The Institute's involvement in SAR simulation for security and reconnaissance applications began with the SAR end-to-end simulator (SETES) during the design phase studies for the SAR-Lupe reconnaissance system in the late 1990s. The lack of experience with high-resolution spaceborne SAR sensors demanded tools for tuning system parameters in a synthetic sandbox environment. With the launch of several spaceborne SAR missions around 2007, which provided a spatial resolution of around one meter, a multitude of SAR image data became available. Since then, the need for tools that interpret radar signatures and their specific effects increased considerably. This changed the paradigm for the design of a simulator from purely scientific, to an easy-to-use software that could also be applied by non-radar experts. With the intention of assisting users in their daily operational work, the new SAR Effects simulator (SAREF) was developed [RC-546].

SAREF: A SAR Simulator with Practical Applications in Image Analysis

SAREF is an in-house standalone simulator used not only as a scientific aid for parametric simulations for the next generation German reconnaissance system SARah, but also as an operational tool for the military [NJ-16]. Additionally, it has been applied in the past as an educational tool in numerous workshops for national and international image analysts. The simulator is currently undergoing a redesign by integrating it into RADIAN using its 3-D viewer as the primary user interface for input preparation. It defines the SAR sensor model for the simulation from real image data or synthetic sensor parameters and prepares a 3-D representation of the scene for the

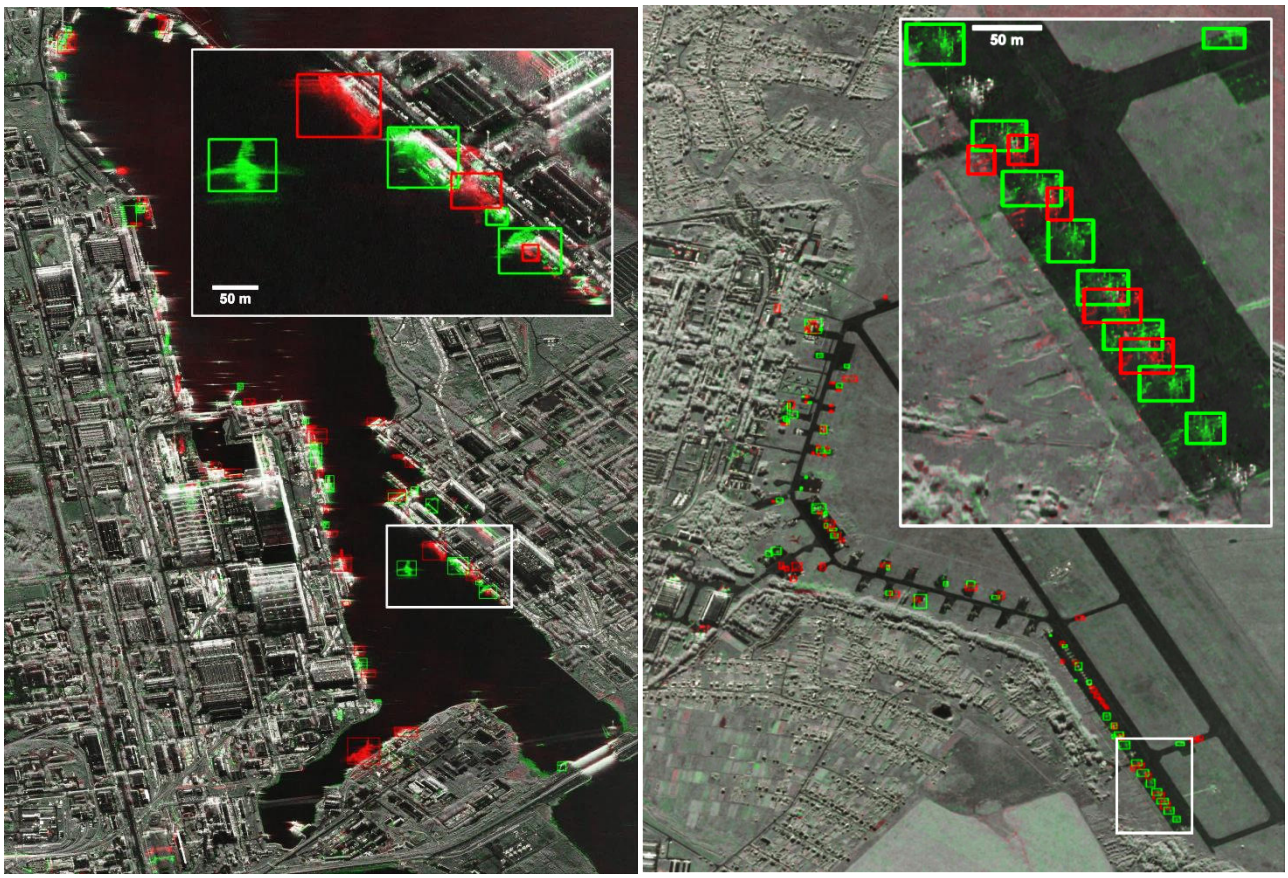

Figure 2.4-16 Automatic detection of changes due to the movement of man-made objects, with examples for monitoring the arrival and departure of ships in a naval base (left), and of airplanes in a military airbase (right). The bounding boxes of the automatically detected objects are drawn over multi-temporal color composite images that highlight the changes in red (object arrivals) and green (object departures) to enable an easy visual validation.

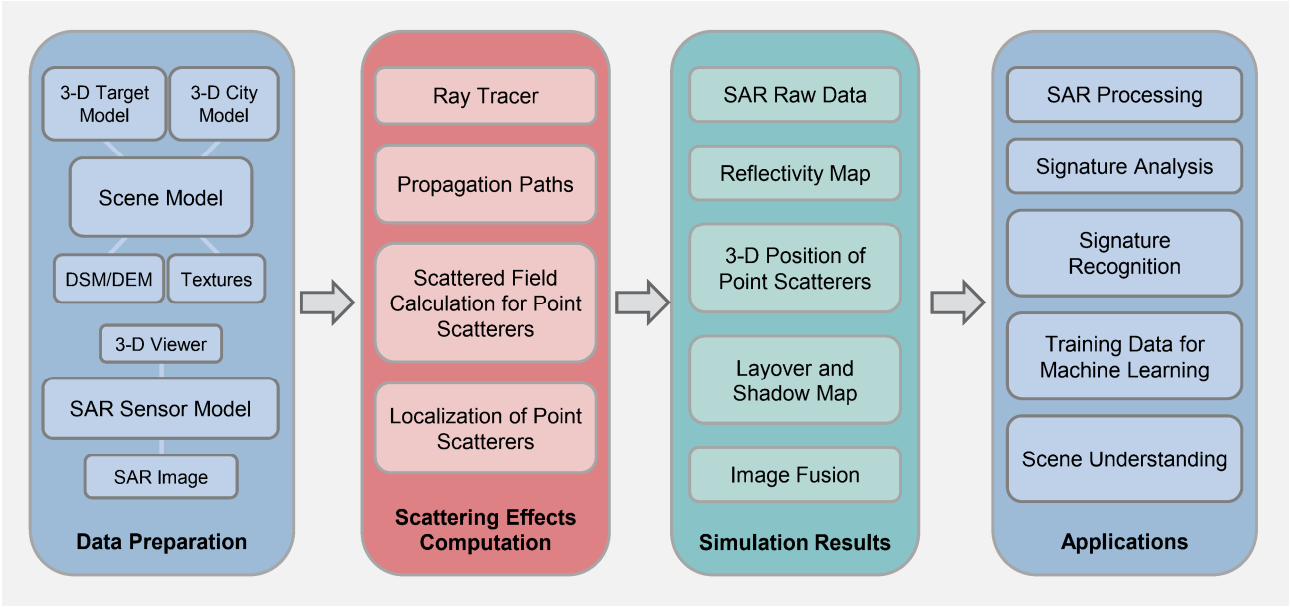

Figure 2.4-17 The conceptual simulation workflow of SAREF: Data preparation sends a 3-D scene model along with the SAR sensor parameters to the scattering effects computation block where the location and radiometry of point scatterers are determined. The results are a variety of products that serve a wide range of practical applications.

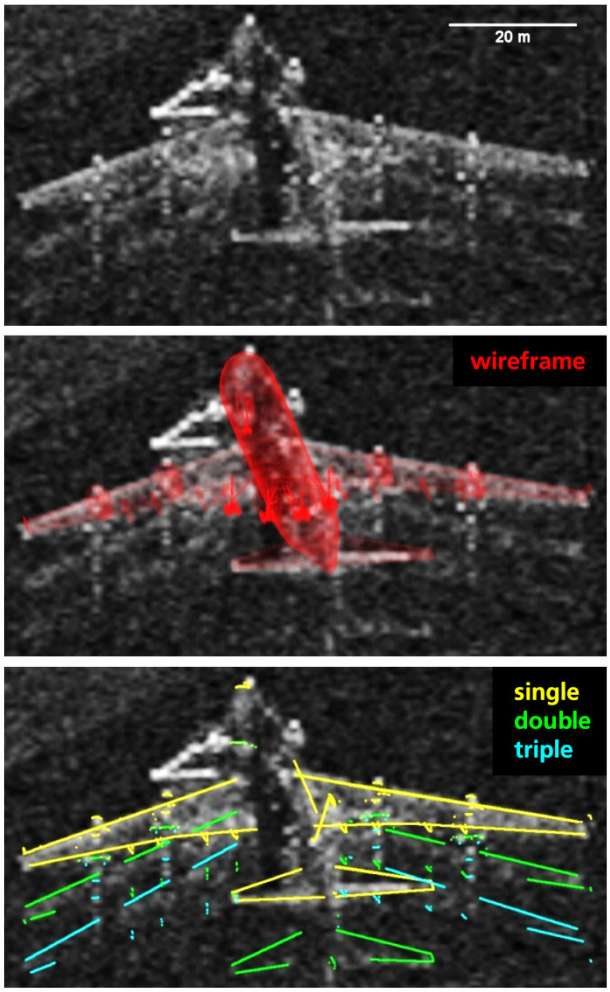

Figure 2.4-18 Recognition of an airplane signature in a TerraSAR-X image: The real signature (top) has been overlaid with a wireframe model of a Boeing 747 (center) and with the simulated signature (bottom). Even the fine triple-bounce effects of the wings are in very good agreement with the SAR signature in the image.

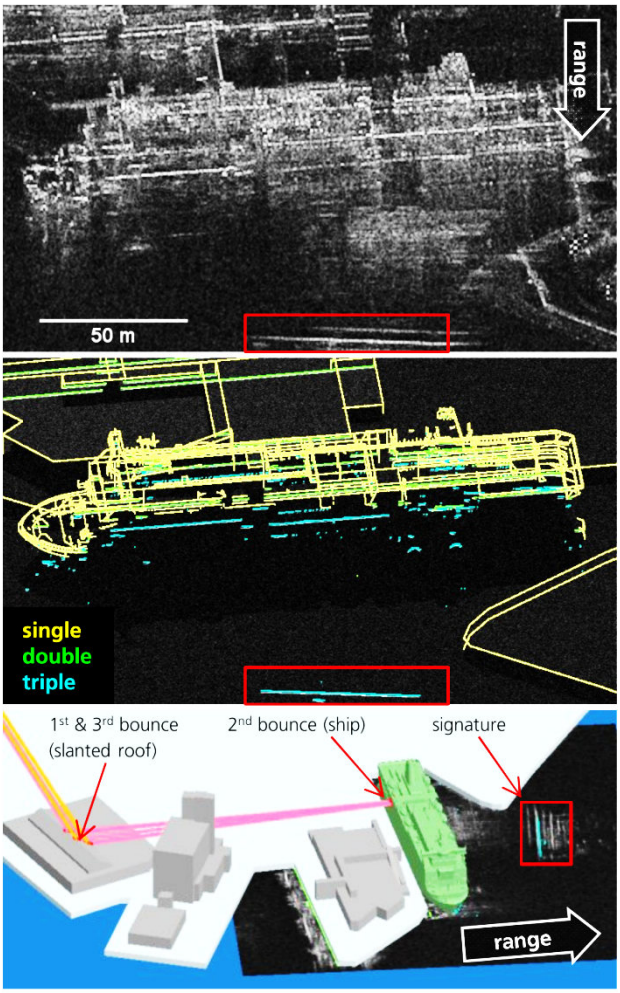

Figure 2.4-19 The TerraSAR-X signature of a ship (top) exhibits many prominent scattering centers, which are in agreement with the simulation (center). This also holds for the highlighted scattering effect (red box) caused by a far-out rooftop of a harbor building for which the propagation ray path is visualized (bottom).

simulation core. Part of the redesign also involves the acceleration of the computational runtime by using Nvidia's high performance ray tracing engine Optix. SAREF is able to perform a vast amount of traces in a split second through GPU processing. The results are propagation paths that represent potential candidates for robust point scatterers. During the next computation phase, these point scatterers are inserted into the 3-D model and their radiometric field return is calculated. A variety of simulation products can subsequently be generated for different kinds of applications (see Figure 2.4-17).

Signature Analysis & Recognition

The simulation concept is especially well suited for user-assisted analysis and recognition of high-resolution target signatures. Great care has been taken to make the process of the simulation chain as user-friendly as possible without losing the high accuracy of the simulation results. The following examples clearly demonstrate this. Figure 2.4-18 shows how SAREF was used for airplane recognition at a civilian airport [RC-341]. With SAREF, it is simple to transparently overlay a 3-D model (in this case a Boeing 747) and the simulated scattering centers with the real signature for visual control. The simulation includes multi-path propagation, which also plays a major role in the maritime example shown in Figure 2.4-19. Due to the simulator's ability to visualize the propagation path, it was possible to identify the characteristic interaction between the ship's body and a distant slanted rooftop [RC-343]. Finally, it is not only possible to use the simulator for single target object signature analysis, but also for the alignment of wide-image scenarios with real image SAR data, optical images and digital elevation models (Figure 2.4-20 and Figure 2.4.21). Figure 2.4-21 shows a sub-pixel accurate geometric alignment of an F-SAR image of the Heligoland island with an optical image on a digital surface model [RC-3]. Such data fusion will become vital for the joint operation of multi-sensor systems.
In the future, the simulator's scattering models will be expanded to other radar imaging configurations (e.g., ground-based, multistatic, through-wall) and to passive imaging technologies, such as radiometry. With the transition to high-performance GPU-based processing, SAREF will be used for automatic target recognition methods to generate extensive training data for machine learning methods [RC-93].

Figure 2.4-20 Image fusion between a TerraSAR-X image (left) and a Pleiades optical image (middle). The layover effect causing the TV tower to overlap with a church in the SAR image is visualized in a 3-D model (right).

Figure 2.4-21 Sub-pixel accurate image fusion between an X-band F-SAR image and an optical image from DLR's airborne sensor system MACS for the whole island of Heligoland. The zoomed detail shows the outstanding accuracy even on a building level through the usage of a very accurate digital surface model.

2.4.8 Ground-Based and Near-Surface Radar Systems

Research on reconnaissance, security and safety applications demands a broad variety of sensor systems with respect to many aspects such as frequency range, spatial resolution, sensitivity, operating distance, penetration capability, polarization, imaging frame rate, ambient conditions, and finally weight and size.
On the one hand, there are a wide range of potential applications, e.g., detection of concealed objects, inspection of wall structures, status monitoring of critical situations, threat detection, freight monitoring, food inspection, target detection, or space observation. On the other hand, applications like these also rely on a variety of platforms, e.g., hand-held, vehicle-based, drone-based, airborne or located at very high altitudes, either piloted or autonomously operated. Consequently, a very large number of different techniques and technologies have to be used, which are discussed along various projects and activities illustrated in the next sections on radar and radiometer systems.

Highly Flexible Experimental Radar System – Gigarad

In the past years, the Institute has developed a very versatile and modular high-resolution radar system for manifold applications that is currently being operated. The so-called Gigarad instrument [J-92], [MaT-29], [MaT-40], [MaT-54], [MaT-60], [BaT-8] is an experimental system operating in X and Ku band (8-14 GHz), which can provide a spatial resolution of a few centimeters. The waveform generation and reception in the baseband is performed by I/Q modulation and demodulation based on full digitization of transmit and receive signals in time domain. The system concept, providing two transmit and two receive channels, allows quasi monostatic, bi-static, or MIMO (multiple-input multiple-output) operation. The standard transmit waveform is a chirp, but any other waveforms like noise or orthogonal – e.g., coded signals – are possible [RC-560]. Based on a coherent system architecture and the realized degree of automation, the applications of the instrument range from RCS measurements, UAV detection, micro-Doppler sensing trough to Imaging of Satellites in Space (IoSiS) [RC-92], [RC-31], [MaT-20], [IC-8]. Figure 2.4-22 left shows a photograph of the radar hardware in 19" construction. Various application examples are shown on the right side. The benefits of very high-resolution imaging and the impacts of radio interference (RFI) on SAR/ISAR imaging, and the detection capabilities of micro-Doppler signatures of humans have been investigated using the Gigarad instrument. However, since 2015 the radar system has been used for the IoSiS system described in a later section.

Landmine and UXO Detection – TIRAMI-SAR

The safe, reliable, and efficient detection and subsequent removal of buried landmines or other unexploded ordnance (UXO) still remains a challenge. Although non-technical surveillance for the identification of contamination is improving slowly, more progress is needed in the basic detection of such threats. Many new technologies have been investigated in the last 20 years, but the classical ones like metal detectors and dogs in cooperation with human operators are still the most common today. Hence, the detection process for many scenarios is unacceptably slow and dangerous for the operators, as they are typically less than one meter away from the threats. A sensor technology enabling a sufficient stand-off distance for safe operation and reliable detection at high area throughput is therefore desirable. Following previous considerations, a SAR system using multiple channels, different polarization combinations, and operating in the UHF range was considered. SAR is an imaging principle based on a side-looking geometry; hence, the radar can move on safe ground, while imaging the hazardous ground. The frequency range should be lower than a few Gigahertz due to penetration depth constraints. In order to use reasonable antenna sizes, the lowest frequency should be at least in the order of a few hundred Megahertz. The constraints of very limited target-to-clutter ratios to be expected for typical landmine/UXO scenarios require advanced methods.

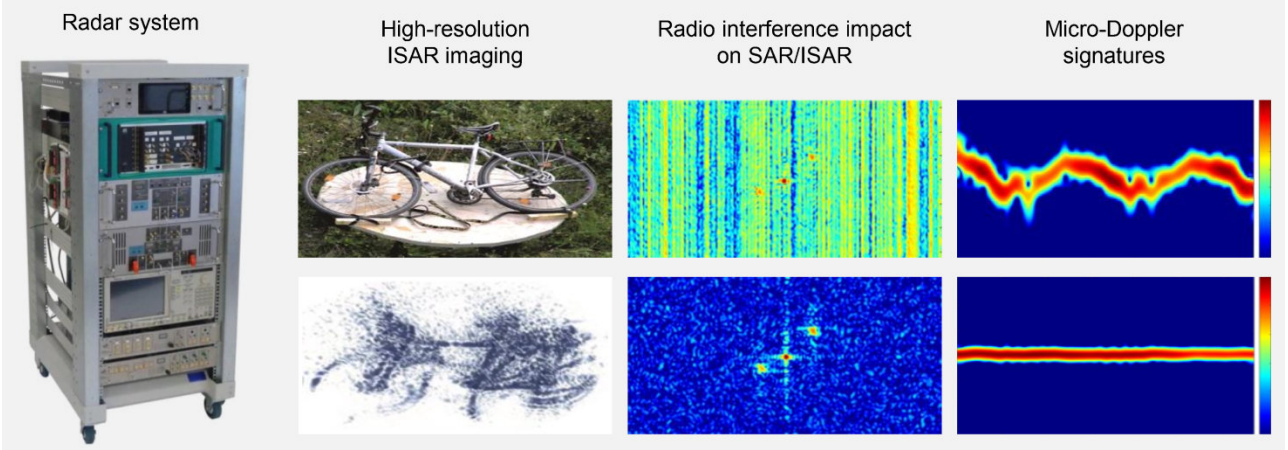

Figure 2.4-22 Gigarad radar system used for various experiments (left). Measurement results shown from left to right: photograph (top) and ISAR image (bottom) of a bicycle at a spatial resolution of 2.5 cm, comparison of a single-frequency CW RFI contaminated ISAR image of three point scatterers (top) and the image without RFI (bottom), micro-Doppler signature (intensity over Doppler/vertical and time/horizontal axis) of a breathing person (top), without breathing (bottom). Color bars are valid for RFI and micro-Doppler images ranging from -40 dB to 0 dB. Doppler frequency ranges from -15 to +15 Hz, and time from 0 to 6.5 s.

From experience it was expected that a man-made target, such as a landmine, typically shows similar signature strengths – even when incidence angle, bistatic angle, and aspect angle of observation are changed considerably – while natural background clutter like vegetation or soil does not.

If the antenna setup for transmit and receive is arranged so that the antenna array produces a certain length in vertical direction, vertical spatial resolution can additionally be achieved by true 3-D imaging capabilities. In addition, the use of polarimetric information is mandatory, since man-made objects often show strong polarimetric predominant directions.

The TIRAMISU project was launched within the EU FP 7 program, in which the Institute was responsible for the development of a vehicle-based SAR system incorporating the features as described before. The top of Figure 2.4-23 shows a photograph of the TIRAMI-SAR radar system [RC-412], [RC-318], [RC-215], [NJ-8], [RC-23], [MaT-21], [BaT-12], [BaT-14], [BaT-16], [InT-16], [IC-5], [IC-34], [IC-57], [IC-58], [IC-64], [IC-65], [IC-97]. On the bottom, a few measurement examples of buried objects, such as mine and grenade simulants and thin wires as indicators for remote activation of improvised explosive devices are shown. The innovative approach allows highly-improved detection of buried objects due to its multi-static and fully polarimetric 3-D imaging capability, making it very useful for detection of thin wires in different configurations as well. However, the TIRAMI-SAR concept still offers a wide range of future investigations towards optimum configurations.

Table 2.4-1 summarizes the main characteristics of both advanced radar systems Gigarad and TIRAMI-SAR, which are used for different applications.

SAR Sensor for Drones – Dronar

For military and also general remote sensing activities, the use of hand-held or vehicle-based sensors is limited with respect to the requirements on forward-looking imaging [IC-56] and in dangerous and restricted access areas. Consequently, sensor operation from a bird's perspective, but within close range of the scene offers attractive advantages. Since the drone market has considerably evolved in the last years, offering very low-cost high-performance airborne capabilities, drones are generally considered as suitable sensor platforms. Hence, a few years ago, the Institute decided to transfer most of TIRAMI-SAR sensing capabilities to a drone platform by launching the Dronar

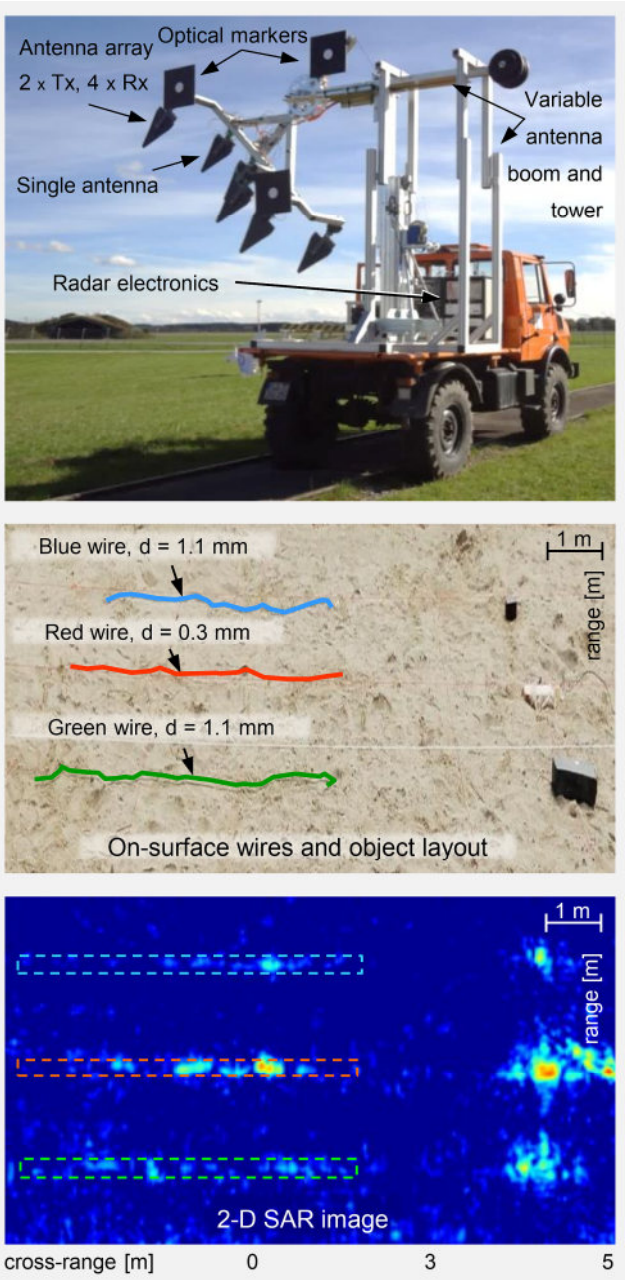

Figure 2.4-23 Top: photograph of the TIRAMI-SAR radar system used for landmine and UXO detection. Optical markers are used for motion compensation. Tx – transmit, Rx – receive. The lower left images show a photograph of a buried object scenario (mine, grenade simulants) and the corresponding 3-D radar image, generated by a stack of 2-D images focused on specific depth levels. Targets appear elongated due to reduced vertical resolution. The lower right images show a photograph (warped) of thin wires (retraced) and some targets on the surface, and the corresponding 2-D radar image (dashed boxes indicate wire signatures). The central target on the right is a wooden pressure plate connected to a wire extending to the right.

activity. Figure 2.4-24 left illustrates the operational principle. For an experimental system, a special drone has been purchased that enables individual absolute flight control, and a first version of a suitable UHF radar module for drone operation has been developed and realized [BaT-2].
Simulation activities are performed to investigate the impact of motion errors and optimum SAR processing. GNSS-based motion tracking is investigated using simulation and experiments to enable motion compensation for high-quality SAR images.
The use of drone-based UHF radar is considered as suitable for many applications, such as concealed threat detection and general ground investigation, serving both military and civilian end users. The first test flights of the whole Dronar system are planned for autumn 2018.

Detection of Drones – LOCASS project

Drones have become novel and excellent platforms for many advanced and new sensor concepts and applications. Their low cost, and broad and commercial spread also make them quite useful for many illegal, criminal or even terrorist activities. It is thus necessary to devise, investigate and prove solutions for early warning, detection and situation compliant removal of such threats. Within the LOCASS (local air surveillance system for security purposes) project, the Institute is developing a multi-sensor concept to address the detection and classification problem in a broad and flexible way. Here, the focus is more on urban scenarios, for which the detection ranges are indeed rather short in the order of a few hundred meters.
However, the environment, which consists of narrow and busy road channels surrounded by high building structures, makes detection challenging due to highly increased clutter levels.
One appropriate sensor solution is a network of advanced high-resolution radar systems providing additional micro-Doppler sensing capabilities, which are arranged in an appropriate grid to observe the areas to be protected from unwanted intrusion by drones. Since the bandwidth of available drones in size, shape, flight capabilities and material decomposition of this highly growing market is extremely large, the radar design must be appropriate to cover most of the typical peculiarities. Consequently, basic investigations on radar cross section signatures as a function of frequency and observation angle, as well as detection experiments of typical flight patterns, are a useful start for research on appropriate radar design. Figure 2.4-25 illustrates the measured results for the RCS of a drone at various frequency bands and a typical flight pattern by opportunity measured in X band using the IoSiS radar system – both for the shown commercial small-sized drone.
Since the drone has a complicated mechanical structure with respect to observation angle, the radar cross section has varying character over azimuth and elevation angle, but not much more than 10 dB. The variation depending on frequency behaves roughly as expected and shows maximum RCS at W band. It is expected that the discrimination from false targets like birds and other clutter can be accomplished from flight pattern measurements – i.e., range profiles over time and corresponding velocity distribution, as shown in Figure 2.4-25. Further research on signatures, especially micro-Doppler behavior, is planned for the near future.

Radar System **Parameter**	**Gigarad**	**TIRAMI-SAR**
Frequency range	8 – 14 GHz	0.5 – 3 GHz
Range resolution	Down to 2.5 cm	Down to 6 cm
Typical scene size	Application dependent, e.g. 300 m x 300 m (imaging of satellites, measured by ISAR in about 30 s)	5 m x 10 m (landmine detection, measured by SAR in about 3 minutes)
Radar type	Pulse radar using chirps (typically)	Pulse/CW radar using chirps (typically)
Channels	2 x Tx, 2 x Rx (all independent)	2 x Tx, 4 x Rx (all independent)
Modulation / demodulation	I/Q, use of upper and lower sideband	None
Tx signal generation	Digital, 12 GS/s (arbitrary waveform possible)	Digital, 12 GS/s (arbitrary waveform possible)
Maximum / typical Tx power at antenna output	Application-dependent, e.g., 4 kW / 4 kW for imaging of satellites	5 W / 100 mW for landmine detection
Rx signal sampling	4 x 8 GS/s, 8 bit, for 2 Rx channels in time domain	4 x 8 GS/s, 8 bit, for 4 Rx channels in time domain
Polarization capability	HH, VV, HV, VH (simultaneously)	HH, VV, HV, VH (in time multiplex)
Scan speed for synthetic aperture	0.8°/s in average (antenna tracking for staring spotlight ISAR)	10 cm/s constantly (truck motion in high-accuracy drive mode for stripmap SAR)

Table 2.4-1 Typical main characteristics of Gigarad and TIRAMI-SAR radar systems

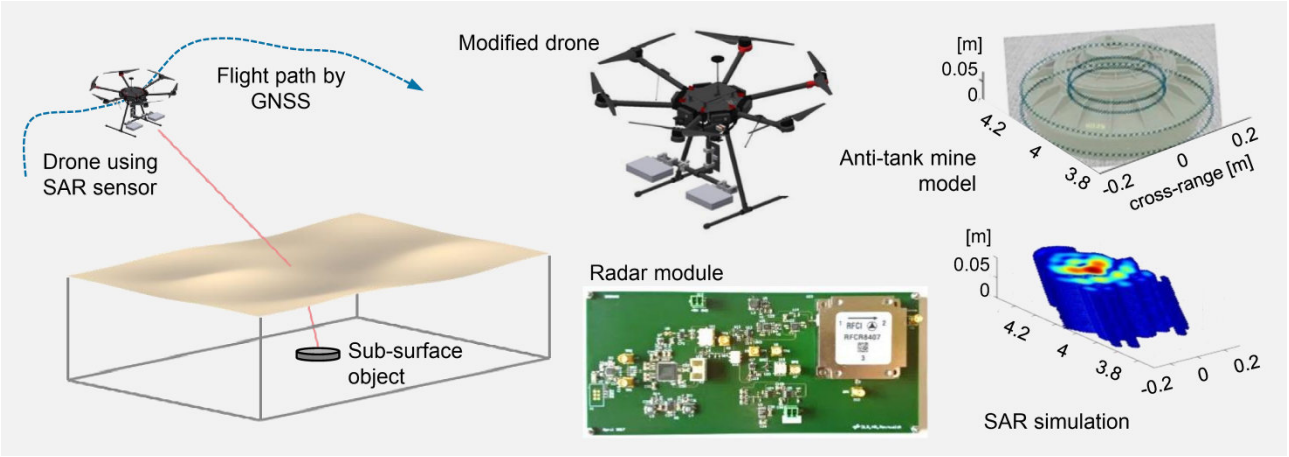

Figure 2.4-24 Operational principle of the drone-based SAR system Dronar (left), photograph of the application-oriented modified drone and the developed UHF radar module (center), wire-grid based model of an anti-tank mine and the corresponding stack of SAR images at various focusing planes assuming linear and ideal sensor motion (right). Axes are given in meters.

Tomography of Buildings – Gtom Radar

By 2050, the German government plans to reduce its primary energy demand by up to 80 percent. One major part of energy consumption is thermal energy, of which 40% is related to buildings. All the buildings constructed before 1979 show higher than average energy consumption. Until the oil crisis in 1979, there was no awareness of thermal insulation, as is the case today, and hence 64% of the building stock remains without any insulation. A clear cost-benefit ratio has to be demonstrated to incentivize house owners to implement suitable insulation. This can only be fulfilled if the optimal solution for each individual building can be determined with sufficient precision. Various DLR institutes and FH Aachen are cooperating in multiple disciplines to address this challenge in the project Gtom (Gebäudetomograph).

The Institute is responsible for investigating radar technology for the analysis of wall structures with regard to the number of layers, layer thickness and material composition [RC-22]. For practical reasons, a simple reflection measurement from outside a building should deliver the desired information. Such a measurement can be made either by recording range profiles locally or by applying SAR techniques to acquire full 3-D images of wall sections.

The forward modeling of wall structures can be accomplished by considering those as a layered medium of slabs of different thickness and permittivity, which is then transferred to an electromagnetic representation by concatenated electric lines and final load impedance. This model allows computing the overall reflection coefficient at the exterior face of the wall and the transmission coefficient at the inside face. The challenge is now to retrieve layer thickness and permittivity from the reflection signature, which is not possible by any direct inversion. Consequently, various methods are being investigated, such as brute-force computation of a larger number of possible configurations and comparison to the actual measurement, evolutionary algorithms using some iterative optimization strategy, or neural networks to be sufficiently trained by appropriate data, both to identify a best solution. In parallel, a multitude of measurements on typical building bricks were performed in order to obtain true signatures, as well as some insight into the type of information that can be extracted. Figure 2.4-26 shows a photograph of the measurement setup, the wall structure arrangement, and measured waterfall plots of radar range measurements for two different frequency bands. It can be seen that a higher bandwidth starting at 2 GHz provides more detail, while the lower bandwidth starting at 1 GHz enables the detection of all three layers, i.e., solid brick, air gap, and hollow brick. Hence, a very wide bandwidth and a very low starting frequency provide optimal frequency coverage to get both sufficient spatial resolution and penetration capability. However, differently structured bricks in combination with several layers of different materials are still a challenge for the retrieval of individual material parameters at a suitable accuracy.

Measurement of General Ground Parameters Using Radar – Ground Check Active

The application of drone- or vehicle-based UHF radar for concealed object or threat detection is strongly related to ground observation, since the ground or soil has a large impact on the signatures to be measured. On the other hand, such radar can deliver valuable information regarding ground parameters on a local scale, e.g., moisture estimation for agricultural purposes or evaluation of trafficability for action or military forces in case of catastrophes or crises, or the exploration of the ground for civil engineering of large traces (sub-surface power lines, pipelines, etc.) and the detection of resources, for instance. Some basic understanding of ground and electromagnetic wave interaction is thus required.

A large amount of modeling is already available in the literature, although the majority was developed for rather large-scale observations (see also Sections 2.2.8 and 2.3.3) and is based on the individual experiments of various research groups in special regions. More detailed knowledge about modeling and its relationship to hardware is necessary to develop suitable microwave sensors and estimate system performances for application in central Europe, Germany or other locations.

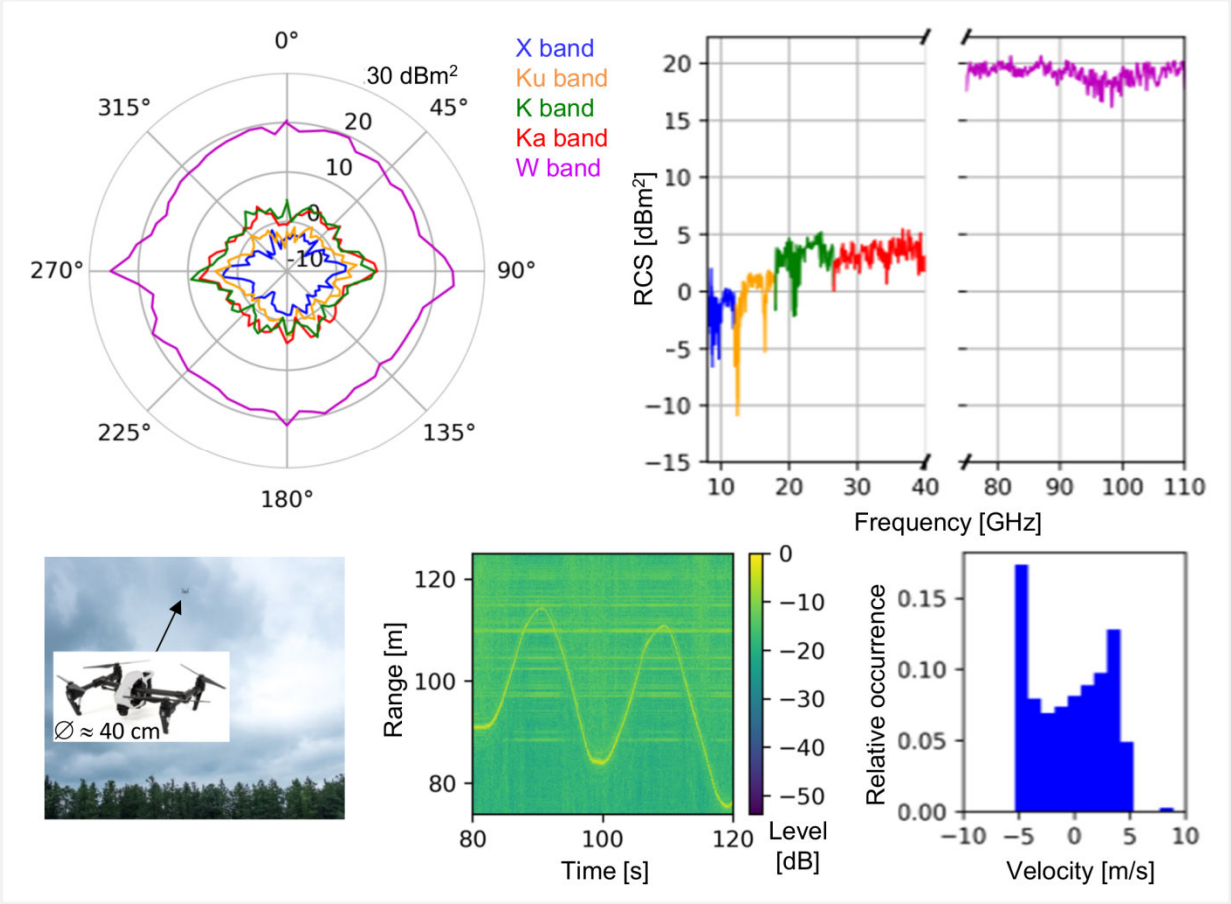

Figure 2.4-25 Top: Measured RCS as a function of azimuth angle for side-view perspective of a commercial drone (left), and corresponding averaged RCS as function of frequency (right); bottom: Photograph of the flying drone scene during radar measurements using the X-band IoSiS system (left), measured range profile over time (center) and corresponding velocity distribution (right).

Hence, the internal project Ground Check Active was initiated performing various basic investigations. In a first step, the sensitivity of various frequency bands to soil moisture dependent on vegetation cover was analyzed [MaT-13]. Figure 2.4-27 left shows the experimental setup. The estimation of soil permittivity from radar in comparison to a commercial Frequency Domain Reflectometer (FDR) device for measurements on a rather densely grown meadow is shown on the right. The comparison is done for permittivity instead of soil moisture in order to avoid additional errors by conversion from permittivity to moisture content via additional modeling. It can be clearly recognized that L band (1-2 GHz) shows the highest sensitivity, as expected, and the radar results are sufficiently correlated to the FDR data, although a slight underestimation of absolute permittivity values can be observed. The sensitivity in S band (2-4 GHz) is still present but shows a much lower variation and a larger offset. All bands above S band appear to be useless for this application, since what is measured is the roughness of the vegetation instead of the reflections from moist soil. It should be noted that the FDR measurements also provide errors in the order of 5 % in absolute values. However, various reports on using C or X band or even higher frequencies for soil moisture estimation are available in the literature, which contradict the presented observations.

Detection of Electronic Devices – Harmony

The detection of threats in the shape of explosive mines or Improvised Explosive Devices (IED) using the analysis of microwave radar signatures is done by evaluating received signals at the exact same frequencies at which they were transmitted. Hence, classical RCS distribution in range and cross-range is compared to estimates of typical threat signatures. In that case, the target signature is often blurred by background clutter, making detection difficult or even impossible. However, a common method to initiate an IED detonation is performed using electronic ignition via remote control, being either a wire-based simple switch mechanism or a more advanced concept using mobile phones or walkie-talkies. Since such devices contain some electronic components like semi-conductors, or at least metal-metal contacts, a non-linear voltage-current relation is realized in theory when activating this transition by an RF signal. Consequently, if such a device is exposed to sufficient RF power at suitable frequencies, the generation of harmonics of the fundamental transmission frequency can be expected. Hence, a suitable receiver able to detect such harmonics is an indicator of the presence of any electronic devices. In addition, the received harmonic signals are rather free of clutter, since non-electronic objects do not produce harmonics.

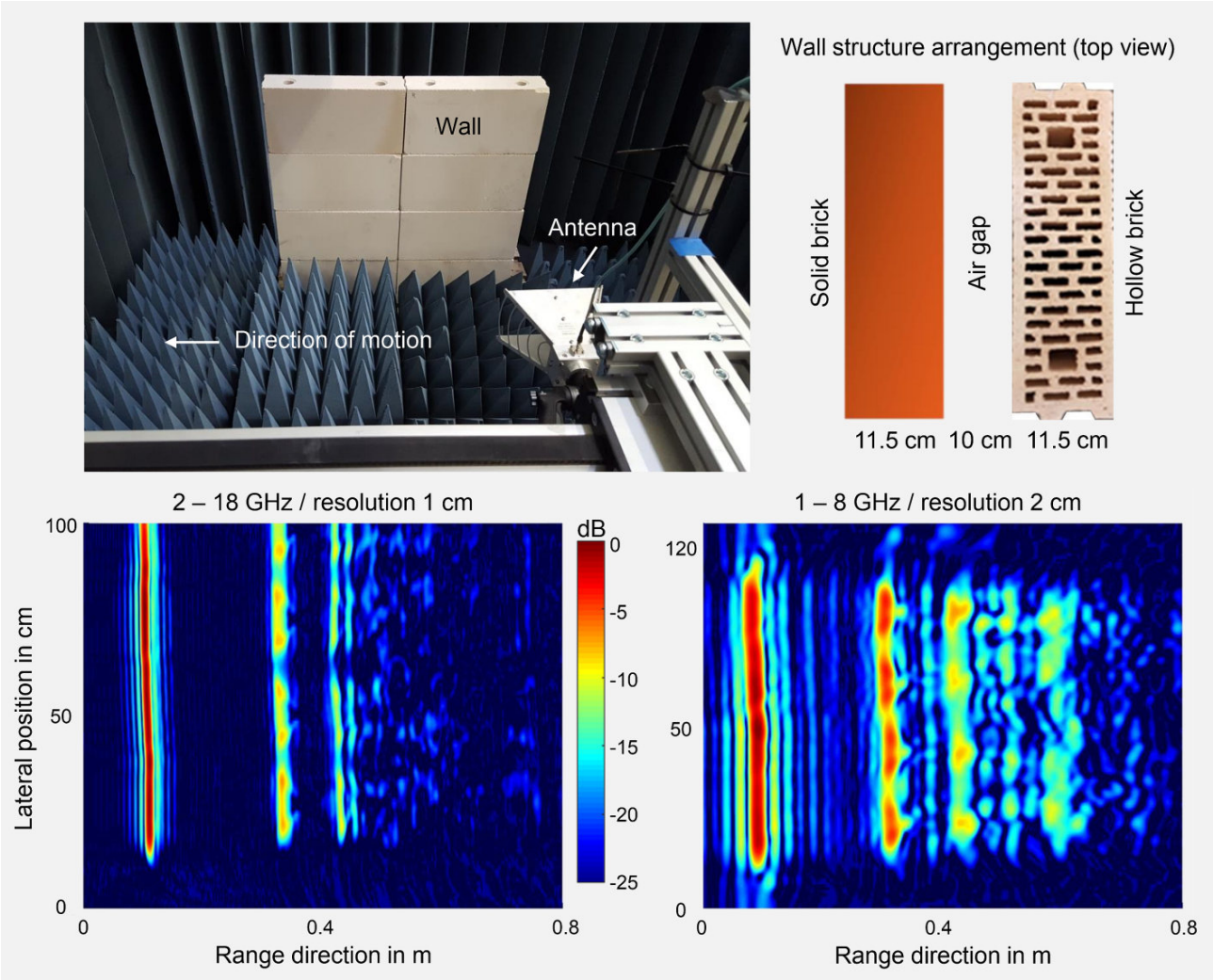

Figure 2.4-26 Photograph of the measurement setup (top left), wall structure arrangement (top right) and waterfall plots of subsequent radar range profiles along the wall structure for two wavebands – broadband 2-18 GHz (bottom left) and broadband 1-8 GHz (bottom right). The radar was located on the left side of the wall structure. The range was computed using a free-space permittivity of 1.0.

Now, an interesting sensor approach is a combination of 'classic radar' looking for 'normal RCS', and 'harmonic radar' looking for 'electronic RCS'. Within the Harmony project, this approach was investigated theoretically by simulation, and experimentally through the development and construction of a special device, being partly based on former research on multi-channel aperture synthesis radiometers [MaT-1], [BaT-11], [InT-3], [InT-7]. A photograph of the system and measurement results are shown in Figure 2.4-28. For range direction, a step-frequency signal is used and processed to range profiles. In cross-range direction the linear array of 3 m length is rotated in order to generate 2-D RCS images for each range bin, resulting in 3-D RCS information for classic and harmonic radar mode. The transmit power for classic radar was about 1-10 mW and 1-10 W for the harmonic radar mode, and the distance to the targets was about 4-5 m. Classic targets indicated by colored boxes are: horizontal metal rail (white), vertical metal rail (green), trihedral radar reflectors (red and yellow). The harmonic target indicated by the violet box is a semi-conductor based frequency doubler connected to both ports of a dual-polarized broadband horn antenna. The results clearly show the different capability of both radar modes within an identical scene, where the classic radar result delivers information on ambient structures and the harmonic radar mode identifies and yields the position of electronic devices.

Detection of Loading Conditions of Trucks – MikroVol

The freight transportation service by truck is a strongly growing market all over the world. However, the road traffic infrastructure in most countries is overstrained and has not grown in an appropriate manner. There is thus a strong demand for optimizing the capacity utilization of trucks to reduce the volume of their traffic on the road. Efficient volume utilization is not always a top priority when freight transportation companies load their trucks. The loading is mostly done according to the experience of the forklift operator. Hence, there is an interest to independently estimate the volume distribution of a truck load with a fast and stand-off monitoring sensor under common driving conditions. Microwave or millimeter-wave sensors like radars and radiometers can provide a significant advantage to this task due to the penetration capabilities through thin dielectric walls, for example plastic or rubber truck tarpaulin.

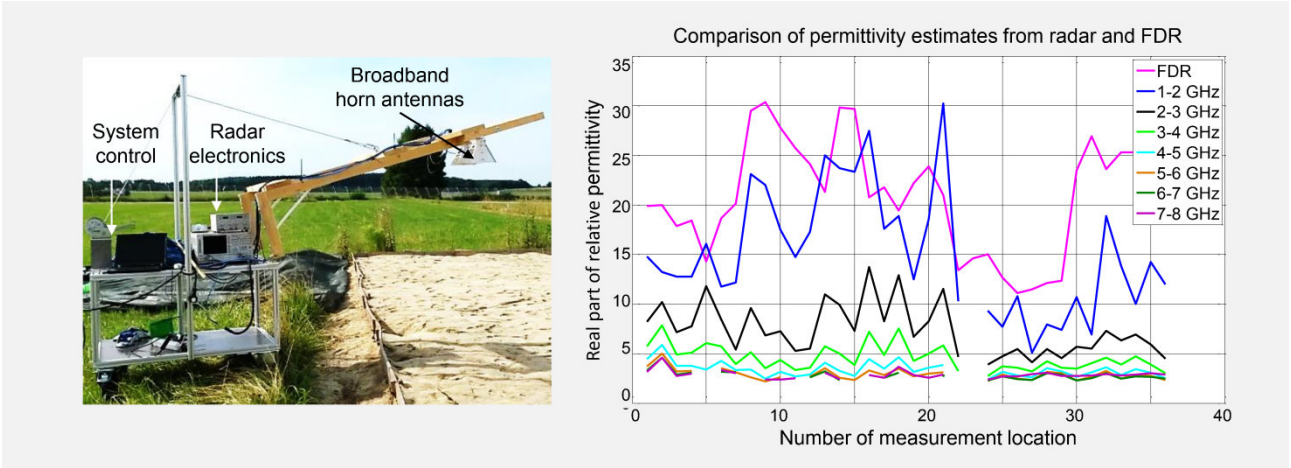

Figure 2.4-27 Photograph of the measurement setup for investigation of radar sensitivity to soil moisture in dependence on frequency bands (left). On the right, relative permittivity estimates of radar measurements are compared to measurements made by a commercial FDR device. Measurements have been carried out at 36 different locations of a large meadow at DLR facilities in Oberpfaffenhofen.

Moreover, these wavebands use non-ionizing radiation, or a purely passive sensing principle, so that there are no constraints about health risks, avoiding expensive infrastructure for safe and legal operation. In addition, such a sensor system could be installed on common roads or selected traffic hubs and perform its measurements in-situ at the normal speed of the trucks, thus not influencing traffic flow.

Within the MikroVol project, the DLR radar system UNIRAD and radiometer line-scanner systems ABOSCA and SUMIRAD have been used in various configurations in order to get a comprehensive picture of the capabilities of such an approach [RC-413], [IC-57]. Figure 2.4-29 shows measurement principles, setups and two results for radar and radiometer imaging of a typical truck with a typical load on its concealed platform.

The radar top-down measurement provides true 3-D information by using the SAR principle along track, a MIMO radar approach in across track, and the radar range measurement capability in the vertical direction. The radiometer provides a repetitive rotational line scan from a slant perspective, and by its own forward motion the truck is also scanned along track in order to finally produce a 2-D image. Note that, in both cases, the load can be clearly identified even through the canvas, despite the use of two completely different microwave imaging principles and two quite different wavebands. Note that for radar, full 3-D information on truck load is available, while for the radiometer a second system on the opposite side of the road, providing another perspective, will be useful for a better 3-D estimation of the load.

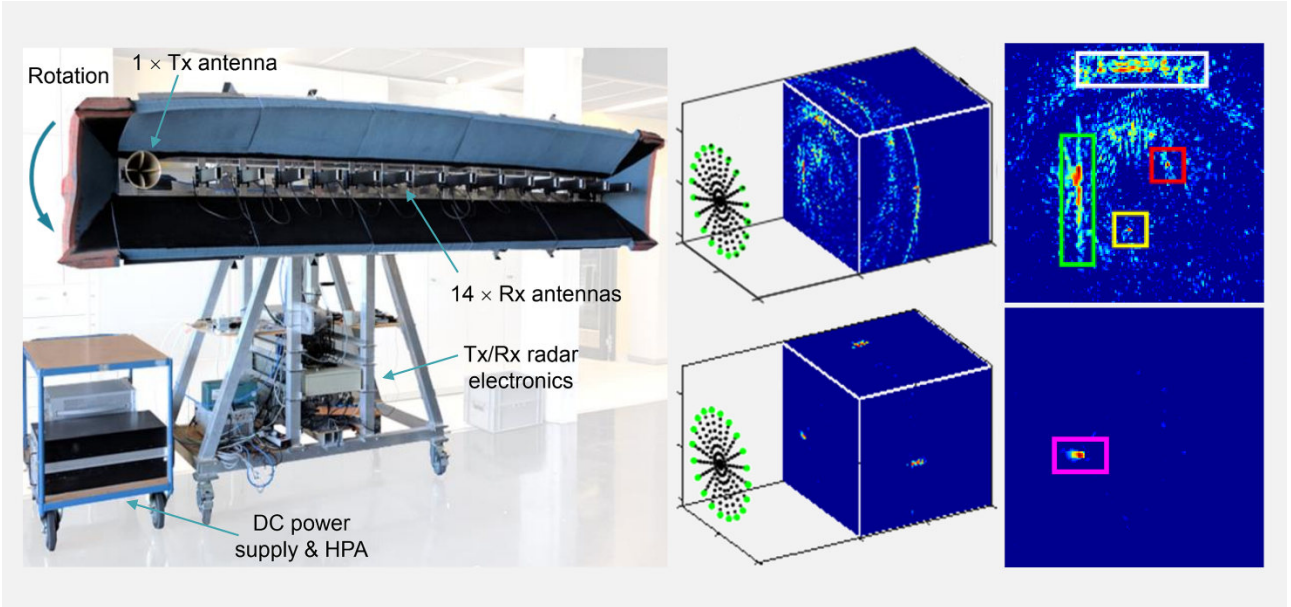

Figure 2.4-28 Photograph of the combined 'classic/harmonic' radar system (left) using one transmitter (Tx) and 14 receivers (Rx) arranged in a linear equidistant array, being rotated for true 3-D imaging. On the right, imaging results for an indoor scene are shown in 3-D (the cubes represent the imaged volume; on the left of the cubes the sampling pattern of the antenna array is shown; the right images represent the front of the cube). Upper results show classic RCS (Tx and Rx 4-7 GHz) and lower ones show harmonic RCS (Tx 2-3 GHz, Rx 4-7 GHz).

Detection of Contamination of Bulk Cargo – Mikrozucker

During the production of high-quality bulk materials it can occur that unwanted metallic and/or non-metallic impurities lower the quality of the final product. In case of food, this may even cause health problems, which cannot be tolerated.
The major problem of detecting such impurities lies in the fact that many bulk materials are moved as a dense material agglomeration during production, so that detection within the bulk cannot be performed by optical/infrared, ultra-sound, magnetic-force or X-ray due to insufficient penetration capability, impurity type or harmful operation for the environment. However, microwave and millimeter-wave imaging technology offers an attractive method for addressing the previously described issues. Now, in case of automatic bulk material transportation, synthetic aperture radar (SAR) technology can be used for in-situ detection during the conventional material flow of the production process.
Following some basic investigations on frequency dependence of RCS for small impurities of sizes around 1 mm or smaller, it was concluded that advanced millimeter-wave ISAR would be an appropriate tool to solve the issue. The approach was designed for impurity detection in granulated sugar during the production process, during long transport on conveyor belts [RC-229], and investigated in the Mikrozucker project. The investigations showed that even thick heaps of granulated sugar can be penetrated sufficiently by W-band radar, and first ISAR approaches have been carried out using a Vector Network Analyzer (VNA) and various metallic spheres of 0.5-5 mm size as low-RCS canonical targets. The intended ISAR concept and a measurement result for typical impurities within bulk sugar are shown in Figure 2.4-30. The impurity targets used were from detections during regular sugar production; these being insects (wasp, bumblebee), glass and aluminum fragments, seal and belt fragments, concrete fragments, percolation backlogs, etc., and all with sizes ranging from between about 1 mm up to 15 mm in diameter. ISAR measurements of the identical scene were carried out in time multiplex for eight different configurations – i.e., combining two bi-static angles (1° and 20°), two polarization bases (0° and 45°) and two polarization combinations for Tx/Rx (V/V and V/H) – resulting in 8 independent ISAR images. Following the positive experience from TIRAMI-SAR research, these 8 images were superimposed incoherently in order to considerably suppress the background

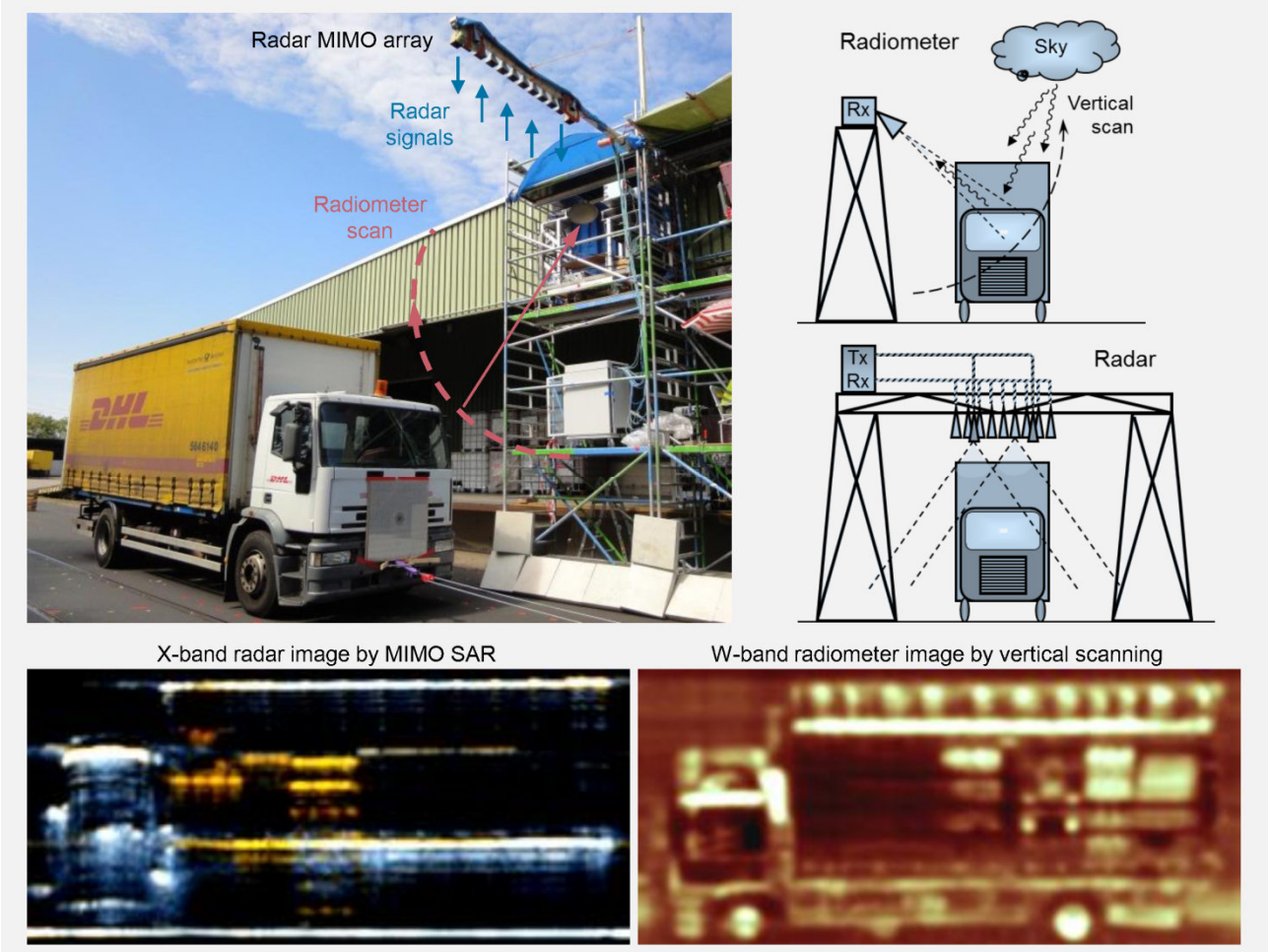

Figure 2.4-29 Photograph (top left) of the measurement setup including radar and radiometer installations, operational principles (top right), and imaging examples (bottom) for radar and radiometer approach. The loading for radar and radiometer was different as is clearly seen in both results. The 3-D radar information has been represented in across-track direction for better comparison.

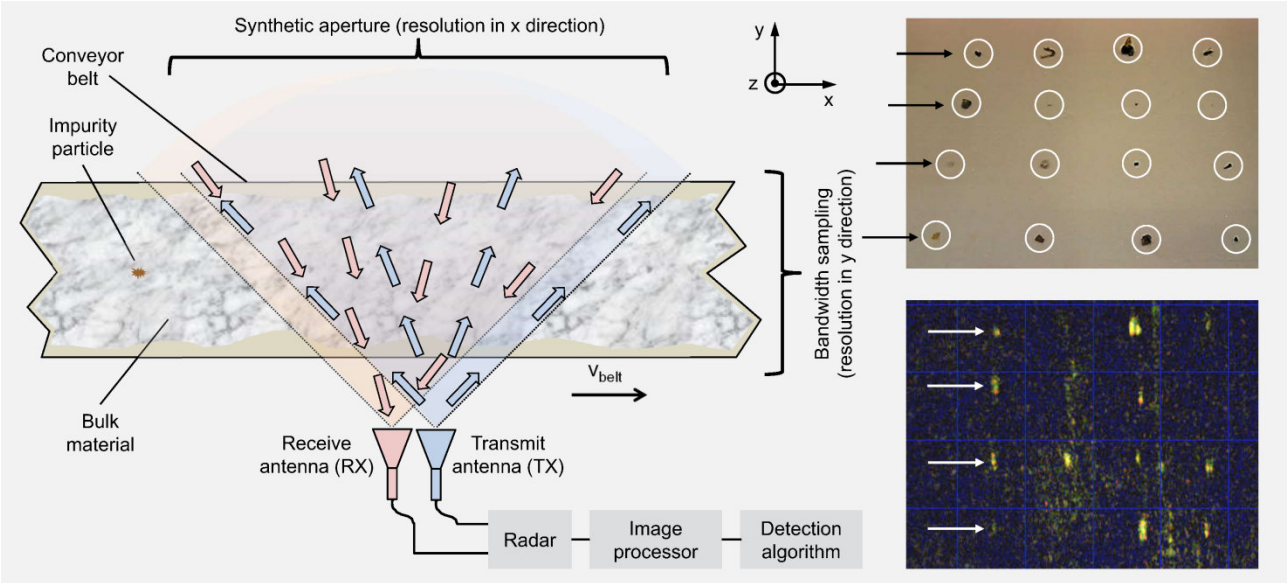

Figure 2.4-30 System concept (left), photograph (top right, slightly warped) and final radar image product (lower right) of an investigated scene. The photograph shows a raster arrangement (4 x 4) of 16 typical impurity targets indicated by white circles. The radar image (W band, 75-110 GHz) is an incoherent superposition of 8 individual ISAR images for advanced clutter suppression. The black and white arrows indicate the 4 target rows of 4 objects for better understanding. At least 12 of the 16 tiny and very low reflecting targets could be clearly identified.

clutter generated by the irregular sugar surface. Consequently, most of the tiny low-reflecting targets could be detected. It is expected that further degrees of freedom in measurement configurations will considerably improve the detection capabilities.

2.4.9 Space Object Imaging

Space is a very important and indispensable part of the living environment and an economic area – at least the low Earth orbit region up to an altitude of about 2000 km above the surface. Consequently, permanent observation and situational awareness is crucial. In Germany, this sovereign task is executed by the German Space Situational Awareness Center (Weltraumlagezentrum WRLageZ) located in Uedem, and jointly operated by the German Bundeswehr and DLR. An important task, in addition to the detection and tracking of space debris, is the high-quality and high-resolution imaging of space objects not classified as debris – e.g., satellites – which can only be done under almost all environmental conditions by adequate imaging radar systems. With approximately 1800 operational satellites and about 3400 tracked non-functional ones in space today, it can be expected that the number of such space objects will considerably increase in the next few decades. Space is used more and more intensely, and many more nations and even private organizations will soon have access to space technology. Consequently, it is absolutely necessary for Germany to have its own space surveillance capabilities, being of course compatible with European and other international networks. The high-quality imaging of space objects must serve various demands – the general and regular inspection of the physical status of operational satellites, threats posed by space weather, space debris and also possible intended harm, the investigation of unknown space objects, and the surveillance and status control of disused satellites during their disposal phase. In view of these challenges and the tremendous increase of space objects in the near future, a comprehensive, scalable, adaptable and future-oriented space surveillance system is required, which cannot be solely realized by classical large dish radar systems. Hence, modern radar techniques and other frequency bands have to be considered. The DLR IoSiS system was designed and developed for this as an experimental basis platform, serving for research on new aperture concepts, very high-resolution challenges, and advanced methods of synthetic aperture radar technology.

Imaging of Satellites in Space – IoSiS

Following basic theoretical investigations and efforts to use existing hardware to the greatest possible extent, the IoSiS radar system was designed based on the multi-functional and multi-purpose radar Gigarad [J-92], [RC-92], [RC-31], [RC-560] and a modified medium-sized steerable dish antenna normally used as redundancy for S-band communication with spacecraft during launch. The imaging operation makes use of inverse synthetic aperture radar (ISAR) imaging, where the radar is kept stationary while the object or scene is in motion. For high cross-range or azimuth resolution, the antenna beam tracks the object to generate the synthetic aperture, and the signal bandwidth provides the range resolution. The final setup of the IoSiS system in spring 2018 is shown in Figure 2.4-31.

The Gigarad radar operating in full X and part of Ku band and further control systems are located in a container from which the whole measurement is controlled. The high-power amplifier is mounted on the counterbalance structure of the large dish antenna, which is only used for transmission (Tx) and has 9 m diameter. The two receive (Rx) antennas, which have diameters of 1 and 2 m, are installed for high isolation between Tx and Rx on both sides. Hence, all antennas, pointing exactly in the identical direction, are steered together when following a space object of interest. Gigarad and the antenna-mounted electronics

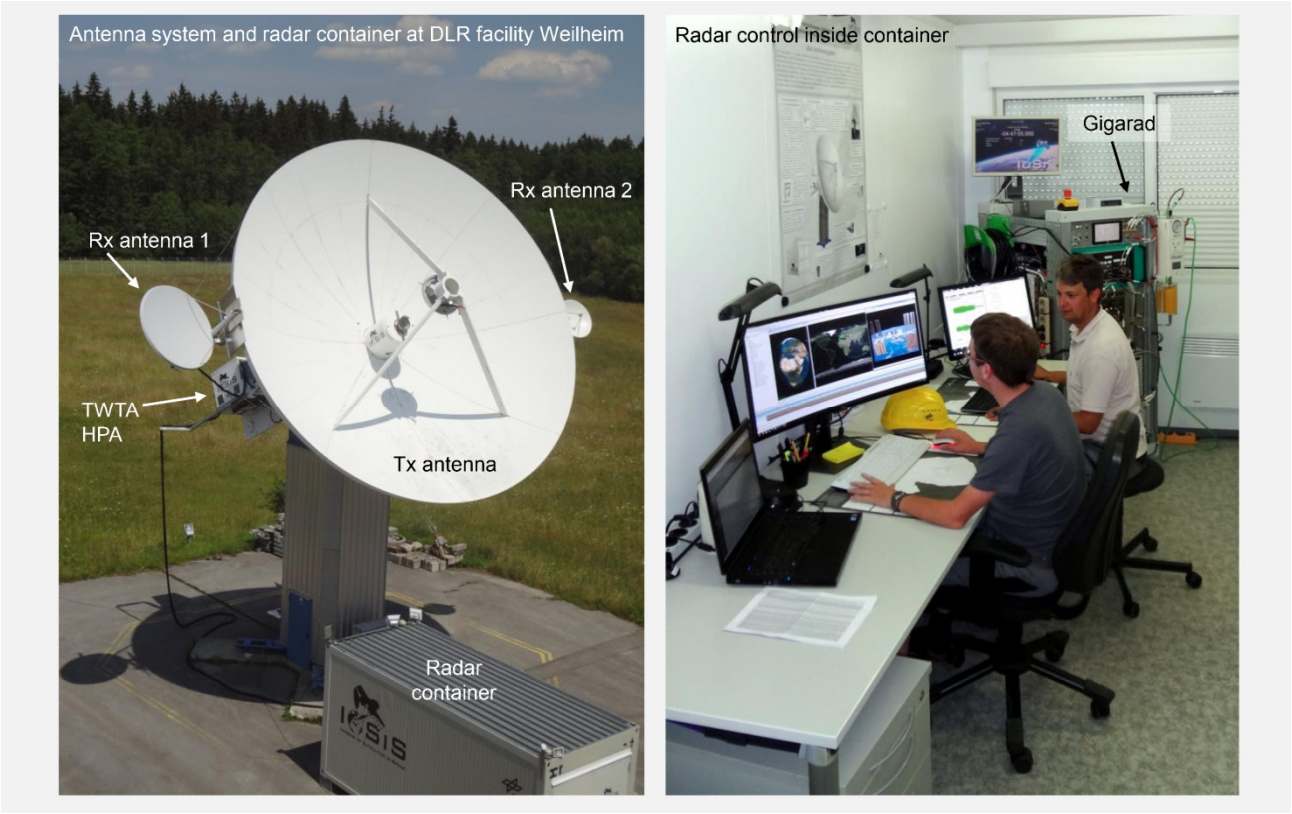

Figure 2.4-31 Photographs of the IoSiS experimental radar system used for basic research on advanced imaging space surveillance systems. Key parameters for operation are: maximum frequency range 8.0-12.4 GHz, maximum transmit peak power 4 kW, typical pulse repetition frequency 200 Hz, typical pulse length 50 µs; Tx – transmit, Rx – receive.

are connected via optical signal links in order to provide lowest losses and to still enable a larger displacement on demand. Following the technical parameters of IoSiS, a maximum range resolution of 3.8 cm can be achieved. For identical cross-range resolution, the synthetic aperture has to be built along a 24° observation angle. Since the whole X-band frequency range is considered for very high spatial resolution, IoSiS operation is legalized by an experimental license issued by German frequency regulation authorities (BNA – Bundesnetzagentur). At present, IoSiS operation is performed without any tracking system support, i.e., the expected orbital path of the object of interest is propagated by software tools based on the last available two-line element (TLE) data from public sources. Orbital data are then fed to the antenna control, which initiates the antenna motion exactly when the object is expected at a certain location, and steers the antenna following a given position over time. The radar operation is started with some advance to the antenna motion. The PRF has to be adjusted from time to time according to the actual range in order to keep the sampling time on Rx and, hence, the data rate as low as possible. Gigarad is a highly digitized radar generating digitally Tx signals and sampling full bandwidth on Rx in time domain.

Figure 2.4-32 shows an imaging example of the International Space Station (ISS) as one of the first successful imaging results. Many details can be extracted from this radar image, and most structures can be assigned to the optical illustration. However, it should be noted that the presented spatial resolution is still about one order worse than what is theoretically possible with IoSiS. This circumstance is due to the insufficient accuracy of public TLE data, especially for the ISS, which generate highly inaccurate propagated position data for the ISAR measurement. As a consequence, it was only possible to track the ISS for an observation angle range of a few degrees, resulting in a reduced azimuth resolution. Presently, various approaches to achieve a sufficiently accurate orbit prediction of space objects are under investigation.

2.4.10 Radiometry Applications

Another attractive microwave sensing technology in addition to radar is microwave radiometry, which is comparable to infrared sensing but at much longer wavelengths. Hence, this technique works purely passively without the need for transmitters. It can operate without causing health issues and without any impact on frequency regulation. Images have a quasi-optical appearance, which considerably simplifies interpretation. The parameter extraction is related at least partly to direct signals from an object due to emission and not only reflection. Microwave radiometry has many applications similar to radar, while the Institute activities are focused on security and safety, as well as Earth observation. In more recent research, investigations on adequate combinations of MMW radar and radiometer data have been initiated [RC-173], [RC-12]. To achieve the maximum benefit of combining active and passive measurements, the main requirement is an almost identical imaging geometry, i.e., an identical orientation of radar and radiometer and, hence, an identical sampling grid. Further investigations on this approach and potential applications such as pilot assistance are planned for the near future.

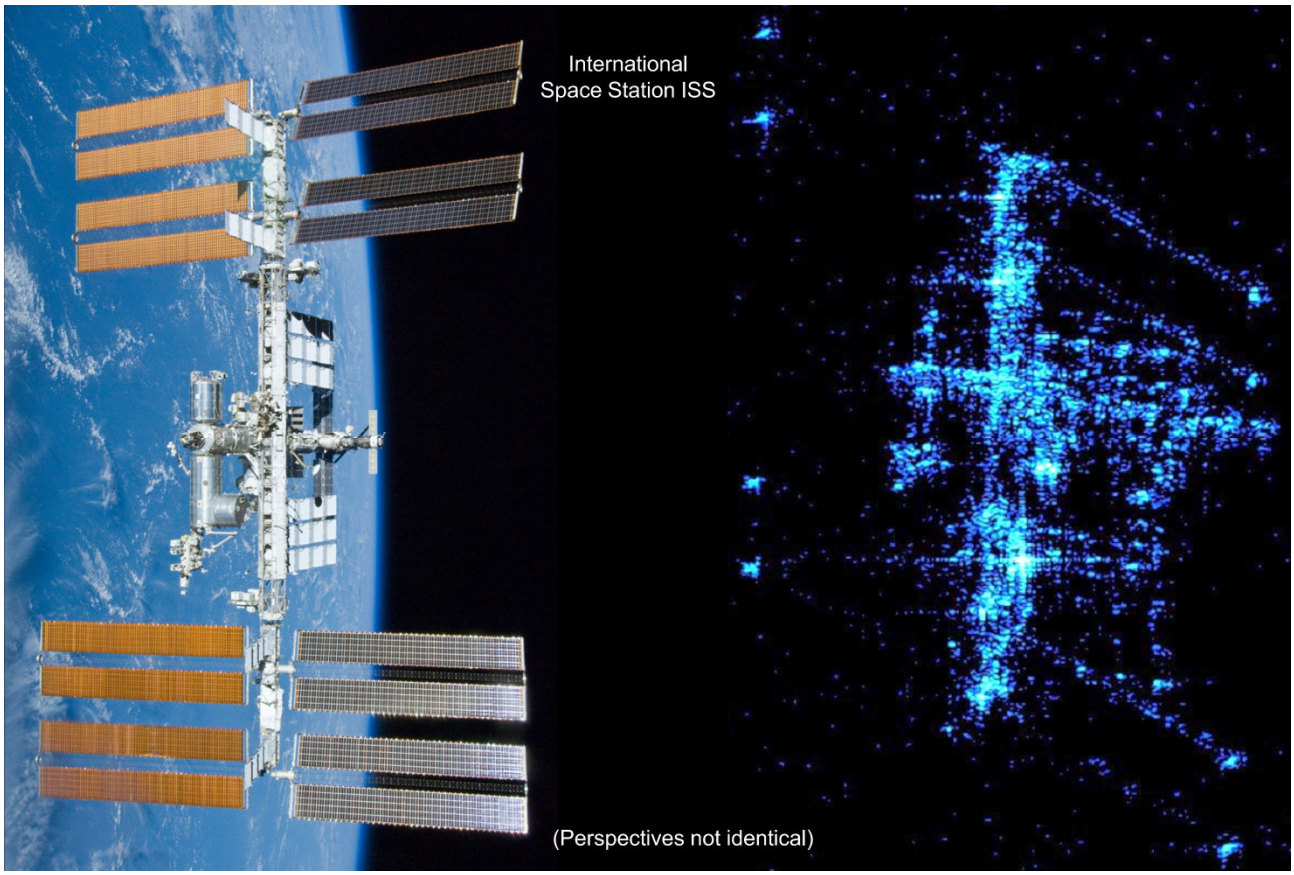

Figure 2.4-32 Artist's impression (left) and IoSiS ISAR image (right) of the ISS for comparison. Relevant ISAR imaging data are: radar range to ISS 570 km, center frequency 9.6 GHz, range resolution 38 cm, azimuth resolution 30 cm. Note that perspectives are not identical and that radar provides different imaging geometry than optical sensors.

Generation of Complementary Threat Information using Radiometric Data – SUMIRAD

Nowadays, peace-keeping forces are heavily confronted with asymmetric warfare. Vehicle patrols and convoys are often threatened by camouflaged IED installed along routes. The patrol or vehicle commander mostly depends on a visual impression of the situation, requiring extensive experience and know-how. Such hardly quantifiable 'information sources' are definitely valuable, but they are not sufficient to enable full-force protection. Consequently, research on advanced technical assistance is mandatory. In order to address this issue, the European Defense Agency (EDA) funded the project SUM (Surveillance in an Urban environment using Mobile sensors). The overall goal of SUM was to develop an advanced vehicle-based multi-sensor system, operating 24 h in all sight conditions. Consequently, a combination of visible and infrared cameras, imaging MMW radar, and imaging MMW radiometer were selected, being supported on demand by auxiliary information from other data sources like satellites or Unmanned Aerial Vehicles (UAV). Threat assessment was carried out by evaluating data using an advanced data fusion engine, and presenting only necessary information via a suitable human-machine interface. The Institute has been responsible for imaging MMW radiometer development and construction, the final sensor system being called SUMIRAD [RC-565], [RC-516], [RC-478], [RC-479], [NJ-18]. Strong constraints concerning limited budget, project duration and high-performance requirements with respect to spatial resolution, sensitivity, image size, frame rate and data rate were considered. The final system design was mounted on a truck and shown in Figure 2.4-33 top in detail. The technical characteristics are: frequency range 82-102 GHz, angular resolution 0.75°, sensitivity < 2 K, image size elevation × azimuth 30° × 80°, and frame rate up to 1 image/s. The image was generated by a repetitive raster scan performed by a crank drive for vertical motion of the antenna beam and a rotating deflection plate for moving the antenna beam horizontally. Since two receivers were used, two independent images are provided in parallel, enabling the selection of horizontal or vertical polarization for each channel. The imaging result shown in Figure 2.4-33 compares the visible and infrared images with the radiometer image for two situations. In the upper result the cardboard box on the roadside is filled with a metal plate simulating part of a possible threat, on the bottom result the cardboard box is empty.

It can be seen that the optical images show no difference, while the radiometer images enables a clear discrimination. It should be noted that this kind of information, together with the location of this optically non-dangerous appearing object, can be an indicator for a potential threat, sharpening the awareness of the convoy or vehicle commander for increased attention.

Impressively demonstrating the capabilities of the approach,

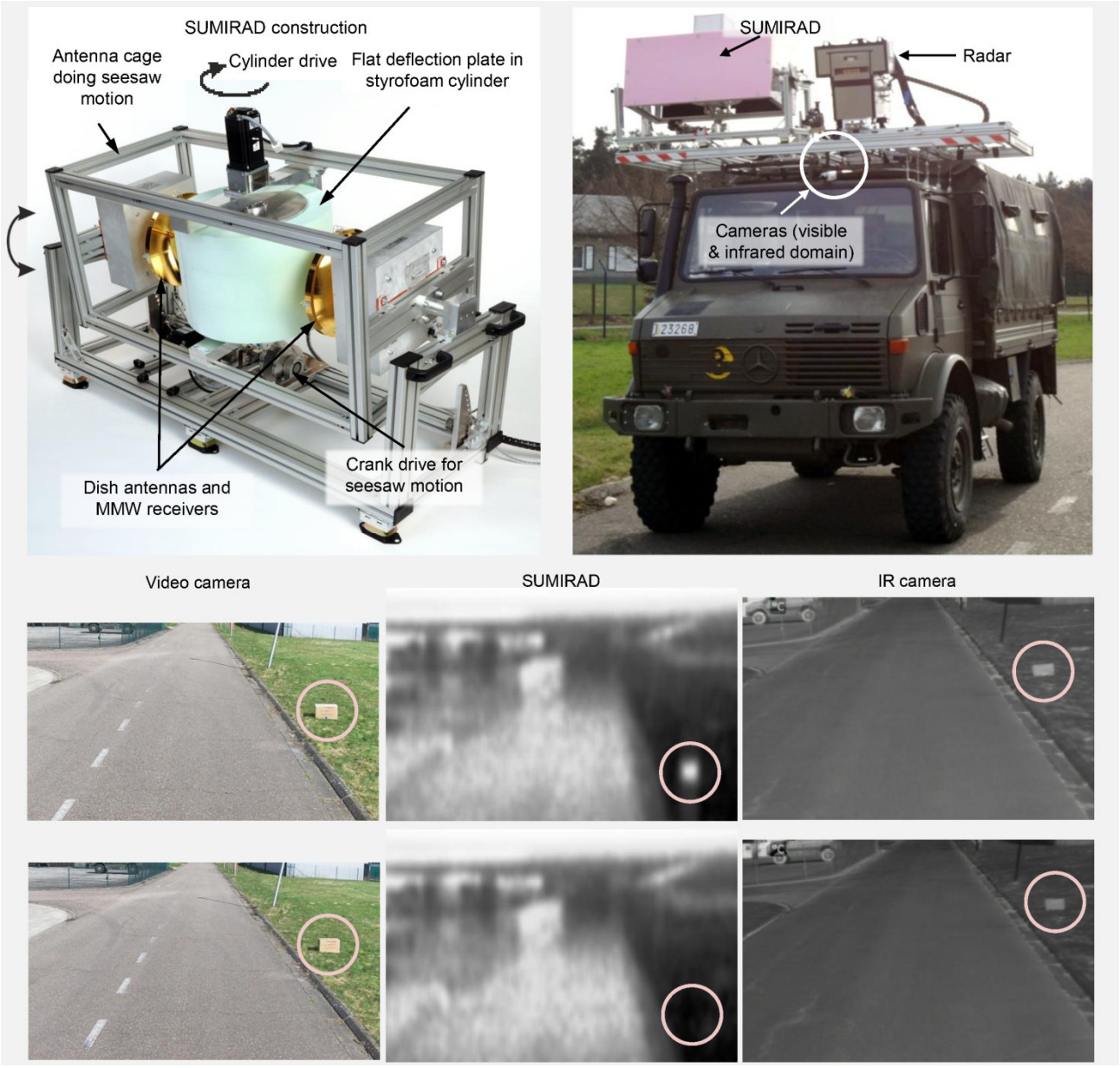

Figure 2.4-33 Top left: photograph of the SUMIRAD system in detail; right the system mounted on a truck; bottom: imaging results of a scenario with a cardboard box on the side of the road (right). The box is empty in the lower images and filled with a metal plate in the top images. Image sizes of different sensors do not exactly match each other.

especially under the use of polarimetric information, a next step can be the development of a multi-channel system in order to increase the frame rate considerably by simultaneously maintaining the large image size. Higher frame rates will enable the use of the system for many other applications, e.g., in the area of search-and-rescue assistance.

Polarimetric Radiometry

The characterization of dielectric materials is of great importance for many applications, being for instance a quality control method during product fabrication or a status control method for outdoor construction work over time. In many outdoor situations the objects of interest have limited accessibility, and the investigation should be carried out without the destruction of any part of the object or health risks to the operator.

Hence, remote sensing from a stand-off position is desirable, and the use of microwaves, millimeter-waves or THz waves offers some penetration capability into matter, depending on its chemical and physical decomposition, and of course, frequency. Many objects of interest consist of a dielectric coating or enclosure, which can electromagnetically be treated as a dielectric layered structure or a dielectric slab surrounded by air. Radar as an active remote sensing technology has great potential for precise range measurements and spatial resolution. However, its mostly monostatic implementation suffers from low or no back reflection of signals in case of plane and tilted surfaces, thus delivering no additional information. In contrast, radiometric imaging as a passive remote sensing technology relies on naturally-generated noise-like radiation of thermal origin, being available everywhere and from all directions. Quite often, the sky can be used as a large illumination source,

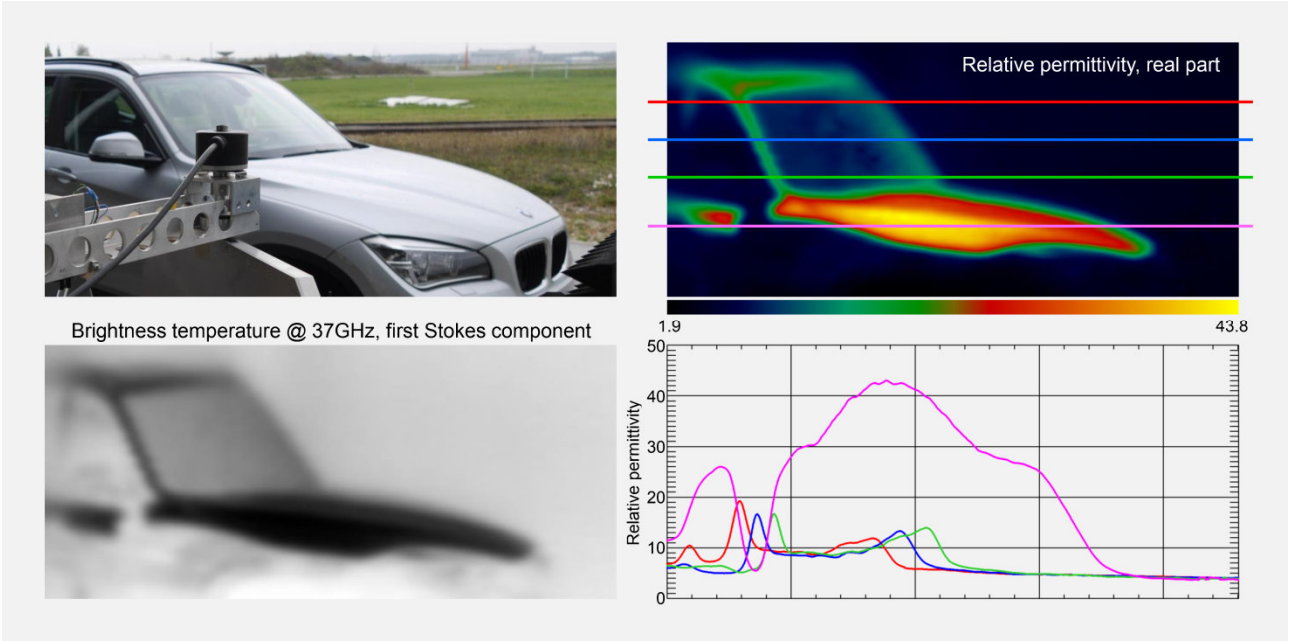

Figure 2.4-34 Top left: photograph of a radiometric scene using a car as the primary target; bottom left: first Stokes component of the Ka-band brightness temperature radiometer images representing the sum of vertical and horizontal polarization; top right: estimated real part of the relative permittivity from the first three Stokes components; bottom right: profiles through the permittivity image according to given colors. The horizontal axis corresponds to identical azimuth angles for all four graphs.

providing rather low radiation power compared to objects on Earth, using frequencies of up to a few hundred GHz. Furthermore, thermal radiation is originally un-polarized, but becomes polarized when reflected partly on a dielectric surface. The use of polarimetric measurements at various incidence angles can thus provide information on the type and structure of the reflecting object.

In the cooperation project LOEWE, a polarizer device was developed by the Technical University of Darmstadt to electronically change the linear polarization state of an input signal continuously from vertical to horizontal or vice versa. The device is based on liquid crystal (LC) technology where varying voltage levels are applied along a waveguide structure filled by LC in order to adjust the orientation of the crystals, gently rotating the linear polarization of the travelling electromagnetic wave from the input to the output. In a proof of concept experiment, the polarizer was installed between the antenna and the receiver of a radiometric imager, being typically used for personnel screening experiments. An imaging result of a car close to the scanner is shown in Figure 2.4-34. Four radiometer images around 37 GHz center frequency for vertical, horizontal, +45°, and -45° linear polarization state were measured in time multiplex and combined to the Stokes vector representation. The car as target has the property that it is mostly composed of metal typically showing no polarimetric behavior. However, the windshield represents a tilted dielectric region reflecting cold sky radiation, for which polarimetric signatures can be expected. From theory, it should be possible to reconstruct the permittivity from the first three components of the Stokes vector, shown as a comparative image on the top right and some corresponding horizontal profiles on the bottom right illustration. In summary, quite reasonable estimates for the real part of the permittivity have been achieved with this approach, i.e., the wind shield permittivity result of around 8-9 is close to literature values for glass, and the painted metal regions are rather high (close to 50), considering the high reflection properties, flat incidence and the spatial resolution with respect to single features. Furthermore, the background and vertically-oriented parts of the car show values close to 1-2, indicating no polarimetric difference in brightness temperature.

By conducting additional experiments and further research on error correction for sensor imperfections, it is expected that more precise results for permittivity of dielectric objects can be acquired, even for layered structures. Further measurements on more practical scenarios shall exploit the use of the approach for remote sensing of material parameters of distant objects.

Measurement of Soil Parameters using Radiometry – Ground Check Passive

In addition to the presented activities in the Ground Check Active project, passive microwave sensing is also considered for many types of ground exploration. Passive polarimetric signatures are of great interest, since they can provide significant information on the surface and sub-surface structure. In addition to airborne or spaceborne geophysical parameter derivation, i.e., soil moisture, sea surface salinity, soil freeze/thaw conditions and cryospheric ice investigations, ground monitoring/observation is essential for task forces within the United Nations or other peace-keeping operations, e.g., those being directly threatened by terrorist attacks on patrol missions. Now, the fully polarimetric radiometer observation in dependence of aspect angle of an optically inconspicuous appearing ground region can allow an assessment of its character within a depth of a few decimeters. This can provide for instance conclusions about the trafficability, former compression due to now invisible traffic

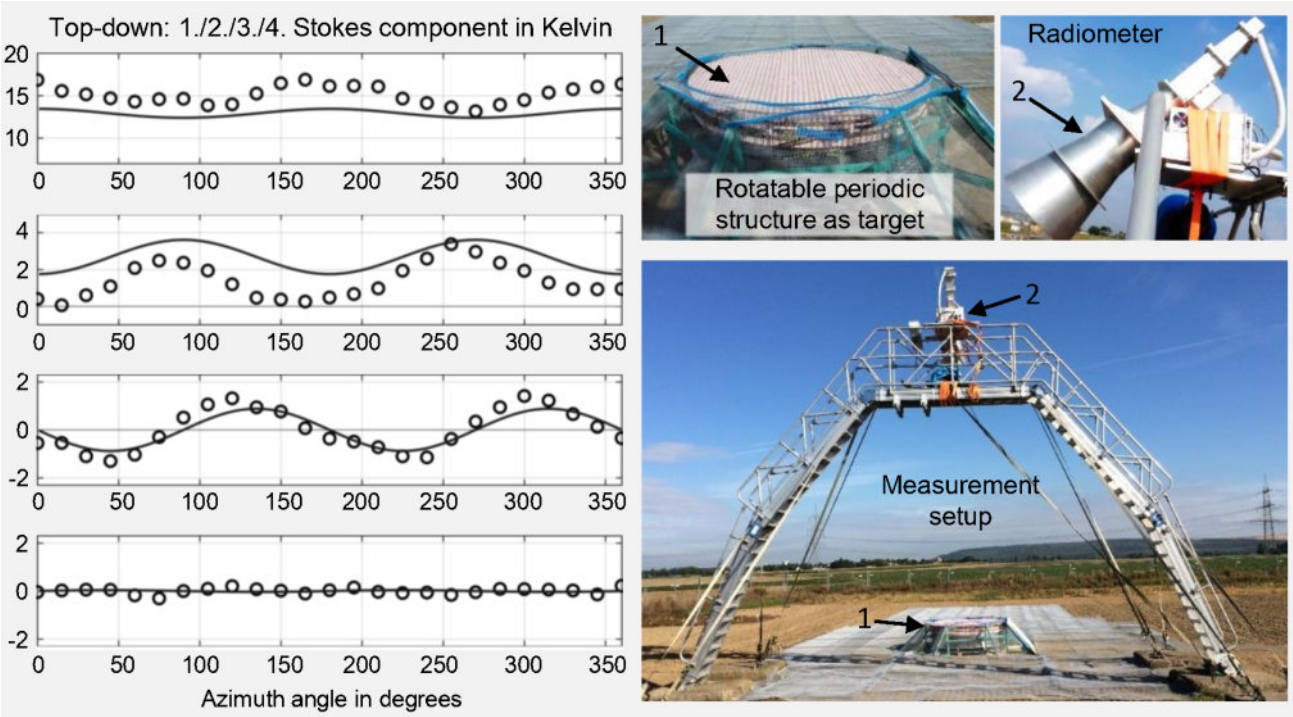

Figure 2.4-35 Left: Comparison of the simulated (solid lines) and measured (dots) four components of the Stokes vector at 1.4 GHz center frequency; right: photographs of the measurement setup, located on a special agricultural demonstration site near Jülich, Germany. The target is a rotatable, 2-m-diameter circularly traced, periodic structure of interleaved wood and Styrofoam panels, providing two different complex permittivities. The fully-polarimetric radiometer is pointing towards the target center at a 45° incidence angle.

lanes, or general redeployment of the ground in case of IED installation.

In theory, such material anisotropy and lateral periodic structures can provide polarimetric signatures in brightness temperature, which can then be used for threat prediction. A large experiment on theoretical prediction and experimental validation of fully polarimetric L-band signatures of bi-anisotropic periodic structures was carried out in cooperation with Forschungszentrum Jülich GmbH (Institute of Bio- and Geosciences), Universite Catholique de Louvain (Earth and Life Institute – Georges Lemaıtre Centre for Earth and Climate Research), and the National Space Institute (Technical University of Denmark).

The experimental setup and the fully polarimetric results for certain periodic bi-anisotropy of an artificial target are shown in Figure 2.4-35. Since the periodicity of the target bi-anisotropy is much smaller than the wavelength in that case, a significant periodic variation in the first three components of the Stokes vector over azimuth angle, and almost no variation in the fourth component, can be observed as predicted by the model. Note that, even despite the rather low amplitudes of the variation, the agreement between theory and experiment is satisfying, demonstrating the applicability for larger structures and longer wavelengths down to UHF range as well.

Given the case of successful application of this methodology to practical situations, a next question could concern the design and development of appropriate radiometric imaging sensors, which are able to deliver sufficient spatial resolution, sensitivity, and fully polarimetric capabilities with sufficient accuracy. Unmanned Aerial Vehicles (UAV), drones or air vehicles at lower altitude can be a suitable platform for providing sufficient near-range resolution in combination with reasonable sensor size, weight and power consumption, to observe a single target from multiple directions.

2.4.11 Radar Signatures

Radar cross section (RCS) is a measure of detectability of an object by radar. A reduction of RCS and therefore of the detectability of an object can be achieved by the following measures: shaping, application of anti-reflection coatings, cloaking and optimization of the position and orientation of the object with respect to the radar – e.g., through the choice of a trajectory in the case of an aircraft.

Signature Determination and Reduction

An accurate prediction of RCS at microwave frequencies is often a challenging task, particularly when the object is electrically large, that is, much larger than the wavelength of the radar radiation. Numerical simulation of RCS of such objects with commercially available electromagnetic solvers is hardly possible due to the large number of unknowns upon discretization of the problem and the associated unrealistic requirements for computer memory and execution time. Experimental determination of RCS of electrically large objects is complicated by the need to measure in the far-field zone of the object, which in the case of an aircraft and a frequency in the X band has to be located several kilometers from the object.

The Physical Optics (PO) method is often the only possible approach to calculate RCS of electrically large objects. Multiple reflections between parts of the scattering geometry may lead to significant contributions to the scattered field, which makes a corresponding extension of the PO method necessary. For example, a reliable prediction of the cross-pol components in the scattered field often requires accounting for at least double reflection. The PO-based simulation tool BISTRO has been extended to account for multiple reflections through the implementation of an iterative technique.

A perfect 3-D cloak, which guides an incident electromagnetic wave around an object as if no object were present, could hardly be realized in the foreseeable future and continues to be more of a theoretical concept. Two-dimensional cloaks for concealing cylindrical objects are much easier to realize. Two such cloaks designed and manufactured by partners at Aalto University, Finland, have been experimentally characterized at the Institute's TechLab measurement facilities. Both cloaks consist of a stack of metal conical plates with a space in the interior for concealing the object – in our case a metal cylinder or a bunch of metal wires. For example, the total scattering width of a metal cylinder with a 30 mm diameter was reduced by more than 50% from 9 to 11 GHz, which corresponds to half of the X-band bandwith [J-178], [J-179], [RC-562].

Metamaterial technologies (see Section 2.4.12) enable creating novel anti-reflection coatings with properties not achievable with natural materials. For example, it is possible to design coatings such that within a certain range of frequencies and incidence angles the surface impedance is almost equal to the wave impedance of the surrounding medium (impedance-matched coating). Electromagnetic scattering and reflection from objects with such coatings show a number of peculiar and extremal properties, which includes vanishing axial backscattering from bodies of revolution, minimum reflectivity of planar interfaces and the generally lower level of bistatic scattering from arbitrarily shaped bodies [IC-192], [RC-598], [J-130], [RC-401], [J-98], [RC-283]. Simulation of electromagnetic scattering from impedance-matched bodies has required an extension of the conventional PO/PTD methods [J-131], [IC-154]. Figure 2.4-36 shows the reduction of the bistatic cross section of a generic UAV by approximately 20 dB by means of an impedance-matched coating.

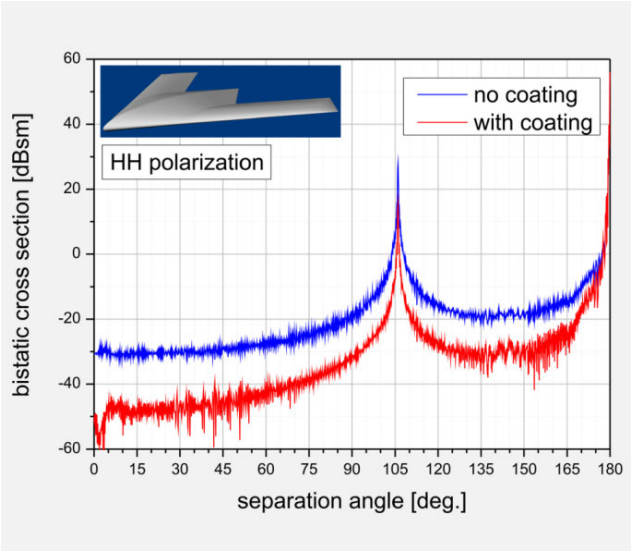

Figure 2.4-36 Bistatic RCS of a generic UAV (nose-on illumination, horizontal plane, horizontal polarization) with and without impedance-matched coating

Seeker Radar and Radome Technology

Today, the threat posed by modern and far-reaching weapon systems even from terrorist organizations is high, due to either proliferation or even own production capabilities. Hence, the reliable and effective defense against highly agile and intelligent missiles or other threats of highly destructive potential require adequate technical solutions. In order to provide cutting-edge technology knowledge and adequate consultancy for the German Armed Forces, the Institute carries out research on advanced concepts for missile seeker radar based on digital beamforming and suitable system and scene modeling in order to evaluate different solutions according to missile designs for various defense purposes.

As an example, a radome is an integral part of most seeker radars, protecting the antenna system and the electronics from hostile exterior conditions (aerodynamic drag, humidity, ice, heat, debris, electromagnetic interference, etc.). Missile radomes are exposed to extreme temperatures and aerodynamic forces, implying the use of particularly heat-resistant and mechanically stable materials at the cost of microwave transparency. The distorted transmission results in losses and a degrading performance of the radar antenna. The consequences for the radar can be reduced operational range and beam alignment and focusing errors. A possible solution may consist in shaping that material, which is often located in the interior of the radome for thermal protection of seeker electronics, as a special microwave lens in order to compensate for the mentioned distortions of the penetrating wave fronts [RC-165], [RC-174], [RC-411], [RC-582]. Figure 2.4-37 shows the distribution of the phase of the transmitted wave on the basis of a radome with and without a lens. The lens, which is made from a heat-resistant silicon-based material (geopolymer), leads to an almost homogeneous distribution of the phase. Another approach based on the use of the so-called metasheets is described in Section 2.4.12.

Material Characterization

Material characterization measurements for microwave frequencies have become significantly important in recent years. Special coatings, innovative composites and metamaterials enable novel possibilities to influence reflected or transmitted fields. Several of the team's experimental setups have been rebuilt, adapted and improved. Free space setups are realized for several microwave frequency bands, the waveguide setup is operating between 1.1 and 110 GHz. Even fluids and powders have been measured successfully in free space as well as in waveguides. Free space measurements of very thin samples such as films and nets, but also very thick ones are quite challenging, which also includes the significant calibration procedure.

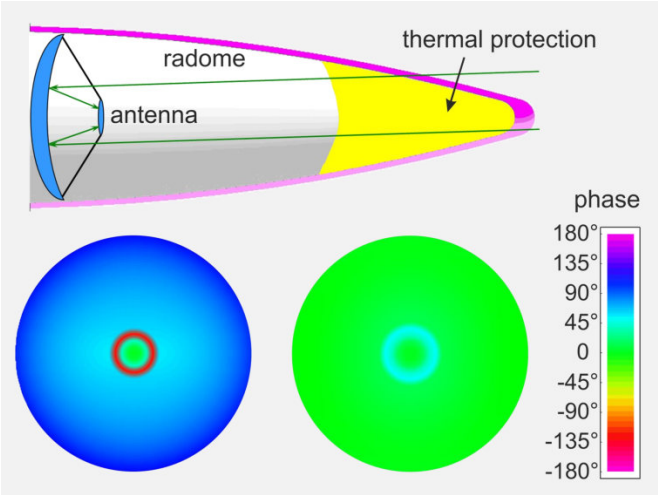

Figure 2.4-37 Top: a generic radome (thickness: 3 mm, material: WHIPOX, base diameter: 200 mm) with a piece of thermal protection shaped as a lens (lens material: geopolymer, maximum lens thickness: 7 mm). Below: distribution of the phase of the transmitted wave on the basis of the radome without the lens (left) and with the lens (right) at 34 GHz.

Figure 2.4-38 shows one of the free space setups (with broadband antennas and plastic lenses) and an evaluation on a liquid fuel [RC-583]. For S-band measurements, the fuel was poured in the vertical waveguide above a plastic slab. X-band measurements were operated in free space.

One important topic is the determination of reflection and transmission coefficients of an electromagnetic wave on a planar material sample, optionally dispersive. Calculating the complex permittivity and permeability of a sample is possible by applying tools, which have been developed and tested. Currently, both material constants of single-layered materials and the permittivity of each laminate layer are computable, assuming isotropic layers. The multilayer computation uses a regressive model that takes a dispersive characteristic of the permittivity and the thickness of the layers into account. Moreover, this regressive model also enables the investigation of artificial materials with very special dispersive behavior, such as metamaterials. An evolutionary algorithm has been developed to increase the quality of regression results. Considering the thicknesses of the layers as additional parameters of the regression model significantly improves the results. The reason for this is that the individual layer thicknesses of laminates are very often not measureable with sufficient accuracy.

To calculate the reflection and transmission coefficients as well as for computing electromagnetic material constants, independent software packages have been developed, which are now integrated in a combined graphical user interface that also provides quick-look graphs of the data.

2.4.12 Metamaterials

Metamaterials are man-made artificial materials with tailored electromagnetic properties which allow for the manipulation of electromagnetic waves in a desired way. In most cases, metamaterials are periodic arrays of resonators located in or on a dielectric substrate, with unit cells significantly smaller than the wavelength of the electromagnetic wave. Therefore, the structure appears to be effectively homogeneous with effective electromagnetic parameters that can be adjusted to almost any desired values. The design of metamaterials has become possible due to the performance of today's computing systems and the advancements in manufacturing techniques for submillimeter conducting structures. Today, research in the field of microwave metamaterials includes the design of thin, inexpensive and lightweight absorbers, cloaks, deflectors and radomes with tunable transmission properties.

Superlensing

A planar metamaterial layer with negative unit values of the relative electric and magnetic constants operates as a superlens, producing a perfect image of a source. However, any practical realization of a superlens necessarily involves small deviations from the ideal values of the material parameters, which leads to various distortions of the image. Unequal transmission of differently polarized fields is a new kind of distortion in imperfect superlenses, which was described in [J-117], [RC-654].

Thin Metamaterial Absorbers

Metamaterials consisting of a single layer of resonators are called metasheets or metasurfaces. Such structures can be used for building antireflection coatings which are thinner and more flexible than commercially available absorbers. Furthermore, a weight reduction to less than 1% has been achieved

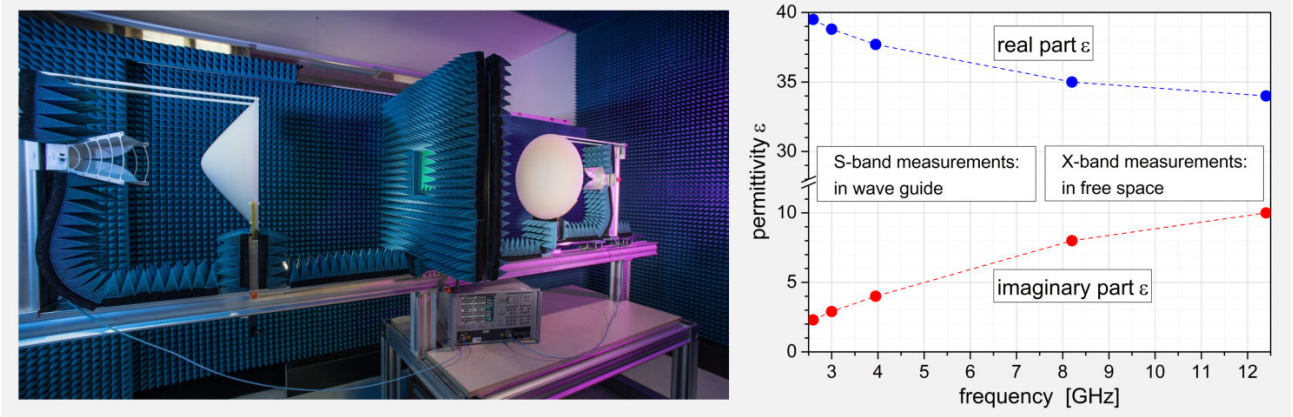

Figure 2.4-38 Left: free-space material characterization setup (transmission and reflection measurements on flat samples for 2 to 8 GHz). Right: evaluated complex permittivity vs. frequency of liquid fuel based on waveguide measurements from 2 to 13 GHz.

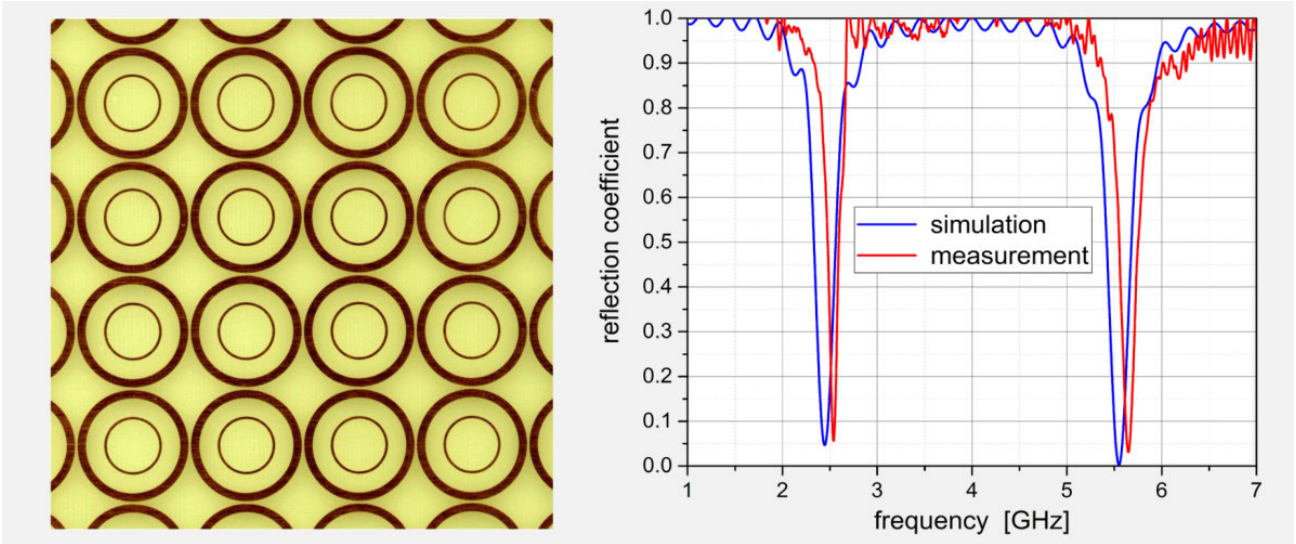

Figure 2.4-39 Left: detail of the double concentric ring Wi-Fi metamaterial; inner and outer radii of the rings: 4.6 mm, 5.1 mm, 8.3 mm, 9.8 mm. Right: simulated and measured reflection coefficients vs. frequency.

[NJ-20], [IC-144]. In the case of absorbing metamaterials, narrowband and broadband absorbers can be distinguished. The unit cell (20 mm x 20 mm) shown in Figure 2.4-39 consists of two concentric conducting rings located on a dielectric FR4 substrate, which is backed by a conducting foil. It acts as a polarization-independent absorber at two common Wi-Fi frequencies in L and C band. The sharply-defined absorption frequencies can be adjusted by a proper choice of the radii of the rings. The small difference in the resonance frequencies is mainly due to a discrepancy in the permittivity of the substrate of the fabricated sample compared to the simulated one. An X-band absorber was designed to demonstrate a broadband absorbing metamaterial.

The key idea of turning the structure in Figure 2.4-40 to a broadband absorber is the introduction of loss by means of surface mount resistors. The performance of both, narrow and broadband absorbers has been experimentally checked. Simulated and measured data depicted on the right halves of Figures 2.4-39 and 2.4-40 are in good agreement with each other.

In the future, the idea of actively controlling the properties of certain types of metamaterial will be pursued. Possible applications are switching back and forth between narrow and broadband absorption or controlling the phase of a reflected wave by an external signal. Furthermore, techniques for printing thin conducting coatings with desired predefined conductivity will be investigated to achieve a cost-efficient reflection attenuation of large areas.

Modeling and Simulation of Metasurfaces

Numerical simulation of metamaterial absorbers with commercial electromagnetic solvers is only possible under the assumption of an infinite planar periodic configuration if the simulation volume can be reduced to a single unit cell of the metamaterial array. For non-periodic configurations, e.g., bounded and/or curved, the whole structure with many electrically small resonators distributed over an electrically large area must be simulated, which results in numerical problems that can hardly be solved, even with modern computing facilities. A practical approach consists of modeling the metamaterial surface with effective surface impedance. The

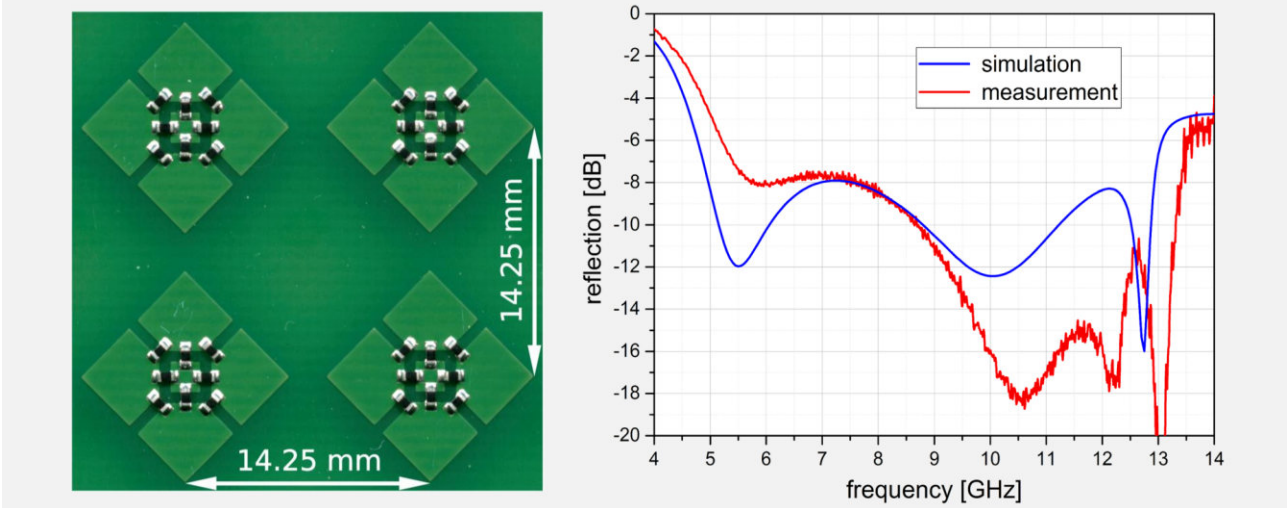

Figure 2.4-40 Left: detail of the broadband metamaterial with 8 surface-mounted resistors (1 mm x 0.5 mm x 0.35 mm) per unit cell; substrate: FR4. Right: simulated and measured reflection coefficient vs. frequency.

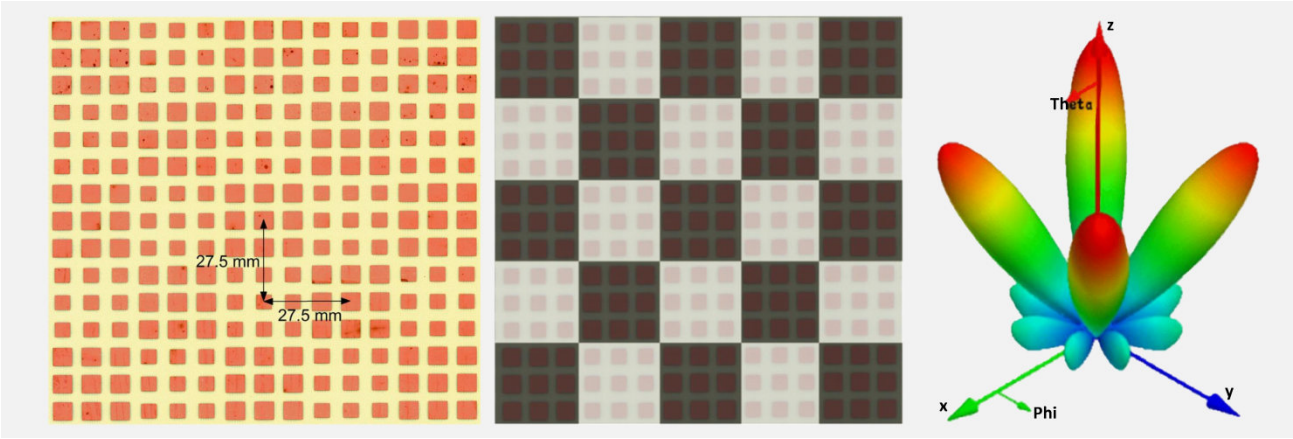

Figure 2.4-41 Left: X-band chessboard on substrate FR4; red squares: copper; middle: sketch to illustrate the chessboard design. Right: example of a 3-D scattering diagram of a perpendicularly incident wave.

impedance formulation results in much more tractable simulation problems with classical boundary conditions, which can be handled by using exact (MoM, FEM, FDTD) or asymptotic methods (GTD/UTD, PO/PTD) [IC-178], [J-152], [RC-364]. The efficiency and accuracy of the impedance approach have been validated by scattering measurements of coated cubes and cylinders [IC-193], [IC-144].

Metamaterial Chessboard-Patterned Deflectors

So-called chessboard structures belong to another class of metamaterial devices for controlling electromagnetic scattering. The structures are periodic arrays of metamaterial squares such that the neighboring squares reflect the incident field with a phase difference of 180°, which leads to destructive interference of the reflected contributions and vanishing backscattering from the surface. In contrast to metamaterial absorbers, chessboard structures do not absorb the incident power, but rather redirect it to side lobes of the array off the direction of the specular reflection. Chessboard structures are broadband with a relative bandwidth of 20% and more [R-210].

The impedance approach permits a rapid simulation of electromagnetic scattering from chessboard structures [IC-19]. Figure 2.4-41 shows a chessboard plate designed and tested at the Institute's X-band bistatic measurement facility.

Metasheets and Metaradomes

Transparent metamaterial structures consisting of a single layer of periodically arranged resonators located on a penetrable substrate material are called metasheets. These structures are characterized by frequency- and polarization-dependent transmission and permit full control of the transmitted radiation. Hybridization of metasheets with antenna radomes results in a new class of metamaterial devices called metaradomes [IC-85], [J-25], [NJ-2]. Figure 2.4-42 illustrates the frequency and polarization-selective properties of a metasheet designed and measured using the X-band transmission measurement setup. Simulation of bounded and non-planar metasheets can be made possible by considering the sheet as being effectively homogeneous and modeling it as a quasi-homogeneous material layer [J-24].

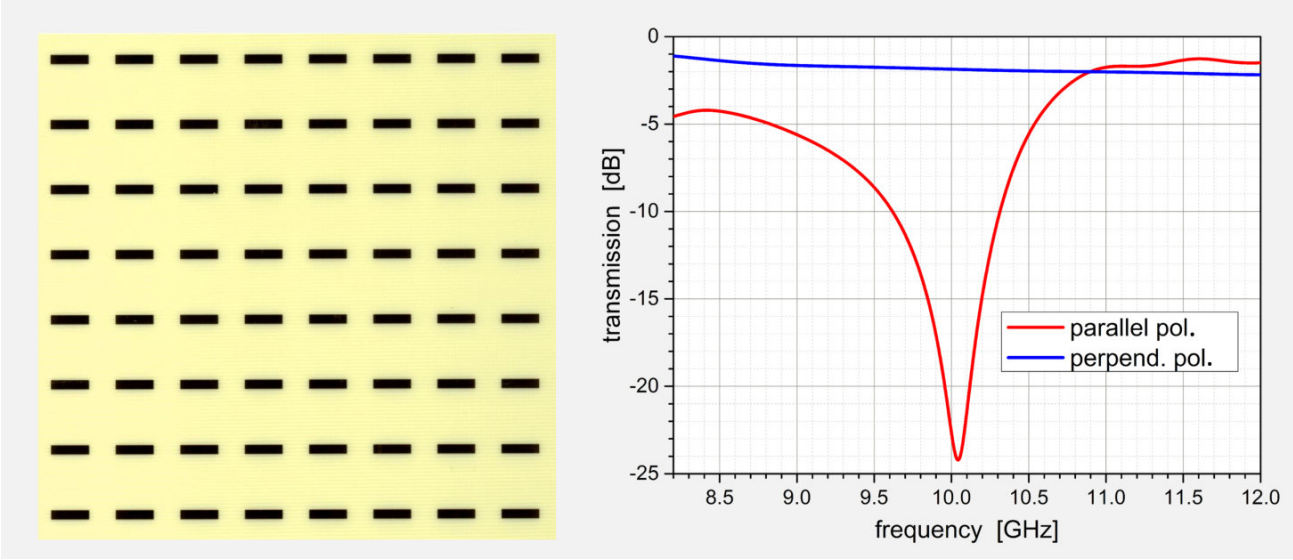

Figure 2.4-42 Left: detail of the cut-wire transmission metamaterial; unit cell size: 14 mm x 14 mm; substrate: FR4. Right: X-band transmission measurement data.

3 Documentation

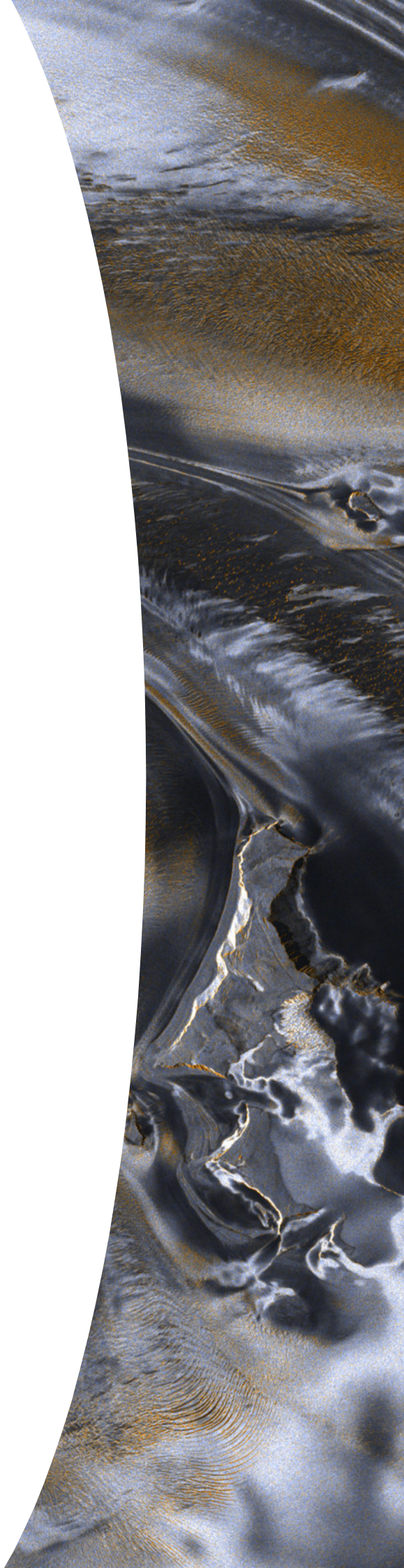

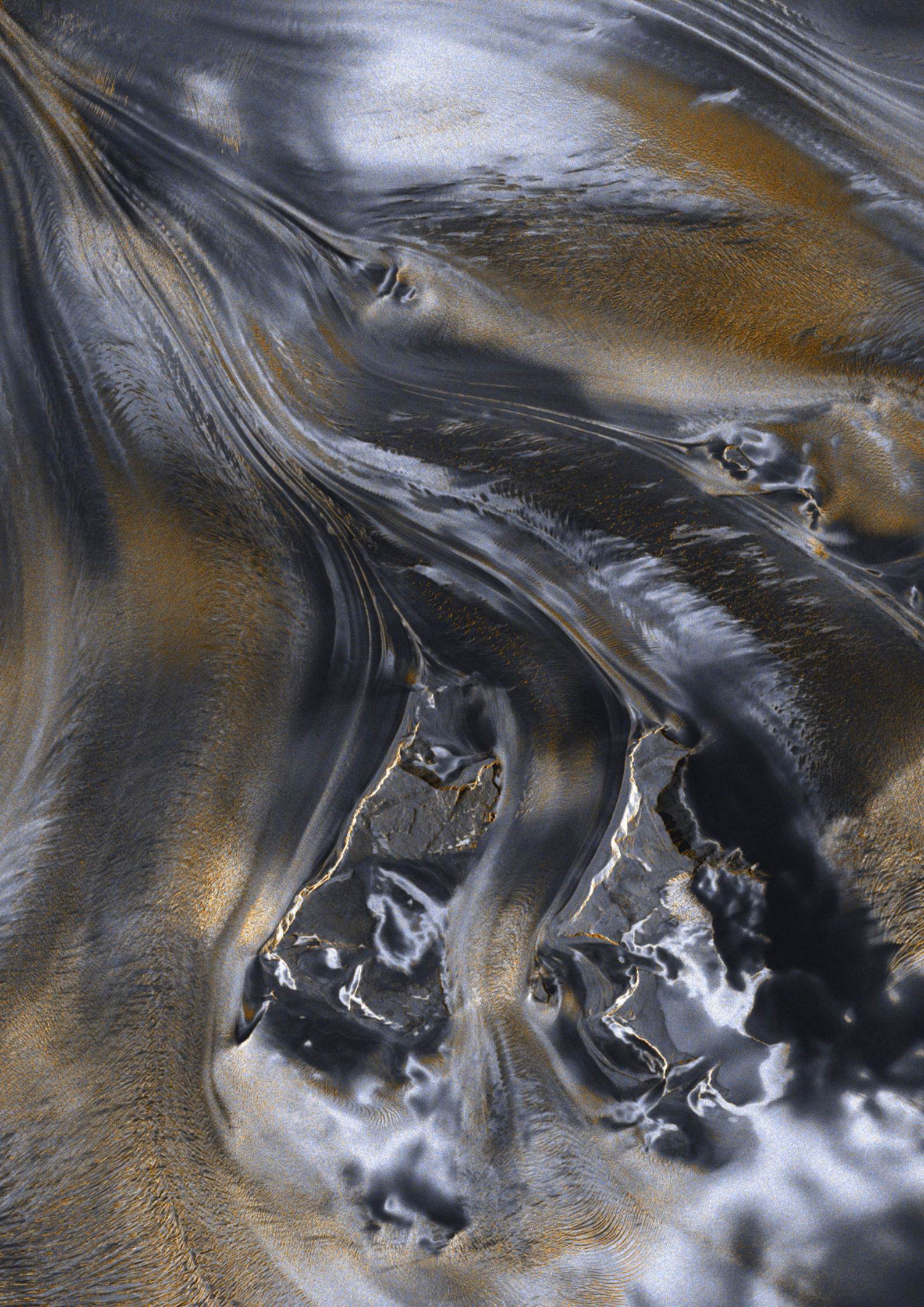

The following pages present the scientific and technical achievements and activities of the Institute in the period between 2011 and 2017.

3.1 Academic Degrees

Professorship Appointments

Name	Appointment	University	Year
Younis, Marwan	Professor	Karlsruher Institut für Technologie (KIT)	since 2017
López-Dekker, Francisco	Associate Professor	Delft University of Technology (TU Delft), The Netherlands	since 2016
Reigber, Andreas	Associate Professor	Technische Universität Berlin	since 2016
Hajnsek, Irena	Full Professor Associate Professor	Eidgenössische Technische Hochschule ETH Zurich, Switzerland	since 2016 2009-2015
Moreira, Alberto	Professor	Karlsruher Institut für Technologie (KIT)	since 2001
Keydel, Wolfgang	Honorary Professor	Ludwig-Maximilians-Universität (LMU) München	since 2008
Süß, Helmut	Honorary Professor	Universität der Bundeswehr München	since 2006

Doctoral Theses

Name	Subject	University	Year
Jörg, Hannah	Multi-Frequency Polarimetric SAR Tomography for the 3-D Characterization and Monitoring of Agricultural Crops	Eidgenössische Technische Hochschule ETH Zurich, Switzerland	2017
Queiroz De Almeida, Felipe	Multichannel Staggered SAR for High-Resolution Wide-Swath Imaging	Karlsruher Institut für Technologie (KIT)	2017
Dexin, Li	Processing Aspects, Simulation and Analysis of the Impact of the Atmosphere on GEO SAR Observations	National University of Defense Technology (NUDT), Changsha, China	2017
Ponce, Octavio	Multicircular Holographic SAR Tomography over Forested Areas	Eidgenössische Technische Hochschule ETH Zurich, Switzerland	2016
Pinheiro, Muriel	Multi-Mode SAR Interferometry for High-Precision DEM Generation	Karlsruher Institut für Technologie (KIT)	2016
Toraño Caicoya, Astor	Allometric Estimation of Aboveground Forest Biomass Using Forest Structure Parameters Estimated by Means of Multibaseline SAR Measurements	Technische Universität München (TUM)	2016
Gramini Ganesan, Ponnurangam	Retrieval of Soil Moisture Using Polarimetric SAR Remote Sensing	Indian Institute of Technology Bombay (IIT Bombay), India	2016
Eilers, Jan	Planning Procedures for SAR Satellite Systems for Interferometric Product Generation	Universität der Bundeswehr München	2016
Villano, Michelangelo	Staggered Synthetic Aperture Radar	Karlsruher Institut für Technologie (KIT)	2016
Döring, Björn	Traceable Radiometric Calibration of Synthetic Aperture Radars	Karlsruher Institut für Technologie (KIT)	2016

Name	Subject	University	Year
Kugler, Florian	Pol-InSAR Forest Height Estimation at Different Frequencies: Opportunities and Limitations	Technische Universität München (TUM)	2015
Parrella, Giuseppe	Characterization of Glacier Facies Using SAR Polarimetry at Long Wavelengths	Eidgenössische Technische Hochschule ETH Zurich, Switzerland	2015
Bachmann, Markus	Antenna Pattern Modeling and Calibration for Spaceborne SAR Systems	Karlsruher Institut für Technologie (KIT)	2015
Zonno, Mariantonietta	SAR Image Processing: Advancements in GB-SAR Data Focusing and InSAR Applications	Politecnico di Bari, Italy	2015
Anglberger, Harald	Simulation and Analysis of High Resolution SAR Signatures	Universität der Bundeswehr München	2015
Aguilera, Esteban	Synthetic Aperture Radar Tomography-Compressed Sensing Models and Algorithms	Technische Universität Berlin	2014
Baumgartner, Stefan	Traffic Monitoring with Air- and Spaceborne Synthetic Aperture Radar	Karlsruher Institut für Technologie (KIT)	2014
Bräutigam, Benjamin	Instrument Calibration of Spaceborne SAR Systems	Karlsruher Institut für Technologie (KIT)	2014
Huber, Sigurd	Spaceborne SAR Systems with Digital Beamforming and Reflector Antennas	Karlsruher Institut für Technologie (KIT)	2014
Schreiber, Eric	Fully Electronic Passive Microwave Imaging System Using Beam Steering by Frequency Shift and Aperture Synthesis	Karlsruher Institut für Technologie (KIT)	2014
Al-Kahachi, Noora	Polarimetric SAR Modelling of a Two-Layer Structure – A Case Study Based on Subarctic Lakes	Technische Universität München (TUM)	2013
Gabele, Martina	SAR/GMTI for Space-Based Radar with Two-Dimensional Antenna Arrays	Karlsruher Institut für Technologie (KIT)	2013
Kim, JunSu	Development of Ionosphere Estimation Techniques for the Correction of SAR Data	Eidgenössische Technische Hochschule ETH Zurich, Switzerland	2013
Sanjuan-Ferrer, Maria-José	Detection of Coherent Scatterers in SAR Data: Algorithms and Applications	Eidgenössische Technische Hochschule ETH Zurich, Switzerland	2013
Rodríguez-Cassolà, Marc	Bistatic Synthetic Aperture Radar Data Processing	Karlsruher Institut für Technologie (KIT)	2012
Lee, Seung-Kuk	Forest Parameter Estimation Using Polarimetric SAR Interferometry Techniques at Low Frequencies	Eidgenössische Technische Hochschule ETH Zurich, Switzerland	2012
Culhaoglu, Ali Eren	Microwave Metamaterials: Superlensing and Design of Low Reflection Coatings	Technische Universität München (TUM)	2012
Jagdhuber, Thomas	Soil Parameter Retrieval under Vegetation Cover Using SAR Polarimetry	Universität Potsdam	2012
Kim, Junghyo	Multiple-Input Multiple-Output Synthetic Aperture Radar for Multimodal Operation	Karlsruher Institut für Technologie (KIT)	2011
Jirousek, Matthias	Imaging Microwave Spectrometer with Aperture Synthesis	Karlsruher Institut für Technologie (KIT)	2011
Jochim, Fritz	The Application of Hansen-Systems in Celestial Mechanics and Astro Dynamics	Universität der Bundeswehr München	2011

Diploma, Master and Bachelor Theses

Name	Thesis	Subject	University	Year
Baris, Ismail	Bachelor	Physikalische Integration von Streumodellen für Mikrowellen und optische Wellenlängen	Georg-August-Universität Göttingen	2017
Bischeltsrieder, Florian	Master	Untersuchung zu einem abbildenden harmonischen Radar mit digitaler Strahlformung	Technische Universität München (TUM)	2017
Engel, Marius	Bachelor	Entwicklung und Anaylse von Teilkomponenten eines Ultraleicht-UWB-Radars	Hochschule für angewandte Wissenschaften Würzburg-Schweinfurt	2017
Heiderich, Lennart	Master	Performance Analysis of Multi-Static SAR Satellite Data	Hochschule für angewandte Wissenschaften München	2017
Kousidis, Konstantinos Antonios	Master	Multi-Dimensional SAR Imaging Based on Compressive Sensing	Technische Universität München (TUM)	2017
Link, Moritz	Master	Potential and Limitations of Soil Moisture Induced Active-Passive Microwave Covariation: A Modeling Study for the Mono- and Dual-Frequency Case	Ludwig-Maximilians-Universität (LMU) München	2017
Mouthaan, Koen	Master	Digital Beamforming for Spaceborne Reflector SAR Systems via FIR Filter Networks in the Presence of Uncertainties	Technische Universität Berlin	2017
Pawar, Bushan R.V.	Master	Concept and Demonstration of a SAR Receiver with Intra-Drift Correction	Ernst-Abbe-Hochschule Jena	2017
Pulella, Andrea	Master	An Analysis of the Potentials of TanDEM-X Data to Characterize Tropical Forest Horizontal Heterogeneity	Università di Pisa, Italy	2017
Weber, Christoph	Master	Entwicklung von innovativen Prozessierungsverfahren für experimentelle bistatische SAR Aufnahmen	Technische Universität München (TUM)	2017
van Kempen, Michel	Bachelor	Refokussierungsverfahren für Schiffe in flugzeuggestützten SAR Bildern	Duale Hochschule Baden-Württemberg Mannheim	2017
Yelahanka Nagaraja, Sharath Babu	Master	Visualization, Detection and Reconstruction of Trees in Fully Polarimetric Long Wavelength SAR Imagery	Technische Universität Chemnitz	2017
Dirscherl, Mariel Christina	Master	Topographic Change Quantification and DEM Uncertainty Assessment Using TanDEM-X and F-SAR DEM Time Series and Quality Maps: Application to the 2014-2015 Bárðarbunga Volcanic Eruption, Iceland	University College London, UK	2016
Aitha, Sravan	Master	Development, Manufacturing, and Testing of a P- and L-Band Outdoor Horn Antenna	Universität Kassel	2016
Raab, Sebastian	Master	Development and Implementation of an Efficient Temperature Management System for SAR System Calibration Transponders	Hochschule für angewandte Wissenschaften Würzburg-Schweinfurt	2016
Freitas Carvalho, Rayssa	Diploma	A Posteriori Knowledge Based Digital Beamforming Concepts Demonstrated with Multi-Channel SAR Data	Instituto Tecnológico de Aeronáutica (ITA), Brazil	2016
Kaschke, Markus	Bachelor	Charakterisierung mehrschichtiger Materialien für Mikrowellenfrequenzen mit Hilfe eines evolutionären Algorithmus	Duale Hochschule Baden-Württemberg Mannheim	2016
Kraus, Luca	Master	Theoretische und experimentelle Untersuchungen zur Bestimmung von Bodenfeuchte mit breitbandigem Radar	Universität Augsburg	2016
Kroll, Jan Paul	Master	Untersuchung und Modellierung von Hardwareeinflüssen auf MIMO Radarsysteme	Karlsruher Institut für Technologie (KIT)	2016
Möhring, Björn	Master	Modulare Simulation of a Compact Antenna Test Range	Technische Universität München (TUM)	2016

Name	Thesis	Subject	University	Year
Pozza, Daniele	Master	Analysis of Vertical Structure of Forests at X-Band and Synergies with Lidar	Università degli Studi di Trento, Italy	2016
Valdo, Paolo	Master	Detection of Changes in Agricultural Scenarios by Means of TanDEM-X Data	Università degli Studi di Trento, Italy	2016
Bertoluzza, Manuel	Master	Monitoring Forest Height Dynamics by Means of L-Band Multibaseline PolInSAR Data	Università degli Studi di Trento, Italy	2015
Braun, Sarah	Bachelor	An Integer Linear Programming Approach to Multi-Satellite Mission Planning	Technische Universität München (TUM)	2015
Ditton, Benjamin	Bachelor	Parametrische Abschätzung der zu erwartenden Bildqualität für flugzeuggestützte SAR Sensoren	Duale Hochschule Baden-Württemberg Mannheim	2015
Haas, Alexander	Diploma	Entwicklung einer breitbandigen Speiseantenne für ein Cassegrain-Antennensystem in der Radarfernerkundung	Karlsruher Institut für Technologie (KIT)	2015
Heinzel, Andreas	Master	Untersuchung von Fokussierungsmöglichkeiten einer SAR-Abbildung bei Halbräumen unterschiedlicher Permittivität	Technische Universität München (TUM)	2015
Linde Cerezo, Alejandro	Bachelor	Performance Assessment and Design of Advance Processing Techniques for Innovative SAR Acquisitions	Universidad de Alcalá, Spain	2015
Marcinkowski, Bartosz	Bachelor	Investigation in Basic Micro Doppler Analysis with a High-Resolution Pulse Radar	Karlsruher Institut für Technologie (KIT)	2015
Marongiu, Sara	Master	Estimation of Vertical Structure of Forests from Multibaseline SAR Data: A Performance Analysis	Università di Pisa, Italy	2015
Severino, Carlos Henrique	Master	Compact Feeding System for a P-Band Circular Horn Antenna	Instituto Tecnológico de Aeronáutica (ITA), Brazil	2015
Szulc, Zbigniew	Bachelor	Development of a Broadband Slotted-Waveguide Antenna at X-Band for Radiometric Applications	Karlsruher Institut für Technologie (KIT)	2015
Telega, Mikolaj	Bachelor	Parametrische Berechnung der Einflüsse von Verformungen bei Corner Reflektoren auf den RCS	Karlsruher Institut für Technologie (KIT)	2015
Tiwari, Sulabh	Master	Spaceborne-Airborne Bistatic SAR: Data Processing and Calibration of an Experimental Acquisition between TanDEM-X and F-SAR	Universität Kassel	2015
Trumpp, Julia	Bachelor	Untersuchung zu Techniken der elektronischen Strahlformung für abbildende Mikrowellenradiometer	Karlsruher Institut für Technologie (KIT)	2015
Wallner, Daniel	Master	Untersuchungen zur radartechnischen Erweiterung eines radiometrischen Abbildungssystems	Technische Universität München (TUM)	2015
Weiss, Thomas	Master	Polarimetric Analyses of SAR Data towards Plant Moisture Estimation	Ludwig-Maximilians-Universität (LMU) München	2015
Albers, Tobias	Master	Aufbau eines Radarsystems zur Detektion von Verunreinigungen	Hochschule für angewandte Wissenschaften Würzburg-Schweinfurt	2014
Axt, Heinrich	Diploma	Vergleichende Analyse von Antennenkonzepten und Antennenentwicklung für P-Band Kalibriertransponder	Hochschule für angewandte Wissenschaften Würzburg-Schweinfurt	2014
Bischeltsrieder, Florian	Bachelor	Untersuchungen von Verfahren zur Bewegungskompensation bei höchstauflösenden SAR-Systemen	Hochschule für angewandte Wissenschaften München	2014
de Sousa Rego, Erich Rommel	Bachelor	Theoretical Investigation of High-Resolution SAR for Buried Object Detection	Instituto Tecnológico de Aeronáutica (ITA), Brazil	2014
Eckermann, Silvio	Diploma	Zeitreihenanalyse von SAR-Bildmaterial am Beispiel ausgewählter Hafenanlagen	Universität der Bundeswehr München	2014

Name	Thesis	Subject	University	Year
Gehrig, Sebastian	Diploma	Untersuchung zur Abbildungsqualität und Absolutwertgenauigkeit eines hochauflösenden Pulsradars	Hochschule für angewandte Wissenschaften Würzburg-Schweinfurt	2014
Grill, Johannes	Master	Analyse von SAR-Bildmaterial in der Umgebung von Minenfeldern in semiariden Gebieten	Universität der Bundeswehr München	2014
Iff, Sebastian	Master	Untersuchungen zum Nachweis von SAR-Bildqualitätsparametern	Hochschule für angewandte Wissenschaften Würzburg-Schweinfurt	2014
Lloredo, Jesus	Master	Joint Phase Unwrapping for Multi-Frequency SAR Interferometry	Ecole nationale supérieure de l'électronique et de ses applications ENSEA, France	2014
Melo Galvao Machado, Bruno	Diploma	Performance Analysis of Rotating SAR (RoSAR)	Instituto Tecnológico de Aeronáutica (ITA), Brazil	2014
Özis, Ezgi	Master	Metamaterial Technologies for Microwave Radomes	Technische Universität München (TUM)	2014
Rauh, Leonhard	Bachelor	Entwicklung und Optimierung einer Wendelantenne für den Einsatz in einem Mikrowellen-Autoklav	Hochschule für angewandte Wissenschaften München	2014
Rosigkeit, Daniel	Master	Verwendbarkeit von LTE im DLR Forschungsflugzeug DO 228-212	Fachhochschule Lübeck	2014
Sorrentino, Aniello	Master	Investigation of Polarimetric Active/Passive Microwave Scattering towards Soil Moisture Estimation	Università degli Studi di Napoli Federico II, Italy	2014
Stambouli, Fairouz	Bachelor	Digitale Kalibrierung mehrkanaliger SAR-Systeme	Karlsruher Institut für Technologie (KIT)	2014
Brancato, Virginia	Master	Electromagnetic Modeling of P-Band Polarimetric SAR Signatures of Polythermal Ice Cap	Università degli Studi di Napoli Federico II, Italy	2013
Cantini, Andrea	Master	3-D Structure of a Forest at L-Band: Experiments Towards a Spaceborne Implementation	Università di Pisa, Italy	2013
Caputo, Maurizio	Master	Soil Moisture Retrieval under a Changing Vegetation Cover Using Dual Polarimetric Data at X-Band	Università degli Studi di Napoli Federico II, Italy	2013
Heinzel, Andreas	Bachelor	Untersuchungen über die Verwendung von UHF-SAR im Nahbereich zur Detektion verborgener Objekte	Technische Universität München (TUM)	2013
Iff, Sebastian	Diploma	Untersuchungen zur Fehleranalyse und zu Kalibrationsmethoden für ein breitbandiges Pulsradar	Hochschule für angewandte Wissenschaften Würzburg-Schweinfurt	2013
Kötschau, Christian	Diploma	Frequency Analysis of Radar Backscatter in X-Band Using F-SAR Data	Karlsruher Institut für Technologie (KIT)	2013
Liebschwager, Toni	Master	Erste Untersuchungen zu einem radarbasierten SSA-Systemverbund	Universität der Bundeswehr München	2013
Lopes Melo, Rafaela	Diploma	Hardware Extension and Experiments for the Digital Beamforming Radar Ground Demonstrator	Instituto Tecnológico de Aeronáutica (ITA), Brazil	2013
Madanahalli Jai Prakash, Adithya Kumar	Master	Investigations of OFDM Signals for Imaging Radar Applications	Technische Universität München (TUM)	2013
Nau, Christopher	Diploma	Koregistrierungsmethoden zur stererometrischen Gewinnung von Höheninformation aus raumgestützten SAR-Daten	Universität der Bundeswehr München	2013
Posovszky, Philipp	Bachelor	Entwicklung einer 3D-Animations-Bibiliothek für Java zur Darstellung von Flugobjekten und Flugtrajektorien	Duale Hochschule Baden-Württemberg Mannheim	2013
Raab, Sebastian	Diploma	Planung und Durchführung einer Freifeld-RCS-Messreihe zur genauen Kalibrierung von Referenzzielen	Hochschule für angewandte Wissenschaften Würzburg-Schweinfurt	2013
Stockamp, Julia	Master	Multi-Frequency Analysis of Snow-Covered Areas Using SAR Polarimetry	Ludwig-Maximilians-Universität (LMU) München	2013

Name	Thesis	Subject	University	Year
Wiese, Tilo	Diploma	Potentielle Anwendungen moderner Inpainting-Algorithmen für die Verarbeitung von Höhenmodellen in der Fernerkundung	Technische Universität Dresden	2013
Albers, Tobias	Diploma	Optimierung und messtechnische Verifikation eines Millimeterwellen-FMCW-Radars	Hochschule für angewandte Wissenschaften Würzburg-Schweinfurt	2012
Anger, Simon	Master	Experimenteller Aufbau und Untersuchung integrierter Empfangsmodule für die Apertursynthese	Universität Ulm	2012
Balkoski, Jovana	Master	Nadir Echo Properties and Suppression in Spaceborne Synthetic Aperture Radar Systems-A Study Based on TerraSAR-X Data	University of Belgrade, Serbia	2012
Dabrowski, Slawomir	Diploma	Untersuchung der Auswirkungen block-adaptiver Quantisierung (BAQ) von SAR-Rohdaten auf die Bildqualität	Karlsruher Institut für Technologie (KIT)	2012
Della Corte, Annalisa	Master	Snow Properties Retrieval Using TerraSAR-X Dual-Polarization Data	Università degli Studi di Napoli Federico II, Italy	2012
Festi, Giorgio	Master	Development and Implementation of a Digital Internal Calibration Strategy for Precise SAR Reference Targets	Università degli Studi di Trento, Italy	2012
Kant, Przemyslaw	Diploma	Systemanalysen und Verfahren zur Kalibrierung eines breitbandigen digitalen Pulsradars	Karlsruher Institut für Technologie (KIT)	2012
Masseroli, Gianpaolo	Master	Crop Volume Characterization Using Dual Polarimetric SAR in X-Band	Università degli Studi di Napoli Federico II, Italy	2012
Profelt, Juliane	Master	Anwendung elastischer Koregistrierungsverfahren auf hoch auflösende Radar-Bildpaare	Technische Universität München (TUM)	2012
Queiroz de Almeida, Vinicius	Diploma	Performance Analysis of Medium Earth Orbit and Geosynchronous Synthetic Aperture Radar	Instituto Tecnológico de Aeronáutica (ITA), Brazil	2012
Rückel, Thomas	Diploma	Signaturanalysen polarimetrischer SAR-Daten von Radarsat-2 und F-SAR	Universität der Bundeswehr München	2012
Simon, David	Master	Weiterentwicklung einer Hohlleiterschlitzantenne für elektronisches Schwenken der Antennenkeule bei radiometrischen Abbildungen	Universität Kassel	2012
Thiemer, Patrick	Diploma	Aufbau und messtechnische Verifikation eines breitbandigen digitalen Pulsradars	Hochschule für angewandte Wissenschaften Würzburg-Schweinfurt	2012
Antonello, Arthur	Diploma	Implementation of Compressed Sensing Algorithms in Python	Instituto Tecnológico de Aeronáutica (ITA), Brazil	2011
Bianco, Vittorio	Master	Phase Calibration of Multibaseline PolInSAR Data Stacks	Università degli Studi di Napoli Federico II, Italy	2011
Eyssartier, Kevin	Diploma	Monitoring the Petermann Ice Island (2010) Using TanDEM-X Satellites	Institute National Polytechnique de Grenoble, France	2011
Helbig, Daniel	Diploma	Genauigkeitsanalyse der Georeferenzierung für SAR Bildprodukte	Universität der Bundeswehr München	2011
Hepner, Christopher	Master	Erstellung dreidimensionaler Radarsignaturen aus Turm-Drehstands-Messungen mit ausgedünnter Apertur	Hochschule Ulm	2011
Künemund, Maren	Bachelor	Hochauflösende Prozessierung flugzeuggestützter SAR Daten auf GPU	Duale Hochschule Baden-Württemberg Mannheim	2011
Pereira Vicente, Luis Gustavo	Diploma	Correlating SAR: Concepts and Simulation	Instituto Tecnológico de Aeronáutica (ITA), Brazil	2011
Pisciottano, Iole	Master	First Analysis on Snow Cover Change Using Polarimetric TerraSAR-X Data	Università degli Studi di Napoli Federico II, Italy	2011

Name	Thesis	Subject	University	Year
Scheuerer, Lars	Diploma	Integration eines Mehrkanal-Analog-Digital-Wandlers in das Apertursynthese-Radiometer ANSAS	Hochschule für angewandte Wissenschaften Würzburg-Schweinfurt	2011
Simon, David	Diploma	Untersuchung möglicher Leitungsübergänge von Hohlleiter auf Streifenleitung für radiometrische Anwendungen	Universität Kassel	2011
Toraño Caicoya, Astor	Diploma	Forest Biomass Estimation Derived from 3D Forest Structure	Technische Universität München (TUM)	2011

3.2 Scientific Exchange

Guest Scientists

Name	Home Institution	Period
Pyne, Budhaditya	University of Tokyo and JAXA, Japan	Dec. 2017-Mar. 2018
Amao Oliva, Joel Alfredo	Centro de Investigación y de Estudios Avanzados del Instituto Politécnico Nacional CINVESTAV-IPN, Mexico	Jun. 2017-Nov. 2017
Dexin, Li	National University of Defense Technology (NUDT), Changsha, China	Nov. 2015-Oct. 2017
Perez Perez, Fabricio Otoniel	Centro de Investigación en Matemáticas A.C. CIMAT, Mexico	Aug. 2016-July 2017
Pourshamsi, Maryam	University of Leicester, UK	May 2017, April 2018
Da Conceicao Bispo, Polyanna	University of Leicester, UK	May 2017, Apr.-June 2016, June 2013
Pinho Perrut, Rapahael Heleno	Diretoria de Serviço Geográfico, Brazil	July-Dec. 2015
Feng, He	National University of Defense Technology (NUDT), Changsha, China	Apr.-Sept. 2015
Martin del Campo Becerra, Gustavo	Centro de Investigación y de Estudios Avanzados del Instituto Politécnico Nacional CINVESTAV-IPN, Mexico	Jan. 2015 -July 2015
Wang, Xiao	Fudan University Graduate School, China	Mar.-June 2015
Heine, Iris	Deutsches GeoForschungsZentrum GFZ, Potsdam	Apr.-May 2015
Knapp, Nikolai	Zentrum für Umweltforschung UfZ, Leipzig	Apr.-May 2015
Schröter, Ingmar	Zentrum für Umweltforschung UfZ, Leipzig	Apr.-May 2015
Pathe, Karsten	Friedrich-Schiller-Universität Jena	December 2014
Salepci, Nesrin	Friedrich-Schiller-Universität Jena	December 2014
Fischer, Rico	Zentrum für Umweltforschung UfZ, Leipzig	December 2014
Paulick, Sebastian	Zentrum für Umweltforschung UfZ, Leipzig	December 2014
Indrio, Gianfranco	Zentrum für Umweltforschung UfZ, Leipzig	Nov. 2013-Dec. 2014
Spengler, Daniel	Deutsches GeoForschungsZentrum GFZ, Potsdam	Nov.-Dec. 2014
Garcia, Daniel Maximo	Diretoria de Serviço Geográfico, Brazil	July-Dec. 2014
Brancato, Virginia	Eidgenössische Technische Hochschule ETH Zurich, Switzerland	July-Nov. 2014

Name	Home Institution	Period
Ishitsuka, Kazuya	Kyoto University, Japan	Oct.-Nov. 2014
Kawano, Noriyuki	JAXA, Japan	July 2013-Oct. 2014
Avtar, Ram	United Nations University, Tokyo, Japan	July-Aug. 2014
Qi, Wenlu	University of Texas at Dallas, USA	Apr.-July 2014
Voormansik, Kaupo	University of Tartu, Estonia	Feb.-Apr. 2014
Zonno, Mariantonietta	Politecnico di Bari, Italy	Sept. 2013-Apr. 2014
Barreto da Silva, Wagner	Instituto Militar de Engenharia, Brazil	Sept. 2013-Mar. 2014
Makhoul Varona, Eduardo	Universitat Politècnica de Catalunya UPC, Spain	April-Aug. 2013
Abdullahi, Sahra	Technische Universität München (TUM)	May-June 2013
Junqueira, Cynthia	Departamento de Ciência e Tecnologia Aeroespacial DCTA, Brazil	July 2012
Kusano, Shunishi	Tohoku University, Sendai, Japan	June 2011-May 2012
Naiara, Pinto	University of Maryland, USA	May 2012
Brolly, Mathew	University of Maryland, USA	May 2012
Voormansik, Kaupo	University of Tartu, Estonia	Feb.-Apr. 2012
Erten, Esra	Eidgenössische Technische Hochschule ETH Zurich, Switzerland	August 2011
Kumar, Vishvendra	Indien, DAAD Fachpraktikum	May-July 2011
Alitalo, Pekka	Aalto University, Finland	May-July 2011
Deledalle, Charles	Télécom ParisTech, France	Apr.-May 2011

Scientific Sabbaticals

Name	Host Institution	Period
Kim, Jun Su	University of Fairbanks, Alaska	Aug.-Oct. 2017
Baur, Martin	Massachusetts Institute of Technology MIT, USA	Jul.-Aug. 2017
Jagdhuber, Thomas	Massachusetts Institute of Technology MIT, USA	Jul.-Aug. 2017
Link, Moritz	Massachusetts Institute of Technology MIT, USA	Jul.-Aug. 2017, Sep. 2016-Jan. 2017
Pardini, Matteo	University of Maryland, USA	June-July 2017
Rommel, Tobias	NASA/Goddard, USA	Apr.-July 2017
Villano, Michelangelo	NASA/JPL, USA	Apr.-June 2017
Jagdhuber, Thomas	Massachusetts Institute of Technology MIT, USA	July 2016
Link, Moritz	University of Rome Tor Vergata, Italy	June-July 2016
Jagdhuber, Thomas	Massachusetts Institute of Technology MIT, USA	March 2015
Jagdhuber, Thomas	Massachusetts Institute of Technology MIT, USA	October 2014
Younis, Marwan	DLR-Forschungssemester, NASA/JPL, USA	Mar.-June 2013
Mittermayer, Josef	Forschungssemester, Universitat Politècnica de Catalunya UPC, Spain	Mar.-June 2012
Süß, Helmut	DLR-Forschungssemester, Naval Postgraduate School, Monterey, USA	Apr.-July 2011

3.3 Scientific Awards and Recognitions

Award	Institution	Laureate	Year
Letter Prize Paper Award (IEEE GRSL)	IEEE Geoscience and Remote Sensing Society	Villano, Michelangelo; Krieger, Gerhard; Moreira, Alberto	2017
Best Poster Award	ESA World Cover Conference	Rizzoli, Paola; Martone, Michele; Wecklich, Christopher; Gonzalez, Carolina; Bueso Bello, José Luis; Valdo, Paolo; Krieger, Gerhard; Zink, Manfred	2017
Otto Lilienthal Sabbatical	Gesellschaft von Freunden des DLR (GvF)	Younis, Marwan	2017
Young Scientist Award for Excellence	URSI Kleinheubacher Tagung	Jörg, Hannah	2017
ITG Dissertation Award	Informationstechnische Gesellschaft	Villano, Michelangelo	2017
Young Scientist Award	Werner-von-Siemens-Ring Foundation	Villano, Michelangelo	2017
Best Paper Award	European Conference on Synthetic Aperture Radar (EUSAR)	Krieger, Gerhard; Rommel, Tobias; Moreira, Alberto	2016
DLR Science Award	German Aerospace Center – DLR	Villano, Michelangelo	2016
OHB Award "Future of Radar Based Earth Observation"	SCG Space Generation Congress / IAC International Astronautical Congress, Mexico	Ponce, Octavio; Queiroz de Almeida, Felipe; Rommel, Tobias	2016
Recognition in Young Scientist Contest	International Radar Symposium (IRS)	Que, Russel	2016
SET Panel Excellence Award	NATO	Osipov, Andrey	2016
Transactions Prize Paper Award (IEEE TGRS)	IEEE Geoscience and Remote Sensing Society	Reigber, Andreas; Jäger, Marc	2016
Young Scientist Award for Excellence	URSI Kleinheubacher Tagung	Pinheiro, Muriel	2016
Best Poster Award	German Microwave Conference (GeMiC)	Rudolf, Daniel; Raab, Sebastian; Döring, Björn; Jirousek, Matthias; Reimann, Jens; Schwerdt, Marco	2015
Culmann Award	Eidgenössische Technische Hochschule ETH Zurich, Switzerland	Kim, Jun Su	2015
Franz-Xaver-Erlacher-Förderpreis	Gesellschaft von Freunden des DLR (GvF)	Queiroz de Almeida, Felipe	2015
IEEE Fellow	IEEE	Reigber, Andreas	2015
Letter Prize Paper Award (IEEE GRSL)	IEEE Geoscience and Remote Sensing Society	Villano, Michelangelo; Krieger, Gerhard; Moreira, Alberto	2015
Otto Lilienthal Sabbatical	Gesellschaft von Freunden des DLR (GvF)	López-Dekker, Francisco	2015
Student Paper Award	APSAR Asia-Pacific Synthetic Aperture Radar Conference, Singapore	Villano, Michelangelo	2015
Transactions Prize Paper Award (IEEE TGRS)	IEEE Geoscience and Remote Sensing Society	Krieger, Gerhard	2015
DLR Center of Excellence on Spaceborne SAR	German Aerospace Center – DLR	Institute HR (together with EOC)	2014-2016
Asto Aerospace Promotion Prize	Gesellschaft von Freunden des DLR (GvF)	Heister, Anton	2014
Certificate of Merit and Young Scientist Award	URSI Kleinheubacher Tagung	Villano, Michelangelo	2014

Award	Institution	Laureate	Year
DLR Science Award	German Aerospace Center – DLR	Jagdhuber, Thomas	2014
IEEE Distinguished Achievement Award	IEEE Geoscience and Remote Sensing Society	Moreira, Alberto	2014
IEEE Fellow	IEEE	Hajnsek, Irena; Papathanassiou, Kostas	2014
Student Paper Award, first place	European Conference on Synthetic Aperture Radar (EUSAR)	Villano, Michelangelo	2014
Student Paper Award, second place	European Conference on Synthetic Aperture Radar (EUSAR)	Ponce, Octavio	2014
Student Paper Award, third place	European Conference on Synthetic Aperture Radar (EUSAR)	Kim, Jun Su	2014
Young Scientist Award	International Radar Symposium (IRS), Poland	Ponce, Octavio; Rommel, Tobias; Younis, Marwan; Prats, Pau; Moreira, Alberto	2014
Certificate of Merit and Young Scientist Award Finalist	URSI Kleinheubacher Tagung	Rommel, Tobias	2013
DLR Science Slam winner	German Aerospace Center – DLR	Tello Alonso, Maria; Martone, Michele	2013
DLR Forschungssemester	German Aerospace Center – DLR	Younis, Marwan	2013
IEEE Fellow	IEEE	Krieger, Gerhard	2013
IEEE Senior Member	IEEE Geoscience and Remote Sensing Society	Prats, Pau	2013
ITG Dissertation Award	Informationstechnische Gesellschaft	Culhaoglu, Ali Eren	2013
Student Paper Award, second place	IEEE Geoscience and Remote Sensing Symposium (IGARSS)	Ponce, Octavio	2013
Best Diploma Thesis	Hochschule Würzburg-Schweinfurt & Hans-Wilhelm-Renkhoff-Stiftung	Thiemer, Patrick	2012
Certificate of Recognition of TanDEM-X Achievements and Impact	European Conference on Synthetic Aperture Radar (EUSAR)	The team of satellite mission TanDEM-X (Institutes HR, EOC and GSOC)	2012
DLR Forschungssemester	German Aerospace Center – DLR	Mittermayer, Josef	2012
DLR IDEA Award 2011	German Aerospace Center – DLR	Peichl, Markus; Dill, Stephan	2012
DLR Science Award	German Aerospace Center – DLR	Prats, Pau	2012
Deutscher Zukunftspreis des Bundespräsidenten für Technik und Innovation, Nomination as one of four Finalists	Bundespräsident	Moreira, Alberto; Krieger, Gerhard; Zink, Manfred	2012
DLR Senior Scientist	German Aerospace Center – DLR	Hajnsek, Irena	2012
IEEE W.R.G. Baker Award	IEEE Geoscience and Remote Sensing Society	Krieger, Gerhard; Moreira, Alberto; Fiedler, Hauke; Hajnsek, Irena; Werner, Marian; Younis, Marwan; Zink, Manfred	2012
Student Paper Award Finalist	International Conference on Radar Systems, Glasgow, UK	Villano, Michelangelo	2012
Young Scientist Award	URSI	Aguilera, Esteban	2011
Franz-Xaver-Erlacher-Förderpreis	Gesellschaft von Freunden des DLR (GvF)	Toraño Caicoya, Astor	2011
DLR Forschungssemester	German Aerospace Center – DLR	Süß, Helmut	2011
DLR Senior Scientist	German Aerospace Center – DLR	Papathanassiou, Konstantinos	2011
Sustainable Resource Management (SRM) Award	Audi Stiftung für Umwelt	Toraño Caicoya, Astor	2011
ARGUS-Preis	EADS Cassidian	Hepner, Christopher	2011

3.4 Lectures at Universities

Lecturer	University	Subject	2011	2012	2013	2014	2015	2016	2017
Baumgartner, Stefan	Friedrich-Alexander-Universität Erlangen-Nürnberg	Radarfernerkundung mit Satelliten (SatRadar)						■	■
Hajnsek, Irena	Eidgenössische Technische Hochschule ETH Zurich, Switzerland	Methodologies for Image Processing of Remote Sensing	■	■	■	■	■	■	■
	Friedrich-Schiller-Universität Jena	Fernerkundung		■					
Jagdhuber, Thomas	Friedrich-Schiller-Universität Jena	Spezielle angewandte Fernerkundung: Polarimetrie			■	■	■	■	■
	Universität Augsburg	Radarfernerkundung für Geographische Anwendungen				■	■	■	■
Jirousek, Matthias	Karlsruher Institut für Technologie (KIT)	Spaceborne Microwave Radiometry – Advanced Methods and Applications					■	■	■
Krieger, Gerhard	Friedrich-Alexander-Universität Erlangen-Nürnberg	Radarfernerkundung mit Satelliten (SatRadar)			■	■	■	■	■
Moreira, Alberto	Karlsruher Institut für Technologie (KIT)	Spaceborne Radar Remote Sensing	■	■	■	■	■	■	■
Papathanassiou, Konstantinos	Ludwig-Maximilians-Universität (LMU) München	Moderne Verfahren der Radarfernerkundung				■	■	■	■
	Friedrich-Schiller-Universität Jena	Spezielle angewandte Fernerkundung: Polarimetrie	■		■		■		
Pardini, Matteo	Eidgenössische Technische Hochschule ETH Zurich, Switzerland	SAR Tomography					■	■	■
Reigber, Andreas	Technische Universität Berlin	Optical Remote Sensing	■						
	Technische Universität Berlin	Microwave and Radar Remote Sensing	■	■	■	■	■	■	■
Rommel, Tobias	Technische Universität Chemnitz	Hochfrequenztechnik und Photonik		■	■	■	■	■	■
	Technische Universität Chemnitz	Basics of Microwave and Photonic Systems					■	■	■
	Technische Universität Chemnitz	Aerospace Remote Sensing					■	■	■
Süß, Helmut	Karlsruher Institut für Technologie (KIT)	Mikrowellenradiometrie-Grundlagen und neuartige Anwendungen	■	■	■	■			
	Universität der Bundeswehr München	Radar- und Lasermethoden	■	■	■	■	■	■	■
	Universität der Bundeswehr München	Einführung in die Fernerkundung				■			
Younis, Marwan	Karlsruher Institut für Technologie (KIT)	Spaceborne Radar Remote Sensing		■		■	■	■	■
	Karlsruher Institut für Technologie (KIT)	Advanced Radio Communication I		■	■	■	■	■	■

3.5 Tutorials and Annual Courses

Lecturer	Course	Lecture	2011	2012	2013	2014	2015	2016	2017
Anglberger, Harald	SAR Course for Military Image Analysis	SAR Image Analysis		■	■	■	■	■	■
Bachmann, Markus	CCG Course: Radar und Messtechnik	Entwicklung eines Antennenmodells	■						
	CCG Course: SAR Principles and Applications	TerraSAR-X & TanDEM-X	■						
	CCG Course: SAR Principles and Applications	SAR Moving Targets Techniques						■	
Bräutigam, Benjamin	CCG Course: Radar und Messtechnik	Instrument-Verifikation im Orbit	■						
	CCG Course: Radar und Messtechnik	Interne Kalibrierung von SAR-Systemen	■						
Chiari, Martin Freiherr von	CCG Course: Future Sensor Technology	Multi-Sensor Data Fusion-Principles and Applications	■	■					
Culhaoglu, Ali Eren	CCG Course: Radar- und Infrarottarnung: Technik und Anwendung	Radartarnung mit Metamaterialien	■	■					
De Zan, Francesco	Training Course on Radar Remote Sensing Technology and Environmental Applications 2012, Tartu, Estonia	SAR Interferometry		■					
Dietrich, Björn	BKA-Workshop	Detektion und Abwehr ziviler UAS					■		
	CCG Course: Future Sensor Technology	SAR-Grundlagen für Aufklärungssysteme	■	■					
Döring, Björn	CCG Course: Radar und Messtechnik	Akkurate Referenzziele	■						
Eilers, Jan; Neff, Thomas	Lehrgang Luft, Militärische Anwendungen in der Raumfahrt, BiZBw, Mannheim	Schutz von Raumfahrtsystemen	■	■	■	■	■	■	■
	Lehrgang Luft, Qualitätssicherung in der Raumfahrt, BiZBw, Mannheim	Bahnmechanik & Simulation	■	■	■	■	■	■	■
Hajnsek, Irena	7th ESA Advanced Training Course on Land Remote Sensing, Godollő, Hungary	Introduction to SAR and InSAR							■
	Advanced course on RADAR Polarimetry 2011, ESRIN, Italy	PolSAR-Surface Parameters Estimation Intro & Basic and Advanced Concepts	■		■		■		■
	CCG Course: SAR Principles and Applications	SAR Polarimetry I & II	■	■	■	■	■	■	■
	ESA Advanced Training Course in Land Remote Sensing 2011, Krakow, Poland	Advanced SAR 2, POLInSAR Exploitation	■						
	The first Algerian Geoscience and Remote Sensing Spring School 2017, "Applications of Optical Imaging and Radar Sensors", Algeria	Radar Remote Sensing: TanDEM-X : Mission Status							■
	Tutorial at European Conference on Synthetic Aperture Radar (EUSAR) 2014, Berlin	Surface Parameter Estimation: Basics and Advanced Concepts				■			

Lecturer	Course	Lecture	2011	2012	2013	2014	2015	2016	2017
Horn, Ralf	CCG Course: SAR Principles and Applications	DLR Airborne SAR Activities	■	■	■	■	■	■	■
Jagdhuber, Thomas	SAR-EDU Summer School for Applied Radar Remote Sensing, Jena	SAR-Polarimetry: Theory and Applications					■	■	■
	SUNSAR Symposium 2017	Advanced SAR Techniques and Applications							■
Kemptner, Erich	CCG Course: Radar- und Infrarottarnung: Technik und Anwendung	Numerische Methoden zur RCS-Simulation	■	■			■		
	CCG Course: Radar- und Infrarottarnung: Technik und Anwendung	Radartarnung mit Metamaterialien					■		
Krieger, Gerhard	CCG Course: Intelligente Sensorik II ("Future Sensor Technologies" until 2013)	SAR-Systeme: Überblick und neue Konzepte	■	■	■	■	■	■	
	CCG Course: SAR Principles and Applications	Innovative SAR Missions and Sensor Concepts	■	■	■	■	■		■
	Invited Tutorial at EuRAD, European Microwave Week	Advanced Spaceborne SAR Concepts			■				
	Invited Tutorial at IGARSS 2012, Munich	New SAR Missions and Concepts		■					
López-Dekker, Francisco	Radar Remote Sensing Course 2011, Hungary	Introduction to SAR	■						
López-Dekker, Francisco; Reigber, Andreas	Invited Tutorial at IGARSS 2012, Munich	SAR Imaging, Polarimetry, Interferometry and Tomography		■					
López-Dekker, Francisco	Tutorial at European Conference on Synthetic Aperture Radar (EUSAR) 2014, Berlin	Bistatic and Multistatic SAR				■			
Moreira, Alberto	4th Advanced Training Course in Land Remote Sensing, Greece	Synthetic Aperture Radar (SAR): Principles and Applications			■				
	CCG Course: SAR Principles and Applications	SAR Basics	■	■	■	■	■	■	■
	CCG Course: SAR Principles and Applications	SAR Theory	■	■	■	■	■	■	■
	CCG Course: SAR Principles and Applications	Advanced and Future SAR Systems	■	■	■	■	■	■	■
	Tutorial at IGARSS 2016, China; IGARSS 2017, USA	SAR Principles & Applications						■	■
Osipov, Andrey	CCG Course: Radar- und Infrarottarnung: Technik und Anwendung	Grundlagen der elektromagnetischen Streuung	■	■			■	■	■
	CCG Course: Radar- und Infrarottarnung: Technik und Anwendung	Numerische Methoden zur RCS-Simulation					■	■	■
	CCG Course: Radar- und Infrarottarnung: Technik und Anwendung	Radartarnung mit Metamaterialien						■	■

Lecturer	Course	Lecture	2011	2012	2013	2014	2015	2016	2017
Papathanassiou, Konstantinos	1st Advanced Course on Radar Polarimetry 2011, ESA, Italy	Polarimetric SAR Interferometry	■						
	2nd Advanced Course on Radar Polarimetry 2013, ESRIN, The Netherlands	Polarimetric SAR Interferometry			■				
	3rd CEOS Synthetic Aperture Radar (SAR) Workshop, Gabon	PolIn-SAR and Tomo-SAR Principles and Applications							■
	4th ESA Advanced Training Course on Land Remote Sensing, Greece	SAR Basic Concepts			■				
	5th ESA Advanced Training Course on Land Remote Sensing, Spain	Advanced SAR					■		
	7th ESA Advanced Training Course on Land Remote Sensing, Hungary	Introduction to SAR and InSAR Forest Retrievals Using SAR							■
	CCG Course: SAR Principles and Applications	Polarimetric SAR Interferometry I & II	■	■	■	■	■	■	■
	ESA-AGEOS AfriSAR Workshop, Gabon	SAR, Pol-SAR, and In-SAR Principles and Applications							■
	Invited Tutorial at IGARSS 2012, Munich	Deriving Vegetation Structure from Lidar and SAR		■					
	NASA Carbon Cycle & Ecosystems Science Workshop, Alexandria, USA	Polarimetric SAR Interferometry (Pol-InSAR)	■						
	SAR-EDU Summer School for Applied Radar Remote Sensing, Jena	Forest Biomass from SAR						■	
	Tutorial at European Conference on Synthetic Aperture Radar (EUSAR) 2014, Berlin	Pol-InSAR Concepts and Applications; SAR Contribution for Vegetation Mapping				■			
	Tutorial at the European Conference on Synthetic Aperture Radar (EUSAR) 2012, Nuremberg	Application of Pol and Pol-InSAR		■					
Pardini, Matteo	3rd Advanced Course on Radar Polarimetry 2015, ESA, Italy	Polarimetric SAR Interferometry				■			
Peichl, Markus	CCG Course: Intelligente Sensorik II ("Future Sensor Technologies" until 2013)	Technologien und Anwendungen Abbildender Mikrowellen-Radiometrie	■	■	■	■	■	■	■
	CCG Course: Spaceborne Remote Sensing	Basics of Microwave Radiometry Technology; Spaceborne Microwave Radiometry				■	■	■	■
	Lehrgang "Moderne Verfahren der Radartechnik", BiZBw Mannheim	SAR und ISAR – Theorie und Praxis						■	
Reigber, Andreas	Invited Lecture at Karlsruhe Institute of Technology (KIT)	3D Imaging with SAR Tomography			■				
	Invited Tutorial at IGARSS 2012, Munich	3D Imaging with SAR Tomography		■					
	Tutorial at European Conference on Synthetic Aperture Radar	SAR Tomography				■			

Lecturer	Course	Lecture	2011	2012	2013	2014	2015	2016	2017
	(EUSAR) 2014, Berlin								
Rizzoli, Paola	Invited Tutorial at EuRAD, European Microwave Week	Spaceborne SAR Interferometry and TanDEM-X							■
Rommel, Tobias	Invited Tutorial at Atlantic Radio Science Conference (URSI AT-RASC), Spain	Polarization and Waveform Diversity Radar Methods and their Application in Disaster Management					■		
	Invited Tutorial at VDE ITG Fachausschuss	Waveform Diversity Methods for Multi-Parameter Radar Applications					■		
Schwerdt, Marco	CCG Course: Radar und Messtechnik	Kalibrierkonzepte	■						
	CCG Course: Radar und Messtechnik	Akkurate Referenzziele	■						
	CCG Course: Radar und Messtechnik	Externe Kalibrierung von SAR-Systemen	■						
Villano, Michelangelo	CCG Course: Intelligente Sensorik II	SAR-Systeme: Überblick und neue Konzepte							■
	CCG Course: SAR Principles and Applications	Innovative SAR Missions and Sensor Concepts						■	
Younis, Marwan	6th ESA Advanced Training Course on Land Remote Sensing 2015, Romania	Introduction to SAR Remote Sensing; Advanced SAR I					■		
	CCG Course: Radartechnik für Entwickler und Systemingenieure	Synthetic Aperture Radar (SAR) Principles	■	■	■	■	■	■	■
	Invited Tutorial at EuRAD, European Microwave Week	Synthetic Aperture Radar: Principles, Theory and Applications			■				■
	Tutorial at European Conference on Synthetic Aperture Radar (EUSAR) 2014, Berlin	Digital Beamforming Concepts				■			
Zink, Manfred	CCG Course: Radar und Messtechnik	SAR-Systeme – Einführung	■						
	Invited Tutorial at IGARSS 2012, Munich	New SAR Missions and Concepts		■					
	Invited Tutorial at EuRAD, European Microwave Week	Spaceborne SAR Interferometry and TanDEM-X			■				

3.6 Conference Organization

Event	Function	Years
Conference Highlights:		
IEEE International Geoscience and Remote Sensing Symposium (IGARSS) 2012, Munich, Germany	Main Organizer, Co-Chair, Technical Chair, Organising Committee Member, Technical Program Committee Member, Session Organizer and Chair	2012
European Conference on Synthetic Aperture Radar (EUSAR) 2014, Berlin, Germany	Main Organizer, General Chair, Technical Chair, Technical Program Committee Member	2014
European Conference on Synthetic Aperture Radar (EUSAR) 2016, Hamburg, Germany	Co-Chair, Technical Program Committee Member	2016

Event	Function	Years
Recurring Conferences:		
European Conference on Synthetic Aperture Radar (EUSAR), Germany	Technical Program Committee Member, Session Organizer, Session Chair	Since 1996 (biannual)
IEEE International Geoscience and Remote Sensing Symposium (IGARSS)	Technical Program Committee Member, Session Organizer, Session Chair	Since 2000
ESA International Workshop on Science and Applications of SAR Polarimetry and Polarimetric Interferometry (PolInSAR)	Technical Program Committee Member, Session Organizer, Session Chair	Since 2003
International Radar Symposium (IRS) (odd years in Germany, even years in East Europe)	Technical Program Committee Member, Session Organizer, Session Chair	Since 2006
Committee on Earth Observation Satellites (CEOS) Working Group on Calibration and Validation (WGCV), SAR Subgroup, Synthetic Aperture Radar Workshop	Co-Chair (2015, 2016), Technical Program Committee Member, Session Organizer, Session Chair	Since 1991
Regular Conferences:		
TerraSAR-X / TanDEM-X Science Team Meetings	Main Organizer, General Chair, Organising Committee Member, Technical Program Committee Member	2011, 2013, 2016
HGF Alliance "Remote Sensing and Earth System Dynamics" (EDA) Week, Garmisch-Partenkirchen, Germany	Main Organizer, General Chair, Technical Program Committee Member	2013 -2017
Committee on Earth Observation Satellites (CEOS) Working Group on Calibration and Validation (WGCV), SAR Subgroup, Synthetic Aperture Radar Workshop	Co-Chair	2015, 2016
ARSI Advanced RF Sensors and Remote Sensing Instruments Workshop	Technical Program Committee Member, Session Chair	2014
ESA Living Planet Symposium	Technical Program Committee Member	2013, 2016
European Microwave Week	Technical Program Committee Member	2013, 2015, 2016, 2017
FRINGE, Frascati, Italy	Technical Program Committee Member	2015, 2017
German Microwave Conference (GeMiC), Germany	Technical Program Committee Member	2011, 2014, 2015, 2016
IEEE Young Professionals Conference on Remote Sensing	Main Organizer, Technical Program Committee Member	2014, 2016, 2017
Joint Urban Remote Sensing Event (JURSE)	Technical Program Committee Member	2011, 2013
NATO SCO AVT-257, Specialists' Meeting "Best Practices for Risk Reduction for Overall Space Systems"	Technical Program Committee Member	2016
SPIE, San Diego, USA	Technical Program Committee Member	2017
URSI General Assembly and Scientific Symposium	Technical Program Committee Member, Session Organizer, Session Chair	2013, 2017
Asian Pacific SAR Conference (APSAR)	Technical Program Committee Member	2015, 2017
Advanced SAR Workshop (ASAR Workshop)	Technical Program Committee Member	2011, 2013, 2015, 2017
PIERS, St. Petersburg, Russia	Technical Program Committee Member	2017
International Conference on Electromagnetics in Advanced Applications (ICEAA)	Session Organizer, Session Chair	2012, 2017
URSI Commission B International Symposium on Electromagnetic Theory (EMTS)	Session Organizer, Session Chair	2013, 2016
ESA Ocean Currents Workshop	Session Chair	2015
International Earth Observation Convoy and Constellation Concepts Workshop	Session Chair	2013

3.7 Participation in Scientific and Technical Committees

Name	Committee and Function	Years
Anglberger, Harald	Member of NATO SET-215-Model-based SAR Automatic Target Recognition	Since 2014
Bachmann, Markus	Member of the Committee on Earth Observation Satellites (CEOS) Working Group on Calibration & Validation (WGCV) SAR Subgroup	Since 2008
Bräutigam, Benjamin	Member of the Committee on Earth Observation Satellites (CEOS) Working Group on Calibration & Validation (WGCV) SAR Subgroup	Since 2008
Buckreuß, Stefan	Member of the Advisory Board (Fachbeirat) of Deutsches Museum	Since 2016
	Member of the TerraSAR-X/TanDEM-X Advisory Board	Since 2016
	Head of the TerraSAR-X/TanDEM-X Mission Board	2007-2015
	Member of the TerraSAR-X/TanDEM-X Joint Steering Committee	2007-2015
Busche, Thomas	Deputy Coordinator of the TanDEM-X Science Team	Since 2007
Döring, Björn	Member of the Committee on Earth Observation Satellites (CEOS) Working Group on Calibration & Validation (WGCV) SAR Subgroup	Since 2008
Eilers, Jan	Member of CEN/CLC/TC5 WG3 Earth Observation, DIN Standards Committee Aerospace, DIN Deutsches Institut für Normung e. V.	Since 2013
Hager, Manfred	Member of NATO SET-220-Geospatial Information Extraction from Spaceborne SAR-Images for NATO-Operations	Since 2014
Hajnsek, Irena	Member of the Helmholtz Association Committee "Think Tank"	Since 2017
	Member of the Steering Committee CIRFA Center for Integrated Remote Sensing and Forecasting for Arctic Operations	Since 2016
	Mentor as part of the MARIA-REICHE-Mentoring Program to support academic careers of female post-doc researchers	Since 2016
	Mentor as part of the Helmholtz Mentoring Program 'Taking the Lead'	Since 2015
	Chair of Small Conferences and Symposia, IEEE Geoscience and Remote Sensing Society (GRSS)	Since 2015
	Member of the Steering Committee of MOSES "Erde und Umwelt"	Since 2015
	Member of the Advisory Board of GlobeBiomass	Since 2015
	Science coordinator of the TanDEM-X mission, DLR	2007-2015
	IEEE Geoscience and Remote Sensing (GRSS) Women Mentoring Program	Since 2014
	Member of the IEEE TGRS AdCom	Since 2013
	Member of the HGF-Alliance "Remote Sensing and Earth System Dynamics" (EDA) Steering Committee	since 2013
	TERENO/ACROSS Steering Committee	Since 2008
	Member of the Swiss Commission of Remote Sensing (SKF)	since 2011
	Member of IDA-FERN, Interdepartementale Arbeitsgruppe Fernerkundung des Bundes, CH	since 2011
	Vice President of Technical Activities of IEEE Geoscience and Remote Sensing (GRSS) AdCOM	Since 2008
	Chair of the German Chapter of the IEEE Geoscience and Remote Sensing (GRSS)	Since 2008
	Coordinator of the Tandem-L Science Team, DLR	Since 2008
Kempf, Timo	Member of NATO SET-215-Model-based SAR Automatic Target Recognition	Since 2014
	Member of NATO SET-163-Aspects of Multi-Parameter Radar ATR in Complex Environments	2009-2014

Name	Committee and Function	Years
Kemptner, Erich	Member of the METAMORPHOSE (Virtual Institute for Artificial EM Materials and Metamaterials)	Since 2008
Klenk, Patrick	Member of the Committee on Earth Observation Satellites (CEOS) Working Group on Calibration & Validation (WGCV) SAR Subgroup	Since 2016
López-Dekker, Francisco	Member of the SAOCOM Expert Science Group, ESA	Since 2014
Moreira, Alberto	Chair of the IEEE Geoscience and Remote Sensing Society (GRSS) Major Awards Committee	Since 2017
	Spokesman of DLR's Center of Excellence on Synthetic Aperture Radar	2000-2015
	Principal Investigator and member of the HGF-Alliance "Remote Sensing and Earth System Dynamics" (EDA) Steering Committee	Since 2013
	Past President of the Administrative Committee (AdCom) of the IEEE Geoscience and Remote Sensing Society (GRSS)	2011-2013
	Member of the Nominations & Appointments Committee, IEEE Aerospace and Electronic Systems Society, AESS	2012
	Principal Investigator for Tandem-L	Since 2008
	Member of the URSI National Commission F	Since 2007
	Principal Investigator for TanDEM-X	Since 2006
	Member of the ITG Fachausschuss 7.3 "Mikrowellentechnik"	Since 2005
	Member of the European Space Agency (ESA) Mission Advisory Group for Sentinel-1	2003-2016
	Member of the CEOS Working Group on Calibration & Validation (WGCV) SAR Subgroup	Since 2000
	Spokesman of the DLR Leadership Circle at Oberpfaffenhofen	2009-2011
Neff, Thomas	Member of NATO STO AVT-257-Best Practices for Risk Reduction for Overall Space Systems	2015-2016
	Member of NATO SET-147-Microsatellites and Surveillance of Space	2008-2014
	Chair of CEN/CLC/TC5 WG3 Earth Observation, DIN Standards Committee Aerospace	Since 2013
	Member of NATO SCI-ET 205-Emerging Space Systems Concepts	2011-2012
	Head of the Task Force 7, Standardisation of User Ground Segment Interfaces for Earth Observation Systems, CEN/BT/WG 202, ESA	2011-2012
Osipov, Andrey	Member of NATO STO SET-252- "Development of a Validation Model of a Stealth UCAV"	Since 2017
	Member of NATO STO SET-181-Metamaterials for Defence and Security Applications	2011-2013
	Member of the METAMORPHOSE (Virtual Institute for Artificial EM Materials and Metamaterials)	Since 2008
Papathanassiou, Konstantinos	Global Ecosystem Dynamics Investigation (GEDI) Science Team	Since 2016
	Member of the SAOCOM Expert Science Group, ESA	Since 2014
	Member of the HGF-Alliance "Remote Sensing and Earth System Dynamics" (EDA) Steering Committee	Since 2013
	Member of the ALOS Carbon & Kyoto Panel, JAXA	Since 2012
	Member of the ALOS-2 Cal-Val Panel, JAXA	Since 2012
	Member of the BIOMASS Mission Advisory Group, ESA	Since 2008
	Member of the Tandem-L Science Team	Since 2008
	Member of the Committee on Earth Observation Satellites (CEOS) Working Group on Calibration & Validation (WGCV) SAR Subgroup	Since 2000
Pardini, Matteo	Member of the SAOCOM Expert Science Group, ESA	Since 2015
Peichl, Markus	Member of NATO SET-238-Side-Attack Threat Detection Strategies, Technologies and Techniques	Since 2017
	Member of NATO SET-215-Model-based SAR Automatic Target Recognition	Since 2015

Name	Committee and Function	Years
Peichl, Markus	Member of VDI Technical Committee on Terahertz Systems	Since 2014
	Member of NATO SET-163-Aspects of Multi-Parameter Radar ATR in Complex Environments	2009-2014
	Member of NATO SET-135-High Performance Passive / Active Radiometric Millimeterwave Imaging using Thinned Arrays	2008-2011
Reigber, Sandra	Member of the HGF-Alliance "Remote Sensing and Earth System Dynamics" (EDA) Steering Committee	Since 2013
Reimann, Jens	Member of the Committee on Earth Observation Satellites (CEOS) Working Group on Calibration & Validation (WGCV) SAR Subgroup	Since 2015
Rodriguez-Cassola, Marc	Member of the SAOCOM Expert Science Group, ESA	Since 2016
Scheiber, Rolf	Member of the Committee on Earth Observation Satellites (CEOS) Working Group on Calibration & Validation (WGCV) SAR Subgroup	Since 2013
Schmidt, Kersten	Member of the Sentinel-1 Quality Working Group	Since 2015
	Member of the Committee on Earth Observation Satellites (CEOS) Working Group on Calibration & Validation (WGCV) SAR Subgroup	Since 2013
Schulze, Daniel	Member of the Committee on Earth Observation Satellites (CEOS) Working Group on Calibration & Validation (WGCV) SAR Subgroup	Since 2013
Schwerdt, Marco	Member of the Committee on Earth Observation Satellites (CEOS) Working Group on Calibration & Validation (WGCV) SAR Subgroup	Since 2000
Speck, Rainer	Member of NATO SET-145-Extraction of Geospatial Intelligence Information from Spaceborne SAR-Sensors	2009-2012
Steinbrecher, Ulrich	Member of the Technical/Scientific Council (WTR) of DLR	Since 2010
Süß, Helmut	Member of the scientific council of "Zentrum für Geoinformationswesen der Bundeswehr", ZGeoBw	2012-2015
	Chairman NATO Science and Technology Organization	2009-2012
	Member of NATO SET-145-Extraction of Geospacial Intelligence Information from Space Borne SAR Sensors	2009-2012
Thurner, Stefan	Member of the METAMORPHOSE (Virtual Institute for Artificial EM Materials and Metamaterials)	Since 2008
Weigt, Mathias	Member of the Committee on Earth Observation Satellites (CEOS) Working Group on Calibration & Validation (WGCV) SAR Subgroup	2011-2016
Younis, Marwan	Member of the Administrative Committee (AdCom) of the IEEE Geoscience and Remote Sensing Society (GRSS)	2017-2020
	Director of Corporate Relations, IEEE Geoscience and Remote Sensing Society (GRSS)	2015-2017
	Co-Chair of the IEEE Geoscience and Remote Sensing Society (GRSS) Technical Committee on Instrumentation and Future Technologies	Since 2016
	Chair of the IEEE Geoscience and Remote Sensing Society (GRSS) Technical Committee on Instrumentation and Future Technologies	2013-2015
	Lead of Active Microwave – Radar and SAR Working Group, IEEE GRSS Instrumentation and Future Technologies	2011-2012
	Member of the Committee on Earth Observation Satellites (CEOS) Working Group on Calibration & Validation (WGCV) SAR Subgroup	Since 2005
Zink, Manfred	Chair of the CEOS Working Group on Calibration & Validation (WGCV) SAR Subgroup	2011-2017
	Member of the TerraSAR-X/TanDEM-X Joint Steering Committee	2006-2015

3.8 Editorial Boards and Journal Reviews

Guest and Associate Editorships

Journal	Position	Years	Editor
IEEE Transactions on Geoscience and Remote Sensing (TGRS)	Associate Editor	Since 2005	Moreira, Alberto
		2012-2016	López-Dekker, Francisco
		since 2012	Krieger, Gerhard
IEEE Geoscience and Remote Sensing Letters (GRSL)	Associate Editor	Since 2011	Younis, Marwan
IEEE Geoscience and Remote Sensing Magazine (GRSM)	Associate Editor	Since 2012	Hajnsek, Irena
		2015-2017	Younis, Marwan
		2013-2015	Moreira, Alberto
IEEE Journal of Selected Topics in Applied Earth Observations and Remote Sensing (JSTARS)	Associate Editor	Since 2012	Hajnsek, Irena
SPIE Journal of Applied Remote Sensing	Associate Editor	2015	Papathanassiou, Kostas
Special Issue on the 2012 IGARSS, IEEE Journal of Selected Topics in Applied Earth Observations and Remote Sensing, 2013	Guest Editor	2013	Hajnsek, Irena
Special Issue "Advances in Antenna Array Processing for Radar" of the International Journal of Antennas and Propagation	Guest Editor	2013, 2014, 2015	Papathanassiou, Kostas
Special Issue "Advances in SAR and Radar Technology" , IEEE Journal of Selected Topics in Applied Earth Observations and Remote Sensing (JSTARS), 2015	Guest Editor	2015	Zink, Manfred
Special Issue on Synthetic Aperture Radar (SAR) – New Techniques, Missions and Applications, IEEE Journal of Selected Topics in Applied Earth Observations and Remote Sensing (JSTARS), 2016	Guest Editor	2016	Krieger, Gerhard; Moreira, Alberto; Zink, Manfred;
Final Report, NATO SCO AVT-257, Specialists' Meeting "Best Practices for Risk Reduction for Overall Space Systems"	Guest Editor	2016	Neff, Thomas
Transactions on Computational Imaging	Guest Editor	2016	Reigber, Andreas
Special Issue "Recent Advances in Polarimetric SAR Interferometry", Remote Sensing, 2017	Guest Editor	2017	Hajnsek, Irena

Journal Reviews

Journal Title	Journal Title
▪ Advances in Radio Science ▪ Canadian Journal of Remote Sensing (CJRS) ▪ European Journal of Remote Sensing (EJRS) ▪ Heliyon Journal, Elsevier ▪ Frequenz ▪ IEE Vision, Image and Signal Processing ▪ IEEE Aerospace and Electronic Systems Magazine (AESS) ▪ IEEE Antennas and Propagation Magazine ▪ IEEE Antennas and Wireless Propagation Letters (AWPL) ▪ IEEE Geoscience and Remote Sensing Letters (GRSL) ▪ IEEE Geoscience and Remote Sensing Magazine ▪ IEEE Journal of Selected Topics in Applied Earth Observations and Remote Sensing (JSTARS) ▪ IEEE Microwave and Components Letters (MWCL) ▪ IEEE Microwave and Wireless Components Letters ▪ IEEE Radar, Sonar & Navigation (RSN) ▪ IEEE Signal Processing Letters (SPL) ▪ IEEE Transactions on Aerospace and Electronic Systems (TAES) ▪ IEEE Transactions on Antennas and Propagation (TAP) ▪ IEEE Transactions on Geoscience and Remote Sensing (TGRS) ▪ IEEE Transactions on Image Processing (TIP) ▪ IEEE Transactions on Plasma Science (TPS) ▪ IEEE Transactions on Signal Processing (TSP) ▪ IEEE Transactions on Terahertz Science and Technology (TTST) ▪ IET Proceedings – Radar, Sonar & Navigation ▪ International Journal of Antennas and Propagation (IJAP) ▪ International Journal of Digital Earth ▪ International Journal of Remote Sensing (IJRS) ▪ International Journal on Infrared, Millimeter and Terahertz Waves ▪ SPRS Journal of Photogrammetry and Remote Sensing ▪ Journal of Aerospace Technology and Management (JATM)	▪ Journal of Applied Physics (JAP) ▪ Journal of Applied Sciences ▪ Journal of Electromagnetic Waves and ApplicationsJournal of Electronic Imaging ▪ Journal of EM Waves and Applications (PIER-JEMWA) ▪ Journal of Geophysical Research (JGR) ▪ Journal of Hydrology ▪ Journal of Infrared, Millimeter, and Terahertz Waves (IMTW) ▪ Journal of Mechanics and Applied Mathematics (QJMAM) ▪ Journal of Microwaves, Optoelectronics and EM Applications (JMOe) ▪ Journal of Modern Optics ▪ Journal of Physics and Chemistry of the Earth (JPCE) ▪ Journal of Sound and Vibration ▪ Journal on Advances in Signal Processing (EURASIP) ▪ MDPI Remote Sensing ▪ MDPI Sensors ▪ Natural Hazards and Earth System Sciences (NHESS) ▪ Optical Engineering ▪ Photogrammetrie, Fernerkundung, Geoinformation (PFG) ▪ PLOS ONE Journal ▪ Proceedings of the IEEE Progress In Electromagnetics Research (PIER) ▪ Radio Science ▪ Remote Sensing Letters (RSL) ▪ Remote Sensing of Environment (ERS) ▪ Results in Physics (RINP) ▪ Science of the Total Environment (STOTEN) ▪ SIAM Journal of Applied Mathematics (SIAP) ▪ Water Resources Research ▪ Wave Motion

3.9 Project Review Panel Members

Project Review	Reviewer	Year
HRWS Mission Definition Review (MDR)	Zink, Manfred Neff, Thomas	May 2017
Sentinel-1B Flight Acceptance Review (FAR)	Zink, Manfred	January 2016
Sentinel-1A Qualification and Flight Acceptance Review (QAR + FAR)	Zink, Manfred	January 2014
GOSSAMER Preliminary Design Review (PDR)	Zink, Manfred	June 2013
TerraSAR-X2 Preliminary Requirements Review (PRR)	Zink, Manfred	March 2012
GMES Sentinel-1 Commissioning Phase Calibration and Performance Analysis Facility, Critical Design Reviews (CDR)	Schwerdt, Marco	November 2011
GMES Sentinel-1 Commissioning Phase Calibration and Performance Analysis Facility, Preliminary Design Review (PDR)	Schwerdt, Marco	June 2011
NASA, Terrestrial Ecology Program, Research Proposal Reviewer	Papathanassiou, Konstantinos Pardini, Matteo	2013, 2014

3.10 Airborne SAR Campaigns

Campaign (Acronym)	Field Phase	Region	Brief Description
17TMPSAR	May 2017	Traunstein, Froschham	F-SAR – dual-frequency SAR tomography
17SARTOM	May 2017	Traunstein, Froschham	F-SAR – dual-frequency SAR tomography
17OP17AF	May-June 2017	Kaufbeuren	F-SAR – instrument calibration
17DBFTST	March, October 2017	Kaufbeuren, Starnberger See	DBFSAR – instrument functional tests
17ATRSAR	June 2017	Oksboel, Denmark	F-SAR – multi-frequency polarimetric imaging and change detection (under contract by Terma A/S)
16VABENE	June 2016	Osterseen, Simbach-Rott, Scharhoern, Cuxhaven & Helgoland	F-SAR – natural disaster monitoring, ship traffic monitoring & high-resolution imaging
16TMPSAR	June 2016	Traunstein, Froschham & Haspelmoor	F-SAR – multi-temporal Pol-InSAR measurements
16OP16CF	Oct.-Nov. 2016	Kaufbeuren, Starnberger See	F-SAR – instrument calibration
16OP16BF	June 2016	Kaufbeuren	F-SAR – instrument calibration
16OP16AF	January, March 2016	Kaufbeuren	F-SAR – instrument calibration
16FOREST	Oct.-Nov. 2016	Bayrischer Wald	F-SAR – dual-frequency tomographic SAR trials on forest on difficult terrain
16DBFTST	Nov.-Dec. 2016	Kaufbeuren	DBFSAR – instrument functional tests
16AFRISR	February 2016	La Lopé NP, Mondah, Rabi, Mabounie, Pongara NP, Nkok, Gabon	F-SAR trials in Gabon for BIOMASS (ESA) and Tandem-L (DLR) spaceborne SAR missions ; L-P dual-frequency Pol-InSAR and tomography SAR measurements (in cooperation with ESA, ONERA, AGEOS & NASA)
15TMPSAR	June, October 2015	Traunstein, Stadtrodaer Wald	F-SAR – multi-temporal Pol-InSAR measurements
15SOIMEX	July 2015	Ammer catchment	TERENO; F-SAR trials on soil moisture estimation
15OP15BF	October 2015	Kaufbeuren	F-SAR – instrument calibration
15OP15AF	Feb.-July 2015	Kaufbeuren & Voralpen	F-SAR – instrument calibration
15ICESAR	March 2015	Findel glacier, Switzerland	F-SAR – multi-temporal, dual-frequency tomographic SAR trials on snow and ice; Part 2
15ICELND	June 2015	Skjaldbreidur, Vogar, Central Rift, Katla, Bardarbunga, Iceland	F-SAR – multi-frequency interferometric SAR trials on volcanic rock and glaciers (in cooperation with NASA)
15CROPEX	July 2015	Wallerfing	F-SAR – multi-frequency tomographic SAR trials on agricultural crops
15ARCTIC	Apr.-May 2015	Southern Greenland & Davis Strait	F-SAR – multi-frequency, Pol-InSAR and tomography trials on Greenlandic ice and glaciers & sea ice (in cooperation with DALO)
14VABENE	May-June 2014	Nuerburg Ring	VABENE; F-SAR traffic monitoring and change detection trials ('Rock am Ring')
14TMPSAR	May-Oct. 2014	Traunstein, Hohes Holz, Blauberge	F-SAR – multi-temporal, multi-frequency tomographic SAR trials on forests
14OP14AF	May-Oct. 2014	Kaufbeuren	F-SAR – instrument calibration
14ICESAR	September 2014	Rhone & Findel glaciers, Switzerland	F-SAR – multi-temporal, dual-frequency tomographic SAR trials on snow and ice; Part 1
14DALOEX	October 2014	Sjaellands Odde, Great Belt Bridge, Denmark	F-SAR trials on polarimetric imaging and change detection (under contract by DALO)

Campaign (Acronym)	Field Phase	Region	Brief Description
14CROPEX	May-Sept. 2014	Wallerfing	F-SAR – multi-temporal, multi-frequency tomographic SAR trials on agricultural crops
14ARCHEO	May 2014	Eining a.d. Donau, Erlstaett	F-SAR – radar archaeology
13VABENE	Oct.-Nov. 2013	Greifenberg, Inning, Kaufbeuren	VABENE; F-SAR traffic monitoring trials; OBP tests
13TOPSAR	April, July 2013	Jadebusen, Juist	F-SAR trials on SAR interferometry for high-resolution DEM generation of coastal wetlands (under contract by BfG)
13TMPSAR	April, May, July 2013	Traunstein, Stadtrodaer Wald	F-SAR – multi-temporal Pol-InSAR measurements
13SWISAR	October 2013	Memmingen, Kaufbeuren; Meiringen, Haerkingen, Rapperswil, Mt. Crosin, Cressier & Goesgen, Switzerland	F-SAR trials on traffic monitoring, change detection and circular SAR imaging (contract by armasuisse)
13SOIMEX	Apr.-May 2013	Rur, Bode & Ammer catchments, Jülich, Monschau	F-SAR multi-temporal trials on soil moisture estimation; L-band SAR combined with PLMR & Thermal Camera (under contract by FZ Juelich)
13SNWSAR	March 2013	Leutasch, Rotmoostal & Mittelbergferner, Austria	F-SAR experiment on Snow and Ice; linked to the CoReH2O mission (ESA); Part 2
13OP13CF	October 2013	Kaufbeuren	F-SAR – instrument calibration
13OP13BF	July 2013	Kaufbeuren	F-SAR – instrument calibration
13OP13AF	Mar.-May 2013	Kaufbeuren	F-SAR – instrument calibration
13CRSORB	April 2013	Kaufbeuren	'Crossing Orbits' tomographic SAR experiment
13CROPEX	March, July 2013	Wallerfing	F-SAR Pol-InSAR trials on agricultural crops
12VABENE	July 2012	Kaufbeuren, Neugablonz, Kaltenberg	VABENE; F-SAR traffic monitoring trials
12TOPSAR	April, November 2012	Jadebusen, Juist, Wilhelmshaven	F-SAR trials on SAR interferometry for high-res DEM generation of coastal wetlands (contract by BfG)
12TMPSAR	November 2012	Traunstein	F-SAR – Multi-temporal Pol-InSAR measurements
12SOIMEX	May 2012	Bode, Ammer & Uecker catchments, Jülich, Monschau	TERENO; F-SAR trials on soil moisture estimation
12SNWSAR	November 2012	Leutasch, Rotmoostal & Mittelbergferner, Austria	F-SAR experiment on Snow and Ice; linked to the CoReH2O mission (ESA); Part 1
12OP12DF	November 2012	Kaufbeuren	F-SAR – instrument calibration
12OP12CF	July 2012	Kaufbeuren, Ammer Catchment	F-SAR – tests incl. PLMR and Thermal Camera
12OP12BF	May 2012	Kaufbeuren	F-SAR – tests incl. PLMR and Thermal Camera
12OP12AF	March 2012	Vordemwald, Switzerland	F-SAR – first P-band instrument tests
11VABENE	July, November 2011	Divers sites in Bavaria	VABENE; F-SAR traffic monitoring trials
11TMPSAR	June 2011	Traunstein	F-SAR – multi-temporal Pol-InSAR measurements
11TDXUFL	November 2011	Kaufbeuren	F-SAR – TDX bi-static SAR experiment
11SOIMEX	May-June 2011	Rur, Bode & Ammer catchments	TERENO; F-SAR trials on soil moisture estimation
11OP11CF	November 2011	Kaufbeuren	F-SAR – interferometry and mosaicking
11OP11BF	September 2011	Kaufbeuren	F-SAR – instrument calibration
11OP11AF	May-June 2011	Kaufbeuren	F-SAR – L-band instrument calibration
11CIRCUS	June 2011	Kaufbeuren	F-SAR – first L-band circular SAR experiment

3.11 Spaceborne Calibration Campaigns

Mission	Topic / Subject	Customer	Years
Sentinel-1A/B Routine Operation	DLR calibration support for routine operation of Sentinel-1 A/B constellation	ESA/ESRIN	since October 2016
Sentinel-1B Commissioning Phase	Independent SAR system calibration, South Germany	ESA/ESTEC	Apr.-Sept. 2016
TerraSAR-X, TanDEM-X	Calibration campaign for the dual receive antenna (DRA) mode, South Germany	DLR	Jan.-Feb. 2015
Sentinel-1A Routine Operation	DLR calibration support for Sentinel-1A routine operation	ESA/ESRIN	since October 2014
Sentinel-1A Commissioning Phase	Independent SAR system calibration, South Germany	ESA/ESTEC	Apr.-Sept. 2014

3.12 Patents

Inventors	Patent Title	Patent No.	Prio	Patent granted on	Countries
Baumgartner, S., Schaefer, C.	Synthetic Aperture Radar for Simultaneous Imaging and Moving Target Detection	EP000002725382B1	■	18 January 2017	EP
Mittermayer, J., **López-Dekker, F.**, **Prats-Iraola, P.**, **Kraus, T.**, **Krieger, G.**, **Moreira, A.**	Verfahren zur Erstellung eines Erdbeobachtungsbildes einer Region mittels eines Radars mit synthetischer Apertur	DE102016209803B3	■	12 October 2017	DE
Queiroz de Almeida, F., **Younis, M.**, **Krieger, G.**, **López-Dekker, F.**, **Moreira, A.**	Synthetik-Apertur-Radarverfahren und Synthetik-Apertur-Radarvorrichtung	DE102016208899B3	■	08 June 2017	DE
Reimann, J., **Döring, B.**, **Schwerdt, M.**, **Rudolf, D.**, **Raab, S.**	Verfahren zur Kalibrierung eines aktiven Sensorsystems	DE102016101898B3	■	13 April 2017	DE
Huber, S., **Krieger, G.**, **Younis, M.**	Reflector Antenna for a Synthetic Aperture Radar	EP000002735055B1	■	10 February 2016	DE
		US000009531081B2	-	27 December 2016	US
Martone, M., **Krieger, G.**, **Bräutigam, B.**	Verfahren und Vorrichtung zur rechnergestützten Verarbeitung von SAR-Rohdaten	DE102012209113B4	■	02 June 2016	DE
Villano, M., **Krieger, G.**, **Moreira, A.**	Synthetik-Apertur-Radarverfahren und Synthetik-Apertur-Radarvorrichtung	DE102012219225B4	■	04 August 2016	DE
Döring, B., **Schwerdt, M.**, **Jirousek, M.**, **Rudolf, D.**, **Reimann, J.**, **Raab, S.**	Method for Absolute Radiometric Calibration of the Radar Cross-Section of Radar Targets	DE102014110079B3	■	09 July 2015	DE
Hounam, D., **Limbach, M.**	Method for Localizing Objects by Means of an Imaging Radar System and Transponder for Localizing Objects by Means of such Radar Systems	EP000002018578B1	■	09 September 2015	EP

Inventors	Patent Title	Patent No.	Prio	Patent granted on	Countries
Peichl, M., **Dill, S.**, **Albers, T.**	Inverses Synthetisches Apertur Radar (ISAR) und Verfahren zur Erfassung von Verunreinigungen in einem Material	DE102014106892B3	■	22 October 2015	DE
de Florio, S.	Monitoring Data Delivery System for Earth Monitoring Satellite, has Small/Micro Courier Satellite Provided as Inter Satellite Connection for Delivery of Command from Earth Station to Monitoring Satellite or for Bridging Satellites	DE102008006432B4	■	31 December 2014	DE
Rodríguez-Cassola, M., Pinheiro, M., Prats-Iraola, P., Krieger, G.	Method for the Computer-Assisted Processing of SAR Data	DE102013213304B3	■	04 September 2014	DE
Younis, M., **Bordoni, F.**, **Krieger, G.**, **López-Dekker, F.**, **De Zan, F.**	Synthetic Aperture Radar Method	DE102013221756B3	■	16 October 2014	DE
Brand, B., Zehetbauer, T.	Method for Reducing the Data Age of Image Products Obtained by Earth Observation Satellites	FR000002893794B1	-	15 February 2013	FR
López Martinez, C., **Papathanassiou, K.**	Method for Estimating the Topography of the Earth's Surface in Areas with Plant Cover	ES000002384922B1	■	11 June 2013	ES
Peichl, M., **Dill, S.**, **Jirousek, M., Berthel , D.**	Device for Two-Dimensional Imaging of Scenes by Microwave Scanning	EP000002099095B1	-	20 November 2013	EP
Gebert, N., **Krieger, G.**	Synthetic Aperture Radar Process	US000008134490B2	-	13 March 2012	US
Scheiber, R.	Method for Examining an Ice Region or Dry Region Using Radar Echo Sounding	US000008159384B2	-	17 April 2012	US
Gebert, N., Krieger, G.	Synthetic Aperture Radar Process	EP000002191297B1	-	02 March 2011	EP
Krieger, G., Gebert, N., Moreira, A.	High-Resolution Synthetic Aperture Side View Radar System Used By Means of Digital Beamforming	US000007944390B2	-	17 May 2011	US
Krieger, G., Gebert, N., Moreira, A.	High-Resolution Synthetic Aperture Side View Radar System Used By Means of Digital Beamforming	EP000002018577B1	■	27 April 2011	EP
Peichl, M., Dill, S., Jirousek, M., Berthel , D.	Device for Two-Dimensional Imaging of Scenes by Microwave Scanning	US000008009116B2	-	30 August 2011	US
Prats Iraola, P., Mittermayer, J., Scheiber, R., Moreira, A.	Method for Processing TOPS (Terrain Observation by Progressive Scan)-SAR (Synthetic Aperture Radar)-Raw Data	US000008049657B2	-	01 November 2011	US
Scheiber, R.	Method for Examining an Ice Region or Dry Region Using Radar Echo Sounding	EP000002130062B1	-	31 August 2011	EP

Bold face = HR Institute employees, Christoph Schäfer is with Airbus Defence and Space, Germany, and Carlos López Martinez is with University Catalunya Politechnica, Spain.

Prio = Priority establishing patent, EP = European Patent, DE = German Patent, FR = French Patent, ES = Spanish Patent, US = US Patent

3.13 Publications

The list of publications is organized as follows:

[J-] Publications in ISI or Scopus Journals
[NJ-] Publications in Non-ISI-Scopus Journals
[B-] Books and Book Chapters
[IC-] Invited Conference Contributions
[RC-] Regular Conference Contributions
[R-] Technical and Project Reports
[PhD-] Doctoral Theses
[MaT-] Diploma and Master Theses
[P-] Patents

The number of publications from 2011 to 2017 totals 1844. The complete list of publications including year 2018 can be found on the website of the Institute www.dlr.de/hr/publications.

Authors of the Institute in the list below are marked in boldface.

Publications in ISI or Scopus Journals

2017

[J-1] **Barros Cardoso da Silva, A.**, **Baumgartner, S.**, Novel Post-Doppler STAP with a Priori Knowledge Information for Traffic Monitoring Applications: Basic Idea and First Results, *Advances in Radio Sci. – Kleinheubacher Berichte*, pp. 77-82, 2017.

[J-2] **Brancato, V.**, Liebisch, F., **Hajnsek, I.**, Impact of Plant Surface Moisture on Differential Interferometric Observables: A Controlled Electromagnetic Experiment, *IEEE Trans. Geosci. Rem. Sens.*, 55(7), pp. 3949-3964, 2017.

[J-3] **Bueso Bello, J.**, **Martone, M.**, **Prats Iraola, P.**, **Gonzalez, C.**, **Kraus, T.**, **Reimann, J.**, **Jäger, M.**, **Bräutigam, B.**, **Rizzoli, P.**, **Zink, M.**, Performance Analysis of TanDEM-X Quad Polarization Products in Pursuit Monostatic Mode, *IEEE Journal of Selected Topics in Applied Earth Observations and Remote Sensing*, 10(5), pp. 1853-1869, 2017.

[J-4] Dierking, W., Lang, O., **Busche, T.**, Sea Ice Local Surface Topography from Single-Pass Satellite InSAR Measurements: A Feasibility Study, *The Cryosphere*, 11(4), pp. 1967-1985, 2017.

[J-5] Ren, Y., Li, X., Gao, G., **Busche, T.**, Derivation of Sea Surface Tidal Current From Spaceborne SAR Constellation Data, *IEEE Trans. Geosci. Rem. Sens.*, 55(6), pp. 3236-3247, 2017.

[J-6] Johansson, M., King, J., Doulgeris, A., Gerland, S., Singha, S., Spreen, G., **Busche, T.**, Combined Observations of Arctic Sea Ice with Near-Coincident Co-Located X, C and L-Band SAR Satellite Remote Sensing and Helicopter-borne Measurements, *J. Geophys. Res. - Oceans*, 122(1), pp. 669-691, 2017.

[J-7] **Cazcarra Bes, V.**, **Tello Alonso, M.**, Fischer, R., Heym, M., **Papathanassiou, K.**, Monitoring of Forest Structure Dynamics by Means of L-Band SAR Tomography, *Remote Sensing*, 9(1229), 2017.

[J-8] Yuzugullu, O., **Erten, E.**, **Hajnsek, I.**, A Multi-Year Study on Rice Morphological Parameter Estimation with X-Band Polsar Data, *Applied Sciences*, 7 (6)(602), 2017.

[J-9] Yuzugullu, O., Marelli, S., **Erten, E.**, **Hajnsek, I.**, Determining Rice Growth Stage with X-Band SAR: A Metamodel-Based Inversion, *Remote Sensing*, 9(460), 2017.

[J-10] Yuzugullu, O., **Erten, E.**, **Hajnsek, I.**, Estimation of Rice Crop Height from X- and C-Band PolSAR by Metamodel-Based Optimization, *IEEE Journal of Selected Topics in Applied Earth Observations and Remote Sensing*, 10(1), pp. 194-204, 2017.

[J-11] **Fischer, J.**, On the Duality of Regular and Local Functions, *Mathematics*, 5(41), pp. 1-14, 2017.

[J-12] Lucas, C., Leinss, S., Bühler, Y., Marino, A., **Hajnsek, I.**, Multipath Interferences in Ground-Based Radar Data: A Case Study, *Remote Sensing*, 9(12), 2017.

[J-13] Zwieback, S., **Hajnsek, I.**, Edwards-Smith, A., Morrison, K., Depth-Resolved Backscatter and Differential Interferometric Radar Imaging of Soil Moisture Profiles: Observations and Models of Subsurface Volume Scattering, *IEEE Journal of Selected Topics in Applied Earth Observations and Remote Sensing*, 10(7), pp. 3281-3296, 2017.

[J-14] Round, V., Leinss, S., Huss, M., Haemmig, C., **Hajnsek, I.**, Surge Dynamics and Lake Outbursts of Kyagar Glacier, Karakoram, *The Cryosphere*, 11(2), pp. 723-739, 2017.

[J-15] Seppänen, J., Antropov, O., **Jagdhuber, T.**, Hallikainen, M., Heiskanen, J., Praks, J., Improved Characterization of Forest Transmissivity within the L-MEB Model Using Multisensor SAR Data, *IEEE Geosci. Rem. Sens. Lett.*, 14(8), pp. 1408-1412, 2017.

[J-16] Ullmann, T., Banks, S., Schmitt, A., **Jagdhuber, T.**, Scattering Characteristics of X-, C- and L-Band PolSAR Data Examined for the Tundra Environment of the Tuktoyaktuk Peninsula, Canada, *Applied Sciences*, 7(6), pp. 1-28, 2017.

[J-17] **Jörg, H.**, **Pardini, M.**, **Hajnsek, I.**, **Papathanassiou, K.**, On the Separation of Ground and Volume Scattering Using Multibaseline SAR Data, *IEEE Geosci. Rem. Sens. Lett.*, 14(9), pp. 1570-1574, 2017.

[J-18] **Kim, J.**, **Papathanassiou, K.**, Sato, H., Quegan, S., Detection and Estimation of Equatorial Spread F Scintillation Using Synthetic Aperture Radar, *IEEE Trans. Geosci. Rem. Sens.*, 55(12), pp. 6713-6725, 2017.

[J-19] Bohleber, P., Sold, L., Hardy, D., Schwikowski, M., **Klenk, P.**, Fischer, A., Sirguey, P., Cullen, N., Potocki, M., Hoffmann, H., Mayewski, P., Ground-Penetrating Radar Reveals Ice Thickness and Undisturbed Englacial Layers at Kilimanjaro's Northern Ice Field, *The Cryosphere*, 11(1), pp. 469-482, 2017.

[J-20] Tian, J., Schneider, T., Straub, C., **Kugler, F.**, Reinartz, P., Exploring Digital Surface Models from Nine Different Sensors for Forest Monitoring and Change Detection, *Remote Sensing*, 9(3), 2017.

[J-21] **Li, D.**, **Rodríguez Cassolà, M.**, **Prats Iraola, P.**, Wu, M., **Moreira, A.**, Reverse Backprojection Algorithm for the Accurate Generation of SAR Raw Data of Natural Scenes, *IEEE Geosci. Rem. Sens. Lett.*, 14(11), pp. 2072-2076, 2017.

[J-22] **Li, D.**, **Rodríguez Cassolà, M.**, **Prats Iraola, P.**, Dong, Z., Wu, M., **Moreira, A.**, Modelling of Tropospheric Delays in Geosynchronous Synthetic Aperture Radar, *Science China Information Sciences*, 2017.

[J-23] **Martone, M.**, **Gonzalez, C.**, **Bueso Bello, J.**, **Bräutigam, B.**, Bandwidth Considerations for Interferometric Applications Based on TanDEM-X, *IEEE Geosci. Rem. Sens. Lett.*, 14(2), pp. 203-207, 2017.

[J-24] **Özis, E.**, **Osipov, A.**, Eibert, T., Physical Optics and Full-Wave Simulations of Transmission of Electromagnetic Fields through Electrically Large Planar Meta-sheets, *Advances in Radio Sci.*, pp. 29-35, 2017.

[J-25] **Özis, E.**, **Osipov, A.**, Eibert, T., Metamaterials for Microwave Radomes and the Concept of a Meta-Radome: Review of the Literature, *Int. J. Antenn. Propag.*, 2017(135610), pp. 1-13, 2017.

[J-26] Steele-Dunne, S., McNairn, H., Monsivais-Huertero, A., Judge, J., Liu, P., **Papathanassiou, K.**, Radar Remote Sensing of Agricultural Canopies: A Review, *IEEE Journal of Selected Topics in Applied Earth Observations and Remote Sensing*, 10(5), pp. 2249-2273, 2017.

[J-27] **Pardini, M.**, **Papathanassiou, K.**, On the Estimation of Ground and Volume Polarimetric Covariances in Forest Scenarios with SAR Tomography, *IEEE Geosci. Rem. Sens. Lett.*, 14(10), pp. 1860-1864, 2017.

[J-28] **Pinheiro, M.**, **Reigber, A.**, **Moreira, A.**, Large-Baseline InSAR for Precise Topographic Mapping: a Framework for TanDEM-X Large-Baseline Data, *Advances in Radio Sci.*, pp. 231-241, 2017.

[J-29] Nikkhoo, M., Walter, T., Lundgren, P., **Prats Iraola, P.**, Compound Dislocation Models (CDMs) for Volcano Deformation Analyses, *Geophysical Journal International*, 208(2), pp. 877-894, 2017.

[J-30] **Reimann, J.**, **Schwerdt, M.**, **Schmidt, K.**, **Tous Ramon, N.**, **Castellanos Alfonzo, G.**, **Döring, B.**, **Rudolf, D.**, **Raab, S.**, **Walter Antony, J.**, **Zink, M.**, The DLR Spaceborne SAR Calibration Center, *Frequenz*, 2017.

[J-31] **Rizzoli, P.**, **Martone, M.**, **Gonzalez, C.**, **Wecklich, C.**, **Borla Tridon, D.**, **Bräutigam, B.**, **Bachmann, M.**, **Schulze, D.**, Fritz, T., Huber, M., Wessel, B., **Krieger, G.**, **Zink, M.**, **Moreira, A.**, Generation and Performance Assessment of the Global TanDEM-X Digital Elevation Model, *ISPRS Journal of Photogrammetry and Remote Sensing*, no.132, pp. 119-139, 2017.

[J-32] **Rizzoli, P.**, **Martone, M.**, Rott, H., **Moreira, A.**, Characterization of Snow Facies on the Greenland Ice Sheet Observed by TanDEM-X Interferometric SAR Data, *Remote Sensing*, 2017.

[J-33] Mao, C., Gao, S., Luo, Q., **Rommel, T.**, Chu, Q., Low-Cost X/Ku/Ka-Band Dual-Polarized Array with Shared Aperture, *IEEE Trans. Antenn. Propag.*, 65(7), pp. 3520-3527, 2017.

[J-34] **Schwerdt, M.**, **Schmidt, K.**, **Tous Ramon, N.**, **Klenk, P.**, **Yague-Martinez, N.**, **Prats Iraola, P.**, **Zink, M.**, Geudtner, D., Independent System Calibration of Sentinel-1B, *Remote Sensing*, 9(6), 2017.

[J-35] Mao, C., Gao, S., **Tienda Herrero, C.**, **Rommel, T.**, **Patyuchenko, A.**, **Younis, M.**, Boccia, L., Arnieri, E., Glisic, S., Yodprasit, U., Penkala, P., Krstic, M., Qin, F., Schrape, O., Koczor, A., Amendola, G., Petrovic, V., X/Ka-Band Dual-Polarized Digital Beamforming Synthetic Aperture Radar, *IEEE Transactions on Microwave Theory and Techniques*, 65(11), pp. 4400-4407, 2017.

[J-36] **Villano, M.**, **Krieger, G.**, **Jäger, M.**, **Moreira, A.**, Staggered SAR: Performance Analysis and Experiments with Real Data, *IEEE Trans. Geosci. Rem. Sens.*, 55(11), pp. 6617-6638, 2017.

[J-37] **Villano, M.**, **Krieger, G.**, **Moreira, A.**, New Insights into Ambiguities in Quad-Pol SAR, *IEEE Trans. Geosci. Rem. Sens.*, 55(6), pp. 3287-3308, 2017.

[J-38] Koppel, K., Zalite, K., **Voormansik, K.**, **Jagdhuber, T.**, Sensitivity of Sentinel-1 Backscatter to Characteristics of Buildings, *Int. J. Rem. Sens.*, 38(22), pp. 6298-6318, 2017.

[J-39] **Wollstadt, S.**, **López-Dekker, F.**, De Zan, F., **Younis, M.**, Design Principles and Considerations for Spaceborne ATI SAR-Based Observations of Ocean Surface Velocity Vectors, *IEEE Trans. Geosci. Rem. Sens.*, 55(8), pp. 4500-4519, 2017.

[J-40] **Yague-Martinez, N.**, De Zan, F., **Prats Iraola, P.**, Coregistration of Interferometric Stacks of Sentinel-1 TOPS Data, *IEEE Geosci. Rem. Sens. Lett.*, 14(7), pp. 1002-1006, 2017.

2016

[J-41] **Abdullahi, S.**, **Kugler, F.**, Pretzsch, H., Prediction of Stem Volume in Complex Temperate Forest Stands Using TanDEM-X SAR Data, *Remote Sensing of Environment*, no.174, pp. 197-211, 2016.

[J-42] **Baumgartner, S.**, **Krieger, G.**, Dual-Platform Large Along-Track Baseline GMTI, *IEEE Trans. Geosci. Rem. Sens.*, 54(3), pp. 1554-1574, 2016.

[J-43] **Bueso Bello, J.**, **Martone, M.**, **Prats Iraola, P.**, **Bräutigam, B.**, First Characterization and Performance Evaluation of Bistatic TanDEM-X Experimental Products, *IEEE Journal of Selected Topics in Applied Earth Observations and Remote Sensing*, 9(3), pp. 1058-1071, 2016.

[J-44] **Döring, B.**, **Schwerdt, M.**, The SAR Passband Problem: Analytical Model and Possible Practical Solutions, *IEEE Trans. Geosci. Rem. Sens.*, 54(3), pp. 1647-1658, 2016.

[J-45] **Erten, E.**, Lopez-Sanchez, J., Yuzugullu, O., **Hajnsek, I.**, Retrieval of Agricultural Crop Height from Space: A Comparison of SAR Techniques, *Remote Sensing of Environment*, pp. 130 -144, 2016.

[J-46] **Gramini Ganesan, P.**, **Jagdhuber, T.**, **Hajnsek, I.**, **Rao, Y.**, Soil-Moisture Estimation Using Hybrid Polarimetric SAR Data of RISAT-1, *IEEE Trans. Geosci. Rem. Sens.*, 54(4), pp. 2033-2049, 2016.

[J-47] Round, V., Leinss, S., Huss, M., Haemmig, C., **Hajnsek, I.**, Surge Dynamics and Lake Outbursts of Kyagar Glacier, Karakoram, *The Cryosphere*, 2016.

[J-48] Wolf, B., Chwala, C., Fersch, B., Garvelmann, J., Junkermann, W., Zeeman, M., Angerer, A., Adler, B., Beck, C., Brosy, C., Brugger, P., Emeis, S., Dannenmann, M., DeRoo, F., Diaz-Pines, E., Haas, E., Hagen, M., **Hajnsek, I.**, Jacobeit, J., **Jagdhuber, T.**, Kalthoff, N., Kiese, R., Kunstmann, H., Kosak, O., Krieg, R., Malchow, C., Mauder, M., Merz, R., Notarnicola, C., Philipp, A., Reif, W., Reineke, S., Rödiger, T., Rühr, N., Schäfer, K., Schrön, M., Senatore, A., Shupe, H., Völksch, I., Wanninger, C., Zacharias, S., Schmid, H., The ScaleX Campaign: Scale-Crossing Land-surface and Boundary Layer Processes in the TERENO-PreAlpine Observatory, *Bulletin of the American Meteorological Society*, pp. 1-51, 2016.

[J-49] Zwieback, S., Liu, X., Antonova, S., Heim, B., Bartsch, A., Boike, J., **Hajnsek, I.**, A Statistical Test of Phase Closure to Detect Influences on DInSAR Deformation Estimates Besides Displacements and Decorrelation Noise: Two Case Studies in High-Latitude Regions, *IEEE Trans. Geosci. Rem. Sens.*, 54(9), pp. 5588-5601, 2016.

[J-50] Pichierri, M., **Hajnsek, I.**, **Papathanassiou, K.**, A Multibaseline Pol-InSAR Inversion Scheme for Crop Parameter Estimation at Different Frequencies, *IEEE Trans. Geosci. Rem. Sens.*, 54(8), pp. 4952-4970, 2016.

[J-51] Siddique, M., Wegmuller, U., **Hajnsek, I.**, Frey, O., Single-Look SAR Tomography as an Add-On to PSI for Improved Deformation Analysis in Urban Areas, *IEEE Trans. Geosci. Rem. Sens.*, 54(10), pp. 6119-6137, 2016.

[J-52] Zwieback, S., **Hajnsek, I.**, Influence of Vegetation Growth on the Polarimetric Zero-Baseline DInSAR Phase Diversity – Implications for Deformation Studies, *IEEE Trans. Geosci. Rem. Sens.*, 54(5), 2016.

[J-53] **Heine, I.**, **Jagdhuber, T.**, Itzerott, S., Classification and Monitoring of Reed Belts Using Dual-Polarimetric TerraSAR-X Time Series, *Remote Sensing*, 8(552), pp. 1-24, 2016.

[J-54] Ullmann, T., Schmitt, A., **Jagdhuber, T.**, Two Component Decomposition of Dual Polarimetric HH/VV SAR Data: Case Study for the Tundra Environment of the Mackenzie Delta Region, Canada, *Remote Sensing*, 8(1027), pp. 1-24, 2016.

[J-55] **Jagdhuber, T.**, An Approach to Extended Fresnel Scattering for Modeling of Depolarizing Soil-Trunk Double-Bounce Scattering, *Remote Sensing*, 8(818), pp. 1-25, 2016.

[J-56] Wang, H., Magagi, R., Goita, K., **Jagdhuber, T.**, **Hajnsek, I.**, Evaluation of Polarimetric Decomposition for Soil Moisture Retrieval over Vegetated Agricultural Fields, *Remote Sensing*, 8(142), pp. 1-38, 2016.

[J-57] Montzka, C., **Jagdhuber, T.**, **Horn, R.**, Bogena, H., **Hajnsek, I.**, **Reigber, A.**, Vereecken, H., Investigation of SMAP Fusion Algorithms with Airborne Active and Passive L-Band Microwave Remote Sensing, *IEEE Trans. Geosci. Rem. Sens.*, 54(7), pp. 3878-3889, 2016.

[J-58] **Kraus, T.**, **Bräutigam, B.**, **Mittermayer, J.**, **Wollstadt, S.**, **Grigorov, C.**, TerraSAR-X Staring Spotlight Mode Optimization and Global Performance Predictions, *IEEE Journal of Selected Topics in Applied Earth Observations and Remote Sensing*, 9(3), pp. 1015-1027, 2016.

[J-59] **López-Dekker, F.**, **Rodriguez-Cassola, M**, De Zan, F., **Krieger, G.**, **Moreira, A.**, Correlating Synthetic Aperture Radar (CoSAR), *IEEE Trans. Geosci. Rem. Sens.*, vol. 54, no. 4, pp. 2268-2284, April 2016

[J-60] **Martone, M.**, **Rizzoli, P.**, **Krieger, G.**, Volume Decorrelation Effects in TanDEM-X Interferometric SAR Data, *IEEE Geosci. Rem. Sens. Lett.*, 13(12), pp. 1812-1816, 2016.

[J-61] **Martone, M.**, **Bräutigam, B.**, **Rizzoli, P.**, **Yague-Martinez, N.**, **Krieger, G.**, Enhancing Interferometric SAR Performance over Sandy Areas: Experience from the TanDEM-X Mission, *IEEE Journal of Selected Topics in Applied Earth Observations and Remote Sensing*, 9(3), pp. 1036-1046, 2016.

[J-62] **Mittermayer, J.**, **Kraus, T.**, **López-Dekker, F.**, **Prats Iraola, P.**, **Krieger, G.**, **Moreira, A.**, Wrapped Staring Spotlight SAR, *IEEE Trans. Geosci. Rem. Sens.*, Vol 54(10), pp. 5745-5764, 2016.

[J-63] Xu, F., Ya-Qiu, L., **Moreira, A.**, A Preliminary Study on SAR Advanced Information Retrieval and Scene Reconstruction, *IEEE Geosci. Rem. Sens. Lett.*, 13(10), pp. 1443-1447, 2016.

[J-64] **Nannini, M.**, **Prats Iraola, P.**, De Zan, F., Geudtner, D., TOPS Time Series Performance Assessment with TerraSAR-X Data, *IEEE Journal of Selected Topics in Applied Earth Observations and Remote Sensing*, pp. 3832 -3848, 2016.

[J-65] **Parrella, G.**, **Hajnsek, I.**, **Papathanassiou, K.**, Polarimetric Decomposition of L-Band PolSAR Backscattering Over the Austfonna Ice-Cap, *IEEE Trans. Geosci. Rem. Sens.*, 54(3), pp. 1267-1281, 2016.

[J-66] **Parrella, G.**, **Hajnsek, I.**, **Papathanassiou, K.**, On the Interpretation of Polarimetric Phase Differences in SAR Data over Land Ice, *IEEE Geosci. Rem. Sens. Lett.*, 13(2), pp. 192-196, 2016.

[J-67] **Ponce Madrigal, O.**, **Prats Iraola, P.**, **Scheiber, R.**, **Reigber, A.**, **Moreira, A.**, First Airborne Demonstration of Holographic SAR Tomography with Fully Polarimetric Multicircular Acquisitions at L-Band, *IEEE Trans. Geosci. Rem. Sens.*, 54(10), pp. 6170-6196, 2016.

[J-68] Diao, F., Walter, T., Minati, F., Wang, R., Costantini, M., Ergintav, S., Xiong, X., **Prats Iraola, P.**, Secondary Fault Activity of the North Anatolian Fault near Avcilar, Southwest of Istanbul: Evidence from SAR Interferometry Observations, *Remote Sensing*, 8(10), pp. 1-17, 2016.

[J-69] **Reimann, J.**, Hagen, M., Antenna Pattern Measurements of Weather Radars Using the Sun and a Point Source, *Journal of Atmospheric and Oceanic Technology*, 33(5), pp. 891-898, 2016.

[J-70] **Schwerdt, M.**, **Schmidt, K.**, **Tous Ramon, N.**, **Castellanos Alfonzo, G.**, **Döring, B.**, **Zink, M.**, **Prats Iraola, P.**, Independent Verification of the Sentinel-1A System Calibration, *IEEE Journal of Selected Topics in Applied Earth Observations and Remote Sensing*, Vol 9(3), pp. 994-1007, 2016.

[J-71] **Toraño Caicoya, A.**, **Kugler, F.**, **Hajnsek, I.**, **Papathanassiou, K.**, Large Scale Biomass Classification in Boreal Forests with TanDEM-X Data, *IEEE Trans. Geosci. Rem. Sens.*, 54(10), pp. 5935-5951, 2016.

[J-72] **Villano, M.**, **Krieger, G.**, **Moreira, A.**, Onboard Processing for Data Volume Reduction in High-Resolution Wide-Swath SAR, *IEEE Geosci. Rem. Sens. Lett.*, 13(8), pp. 1173-1177, 2016.

[J-73] Hu, H., Wang, X., **Villano, M.**, Khwaja, A., Mar, J., Xie, W., Advances in Antenna Array Processing for Radar 2016, *Int. J. Antenn. Propag.*, 2016.

[J-74] **Voormansik, K.**, **Jagdhuber, T.**, Zalite, K., Noorma, M., **Hajnsek, I.**, Observations of Cutting Practices in Agricultural Grasslands using Polarimetric SAR, *IEEE Journal of Selected Topics in Applied Earth Observations and Remote Sensing*, 9(4), pp. 1382-1396, 2016.

[J-75] **Yague-Martinez, N.**, **Prats Iraola, P.**, Rodriguez Gonzalez, F., Brcic, R., Shau, R., Geudtner, D., Eineder, M., Bamler, R., Interferometric Processing of Sentinel-1 TOPS Data, *IEEE Trans. Geosci. Rem. Sens.*, 54(04), pp. 2220-2234, 2016.

2015

[J-76] Bieniarz, J., **Aguilera, E.**, Zhu, X., Müller, R., Reinartz, P., Joint Sparsity Model for Multilook Hyperspectral Image Unmixing, *IEEE Geosci. Rem. Sens. Lett.*, 12(4), pp. 696-700, 2015.

[J-77] **Baumgartner, S.**, **Krieger, G.**, Simultaneous High-Resolution Wide-Swath SAR Imaging and Ground Moving Target Indication: Processing Approaches and System Concepts, *IEEE Journal of Selected Topics in Applied Earth Observations and Remote Sensing*, 8(11), pp. 5015-5029, 2015.

[J-78] Makhoul, E., **Baumgartner, S.**, **Jäger, M.**, Broquetas, A., Multichannel SAR-GMTI in Maritime Scenarios with F-SAR and TerraSAR-X Sensors, *IEEE Journal of Selected Topics in Applied Earth Observations and Remote Sensing*, 8(11), pp. 5052-5067, 2015.

[J-79] **Bertl, S.**, **López-Dekker, F.**, **Younis, M.**, **Krieger, G.**, Along-Track SAR Interferometry Using a Single Reflector Antenna, *IET Radar Sonar & Navigation*, 9(8), pp. 942-947, 2015.

[J-80] De Zan, F., **Zonno, M.**, **López-Dekker, F.**, Phase Inconsistencies and Multiple Scattering in SAR Interferometry, *IEEE Trans. Geosci. Rem. Sens.*, 53(12), pp. 6608-6616, 2015.

[J-81] De Zan, F., **Prats Iraola, P.**, **Rodríguez Cassolà, M.**, On the Dependence of Delta-K Efficiency on Multilooking, *IEEE Geosci. Rem. Sens. Lett.*, 12(8), pp. 1745-1749, 2015.

[J-82] **Döring, B.**, **Reimann, J.**, **Raab, S.**, **Jirousek, M.**, **Rudolf, D.**, **Schwerdt, M.**, The Three-Transponder Method: A Novel Method for Accurate Transponder RCS Calibration, *Electromagn. Waves B*, pp. 297-315, 2015.

[J-83] Yuzugullu, O., **Erten, E.**, **Hajnsek, I.**, Rice Growth Monitoring by Means of X-Band Co-Polar SAR: Feature Clustering and BBCH Scale, *IEEE Geosci. Rem. Sens. Lett.*, 12(6), pp. 1218 - 1222, 2015.

[J-84] **Gonzalez, C.**, **Bräutigam, B.**, Relative Height Accuracy Estimation Method for InSAR-Based DEMs, *IEEE Journal of Selected Topics in Applied Earth Observations and Remote Sensing*, 8(11), pp. 5352-5360, 2015.

[J-85] Leinss, S., Löwe, H., Proksch, M., Lemmetyinen, J., Wiesmann, A., **Hajnsek, I.**, Anisotropy of Seasonal Snow Measured by Polarimetric Phase Differences in Radar Time Series, *The Cryosphere*, 9(6), pp. 6061-6123, 2015.

[J-86] Marino, A., **Hajnsek, I.**, Ship Detection with TanDEM-X Data Extending the Polarimetric Noth Filter, *IEEE Geosci. Rem. Sens. Lett.*, 12(10), pp. 2160-2164, 2015.

[J-87] Zwieback, S., Hensley, S., **Hajnsek, I.**, A Polarimetric First-Order Model of Soil Moisture Effects on the DInSAR Coherence, *Remote Sensing*, 7(6), pp. 7571-7596, 2015.

[J-88] Zwieback, S., Hensley, S., **Hajnsek, I.**, Assessment of Soil Moisture Effects on L-Band Radar Interferometry, *Remote Sensing of Environment*, pp. 77-89, 2015.

[J-89] Leinss, S., Wiesmann, A., Lemmetyinen, J., **Hajnsek, I.**, Snow Water Equivalent of Dry Snow Measured by Differential Interferometry, *IEEE Journal of Selected Topics in Applied Earth Observations and Remote Sensing*, 8(8), pp. 3773 -3790, 2015.

[J-90] **Huber, S.**, **Younis, M.**, **Krieger, G.**, **Moreira, A.**, Wiesbeck, W., A Reflector Antenna Concept Robust Against Feed Failures for Satellite Communications, *IEEE Trans. Antenn. Propag.*, 63(4), pp. 1218-1224, 2015.

[J-91] **Jagdhuber, T.**, **Hajnsek, I.**, **Papathanassiou, K.**, An Iterative Generalized Hybrid Decomposition for Soil Moisture Retrieval under Vegetation Cover Using Fully Polarimetric SAR, *IEEE Journal of Selected Topics in Applied Earth Observations and Remote Sensing*, 8(8), pp. 3911-3922, 2015.

[J-92] **Jirousek, M.**, **Iff, S.**, **Anger, S.**, **Peichl, M.**, GigaRad – a Multi-Purpose High-Resolution Ground-Based Radar-system Concept, Error Correction Strategies and Performance Verification, *International Journal of Microwave and Wireless Technologies*, pp. 443-451, 2015.

[J-93] **Kim, J.**, **Papathanassiou, K.**, **Scheiber, R.**, Quegan, S., Correcting Distortion of Polarimetric SAR Data Induced by Ionospheric Scintillation, *IEEE Trans. Geosci. Rem. Sens.*, 53(12), pp. 6319-6335, 2015.

[J-94] **Kim, J.**, **Younis, M.**, **Moreira, A.**, Wiesbeck, W., Spaceborne MIMO Synthetic Aperture Radar for Multimodal Operation, *IEEE Trans. Geosci. Rem. Sens.*, 53(5), pp. 2453-2466, 2015.

[J-95] **Kugler, F.**, **Lee, S.**, **Hajnsek, I.**, **Papathanassiou, K.**, Forest Height Estimation by Means of Pol-InSAR Data Inversion: The Role of the Vertical Wavenumber, *IEEE Geoscience and Remote Sensing Magazine (GRSM)*, 53(10), pp. 5294 -5311, 2015.

[J-96] **Martone, M.**, **Bräutigam, B.**, **Krieger, G.**, Quantization Effects in TanDEM-X Data, *IEEE Trans. Geosci. Rem. Sens.*, 53(2), pp. 583-597, 2015.

[J-97] **Moreira, A.**, **Krieger, G.**, **Hajnsek, I.**, **Papathanassiou, K.**, **Younis, M.**, **López-Dekker, F.**, **Huber, S.**, **Villano, M.**, **Pardini, M.**, Eineder, M., De Zan, F., Parizzi, A., Tandem-L: A Highly Innovative Bistatic SAR Mission for Global Observation of Dynamic Processes on the Earth's Surface, *IEEE Geoscience and Remote Sensing Magazine (GRSM)*, 3(2), pp. 8-23, 2015.

[J-98] **Osipov, A.**, Scattering Cross Sections of Impedance-Matched Bodies, *IEEE Trans. Antenn. Propag.*, 63(7), pp. 3122-3126, 2015.

[J-99] Ra'di, Y., Asadchy, V., Kosulnikov, S., Omelyanovich, M., Morits, D., **Osipov, A.**, Simovski, C., Tretyakov, S., Full Light Absorption in Single Arrays of Spherical Nanoparticles, *ACS Photonics*, 2(5), pp. 653-660, 2015.

[J-100] Qin, F., Gao, S., Mao, C., Wang, Z., **Patyuchenko, A.**, **Younis, M.**, **Krieger, G.**, Smart Antennas for Spaceborne Synthetic Aperture Radars, *Applied Physics A: Materials Science & Processing*, pp. 1-7, 2015.

[J-101] **Pinheiro, M.**, **Rodríguez Cassolà, M.**, **Prats Iraola, P.**, **Reigber, A.**, **Krieger, G.**, **Moreira, A.**, Reconstruction of Coherent Pairs of Synthetic Aperture Radar Data Acquired in Interrupted Mode, *IEEE Trans. Geosci. Rem. Sens.*, 53(4), pp. 1876-1893, 2015.

[J-102] Diao, F., Walter, T., Motagh, M., **Prats Iraola, P.**, Wang, R., Samsonov, S., The 2015 Gorkha Earthquake Investigated from Radar Satellites: Slip and Stress Modeling along the MHT, *Frontiers in Earth Science*, 3(65), pp. 1-9, 2015.

[J-103] **Prats Iraola, P.**, **Rodríguez Cassolà, M.**, De Zan, F., **Scheiber, R.**, **López-Dekker, F.**, Barat, I., Geudtner, D., Role of the Orbital Tube in Interferometric Spaceborne SAR Missions, *IEEE Geosci. Rem. Sens. Lett.*, 12(7), pp. 1486-1490, 2015.

[J-104] Deledalle, C., Denis, L., Tupin, F., **Reigber, A.**, **Jäger, M.**, NL-SAR: A Unified Nonlocal Framework for Resolution-Preserving PolInSAR Denoising, *IEEE Trans. Geosci. Rem. Sens.*, 53(4), pp. 2021-2038, 2015.

[J-105] **Rizzoli, P.**, **Martone, M.**, **Bräutigam, B.**, Global Mosaics of the Relative Height Error From TanDEM-X Quicklooks, *IEEE Geosci. Rem. Sens. Lett.*, 12(9), pp. 1928-1932, 2015.

[J-106] **Rodríguez Cassolà, M.**, **Prats Iraola, P.**, De Zan, F., **Scheiber, R.**, **Reigber, A.**, Geudtner, D., **Moreira, A.**, Doppler-Related Distortions in TOPS SAR Images, *IEEE Trans. Geosci. Rem. Sens.*, 53(1), pp. 25-35, 2015.

[J-107] **Sanjuan Ferrer, M.**, **Hajnsek, I.**, **Papathanassiou, K.**, **Moreira, A.**, A New Detection Algorithm for Coherent Scatterers in SAR Data, *IEEE Trans. Geosci. Rem. Sens.*, 53(11), pp. 6293-6307, 2015.

[J-108] Marino, A., **Sanjuan Ferrer, M.**, **Hajnsek, I.**, Ouchi, K., Ship Detection with Spectral Analysis of Synthetic Aperture Radar: a Comparison of New and Well-known Algorithms, *Remote Sensing*, 7(5), pp. 5416-5439, 2015.

[J-109] **Scheiber, R.**, **Jäger, M.**, **Prats Iraola, P.**, De Zan, F., Geudtner, D., Speckle Tracking and Interferometric Processing of TerraSAR-X TOPS Data for Mapping Nonstationary Scenarios, *IEEE Journal of Selected Topics in Applied Earth Observations and Remote Sensing*, 8(4), pp. 1709-1720, 2015.

[J-110] **Toraño Caicoya, A.**, **Pardini, M.**, **Hajnsek, I.**, **Papathanassiou, K.**, Forest Above-Ground Biomass Estimation from Vertical Reflectivity Profiles at L-Band, *IEEE Geosci. Rem. Sens. Lett.*, 12(12), pp. 2379-2383, 2015.

[J-111] **Toraño Caicoya, A.**, **Kugler, F.**, **Papathanassiou, K.**, Pretzsch, H., Forest Vertical Structure Characterization Using Ground Inventory Data for the Estimation of Forest Aboveground Biomass, *Canadian Journal of Forest Research*, 2015.

[J-112] **Villano, M.**, Student Research Highlight Staggered Synthetic Aperture Radar, *IEEE Aero. Electron. Syst. Mag.*, 30(7), pp. 30-32, 2015.

[J-113] Hu, H., Qi, H., **Villano, M.**, Khwaja, A., Advances in Antenna Array Processing for Radar 2014, *Int. J. Antenn. Propag.*, 2015.

[J-114] **Younis, M.**, **Rommel, T.**, **Bordoni, F.**, **Krieger, G.**, **Moreira, A.**, On the Pulse Extension Loss in Digital Beamforming SAR, *IEEE Geosci. Rem. Sens. Lett.*, 12(7), pp. 1436-1440, 2015.

2014

[J-115] Erasmi, S., Rosenbauer, R., Buchbach, R., **Busche, T.**, Rutishauser, S., Evaluating the Quality and Accuracy of TanDEM-X Digital Elevation Models at Archaeological Sites in the Cilician Plain, Turkey, *Remote Sensing*, 6(10), pp. 9475-9493, 2014.

[J-116] Linck, R., **Busche, T.**, **Buckreuß, S.**, Visual Analysis of TerraSAR-X Backscatter Imagery for Archaeological Prospection, *Photogrammetrie Fernerkundung Geoinformation*, 2014(1), pp. 55-65, 2014.

[J-117] **Culhaoglu, A.**, **Osipov, A.**, Russer, P., Imaging by a Double Negative Metamaterial Slab Excited with an Arbitrarily Oriented Dipole, *Radio Sci.*, 49(1), pp. 68-79, 2014.

[J-118] **De Zan, F.**, Accuracy of Incoherent Speckle Tracking for Circular Gaussian Signals, *IEEE Geosci. Rem. Sens. Lett.*, 11(1), pp. 264-267, 2014.

[J-119] **De Zan, F.**, Parizzi, A., **Prats Iraola, P.**, **López-Dekker, F.**, A SAR Interferometric Model for Soil Moisture, *IEEE Trans. Geosci. Rem. Sens.*, 52(1), pp. 418-425, 2014.

[J-120] Marino, A., **Hajnsek, I.**, A Change Detector Based on an Optimization with Polarimetric SAR Imagery, *IEEE Trans. Geosci. Rem. Sens.*, 52(8), pp. 4781-4798, 2014.

[J-121] Zwieback, S., **Hajnsek, I.**, Statistical Tests for Symmetries in Polarimetric Scattering Coherency Matrices, *IEEE Geosci. Rem. Sens. Lett.*, 11(1), pp. 308 -312, 2014.

[J-122] **Jagdhuber, T.**, **Stockamp, J.**, **Hajnsek, I.**, Ludwig, R., Identification of Soil Freezing and Thawing States Using SAR Polarimetry at C-Band, *Remote Sensing*, 6(3), pp. 2008-2023, 2014.

[J-123] Rogers, N., Quegan, S., **Kim, J.**, **Papathanassiou, K.**, Impacts of Ionospheric Scintillation on the BIOMASS P-Band Satellite SAR, *IEEE Trans. Geosci. Rem. Sens.*, 52(3), pp. 1856-1868, 2014.

[J-124] **Krieger, G.**, MIMO-SAR: Opportunities and Pitfalls, *IEEE Trans. Geosci. Rem. Sens.*, 52(5), pp. 2628-2645, 2014.

[J-125] **Krieger, G.**, **De Zan, F.**, Relativistic Effects in Bistatic Synthetic Aperture Radar, *IEEE Trans. Geosci. Rem. Sens.*, 52(2), pp. 1480-1488, 2014.

[J-126] **Kugler, F.**, **Schulze, D.**, **Hajnsek, I.**, Pretzsch, H., **Papathanassiou, K.**, TanDEM-X Pol-InSAR Performance for Forest Height Estimation, *IEEE Trans. Geosci. Rem. Sens.*, 52(10), pp. 6404-6422, 2014.

[J-127] Iglesias, R., Mallorqui, J., **López-Dekker, F.**, DInSAR Pixel Selection Based on Sublook Spectral Correlation Along Time, *IEEE Trans. Geosci. Rem. Sens.*, 52(7), pp. 3788-3799, 2014.

[J-128] **Martone, M.**, **Bräutigam, B.**, **Krieger, G.**, Azimuth-Switched Quantization for SAR Systems and Performance Analysis on TanDEM-X Data, *IEEE Geosci. Rem. Sens. Lett.*, 11(1), pp. 181-185, 2014.

[J-129] **Mittermayer, J.**, **Wollstadt, S.**, **Prats Iraola, P.**, **Scheiber, R.**, The TerraSAR-X Staring Spotlight Mode Concept, *IEEE Trans. Geosci. Rem. Sens.*, 52(6), pp. 3695-3706, 2014.

[J-130] **Osipov, A.**, Minimum Reflection Properties of Planar Impedance-Matched Boundaries, *IEEE Trans. Antenn. Propag.*, 62(11), pp. 5666-5670, 2014.

[J-131] **Osipov, A.**, Physical Theory of Diffraction for Scatterers with Low-Reflection Surface, *Radio Sci.*, 49(11), pp. 1052-1064, 2014.

[J-132] Leinss, S., **Parrella, G.**, **Hajnsek, I.**, Snow Height Determination by Polarimetric Phase Differences in X-Band SAR Data, *IEEE Journal of Selected Topics in Applied Earth Observations and Remote Sensing*, 7(9), pp. 3794-3810, 2014.

[J-133] **Ponce Madrigal, O.**, **Prats Iraola, P.**, **Pinheiro, M.**, **Rodríguez Cassolà, M.**, **Scheiber, R.**, **Reigber, A.**, **Moreira, A.**, Fully-Polarimetric High-Resolution 3-D Imaging with Circular SAR at L-Band, *IEEE Trans. Geosci. Rem. Sens.*, 52(6), pp. 3074-3090, 2014.

[J-134] **Ponce Madrigal, O.**, **Prats Iraola, P.**, **Scheiber, R.**, **Reigber, A.**, **Moreira, A.**, **Aguilera, E.**, Polarimetric 3-D Reconstruction from Multi-Circular SAR at P-Band, *IEEE Geosci. Rem. Sens. Lett.*, 11(4), pp. 803-807, 2014.

[J-135] **Prats Iraola, P.**, **Scheiber, R.**, **Rodríguez Cassolà, M.**, **Mittermayer, J.**, **Wollstadt, S.**, **De Zan, F.**, **Bräutigam, B.**, **Schwerdt, M.**, **Reigber, A.**, **Moreira, A.**, On the Processing of Very High-Resolution Spaceborne SAR Data, *IEEE Trans. Geosci. Rem. Sens.*, 52(10), pp. 6003-6016, 2014.

[J-136] **Prats Iraola, P.**, **Rodríguez Cassolà, M.**, **De Zan, F.**, **López-Dekker, F.**, **Scheiber, R.**, **Reigber, A.**, Efficient Evaluation of Fourier-Based SAR Focusing Kernels, *IEEE Geosci. Rem. Sens. Lett.*, 11(9), pp. 1489-1493, 2014.

[J-137] **Rizzoli, P.**, **Martone, M.**, **Bräutigam, B.**, Global Interferometric Coherence Maps From TanDEM-X Quicklook Data, *IEEE Geosci. Rem. Sens. Lett.*, 11(11), pp. 1861-1865, 2014.

[J-138] **Rizzoli, P.**, **Bräutigam, B.**, Radar Backscatter Modeling Based on Global TanDEM-X Mission Data, *IEEE Trans. Geosci. Rem. Sens.*, 52(9), pp. 5974-5988, 2014.

[J-139] Kuk, B., **Schmidt, K.**, Lee, G., On Network Performance and Data Quality of a Lightning Detection Network in Korea (KLDN), *Atmospheric Research*, pp. 136-153, 2014.

[J-140] **Villano, M.**, **Krieger, G.**, **Moreira, A.**, A Novel Processing Strategy for Staggered SAR, *IEEE Geosci. Rem. Sens. Lett.*, 11(11), pp. 1891-1895, 2014.

[J-141] **Villano, M.**, **Krieger, G.**, **Moreira, A.**, Staggered SAR: High-Resolution Wide-Swath Imaging by Continuous PRI Variation, *IEEE Trans. Geosci. Rem. Sens.*, 52(7), pp. 4462-4479, 2014.

[J-142] **Villano, M.**, **Krieger, G.**, Spectral-Based Estimation of the Local Azimuth Ambiguity-to-Signal Ratio in SAR Images, *IEEE Trans. Geosci. Rem. Sens.*, 52(5), pp. 2304-2313, 2014.

[J-143] **Villano, M.**, SNR and Noise Variance Estimation in Polarimetric SAR data, *IEEE Geosci. Rem. Sens. Lett.*, 11(1), pp. 278-282, 2014.

[J-144] **Zink, M.**, **Bachmann, M.**, **Bräutigam, B.**, Fritz, T., **Hajnsek, I.**, **Krieger, G.**, **Moreira, A.**, Wessel, B., TanDEM-X: The New Global DEM Takes Shape, *IEEE Geoscience and Remote Sensing Magazine (GRSM)*, 2(2), pp. 8-23, 2014.

2013

[J-145] **Aguilera, E.**, **Nannini, M.**, **Reigber, A.**, Wavelet-Based Compressed Sensing for SAR Tomography of Forested Areas, *IEEE Trans. Geosci. Rem. Sens.*, 51(12), pp. 5283-5295, 2013.

[J-146] **Aguilera, E.**, **Nannini, M.**, **Reigber, A.**, A Data-Adaptive Compressed Sensing Approach to Polarimetric SAR Tomography of Forested Areas, *IEEE Geosci. Rem. Sens. Lett.*, 10(3), pp. 543-547, 2013.

[J-147] **Bachmann, M.**, **Schwerdt, M.**, **Castellanos Alfonzo, G.**, **Schrank, D.**, Phase Pattern Calibration for Interferometric Applications in Spaceborne SAR Systems, *Int. J. Antenn. Propag.*, no.2013, pp. 1-8, 2013.

[J-148] Linck, R., **Busche, T.**, **Buckreuß, S.**, Fassbinder, J., Seren, S., Possibilities of Archaeological Prospection by High-Resolution X-Band Satellite Radar – a Case Study from Syria, *Archaeological Prospection*, pp. 97-108, 2013.

[J-149] **Castellanos Alfonzo, G.**, **Schwerdt, M.**, **Wollstadt, S.**, **Bachmann, M.**, **Döring, B.**, Geudtner, D., First TerraSAR-X TOPS Mode Antenna Pattern Measurements Using Ground Receivers, *Int. J. Antenn. Propag.*, 2013.

[J-150] Alitalo, P., **Culhaoglu, A.**, Simovski, C., Tretyakov, S., Experimental Study of Anti-Resonant Behavior of Material Parameters in Periodic and Aperiodic Composite Materials, *Journal of Applied Physics*, 113(22), 2013.

[J-151] Alitalo, P., Valagiannopoulos, C., **Culhaoglu, A.**, Design and Free-space Measurements of a Simple Electromagnetic Cloak for Conducting Cylindrical Objects, *AIP Advances*, 3(4), 2013.

[J-152] **Culhaoglu, A.**, **Osipov, A.**, Russer, P., Mono- and Bistatic Scattering Reduction by a Metamaterial Low Reflection Coating, *IEEE Trans. Antenn. Propag.*, 61(1), pp. 462-466, 2013.

[J-153] **De Zan, F.**, **Krieger, G.**, **López-Dekker, F.**, On Some Spectral Properties of TanDEM-X Interferograms over Forested Areas, *IEEE Geosci. Rem. Sens. Lett.*, 10(1), pp. 71-75, 2013.

[J-154] **Döring, B.**, **Schmidt, K.**, **Jirousek, M.**, **Rudolf, D.**, **Reimann, J.**, **Raab, S.**, **Schwerdt, M.**, Hierarchical Bayesian Data Analysis in Radiometric SAR System Calibration: A Case Study on Transponder Calibration with RADARSAT-2 Data, *Remote Sensing*, pp. 6667-6690, 2013.

[J-155] **Döring, B.**, **Schwerdt, M.**, The Radiometric Measurement Quantity for SAR Images, *IEEE Trans. Geosci. Rem. Sens.*, PP(99), 2013.

[J-156] **Gebert, N.**, **Villano, M.**, **Krieger, G.**, **Moreira, A.**, Correction to "Multichannel Azimuth Processing in ScanSAR and TOPS Mode Operation", *IEEE Trans. Geosci. Rem. Sens.*, 51(8), pp. 4611-4611, 2013.

[J-157] **Gebert, N.**, **Villano, M.**, **Krieger, G.**, **Moreira, A.**, Errata: Digital Beamforming on Receive: Techniques and Optimization Strategies for High-Resolution Wide-Swath SAR Imaging, *IEEE Trans. Aero. Electron. Syst.*, 49(3), pp. 2110-2110, 2013.

[J-158] **Huber, S.**, **Younis, M.**, **Krieger, G.**, **Moreira, A.**, A Dual-Focus Reflector Antenna Concept for Spaceborne SAR Systems with Digital Beamforming, *IEEE Trans. Antenn. Propag.*, 2013.

[J-159] **Jagdhuber, T.**, **Hajnsek, I.**, Bronstert, A., **Papathanassiou, K.**, Soil Moisture Estimation under Low Vegetation Cover Using a Multi-Angular Polarimetric Decomposition, *IEEE Trans. Geosci. Rem. Sens.*, 51(4), pp. 2201-2215, 2013.

[J-160] **Kim, J.**, **Younis, M.**, **Moreira, A.**, Wiesbeck, W., A Novel OFDM Chirp Waveform Scheme for Use of Multiple Transmitters in SAR, *IEEE Geosci. Rem. Sens. Lett.*, 10(3), pp. 568-572, 2013.

[J-161] **Kim, J.**, **Younis, M.**, **Prats Iraola, P.**, **Gabele, M.**, **Krieger, G.**, First Spaceborne Demonstration of Digital Beamforming for Azimuth Ambiguity Suppression, *IEEE Trans. Geosci. Rem. Sens.*, 51(1), pp. 579-590, 2013.

[J-162] **Krieger, G.**, **Zink, M.**, **Bachmann, M.**, **Bräutigam, B.**, **Schulze, D.**, **Martone, M.**, **Rizzoli, P.**, **Steinbrecher, U.**, Walter Anthony, J., **De Zan, F.**, **Hajnsek, I.**, **Papathanassiou, K.**, **Kugler, F.**, **Rodríguez Cassolà, M.**, **Younis, M.**, **Baumgartner, S.**, **López-Dekker, F.**, **Prats Iraola, P.**, **Moreira, A.**, TanDEM-X: A Radar Interferometer with Two Formation Flying Satellites, *Acta Astronautica*, pp. 83-98, 2013.

[J-163] **Lee, S.**, **Kugler, F.**, **Papathanassiou, K.**, **Hajnsek, I.**, Quantification of Temporal Decorrelation Effects at L-Band for Polarimetric SAR Interferometry Applications, *IEEE Journal of Selected Topics in Applied Earth Observations and Remote Sensing*, 6(3), pp. 1351-1367, 2013.

[J-164] Farquharson, G., **López-Dekker, F.**, Frasier, S., Contrast-based Phase Calibration for Remote Sensing Systems with Digital Beamforming Antennas, *IEEE Trans. Geosci. Rem. Sens.*, 51(3), pp. 1744-1754, 2013.

[J-165] **Martone, M.**, **Rizzoli, P.**, **Bräutigam, B.**, **Krieger, G.**, First Two Years of TanDEM-X mission: Interferometric Performance Overview, *Radio Sci.*, pp. 1-11, 2013.

[J-166] **Mittermayer, J.**, **Wollstadt, S.**, **Prats Iraola, P.**, **López-Dekker, F.**, **Krieger, G.**, **Moreira, A.**, Bidirectional SAR Imaging Mode, *IEEE Trans. Geosci. Rem. Sens.*, 51(1), pp. 601-614, 2013.

[J-167] **Moreira, A.**, **Prats Iraola, P.**, **Younis, M.**, **Krieger, G.**, **Hajnsek, I.**, **Papathanassiou, K.**, A Tutorial on Synthetic Aperture Radar, *IEEE Geoscience and Remote Sensing Magazine (GRSM)*, 1(1), pp. 6-43, 2013.

[J-168] **Osipov, A.**, Kobayashi, H., Suzuki, H., An Improved Image-Based Circular Near-Field-to-Far-Field Transformation, *IEEE Trans. Antenn. Propag.*, 61(2), pp. 989-993, 2013.

[J-169] **Reigber, A.**, **Scheiber, R.**, **Jäger, M.**, **Prats Iraola, P.**, **Hajnsek, I.**, **Jagdhuber, T.**, **Papathanassiou, K.**, **Nannini, M.**, **Aguilera, E.**, **Baumgartner, S.**, **Horn, R.**, **Nottensteiner, A.**, **Moreira, A.**, Very-High-Resolution Airborne Synthetic Aperture Radar Imaging: Signal Processing and Applications, *Proc. IEEE*, 101(3), pp. 759-783, 2013.

[J-170] **Sharma, J.**, **Hajnsek, I.**, **Papathanassiou, K.**, **Moreira, A.**, Estimation of Glacier Ice Extinction Using Long-Wavelength Airborne Pol-InSAR, *IEEE Trans. Geosci. Rem. Sens.*, 51(6), pp. 3715-3732, 2013.

[J-171] **Villano, M.**, Colone, F., Lombardo, P., Antenna Array for Passive Radar: Configuration Design and Adaptive Approaches to Disturbance Cancellation, *Int. J. Antenn. Propag.*, 2013.

[J-172] **Voormansik, K.**, **Jagdhuber, T.**, Olesk, A., **Hajnsek, I.**, **Papathanassiou, K.**, Towards a Detection of Grassland Cutting Practices with Dual Polarimetric TerraSAR-X Data, *Int. J. Rem. Sens.*, 34(22), pp. 8081-8103, 2013.

[J-173] **Walter Antony, J.**, Hueso González, J., **Schwerdt, M.**, **Bachmann, M.**, **Krieger, G.**, **Zink, M.**, Results of the TanDEM-X Baseline Calibration, *IEEE Journal of Selected Topics in Applied Earth Observations and Remote Sensing*, 6(3), pp. 1495-1501, 2013.

2012

[J-174] **Aguilera, E.**, **Nannini, M.**, **Reigber, A.**, Multisignal Compressed Sensing for Polarimetric SAR Tomography, *IEEE Geosci. Rem. Sens. Lett.*, 9(5), pp. 871-875, 2012.

[J-175] **Baumgartner, S.**, **Krieger, G.**, Fast GMTI Algorithm For Traffic Monitoring Based On A Priori Knowledge, *IEEE Trans. Geosci. Rem. Sens.*, 50(11), pp. 4626-4641, 2012.

[J-176] **Bordoni, F.**, **Younis, M.**, **Krieger, G.**, Ambiguity Suppression by Azimuth Phase Coding in Multichannel SAR Systems, *IEEE Trans. Geosci. Rem. Sens.*, 50(2), pp. 617-629, 2012.

[J-177] Ben Khadhra, K., **Börner, T.**, **Hounam, D.**, Chandra, M., Surface Parameter Estimation Using Bistatic Polarimetric X-Band Measurements, *Electromagn. Waves B*, pp. 197-223, 2012.

[J-178] Alitalo, P., **Culhaoglu, A.**, **Osipov, A.**, **Thurner, S.**, **Kemptner, E.**, Tretyakov, S., Experimental Characterization of a Broadband Transmission-Line Cloak in Free Space, *IEEE Trans. Antenn. Propag.*, 60(10), pp. 4963-4968, 2012.

[J-179] Alitalo, P., **Culhaoglu, A.**, **Osipov, A.**, **Thurner, S.**, **Kemptner, E.**, Tretyakov, S., Bistatic Scattering Characterization of a Three-Dimensional Broadband Cloaking Structure, *Journal of Applied Physics*, 111(034901), pp. 1-5, 2012.

[J-180] **Döring, B.**, **Looser, P.**, **Jirousek, M.**, **Schwerdt, M.**, Reference Target Correction Based on Point Target SAR Simulation, *IEEE Trans. Geosci. Rem. Sens.*, 50(3), pp. 951-959, 2012.

[J-181] **Erten, E.**, **Reigber, A.**, Ferro-Famil, L., A New Coherent Similarity Measure for Temporal Multichannel Scene Characterization, *IEEE Trans. Geosci. Rem. Sens.*, 50(7), pp. 2839-2851, 2012.

[J-182] Lopez-Sanchez, J., **Hajnsek, I.**, Ballester-Berman, D., First Demonstration of Agriculture Height Retrieval with PolInSAR Airborne Data, *IEEE Geosci. Rem. Sens. Lett.*, 9(2), pp. 242-246, 2012.

[J-183] **Huber, S.**, **Younis, M.**, **Krieger, G.**, **Patyuchenko, A.**, **Moreira, A.**, Spaceborne Reflector SAR Systems with Digital Beamforming, *IEEE Trans. Aero. Electron. Syst.*, 48(4), pp. 3473-3493, 2012.

[J-184] **Hueso Gonzalez, J.**, **Walter Antony, J.**, **Bachmann, M.**, **Krieger, G.**, **Zink, M.**, **Schrank, D.**, **Schwerdt, M.**, Bistatic System Calibration in TanDEM-X to Ensure the Global Digital Elevation Model Quality, *ISPRS Journal of Photogrammetry and Remote Sensing*, pp. 3-11, 2012.

[J-185] Merlano-Duncan, J., Mallorquí, J., **López-Dekker, F.**, Carrier Phase Synchronisation Scheme for very Long Baseline Coherent Arrays, *Electronics Letters*, 48(15), pp. 950-951, 2012.

[J-186] Makhoul, E., Broquetas, A., **López-Dekker, F.**, Closa, J., Saameno, P., Evaluation of the Internal Calibration Methodologies for Spaceborne Synthetic Aperture Radars with Active Phased Array Antennas, *IEEE Journal of Selected Topics in Applied Earth Observations and Remote Sensing*, 5(3), pp. 909-918, 2012.

[J-187] **Martone, M.**, **Bräutigam, B.**, **Rizzoli, P.**, **Gonzalez, C.**, **Bachmann, M.**, **Krieger, G.**, Coherence Evaluation of TanDEM-X Interferometric Data, *ISPRS Journal of Photogrammetry and Remote Sensing*, pp. 21-29, 2012.

[J-188] **Nannini, M.**, **Scheiber, R.**, **Horn, R.**, **Moreira, A.**, First 3-D Reconstructions of Target Hidden Beneath Foliage by Means of Polarimetric SAR Tomography, *IEEE Geosci. Rem. Sens. Lett.*, 9(1), pp. 60-64, 2012.

[J-189] Lombardini, F., **Pardini, M.**, Superresolution Differential Tomography: Experiments on Identification of Multiple Scatterers in Spaceborne SAR Data, *IEEE Trans. Geosci. Rem. Sens.*, 50(4), pp. 1117-1129, 2012.

[J-190] **Prats Iraola, P.**, **Scheiber, R.**, Marotti, L., **Wollstadt, S.**, **Reigber, A.**, TOPS Interferometry with TerraSAR-X, *IEEE Trans. Geosci. Rem. Sens.*, 50(8), pp. 3179-3188, 2012.

[J-191] Huang, Y., Ferro-Famil, L., **Reigber, A.**, Under-Foliage Object Imaging Using SAR Tomography and Polarimetric Spectral Estimators, *IEEE Trans. Geosci. Rem. Sens.*, 50(6), pp. 2213-2225, 2012.

[J-192] **Rizzoli, P.**, **Bräutigam, B.**, **Kraus, T.**, **Martone, M.**, **Krieger, G.**, Relative Height Error Analysis of TanDEM-X Elevation Data, *ISPRS Journal of Photogrammetry and Remote Sensing*, pp. 30-38, 2012.

[J-193] **Rodríguez Cassolà, M.**, **Prats Iraola, P.**, **Schulze, D.**, **Tous Ramon, N.**, **Steinbrecher, U.**, Marotti, L., **Nannini, M.**, **Younis, M.**, **López-Dekker, F.**, **Zink, M.**, **Reigber, A.**, **Krieger, G.**, **Moreira, A.**, First Bistatic Spaceborne SAR Experiments with TanDEM-X, *IEEE Geosci. Rem. Sens. Lett.*, 9(1), pp. 33-37, 2012.

[J-194] **Villano, M.**, **Krieger, G.**, Impact of Azimuth Ambiguities on Interferometric Performance, *IEEE Geosci. Rem. Sens. Lett.*, 9(5), pp. 896-900, 2012.

[J-195] **Wollstadt, S.**, **Prats Iraola, P.**, **Bachmann, M.**, **Mittermayer, J.**, **Scheiber, R.**, Scalloping Correction in TOPS Imaging Mode SAR Data, *IEEE Geosci. Rem. Sens. Lett.*, 9(4), pp. 614-618, 2012.

2011

[J-196] Krumpen, T., Hölemann, J., Willmes, S., Morales Maqueda, M., **Busche, T.**, Dmitrenko, I., Gerdes, R., Haas, C., Heinemann, G., Hendricks, S., Kassens, H., Rabenstein, L., Schröder, D., Sea Ice Production and Water Mass Modification in the Eastern Laptev Sea, *J. Geophys. Res. - Oceans*, 116(C05014), pp. 1-17, 2011.

[J-197] **De Zan, F.**, Coherent Shift Estimation for Stacks of SAR Images, *IEEE Geosci. Rem. Sens. Lett.*, 8(6), pp. 1095-1099, 2011.

[J-198] **De Zan, F.**, **López-Dekker, F.**, SAR Image Stacking for the Exploitation of Long-Term Coherent Targets, *IEEE Geosci. Rem. Sens. Lett.*, 8(3), pp. 502-506, 2011.

[J-199] **Gebert, N.**, **Queiroz de Almeida, F.**, **Krieger, G.**, Airborne Demonstration of Multichannel SAR Imaging, *IEEE Geosci. Rem. Sens. Lett.*, 8(5), pp. 963-967, 2011.

[J-200] Bronstert, A., Creutzfeldt, C., Gräff, T., **Hajnsek, I.**, Heistermann, M., Itzerott, S., **Jagdhuber, T.**, Kneis, D., Lück, E., Reusser, D., Potentials and Constraints of Different Type of Soil Moisture Observations for Flood Simulations in Headwater Catchments, *Nat. Hazards*, 60(3), pp. 879-914, 2011.

[J-201] Zacharias, S., Bogena, H., Samaniego, L., Mauder, M., Fuß, R., Pütz, T., Frenzel, M., Schwank, M., Baessler, C., Butterbach-Bahl, K., Bens, O., Borg, E., Brauer, A., Dietrich, P., **Hajnsek, I.**, Helle, G., Kiese, R., Kunstmann, H., Klotz, S., Munch, J., Papen, H., Priesack, E., Schmid, H., Steinbrecher, R., Rosenbaum, U., Teutsch, G., Vereecken, H., A Network of Terrestrial Environmental Observatories in Germany, *Vadose Zone Journal*, 10(3), pp. 955-973, 2011.

[J-202] Lopez-Sanchez, J., Ballester-Berman, J., **Hajnsek, I.**, First Results of Rice Monitoring Practices in Spain by Means of Time Series of TerraSAR-X Dual-Pol Images, *IEEE Journal of Selected Topics in Applied Earth Observations and Remote Sensing*, 4(2), pp. 412-422, 2011.

[J-203] **Jochim, F.**, **Fiedler, H.**, **Krieger, G.**, Fuel Consumption and Collision Avoidance Strategy in Multi-static Orbit Formations, *Acta Astronautica*, 68(7-8), pp. 1002-1014, 2011.

[J-204] **López-Dekker, F.**, **Prats Iraola, P.**, **De Zan, F.**, **Schulze, D.**, **Krieger, G.**, **Moreira, A.**, TanDEM-X First DEM Acquisition: A Crossing Orbit Experiment, *IEEE Geosci. Rem. Sens. Lett.*, 8(5), pp. 943-947, 2011.

[J-205] Le Toan, T., Quegan, S., Davidson, M., Baltzer, H., Paillou, P., **Papathanassiou, K.**, Plummer, S., Rocca, F., Saatchi, S., Shugart, H., Ulander, L., The BIOMASS Mission: Mapping Global Forest Biomass to Better Understand the Terrestrial Carbon Cycle, *Int. J. Rem. Sens.*, 115(11), 2011.

[J-206] **Rizzoli, P.**, **Bräutigam, B.**, **Wollstadt, S.**, **Mittermayer, J.**, Radar Backscatter Mapping Using TerraSAR-X, *IEEE Trans. Geosci. Rem. Sens.*, 49(10), pp. 3538-3547, 2011.

[J-207] **Rodríguez Cassolà, M.**, **Prats Iraola, P.**, **Krieger, G.**, **Moreira, A.**, Efficient Time-Domain Image Formation with Precise Topography Accommodation for General Bistatic SAR Configurations, *IEEE Trans. Aero. Electron. Syst.*, 47(4), pp. 2949-2966, 2011.

[J-208] **Sauer, S.**, Ferro-Famil, L., **Reigber, A.**, Pottier, E., Three-Dimensional Imaging and Scattering Mechanism Estimation Over Urban Scenes Using Dual-Baseline Polarimetric InSAR Observations at L-Band, *IEEE Trans. Geosci. Rem. Sens.*, 49(11), pp. 4616-4629, 2011.

[J-209] **Sharma, J.**, **Hajnsek, I.**, **Papathanassiou, K.**, **Moreira, A.**, Polarimetric Decomposition over Glacier Ice Using Long-Wavelength Airborne PolSAR, *IEEE Trans. Geosci. Rem. Sens.*, 49(1), pp. 519-535, 2011.

Publications in Non-ISI-Scopus Journals

2017

[NJ-1] **Dietrich, B.**, **Iff, S.**, **Profelt, J.**, **Albers, T.**, **Blaschke, K.**, Development of a Local Air Surveillance System for Security Purposes – Design and Core Characteristics, *European Journal for Security Research*, 2017.

[NJ-2] **Kemptner, E.**, **Osipov, A.**, **Özis, E.**, Metamaterials for Microwave Radomes, *Annual Military Scientific Research*, pp. 42-43, 2017.

[NJ-3] **Kemptner, E.**, **Osipov, A.**, **Özis, E.**, Metamaterialien für Mikrowellenradome, *Wehrwissenschaftliche Forschung*, pp. 42-43, 2017.

2016

[NJ-4] **Baumgartner, S.**, Clevere List gegen Nebel und Finsternis, *DLR-Magazin*, no.149, pp. 42-45, 2016.

[NJ-5] **Eilers, J.**, **Anger, S.**, **Neff, T.**, Radar-Based System for Space Situational Awareness, *The Journal of Space Operations & Communicator*, 13(4), pp. 1-13, 2016.

[NJ-6] Bogena, H., Borg, E., Brauer, A., Dietrich, P., **Hajnsek, I.**, Heinrich, I., Kiese, R., Kunkel, R., Kunstmann, H., Merz, B., Priesack, E., Pütz, T., Schmidt, H., Wollschläger, U., Vereecken, H., Zacharias, S., TERENO: German Network of Terrestrial Environmental Observatories, *Journal of Large-Scale Research Facilities JLSRF*, A52(2), pp. 1-8, 2016.

[NJ-7] **Jochim, F.**, Rectilinear Motion: A Basis for the Adaptation of Arbitrary Motion, *The Journal of Space Operations & Communicator*, 13(2), pp. 1-29, 2016.

[NJ-8] **Peichl, M.**, **Schreiber, E.**, **Heinzel, A.**, **Dill, S.**, Novel Imaging Radar Technology for Detection of Landmines and Other Unexploded Ordnance, *European Journal for Security Research*, 1(2), pp. 1-15, 2016.

[NJ-9] **Zink, M.**, **Moreira, A.**, Tandem Satellite Mission on Course for Success, *DLR Magazine*, no.148, pp. 40-43, 2016.

2015

[NJ-10] **Jochim, F.**, The Circle will Now be Closed, Finally (On the Inability to Adapt Circular Motion to Arbitrary Motions), *The Journal of Space Operations & Communicator*, 12(2), pp. 1-21, 2015.

[NJ-11] **Scheiber, R.**, **Pinheiro, M.**, Über Höhen und Tiefen besser im Bild, *DLR-Magazin*, no.146, pp. 10-15, 2015.

[NJ-12] **Zink, M.**, **Moreira, A.**, Satelliten-Tandem auf Erfolgskurs – 3D Karte der Erde steht kurz vor der Fertigstellung, *DLR-Magazin*, no.148, pp. 22-27, 2015.

2014

[NJ-13] **Borla Tridon, D.**, **Bachmann, M.**, **Schulze, D.**, **Ortega-Míguez, C.**, **Polimeni, M.**, **Martone, M.**, **Böer, J.**, **Zink, M.**, TanDEM-X: DEM Acquisition in the Third Year Era, *International Journal of Space Science and Engineering*, 1(4), pp. 367-381, 2014.

[NJ-14] **Kemptner, E.**, **Peichl, M.**, Radarsignaturen und ihre Veränderung durch Metamaterialien, *Wehrtechnische Forschung im DLR*, pp. 56-57, 2014.

[NJ-15] Wermuth, M., König, R., Moon, Y., **Walter Antony, J.**, Montenbruck, O., Two Years of TanDEM-X Baseline Determination, *International Journal of Space Science and Engineering*, 2(1), pp. 35-48, 2014.

2013

[NJ-16] **Anglberger, H.**, **Speck, R.**, **Süß, H.**, Simulation Techniques for High-Resolution Spaceborne SAR Systems, *Annual Military Scientific Research Report 2012*, pp. 40-41, 2013.

[NJ-17] **Anglberger, H.**, **Speck, R.**, **Süß, H.**, Verfahren zur Simulation von raumgestützten SAR-Systemen mit hoher Auflösung, *Wehrwissenschaftliche Forschung – Jahresbericht 2012*, pp. 40-41, 2013.

[NJ-18] **Dill, S.**, **Peichl, M.**, SUMIRAD - A Fast MMW Radiometer Imager for Enhanced Reconnaissance Capability on Military Patrol Vehicles, *Annual Military Scientific Research Report - 2012*, pp. 42-43, 2013.

[NJ-19] **Dill, S.**, **Peichl, M.**, SUMIRAD - ein schneller MMW-Radiometerscanner zur verbesserten Aufklärungsfähigkeit militärischer Fahrzeuge, *Wehrwissenschaftliche Forschung – Jahresbericht 2012*, pp. 42-43, 2013.

2012

[NJ-20] **Culhaoglu, A.**, **Osipov, A.**, Metamaterialien zur Reduzierung der Radarsignatur, *Wehrwissenschaftliche Forschung – Jahresbericht 2011*, pp. 44-45, 2012.

[NJ-21] **Jochim, F.**, The Significance of the Hansen Ideal Space Frame, *Astronimical Notes*, 333(8), pp. 774-783, 2012.

2011

[NJ-22] **Baumgartner, S.**, **Krieger, G.**, Traffic Monitoring via Satellite, *PositionIT*, pp. 57-62, 2011.

[NJ-23] **Culhaoglu, A.**, **Osipov, A.**, Metamaterials for Radar Signature Reduction, *Annual Military Scientific Research*, pp. 44-45, 2011.

[NJ-24] **Peichl, M.**, Modern Radar Technology and Applications for Remote Sensing, *European Journal of Navigation*, 9(3), pp. 29-39, 2011.

Books and Book Chapters

2017

[B-1] **Osipov, A.**, Tretyakov, S., Modern Electromagnetic Scattering Theory with Applications, John Wiley & Sons, 2017.

[B-2] **Villano, M.**, Radar mit synthetischer Apertur: Eine leistungsstarke Technologie zur Beobachtung der Erde aus dem All, In: "*Faszination Technik- und Naturwissenschaften – Ausgezeichnete Forschungsbeiträge 2017*", VDE Verlag GmbH, pp. *76-85*, 2017.

2016

[B-3] Peichl, M., Handbook of Antenna Technologies – Chapter Radiometer Antennas, In: "*Handbook of Antenna Technologies*", Series "*Springer Reference*", Springer Science+Business Media Singapore, pp. *2727-2794*, 2016.

[B-4] Zink, M., **Bachmann, M.**, **Bräutigam, B.**, Fritz, T., **Hajnsek, I.**, **Krieger, G.**, **Moreira, A.**, Wessel, B., TanDEM-X: Das neue globale Höhenmodell der Erde, In: "*Handbuch der Geodäsie*", Series "*Springer Reference Naturwissenschaften*", Springer-Verlag Berlin Heidelberg, pp. *1-30*, 2016.

2015

[B-5] Oppelt, N., **Scheiber, R.**, Gege, P., Wegmann, M., Taubenböck, H., Berger, M., Fundamentals of Remote Sensing for Terrestrial Applications: Evolution, Current State of the Art, and Future Possibilities, In: "*Remote Sensing Handbook, Vol. I: Remotely Sensed Data Characterization, Classification, and Accuracies*", CRC Press, pp. *61-86*, 2015.

2014

[B-6] Börner, T., **López-Dekker, F.**, **Krieger, G.**, **Bachmann, M.**, **Moreira, A.**, Müller, H., Passive Interferometric Ocean Currents Observation Synthetic Aperture Radar (PICOSAR), In: "*Small Satellites for Earth Observation - Missions & Technologies, Operational Responsive Space, Commercial Constellations*", Series "*IAA Book Series*", International Academy of Astronatics (IAA), pp. *53-60*, 2014.

2013

[B-7] Baumgartner, S., **Krieger, G.**, Multi-Channel SAR for Ground Moving Target Indication, In: "*Academic Press Library in Signal Processing - Communications and Radar Signal Processing*", Series "*Academic Press Library in Signal Processing*", ELSEVIER (Academic Press), pp. *911-986*, 2013.

2012

[B-8] Krieger, G., **Zink, M.**, **Bachmann, M.**, **Bräutigam, B.**, Breit, H., **Fiedler, H.**, Fritz, T., **Hajnsek, I.**, **Hueso Gonzalez, J.**, Kahle, R., König, R., Schättler, B., **Schulze, D.**, Ulrich, D., Wermuth, M., Wessel, B., **Moreira, A.**, TanDEM-X, In: "*Distributed Space Missions for Earth System Monitoring*", Series "*Space Technology Library*", Springer, pp. *387-435*, 2012.

[B-9] López-Dekker, F., **Krieger, G.**, **Moreira, A.**, Multistatic Radar Systems, In: "*Distributed Space Missions for Earth System Monitoring*", Series "*Space Technology Library*", Springer New York, pp. *61-122*, 2012.

[B-10] Rommel, T., Schmied, J., Laplace-Transformation in der Praxis, Pro BUSINESS GmbH, pp. *1-238*, 2012.

Invited Conference Contributions

2017

[IC-1] Baumgartner, S., Moving Target Indication (MTI) with SAR, Proc. *EuRAD*, Nuremberg, Germany, Oct. 2017.

[IC-2] Baumgartner, S., **López-Dekker, F.**, **Laskowski, P.**, Völker, M., Klein, R., Schaefer, C., **Laux, C.**, Marques, P., **Börner, T.**, **Younis, M.**, **Bertl, S.**, García Moliná, J., Study of Multi-Channel Ka-Band SARs for Moving Target Indication, Proc. *ESA/ESTEC Final Presentation Days "RF Payload, Subsystems, Products and Technologies for Navigation, Communication and Remote Sensing*", Noordwijk, The Netherlands, Feb. 2017.

[IC-3] Buchelt, S., **Jörg, H.**, **Hajnsek, I.**, **Papathanassiou, K.**, Influences of Planting Row Orientation on Polarimetric SAR over Corn Fields at C-Band, Proc. *HGF Alliance Week*, Garmisch-Partenkirchen, Germany, Jun. 2017.

[IC-4] Buckreuß, S., 10 Jahre TerraSAR-X: Blut, Schweiß und Tränen, Proc. *10 Jahre TerraSAR-X*, Oberpfaffenhofen, Germany, Jun. 2017.

[IC-5] Heinzel, A., **Schreiber, E.**, **Peichl, M.**, **Dill, S.**, Detection of Landmines, UXO, and IEDs Using Advanced Synthetic Aperture Radar Technology, Proc. *Mine Detection Symposium*, Basel, Switzerland, Nov. 2017.

[IC-6] Horn, R., **Jäger, M.**, **Keller, M.**, **Limbach, M.**, **Nottensteiner, A.**, **Pardini, M.**, **Reigber, A.**, **Scheiber, R.**, F-SAR – Recent Upgrades and Campaign Activities, Proc. *IRS*, Prague, Czech Republic, Jun. 2017.

[IC-7] Das, N., Entekhabi, D., Kim, S., **Jagdhuber, T.**, Dunbar, S., Yueh, S., Colliander, A., High-Resolution Enhanced Product Based on SMAP Active-Passive Approach Using Sentinel-1 Data and its Applications, Proc. *IGARSS*, Fort Worth, USA, Jul. 2017.

[IC-8] Jirousek, M., **Anger, S.**, **Peichl, M.**, **Dill, S.**, **Schreiber, E.**, The IOSIS Space Object Imaging Radar, Proc. *Astrodynamics Community of Interest (ACI) Workshop*, London, Great Britain, Nov. 2017.

[IC-9] Jörg, H., **Pardini, M.**, **Hajnsek, I.**, New Insights on 3D Radar Remote Sensing in the Context of Agricultural Soil and Plant Water Dynamics: Actual Status, Future Potential and Challenges, Proc. *Water Research Horizon Conference*, Hamburg, Germany, Sep. 2017.

[IC-10] Jörg, H., **Pardini, M.**, **Hajnsek, I.**, **Papathanassiou, K.**, Analysis of a Fully Polarimetric Tomographic Time Series over Agricultural Crops for Monitoring Bio- and Geophysical Changes, Proc. *HGF Alliance Week*, Garmisch-Partenkirchen, Germany, Jun. 2017.

[IC-11] Krieger, G., **Zonno, M.**, **Rodríguez Cassolà, M.**, **López-Dekker, F.**, **Mittermayer, J.**, **Younis, M.**, **Huber, S.**, **Villano, M.**, **Queiroz de Almeida, F.**, **Prats Iraola, P.**, **Moreira, A.**, MirrorSAR: A Fractionated Space Radar for Bistatic, Multistatic and High-Resolution Wide-Swath SAR Imaging, Proc. *IGARSS*, Fort Worth, USA, Jul. 2017.

[IC-12] Krieger, G., **Queiroz de Almeida, F.**, **Huber, S.**, **Villano, M.**, **Younis, M.**, **Moreira, A.**, **del Castillo, J.**, **Rodríguez Cassolà, M.**, **Prats Iraola, P.**, Petrolati, D., Ludwig, M., Buck, C., Suess, M., **Gebert, N.**, Advanced L-Band SAR System Concepts for High-Resolution Ultra-Wide-Swath SAR Imaging, Proc. *ESA ARSI*, Noordwijk, The Netherlands, Sep. 2017.

[IC-13] Moreira, A., A Vision for Spaceborne Radar Remote Sensing, Proc. *URSI Kleinheubacher Tagung*, Miltenberg, Germany, Sep. 2017.

[IC-14] Moreira, A., Tandem-L: Highly Innovative Interferometric Radar Satellite Mission for Climate Research and Environmental Monitoring, Proc. *DPG-Frühjahrstagung*, Bremen, Germany, Mar. 2017.

[IC-15] Moreira, A., The TanDEM-X Mission: A New Measurement of the Earth`s Topography and Much More, Proc. *IRS*, Prague, Czech Republic, Jun. 2017.

[IC-16] Nannini, M., **Martone, M.**, **Rizzoli, P.**, **Prats Iraola, P.**, **Rodríguez Cassolà, M.**, **Moreira, A.**, Spaceborne Demonstration of Coherent SAR Tomography for Future Companion Satellite SAR Missions, Proc. *IGARSS*, Fort Worth, USA, Jul./Aug. 2017.

[IC-17] Neff, T., Neue Entwicklungen in der Raumaufklärung, Proc. *Symposium Radarsystemtechnologie für die Bundeswehr*, Mannheim, Jan. 2017.

[IC-18] Osipov, A., Backscattering from Electrically Large Low-Absorption Spheres: an Explanation of Solar Glories, Proc. *URSI GASS*, Montreal, Canada, Aug. 2017.

[IC-19] Osipov, A., **Culhaoglu, A.**, **Kemptner, E.**, Impedance Modeling of Electromagnetic Scattering from Canonical Bodies with Metamaterial Absorbers and Chessboard-Patterned Deflectors, Proc. *ICEAA*, Verona, Italy, Sep. 2017.

[IC-20] Osipov, A., **Kemptner, E.**, **Özis, E.**, Kobayashi, H., Microwave Metamaterials for Increased Survivability of Future Systems, Proc. *IEICE Workshop of Technical Committee on Space, Aeronautical and Navigational Electronics (IEICE-SANE)*, Nagasaki, Japan, vol. 116, Jan. 2017.

[IC-21] Papathanassiou, K., Science Challenges of Retrieving Forest Height from SAR, Proc. *ISSI Workshop*, Bern, Switzerland, Nov. 2017.

[IC-22] Papathanassiou, K., Structure Parameter Estimation of Natural Scatteres by Means of Multibaseline Pol-InSAR Techniques: Status and Challenges, Proc. *IGARSS*, Fort Worth, USA, Jul. 2017.

[IC-23] Papathanassiou, K., **Kim, J.**, Polarimetric System Calibration in the Presence of Faraday Rotation, Proc. *IGARSS*, Fort Worth, USA, Jul. 2017.

[IC-24] Pardini, M., **Tello Alonso, M.**, **Cazcarra Bes, V.**, **Papathanassiou, K.**, **Hajnsek, I.**, What Can We Learn about Vertical Forest Structure from TomoSAR at L- and P-Band and How Does it Compare to Full Waveform Lidar Profiles?, Proc. *ISSI Workshop*, Bern, Switzerland, Nov. 2017.

[IC-25] Pardini, M., **Kim, J.**, **Papathanassiou, K.**, **Hajnsek, I.**, Height Estimation and 3-D Structure Observation of African Tropical Forests With Multibaseline SAR: Results from the AfriSAR Campaign, Proc. *IGARSS*, Fort Worth, USA, Jul. 2017.

[IC-26] Prats Iraola, P., **Nannini, M.**, **Yague-Martinez, N.**, **Pinheiro, M.**, Kim, J., Vecchioli, F., Minati, F., Costantini, M., Borgstrom, S., De Martino, P., Siniscalchi, V., Foumelis, M., Desnos, Y., Interferometric Investigations with the Sentinel-1 Constellation, Proc. *IGARSS*, Fort Worth, USA, Jul. 2017.

[IC-27] Prats Iraola, P., **Rodríguez Cassolà, M.**, **López-Dekker, F.**, **Zonno, M.**, **Yague-Martinez, N.**, **Nannini, M.**, Technical Aspects in SAR Image Formation and Interferometric Processing of Companion Satellite SAR Missions, Proc. *IGARSS*, Fort Worth, USA, Jul. 2017.

[IC-28] Prats Iraola, P., **Nannini, M.**, **Yague-Martinez, N.**, **Pinheiro, M.**, **Kim, J.**, Vecchioli, F., Minati, F., Costantini, M., Borgstrom, S., de Martino, P., Siniscalchi, V., Foumelis, M., Desnos, Y., Interferometric Investigations with the Sentinel-1 Constellation and Results, Proc. *ESA FRINGE Workshop*, Helsinki, Finland, Jun. 2017.

[IC-29] Pulella, A., Bispo, P., **Pardini, M.**, **Kugler, F.**, **Cazcarra Bes, V.**, **Tello Alonso, M.**, **Papathanassiou, K.**, Balzter, H., Rizaev, I., Dos Santos, M., Dos Santos, J., Spinelli-Araujo, L., Tansey, K., Tropical Forest Structure Observation with TanDEM-X Data, Proc. *IGARSS*, Fort Worth, USA, Jul. 2017.

[IC-30] Reigber, A., DLR's Airborne SAR Research: Preparing Future Satellite Missions, Proc. *CIRFA*, Tromsø, Norway, Oct. 2017.

[IC-31] Reigber, A., DLR's Airborne F-SAR System, Proc. *Photogrammetric Week*, Stuttgart, Germany, Sep. 2017.

[IC-32] Hagen, M., **Reimann, J.**, Propagation Effects in the Application of Weather Radar – Positive and Negative Impact, Proc. *European Conference on Antennas and Propagation (EUCAP)*, Paris, France, Mar. 2017.

[IC-33] Rodríguez Cassolà, M., **Prats Iraola, P.**, **Zonno, M.**, **Nannini, M.**, **López-Dekker, F.**, Carnicero Dominguez, B., Rommen, B., **Moreira, A.**, End-TO-End Performance Anasysis of Companion SAR Missions, Proc. *IGARSS*, Fort Worth, USA, Jul. 2017.

[IC-34] Schreiber, E., Hoch-Performantes Radarsystem zur Detektion verborgener Objekte, Proc. *Symposium Radarsystemtechnologie für die Bundeswehr*, Mannheim, Germany, Jan. 2017.

[IC-35] Yague-Martinez, N., **Prats Iraola, P.**, **Wollstadt, S.**, North-Sound Ground Displacement Retrieval with Burst-Mode SAR Systems: Experimental Modes and Results with TerraSAR-X., Proc. *Mesure de la Déformation par Imagerie Spatiale*, Clermont-Ferrand, Besse-en-Chandesse, France, Oct. 2017.

[IC-36] Zink, M., **Moreira, A.**, **Bachmann, M.**, **Rizzoli, P.**, Fritz, T., **Hajnsek, I.**, **Krieger, G.**, Wessel, B., The Global TanDEM-X Dem – A Unique Data Set, Proc. *IGARSS*, Fort Worth, USA, Jul. 2017.

2016

[IC-37] Wessel, B., Breunig, M., **Bachmann, M.**, Huber, M., **Martone, M.**, Lachaise, M., Fritz, T., **Zink, M.**, Concept and First Example of TanDEM-X High-Resolution DEM, Proc. *EUSAR*, Hamburg, Germany, Jun. 2016.

[IC-38] Baumgartner, S., **Nottensteiner, A.**, **Rosigkeit, D.**, Usability of LTE for Transmitting Radar Data from DLR's Research Aircraft DO228-212, Proc. *European Telemetry and Test Conference (ETC)*, Nuremberg, Germany, May 2016.

[IC-39] Buckreuß, S., **Zink, M.**, TerraSAR-X and TanDEM-X Mission Status, Proc. *TerraSAR-X Science Team Meeting*, Oberpfaffenhofen, Germany, Oct. 2016.

[IC-40] Buckreuß, S., **Zink, M.**, TerraSAR-X and TanDEM-X Mission Status, Proc. *EUSAR*, Hamburg, Germany, Jun. 2016.

[IC-41] Eilers, J., **Calaminus, B.**, **Brand, B.**, **Blaschke, K.**, Performance Estimation of Small Satellite Systems, Proc. *Specialists' Meeting AVT-257/RSM-041*, Zaragoza, Spain, Sep. 2016.

[IC-42] Yuzugullu, O., Marelli, S., **Erten, E.**, Sudret, B., **Hajnsek, I.**, Global Sensitivity Analysis of a Morphology Based Electromagnetic Scattering Model, Proc. *IGARSS*, Milan, Italy, Jul. 2015/Jul. 2016.

[IC-43] Hager, M., Einsatz von Corner Reflektoren zur Kalibrierung von weltraumgestützten hochauflösenden SAR-Sensoren, Proc. *ATCx – Electromagnetics*, Böblingen, Germany, Sep. 2016.

[IC-44] Siddique, M., Wegmuller, U., **Hajnsek, I.**, Frey, O., SAR Tomography for Spatio-temporal Inversion of Point-Like Scatterers in Urban Areas, Proc. *IGARSS*, Milan, Italy, Jul. 2015/Jul. 2016.

[IC-45] Boerner, W., Erricolo, D., Negishi, T., Yang, R., **Krieger, G.**, **Reigber, A.**, **Moreira, A.**, International Development of Multi-band Pol-InSAR Satellite Sensors for Protecting the Flora and Fauna as well as Natural Land and Coastal Environment within the Equatorial Belt of +/-23.77 deg, +/-18 deg, +/-12 deg and +/-8 deg Latitude, Proc. *IGARSS*, Beijing, China, Jul. 2016.

[IC-46] **Krieger, G.**, **Moreira, A.**, **Zink, M.**, **Hajnsek, I.**, **Huber, S.**, **Villano, M.**, **Papathanassiou, K.**, **Younis, M.**, **López-Dekker, F.**, **Pardini, M.**, **Schulze, D.**, **Bachmann, M.**, **Borla Tridon, D.**, **Reimann, J.**, **Bräutigam, B.**, **Steinbrecher, U.**, **Tienda Herrero, C.**, **Sanjuan Ferrer, M.**, **Zonno, M.**, Eineder, M., De Zan, F., Parizzi, A., Fritz, T., Diedrich, E., Maurer, E., Münzenmayer, R., Grafmüller, B., Wolters, R., te Hennepe, F., Ernst, R., Bewick, C., Tandem-L: Main Results of the Phase A Feasibility Study, Proc. *IGARSS*, Beijing, China, Jul. 2016.

[IC-47] **Matar, J.**, **López-Dekker, F.**, **Krieger, G.**, Potentials and Limitations of MEO SAR, Proc. *EUSAR*, Hamburg, Germany, Jun. 2016.

[IC-48] **Moreira, A.**, Tandem-L: Highly Innovative Radar Satellite Mission for Climate Research and Environmental Monitoring, Proc. *United Nations / Austria Symposium on "Integrated Space Technology Applications for Climate Change*", Graz, Austria, Sep. 2016.

[IC-49] **Moreira, A.**, A Vision for Spaceborne Synthetic Aperture Radar (SAR), Proc. *International Society for Photogrammetry and Remote Sensing (ISPRS) Congress*, Prague, Czech Republic, Jul. 2016.

[IC-50] **Osipov, A.**, Backscattering from Electrically Large Low-Absorption Spheres, Proc. *EMTS*, Espoo, Finland, Aug. 2016.

[IC-51] **Papathanassiou, K.**, **Kim, J.**, Pol-InSAR Calibration of ALOS-2: Analysis and Results from the CAL-VAL Phase, Proc. *IGARSS*, Beijing, China, Jul. 2016.

[IC-52] **Papathanassiou, K.**, **Pardini, M.**, **Hajnsek, I.**, Volume Structure Characterisation by Means of Multibaseline Pol-InSAR: Status and Challenges, Proc. *IGARSS*, Beijing, China, Jul. 2016.

[IC-53] **Parrella, G.**, **Fischer, G.**, **Pardini, M.**, **Hajnsek, I.**, **Papathanassiou, K.**, Potential of P-Band SAR for Ice Sheet Subsurface Investigations, Proc. *ESA Living Planet Symposium*, Prague, Czech Republic, May 2016.

[IC-54] **Peichl, M.**, SAR und ISAR: Theorie und Praxis, Proc. *Lehrgang „Moderne Verfahren der Radartechnik"*, Mannheim, Germany, Nov. 2016.

[IC-55] **Peichl, M.**, Detection of Explosives in a Flow of Vehicles, Proc. *Technology for Countering the CBRN-E Threats*, Les Bons Villers, Belgium, Oct. 2016.

[IC-56] **Peichl, M.**, Forward-Looking Radar, Proc. *Nationale Counter-IED-Konferenz*, Mannheim, Germany, Sep. 2016.

[IC-57] **Peichl, M.**, Potenziale von MW-Messverfahren zur Detektion verborgener Objekte, Proc. *KSK-Symposium Rüstung*, Calw, Germany, Sep. 2016.

[IC-58] **Peichl, M.**, Modern Radar Technology for Efficient Detection of Landmines and UXO, Proc. *Improvised Explosive Devices and Antipersonnel Mines meeting the Challenges*, Brussels, Belgium, May 2016.

[IC-59] **Ponce Madrigal, O.**, **Queiroz de Almeida, F.**, **Rommel, T.**, Multiple-Input Multiple-Output Circular SAR for High Altitude Pseudo-Satellites, Proc. *International Astronautical Congress (IAC)*, Guadalajara, Mexico, Sep./Oct. 2016.

[IC-60] **Ponce Madrigal, O.**, **Martinez del Hoyo, A.**, **Scheiber, R.**, **Hajnsek, I.**, **Reigber, A.**, Multi-Dimensional Airborne Holographic SAR Tomography Reconstruction for Glaciers at L-/P-Band, Proc. *IGARSS*, Beijing, China, Jul. 2016.

[IC-61] **Prats Iraola, P.**, **Nannini, M.**, **Yague-Martinez, N.**, **Scheiber, R.**, Minati, F., Vecchioli, F., Costantini, M., Borgstrom, S., De Martino, P., Siniscalchi, V., Walter, T., Nikkhoo, M., Foumelis, M., Desnos, Y., Sentinel-1 Assessment of the Interferometric Wide-Swath Mode, Proc. *IGARSS*, Beijing, China, Jul. 2016.

[IC-62] **Reigber, A.**, **Jäger, M.**, Krogager, E., Polarimetric SAR Change Detection in Multiple Frequency Bands for Environmental Monitoring in Arctic Regions, Proc. *IGARSS*, Beijing, China, Jul. 2016.

[IC-63] **Rodríguez Cassolà, M.**, **López-Dekker, F.**, **Nannini, M.**, **Zonno, M.**, **Prats Iraola, P.**, Gebert, N., Davidson, M., Carnicero Dominguez, B., SAOCOM/CS Mission: Interferometric/Tomographic Performance and Suggested Calibration Concept, Proc. *ESA Living Planet Symposium*, Prague, Czech Republic, May 2016.

[IC-64] **Schreiber, E.**, Radarsensor mit synthetischer Apertur zur Detektion von vergrabenen Objekten aus sicherer Distanz, Proc. *Wehrtechnisches F&T Symposium „Safety und Security in militärischen Waffensystemen"*, Mannheim, Germany, Jun. 2016.

[IC-65] **Schreiber, E.**, **Peichl, M.**, Radarsensor mit synthetischer Apertur zur Detektion von vergrabenen Objekten aus sicherer Distanz, Proc. *Wehrtechnisches F&T Symposium "Safety und Security in militärischen Waffensystemen*", Mannheim, Germany, Jun. 2016.

[IC-66] **Schwerdt, M.**, **Schmidt, K.**, **Tous Ramon, N.**, **Castellanos Alfonzo, G.**, **Döring, B.**, **Zink, M.**, **Prats Iraola, P.**, Sentinel-1B Independent In-Orbit System Calibration - First Results -, Proc. *EUSAR*, Hamburg, Germany, Jun. 2016.

[IC-67] **Wecklich, C.**, **Gonzalez, C.**, **Bräutigam, B.**, **Rizzoli, P.**, Height Accuracy and Data Coverage Status of the Global TanDEM-X DEM, Proc. *EUSAR*, Hamburg, Germany, Jun. 2016.

[IC-68] **Yague-Martinez, N.**, **Prats Iraola, P.**, **Kraus, T.**, **Wollstadt, S.**, **Scheiber, R.**, Experimental Validation with TerraSAR-X/TanDEM-X of Advanced Interferometric Modes for Accurate Retrieval of Azimuthal Displacements, Proc. *IGARSS*, Beijing, China, Jul. 2016.

[IC-69] **Younis, M.**, **Queiroz de Almeida, F.**, **López-Dekker, F.**, **Krieger, G.**, Techniques and Modes for Multi-Channel SAR Instruments, Proc. *EUSAR*, Hamburg, Germany, Jun. 2016.

[IC-70] **Zink, M.**, **Moreira, A.**, **Bachmann, M.**, **Bräutigam, B.**, Fritz, T., **Hajnsek, I.**, **Krieger, G.**, Wessel, B., TanDEM-X Mission Status: The Complete New Topography of the Earth, Proc. *IGARSS*, Beijing, China, Jul. 2016.

2015

[IC-71] **Alonso-González, A.**, Lopez-Martinez, C., **Hajnsek, I.**, Processing Polarimetric SAR Time Series over Urban Areas with Binary Partition Trees, Proc. *International Workshop on the Analysis of Multitemporal Remote Sensing Images*, Annecy, France, Jul. 2015.

[IC-72] **Anglberger, H.**, Modern Spaceborne Radar – A Comprehensive Tool for High-Performance Reconnaissance and Surveillance, Proc. *3NATO SET Business Panel Meeting*, Norfolk, USA, May 2015.

[IC-73] **Bräutigam, B.**, **Martone, M.**, **Rizzoli, P.**, **Gonzalez, C.**, **Wecklich, C.**, **Bachmann, M.**, **Schulze, D.**, **Zink, M.**, Quality Assessment of the TanDEM-X Global Digital Elevation Model, Proc. *International Symposium on Remote Sensing of Environment (ISRSE)*, Berlin, Germany, vol. XL-7/W, May 2015.

[IC-74] **Bräutigam, B.**, Germany's Spaceborne Radar Program: TerraSAR-X, TanDEM-X and Beyond, Proc. *Global Space & Technology Convention (GSTC)*, Singapore, Feb. 2015.

[IC-75] Yuzugullu, O., **Erten, E.**, **Hajnsek, I.**, Scattering Function Optimization for Growth Stage Determination of Rice Fields: Preliminary Results, Proc. *ESA POLinSAR Workshop*, Frascati, Italy, Jan. 2015.

[IC-76] Siddique, M., **Hajnsek, I.**, Wegmuller, U., Frey, O., Investigating the Combined Use of Differential SAR Tomography and PSI for Spatio-Temporal Inversion, Proc. *Joint Urban Remote Sensing Event (JURSE)*, Lausanne, Switzerland, vol. 26453, Mar./Apr. 2015.

[IC-77] Siddique, M., **Hajnsek, I.**, Wegmuller, U., Frey, O., Towards the Integration of SAR Tomography and PSI for Improved Deformation Assessment in Urban Areas, Proc. *ESA FRINGE Workshop*, Frascati, Italy, Mar. 2015.

[IC-78] Alemohammad, S., Konnings, A., **Jagdhuber, T.**, Entekhabi, D., Retrieving Vegetation and Soil Parameters from Active Polarimetric P-Band Observations, Proc. *IGARSS*, Milan, Italy, Jul. 2015.

[IC-79] **Jäger, M.**, **Pinheiro, M.**, **Ponce Madrigal, O.**, **Reigber, A.**, **Scheiber, R.**, A Survey of Novel Airborne SAR Signal Processing Techniques and Applications for DLR's F-SAR Sensor, Proc. *IRS*, Dresden, Germany, Jun. 2015.

[IC-80] Boerner, W., **Krieger, G.**, **Reigber, A.**, **Hajnsek, I.**, Schmullius, C., **Moreira, A.**, Eineder, M., Bamler, R., Meyer, F., Hensley, S., van Zyl, J., Neumann, M., Shimada, M., Ohki, M., Sumantyo, J., Hattori, K., Ocampo-Torres, F., **Ponce Madrigal, O.**, Moreira, J., Campos, J., Lu, Y., Dubois-Fernandez, P., Pottier, E., Le Toan, T., Surussavadee, C., Koo, V., Lim, V., Triharjanto, R., Hasbi, W., Mohan, S., Singh, G., Development of New Multi-band Equatorially Orbiting PoLinSAR Satellite Sensors System Configurations for Varying Latitudinal Coverage within Total Tropical Belt (Invited Group presentation for establishing an associated Consortium), Proc. *Asian Pacific Conference on Synthetic Aperture Radar (APSAR)*, Singapore, Sep. 2015.

[IC-81] **Krieger, G.**, **Huber, S.**, **Villano, M.**, **Younis, M.**, **Rommel, T.**, **López-Dekker, F.**, **Queiroz de Almeida, F.**, **Moreira, A.**, CEBRAS: Cross Elevation Beam Range Ambiguity Suppression for High-Resolution Wide-Swath and MIMO-SAR Imaging, Proc. *IGARSS*, Milan,Italy, Jul. 2015.

[IC-82] **Moreira, A.**, Radaraugen im All: Einzigartiger Blick auf Erde und Umwelt, Proc. *Wissenschaftliches Symposium im Rahmen des 20-jährigen Helmholtz-Jubiläums*, Berlin, Germany, Jun. 2015.

[IC-83] **Moreira, A.**, **Ponce Madrigal, O.**, **Nannini, M.**, **Pardini, M.**, **Prats Iraola, P.**, Multibaseline Imaging: A Vision for Spaceborne SAR, Proc. *IRS*, Dresden, Germany, Jun. 2015.

[IC-84] **Moreira, A.**, Global Trends and Challenges in Remote Sensing Technology: New Approaches in SAR Imaging, Proc. *International Symposium on Remote Sensing of Environment (ISRSE)*, Berlin, Germany, May 2012/May 2015.

[IC-85] **Özis, E.**, **Osipov, A.**, Eibert, T., Metamaterials for Microwave Radomes: An Overview, Proc. *PIERS*, Prague, Czech Republic, Jul. 2015.

[IC-86] **Osipov, A.**, Tretyakov, S., Analytical Approximations of Low-Frequency Scattering from Homogeneous Spheres, Proc. *URSI Atlantic Radio Science Conference (URSI AT-RASC)*, Spain, May 2015.

[IC-87] **Papathanassiou, K.**, Volume Structure Parameter Estimation by Means of Pol-InSAR Techniques: Status and Challenges, Proc. *IGARSS*, Milan, Italy, Jul. 2015.

[IC-88] **Papathanassiou, K.**, **Kim, J.**, Calibration of Pol-InSAR ALOS-2 Data: Analysis and Results from the Cal-Val Phase, Proc. *IGARSS*, Milan, Italy, Jul. 2015.

[IC-89] **Pardini, M.**, **Papathanassiou, K.**, First Investigation on the Information Content of Multibaseline PolInSAR Data at S-Band for Forest Structure Observation, Proc. *IGARSS*, Milan, Italy, Jul. 2015.

[IC-90] **Pardini, M.**, **Papathanassiou, K.**, Spaceborne SAR Tomography Over Forests: Performance and Trade-Offs for Repeated Single Pass PolInSAR Acquisitions, Proc. *IGARSS*, Milan, Italy, Jul. 2015.

[IC-91] **Prats Iraola, P.**, **Nannini, M.**, **Scheiber, R.**, De Zan, F., **Wollstadt, S.**, Minati, F., Vecchioli, F., Costantini, M., Borgstrom, S., Walter, T., Foumelis, M., Desnos, Y., Assessment of the Sentinel-1 Interferometric Capabilities in the Interferometric Wide-Swath Mode, Proc. *International Symposium on Remote Sensing of Environment (ISRSE)*, Berlin, Germany, May 2015.

[IC-92] **Prats Iraola, P.**, **Nannini, M.**, **Scheiber, R.**, De Zan, F., **Wollstadt, S.**, Minati, F., Costantini, M., Bucarelli, A., Borgstrom, S., Walter, T., Foumelis, M., Desnos, Y., Investigations with the Sentinel-1 Interferometric Wide-Swath Mode, Proc. *ESA FRINGE Workshop*, Frascati, Italy, Mar. 2015.

[IC-93] **Reigber, A.**, Lombardini, F., Viviani, F., **Nannini, M.**, **Martinez del Hoyo, A.**, Three-Dimensional and Higher-Order Imaging with Tomographic SAR: Techniques, Applications, Issues, Proc. *IGARSS*, Milan, Italy, Jul. 2015.

[IC-94] **Reigber, A.**, **Nannini, M.**, **Martinez del Hoyo, A.**, **Martín del Campo Becerra, G.**, Shkvarko, Y., A Comparative Study of Tomographic SAR Focusing Methods, Proc. *EuRAD*, Paris, France, Sep. 2015.

[IC-95] **Rommel, T.**, Waveform Diversity Methods for Multi-Parameter Radar Applications, Proc. *ITG Fachausschuss 7.5*, Chemnitz, Germany, Feb. 2015.

[IC-96] Hagen, M., Höller, H., **Schmidt, K.**, Evaluation of Mesoscale Events Using Dual-Polarization and Doppler Radar Observations, Proc. *VII. Atmospheric Science Symposium*, Istanbul, Turkey, Apr. 2015.

[IC-97] **Schreiber, E.**, **Peichl, M.**, **Dill, S.**, **Jirousek, M.**, **Kempf, T.**, Application of Passive Millimeterwave Imaging and UHF-based Synthetic Aperture Radar for Threat Detection, Proc. *Counter IED Technology Workshop*, Madrid, Spain, Jun. 2015.

[IC-98] Wiesbeck, W., Sit, L., **Younis, M.**, **Krieger, G.**, **Moreira, A.**, Radar 2020: The Future of Radar Systems, Proc. *IGARSS*, Milan, Italy, Jul. 2015.

[IC-99] **Zink, M.**, DLR's Current & Future SAR Missions: TerraSAR-X, TanDEM-X & Tandem-L, Proc. *Polar Space Task Group*, Oberpfaffenhofen, Germany, Oct. 2015.

[IC-100] **Zink, M.**, **Bachmann, M.**, **Bräutigam, B.**, Fritz, T., **Hajnsek, I.**, **Krieger, G.**, **Moreira, A.**, Wessel, B., TanDEM-X: A Single-Pass SAR Interferometer for global DEM Generation and Demonstration of New SAR Techniques, Proc. *IGARSS*, Milan, Italy, Jul. 2015.

[IC-101] **Zink, M.**, TanDEM-X Mission Status, Proc. *International Symposium on Remote Sensing of Environment (ISRSE)*, Berlin, Germany, vol. XL-7/W, May 2015.

[IC-102] **Zink, M.**, Radaranwendungen in der Raumfahrt: TerraSAR-X, TanDEM-X & zukünftige Entwicklungen, Proc. *Symposium Radar*, Mannheim, Germany, Jan. 2015.

[IC-103] **Zink, M.**, **Moreira, A.**, TanDEM-X: A Challenging Radar Mission for Generating a Next-Generation Earth's Topography, Proc. *Geomorphometry*, Poznan, Poland, Jun. 2015.

2014

[IC-104] **Anglberger, H.**, Aufklärung mittels Optik-Radar Datenfusion, Proc. *Angewandte Forschung für Verteidigung und Sicherheit in Deutschland*, Berlin, Germany, Feb. 2014.

[IC-105] **Bertl, S.**, **López-Dekker, F.**, **Younis, M.**, **Krieger, G.**, Flexible Generation of Equivalent Beams for Digital Beamforming SAR Systems with Different Antenna Structures, Proc. *ARSI & Ka-Band Earth Observation Radar Missions Workshop (KEO)*, Noordwijk, The Netherlands, Nov. 2014.

[IC-106] Bräutigam, B., **Bachmann, M.**, **Schulze, D.**, **Borla Tridon, D.**, **Rizzoli, P.**, **Martone, M.**, **Gonzalez, C.**, **Zink, M.**, **Krieger, G.**, TanDEM-X Global DEM Quality Status and Acquisition Completion, Proc. *IGARSS*, Québec, Canada, Jul. 2014.

[IC-107] Culhaoglu, A., Microwave Metamaterials for Radar Signature Reduction, Proc. *Hauptseminar Nano,* Technische Universität Munich (TUM), Munich, Germany, Nov. 2014.

[IC-108] De Zan, F., **Zonno, M.**, **López-Dekker, F.**, Lack of Triangularity in SAR Interferometric Phases, Proc. *EUSAR*, Berlin, Germany, Jun. 2014.

[IC-109] Erten, E., Rossi, C., Yuzugullu, O., **Hajnsek, I.**, Phenological Growth Stages of Paddy Rice according to the BBCH Scale and SAR Images, Proc. *IGARSS*, Quebec City, Canada, Jul. 2014.

[IC-110] Zwieback, S., **Hajnsek, I.**, The Impact of Vegetation Growth on DInSAR Coherence Regions and Estimated Deformations, Proc. *IGARSS*, Quebec City, Canada, Jul. 2014.

[IC-111] Frey, O., **Hajnsek, I.**, Wegmuller, U., Werner, C., SAR Tomography Based 3-D Point Cloud Extraction of Point-Like Scatterers in Urban Areas, Proc. *IGARSS*, Quebec City, Canada, Jul. 2014.

[IC-112] Hajnsek, I., **Busche, T.**, TanDEM-X: Science Activities, Proc. *EUSAR*, Berlin, Germany, Jun. 2014.

[IC-113] Hajnsek, I., Shimada, M., Eineder, M., **Papathanassiou, K.**, Motooka, T., Watanabe, M., Ohki, M., **De Zan, F.**, **López-Dekker, F.**, **Krieger, G.**, **Moreira, A.**, Tandem-L: Science Requirements and Mission Concept, Proc. *EUSAR*, Berlin, Germany, Jun. 2014.

[IC-114] Marino, A., **Hajnsek, I.**, Ship Detection with TanDEM-X Data: a Statistical Test for a Polarimetric Notch Filter, Proc. *EUSAR*, Berlin, Germany, Jun. 2014.

[IC-115] Zwieback, S., **Hajnsek, I.**, Hensley, S., Modelling the Impact of Moisture Changes in a Heterogeneous Soil on Differential Interferometry, Proc. *IGARSS*, Quebec City, Canada, Jul. 2014.

[IC-116] Jagdhuber, T., **Hajnsek, I.**, **Papathanassiou, K.**, Polarimetric Soil Moisture Retrieval Using An Iterative Generalized Hybrid Decomposition Technique, Proc. *IGARSS*, Quebec City, Canada, Jul. 2014.

[IC-117] Jagdhuber, T., **Hajnsek, I.**, **Papathanassiou, K.**, Progress in Surface Soil Moisture Derivation under Agricultural Vegetation Cover, Proc. *HGF Alliance Week*, Garmisch-Partenkirchen, Germany, Jul. 2014.

[IC-118] Jagdhuber, T., **Hajnsek, I.**, **Papathanassiou, K.**, An Iterative, Generalized, Hybrid Decomposition on Fully Polarimetric SAR Data for Soil Moisture Retrieval under Vegetation, Proc. *EUSAR*, Berlin, Germany, Jun. 2014.

[IC-119] Jäger, M., **Reigber, A.**, A Non-Parametric Texture Descriptor for Polarimetric SAR Data with Applications to Supervised Classification, Proc. *EUSAR*, Berlin, Germany, Jun. 2014.

[IC-120] Jäger, M., **Gabler, B.**, **Reigber, A.**, High-Precision Antenna Characterization for Broadband Synthetic Aperture Radar Processing, Proc. *EuCAP*, The Hague, The Netherlands, Apr. 2014.

[IC-121] Jäger, M., Hellwich, O., A Cascaded Ensemble Classifier for Object Segmentation in High-Resolution Polarimetric SAR Data, Proc. *IGARSS*, Quebec City, Canada, Jul. 2014.

[IC-122] Ludwig, M., Germani, C., Venturini, R., Schaefer, C., **López-Dekker, F.**, Digital Beamforming for Ka-Band InSAR Instruments, Proc. *EUSAR*, Berlin, Germany, Jun. 2014.

[IC-123] Moreira, A., A Golden Age for Spaceborne SAR Systems, Proc. *International Conference Microwave and Radar Week (MRW)*, Gdańsk, Poland, Jun. 2014.

[IC-124] Moreira, A., Radaraugen im All: Einzigartiger Blick auf Erde und Umwelt, Proc. *Internationale Fachmesse und Kongress für Elektromagnetische Verträglichkeit (EMV)*, Duesseldorf, Germany, Mar. 2014.

[IC-125] Nannini, M., **Prats Iraola, P.**, **De Zan, F.**, DInSAR Performance Investigations with the TOPS Mode, Proc. *EUSAR*, Berlin, Germany, Jun. 2014.

[IC-126] Pardini, M., **Cantini, A.**, **Kugler, F.**, **Papathanassiou, K.**, Lombardini, F., Monitoring Dynamics in Time of Forest Vertical Structure with Multibaseline PolInSAR Data, Proc. *IGARSS*, Quebec City, Canada, Jul. 2014.

[IC-127] Pardini, M., **Cantini, A.**, Lombardini, F., **Papathanassiou, K.**, 3-D Structure of Forests: First Analysis of Tomogram Changes due to Weather and Seasonal Effects at L-Band, Proc. *EUSAR*, Berlin, Germany, Jun. 2014.

[IC-128] Parrella, G., **Hajnsek, I.**, **Papathanassiou, K.**, Polarimetric Decomposition of L- and P-Band SAR Backscatter Over the Superimposed Ice Zone of a Sub-Polar Ice-Cap, Proc. *EUSAR*, Berlin, Germany, Jun. 2014.

[IC-129] Ponce Madrigal, O., Synthetic Aperture Radar (SAR) for Earth Observation, Proc. *United Nations / Mexico Symposium on Basic Space Technology "Making Space Technology Accessible and Affordable"*, Ensenada, Baja California, Mexico, Oct. 2014.

[IC-130] Scheiber, R., **Prats Iraola, P.**, **Nannini, M.**, **Villano, M.**, Morrison, K., **Gebert, N.**, Comparison of Digital Beamforming Techniques for Enhanced Ice Sounding Radar Data Processing, Proc. *EUSAR*, Berlin, Germany, Jun. 2014.

[IC-131] Schulze, D., **Bachmann, M.**, **Bräutigam, B.**, **Borla Tridon, D.**, **Rizzoli, P.**, **Martone, M.**, **Zink, M.**, **Krieger, G.**, Status of TanDEM-X DEM Acquisition, Calibration and Performance, Proc. *EUSAR*, Berlin, Germany, Jun. 2014.

[IC-132] Schwerdt, M., **Schmidt, K.**, **Tous Ramon, N.**, **Castellanos Alfonzo, G.**, **Döring, B.**, **Zink, M.**, Independent Verification of the Sentinel-1A System Calibration - First Results -, Proc. *EUSAR*, Berlin, Germany, Jun. 2014.

[IC-133] Balss, U., Breit, H., Fritz, T., **Steinbrecher, U.**, Gisinger, C., Eineder, M., Analysis of Internal Timings and Clock Rates of TerraSAR-X, Proc. *IGARSS*, Quebec City, Canada, Jul. 2014.

[IC-134] Toraño Caicoya, A., **Kugler, F.**, **Pardini, M.**, **Hajnsek, I.**, **Papathanassiou, K.**, Vertical Forest Structure Characterization for the Estimation of Above Ground Biomass: First Experimental Results Using SAR Vertical Reflectivity Profiles, Proc. *IGARSS*, Quebec City, Canada, Jul. 2014.

[IC-135] Younis, M., **Laux, C.**, **Al-Kahachi, N.**, **López-Dekker, F.**, **Krieger, G.**, **Moreira, A.**, Calibration of Multi-Channel Spaceborne SAR - Challenges and Strategies -, Proc. *EUSAR*, Berlin, Germany, Jun. 2014.

[IC-136] Zink, M., TanDEM-X: Key Features and Mission Status, Proc. *EUSAR*, Berlin, Germany, Jun. 2014.

2013

[IC-137] Bachmann, M., **Borla Tridon, D.**, **Böer, J.**, **Bräutigam, B.**, **Grigorov, C.**, **Kraus, T.**, **Krieger, G.**, **Martone, M.**, **Ortega Miguez, C.**, **Rizzoli, P.**, **Steinbrecher, U.**, **Schulze, D.**, **Walter Antony, J.**, **Weigt, M.**, **De Zan, F.**, **Zink, M.**, TanDEM-X Acquisition Status and DEM Performance, Proc. *TerraSAR-X / TanDEM-X Science Team Meeting*, Oberpfaffenhofen, Germany, Jun. 2013.

[IC-138] Bräutigam, B., **Zink, M.**, **Hajnsek, I.**, **Krieger, G.**, The TanDEM-X Mission: Earth Observation in 3D, Proc. *Geomorphometry*, Nanjing, China, Oct. 2013.

[IC-139] Bräutigam, B., **Rizzoli, P.**, **Martone, M.**, **Bachmann, M.**, **Schulze, D.**, **Krieger, G.**, **Zink, M.**, TanDEM-X Acquisition and Quality Overview with Two Global Coverages, Proc. *IGARSS*, Melbourne, Australia, Jul. 2013.

[IC-140] Buckreuß, S., TerraSAR-X Mission Status, Proc. *TerraSAR-X / TanDEM-X Science Team Meeting*, Oberpfaffenhofen, Germany, Jun. 2013.

[IC-141] Buckreuß, S., Die Missionen TerraSAR-X und TanDEM-X, Proc. *Wehrtechnisches Symposium Sensortechnologien*, Mannheim, Germany, Jun. 2013.

[IC-142] Linck, R., **Buckreuß, S.**, Seren, S., Determination of the Applicability of High-Resolution X-Band Satellite Radar for the Archaeological Prospection by a Comparison with a Ground-Based Survey, Proc. *Archaeological Prospection*, Vienna, Austria, May/Jun. 2013.

[IC-143] Albooyeh, M., Alitalo, P., Andryieuski, A., **Culhaoglu, A.**, Lavrinrnko, A., Morits, D., Simovski, C., Tretyakov, S., Modeling and Understanding of Effects of Randomness in Arrays of Resonant Meta-Atoms, Proc. *SPIE Optics and Photonics*, San Diego, USA, Aug. 2013.

[IC-144] Culhaoglu, A., **Kemptner, E.**, **Osipov, A.**, Modeling and Simulation of Electromagnetic Scattering from Electrically Large Bodies Coated with CLS-based Metamaterial Absorbers, Proc. *EuCAP*, Gothenburg, Sweden, Apr. 2013.

[IC-145] Jagdhuber, T., **Hajnsek, I.**, Radar Environmental Sensing within TERENO, Proc. *TERENO Advisory Board Meeting*, Klink, Germany, Sep. 2013.

[IC-146] Jagdhuber, T., **Hajnsek, I.**, **Papathanassiou, K.**, Refined Soil Moisture Estimation by Means of L-Band Polarimetry, Proc. *IEEE International Symposium on Geoscience and Remote Sensing (IGARSS)*, Melbourne, Australia, Jul. 2013.

[IC-147] Krieger, G., **Zink, M.**, **Moreira, A.**, Global Topography Measurements with TanDEM-X, Proc. *Hotine Marussi Symposium*, Rome, Italy, Jun. 2013.

[IC-148] Moreira, A., The German Spaceborne Radar Program: Looking Back and Ahead, Proc. *CSA ASAR Workshop*, Montreal, Canada, Oct. 2013.

[IC-149] Moreira, A., Synthetic Aperture Radar (SAR): Principles and Applications, Proc. *Advanced Training Course in Land Remote Sensing*, Harokopio University, Athens, Greece, Jul. 2013.

[IC-150] Moreira, A., German Spaceborne Radar Program: TerraSAR-X, TanDEM-X and Beyond, Proc. *First German-Japanese Science and Application Workshop for Next Generation SAR*, Tokyo, Japan, Jun. 2013.

[IC-151] Moreira, A., Digital Beamforming: A Paradigm Shift for Spaceborne SAR, Proc. *IRS*, Dresden, Germany, Jun. 2013.

[IC-152] Moreira, A., Radaraugen im All: Revolutionäre Technologien für Erde und Umwelt, Proc. *Plenarversammlung des Fakultätentages der Fakultät für Elektrotechnik und Informationstechnik*, Munich, Germany, May 2013.

[IC-153] Moreira, A., A Paradigm Shift for Spaceborne Synthetic Aperture Radar (SAR) Systems, Proc. *EuRAD*, Nuremberg, Germany, Oct. 2013.

[IC-154] Osipov, A., Physical Theory of Diffraction for Scatterers with Low Reflection Surface, Proc. *EMTS*, Hiroshima, Japan, May 2013.

[IC-155] Ponce Madrigal, O., **Reigber, A.**, **Prats Iraola, P.**, **Scheiber, R.**, **Jäger, M.**, **Pinheiro, M.**, **Horn, R.**, **Keller, M.**, **Fischer, J.**, F-SAR System - DLR's Advanced Airborne SAR System, Proc. *Science and Technology Development for Earth Observation from Space with Synthetic Aperture Radar (SAR)*, Merida, Yucatan, Mexico, Oct. 2013.

[IC-156] Ponce Madrigal, O., **Prats Iraola, P.**, **Scheiber, R.**, **Reigber, A.**, **Moreira, A.**, Analysis and Optimization of Multi-Circular SAR for Fully Polarimetric Holographic Tomography over Forested Areas, Proc. *IGARSS*, Melbourne, Australia, Jul. 2013.

[IC-157] Reigber, A., **Papathanassiou, K.**, **Jäger, M.**, **Scheiber, R.**, First Results of Multispectral Polarimetry and Single-Pass PolInSAR with the F-SAR Airborne SAR Instrument, Proc. *IGARSS*, Melbourne, Australia, Jul. 2013.

[IC-158] Reigber, A., **Jäger, M.**, **Scheiber, R.**, **Prats Iraola, P.**, **Horn, R.**, Nottensteiner, A., Multispectral, Polarimetric and Interferometric SAR Imaging with the F-SAR Airborne SAR Instrument, Proc. *IRS*, Dresden, Germany, Jun. 2013.

[IC-159] Rommel, T., Future SAR-Missions - Concepts and Challenges in Waveform Design, Proc. *TU Munich Seminar*, Munich, Germany, Jun. 2013.

[IC-160] Schulze, D., **Bachmann, M.**, **Borla Tridon, D.**, **Zink, M.**, **Krieger, G.**, TanDEM-X Acquisition Planning and DEM Performance in the Third Year of Operation, Proc. *CSA ASAR Workshop*, Montreal, Canada, Oct. 2013.

[IC-161] Younis, M., **Krieger, G.**, **Moreira, A.**, MIMO SAR Techniques and Trades, Proc. *EuRAD*, Nuremberg, Germany, Oct. 2013.

[IC-162] Younis, M., **López-Dekker, F.**, **Bordoni, F.**, **Laskowski, P.**, **Krieger, G.**, Exploring the Trade-Space of MIMO SAR, Proc. *IGARSS*, Melbourne, Australia, Jul. 2013.

[IC-163] Zink, M., TanDEM-X Mission Status, Proc. *CEOS SAR CalVal Workshop*, Montreal, Canada, Oct. 2013.

[IC-164] Zink, M., Spaceborne SAR Interferometry and TanDEM-X, Proc. *European Microwave Week*, Nuremberg, Germany, Oct. 2013.

[IC-165] Zink, M., TanDEM-X: Operational DEM Generation and Pre-Cursor for Future SAR Missions, Proc. *Asia-Pacific Conference on Synthetik Aperture Radar (APSAR)*, Tsukuba, Japan, Sep. 2013.

[IC-166] Zink, M., **Moreira, A.**, TanDEM-X Mission: Overview, Challenges and Status, Proc. *IGARSS*, Melbourne, Australia, Jul. 2013.

[IC-167] Zink, M., TanDEM-X - Hochpräzise 3D-Landvermessung aus dem All, Proc. *Seminarreihe an der Hochschule Kempten*, Kempten, Germany, Jul. 2013.

[IC-168] Zink, M., TanDEM-X Mission Status, Proc. *TerraSAR-X / TanDEM-X Science Team Meeting*, Oberpfaffenhofen, Germany, Jun. 2013.

2012

[IC-169] Aguilera, E., **Nannini, M.**, **Reigber, A.**, A Data Adaptive Compressed Sensing Approach to Polarimetric SAR Tomography, Proc. *IGARSS*, Munich, Germany, Jul. 2012.

[IC-170] Aguilera, E., **Nannini, M.**, **Reigber, A.**, Wavelet-Based Compressed Sensing for SAR Tomography of Forested Areas, Proc. *EUSAR*, Nuremberg, Germany, Apr. 2012.

[IC-171] Al-Kahachi, N., **Papathanassiou, K.**, Polarimetric Scattering Model for Methane Bubbles Trapped in the Ice of Sub-Artic Lakes, Proc. *IGARSS*, Munich, Germany, Jul. 2012.

[IC-172] Anglberger, H., **Süß, H.**, Application Range of the SAR-Simulator SAREF, Proc. *EUSC SAR-Workshop*, Madrid, Mar. 2012.

[IC-173] Bachmann, M., **Schulze, D.**, **Ortega-Míguez, C.**, **Polimeni, M.**, **Böer, J.**, **Hueso Gonzalez, J.**, **Walter Antony, J.**, **Krieger, G.**, **Bräutigam, B.**, **Schwerdt, M.**, **Zink, M.**, TanDEM-X Acquisition Status and Calibration of the Interferometric System, Proc. *IGARSS*, Munich, Germany, Jul. 2012.

[IC-174] **Bachmann, M.**, **Hueso Gonzalez, J.**, **Krieger, G.**, **Schwerdt, M.**, **Walter Antony, J.**, **De Zan, F.**, Calibration of the Bistatic TanDEM-X Interferometer, Proc. *EUSAR*, Nuremberg, Germany, Apr. 2012.

[IC-175] **Bräutigam, B.**, **Martone, M.**, **Rizzoli, P.**, **Bachmann, M.**, **Krieger, G.**, Interferometric Performance of TanDEM-X Global DEM Acquisitions, Proc. *EUSAR*, Nuremberg, Germany, Apr. 2012.

[IC-176] Linck, R., Fassbinder, J., **Buckreuß, S.**, Satellite-Based Geophysical Prospection of the Roman Fortress of Qreiye-Ayyāš in Syria, Proc. *Recent Work In Archaeological Geophysics - December*, London, UK, Dec. 2012.

[IC-177] **Buckreuß, S.**, **Zink, M.**, TerraSAR-X / TanDEM-X Mission Status, Proc. *EUSC SAR Workshop*, Torrejon de Ardoz, Spain, Mar. 2012.

[IC-178] **Culhaoglu, A.**, **Osipov, A.**, Reduction of RCS of a Canonical Shape with a Metamaterial Coating, Proc. *IEEE International Symposium on Antennas and Propagation and USNC-URSI National Radio Science Meeting*, Chicago, USA, Jul. 2012.

[IC-179] Garcia, J., **Eyssartier, K.**, **López-Dekker, F.**, **Prats Iraola, P.**, **De Zan, F.**, **Krieger, G.**, **Busche, T.**, Monitoring the Petermann Ice Island with TanDEM-X, Proc. *IGARSS*, Munich, Germany, Jul. 2012.

[IC-180] Montzka, C., Hasan, S., Bogena, H., **Hajnsek, I.**, **Horn, R.**, **Jagdhuber, T.**, **Reigber, A.**, Hermes, N., Rüdiger, C., Vereecken, H., Active and Passive Airborne Microwave Remote Sensing for Soil Moisture Retrieval in the Rur Catchment, Germany, Proc. *IGARSS*, Munich, Germany, Jul. 2012.

[IC-181] **Jagdhuber, T.**, **Kohling, M.**, **Hajnsek, I.**, **Papathanassiou, K.**, Soil Moisture Retrieval Under Vegetation: Validation on TERENO Observatories, Proc. *IGARSS*, Munich, Germany, Jul. 2012.

[IC-182] **Kempf, T.**, **Anglberger, H.**, **Süß, H.**, Depth-of-Focus Issues on Spaceborne Very High-Resolution SAR, Proc. *IGARSS*, Munich, Germany, Jul. 2012.

[IC-183] **Kohling, M.**, **Jagdhuber, T.**, **Hajnsek, I.**, Pause, M., Montzka, C., Chwala, C., **Papathanassiou, K.**, TERENO Data Validation: Polarimetrically Derived vs. Ground Measured Soil Moisture, Proc. *TERENO Workshop*, Potsdam, Germany, Jan. 2012.

[IC-184] **Krieger, G.**, **Zink, M.**, **Moreira, A.**, TanDEM-X: A Radar Interferometer with Two Formation Flying Satellites, Proc. *International Astronautical Congress (IAC)*, Naples, Italy, Oct. 2012.

[IC-185] **Krieger, G.**, **Younis, M.**, **Huber, S.**, **Bordoni, F.**, **Patyuchenko, A.**, **Kim, J.**, **Laskowski, P.**, **Villano, M.**, **Rommel, T.**, **López-Dekker, F.**, **Moreira, A.**, MIMO-SAR and the Orthogonality Confusion, Proc. *IGARSS*, Munich, Germany, Jul. 2012.

[IC-186] **Krieger, G.**, **De Zan, F.**, Relativistic Effects in Bistatic SAR Processing and System Synchronization, Proc. *EUSAR*, Nuremberg, Germany, Apr. 2012.

[IC-187] **Krieger, G.**, **Younis, M.**, **Huber, S.**, **Bordoni, F.**, **Patyuchenko, A.**, **Kim, J.**, **Laskowski, P.**, **Villano, M.**, **Rommel, T.**, **López-Dekker, F.**, **Moreira, A.**, Digital Beamforming and MIMO SAR: Review and New Concepts, Proc. *EUSAR*, Nuremberg, Germany, Apr. 2012.

[IC-188] **Kugler, F.**, **Hajnsek, I.**, **Papathanassiou, K.**, Dual Pol-InSAR Forest Height Estimation By Means Of TANDEM-X Data, Proc. *IGARSS*, Munich, Germany, Jul. 2012.

[IC-189] **Moreira, A.**, **Krieger, G.**, **Zink, M.**, Revolutionäre Technik für Erde und Umwelt, Proc. *Nominierung für den Deutschen Zukunftspreis*, Deutsches Museum, Munich, Germany, Sep. 2012.

[IC-190] **Moreira, A.**, 30 Jahre Radar im Weltall: Rückblick und Ausblick, Proc. *Festkolloquium – Fortschritte der Hochfrequenz-sensorik*, Technische Universität Munich, Munich, Germany, Jul. 2012.

[IC-191] **Moreira, A.**, The Earth Seen from Space by Radar Remote Sensing - a Vision for 2025, Proc. *IEEE Technology Time Machine (TTM)*, Dresden, Germany, May 2012.

[IC-192] **Osipov, A.**, Mechanisms of High-Frequency Scattering from Impedance Bodies with Unit Relative Surface Impedance, Proc. *International Conference on Electromagnetics in Advanced Applications (ICEAA)*, Cape Town, South Africa, Sep. 2012.

[IC-193] **Osipov, A.**, **Culhaoglu, A.**, **Kemptner, E.**, **Thurner, S.**, Electromagnetic Scattering from Electrically Large Simply Shaped Bodies Coated with Metamaterial Absorbers, Proc. *Progress in Electromagnetics Research Symposium (PIERS)*, Moscow, Russia, Aug. 2012.

[IC-194] **Peichl, M.**, **Dill, S.**, Detecting RFI Using Microwave Radiometers, Proc. *IGARSS*, Munich, Germany, vol. IEEE C, Jul. 2012.

[IC-195] **Peichl, M.**, Microwave Sensing Capabilities of DLR-HR for Maritime Operations, Proc. *MPC EWT Meeting*, Frederikshavn, Denmark, Jun. 2012.

[IC-196] **Peichl, M.**, TerraSAR & Some Maritime Applications, Proc. *MPC EWT Meeting*, Frederikshavn, Denmark, Jun. 2012.

[IC-197] **Ponce Madrigal, O.**, **Prats Iraola, P.**, **Scheiber, R.**, **Reigber, A.**, **Moreira, A.**, Polarimetric 3-D Reconstruction from Multicirular SAR at P-Band, Proc. *IGARSS*, Munich, Germany, Jul. 2012.

[IC-198] **Ponce Madrigal, O.**, **Prats Iraola, P.**, **Scheiber, R.**, **Reigber, A.**, **Moreira, A.**, Multibaseline 3-D Circular SAR Imaging at L-Band, Proc. *EUSAR*, Nuremberg, Germany, Apr. 2012.

[IC-199] **Rodríguez Cassolà, M.**, **Prats Iraola, P.**, **Steinbrecher, U.**, **Horn, R.**, **Nottensteiner, A.**, **Schulze, D.**, **Keller, M.**, **Pinheiro, M.**, **Zink, M.**, **Reigber, A.**, **Krieger, G.**, **Moreira, A.**, Bistatic SAR Experiments with the TanDEM-X Constellation, Proc. *IGARSS*, Munich, Germany, Jul. 2012.

[IC-200] **Sanjuan Ferrer, M.**, **Hajnsek, I.**, **Papathanassiou, K.**, Analysis of the Detection Performance of Coherent Scatterers in SAR Images, Proc. *IGARSS*, Munich, Germany, Jul. 2012.

[IC-201] **Wollstadt, S.**, **Hajnsek, I.**, **Zink, M.**, **Bachmann, M.**, TanDEM-X: Mission Status and Science Activities, Proc. *International Society for Photogrammetry and Remote Sensing (ISPRS) Congress*, Melbourne, Australia, Aug./Sep. 2012.

[IC-202] **Zink, M.**, TanDEM-X Mission Status, Proc. *IGARSS*, Munich, Germany, Jul. 2012.

[IC-203] **Zink, M.**, Bartusch, M., Ulrich, D., TanDEM-X Mission Status, Proc. *EUSAR*, Nuremberg, Germany, Apr. 2012.

2011

[IC-204] **Aguilera, E.**, **Nannini, M.**, **Reigber, A.**, Multi-Signal Compressed Sensing for Polarimetric SAR Tomography, Proc. *IGARSS*, Vancouver, Canada, Jul. 2011.

[IC-205] **Bachmann, M.**, **Zink, M.**, The TanDEM-X Mission – Bistatic SAR for a Global DEM, Proc. *Asia-Pacific Conference on Synthetic Aperture Radar (APSAR)*, Seoul, Korea, Sep. 2011.

[IC-206] **Bachmann, M.**, **Buckreuß, S.**, The TerraSAR-X and TanDEM-X Missions, Proc. *Visit of Industrial College of the Armed Forces, National Defense University, USA*, Oberpfaffenhofen, Germany, May 2011.

[IC-207] **Buckreuß, S.**, **Zink, M.**, The Missions TerraSAR-X and TanDEM-X: Status, Challenges, Future Perspectives, Proc. *URSI General Assembly and Scientific Symposium (GASS)*, Istanbul, Turkey, Aug. 2011.

[IC-208] **Buckreuß, S.**, Werninghaus, R., **Zink, M.**, TerraSAR-X / TanDEM-X Mission Status, Proc. *CSA ASAR Workshop*, Montreal, Canada, Jun. 2011.

[IC-209] **Buckreuß, S.**, TerraSAR-X / TanDEM-X Mission Status, Proc. *TerraSAR-X Science Team Meeting*, Oberpfaffenhofen, Germany, Feb. 2011.

[IC-210] Chandra, M., **Danklmayer, A.**, Tropospheric-Propagation Induced Distortion of Wideband Signals, Proc. *International Conference on Electromagnetics and Advanced Applications (ICEAA)*, Torino, Italy, Sep. 2011.

[IC-211] **Dill, S.**, **Peichl, M.**, **Rudolf, D.**, Investigation of Security Related Fully Polarimetric Signatures of Radiometer Measurements at W-Band, Proc. *SPIE Security, Defense + Sensing*, Prag, Tchechien, vol. 8188, Sep. 2011.

[IC-212] Eineder, M., **Hajnsek, I.**, **Moreira, A.**, Bamler, R., **Krieger, G.**, Minet, C., **De Zan, F.**, Tandem-L: A Radar Mission Proposal to Capture Earth Dynamics, Proc. *FRAGILE EARTH International Conference*, Munich, Germany, Sep. 2011.

[IC-213] **Hajnsek, I.**, **Krieger, G.**, **Papathanassiou, K.**, **Baumgartner, S.**, **Rodríguez Cassolà, M.**, **Prats Iraola, P.**, **López-Dekker, F.**, TanDEM-X: Science Status and Scientific Experiments, Proc. *IGARSS*, Vancouver, Canada, Jul. 2011.

[IC-214] **Hajnsek, I.**, **Papathanassiou, K.**, TanDEM-X: Pol-InSAR over Agricultural Areas, Proc. *IGARSS*, Vancouver, USA, Jul. 2011.

[IC-215] Lee, J., Ainsworth, T., Chen, K., **Hajnsek, I.**, Terrain Categorization Based on Scattering Mechanisms for Single-Pol High-Resolution TerraSAR-X Images, Proc. *IGARSS*, Vancouver, Canada, Jul. 2011.

[IC-216] Rott, H., Cline, D., Duguay, C., Essery, R., Etchevers, P., **Hajnsek, I.**, Yueh, S., CoReh20, a Dual Frequency Radar Satellite for Cold Regions Hydrology, Proc. *IGARSS*, Vancouver, Canada, Jul. 2011.

[IC-217] **Kim, J.**, **Younis, M.**, **Gabele, M.**, **Prats Iraola, P.**, **Krieger, G.**, Contribution of TerraSAR-X to Digital Beamforming Experiment for Future SAR Techniques, Proc. *Asia-Pacific Conference on Synthetic Aperture Radar (APSAR)*, Seoul, South Korea, Sep. 2011.

[IC-218] **Kim, J.**, **Danklmayer, A.**, **Papathanassiou, K.**, Correction of Ionospheric Distortions in Low Frequency Interferometric SAR Data, Proc. *IGARSS*, Vancouver, Canada, Jul. 2011.

[IC-219] Meyer, F., **Kim, J.**, Brcic, R., Pi, X., Potential Contributions of the DESDynI Mission to Ionospheric Research, Proc. *IGARSS*, Vancouver, Canada, Jul. 2011.

[IC-220] **Kim, J.**, **Danklmayer, A.**, **Papathanassiou, K.**, An Ionospheric Calibration Scheme for the BIOMASS Pol-InSAR Data Space, Proc. *ESA POLinSAR Workshop*, Frascati, Italy, Jan. 2011.

[IC-221] **Hueso González, J.**, **Krieger, G.**, **Walter Antony, J.**, **Bachmann, M.**, **Schrank, D.**, **Schwerdt, M.**, **De Zan, F.**, **Rodríguez Cassolà, M.**, Baseline and Bistatic System Calibration in the TanDEM-X Mission, Proc. *IGARSS*, Vancouver, Canada, Jul. 2011.

[IC-222] **Krieger, G.**, **Hajnsek, I.**, **López-Dekker, F.**, **Baumgartner, S.**, **Rodríguez Cassolà, M.**, **De Zan, F.**, **Prats Iraola, P.**, **Papathanassiou, K.**, **Zink, M.**, **Moreira, A.**, TanDEM-X Scientific Results and Future Formation Flying SAR Missions, Proc. *International Conference on Spacecraft Formation Flying Missions & Technologies (SFFMT)*, St-Hubert, Québec, Canada, May 2011.

[IC-223] **Krieger, G.**, **Zink, M.**, **Schulze, D.**, **Hajnsek, I.**, **Moreira, A.**, TanDEM-X: Mission Overview and Status, Proc. *International Conference on Spacecraft Formation Flying Missions & Technologies (SFFMT)*, St-Hubert, Québec, Canada, May 2011.

[IC-224] **Kugler, F.**, **Hajnsek, I.**, Forest Characterisation by Means of TerraSAR-X and TanDEM-X (Polarimetric and) Interferometric Data, Proc. *IGARSS*, Vancouver, Canada, vol. IEEE C, Jul. 2011.

[IC-225] **Kugler, F.**, **Hajnsek, I.**, **Papathanassiou, K.**, Cloude, S., Forest Characterisation by Means of TerraSAR-X and TanDEM-X Polarimetric Interferometric Data, Proc. *DRAGON 2 Symposium*, Prague, Czech Republic, Jun. 2011.

[IC-226] **Lee, S.**, **Sauer, S.**, **Kugler, F.**, **Hajnsek, I.**, **Papathanassiou, K.**, Potential & Challenges of Polarimetric SAR Interferometry Techniques for Forest Parameter Estimation in the Context of the BIOMASS Mission, Proc. *IGARSS*, Vancouver, Canada, Jul. 2011.

[IC-227] **Moreira, A.**, Germany's Spaceborne Radar Program: TerraSAR-X, TanDEM-X and Beyond, Proc. *Asia-Pacific Conference on Synthetic Aperture Radar (APSAR)*, Seoul, Korea, Sep. 2011.

[IC-228] **Moreira, A.**, TanDEM-X: A High-Resolution Radar Topography Mission, Proc. *IRS*, Leipzig, Germany, Sep. 2011.

[IC-229] **Moreira, A.**, Synthetic Aperture Radar: State of the Art and Future Developments, Proc. *International Congress on Technologies and Applications of Synthetic Aperture Radar*, INTA, Madrid, Spain, May 2011.

[IC-230] **Ortega-Míguez, C.**, **Schulze, D.**, **Zink, M.**, **Krieger, G.**, **Moreira, A.**, TanDEM-X Mission Status, Proc. *ARSI*, Noordwijk, The Netherlands, Sep. 2011.

[IC-231] **Osipov, A.**, Research on Microwave Metamaterials at the DLR, Proc. *German-Israeli Workshop on Advances in Electromagnetic Fields and Waves*, Yad-Hashmona Guesthouse, Israel, Mar./Apr. 2011.

[IC-232] Lopez-Martinez, C., **Papathanassiou, K.**, Alonso, A., Fabregas, X., Analysis of Volumetric Scatterers Based on TanDEM-X Polarimetric Interferometric SAR Data, Proc. *IGARSS*, Vancouver, Canada, Jul. 2011.

[IC-233] **Papathanassiou, K.**, **Kugler, F.**, **Hajnsek, I.**, Exploring the Potential of Pol-InSAR Techniques at X-Band – First Results and Experiments from TanDEM-X, Proc. *IGARSS*, Vancouver, Canada, Jul. 2011.

[IC-234] **Papathanassiou, K.**, **Kugler, F.**, **Hajnsek, I.**, Exploring the Potential Pol-InSAR Techniques at X-Band: First Results and Experiments from TanDEM-X, Proc. *ESA POLinSAR Workshop*, Frascati, Italy, Jan. 2011.

[IC-235] Lopez-Martinez, C., **Papathanassiou, K.**, Alonso, A., Fabregas, X., Separation of Scattering Contributions in Polarimetric SAR Interferometry, Proc. *ESA POLinSAR Workshop*, Frascati, Italy, Jan. 2011.

[IC-236] **Pardini, M.**, **Toraño Caicoya, A.**, **Lee, S.**, **Kugler, F.**, **Hajnsek, I.**, **Papathanassiou, K.**, Tandem-L: Estimation of Vertical Forest Structure by Means of Multibaseline Pol-InSAR at L-Band for Global Biomass Mapping, Proc. *IGARSS*, Vancouver, Canada, Jul. 2011.

[IC-237] **Peichl, M.**, Mikrowellenfernerkundung – Sehen und Untersuchen mit großen Wellenlängen, Proc. *Kolloquium des VDI-Arbeitskreis Technikgeschichte*, Munich, Germany, Sep. 2011.

[IC-238] **Peichl, M.**, **Süß, H.**, **Dill, S.**, **Jirousek, M.**, **Schreiber, E.**, **Rudolf, D.**, Radiometric Remote Sensing – Present Capabilities and Limitations, Proc. *URSI Commission F - Triennial Open Symposium on Radio Wave Propagation and Remote Sensing*, Garmisch-Partenkirchen, Germany, Mar. 2011.

[IC-239] **Prats Iraola, P.**, **López-Dekker, F.**, **De Zan, F.**, **Wollstadt, S.**, **Bachmann, M.**, **Steinbrecher, U.**, **Scheiber, R.**, **Reigber, A.**, **Krieger, G.**, Distributed Imaging with TerraSAR-X and TanDEM-X, Proc. *IGARSS*, Vancouver, Canada, Jul. 2011.

[IC-240] **Reigber, A.**, 3D Imaging with SAR Tomography, Proc. *IGARSS*, Munich, Germany, Jul. 2012/Jul. 2011.

[IC-241] **Sanjuan Ferrer, M.**, **Hajnsek, I.**, Papathanassiou, K., Coherent Scatterers Detection: Application over Glacier Terrain Using TerraSAR-X Time Series Data, Proc. *IGARSS*, Vancouver, Canada, Jul. 2011.

[IC-242] **Schulze, D.**, **Martone, M.**, **Rizzoli, P.**, **Bräutigam, B.**, **Krieger, G.**, In-Orbit Performance of TSX-1 & TDX-1, Proc. *IGARSS*, Vancouver, Canada, Jul. 2011.

[IC-243] **Schwerdt, M.**, **Hueso Gonzalez, J.**, **Bachmann, M.**, **Schrank, D.**, **Döring, B.**, **Tous Ramon, N.**, **Walter Antony, J.**, In-Orbit Calibration of the TanDEM-X System, Proc. *IGARSS*, Vancouver, Canada, Jul. 2011.

[IC-244] **Steinbrecher, U.**, **Baumgartner, S.**, **Mittermayer, J.**, **Wollstadt, S.**, Suchandt, S., Breit, H., **Scheiber, R.**, **Schulze, D.**, Experimental Radar-Modes with TerraSAR-X und TanDEM-X, Proc. *20 Years Antarctic Research Station GARS O'Higgins Symposium*, Punta Arenas, Chile, Nov. 2011.

[IC-245] Schättler, B., Kahle, R., Metzig, R., **Steinbrecher, U.**, **Zink, M.**, The Joint TerraSAR-X / TanDEM-X Ground Segment, Proc. *IGARSS*, Vancouver, Canada, Jul. 2011.

[IC-246] **Toraño Caicoya, A.**, Sustainable Research Management AUDI Award, Proc. *Sustainable Research Management Anniversary*, Freising, Germany, Nov. 2011.

[IC-247] **Voormansik, K.**, **Jagdhuber, T.**, **Hajnsek, I.**, **Papathanassiou, K.**, Improving Semi-Natural Grassland Administration with TerraSAR-X, Proc. *GeoCAP Conference*, Tallinn, Estonia, Nov. 2011.

[IC-248] Hoffmann, H., Jaumann, R., Hiesinger, H., Claasen, F., Spohn, T., Mall, U., Helbert, J., Kappelmann, N., Werner, K., Wimmer-Schweingruber, R., Srama, R., Oberst, J., Flohrer, J., **Werner, M.**, Neukum, G., Van Gasselt, S., Schmitz, N., Eichentopf, K., Knigge, T., Kummer, U., Langemann, M., Müller, H., Haarmann, R., A Dedicated Small Lunar Exploration Orbiter and a Mobile Surface Element, Proc. *2011 Annual Meeting of the Lunar Exploration Working Group*, Houston, USA, Nov. 2011.

[IC-249] **Younis, M.**, **Patyuchenko, A.**, **Huber, S.**, **Krieger, G.**, Design and Optimization Aspects for Reflector-Based Synthetic Aperture Radar, Proc. *IGARSS*, Vancouver, Canada, Jul. 2011.

[IC-250] **Zink, M.**, TerraSAR-X / TanDEM-X Mission Status & Results, Proc. *Radarforum*, Ulm, Germany, Dec. 2011.

[IC-251] **Zink, M.**, TanDEM-X – Hochpräzise 3D-Landvermessung aus dem All, Proc. *Wissenschaft für Jedermann*, Munich, Germany, Nov. 2011.

[IC-252] **Zink, M.**, TanDEM-X – The First Bistatic SAR Formation in Space, Proc. *IAA International Conference on Space Technologies*, Athens, Greece, Sep. 2011.

[IC-253] **Zink, M.**, Bartusch, M., Miller, D., TanDEM-X Mission Status, Proc. *IGARSS*, Vancouver, Canada, Jul. 2011.

[IC-254] **Zink, M.**, TanDEM-X: Actual Status & Future Perspectives, Proc. *RSL Remote Sensing Colloquium*, University of Zurich, Zurich, Switzerland, Apr. 2011.

[IC-255] **Zink, M.**, TanDEM-X Mission Status, *WorldDEM Project and Future German Radar Missions*, Library of Congress, Washington D.C., USA, Mar. 2011.

[IC-256] **Zink, M.**, The TanDEM-X Mission: Challenges, Innovations & Current Status, Proc. *URSI Commission F - Triennial Open Symposium on Radio Wave Propagation and Remote Sensing*, Garmisch-Partenkirchen, Germany, Feb. 2011.

Regular Conference Contributions

2017

[RC-1] **Alonso-González, A.**, **Brancato, V.**, **Jörg, H.**, Multi-Frequency Polarimetric SAR Time Series for Agricultural Monitoring, Proc. *HGF Alliance Week*, Garmisch-Partenkirchen, Germany, Jun. 2017.

[RC-2] **Alonso-González, A.**, **Jörg, H.**, **Papathanassiou, K.**, **Hajnsek, I.**, Multi-Frequency PolSAR Change Analysis for Agricultural Monitoring, Proc. *ESA POLinSAR Workshop*, Frascati (Rome), Italy, Jan. 2017.

[RC-3] **Anglberger, H.**, **Speck, R.**, Mapping Detailed 3D Information onto High-Resolution SAR Signatures, Proc. *SPIE Defense + Security*, Anaheim, USA, Apr. 2017.

[RC-4] **Barros Cardoso da Silva, A.**, **Baumgartner, S.**, STAP Moving Target Position Estimation Accuracy Improvement and False Detection Recognition Using a Priori Road Information, Proc. *IRS*, Prague, Czech Republic, Jun. 2017.

[RC-5] **Baumgartner, S.**, **Scheiber, R.**, **Bordoni, F.**, **Krieger, G.**, **Peichl, M.**, HAPS: Potentials, Applications and Requirements for Radar Remote Sensing, Proc. *HAPS4ESA – Towards an ESA Stratospheric High Altitude Pseudo-Satellites (HAPS) Programme for Earth Observation, Telecommunications and Navigation*, Noordwijkerhout, The Netherlands, Oct. 2017.

[RC-6] **Baumgartner, S.**, Linear and Circular ISAR Imaging of Ships Using DLR's Airborne Sensor F-SAR, Proc. *IET International Conference on Radar Systems (Radar)*, Belfast, UK, Oct. 2017.

[RC-7] **Baur, M.**, **Jagdhuber, T.**, **Link, M.**, Piles, M., Entekhabi, D., **Fink, A.**, Estimation of Vegetation Loss Coefficients and Canopy Penetration Depths from SMAP Radiometer and ICESat Lidar Data, Proc. *IGARSS*, Fort Worth, USA, Jul. 2017.

[RC-8] **Bordoni, F.**, **López-Dekker, F.**, **Sanjuan Ferrer, M.**, Beam-Switch Wide-Swath Mode for Interferometrically Compatible Products of the Post-Sentinel HRWS SAR System, Proc. *IRS*, Prague, Czech Republic, Jun. 2017.

[RC-9] **Borla Tridon, D.**, **Bachmann, M.**, De Zan, F., **Krieger, G.**, **Zink, M.**, **Schulze, D.**, **Moreira, A.**, Tandem-L Observation Concept - Contributions and Challenges of Systematic Monitoring of Earth System Dynamics, Proc. *IRS*, Prague, Czech Republic, Jun. 2017.

[RC-10] Johansson, M., Singha, S., King, J., Doulgeris, A., Gerland, S., Spreen, G., Ressel, R., **Busche, T.**, Investigating Monostatic TS-X DRA Acquisitions and Near-Coincident C- and L-Band Fully Polarimetric SAR for Arctic Sea Ice Characterization, Proc. *TerraSAR-X/TanDEM-X Science Team Meeting*, DLR Oberpfaffenhofen, Germany, Oct. 2017.

[RC-11] **Cazcarra Bes, V.**, **Tello Alonso, M.**, **Papathanassiou, K.**, **Pardini, M.**, Evaluation of Tomographic SAR Inversion Algorithms for Forest Applications, Proc. *ESA POLinSAR Workshop*, Rome, Italy, Jan. 2017.

[RC-12] **Dill, S.**, **Peichl, M.**, **Schreiber, E.**, **Anglberger, H.**, Improved Characterization of Scenes with a Combination of MMW Radar and Radiometer Information, Proc. *SPIE Symposium on Defense and Commercial Sensing*, Anaheim, USA, vol. 10189, Apr. 2017.

[RC-13] Estevam Schmiedt, J., Cerra, D., Dahlke, D., **Dill, S.**, Ge, N., Göttsche, J., **Haas, A.**, Heiden, U., Israel, M., Kurz, F., Linkiewicz, M., Patel, D., **Peichl, M.**, Plattner, S., Pless, S., Schiricke, B., Schorn, C., Tiddens, A., Zhu, X., Remote Sensing Techniques for Building Models and Energy Performance Studies of Buildings, Proc. *EBC Annex 71: Building energy performance assessment based on in-situ measurements*, Loughborough, UK, Apr. 2017.

[RC-14] **Weidenhaupt, K.**, **Döring, B.**, **Jirousek, M.**, **Raab, S.**, **Rudolf, D.**, **Schwerdt, M.**, DLR's Innovative Point Targets for SAR System Calibration and their Application to Sentinel-1, Proc. *CSA ASAR Workshop*, Montreal, Canada, Jun. 2017.

[RC-15] **Fischer, G.**, **Papathanassiou, K.**, **Hajnsek, I.**, Influence of Vertical Subsurface Structure of Ice Sheets on Interferometric Phase Center Depths, Proc. *HGF Alliance Week*, Garmisch-Partenkirchen, Germany, Jun. 2017.

[RC-16] **Fischer, G.**, **Hajnsek, I.**, Investigation of Penetration Bias of Surface Elevation Models From SAR Interferometry in Dependence of Subsurface Structure, Frequency and Polarization, Proc. *EARSeL Workshop on Land Ice and Snow*, Bern, Switzerland, Feb. 2017.

[RC-17] **Fischer, G.**, **Parrella, G.**, **Papathanassiou, K.**, **Hajnsek, I.**, Impact of Vertical Subsurface Structure, Frequency and Polarization on the Accuracy of InSAR Phase Center Depth Modelling for Glaciers and Ice Sheets, Proc. *ESA POLinSAR Workshop*, Frascati, Italy, Jan. 2017.

[RC-18] **Fischer, G.**, **Parrella, G.**, **Papathanassiou, K.**, **Hajnsek, I.**, Sensitivity of Polarimetric SAR Interferometry Data to Different Vertical Subsurface Structures of the Greenland Ice Sheet, Proc. *IGARSS*, Forth Worth, USA, Jul./Aug. 2017.

[RC-19] **Fischer, J.**, **Baumgartner, S.**, **Pinheiro, M.**, **Horn, R.**, Leppig, B., Stahl, N., Die Flutkatastrophe von Simbach am Inn im Juni 2016 aus Sicht eines hochauflösenden abbildenden Radarsystems, Proc. *Raum Zeit Risiko*, Munich, Germany, Oct. 2017.

[RC-20] **Gonzalez, C.**, **Rizzoli, P.**, **Martone, M.**, **Wecklich, C.**, **Borla Tridon, D.**, **Bachmann, M.**, Fritz, T., Wessel, B., **Krieger, G.**, **Zink, M.**, The New Global Digital Elevation Model: TanDEM-X DEM and its Final Performance, Proc. *European Geosciences Union (EGU)*, Vienna, Austria, Apr. 2017.

[RC-21] **Gonzalez, C.**, **Rizzoli, P.**, **Martone, M.**, **Wecklich, C.**, **Bueso Bello, J.**, **Krieger, G.**, **Zink, M.**, First Results of the Performance of the Global Forest/Non-Forest Map Derived from TanDEM-X Interferometric Data, Proc. *European Geosciences Union (EGU)*, Vienna, Austria, Apr. 2017.

[RC-22] **Haas, A.**, **Peichl, M.**, **Dill, S.**, Theoretical and Experimental Investigations of Microwave Signatures for Characterization of Building Structures, Proc. *IRS*, Prague, Czech Republic, Jul. 2017.

[RC-23] **Heinzel, A.**, **Peichl, M.**, **Schreiber, E.**, **Dill, S.**, Investigations on the Detection of Thin Wires Using MIMO SAR, Proc. *SPIE Defense + Security*, Anaheim USA, Apr. 2017.

[RC-24] **Heister, A.**, **Scheiber, R.**, Demonstration of Sparse Signal Reconstruction for Radar Imaging of Ice Sheets, Proc. *European Geosciences Union (EGU)*, Vienna, Austria, Apr. 2017.

[RC-25] **Huber, S.**, **Younis, M.**, **Krieger, G.**, Tandem-L: SAR System Design Aspects, Proc. *ESA ARSI*, Noordwijk, The Netherlands, Sep. 2017.

[RC-26] Fersch, B., **Jagdhuber, T.**, Schrön, M., Synergistic Soil Moisture Observation: An Interdisciplinary Multi-Sensor Approach to Yield Improved Estimates Across Scales, Proc. *AGU Fall Meeting*, New Orleans, USA, Dec. 2017.

[RC-27] Piles, M., Chaparro, D., Entekhabi, D., Konings, A., **Jagdhuber, T.**, Camps-Valls, G., Remote Sensing of Vegetation Dynamics in Agro-Ecosystems Using SMAP Vegetation Optical Depth and Optical Vegetation Indices, Proc. *IGARSS*, Fort Worth, USA, Jul. 2017.

[RC-28] **Jagdhuber, T.**, **Baur, M.**, **Link, M.**, Piles, M., Entekhabi, D., Montzka, C., Seppänen, J., Antropov, O., Praks, J., Löw, A., Physics-based Retrieval of Scattering Albedo and Vegetation Optical Depth Using Multi-Sensor Data Integration, Proc. *IGARSS*, Fort Worth, USA, Jul. 2017.

[RC-29] Das, N., Entekhabi, D., Kim, S., **Jagdhuber, T.**, Dunbar, S., Yueh, S., Colliander, A., Lopez-baeza, E., Martinez-Fernandez, J., High-Resolution Enhanced Product Based on SMAP Active-Passive Approach Using Sentinel-1A and 1B SAR Data, Proc. *IGARSS*, Fort Worth, USA, Jul. 2017.

[RC-30] **Jagdhuber, T.**, Entekhabi, D., Das, N., **Link, M.**, Montzka, C., Kim, S., Yueh, S., Microwave Covariation Modeling and Retrieval for the Dual-Frequency Active-Passive Combination of Sentinel-1 AND SMAP, Proc. *IGARSS*, Fort Worth, USA, Jul. 2017.

[RC-31] **Jirousek, M.**, **Anger, S.**, **Dill, S.**, **Peichl, M.**, IoSiS: A Radar System for Imaging of Satellites in Space, Proc. *SPIE Defense + Security*, Anaheim, USA, vol. 10188, Apr. 2017.

[RC-32] **Jäger, M.**, **Scheiber, R.**, A Novel Approach to the External Calibration of Multi-Channel SAR Sensors Based on Range Compressed Data, Proc. *Earth Observation Summit*, Montreal, Canada, Jun. 2017.

[RC-33] Singha, S., **Jäger, M.**, Arctic Sea Ice Characterization Using Multi-Frequency Fully Polarimetric Airborne DLR-FSAR System, Proc. *ESA POLinSAR Workshop*, Frascati, Italy, Jan. 2017.

[RC-34] **Jörg, H.**, **Pardini, M.**, **Hajnsek, I.**, Polarimetric SAR Tomography for Monitoring Changes in Agricultural Crops, Proc. *URSI Kleinheubacher Tagung*, Miltenberg, Germany, Sep. 2017.

[RC-35] **Jörg, H.**, **Pardini, M.**, **Hajnsek, I.**, **Papathanassiou, K.**, Fully Polarimetric Tomographic Time Series for Monitoring Phenological Changes of Agricultural Crops at Different Frequencies, Proc. *ESA POLinSAR Workshop*, Frascati, Italy, Jan. 2017.

[RC-36] **Klenk, P.**, **Moreira, A.**, **Krieger, G.**, **Borla Tridon, D.**, Eineder, M., **Hajnsek, I.**, **Huber, S.**, **Papathanassiou, K.**, Parizzi, A., **Reimann, J.**, **Villano, M.**, **Younis, M.**, De Zan, F., **Zink, M.**, **Zonno, M.**, Tandem-L: A Highly Innovative Bistatic SAR Mission for Monitoring Earth's Dynamic Processes, Proc. *EO Summit*, Montreal, Canada, Jun. 2017.

[RC-37] **Klenk, P.**, **Reimann, J.**, **Schwerdt, M.**, **Zink, M.**, SAR Antenna Pointing Determination: Results from the Sentinel-1B Commissioning Phase and Novel Approaches, Proc. *EO Summit*, Montreal, Canada, Jun. 2017.

[RC-38] **Kraus, T.**, **Bachmann, M.**, **Heiderich, L.**, **Krieger, G.**, **Moreira, A.**, Multistatic SAR Imaging: Comparison of Simulation Results and Experimental Data, Proc. *IET International Conference on Radar Systems (Radar)*, Belfast, UK, Oct. 2017.

[RC-39] **Link, M.**, Entekhabi, D., **Jagdhuber, T.**, Ferrazzoli, P., Guerriero, L., **Baur, M.**, Ludwig, R., Simulating L/L-Band and C/L-Band Active-Passive Covariation of Crops with the Tor Vergata Scattering and Emission Model for a SMAP-SENTINEL-1 Combination, Proc. *IGARSS*, Fort Worth, USA, Jul. 2017.

[RC-40] **Martone, M.**, **Rizzoli, P.**, **Bachmann, M.**, **Borla Tridon, D.**, **Schulze, D.**, **Wecklich, C.**, **Bueso Bello, J.**, **Gonzalez, C.**, **Zink, M.**, **Krieger, G.**, The TanDEM-X Mission: Global Performance of the Digital Elevation Model and Beyond, Proc. *IET International Conference on Radar Systems (Radar)*, Belfast, Great Britain, Oct. 2017.

[RC-41] **Martone, M.**, **Rizzoli, P.**, **Krieger, G.**, Efficient On-Board Quantization for Interferometric and Multi-Channel SAR Systems, Proc. *IET International Conference on Radar Systems (Radar)*, Belfast, Great Britain, Oct. 2017.

[RC-42] **Martone, M.**, **Rizzoli, P.**, **Krieger, G.**, Potentials of TanDEM-X Interferometric Data for Global Land Classification, Proc. *TerraSAR-X Science Team Meeting*, Munich, Germany, Oct. 2017.

[RC-43] **Moreira, A.**, **Krieger, G.**, **Borla Tridon, D.**, Eineder, M., **Hajnsek, I.**, **Huber, S.**, **Klenk, P.**, **Papathanassiou, K.**, Parizzi, A., **Reimann, J.**, **Rizzoli, P.**, **Villano, M.**, **Younis, M.**, De Zan, F., **Zonno, M.**, **Zink, M.**, **Bueso Bello, J.**, Tandem-L: A Highly Innovative Bistatic SAR Mission for Monitoring Dynamic Earth Processes, Proc. *Seminario de Monitoramento Integrado com Radar Orbital*, Brasilia, Brasil, Sep. 2017.

[RC-44] **Moreira, A.**, **Krieger, G.**, **Hajnsek, I.**, **Papathanassiou, K.**, **Younis, M.**, **Huber, S.**, **Villano, M.**, **Pardini, M.**, **Zink, M.**, **Zonno, M.**, **Sanjuan Ferrer, M.**, **Borla Tridon, D.**, **Rizzoli, P.**, Eineder, M., **De Zan, F.**, Parizzi, A., Tandem-L: Global Observation of the Earth´s Surface with DinSAR, PolinSAR and Tomography, Proc. *ESA FRINGE Workshop*, Helsinki, Finland, Jun. 2017.

[RC-45] **Möhring, B.**, **Gabler, B.**, **Limbach, M.**, **Di Maria, A.**, Modular Simulation of a Compact Antenna Test Range, Proc. *EuCAP*, Paris, France, Mar. 2017.

[RC-46] **Nannini, M.**, **Prats Iraola, P.**, **Yague-Martinez, N.**, Costantini, M., Minati, F., Vecchioli, F., **Schmidt, K.**, **Schwerdt, M.**, Geolocation Accuracy Investigations with Sentinel-1, Proc. *ESA FRINGE Workshop*, Helsinki, Finland, Jun. 2017.

[RC-47] **Özis, E.**, **Osipov, A.**, Eibert, T., A Semi-Analytical Model for Transmission Coefficient Calculation for Metal Planar Rings in Meta-Sheets in the Microwave Region, Proc. *PIERS*, Singapore, Nov. 2017.

[RC-48] **Özis, E.**, **Osipov, A.**, Eibert, T., An Approximation for Reflection and Transmission Coefficients of Periodic Arrays of Metal Rings and Circular Slots, Proc. *URSI Kleinheubacher Tagung*, Miltenberg, Germany, Sep. 2017.

[RC-49] **Parrella, G.**, **Fischer, G.**, **Papathanassiou, K.**, **Hajnsek, I.**, Multi-Frequency Modeling of Polarimetric Signatures over the Greenland Ice Sheet, Proc. *ESA POLinSAR Workshop*, Frascati, Italy, Jan. 2017.

[RC-50] Geudtner, D., **Prats Iraola, P.**, **Yague-Martinez, N.**, De Zan, F., Breit, H., Larsen, Y., Monti-Guarnieri, A., Barat, I., Navas Traver, I., Torres, R., Sentinel-1 Constellation SAR Interferometry Performance Verification, Proc. *ESA FRINGE Workshop*, Helsinki, Finland, Jun. 2017.

[RC-51] **Prats Iraola, P.**, **López-Dekker, F.**, De Zan, F., **Yague-Martinez, N.**, **Zonno, M.**, **Rodríguez Cassolà, M.**, 3-D Surface Deformation Performance for Simultaneous Squinted SAR Acquisitions, Proc. *ESA FRINGE Workshop*, Helsinki, Finland, Jun. 2017.

[RC-52] **Queiroz de Almeida, F.**, **Younis, M.**, **Krieger, G.**, **Moreira, A.**, An Analytical Error Model for Spaceborne SAR Multichannel Azimuth Reconstruction, Proc. *IET International Conference on Radar Systems (Radar)*, Belfast, Northern Ireland, Oct. 2017.

[RC-53] **Queiroz de Almeida, F.**, **Younis, M.**, **Krieger, G.**, **Moreira, A.**, Multichannel Staggered SAR with Reflector Antennas: Discussion and Proof of Concept, Proc. *IRS*, Prague, Czech Republic, Jun. 2017.

[RC-54] **Reigber, A.**, **Nottensteiner, A.**, **Limbach, M.**, **Jäger, M.**, **Kosc, A.**, **Scheiber, R.**, **Fischer, J.**, **Di Maria, A.**, **Müller, G.**, **Que, R.**, **Künemund, M.**, **Trappschuh, K.**, **Pasch, S.**, **Geßwein, D.**, **Höflmayer, D.**, **Gabler, B.**, **Keller, M.**, **Horn, R.**, **Moreira, A.**, DBFSAR: An Airborne Very High-Resolution Digital Beamforming SAR System, Proc. *EuRAD*, Nuremberg, Germany, Oct. 2017.

[RC-55] **Reigber, A.**, **Jäger, M.**, PyRAT: An Open-Source SAR Image Processing Framework in Python, Proc. *ESA POLinSAR Workshop*, Frascati, Italy, Jan. 2017.

[RC-56] **Reimann, J.**, **Klenk, P.**, **Schwerdt, M.**, **Zink, M.**, New Approach for SAR Antenna Pointing Determination, Proc. *CEOS SAR CalVal Workshop*, Pasadena, USA, Nov. 2017.

[RC-57] **Reimann, J.**, **Schwerdt, M.**, **Zink, M.**, Definition of the Calibration Terminology for the Tandem-L Mission, Proc. *CEOS SAR CalVal Workshop*, Pasadena, USA, Nov. 2017.

[RC-58] Rossi, C., Baier, G., **Rizzoli, P.**, **Bueso Bello, J.**, Topographical Changes Caused by the 2016 Central Italy Earthquake Series, Proc. *IGARSS*, Fort Worth, USA, Jul. 2017.

[RC-59] Rott, H., Wuite, J., Nagler, T., Floricioiu, D., **Rizzoli, P.**, Helm, V., InSAR Scattering Phase Centre of Antarctic Snow - An Experimental Study, Proc. *Fringe*, Helsinki, Finland, Jun. 2017.

[RC-60] **Rizzoli, P.**, **Bueso Bello, J.**, **Valdo, P.**, **Martone, M.**, Sousa Brandão, W., **Zink, M.**, **Moreira, A.**, Gonzales de Oliveira, C., A Novel Concept for Monitoring Amazonas Deforestation by Combining Sentinel-1A/B and TanDEM-X SAR Data, Proc. *Seminario de Monitoramento Integrado com Radar Orbital*, Brasilia, Brasil, Sep. 2017.

[RC-61] **Rizzoli, P.**, **Martone, M.**, **Gonzalez, C.**, **Wecklich, C.**, **Borla Tridon, D.**, **Bachmann, M.**, Fritz, T., Wessel, B., **Krieger, G.**, **Zink, M.**, The Global TanDEM-X Digital Elevation Model: Final Performance Assessment, Proc. *ESA FRINGE Workshop*, Helsinki, Finland, Jun. 2017.

[RC-62] **Rizzoli, P.**, **Martone, M.**, **Gonzalez, C.**, **Wecklich, C.**, Fritz, T., Wessel, B., **Krieger, G.**, **Zink, M.**, Performance Assessment of the Global TanDEM-X Digital Elevation Model, Proc. *CEOS SAR CalVal Workshop*, Pasadena, USA, Nov. 2017.

[RC-63] **Rizzoli, P.**, **Martone, M.**, **Wecklich, C.**, **Gonzalez, C.**, **Bueso Bello, J.**, **Krieger, G.**, **Zink, M.**, A Global Forest/Non-Forest Map from TanDEM-X Interferometric Data, Proc. *ESA FRINGE Workshop*, Helsinki, Finland, Jun. 2017.

[RC-64] **Rizzoli, P.**, **Martone, M.**, **Wecklich, C.**, **Gonzalez, C.**, **Bueso Bello, J.**, **Valdo, P.**, **Krieger, G.**, **Zink, M.**, Deriving Forest/Non-Forest Maps from TanDEM-X Interferometric SAR Data, Proc. *WorldCover*, Frascati, Italy, Mar. 2017.

[RC-65] **Rizzoli, P.**, **Wecklich, C.**, Parizzi, A., De Zan, F., Fritz, T., **Borla Tridon, D.**, **Zonno, M.**, **Nannini, M.**, **Hajnsek, I.**, **Jörg, H.**, **Parrella, G.**, **Fischer, G.**, **Papathanassiou, K.**, **Krieger, G.**, **Zink, M.**, A First Concept for the Validation of Tandem-L Higher Level Products, Proc. *CEOS SAR CalVal Workshop*, Pasadena, USA, Nov. 2017.

[RC-66] Mao, C., Gao, S., **Rommel, T.**, Low-Profile Aperture-Shared X/Ka-Band Dual-Polarized Antenna for DBF-SAR Applications, Proc. *International Workshop on Antenna Technology*, Athens, Greece, Mar. 2017.

[RC-67] Arnieri, E., Boccia, L., Amendola, G., Mao, C., Gao, S., **Rommel, T.**, Glisic, S., Penkala, P., Krstic, M., Ho, A., Yodprasit, U., Schrape, O., **Younis, M.**, A 60-Channels ADC Board for Space Borne DBF-SAR Applications, Proc. *International Symposium on Antennas and Propagation (ISAP)*, San Diego, USA, Jul. 2017.

[RC-68] **Schmidt, K.**, **Tous Ramon, N.**, **Schwerdt, M.**, Radiometric Accuracy and One-Year-Stability of Sentinel-1A Determined using Point Targets, Proc. *EuRAD*, Nuremberg, Germany, Oct. 2017.

[RC-69] **Sica, F.**, **Martone, M.**, **Rizzoli, P.**, InSAR Forest/Non-Forest Classification Exploiting Nonlocal Pixel Similarities, Proc. *ESA FRINGE Workshop*, Helsinki, Finland, Jun. 2017.

[RC-70] **Tello Alonso, M.**, **Cazcarra Bes, V.**, **Pardini, M.**, **Papathanassiou, K.**, SAR Tomography for Forest Structure Characterization: Comparison of Temperate and Tropical Forests at L-Band, Proc. *ESA POLinSAR Workshop*, Rome, Italy, Jan. 2017.

[RC-71] **Villamil López, C.**, **Anglberger, H.**, Stilla, U., Fusion of very High Resolution SAR and Optical Images for the Monitoring of Urban Areas, Proc. *Joint Urban Remote Sensing Event (JURSE)*, Dubai, United Arab Emirates, Mar. 2017.

[RC-72] **Villamil López, C.**, **Kempf, T.**, **Speck, R.**, **Anglberger, H.**, Stilla, U., Automatic Change Detection Using very High-Resolution SAR Images and Prior Knowledge about the Scene, Proc. *SPIE Defense + Security*, Anaheim, USA, Apr. 2017.

[RC-73] Rosen, P., Hensley, S., Gurrola, E., Harcke, L., Kim, Y., Shaffer, S., Veeramachaneni, C., **Villano, M.**, NISAR Mission Overview and Performance Summary, Proc. *CEOS SAR CalVal Workshop*, Pasadena, USA, Nov. 2017.

[RC-74] **Villano, M.**, **Krieger, G.**, **Moreira, A.**, Advanced Spaceborne SAR Systems with Planar Antenna, Proc. *RadarCon*, Seattle, USA, May 2017.

[RC-75] **Wecklich, C.**, **Gonzalez, C.**, **Rizzoli, P.**, TanDEM-X Height Performance and Data Coverage, Proc. *IGARSS*, Forth Worth, USA, Jun. 2017.

[RC-76] **Wecklich, C.**, **Martone, M.**, **Rizzoli, P.**, **Bueso Bello, J.**, **Gonzalez, C.**, **Krieger, G.**, Production of a Global Forest/Non-Forest Map Utilizing TanDEM-X Interferometric SAR Data, Proc. *IGARSS*, Forth Worth, USA, Jun. 2017.

[RC-77] **Wollstadt, S.**, **Younis, M.**, **Rodríguez Cassolà, M.**, **Huber, S.**, **López-Dekker, F.**, Buck, C., A Ka-Band Wavemill Instrument Study for Ocean Surface Velocity Retrieval, Proc. *ESA ARSI*, Noordwijk, The Netherlands, Sep. 2017.

[RC-78] **Yague-Martinez, N.**, **Prats Iraola, P.**, De Zan, F., Coregistration of Interferometric Stacks of Sentinel-1 TOPS Data, Proc. *ESA FRINGE Workshop*, Helsinki, Finland, Jun. 2017.

[RC-79] **Yague-Martinez, N.**, **Prats Iraola, P.**, **Wollstadt, S.**, Time-Series Evaluation of Azimuth Displacements Retrieval with the Experimental TerraSAR-X 2-looks TOPS Acquisition Mode, Proc. *ESA FRINGE Workshop*, Helsinki, Finland, Jun. 2017.

[RC-80] Hensley, S., Smrekar, S., Dyar, M., Perkovic, D., Campbell, B., **Younis, M.**, Venus Interferometric Synthetic Aperture Radar (VISAR) for the Venus Origins Explorer, Proc. *1Meeting of the Venus Exploration Analysis Group (VEXAG)*, Laurel, USA, Nov. 2017.

[RC-81] **Younis, M.**, Adamiuk, G., Loinger, A., **Rommel, T.**, **Jäger, M.**, **Krieger, G.**, Internal Calibration Methodology for Multi-Channel SAR Instruments, Proc. *CEOS SAR CalVal Workshop*, Pasadena, USA, Nov. 2017.

[RC-82] **Younis, M.**, **Queiroz de Almeida, F.**, **Huber, S.**, **Martone, M.**, **Villano, M.**, **Krieger, G.**, Raw Data-Based Internal SAR Instrument Calibration, Proc. *CEOS SAR CalVal Workshop*, Pasadena, USA, Nov. 2017.

[RC-83] **del Castillo, J.**, **Younis, M.**, **Krieger, G.**, A HRWS SAR System Design with Multi-Beam Imaging Capabilities, Proc. *EuRAD*, Nuremberg, Germany, Oct. 2017.

[RC-84] **Younis, M.**, Adamiuk, G., **Queiroz de Almeida, F.**, **Huber, S.**, **Jäger, M.**, Loinger, A., **Martone, M.**, **Rommel, T.**, **Krieger, G.**, An Internal Calibration Approach of Multi-Channel SAR Sensors, Proc. *ESA ARSI*, Noordwijk, The Netherlands, Sep. 2017.

[RC-85] **Younis, M.**, **Rommel, T.**, **Queiroz de Almeida, F.**, **Huber, S.**, **Martone, M.**, **Krieger, G.**, Investigations on the Internal Calibration of Multi-Channel SAR, Proc. *IGARSS*, USA, Jul. 2017.

[RC-86] **Zink, M.**, **Moreira, A.**, **Krieger, G.**, **Bachmann, M.**, Balzer, W., **Borla Tridon, D.**, Eineder, M., **Hajnsek, I.**, **Huber, S.**, **Klenk, P.**, Maurer, E., **Papathanassiou, K.**, Parizzi, A., **Reimann, J.**, **Rizzoli, P.**, **Steinbrecher, U.**, **Villano, M.**, **Younis, M.**, De Zan, **F.**, **Zonno, M.**, Tandem-L: An Innovative Bistatic SAR Mission for Monitoring Earth's Dynamic Processes, Proc. *CEOS SAR CalVal Workshop*, Pasadena, USA, Nov. 2017.

2016

[RC-87] **Albers, T.**, **Peichl, M.**, **Dill, S.**, **Kempf, T.**, MMW ISAR Concept for Detection of Impurities in Sugar Production, Proc. *EUSAR*, Hamburg, Germany, Jun. 2016.

[RC-88] **Alonso-González, A.**, **Brancato, V.**, Zwieback, S., **Jörg, H.**, Monitoring Agricultural Areas with Polarimetric and Interferometric SAR, Proc. *HGF Alliance Week*, Garmisch-Partenkirchen, Germany, Jun./Jul. 2016.

[RC-89] **Alonso-González, A.**, **Hajnsek, I.**, Change Analysis in Polarimetric SAR Time Series Over Agricultural Areas, Proc. *HGF Alliance Week*, Garmisch-Partenkirchen, Germany, Jun./Jul. 2016.

[RC-90] **Alonso-González, A.**, **Jörg, H.**, **Papathanassiou, K.**, **Hajnsek, I.**, Change Analysis and Interpretation in Polarimetric Time Series over Agricultural Fields at C-Band, Proc. *EUSAR*, Hamburg, Germany, Jun. 2016.

[RC-91] **Alonso-González, A.**, **Jörg, H.**, **Papathanassiou, K.**, **Hajnsek, I.**, Dual-Polarimetric Agricultural Change Analysis of Long Baseline TanDEM-X Time Series Data, Proc. *IGARSS*, Beijing, China, Jul. 2016.

[RC-92] **Anger, S.**, **Peichl, M.**, **Dill, S.**, **Jirousek, M.**, **Schreiber, E.**, IoSiS – A High-Performance Imaging Radar for Surveillance of Objects in Low Earth Orbit, Proc. *EUSAR*, Hamburg, Jun. 2016.

[RC-93] **Anglberger, H.**, **Kempf, T.**, A Simulation-Based Approach Towards Automatic Target Recognition of High Resolution Spaceborne Radar Signatures, Proc. *SPIE Remote Sensing*, Edinburgh, UK, Sep. 2016.

[RC-94] **Anglberger, H.**, Militärische Radar-Bildauswertung auf hoch aufgelöste TerraSAR-X Daten, Proc. *Angewandte Forschung für Verteidigung und Sicherheit in Deutschland*, Bonn, Feb. 2016.

[RC-95] **Anglberger, H.**, Hennig, S., Signature Analysis of the Gateway Arch Monument in St. Louis Using TerraSAR-X Staring Spotlight Mode Data, Proc. *EUSAR*, Hamburg, Jun. 2016.

[RC-96] **Bachmann, M.**, **Borla Tridon, D.**, De Zan, F., **Krieger, G.**, **Zink, M.**, Tandem-L Observation Concept - An Acquisition Scenario for the Global Scientific Mapping Machine, Proc. *EUSAR*, Hamburg, Germany, Jun. 2016.

[RC-97] **Barros Cardoso da Silva, A.**, **Baumgartner, S.**, Novel Post-Doppler STAP with a Priori Knowledge Information for Traffic Monitoring Applications, Proc. *URSI Kleinheubacher Tagung*, Miltenberg, Germany, Sep. 2016.

[RC-98] **Barros Cardoso da Silva, A.**, **Baumgartner, S.**, A Priori Knowledge-Based STAP for Traffic Monitoring Applications: First Results, Proc. *EUSAR*, Hamburg, Germany, Jun. 2016.

[RC-99] **Baumgartner, S.**, **Krieger, G.**, Experimental Verification of High-Resolution Wide-Swath Moving Target Indication, Proc. *EUSAR*, Hamburg, Germany, Jun. 2016.

[RC-100] **Bordoni, F.**, **Rodríguez Cassolà, M.**, **Krieger, G.**, SAR Cross-Ambiguities in SAOCOM-CS Large Baseline Bistatic Configuration, Proc. *EUSAR*, Hannover, Germany, Jun. 2016.

[RC-101] **Borla Tridon, D.**, **Bachmann, M.**, **Martone, M.**, **Schulze, D.**, **Zink, M.**, The Future of TanDEM-X: Final DEM and Beyond, Proc. *EUSAR*, Hamburg, Germany, Jun. 2016.

[RC-102] **Bueso Bello, J.**, **Martone, M.**, **Gonzalez, C.**, **Wecklich, C.**, **Schulze, D.**, **Rizzoli, P.**, **Krieger, G.**, **Zink, M.**, TanDEM-X Global Forest/Non-Forest Map Generation, Proc. *IRS*, Prague, Czech Republic, Jun. 2016.

[RC-103] **Bueso Bello, J.**, **Wecklich, C.**, **Borla Tridon, D.**, **Gonzalez, C.**, **Martone, M.**, **Kraus, T.**, **Bachmann, M.**, **Rizzoli, P.**, **Zink, M.**, TanDEM-X Mission Status and Final DEM Performance, Proc. *IRS*, Prague, Czech Republic, Jun. 2016.

[RC-104] **Böer, J.**, **Gonzalez, C.**, **Wecklich, C.**, **Bräutigam, B.**, **Schulze, D.**, **Bachmann, M.**, **Zink, M.**, Performance Assessment of the Final TanDEM-X DEM, Proc. *ESA Living Planet Symposium*, Prague, Czech Republic, Jun. 2016.

[RC-105] **Börner, T.**, **Zonno, M.**, **López-Dekker, F.**, **Wollstadt, S.**, **Huber, S.**, **Younis, M.**, Statistical Analysis of Ambiguity to Signal Ratio Levels Based on Global Backscattering Maps, Proc. *EUSAR*, Hamburg, Germany, Jun. 2016.

[RC-106] Ostberg, J., Wagner, S., **Calaminus, B.**, An Industrial Experience Report on Introduction and Usage of Static Analysis Tools, Proc. *SANER*, Osaka, Japan, Mar. 2016.

[RC-107] **Cazcarra Bes, V.**, **Tello Alonso, M.**, **Pardini, M.**, **Papathanassiou, K.**, Detecting Forest Structure Changes with SAR Tomography, Proc. *HGF Alliance Week*, Garmisch-Partenkirchen, Germany, Jul. 2016.

[RC-108] **Cazcarra Bes, V.**, **Tello Alonso, M.**, **Toraño Caicoya, A.**, **Papathanassiou, K.**, Monitoring Forest Structure Dynamics by Means of TomoSAR Techniques at L-Band, Proc. *EUSAR*, Hamburg, Germany, Jun. 2016.

[RC-109] **Dietrich, B.**, System zur lokalen Luftraumüberwachung für Sicherheitsanwendungen - eine Machbarkeitsstudie, Proc. *Angewandte Forschung für Verteidigung und Sicherheit in Deutschland*, Bonn, Germany, Feb. 2016.

[RC-110] **Döring, B.**, **Reimann, J.**, **Raab, S.**, **Jirousek, M.**, **Rudolf, D.**, **Schwerdt, M.**, The Three-Transponder Method: A Novel Approach for Traceable (E)RCS Calibration of SAR Transponders, Proc. *EUSAR*, Hamburg, Germany, Jun. 2016.

[RC-111] **Döring, B.**, **Schwerdt, M.**, A New Measurement Principle for Determining the Polarization Direction of Calibration Transponder Antennas, Proc. *EUSAR*, Hamburg, Germany, Jun. 2016.

[RC-112] **Eilers, J.**, **Brand, B.**, **Blaschke, K.**, **Calaminus, B.**, Leistungsbestimmung von Kleinsatellitensystemen, Proc. *Angewandte Forschung für Verteidigung und Sicherheit in Deutschland*, Bonn, Feb. 2016.

[RC-113] Yuzugullu, O., **Erten, E.**, **Hajnsek, I.**, Crop Height Estimation of Rice Fields by X- and C-Band PolSAR, Proc. *EUSAR*, Hamburg, Germany, Jun. 2016.

[RC-114] **Fischer, G.**, **Parrella, G.**, **Papathanassiou, K.**, **Hajnsek, I.**, Interpretation of Pol-InSAR Signatures from Glaciers and Ice Sheets at Different Frequencies, Proc. *EUSAR*, Hamburg, Germany, Jun. 2016.

[RC-115] **Fischer, J.**, Flugzeug-SAR-Systeme am DLR – Stand der Entwicklungen und Datenmanagement, Proc. *Data Science Workshop*, Cologne, Germany, Nov. 2016.

[RC-116] **Gonzalez, C.**, **Bräutigam, B.**, **Rizzoli, P.**, Relative Height Accuracy Analysis of TanDEM-X DEM Products, Proc. *EUSAR*, Hamburg, Germany, Jun. 2016.

[RC-117] **Gramini Ganesan, P.**, **Jagdhuber, T.**, **Hajnsek, I.**, **Rao, Y.**, Time Series Investigation of Soil Moisture Estimation Using Compact Polarimetry at L-Band, Proc. *IGARSS*, Beijing, China, Jul. 2016.

[RC-118] **Haas, A.**, **Peichl, M.**, **Anger, S.**, Design of Wide-Band Corrugated Feed Horn for Reflector Antenna in Radar Applications, Proc. *GeMic*, Bochum, Germany, Mar. 2016.

[RC-119] **Hager, M.**, Examples of Incoherent Change Detection of Sentinel-1A Data, Proc. *NATO SET 220 Panel*, Germany, Friedrichshafen, Oct. 2016.

[RC-120] **Hager, M.**, Investigation on Interferometry for SAR Data from Cosmo SkyMed, RadarSat II and TerraSAR-X, Proc. *NATO SET 220 Panel*, The Netherlands, Apr. 2016.

[RC-121] Baffelli, S., Frey, O., Werner, C., **Hajnsek, I.**, System Characterization and Polarimetric Calibration of the Ku-Band Advanced Polarimetric Interferometer, Proc. *EUSAR*, Hamburg, Germany, Jun. 2016.

[RC-122] Brancato, V., **Hajnsek, I.**, Assessment of Leaf Wetness Variation Effect on Differential Interferometric Observables, Proc. *EUSAR*, Hamburg, Germany, Jun. 2016.

[RC-123] **Hajnsek, I.**, **Pardini, M.**, **Horn, R.**, **Scheiber, R.**, **Jäger, M.**, **Keller, M.**, **Geßwein, D.**, **Papathanassiou, K.**, **Reigber, A.**, 3-D SAR Imaging of African Forests: Results from the AfriSAR Campaign at P- and L-Band, Proc. *EUSAR*, Hamburg, Germany, Jun. 2016.

[RC-124] Leinss, S., **Hajnsek, I.**, Ice Volume Changes and Snow Depth for Aletsch Glacier, Switzerland, Proc. *TanDEM-X Science Team Meeting*, Oberpfaffenhofen, Germany, Oct. 2016.

[RC-125] Lucas, C., **Hajnsek, I.**, Marino, A., Böhler, Y., Investigation of Snow Avalanches with Ground Based Ku-Band Radar, Proc. *EUSAR*, Hamburg, Germany, Jun. 2016.

[RC-126] Pichierri, M., **Hajnsek, I.**, Comparing Performances of RVoG and OVoG Crop Height Inversion Schemes from Multi-Frequency SAR Data, Proc. *EUSAR*, Hamburg, Germany, Jun. 2016.

[RC-127] Siddique, M., Wegmöller, U., **Hajnsek, I.**, Frey, O., SAR Tomography as an Add-on to PSI for Improved Deformation Sampling in Urban Areas: A Quality Assessment, Proc. *EUSAR*, Hamburg, Germany, Jun. 2016.

[RC-128] **Heine, I.**, **Jagdhuber, T.**, Kleinschmit, B., Itzerott, S., Monitoring of Natural Lakes in Northeastern Germany Using Dual-Polarimetric (HH/VV) TerraSAR-X Time Series, Proc. *ESA Living Planet Symposium*, Prague, Czech Republic, May 2016.

[RC-129] **Heine, I.**, **Jagdhuber, T.**, Itzerott, S., Classification and Monitoring of Reed Belts Using Dual-Polarimetric TerraSAR-X Time Series, Proc. *European Geosciences Union (EGU) General Assembly*, Vienna, Austria, Apr. 2016.

[RC-130] **Heinzel, A.**, **Peichl, M.**, **Schreiber, E.**, **Bischeltsrieder, F.**, **Dill, S.**, **Anger, S.**, **Kempf, T.**, **Jirousek, M.**, Focusing Methods for Ground Penetrating MIMO SAR Imaging within Half-Spaces of Different Permittivity, Proc. *EUSAR*, Hamburg, Jun. 2016.

[RC-131] **Heister, A.**, **Scheiber, R.**, First Analysis of Sparse Signal Reconstruction for Radar Imaging of Ice Sheets, Proc. *EUSAR*, Hamburg, Germany, Jun. 2016.

[RC-132] **Huber, S.**, **Villano, M.**, **Younis, M.**, **Krieger, G.**, **Moreira, A.**, Grafmüller, B., Wolters, R., Tandem-L: Design Concepts for a Next-Generation Spaceborne SAR System, Proc. *EUSAR*, Hamburg, Germany, Jun. 2016.

[RC-133] Das, N., Entekhabi, D., Kim, S., **Jagdhuber, T.**, Piles, M., Yueh, S., Colliander, A., Lopez-Baeza, E., Martinez-Fernandez, J., High-Resolution Enhanced Product Based on SMAP Active-Passive Approach and Sentinel-1A Radar Data, Proc. *AGU Fall Meeting*, San Francisco, USA, Dec. 2016.

[RC-134] **Jagdhuber, T.**, Das, N., Entekhabi, D., **Baur, M.**, **Link, M.**, Piles, M., Akbar, R., Konings, A., McColl, K., Alemohammad, S., Montzka, C., Kunstmann, H., A Data-Driven and Physics-based Single-Pass Retrieval of Active-Passive Microwave Covariation and Vegetation Parameters for the SMAP Mission, Proc. *AGU Fall Meeting*, San Francisco, USA, Dec. 2016.

[RC-135] Piles, M., Entekhabi, D., Konings, A., Akbar, R., **Jagdhuber, T.**, Chaparro, D., Das, N., Monitoring the Phenology of Global Agroecosystems Using SMAP Multi-temporal Vegetation Optical Depth Retrievals, Proc. *AGU Fall Meeting*, San Francisco, USA, Dec. 2016.

[RC-136] Das, N., Entekhabi, D., Kim, S., Colliander, A., **Jagdhuber, T.**, Yueh, S., Combining SMAP and Sentinel Data for High-Resolution Soil Moisture Product, Proc. *Satellite Soil Moisture Validation and Application Workshop*, New York, USA, Sep. 2016.

[RC-137] **Jagdhuber, T.**, Entekhabi, D., Das, N., **Baur, M.**, Kim, S., Yueh, S., **Link, M.**, Physically-based Covariation Modelling and Retrieval for Mono- (LL) and Multi-Frequency (LC) Active-Passive Microwave Data from SMAP and Sentinel-1, Proc. *Satellite Soil Moisture Validation and Application Workshop*, New York, USA, Sep. 2016.

[RC-138] Lorenz, C., Montzka, C., **Jagdhuber, T.**, Kunstmann, H., Development of a Copula-based Data Merging Framework for Combining Spaceborne Soil Moisture and Ancillary Data, Proc. *Workshop on Data Assimilation in Terrestrial Systems*, Bonn, Germany, Sep. 2016.

[RC-139] Alemohammad, S., **Jagdhuber, T.**, Moghaddam, M., Entekhabi, D., Decomposing Soil and Vegetation Contributions in Polarimetric L- and P-Band SAR Observations, Proc. *IGARSS*, Beijing, China, Jul. 2016.

[RC-140] Alemohammad, S., Konings, A., **Jagdhuber, T.**, Entekhabi, D., Characterizing Vegetation and Soil Parameters Across Different Biomes Using Polarimetric P-Band SAR Measurements, Proc. *IGARSS*, Beijing, China, Jul. 2016.

[RC-141] **Jagdhuber, T.**, Entekhabi, D., Konings, A., McColl, K., Alemohammad, S., Das, N., Montzka, C., Piles, M., Physically-based Retrieval of SMAP Active-Passive Measurements Covariation and Vegetation Structure Parameters, Proc. *IGARSS*, Beijing, China, Jul. 2016.

[RC-142] Lorenz, C., Montzka, C., **Jagdhuber, T.**, Kunstmann, H., Development of a Copula-based Data Combination Framework for Merging Remote-Sensing Based Soil Moisture Data, Proc. *HGF Alliance Week*, Garmisch-Partenkirchen, Germany, Jun./Jul. 2016.

[RC-143] Piles, M., Entekhabi, D., Konings, A., McColl, K., Das, N., **Jagdhuber, T.**, The Multi-Temporal Dual Channel Algorithm: First Microwave Retrievals of Soil Moisture and Vegetation Parameters from SMAP, Proc. *IGARSS*, Beijing, China, Jul. 2016.

[RC-144] Montzka, C., Lorenz, C., **Jagdhuber, T.**, Laux, P., **Hajnsek, I.**, Kunstmann, H., Entekhabi, D., Vereecken, H., A Copula-based Algorithm for Combining Airborne Active and Passive Microwave Observations, Proc. *ESA Living Planet Symposium*, Prague, Czech Republic, May 2016.

[RC-145] Das, N., **Jagdhuber, T.**, Kim, S., Yueh, S., Entekhabi, D., Covariations of Backscatter and Brightness Temperature: Comparison of Observed L-Band and L- and C-Band Pairs, Proc. *MicroRad*, Espoo, Finland, Apr. 2016.

[RC-146] **Jäger, M.**, Krogager, E., **Reigber, A.**, Polarimetric SAR Change Detection in Multiple Frequency Bands for Environmental Monitoring and Surveillance in Arctic Regions, Proc. *EUSAR*, Hamburg, Germany, Jun. 2016.

[RC-147] **Jörg, H.**, **Pardini, M.**, **Hajnsek, I.**, **Papathanassiou, K.**, Detecting Physical Changes in Agricultural Crops Using Multi-Frequency Tomographic SAR Data, Proc. *HGF Alliance Week*, Garmisch-Partenkirchen, Germany, Jun./Jul. 2016.

[RC-148] **Jörg, H.**, **Pardini, M.**, **Papathanassiou, K.**, **Hajnsek, I.**, Analysis of Orientation Effects of Crop Vegetation Volumes by Means of SAR Tomography at Different Frequencies, Proc. *EUSAR*, Hamburg, Germany, Jun. 2016.

[RC-149] **Kim, J.**, Sato, H., **Papathanassiou, K.**, Estimation of Drift of Equatorial Ionoshere of Post Sunset-Sector by Means of Low Frequency Spaceborne SAR, Proc. *IGARSS*, Beijing, China, Jul. 2016.

[RC-150] **Kim, J.**, Sato, H., **Papathanassiou, K.**, Validation of Ionospheric Mapping by Means of SAR through Ground Based Radar and GNSS Measurements, Proc. *EUSAR*, Hamburg, Germany, Jun. 2016.

[RC-151] **Kraus, T.**, **Bräutigam, B.**, **Bachmann, M.**, **Krieger, G.**, Multistatic SAR Imaging: First Results of a Four Phase Center Experiment with TerraSAR-X and TanDEM-X, Proc. *EUSAR*, Hamburg, Germany, Jun. 2016.

[RC-152] **Kraus, T.**, **Bräutigam, B.**, **Bachmann, M.**, **Krieger, G.**, **Mittermayer, J.**, TerraSAR-X and TanDEM-X: A Unique Platform to Demonstrate the Capabilities of Distributed SAR Satellite Systems, Proc. *ONERA-DLR Aerospace Symposium (ODAS)*, Oberpfaffenhofen, Germany, Jun. 2016.

[RC-153] **Krieger, G.**, **Huber, S.**, **Villano, M.**, **Queiroz de Almeida, F.**, **Younis, M.**, **López-Dekker, F.**, **Prats Iraola, P.**, **Rodríguez Cassolà, M.**, **Moreira, A.**, SIMO and MIMO System Architectures and Modes for High-Resolution Ultra-Wide-Swath SAR Imaging, Proc. *EUSAR*, Hamburg, Germany, Jun. 2016.

[RC-154] **Krieger, G.**, **Rommel, T.**, **Moreira, A.**, MIMO-SAR Tomography, Proc. *EUSAR*, Hamburg, Germany, Jun. 2016.

[RC-155] **Limbach, M.**, **Di Maria, A.**, **Kosc, A.**, **Jäger, M.**, **Horn, R.**, DLR – F-SAR P-Band Antenna – Design, Measurements and Results, Proc. *EUSAR*, Hamburg, Germany, Jun. 2016.

[RC-156] **Martone, M.**, **Rizzoli, P.**, **Bräutigam, B.**, **Krieger, G.**, Forest Classification from TanDEM-X Interferometric Data by Means of Multiple Fuzzy Clustering, Proc. *EUSAR*, Hamburg, Germany, Jun. 2016.

[RC-157] **Martone, M.**, **Rizzoli, P.**, **Bräutigam, B.**, **Krieger, G.**, Global Forest Classification from TanDEM-X Interferometric Data: Potentials and First Results, Proc. *ONERA-DLR Aerospace Symposium (ODAS)*, Oberpfaffenhofen, Germany, Jun. 2016.

[RC-158] **Martone, M.**, **Rizzoli, P.**, **Bräutigam, B.**, **Krieger, G.**, Potentials of TanDEM-X Interferometric Data for Global Forest/Non-Forest Classification, Proc. *ESA Living Planet Symposium*, Prague, Czech Republic, May 2016.

[RC-159] **Mittermayer, J.**, **Kraus, T.**, **Prats Iraola, P.**, **Krieger, G.**, **Moreira, A.**, Wrapped Staring Spotlight SAR for TerraSAR-X, Proc. *EUSAR*, Hamburg, Germany, Jun. 2016.

[RC-160] **Mittermayer, J.**, **López-Dekker, F.**, **Kraus, T.**, **Krieger, G.**, Small Satellite Dispersed SAR – An Exemplary Configuration, Proc. *EUSAR*, Hamburg, Germany, Jun. 2016.

[RC-161] **Mittermayer, J.**, **López-Dekker, F.**, **Kraus, T.**, **Krieger, G.**, Small Satellite Dispersed Synthetic Aperture Radar, Proc. *4S Symposium – Small Satellites Systems and Services*, Valletta, Malta, Jun. 2016.

[RC-162] **Moreira, A.**, **Ponce Madrigal, O.**, **Nannini, M.**, **Pardini, M.**, **Prats Iraola, P.**, **Reigber, A.**, **Papathanassiou, K.**, **Krieger, G.**, Multibaseline Spaceborne SAR Imaging, Proc. *IGARSS*, Beijing, China, Jul. 2016.

[RC-163] **Nannini, M.**, **Prats Iraola, P.**, **Scheiber, R.**, **Yague-Martinez, N.**, Minati, F., Vecchioli, F., Costantini, M., Borgstrom, S., De Martino, P., Siniscalchi, V., Walter, T., Foumelis, M., Desnos, Y., Sentinel-1 Mission: Results of the InSARap Project, Proc. *EUSAR*, Hamburg, Germany, Jun. 2016.

[RC-164] **Özis, E.**, **Osipov, A.**, Eibert, T., Physical Optics and Full Wave Simulations of Transmission of Electromagnetic Fields through Electrically Large Planar Meta-Sheets, Proc. *URSI Kleinheubacher Tagung*, Miltenberg, Germany, Sep. 2016.

[RC-165] **Osipov, A.**, **Kemptner, E.**, Einsatz von Metamaterialien zur Reduzierung des Radarstreuquerschnitts im Mikrowellenbereich, Proc. *Angewandte Forschung für Verteidigung und Sicherheit in Deutschland*, Bonn, Germany, Feb. 2016.

[RC-166] **Pardini, M.**, **Parrella, G.**, **Fischer, G.**, **Papathanassiou, K.**, A Multi-Frequency SAR Tomographic Characterization of Sub-Surface Ice Volumes, Proc. *EUSAR*, Hamburg, Germany, Jun. 2016.

[RC-167] **Pardini, M.**, **Qi, W.**, Dubayah, R., **Papathanassiou, K.**, Exploiting TanDEM-X Pol-InSAR Data for Forest Structure Observation and Potential Synergies with NASA's Global Ecosystem Dynamics Investigation Lidar (GEDI) Mission, Proc. *EUSAR*, Hamburg, Germany, Jun. 2016.

[RC-168] **Parrella, G.**, **Fischer, G.**, **Hajnsek, I.**, Identification of Glacier Zones in Western Greenland by Means of SAR Polarimetry, Proc. *HGF Alliance Week*, Garmisch-Partenkirchen, Germany, Jun. 2016.

[RC-169] **Parrella, G.**, Farinotti, D., **Hajnsek, I.**, **Papathanassiou, K.**, Monitoring the Subsurface of an Alpine Glacier Using Polarimetric SAR Observations at L-Band, Proc. *EUSAR*, Hamburg, Germany, Jun. 2016.

[RC-170] **Parrella, G.**, **Pardini, M.**, **Fischer, G.**, **Hajnsek, I.**, Looking under the Subsurface of the Ablation Zone of Greenland with SAR Tomography, Proc. *HGF Alliance Week*, Garmisch-Partenkirchen, Germany, Jun./Jul. 2016.

[RC-171] **Parrella, G.**, **Ponce Madrigal, O.**, **Hajnsek, I.**, **Moreira, A.**, Exploring the Potential of Polarimetric Circular SAR for Glacier Monitoring: the Findel Glacier Case Study, Proc. *ESA Living Planet Symposium*, Prague, Czech Republic, May 2016.

[RC-172] **Peichl, M.**, **Dill, S.**, Enhanced Imaging by Combined Use of MMW Radar and Radiometer Systems, Proc. *International Workshop on Terahertz Technology and Applications*, Kaiserslautern, Germany, Mar. 2016.

[RC-173] **Peichl, M.**, **Dill, S.**, **Wallner, D.**, Combining MMW Radar and Radiometer Images for Enhanced Characterization of Scenes, Proc. *SPIE Symposium on Defense and Commercial Sensing*, Baltimore, USA, Apr. 2016.

[RC-174] **Peichl, M.**, **Kemptner, E.**, **Dill, S.**, **Osipov, A.**, Phänomenologie und Techniken der Mikrowellenfernerkundung auf hochagilen Flugkörpern, Proc. *DWT-Konferenz "Angewandte Forschung für Verteidigung und Sicherheit in Deutschland"*, Bonn, Germany, Feb. 2016.

[RC-175] **Peichl, M.**, **Schreiber, E.**, **Heinzel, A.**, **Dill, S.**, Detection of Landmines and UXO Using Advanced Synthetic Aperture Radar Technology, Proc. *SPIE Symposium on Defense and Commercial Sensing*, Baltimore, USA, Apr. 2016.

[RC-176] **Peichl, M.**, **Schreiber, E.**, **Heinzel, A.**, **Dill, S.**, Detektion von Landminen und Sprengkörpern durch hochentwickelte Radartechnologie mit synthetischer Apertur, Proc. *DWT-Konferenz "Angewandte Forschung für Verteidigung und Sicherheit in Deutschland"*, Bonn, Germany, Feb. 2016.

[RC-177] **Pinheiro, M.**, **Reigber, A.**, Improving TanDEM-X DEMs Accuracy Using Large-Baseline Data from the Science Phase, Proc. *EUSAR*, Hamburg, Germany, Jun. 2016.

[RC-178] **Pinheiro, M.**, **Reigber, A.**, **Moreira, A.**, Large-Baseline InSAR for Precise Topographic Mapping: a Dual-baseline Framework for TanDEM-X Interferometric Data, Proc. *URSI Kleinheubacher Tagung*, Miltenberg, Germany, Sep. 2016.

[RC-179] **Ponce Madrigal, O.**, **Martinez del Hoyo, A.**, **Jörg, H.**, **Prats Iraola, P.**, **Hajnsek, I.**, **Reigber, A.**, First Study on Holographic SAR Tomography over Agricultural Crops at C-/X-Band, Proc. *IGARSS*, Beijing, China, Jul. 2016.

[RC-180] **Bueso-Bello, J.**, **Prats Iraola, P.**, **Martone, M.**, **Rizzoli, P.**, **Bräutigam, B.**, Performance Evaluation of the TanDEM-X Quad Polarization Acquisitions in the Science Phase, Proc. *EUSAR*, Hamburg, Germany, Jun. 2016.

[RC-181] **Prats Iraola, P.**, **Rodríguez Cassolà, M.**, **Moreira, A.**, Investigations on Bistatic SAR Image Formation for the SAOCOM-CS Mission, Proc. *EUSAR*, Hamburg, Germany, Jun. 2016.

[RC-182] **Prats Iraola, P.**, **Yague-Martinez, N.**, **Wollstadt, S.**, **Kraus, T.**, **Scheiber, R.**, Demonstration of the Applicability of 2-Look Burst Modes in Non-Stationary Scenarios with TerraSAR-X, Proc. *EUSAR*, Hamburg, Germany, Jun. 2016.

[RC-183] **Que, R.**, **Ponce Madrigal, O.**, **Baumgartner, S.**, **Scheiber, R.**, Multi-Mode Realtime SAR On-Board Processing, Proc. *EUSAR*, Hamburg, Germany, Jun. 2016.

[RC-184] **Queiroz de Almeida, F.**, **Krieger, G.**, Multichannel Staggered SAR Azimuth Sample Regularization, Proc. *EUSAR*, Hamburg, Germany, Jun. 2016.

[RC-185] **Raab, S.**, **Döring, B.**, **Rudolf, D.**, **Reimann, J.**, **Schwerdt, M.**, Analysis of an Improved Temperature Management Concept for SAR System Calibration Transponders, Proc. *EUSAR*, Hamburg, Germany, Jun. 2016.

[RC-186] Ferro-Famil, L., Huang, Y., El Hajj Chehade, B., **Reigber, A.**, Tebaldini, S., 3-D Imaging Using Polarimetric Diversity, Processing Techniques and Applications, Proc. *EuCAP*, Davos, Switzerland, Apr. 2016.

[RC-187] Hensley, S., Lou, Y., Michel, T., Mullerschoen, R., Hawkins, B., Lavalle, M., Pinto, N., **Reigber, A.**, **Pardini, M.**, UAVSAR PolInSAR and Tomographic Experiments in Germany, Proc. *IGARSS*, Beijing, China, Jul. 2016.

[RC-188] Huang, Y., Levy-Vehel, J., Ferro-Famil, L., **Reigber, A.**, 3D Imaging for Underfoliage Targets Using L-Band Multibaseline PolInSAR Data and Sparse Estimation Methods, Proc. *IGARSS*, Beijing, China, Jul. 2016.

[RC-189] Huang, Y., Levy-Vehel, J., Ferro-Famil, L., **Reigber, A.**, Fortunati, S., 3D Characterization of Underfoliage Targets Using L-Band Tomographic SAR Data and a Wavelet-Based Approach, Proc. *EUSAR*, Hamburg, Germany, Jun. 2016.

[RC-190] Krogager, E., von Platen Rosenmunthe, S., **Reigber, A.**, **Keller, M.**, **Jäger, M.**, Boerner, W., Characterization of Radar Targets - A Review of Polarimetric Descriptors Applied to Recent F-SAR Data, Proc. *EUSAR*, Hamburg, Germany, Jun. 2016.

[RC-191] **Martín del Campo Becerra, G.**, **Reigber, A.**, Shkvarko, Y., Resolution Enhanced SAR Tomography: A Nonparametric Iterative Adaptive Approach, Proc. *IGARSS*, Beijing, China, Jul. 2016.

[RC-192] **Martín del Campo Becerra, G.**, **Reigber, A.**, Shkvarko, Y., Resolution Enhanced SAR Tomography: From Match Filtering to Compressed Sensing Beamforming Techniques, Proc. *EUSAR*, Hamburg, Germany, Jun. 2016.

[RC-193] **Martín del Campo Becerra, G.**, Shkvarko, Y., Lukin, K., **Reigber, A.**, SAR Tomography of Forested Areas: An APES-based Virtual Beamforming Approach, Proc. *International Kharkiv Symposium on Physics and Engineering of Microwaves, Millimeter and Submillimeter Waves (MSMW)*, Kharkiv, Ukraine, Jun. 2016.

[RC-194] **Reigber, A.**, Krogager, E., **Keller, M.**, **Jäger, M.**, **Hajnsek, I.**, **Horn, R.**, The DALO-ARCTIC Campaign: Multi-Spectral SAR Imaging of Ice Features in Greenland, Proc. *EUSAR*, Hamburg, Germany, Jun. 2016.

[RC-195] Shkvarko, Y., **Reigber, A.**, Garcia, G., Feature Enhanced Imaging with Compressed Fractional SAR Sensors: Inverse Problem Formalism and l2–l1 Structured Descriptive Regularization Framework, Proc. *EUSAR*, Hamburg, Germany, Jun. 2016.

[RC-196] Tebaldini, S., Rocca, F., **Reigber, A.**, Ferro-Famil, L., SAR Tomography of Natural Environments: Signal Processing, Applications, and Future Challenges, Proc. *IGARSS*, Beijing, China, Jul. 2016.

[RC-197] **Reimann, J.**, **Schwerdt, M.**, **Döring, B.**, **Zink, M.**, Concepts for the Calibration of Low Frequency Spaceborne SAR Systems, Proc. *EUSAR*, Hamburg, Germany, Jun. 2016.

[RC-198] **Reimann, J.**, **Schwerdt, M.**, **Zink, M.**, Calibration Concepts for Future Low Frequency SAR Missions, Proc. *CEOS SAR CalVal Workshop*, Tokyo, Japan, Sep. 2016.

[RC-199] **Rizzoli, P.**, **Martone, M.**, **Bräutigam, B.**, Rott, H., **Moreira, A.**, Analysis of the Greenland Ice Sheet Snow Facies Using TanDEM-X Interferometric Data., Proc. *ONERA-DLR Aerospace Symposium (ODAS)*, Oberpfaffenhofen, Germany, Jun. 2016.

[RC-200] **Rizzoli, P.**, **Martone, M.**, **Bräutigam, B.**, Rott, H., **Moreira, A.**, Deriving Greenland Ice Sheet Properties from TanDEM-X Mission Data, Proc. *EUSAR*, Hamburg, Germany, Jun. 2016.

[RC-201] **Rizzoli, P.**, **Martone, M.**, **Bräutigam, B.**, Rott, H., **Moreira, A.**, Multi-Temporal Investigation of Greenland Ice Sheet Snow Facies Using TanDEM-X Mission Data, Proc. *ESA Living Planet Symposium*, Prague, Czech Republic, May 2016.

[RC-202] Linde-Cerezo, A., **Rodríguez Cassolà, M.**, Alvarez-Perez, J., **Prats Iraola, P.**, **Moreira, A.**, Numerical SAR Processing Scheme for Generic Very-High-Resolution Spotlight Acquisitions, Proc. *EUSAR*, Hamburg, Germany, Jun. 2016.

[RC-203] **Rodríguez Cassolà, M.**, **López-Dekker, F.**, **Prats Iraola, P.**, De Zan, F., **Krieger, G.**, **Moreira, A.**, Aspects and Challanges of COSAR Image Formation, Proc. *IGARSS*, Beijing, China, Jul. 2016.

[RC-204] **Rodríguez Cassolà, M.**, **López-Dekker, F.**, **Prats Iraola, P.**, De Zan, F., **Krieger, G.**, **Moreira, A.**, CoSAR: Geometrical Analysis and Image Formation Assessment, Proc. *EUSAR*, Hamburg, Germany, Jun. 2016.

[RC-205] **Rodríguez Cassolà, M.**, **Prats Iraola, P.**, **Nannini, M.**, **López-Dekker, F.**, **Moreira, A.**, Carnicero Dominguez, B., Calibration Concept for Weakly-Synchronised SAR Companion Missions: ESA's SAOCOM-CS Case, Proc. *EUSAR*, Hamburg, Germany, Jun. 2016.

[RC-206] Gao, S., Ludwig, M., **Rommel, T.**, Glisic, S., Boccia, L., Krstic, M., Penkala, P., Digital Beamforming Spaceborne Synthetic Aperture Radars, Proc. *EuMW*, London, Great Britain, Oct. 2016.

[RC-207] **Rommel, T.**, **Krieger, G.**, Detection of Multipath Propagation Effects in SAR-Tomography with MIMO Modes, Proc. *EUSAR*, Hamburg, Germany, Jun. 2016.

[RC-208] **Rommel, T.**, **Younis, M.**, Matrix Pencil Method for Direction of Arrival Estimation in DBF-SAR, Proc. *EUSAR*, Hamburg, Germany, Jun. 2016.

[RC-209] **Rommel, T.**, **Younis, M.**, **Krieger, G.**, Demonstration of Simultaneous Quad-Polarization SAR Imaging for Extended Targets in MIMO-SAR, Proc. *GeMiC*, Bochum, Germany, Mar. 2016.

[RC-210] **Rudolf, D.**, **Döring, B.**, **Jirousek, M.**, **Reimann, J.**, **Schwerdt, M.**, A Compact Antenna Rotation Concept for Precise Polarimetric SAR Calibration Transponders, Proc. *EUSAR*, Hamburg, Germany, Jun. 2016.

[RC-211] **Sanjuan Ferrer, M.**, **Pardini, M.**, **Borla Tridon, D.**, **López-Dekker, F.**, **Papathanassiou, K.**, **Bachmann, M.**, Product-Level Performance Models for the Tandem-L Mission: Forest Structure Case Study, Proc. *EUSAR*, Hamburg, Germany, Jun. 2016.

[RC-212] Naghmouchi, J., Michalik, S., **Scheiber, R.**, **Reigber, A.**, Aviely, P., Ginosar, R., Bischoff, O., Gellis, H., Berekovic, M., MacSpace - High-Performance DSP for Onboard Image Processing, Proc. *ESA DSP Day* , Gothenburg, Sweden, Jun. 2016.

[RC-213] **Scheiber, R.**, **Jäger, M.**, Detection and Mitigation of Strong Azimuth Ambiguities in High-Resolution SAR Images, Proc. *EUSAR*, Hamburg, Germany, Jun. 2016.

[RC-214] **Schmidt, K.**, **Schwerdt, M.**, **Castellanos Alfonzo, G.**, **Tous Ramon, N.**, Sentinel-1A Calibration Support during Routine Operation, Proc. *EUSAR*, Hamburg, Germany, Jun. 2016.

[RC-215] **Schreiber, E.**, **Peichl, M.**, **Heinzel, A.**, **Dill, S.**, **Bischeltsrieder, F.**, **Anger, S.**, **Kempf, T.**, **Jirousek, M.**, Challenges for Operational Use of Ground-Based High-Resolution SAR for Landmines and UXO Detection, Proc. *EUSAR*, Hamburg, Germany, Jun./Sep. 2016.

[RC-216] **Schwerdt, M.**, **Schmidt, K.**, **Tous Ramon, N.**, **Klenk, P.**, **Döring, B.**, **Zink, M.**, Final Results of DLR's Independent Sentinel-1B System Calibration, Proc. *CEOS SAR CalVal Workshop*, Tokio, Japan, Sep. 2016.

[RC-217] **Tienda Herrero, C.**, **Younis, M.**, **Krieger, G.**, Reduction of Cross-Polarization on a Single Offset Parabolic Reflector Using Digital Beamforming Techniques and Combination of Elements, Proc. *EUSAR*, Hamburg, Germany, Jun. 2016.

[RC-218] **Tienda Herrero, C.**, **Rommel, T.**, Status Report on the DIFFERENT Project, Proc. *EC Review Meeting DIFFERENT*, Brussels, Belgium, Feb. 2016.

[RC-219] **Tous Ramon, N.**, **Schwerdt, M.**, **Castellanos Alfonzo, G.**, **Schmidt, K.**, Verification of Sentinel-1B Internal Calibration - First Results, Proc. *EUSAR*, Hamburg, Germany, Jun. 2016.

[RC-220] **Valdo, P.**, **Alonso-González, A.**, **Papathanassiou, K.**, Bruzzone, L., Analysis of Agricultural Crops Evolution in Time with TanDEM-X, Proc. *IEEE YP GRSS Conference*, Munich, Germany, Oct. 2016.

[RC-221] **Villamil López, C.**, Petersen, L., **Speck, R.**, Frommholz, D., Registration of Very High Resolution SAR and Optical Images, Proc. *EUSAR*, Hamburg, Germany, Jun. 2016.

[RC-222] **Villano, M.**, **Krieger, G.**, **Moreira, A.**, Reconsideration of Ambiguities in Quad-Pol SAR, Proc. *EUSAR*, Hamburg, Germany, Jun. 2016.

[RC-223] **Walter Antony, J.**, **Schmidt, K.**, **Schwerdt, M.**, **Polimeni, M.**, **Tous Ramon, N.**, **Bachmann, M.**, **Castellanos Alfonzo, G.**, Radiometric Accuracy and Stability of TerraSAR-X and TanDEM-X, Proc. *EUSAR*, Hamburg, Germany, Jun. 2016.

[RC-224] **Wecklich, C.**, **Martone, M.**, **Rizzoli, P.**, **Krieger, G.**, Generation of a Global Forest/non-Forest Map from TanDEM-X Interferometric Data, Proc. *TerraSAR-X Science Team Meeting*, Oberpfaffenhofen, Germany, Oct. 2016.

[RC-225] **Wollstadt, S.**, **López-Dekker, F.**, **Tienda Herrero, C.**, **Younis, M.**, Tesmer, V., Ernst, R., A Dual-beam ATI SAR Mission for Ocean Surface Current Retrieval: Ku- vs. Ka-Band, Proc. *ESA Living Planet Symposium*, Prague, Czech Republic, May 2016.

[RC-226] **Yague-Martinez, N.**, **Prats Iraola, P.**, De Zan, F., Coregistration of Interferometric Stacks of Sentinel-1A TOPS Data, Proc. *EUSAR*, Hamburg, Germany, Jun. 2016.

[RC-227] **Younis, M.**, **Queiroz de Almeida, F.**, **Bordoni, F.**, **López-Dekker, F.**, **Krieger, G.**, Digital Beamforming Techniques for Multi-Channel Synthetic Aperture Radar, Proc. *IGARSS*, Beijing, China, Jul. 2016.

[RC-228] **Zink, M.**, **Bachmann, M.**, Fritz, T., **Rizzoli, P.**, **Schulze, D.**, Wessel, B., Quality of the TanDEM-X DEM, Proc. *CEOS SAR CalVal Workshop*, Tokyo, Japan, Sep. 2016.

2015

[RC-229] **Albers, T.**, **Peichl, M.**, **Dill, S.**, Detection of very Small Impurity Particles in High-Quality Granulated Sugar, Proc. *GeMic*, Nuernberg, Germany, Mar. 2015.

[RC-230] **Alonso-González, A.**, **Papathanassiou, K.**, **Hajnsek, I.**, Physical Interpretation of the Polarimetric SAR Changes Observed over Agricultural Time Series, Proc. *International Workshop on Retrieval of Bio- & Geo-Physical Parameters from SAR Data for Land Applications*, Harwell, UK, Nov. 2015.

[RC-231] **Alonso-González, A.**, **Jagdhuber, T.**, **Hajnsek, I.**, Polarimetric SAR Time Series Change Analysis and Classification over Agricultural Areas, Proc. *HGF Alliance Week*, Garmisch-Partenkirchen, Germany, Jun. 2015.

[RC-232] Alonso-González, A., **Jagdhuber, T.**, **Hajnsek, I.**, Agricultural Monitoring with Polarimetric SAR Time Series, Proc. *International Workshop on the Analysis of Multitemporal Remote Sensing Images*, Annecy, France, Jul. 2015.

[RC-233] Bachmann, M., **Bräutigam, B.**, **Krieger, G.**, **Schulze, D.**, **Wecklich, C.**, **Zink, M.**, TanDEM-X Interferometric System Calibration Review and DEM Quality Status, Proc. *CEOS SAR CalVal Workshop*, Noordwijk, The Netherlands, Oct. 2015.

[RC-234] Bertoluzza, M., **Kim, J.**, **Pardini, M.**, **Papathanassiou, K.**, Bruzzone, L., On the Potentials of PolInSAR Inversion for Monitoring Long-Term Forest Height Dynamics at L-Band, Proc. *ESA POLinSAR Workshop*, Frascati, Italy, Jan. 2015.

[RC-235] Bordoni, F., **Younis, M.**, **Rodríguez Cassolà, M.**, **Prats Iraola, P.**, **López-Dekker, F.**, **Krieger, G.**, SAOCOM-CS SAR Imaging Performance Evaluation in Large Baseline Bistatic Configuration, Proc. *IGARSS*, Milan, Italy, Jul. 2015.

[RC-236] Borla Tridon, D., **Bachmann, M.**, **Böer, J.**, **Bräutigam, B.**, **Gonzalez, C.**, **Kraus, T.**, **Krieger, G.**, **Martone, M.**, **Polimeni, M.**, **Schulze, D.**, **Wecklich, C.**, **Zink, M.**, TanDEM-X Going for the DEM: Acquisition, Performance, and Further Activities, Proc. *Asia-Pacific Conference on Synthetic Aperture Radar (APSAR)*, Singapore, Sep. 2015.

[RC-237] Buckreuß, S., **Steinbrecher, U.**, Schättler, B., The TerraSAR-X Mission, Proc. *Asia-Pacific Conference on Synthetic Aperture Radar (APSAR)*, Singapore, Sep. 2015.

[RC-238] Bueso Bello, J., **Martone, M.**, **Gonzalez, C.**, **Kraus, T.**, **Bräutigam, B.**, First Performance Analysis of Full Polarimetric TanDEM-X Acquisitions in the Pursuit Monostatic Phase, Proc. *IGARSS*, Milan, Italy, Jul. 2015.

[RC-239] Cazcarra Bes, V., **Tello Alonso, M.**, **Papathanassiou, K.**, Forest Structure Estimation by Means of TomoSAR in Front of Weather and Seasonal Variability, Proc. *HGF Alliance Week*, Garmisch-Partenkirchen, Germany, Jun. 2015.

[RC-240] Cazcarra Bes, V., **Tello Alonso, M.**, **Papathanassiou, K.**, Observing the Forest from Lidar and Radar Remote Sensing, Proc. *HGF Alliance Week*, Garmisch-Partenkirchen, Germany, Jun. 2015.

[RC-241] Cazcarra Bes, V., **Tello Alonso, M.**, **Papathanassiou, K.**, 3D Forest Structure Estimation from SAR Tomography by Means of a Full Rank Polarimetric Inversion Based on Compressive Sensing, Proc. *ESA POLinSAR Workshop*, Frascati, Italy, Jan. 2015.

[RC-242] Silva, M., Junqueira, C., **Culhaoglu, A.**, **Kemptner, E.**, Frequency Selective Smart Shield Design for Wireless Signals, Proc. *EuCap*, Lissabon, Portugal, Apr. 2015.

[RC-243] Chandra, M., **Danklmayer, A.**, **Rommel, T.**, Tanzi, T., Polarization and Waveform Diversity Radar Methods and their Application in Disaster Management, Proc. *URSI Atlantic Radio Science Conference*, Gran Canaria, Spain, May 2015.

[RC-244] De Zan, F., **Zonno, M.**, **López-Dekker, F.**, Parizzi, A., Phase Inconsistencies and Water Effects in SAR Interferometric Stacks, Proc. *ESA FRINGE Workshop*, Frascati, Italy, Mar. 2015.

[RC-245] Di Maria, A., **Limbach, M.**, **Horn, R.**, **Reigber, A.**, A P-Band 5-Way Unequal Split High Power Divider for SAR Applications, Proc. *European Microwave Conference (EuMC)*, Paris, France, Sep. 2015.

[RC-246] Döring, B., **Reimann, J.**, **Raab, S.**, **Jirousek, M.**, **Rudolf, D.**, **Schwerdt, M.**, Accurate Transponder Calibrations with the Novel Three-Transponder Method, Proc. *CSA ASAR Workshop*, St. Hubert, Canada, Oct. 2015.

[RC-247] Döring, B., **Reimann, J.**, **Raab, S.**, **Jirousek, M.**, **Rudolf, D.**, **Schwerdt, M.**, Accurate Transponder Calibrations with the Novel Three-Transponder Method, Proc. *CEOS SAR CalVal Workshop*, Noordwijk, The Netherlands, Oct. 2015.

[RC-248] Döring, B., **Schwerdt, M.**, Equivalent Radar Cross Section: What Is It and Why Is It Important?, Proc. *CEOS SAR CalVal Workshop*, Noordwijk, The Netherlands, Oct. 2015.

[RC-249] Fischer, G., **Hajnsek, I.**, Time Series of Pol-InSAR Data as a Proxy for Snow Accumulation and DLR's Airborne SAR Campaign in Greenland, Proc. *HGF Alliance Week*, Garmisch-Partenkirchen, Germany, Jun. 2015.

[RC-250] Fischer, G., **Hajnsek, I.**, Dual-Pol X-Band Pol-InSAR Time Series of a Greenland Outlet Glacier, Proc. *ESA POLinSAR Workshop*, Frascati, Italy, Jan. 2015.

[RC-251] Gabler, B., **Limbach, M.**, A Practical Approach in Applying Validated Reference Values for the Gain-Transfer Method in Antenna Measurements, Proc. *WFMN*, Chemnitz, Germany, Feb. 2015.

[RC-252] Gramini Ganesan, P., **Jagdhuber, T.**, **Hajnsek, I.**, Rao, Y., Retrieval of Soil Moisture Using Multi-Temporal Hybrid Polarimetric RISAT-1 Data, Proc. *IGARSS*, Milano, Italy, Jul. 2015.

[RC-253] Gramini Ganesan, P., **Jagdhuber, T.**, **Hajnsek, I.**, Rao, Y., Time Series Analysis of Hybrid Polarimetric Risat-1 Data for Soil Moisture Estimation, Proc. *Polarimetric and Interferometric SAR Workshop (PI-SAR)*, Frascati, Italy, Jan. 2015.

[RC-254] Grigorov, C., **Schulze, D.**, **Bachmann, M.**, **Bräutigam, B.**, **Zink, M.**, TerraSAR-X and TanDEM-X Mission Status, Proc. *CSA ASAR Workshop*, St. Hubert, Canada, Oct. 2015.

[RC-255] Huber, S., **Krieger, G.**, **Younis, M.**, **Moreira, A.**, Advanced Spaceborne SAR Systems with Array-Fed Reflector Antennas, Proc. *RadarCon*, Washington, USA, May 2015.

[RC-256] Montzka, C., Lorenz, C., **Jagdhuber, T.**, Laux, P., **Hajnsek, I.**, Kunstmann, H., Entekahbi, D., Vereecken, H., Investigating Baseline, Alternative and Copula-based Algorithm for Combining Airborne Active and Passive Microwave Observations in the SMAP Context., Proc. *AGU Fall Meeting*, San Francisco, USA, Dec. 2015.

[RC-257] Alemohammad, S., Konings, A., **Jagdhuber, T.**, Entekhabi, D., Retrieving Vegetation Parameters and Soil Reflection Coefficients with P-Band SAR Polarimetry, Proc. *AGU Fall Meeting*, San Francisco, USA, Dec. 2015.

[RC-258] Marzahn, P., **Jagdhuber, T.**, **Jörg, H.**, **Hajnsek, I.**, Ludwig, R., Estimating Soil Moisture Variability and Uncertainty at Field Scale for Applications in Flood Hydrology, Proc. *Earth Observation for water cycle science*, Frascati, Italy, Oct. 2015.

[RC-259] Wang, H., Magagi, R., Goita, K., **Jagdhuber, T.**, Potential of Polarimetric UAVSAR and RADARSAT-2 Data for Soil Moisture Retrieval over Agricultural fields, Proc. *CSA ASAR Workshop*, Quebec, Canada, Oct. 2015.

[RC-260] Wang, H., Magagi, R., Goita, K., **Jagdhuber, T.**, Soil Moisture Retrieval over Agricultural Fields Using Polarimetric Decomposition, Proc. *CSA ASAR Workshop*, Quebec, Canada, Oct. 2015.

[RC-261] Wang, H., Magagi, R., Goita, K., **Jagdhuber, T.**, Evaluation of Polarimetric Decomposition for Soil Moisture Retrieval over Vegetated, Agricultural Fields, Proc. *IGARSS*, Milan, Italy, Jul. 2015.

[RC-262] Jagdhuber, T., Entekhabi, D., **Hajnsek, I.**, Konnings, A., McColl, K., Alemohammad, S., Das, N., Montzka, C., Physically-based Active-Passive Modelling and Retrieval for Smap Soil Moisture Inversion Algorithm, Proc. *IGARSS*, Milano, Italy, Jul. 2015.

[RC-263] Jagdhuber, T., **Hajnsek, I.**, Montzka, C., Wollschläger, U., **Spengler, D.**, Marzahn, P., Lorenz, C., Kunstmann, H., Retrieval of Soil Moisture under Vegetation Using SAR Polarimetry, Proc. *HGF Alliance Week*, Garmisch-Partenkirchen, Germany, Jun. 2015.

[RC-264] Lorenz, C., **Jagdhuber, T.**, Montzka, C., Entekhabi, D., Copula-based Combination of Active and Passive L-Band Observations for Soil Moisture Estimation, Proc. *HGF Alliance Week*, Garmisch-Partenkirchen, Germany, Jun. 2015.

[RC-265] Montzka, C., Bogena, H., **Jagdhuber, T.**, **Hajnsek, I.**, **Horn, R.**, **Reigber, A.**, Vereecken, H., Investigation of SMAP Fusion Algorithms with Airborne Active and Passive L-Band Microwave Remote Sensing, Proc. *HGF Alliance Week*, Garmisch-Partenkirchen, Germany, Jun. 2015.

[RC-266] Wollschläger, U., Zink, M., **Jagdhuber, T.**, **Schröter, I.**, Schrön, M., **Hajnsek, I.**, Paasche, H., Dietrich, P., Samaniego, L., A Comprehensive Assessment of Soil Moisture at the Catchment Scale Using Remote Sensing, Modeling and Local Observations, Proc. *HGF Alliance Week*, Garmisch-Partenkirchen, Germany, Jun. 2015.

[RC-267] **Jagdhuber, T.**, **Hajnsek, I.**, Entekhabi, D., Montzka, C., **Papathanassiou, K.**, Active-Passive Microwave Polarimetry for Soil Moisture Estimation, Proc. *Polarimetric and Interferometric SAR Workshop (PI-SAR)*, Frascati, Italy, Jan. 2015.

[RC-268] **Jagdhuber, T.**, **Hajnsek, I.**, **Weiß, T.**, **Papathanassiou, K.**, Estimation Of Soil Moisture under Vegetation Cover at Multiple Frequencies, Proc. *Polarimetric and Interferometric SAR Workshop (PI-SAR)*, Frascati, Italy, Jan. 2015.

[RC-269] Eckardt, R., Riedel, T., Eineder, M., Auer, S., Walter, D., **Jagdhuber, T.**, Braun, M., Motagh, M., Pathe, C., Pleskachevsky, A., Thiel, C., **Hajnsek, I.**, Lehner, S., Bock, M., Schmullius, C., SAR-EDU – An Education Initiative for Applied Radar Remote Sensing, Proc. *International Symposium on Remote Sensing of Environment (ISRSE)*, Berlin, Germany, May 2015.

[RC-270] **Jörg, H.**, **Pardini, M.**, **Hajnsek, I.**, Spatial and Temporal Characterisation of Agricultural Crop Volumes Using (Polarimetric) SAR Tomography, Proc. *HGF Alliance Week*, Garmisch-Partenkirchen, Germany, Jun. 2015.

[RC-271] **Jörg, H.**, **Pardini, M.**, **Papathanassiou, K.**, **Hajnsek, I.**, Spatial and Temporal Characterization of Agricultural Crop Volumes by Means of Polarimetric SAR Tomography at C-Band, Proc. *IGARSS*, Milan, Italy, Jul. 2015.

[RC-272] **Jörg, H.**, **Pardini, M.**, **Papathanassiou, K.**, **Hajnsek, I.**, Application of Polarimetric SAR Tomography on Agricultural Vegetation for Scattering Characterisation, Proc. *Polarimetric and Interferometric SAR Workshop (PolinSAR)*, Frascati, Italy, Jan. 2015.

[RC-273] **Jörg, H.**, Picchierri, M., **Pardini, M.**, **Papathanassiou, K.**, **Hajnsek, I.**, Agricultural Crop Structure by Means of Multibaseline Pol-InSAR and SAR Tomography, Proc. *Workshop on Retrieval of Bio- & Geophysical Parameters from SAR Data*, Harwell, UK, Nov. 2015.

[RC-274] **Kemptner, E.**, **Rode, G.**, Radarsignaturbewertung von agilen und hoch gepfeilten Flugzeugkonfigurationen, Proc. *Deutscher Luft- und Raumfahrtkongress*, Rostock, Germany, Sep. 2015.

[RC-275] **Kim, J.**, **Papathanassiou, K.**, On the Separation of Dynamic Scattering and Ionospheric Effects in SAR Data, Proc. *ESA POLinSAR Workshop*, Frascati, Italy, Jan. 2015.

[RC-276] **Krieger, G.**, De Zan, F., **López-Dekker, F.**, **Kim, J.**, **Rodríguez Cassolà, M.**, **Moreira, A.**, Impact of TEC Gradients and Higher-Order Ionospheric Disturbances on Spaceborne Single-Pass SAR Interferometry, Proc. *IGARSS*, Milan,Italy, Jul. 2015.

[RC-277] **Limbach, M.**, **Gabler, B.**, **Horn, R.**, **Kosc, A.**, **Di Maria, A.**, **Scheiber, R.**, New Airborne SAR Antenna at P-Band, Proc. *Fachtagung des ITG Fachausschusses 7.5* "*Wellenausbreitung*", Chemnitz, Germany, Feb. 2015.

[RC-278] **Limbach, M.**, **Gabler, B.**, **Horn, R.**, **Kosc, A.**, **Di Maria, A.**, **Scheiber, R.**, P-Band Antenna Array for Airborne SAR Application and DBF SAR Demonstration, Proc. *EuCAP*, Lisbon, Portugal, Apr. 2015.

[RC-279] **Martone, M.**, **Rizzoli, P.**, **Bräutigam, B.**, **Krieger, G.**, A Method for Generating Forest/Non-Forest Maps from TanDEM-X Interferometric Data, Proc. *IGARSS*, Milan, Italy, Jul. 2015.

[RC-280] **Moreira, A.**, **Krieger, G.**, **Hajnsek, I.**, **Papathanassiou, K.**, **Pardini, M.**, Eineder, M., Shimada, M., Motohka, T., Watanabe, M., Ohki, M., Uematsu, A., Ozawa, S., Tandem-L/ALOS-Next: Monitoring the Earth's Dynamics with PolinSAR, Proc. *ESA POLinSAR Workshop*, Frascati, Italy, Jan. 2015.

[RC-281] **Moreira, A.**, **Krieger, G.**, **Hajnsek, I.**, **Papathanassiou, K.**, **Younis, M.**, **López-Dekker, F.**, **Huber, S.**, Eineder, M., Shimada, M., Motohka, T., Watanabe, M., Ohki, M., Uematsu, A., Ozawa, S., ALOS-Next/Tandem-L: A Highly Innovative SAR Mission for Global Observation of Dynamic Processes on the Earth´s Surface, Proc. *IGARSS*, Milan, Italy, Jul. 2015.

[RC-282] **Özis, E.**, **Osipov, A.**, Eibert, T., Enhancing Microwave Radomes with Metamaterials, Proc. *URSI Kleinheubacher Tagung*, Miltenberg, Deutschland, Sep. 2015.

[RC-283] **Osipov, A.**, Electromagnetic Scattering from Impedance-Matched Bodies, Proc. *EuCAP*, Portugal, Apr. 2015.

[RC-284] **Tello Alonso, M.**, **Cazcarra Bes, V.**, **Pardini, M.**, **Papathanassiou, K.**, Structural Classification of Forest by Means of L-Band Tomographic SAR, Proc. *IGARSS*, Milan, Italy, Jul. 2015.

[RC-285] **Pardini, M.**, **Tello Alonso, M.**, **Kugler, F.**, **Toraño Caicoya, A.**, **Cazcarra Bes, V.**, **Hajnsek, I.**, **Papathanassiou, K.**, Monitoring Forest Change by Means of Multibaseline L-Band SAR Remote Sensing: The Traunstein Test Case, Proc. *NASA Carbon Cycle & Ecosystem Joint Science Workshop*, College Park, USA, Apr. 2015.

[RC-286] **Pardini, M.**, **Tello Alonso, M.**, **Toraño Caicoya, A.**, Heym, M., **Papathanassiou, K.**, A Comparison of P- and L-Band PolInSAR 3-D Forest Structure Estimates: A Study Case in the Traunstein Forest, Proc. *ESA POLinSAR Workshop*, Frascati, Italy, Jan. 2015.

[RC-287] **Parrella, G.**, **Papathanassiou, K.**, **Hajnsek, I.**, 3-D Glacier Subsurface Characterization Using SAR Polarimetry, Proc. *IGARSS*, Milan, Italy, Jul. 2015.

[RC-288] **Parrella, G.**, **Hajnsek, I.**, Characterization Of Glacier Facies Using SAR Polarimetry, Proc. *HGF Alliance Week*, Garmisch Partenkirchen, Germany, Jun. 2015.

[RC-289] Leinss, S., Wiesmann, A., Lemmetyinen, J., **Parrella, G.**, **Hajnsek, I.**, Polarimetric and Interferometric Methods to Determine Snow Depth, SWE, and the Depth of Fresh Snow, Proc. *Polarimetric and Interferometric SAR Workshop (PI-SAR)*, Frascati, Italy, Jan. 2015.

[RC-290] **Parrella, G.**, **Hajnsek, I.**, **Papathanassiou, K.**, A Comparison of L- and P-Band PolSAR Observations of a Sub-Polar Ice-Cap, Proc. *Polarimetric and Interferometric SAR Workshop (PI-SAR)*, Frascati, Italy, Jan. 2015.

[RC-291] Gao, S., Mao, C., Qin, F., **Patyuchenko, A.**, **Tienda Herrero, C.**, **Younis, M.**, **Krieger, G.**, Glisic, S., Debski, W., Boccia, L., Amendola, G., Arnieri, E., Krstic, M., Koczor, A., Penkala, P., Celton, E., Dual-Band Digital Beamforming Synthetic Aperture Radar for Earth Observation, Proc. *Asia-Pacific Microwave Conference (APMC)*, Nanjing, China, vol. 1, Oct. 2015.

[RC-292] Mao, C., Gao, S., Qin, F., Wang, Z., **Patyuchenko, A.**, **Younis, M.**, **Krieger, G.**, Low Profile Shared-Aperture Dual-Band Dual-Polarized Antenna for SAR Applications, Proc. *EuMW*, Paris, France, Sep. 2015.

[RC-293] **Patyuchenko, A.**, **Younis, M.**, **Krieger, G.**, Wang, Z., Gao, S., Qin, F., Mao, C., Glisic, S., Debski, W., Boccia, L., Amendola, G., Arnieri, E., Krstic, M., Celton, E., Highly Integrated DuaL-Band Digital Beamforming Synthetic Aperture Radar, Proc. *EuMW*, Paris, France, Sep. 2015.

[RC-294] **Patyuchenko, A.**, **Younis, M.**, **Krieger, G.**, Compact X/Ka-Band Dual-Polarization Spaceborne Digital Beamforming Synthetic Aperture Radar, Proc. *IRS*, Dresden, Germany, Jun. 2015.

[RC-295] Qin, F., Gao, S., Mao, C., Wang, Z., **Patyuchenko, A.**, **Younis, M.**, **Krieger, G.**, Ka/X DuaL-Band Dual-Polarized Digital Beamforming Smart Antenna for Spaceborne Synthetic Aperture Radars, Proc. *IET Enterprise Workshop*, Edinburgh, UK, Mar. 2015.

[RC-296] **Pinheiro, M.**, **Reigber, A.**, Improving Satellite Derived DEMs by Using Airborne InSAR Data: the TanDEM-X / F-SAR Case of Study, Proc. *IGARSS*, Milan, Italy, Jul. 2015.

[RC-297] **Ponce Madrigal, O.**, **Prats Iraola, P.**, **Scheiber, R.**, **Reigber, A.**, **Moreira, A.**, Polarimetric 3-D Imaging with Airborne Holographic SAR Tomography over Glaciers, Proc. *IGARSS*, Milan, Italy, Jul. 2015.

[RC-298] **Ponce Madrigal, O.**, **Moreira, A.**, **Prats Iraola, P.**, **Scheiber, R.**, **Reigber, A.**, Airborne Holographic SAR Tomography at L- and P-Band, Proc. *Polarimetric and Interferometric SAR Workshop (PI-SAR)*, Frascati, Italy, Jan. 2015.

[RC-299] Ishitsuka, K., **Prats Iraola, P.**, **Nannini, M.**, Surface Displacements of the Kanto Plain, Japan, and Subsurface Structure: Insight from Persistent Scatterer SAR Interferometry, Proc. *SEGJ International Symposium*, Tokyo, Japan, Nov. 2015.

[RC-300] Ishitsuka, K., **Prats Iraola, P.**, **Nannini, M.**, ALOS/PALSAR and TerraSAR-X Persistent Scatterer Interferometry around Tokyo: Interferometric Phase Evaluation and Validation, Proc. *IGARSS*, Milan, Italy, Jul. 2015.

[RC-301] **Prats Iraola, P.**, **Nannini, M.**, **Scheiber, R.**, De Zan, F., **Wollstadt, S.**, Minati, F., Vecchioli, F., Costantini, M., Borgstrom, S., De Martino, P., Siniscalchi, V., Walter, T., Foumelis, M., Desnos, Y., Sentinel-1 Assessment of the Interferometric Wide-Swath Mode, Proc. *IGARSS*, Milan, Italy, Jul. 2015.

[RC-302] **Prats Iraola, P.**, **Rodríguez Cassolà, M.**, **Yague-Martinez, N.**, **López-Dekker, F.**, **Scheiber, R.**, De Zan, F., **Kraus, T.**, **Wollstadt, S.**, Repeat-Pass Interferometric Experiments with the TanDEM-X Constellation for Accurate Along-track Motion Estimation, Proc. *IGARSS*, Milan, Italy, Jul. 2015.

[RC-303] **Prats Iraola, P.**, **Rodríguez Cassolà, M.**, **López-Dekker, F.**, **Scheiber, R.**, De Zan, F., Barat, I., Geudtner, D., Considerations of the Orbital Tube for Interferometric Applications, Proc. *ESA FRINGE Workshop*, Frascati, Italy, Mar. 2015.

[RC-304] **Reimann, J.**, **Schwerdt, M.**, **Döring, B.**, **Raab, S.**, **Rudolf, D.**, **Jirousek, M.**, **Schmidt, K.**, **Tous Ramon, N.**, **Walter Antony, J.**, **Castellanos Alfonzo, G.**, The DLR SAR Calibration Center, Abstract in Proc. *WFMN*, Chemnitz, Germany, Feb. 2015.

[RC-305] **Reimann, J.**, **Schwerdt, M.**, **Döring, B.**, **Raab, S.**, **Rudolf, D.**, **Jirousek, M.**, **Schmidt, K.**, **Tous Ramon, N.**, **Walter Antony, J.**, **Castellanos Alfonzo, G.**, The DLR SAR Calibration Center, Proc. *WFMN*, Chemnitz, Germany, Feb. 2015.

[RC-306] **Reimann, J.**, **Schwerdt, M.**, **Schmidt, K.**, **Tous Ramon, N.**, **Castellanos Alfonzo, G.**, **Döring, B.**, **Rudolf, D.**, **Raab, S.**, **Walter Antony, J.**, **Zink, M.**, The DLR SAR Calibration Center, Proc. *Asia-Pacific Conference on Synthetic Aperture Radar (APSAR)*, Marina Bay Sands, Singapure, Sep. 2015.

[RC-307] **Reimann, J.**, **Schwerdt, M.**, **Zink, M.**, Calibration Concepts for Future Low Frequency SAR Missions, Proc. *CEOS SAR CalVal Workshop*, Noordwijk, The Netherlands, Oct. 2015.

[RC-308] **Rizzoli, P.**, **Bräutigam, B.**, Snow Facies Analysis of the Greenland Ice Sheet Using TanDEM-X Interferometric Coherence, Proc. *IGARSS*, Milan, Italy, Jul. 2015.

[RC-309] **Rizzoli, P.**, **Martone, M.**, **Bräutigam, B.**, **Zink, M.**, Global Maps from Interferometric TanDEM-X Data: Applications and Potentials, Proc. *ESA FRINGE Workshop*, Frascati, Italy, Mar. 2015.

[RC-310] **Rommel, T.**, **Queiroz de Almeida, F.**, **Huber, S.**, **Jäger, M.**, **Krieger, G.**, **Laux, C.**, **Martone, M.**, **Villano, M.**, **Wollstadt, S.**, **Younis, M.**, Calibration Concepts of Multi-Channel Spaceborne SAR, Proc. *CEOS SAR CalVal Workshop*, Tokyo, Japan, Sep. 2015.

[RC-311] **Rommel, T.**, **Younis, M.**, **Krieger, G.**, MIMO SAR Waveforms – A Comparison, Proc. *ITG Fachausschuss 7.5*, Chemnitz, Germany, Feb. 2015.

[RC-312] **Rosigkeit, D.**, **Baumgartner, S.**, **Nottensteiner, A.**, Usability of Long-Term Evolution (LTE) in DLR's Research Aircraft DO228-212, Proc. *GeMiC*, Nuremberg, Germany, Mar. 2015.

[RC-313] **Rudolf, D.**, **Raab, S.**, **Jirousek, M.**, **Döring, B.**, **Reimann, J.**, **Schwerdt, M.**, Absolute Radiometric Calibration of the Novel DLR "Kalibri" Transponder, Proc. *GeMiC*, Nuremberg, Germany, Mar. 2015.

[RC-314] **Sanjuan Ferrer, M.**, **Zonno, M.**, **López-Dekker, F.**, van Leijen, F., Hanssen, R., Towards Product-Level Performance Models for Sentinel-1 Follow-on Missions: Deformation Measurements Case Study, Proc. *IGARSS*, Milan, Italy, Jul. 2015.

[RC-315] **Schmidt, K.**, **Castellanos Alfonzo, G.**, **Bachmann, M.**, **Polimeni, M.**, **Tous Ramon, N.**, **Schwerdt, M.**, Long-Term System Monitoring of Radiometric Stability – Current Status of TerraSAR-X and TanDEM-X, Proc. *CEOS SAR CalVal Workshop*, Noordwijk, The Netherlands, Oct. 2015.

[RC-316] **Schmidt, K.**, **Schwerdt, M.**, **Tous Ramon, N.**, **Castellanos Alfonzo, G.**, **Döring, B.**, **Raab, S.**, **Reimann, J.**, **Rudolf, D.**, **Walter Antony, J.**, Verification of the Sentinel-1A SAR Instrument Calibration Using Active and Passive Point Targets, Proc. *WFMN*, Chemnitz, Germany, Feb. 2015.

[RC-317] **Schmidt, K.**, **Schwerdt, M.**, **Tous Ramon, N.**, **Castellanos Alfonzo, G.**, **Zink, M.**, Sentinel-1A Calibration Support during Routine Operation Using Innovative Point Targets, Proc. *WFMN*, Chemnitz, Germany, Feb. 2015.

[RC-318] **Schreiber, E.**, **Peichl, M.**, **Dill, S.**, **Anger, S.**, **Heinzel, A.**, **Bischeltsrieder, F.**, **Kempf, T.**, **Jirousek, M.**, Theoretical and Experimental Investigations of a Ground-Based High-Resolution SAR for Buried Object Detection, Proc. *European Microwave Week*, Paris, France, Sep. 2015.

[RC-319] **Schwerdt, M.**, **Schmidt, K.**, **Castellanos Alfonzo, G.**, **Tous Ramon, N.**, **Döring, B.**, **Zink, M.**, Independent Sentinel-1A System Calibration, Proc. *CEOS SAR CalVal Workshop*, Noordwijk, The Netherlands, Oct. 2015.

[RC-320] **Spengler, D.**, **Jagdhuber, T.**, Küster, T., Schwonke, F., Itzerott, S., Advances in Estimation of Surface Soil Moisture Using Hyperspectral, Thermal and Microwave Data, Proc. *HGF Alliance Week*, Garmisch-Partenkirchen, Germany, Jun. 2015.

[RC-321] **Tello Alonso, M.**, **Cazcarra Bes, V.**, **Kim, J.**, **Bertoluzza, M.**, **Toraño Caicoya, A.**, **Pardini, M.**, **Papathanassiou, K.**, SAR Tomography for Forest Structure Classification and Monitoring: Actual Status and Perspectives, Proc. *International Workshop on Retrieval of Bio- & Geo-Physical Parameters from SAR Data for Land Applications*, Harwell, UK, Nov. 2015.

[RC-322] **Tello Alonso, M.**, **Cazcarra Bes, V.**, **Pardini, M.**, **Toraño Caicoya, A.**, **Papathanassiou, K.**, 3D Monitoring of Forest Structure by Means of Synthetic Aperture Radar Tomography, Proc. *Der Gepixelte Wald*, Freising, Germany, Mar. 2015.

[RC-323] Cuevas Castillo, J., **Tienda Herrero, C.**, Encinar, J., **Krieger, G.**, Principle of Bifocal Antennas Implemented in a Dual Reflectarray Configuration, Proc. *EuCAP*, Lisbon, Portugal, Apr. 2015.

[RC-324] Cuevas Castillo, J., **Tienda Herrero, C.**, Encinar, J., **Krieger, G.**, Reduction of Cross-Polarization in a Single Offset Parabolic Reflector, Proc. *EuCAP*, Lisbon, Portugal, Apr. 2015.

[RC-325] **Tienda Herrero, C.**, **Bertl, N.**, **Younis, M.**, **Krieger, G.**, Characterization of the Cross-Talk SAR Image Produced by the Cross-Polarization in a Single Offset Parabolic Reflector, Proc. *EuCAP*, Lisbon, Portugal, Apr. 2015.

[RC-326] **Toraño Caicoya, A.**, **Pardini, M.**, **Kugler, F.**, **Papathanassiou, K.**, **Hajnsek, I.**, Above Ground Biomass Estimation from SAR Vertical Reflectivity Profiles, Proc. *ESA POLinSAR Workshop*, Frascati, Italy, Jan. 2015.

[RC-327] **Villano, M.**, **Krieger, G.**, **Moreira, A.**, Ambiguities and Image Quality in Staggered SAR, Proc. *Asia-Pacific Conference on Synthetic Aperture Radar (APSAR)*, Singapore, Sep. 2015.

[RC-328] **Villano, M.**, **Krieger, G.**, **Moreira, A.**, Data Volume Reduction in High-Resolution Wide-Swath SAR Systems, Proc. *Asia-Pacific Conference on Synthetic Aperture Radar (APSAR)*, Singapore, Sep. 2015.

[RC-329] **Villano, M.**, **Papathanassiou, K.**, **Krieger, G.**, **Moreira, A.**, Imaging a Wide-Swath with Full Polarimetry, Proc. *Polarimetric and Interferometric SAR Workshop (PI-SAR)*, Frascati, Italy, Jan. 2015.

[RC-330] **Wecklich, C.**, **Gonzalez, C.**, **Bräutigam, B.**, Height Accuracy for the First Part of the Global TanDEM-X DEM Data, Proc. *Geomorphometry*, Poznan, Poland, Jun. 2015.

[RC-331] **Weiß, T.**, **Jagdhuber, T.**, **Hajnsek, I.**, Marzahn, P., Ludwig, R., Polarimetric Analysis of SAR-Data to Estimate Plant Moisture in Agriculture, Proc. *HGF Alliance Week*, Garmisch-Partenkirchen, Germany, Jun. 2015.

[RC-332] **Wollstadt, S.**, **López-Dekker, F.**, **Younis, M.**, Danielson, R., Tesmer, V., Ernst, R., D'Aliesio, G., Martins-Camelo, L., Lecuyot, A., OSCM #2 - Payload Concept & Performance, Proc. *ESA Ocean Surface Currents Workshop - International Meeting*, Brest, France, Nov. 2015.

[RC-333] **Wollstadt, S.**, **López-Dekker, F.**, De Zan, F., **Younis, M.**, Danielson, R., Tesmer, V., Martins-Camelo, L., A Ku-Band SAR Mission Concept for Ocean Surface Current Measurement using Dual Beam ATI and Hybrid Polarization, Proc. *IGARSS*, Milan, Italy, Jul. 2015.

[RC-334] **Yague-Martinez, N.**, Rodriguez Gonzalez, F., Brcic, R., Shau, R., Interferometric Evaluation of Sentinel-1A TOPS Data, Proc. *FRINGE*, ESRIN, Frascati, Italy, Mar. 2015.

[RC-335] **Younis, M.**, **López-Dekker, F.**, **Krieger, G.**, Signal and Noise Considerations in Multi-Channel SAR, Proc. *IRS*, Dresden, Germany, Jun. 2015.

[RC-336] **Younis, M.**, **López-Dekker, F.**, **Krieger, G.**, **Moreira, A.**, Digital Beamforming Signal-to-Noise Ratio Gain in Multi-Channel SAR, Proc. *IGARSS*, Milan, Italy, Jul. 2015.

[RC-337] **Zink, M.**, **Buckreuß, S.**, TerraSAR-X and TanDEM-X Mission Status, Proc. *CEOS SAR CalVal Workshop*, Noordwijk, The Netherlands, Oct. 2015.

2014

[RC-338] Bieniarz, J., **Aguilera, E.**, Zhu, X., Müller, R., Reinartz, P., Spectral-Spatial Joint Sparsity Unmixing of Hyperspectral Data Using Overcomplete Dictionaries, Proc. *WHISPERS*, Lausanne, Switzerland, Jun. 2014.

[RC-339] **Al-Kahachi, N.**, **Tienda Herrero, C.**, **Younis, M.**, Polarimetric Cross-Talk in SAR System Induced by Antenna Cross-Pol Pattern, Proc. *EUSAR*, Berlin, Germany, Jun. 2014.

[RC-340] **Anger, S.**, **Jirousek, M.**, **Peichl, M.**, GigaRad - A Versatile High-Resolution Ground-Based Pulse Radar for Advanced Remote Sensing Research, Proc. *EUSAR*, Berlin, Jun. 2014.

[RC-341] **Anglberger, H.**, **Hager, M.**, **Kempf, T.**, **Speck, R.**, **Süß, H.**, Simulation-Based Recognition of Airplane Signatures from TerraSAR-X Data, Proc. *EUSAR*, Berlin, Germany, Jun. 2014.

[RC-342] **Anglberger, H.**, Erkennung von maritimen Zielobjekten aus hoch auflösendem TerraSAR-X Bildmaterial, Proc. *Forum Weltraum*, Bonn, Germany, Sep. 2014.

[RC-343] **Anglberger, H.**, **Speck, R.**, **Süß, H.**, Identification of Maritime Target Objects from High Resolution TerraSAR-X Data Using SAR Simulation, Proc. *SPIE Defense + Security*, Baltimore, USA, May 2014.

[RC-344] **Bachmann, M.**, **Castellanos Alfonzo, G.**, **Kraus, T.**, **Steinbrecher, U.**, **Schwerdt, M.**, **Zink, M.**, About the Impact of System Noise in Antenna Pattern Measurements over Rain Forest with TerraSAR-X, Proc. *EUSAR*, Berlin, Germany, Jun. 2014.

[RC-345] **Baumgartner, S.**, **Laskowski, P.**, **Younis, M.**, Schaefer, C., Klein, R., Petrolati, D., Ka-Band Systems and Processing Approaches for Simultaneous High-Resolution Wide-Swath SAR Imaging and Ground Moving Target Indication, Proc. *Advanced RF Sensors and Remote Sensing Instruments (ARSI) and Ka-Band Earth Observation Radar Missions Workshop (KEO)*, Noordwijk, The Netherlands, Nov. 2014.

[RC-346] Makhoul, E., Zhan, Y., Broquetas, A., Ruiz-Rodon, J., **Baumgartner, S.**, Sea Clutter Statistical Characterization Using TerraSAR-X Data, Proc. *IGARSS*, Québec, Canada, Jul. 2014.

[RC-347] **Baumgartner, S.**, Schaefer, C., **Krieger, G.**, Simultaneous Low PRF GMTI and HRWS SAR Imaging without Changing the System Operation Mode, Proc. *EUSAR*, Berlin, Germany, Jun. 2014.

[RC-348] Pál, I., Biemann, R., **Baumgartner, S.**, A Comparison and Validation Approach for Traffic Data, Acquired by Airborne Radar and Optical Sensors Using Parallelized Lucas-Kanade Algorithm, Proc. *EUSAR*, Berlin, Germany, Jun. 2014.

[RC-349] **Bertl, S.**, **López-Dekker, F.**, **Wollstadt, S.**, **Krieger, G.**, Demonstration of Digital Beamforming in Elevation for Spaceborne Synthetic Aperture Radar, Proc. *EUSAR*, Berlin, Germany, Jun. 2014.

[RC-350] **Bertl, S.**, **López-Dekker, F.**, **Younis, M.**, **Krieger, G.**, Equivalency of Multiple Beams and Multiple Phase Centres for Digital Beamforming SAR systems, Proc. *EUSAR*, Berlin, Germany, Jun. 2014.

[RC-351] **Bordoni, F.**, **Laux, C.**, **Wollstadt, S.**, **Younis, M.**, **Mittermayer, J.**, **Krieger, G.**, First Demonstration of Azimuth Phase Coding Technique by TerraSAR-X, Proc. *EUSAR*, Berlin, Germany, Jun. 2014.

[RC-352] **Borla Tridon, D.**, **Bachmann, M.**, **Schulze, D.**, **Polimeni, M.**, **Martone, M.**, **Böer, J.**, **Zink, M.**, TanDEM-X DEM Difficult Terrain & Antarctica Acquisitions towards the Planing of the Science Phase, Proc. *EUSAR*, Berlin, Germany, Jun. 2014.

[RC-353] **Brancato, V.**, **Parrella, G.**, **Hajnsek, I.**, Iodice, A., Electromagnetic Modeling of P-Band Polarimetric SAR Signatures of a Polythermal Ice Cap, Proc. *IEEE GOLD*, Berlin, Germany, Jun. 2014.

[RC-354] **Buckreuß, S.**, TerraSAR-X Mission Status, Proc. *EUSAR*, Berlin, Germany, Jun. 2014.

[RC-355] **Bueso Bello, J.**, **Martone, M.**, **Kraus, T.**, **Prats Iraola, P.**, **Bräutigam, B.**, Performance Evaluation of TanDEM-X Experimental Modes, Proc. *EUSAR*, Berlin, Germany, Jun. 2014.

[RC-356] Casey, J., Beckers, J., **Busche, T.**, Haas, C., Towards the Retrieval of Multi-Year Sea Ice Thickness and Deformation State from Polarimetric C- and X-Band SAR Observations, Proc. *IGARSS*, Quebec City, Canada, Jul. 2014.

[RC-357] Lehner, S., Krumpen, T., Frost, A., Ressel, R., **Busche, T.**, Schwarz, E., First Tests on Near Real Time Ice Type Classification in Antarctica, Proc. *IGARSS*, Quebec City, Canada, Jul. 2014.

[RC-358] **Böer, J.**, **Steinbrecher, U.**, **Bachmann, M.**, **Schulze, D.**, **Bräutigam, B.**, Overview and Status of TerraSAR-X / TanDEM-X Long-Term System Monitoring, Proc. *EUSAR*, Berlin, Germany, Jun. 2014.

[RC-359] **Börner, T.**, **Marull Paretas, G.**, **Baumgartner, S.**, **López-Dekker, F.**, **Sauer, S.**, **Krieger, G.**, D'Addio, S., ATI and GMTI Performance Analysis of Post-Sentinel-1 SAR Systems Based on Simulations Using OASIS, Proc. *EUSAR*, Berlin, Germany, Jun. 2014.

[RC-360] **Castellanos Alfonzo, G.**, **Schwerdt, M.**, **Döring, B.**, **Tous Ramon, N.**, **Schmidt, K.**, First Results of the Sentinel-1A In-Orbit Antenna Characterization Performed by DLR, Proc. *EUSAR*, Berlin, Germany, Jun. 2014.

[RC-361] del Castillo Mena, J., de Porras Bernácer, R., Larrañaga-Sudupe, J., Gomez, B., Sánchez, S., **Castellanos Alfonzo, G.**, PAZ Calibration and Performance Update Based on Precise Antenna Model and Instrument Monitoring Capabilities, Proc. *EUSAR*, Berlin, Germany, Jun. 2014.

[RC-362] **Chiari v., M.**, TimeDAT - A Time Domain Simulation Framework, Proc. *EUSAR*, Berlin, Germany, Jun. 2014.

[RC-363] Russer, J., Xiong, Y., Abdellah, A., **Culhaoglu, A.**, Che, W., Lugli, P., Russer, P., Carbon Nanotube Based Millimeterwave Fishnet, Proc. *4European Microwave Conference (EuMC)*, Rome, Italy, Oct. 2014.

[RC-364] **Culhaoglu, A.**, **Osipov, A.**, An Impedance Formulation to Determine Specular Reflection from Metamaterial Absorbers Composed of Capacitively Loaded Strip Inclusions, Proc. *Metamaterials*, Copenhagen, Denmark, Aug. 2014.

[RC-365] Russer, J., Xiong, Y., Abdellah, A., **Culhaoglu, A.**, Che, W., Lugli, P., Russer, P., Organic Millimeterwave Fishnet Metamaterial Structures, Proc. *Microwave Symposium (IMS)*, Tampa, USA, Jun. 2014.

[RC-366] **De Zan, F.**, **Prats Iraola, P.**, **Scheiber, R.**, Rucci, A., Interferometry with TOPS: Coregistration and Azimuth Shifts, Proc. *EUSAR*, Berlin, Germany, Jun. 2014.

[RC-367] **Del Zoppo, V.**, **Villano, M.**, **Krieger, G.**, A Data Volume Reduction Strategy Based on On-Board Doppler Filtering, Proc. *IEEE GOLD Remote Sensing Conference*, Berlin, Germany, Jun. 2014.

[RC-368] **Di Maria, A.**, Pandolfo, L., De Vita, P., Guida, G., Bercigli, M., Bandinelli, M., High Fidelity Modeling of 30m Near-Field Cassegrain Antenna in X-Band, Proc. *EuCAP*, The Hague, The Netherlands, Apr. 2014.

[RC-369] **Döring, B.**, **Schwerdt, M.**, Introducing Equivalent Radar Cross Section – A First Step Toward New Radiometric Requirement Definitions, Proc. *EUSAR*, Berlin, Germany, Jun. 2014.

[RC-370] **Fischer, G.**, **Hajnsek, I.**, Potential of Dual-Pol X-Band Polarimetric SAR Interferometry over Glaciers, Proc. *HGF Alliance Week*, Garmisch-Partenkirchen, Germany, Jul. 2014.

[RC-371] **Fischer, G.**, **Hajnsek, I.**, **Papathanassiou, K.**, Pol-InSAR Signatures of Glaciers at X-Band: A Preliminary Analysis, Proc. *EUSAR*, Berlin, Germany, Jun. 2014.

[RC-372] **Fischer, G.**, **Hajnsek, I.**, **Papathanassiou, K.**, Temporal Variations of X-Band Pol-InSAR Coherence over Glaciers, Proc. *EARSeL Workshop on Land Ice and Snow*, Bern, Switzerland, Feb. 2014.

[RC-373] **Gabler, B.**, **Horn, R.**, **Jäger, M.**, **Reigber, A.**, Accurate Antenna Characterization for Wideband Synthetic Aperture Radar Processing, Proc. *GeMiC*, Aachen, Germany, Mar. 2014.

[RC-374] **Gonzalez, C.**, **Bräutigam, B.**, **Martone, M.**, **Rizzoli, P.**, Relative Height Error Estimation Method for TanDEM-X DEM Products, Proc. *EUSAR*, Berlin, Germany, Jun. 2014.

[RC-375] **Gramini Ganesan, P.**, **Jagdhuber, T.**, **Hajnsek, I.**, **Rao, Y.**, Soil Moisture Inversion Using Hybrid Polarimetric RISAT-1 Data, Proc. *EUSAR*, Berlin, Germany, Jun. 2014.

[RC-376] **Hajnsek, I.**, Eineder, M., Walter, T., Friedrich, A., Bieber, P., Huth, A., **Papathanassiou, K.**, Montzka, C., Wollschläger, U., Thies, B., Humbert, A., Braun, M., **Krieger, G.**, **Moreira, A.**, Remote Sensing and Earth System Dynamics: The Helmholtz Association Alliance, Proc. *American Geophysical Union*, San Francisco, USA, Dec. 2014.

[RC-377] Anghel, A., Vasile, G., Ioana, C., Cacoveanu, R., Ciochina, S., Ovarlez, J., Boudon, R., d'Urso, G., **Hajnsek, I.**, Scattering Centers Monitoring in Refocused SAR Images on a High-Resolution DEM, Proc. *IGARSS*, Quebec City, Canada, Jul. 2014.

[RC-378] Frey, O., Siddique, M., **Hajnsek, I.**, Wegmüller, U., Werner, C., Combining SAR Tomography and a PSI Approach for High-Resolution 3-D Imaging of an Urban Area, Proc. *EUSAR*, Berlin, Germany, Jun. 2014.

[RC-379] Leinss, S., Lemmetyinen, J., Wiesmann, A., **Hajnsek, I.**, Snow Structure Evolution Measured by Ground Based Polarimetric Phase Differences, Proc. *EUSAR*, Berlin, Germany, Jun. 2014.

[RC-380] Marino, A., **Hajnsek, I.**, Including Overall Amplitude in the Geometrical Perturbation Filters Classifier, Proc. *EUSAR*, Berlin, Germany, Jun. 2014.

[RC-381] Pichierri, M., **Hajnsek, I.**, First Results towards the Retrieval of Agricultural Crop Structure by Means of Polarimetric SAR Interferometry, Proc. *EUSAR*, Berlin, Germany, Jun. 2014.

[RC-382] **Huber, S.**, **Rommel, T.**, **Patyuchenko, A.**, **Laskowski, P.**, A Reflector-Based Digital Beamforming Demonstrator, Proc. *EUSAR*, Berlin, Germany, Jun. 2014.

[RC-383] **Jagdhuber, T.**, **Hajnsek, I.**, **Papathanassiou, K.**, Tereno Observatories – Validation Sites for a SAR-Based Soil Moisture Retrieval under Vegetation Cover, Proc. *International TERENO Conference*, Bonn, Germany, Sep./Oct. 2014.

[RC-384] Montzka, C., Bogena, H., **Jagdhuber, T.**, **Hajnsek, I.**, **Horn, R.**, **Reigber, A.**, Hasan, S., Rüdiger, C., **Jäger, M.**, Vereecken, H., Airborne Active and Passive L-Band Microwave Remote Sensing – A Test Bed for SMAP Fusion Algorithms, Proc. *IGARSS*, Quebec City, Canada, Jul. 2014.

[RC-385] Ballester-Berman, D., **Jagdhuber, T.**, Lopez-Sanchez, J., Vicente-Guijalba, F., Soil Moisture Estimation in Vineyards by Means of C-Band Radar Measurements, Proc. *EUSAR*, Berlin, Germany, Jun. 2014.

[RC-386] **Jagdhuber, T.**, **Hajnsek, I.**, **Caputo, M.**, **Papathanassiou, K.**, Dual-Polarimetry for Soil Moisture Inversion at X-Band, Proc. *EUSAR*, Berlin, Germany, Jun. 2014.

[RC-387] **Jirousek, M.**, **Iff, S.**, **Anger, S.**, **Peichl, M.**, GigaRad – A Multi-Purpose High-Resolution Ground-Based Radar System, Proc. *EuRad*, Rome, Italy, Oct. 2014.

[RC-388] **Jirousek, M.**, **Döring, B.**, **Rudolf, D.**, **Raab, S.**, **Schwerdt, M.**, Development of the Highly Accurate DLR Kalibri Transponder, Proc. *EUSAR*, Berlin, Germany, Jun. 2014.

[RC-389] **Jörg, H.**, **Hajnsek, I.**, Characterisation of Scattering Mechanisms Occurring in Agricultural Vegetation Using Multi-Frequency Multibaseline SAR Data, Proc. *HGF Alliance Week*, Garmisch-Partenkirchen, Germany, Jul. 2014.

[RC-390] **Jörg, H.**, **Pardini, M.**, **Hajnsek, I.**, **Papathanassiou, K.**, First Multi-Frequency Investigation of SAR Tomography for Vertical Structure of Agricultural Crops, Proc. *EUSAR*, Berlin, Germany, Jun. 2014.

[RC-391] **Kim, J.**, **Papathanassiou, K.**, SAR Observation of Ionosphere Using Range/Azimuth Sub-Bands, Proc. *EUSAR*, Berlin, Germany, Jun. 2014.

[RC-392] **Kraus, T.**, **Bräutigam, B.**, **Mittermayer, J.**, **Steinbrecher, U.**, **Grigorov, C.**, **Schulze, D.**, A Global Performance Assessment Approach for the TerraSAR-X Staring Spotlight and Wide ScanSAR Modes, Proc. *EUSAR*, Berlin, Germany, Jun. 2014.

[RC-393] **Krieger, G.**, **De Zan, F.**, **Bachmann, M.**, **López-Dekker, F.**, **Rodríguez Cassolà, M.**, **Kim, J.**, Tropospheric and Ionospheric Effects in Spaceborne Single-Pass SAR Interferometry and Radargrammetry, Proc. *EUSAR*, Berlin, May 2014.

[RC-394] **Limbach, M.**, **Gabler, B.**, **Horn, R.**, **Kosc, A.**, **Di Maria, A.**, New Cavity Backed Capacitively Coupled Stacked Patch Element for P-Band SAR Application, Proc. *European Conference on Antennas and Propagation (EUCAP)*, The Hague, The Netherlands, Apr. 2014.

[RC-395] **Limbach, M.**, **Gabler, B.**, **Horn, R.**, **Kosc, A.**, **Di Maria, A.**, Cavity Backed Capacitively Coupled Stacked Patch Element for Electrically Small P-Band Array, Proc. *GeMiC*, Aachen, Germany, Mar. 2014.

[RC-396] **López-Dekker, F.**, **Rodríguez Cassolà, M.**, **De Zan, F.**, **Krieger, G.**, Imaging Ocean Surface Statistics Using Geosynchronous Correlating SAR (CoSAR), Proc. *EUSAR*, Berlin, Germany, Jun. 2014.

[RC-397] **López-Dekker, F.**, **Rodríguez Cassolà, M.**, **Prats Iraola, P.**, **De Zan, F.**, **Kraus, T.**, **Sauer, S.**, **Mittermayer, J.**, Experimental Bidirectional SAR ATI Acquisitions of the Ocean Surface with TanDEM-X, Proc. *EUSAR*, Berlin, Germany, Jun. 2014.

[RC-398] **López-Dekker, F.**, **De Zan, F.**, **Wollstadt, S.**, **Younis, M.**, Danielson, R., Tesmer, V., Martins Camelo, L., A Ku-band ATI SAR Mission for Total Ocean Surface Current Vector Retrieval: System Concept and Performance, Proc. *ESA ARSI and Ka-Band Earth Observation Radar Missions (KEO)*, Noordwijk, The Netherlands, Nov. 2014.

[RC-399] **Martone, M.**, **Bräutigam, B.**, **Rizzoli, P.**, **Krieger, G.**, TanDEM-X Performance over Sandy Areas, Proc. *EUSAR*, Berlin, Germany, Jun. 2014.

[RC-400] **Özis, E.**, **Osipov, A.**, Eibert, T., Analyzing Scattering and Reflection from Metasheets of Bi-Anisotropic Particles, Proc. *ONERA-DLR Aerospace Symposium (ODAS)*, Cologne, Germany, Jun. 2014.

[RC-401] **Osipov, A.**, On Electromagnetic Scattering from Impedance-Matched Bodies, Proc. *URSI Kleinheubacher Tagung*, Miltenberg, Germany, Sep. 2014.

[RC-402] **Pardini, M.**, **Papathanassiou, K.**, L-Band Tomographic Monitoring of Temperate Forests with TangoSAT – Potentials, Challenges and Synergies, Proc. *SAOCOM Companion Satellite Workshop*, Noordwijk, The Netherlands, Oct. 2014.

[RC-403] **Pardini, M.**, **Kugler, F.**, **Tello Alonso, M.**, **Toraño Caicoya, A.**, **Papathanassiou, K.**, Remote Sensing of Forest 3-D Structure by Means of SAR Tomography at L-Band: Perspectives for Tandem-L, Proc. *International TERENO Conference*, Bonn, Germany, Oct. 2014.

[RC-404] **Pardini, M.**, **Tello Alonso, M.**, **Toraño Caicoya, A.**, **Papathanassiou, K.**, Vertical Forest Structure and Biomass Estimates from SAR Remote Sensing: Status of the Activities and Perspectives, Proc. *HGF Alliance Week*, Garmisch-Partenkirchen, Germany, Jul. 2014.

[RC-405] **Pardini, M.**, **Papathanassiou, K.**, A Two-Step Phase Calibration Method for Tomographic Applications with Airborne SAR Data, Proc. *EUSAR*, Berlin, Germany, Jun. 2014.

[RC-406] **Parrella, G.**, **Hajnsek, I.**, **Papathanassiou, K.**, Relating Polarization Phase Difference in SAR Signals over Land Ice to the Structure of Firn and Metamorphic Snow, Proc. *HGF Alliance Week*, Garmisch Partenkirchen, Germany, Jul. 2014.

[RC-407] **Parrella, G.**, **Papathanassiou, K.**, **Hajnsek, I.**, Relating Co-Polarization Phase Difference at L-Band over Land Ice to the Structure of Snow and Firn Layers, Proc. *IGARSS*, Quebec City, Canada, Jul. 2014.

[RC-408] Qin, F., Gao, S., Mao, C., Wang, Z., **Patyuchenko, A.**, **Younis, M.**, **Krieger, G.**, Smart Antennas for Spaceborne Synthetic Aperture Radars, Proc. *Advanced Electromagnetics Symposium (AES)*, Hangzhou, China, Dec. 2014.

[RC-409] **Patyuchenko, A.**, **Younis, M.**, Wang, Z., Gao, S., Qin, F., Glisic, S., Debski, W., Boccia, L., Amendola, G., Arnieri, E., Krstic, M., Celton, E., Penkala, P., Spaceborne X/Ka-Band Digital Beamforming Synthetic Aperture Radar for Earth Observation, Proc. *ARSI & Ka-Band Earth Observation Radar Missions Workshop (KEO)*, Noordwijk, The Netherlands, Nov. 2014.

[RC-410] **Patyuchenko, A.**, **Tienda Herrero, C.**, **Younis, M.**, **Bertl, S.**, **López-Dekker, F.**, **Krieger, G.**, Digital Beamforming SAR Interferometer Based on a Multi-Beam Reflectarray Antenna, Proc. *EUSAR*, Berlin, Germany, Jun. 2014.

[RC-411] **Peichl, M.**, **Kemptner, E.**, Verifizierung und Optimierung der Hochfrequenzeigenschaften von Flugkörper-Radomen, Proc. *Symposium WSE*, Mannheim, Germany, Oct. 2014.

[RC-412] **Peichl, M.**, **Schreiber, E.**, **Heinzel, A.**, **Kempf, T.**, TIRAMI-SAR – A Synthetic Aperture Radar Approach for Efficient Detection of Landmines and UXO, Proc. *EUSAR*, Berlin, Germany, Jun. 2014.

[RC-413] **Peichl, M.**, **Dill, S.**, **Kempf, T.**, Determination of Truckload by Microwave and Millimeterwave Imaging, Proc. *SPIE Defense + Security*, Baltimore, USA, May 2014.

[RC-414] **Pinheiro, M.**, **Reigber, A.**, **Scheiber, R.**, **Jäger, M.**, DEM Generation Using Large-Baseline Airborne InSAR, Proc. *EUSAR*, Berlin, Germany, Jun. 2014.

[RC-415] **Pinheiro, M.**, **Scheiber, R.**, **Reigber, A.**, Combination of Repeat and Single-Pass Dual-Frequency Airborne InSAR Sata for Accurate Height Estimation, Proc. *IGARSS*, Quebec City, Canada, Jul. 2014.

[RC-416] **Ponce Madrigal, O.**, **Prats Iraola, P.**, **Scheiber, R.**, **Reigber, A.**, **Moreira, A.**, Study of the 3-D Impulse Response Function of Holographic SAR Tomography with Multicircular Acquisitions, Proc. *EUSAR*, Berlin, Germany, Jun. 2014.

[RC-417] **Ponce Madrigal, O.**, **Rommel, T.**, **Younis, M.**, **Prats Iraola, P.**, **Moreira, A.**, Multiple-Input Multiple-Output Circular SAR, Proc. *IRS*, Gdansk, Poland, Jun. 2014.

[RC-418] **Prats Iraola, P.**, **Rodríguez Cassolà, M.**, **De Zan, F.**, **López-Dekker, F.**, **Scheiber, R.**, **Reigber, A.**, Efficient Fourier-Based Evaluation of SAR Focusing Kernels, Proc. *EUSAR*, Berlin, Germany, Jun. 2014.

[RC-419] **Prats Iraola, P.**, **Scheiber, R.**, **Rodríguez Cassolà, M.**, **De Zan, F.**, **Reigber, A.**, **Moreira, A.**, New Aspects of Very High-Resolution Spaceborne SAR Image Formation, Proc. *EUSAR*, Berlin, Germany, Jun. 2014.

[RC-420] **Raab, S.**, **Döring, B.**, **Jirousek, M.**, **Reimann, J.**, **Rudolf, D.**, **Schwerdt, M.**, Comparison of Absolute Radiometric Transponder Calibration Strategies, Proc. *EUSAR*, Berlin, Germany, Jun. 2014.

[RC-421] **Reimann, J.**, Hagen, M., Detection of Electric Fields Using Full Polarimetric C-Band Radar Data, Proc. *European Conference on Radar in Meteorology and Hydrology*, Garmisch-Partenkirchen, Germany, Sep. 2014.

[RC-422] **Reimann, J.**, Hagen, M., Polarimetric Calibration of Weather Radar Using the Sun, Proc. *European Conference on Radar in Meteorology and Hydrology*, Garmisch-Partenkirchen, Germany, Sep. 2014.

[RC-423] **Rizzoli, P.**, **Bräutigam, B.**, Quality and Seasonal Time Dependent Modeling of Radar Backscatter from TanDEM-X Data, Proc. *IGARSS*, Quebec City, Canada, Jul. 2014.

[RC-424] **Rizzoli, P.**, **Bräutigam, B.**, **Zink, M.**, TanDEM-X Large-Scale Study of Tropical Rainforests for Spaceborne SAR Calibration in X-Band, Proc. *EUSAR*, Berlin, Germany, Jun. 2014.

[RC-425] **Rizzoli, P.**, **Martone, M.**, **Bräutigam, B.**, Global Mosaics from TanDEM-X Quicklook Data: First Results and Potentials, Proc. *EUSAR*, Berlin, Germany, Jun. 2014.

[RC-426] **Rodríguez Cassolà, M.**, **Prats Iraola, P.**, **Krieger, G.**, **Reigber, A.**, **Moreira, A.**, Bistatic SAR Image Formation: A Systematic Approach, Proc. *IGARSS*, Quebec City, Canada, Jul. 2014.

[RC-427] **Rodríguez Cassolà, M.**, **Prats Iraola, P.**, **López-Dekker, F.**, **Reigber, A.**, **Krieger, G.**, **Moreira, A.**, Autonomous Time and Phase Calibration of Spaceborne Bistatic SAR Systems, Proc. *EUSAR*, Aachen, Germany, Jun. 2014.

[RC-428] **Rodríguez Cassolà, M.**, **Prats Iraola, P.**, **Scheiber, R.**, **Moreira, A.**, Geometrical Considerations of Spaceborne SAR Surveys, Proc. *EUSAR*, Aachen, Germany, Jun. 2014.

[RC-429] **Rommel, T.**, **Younis, M.**, **Krieger, G.**, An Orthogonal Waveform for Fully Polarimetric MIMO-SAR, Proc. *RadarCon*, Cincinnati, USA, May 2014.

[RC-430] **Rommel, T.**, **Huber, S.**, **Patyuchenko, A.**, **Laskowski, P.**, **Younis, M.**, **Krieger, G.**, An Orthogonal Waveform for MIMO-SAR Applications, Proc. *EUSAR*, Berlin, Germany, Jun. 2014.

[RC-431] **Rudolf, D.**, **Döring, B.**, **Jirousek, M.**, **Reimann, J.**, **Raab, S.**, **Schwerdt, M.**, Absolute Radiometric Calibration of C-Band Transponders with Proven Plausibility, Proc. *EUSAR*, Berlin, Germany, Jun. 2014.

[RC-432] **Sanjuan Ferrer, M.**, **López-Dekker, F.**, **Hajnsek, I.**, **Bordoni, F.**, Adamiuk, G., Hanssen, R., van Leijen, F., Skriver, H., Danielson, R., Nagler, T., Pedersen, L., Lang, O., Gabriele, A., Ludwig, M., Lecuyot, A., High Resolution Wide Swath SAR Applications Study: An Overview, Proc. *ARSI & Ka-Band Earth Observation Radar Missions Workshop (KEO)*, Noordwijk, The Netherlands, Nov. 2014.

[RC-433] Marino, A., **Sanjuan Ferrer, M.**, **Hajnsek, I.**, Ouchi, K., Ship Detectors Exploiting Spectral Analysis of SAR Images, Proc. *IGARSS*, Quebec City, Canada, Jul. 2014.

[RC-434] **Sanjuan Ferrer, M.**, **Hajnsek, I.**, **Papathanassiou, K.**, Detection of Coherent Scatterers in SAR Data: Application for Urban Environments, Proc. *EUSAR*, Berlin, Germany, Jun. 2014.

[RC-435] **Schmidt, K.**, **Castellanos Alfonzo, G.**, **Tous Ramon, N.**, **Bachmann, M.**, **Schwerdt, M.**, Calibration Performance of the TerraSAR-X and TanDEM-X Satellites since Launch, Proc. *EUSAR*, Berlin, Germany, Jun. 2014.

[RC-436] **Schwerdt, M.**, **Schmidt, K.**, **Tous Ramon, N.**, **Castellanos Alfonzo, G.**, **Döring, B.**, **Zink, M.**, **Prats Iraola, P.**, Independent Verification of the Sentinel-1A System Calibration, Proc. *IGARSS*, Quebec City, Canada, Jul. 2014.

[RC-437] **Sorrentino, A.**, **Jagdhuber, T.**, **Hajnsek, I.**, Iodice, A., Investigation of Polarimetric Active/Passive Microwave Scattering Towards Soil Moisture Estimation, Proc. *GOLD Conference*, Berlin, Germany, Jun. 2014.

[RC-438] **Sorrentino, A.**, **Jagdhuber, T.**, **Hajnsek, I.**, Montzka, C., **Papathanassiou, K.**, Investigation of Polarimetric Active/Passive Microwave Scattering towards Soil Moisture Estimation, Proc. *EUSAR*, Berlin, Germany, Jun. 2014.

[RC-439] **Steinbrecher, U.**, **Kraus, T.**, **Castellanos Alfonzo, G.**, **Grigorov, C.**, **Schulze, D.**, **Bräutigam, B.**, TerraSAR-X: Design of the New Operational WideScanSAR Mode, Proc. *EUSAR*, Berlin, Germany, Jun. 2014.

[RC-440] **Stockamp, J.**, **Jagdhuber, T.**, **Hajnsek, I.**, **Parrella, G.**, Ludwig, R., Multi-Frequency Analysis of Snow-Covered Areas Using SAR-Polarimetry, Proc. *Gemeinsame Tagung der DGfK, der DGPF, der GfGI und des GiN*, Hamburg, Germany, Mar. 2014.

[RC-441] **Tello Alonso, M.**, **Pardini, M.**, **Papathanassiou, K.**, Towards Forest Structure Characteristics Retrieval from SAR Tomographic Profiles, Proc. *EUSAR*, Berlin, Germany, Jun. 2014.

[RC-442] **Toraño Caicoya, A.**, **Kugler, F.**, **Hajnsek, I.**, **Papathanassiou, K.**, Vertical Forest Structure Characterization for the Estimation of Above Ground Biomass. Potential and Limitations for Radar Remote Sensing, Proc. *EUSAR*, Berlin, Germany, Jun. 2014.

[RC-443] **Tous Ramon, N.**, **Schwerdt, M.**, **Castellanos Alfonzo, G.**, **Schmidt, K.**, Verification of the Complex Internal Calibration Approach Operated for the Sentinel-1A C-SAR Instrument, Proc. *EUSAR*, Berlin, Germany, Jun. 2014.

[RC-444] **Villano, M.**, **Jäger, M.**, **Steinbrecher, U.**, **Krieger, G.**, **Moreira, A.**, Staggered SAR: Imaging a Wide Continuous Swath by Continuous PRI Variation, Proc. *URSI Kleinheubacher Tagung*, Miltenberg, Germany, Sep./Oct. 2014.

[RC-445] **Villano, M.**, **Krieger, G.**, Staggered SAR: From Concept to Experiments with Real Data, Proc. *EUSAR*, Berlin, Germany, Jun. 2014.

[RC-446] **Villano, M.**, **Krieger, G.**, **Del Zoppo, V.**, On-Board Doppler Filtering for Data Volume Reduction in Spaceborne SAR Systems, Proc. *International Radar Symposium*, Gdansk, Poland, Jun. 2014.

[RC-447] **Villano, M.**, **Martone, M.**, **Del Zoppo, V.**, **Krieger, G.**, Joint Effects of On-Board Doppler Filtering and Quantization in Spaceborne SAR Systems, Proc. *IEEE GOLD Remote Sensing Conference*, Berlin, Germany, Jun. 2014.

[RC-448] **Weigt, M.**, **Grigorov, C.**, **Steinbrecher, U.**, **Schulze, D.**, TanDEM-X Mission: Long Term in Orbit Synchronisation Link Performance Analysis, Proc. *EUSAR*, Berlin, Germany, Jun. 2014.

[RC-449] **Wollstadt, S.**, **Prats Iraola, P.**, Geudtner, D., TOPS Imaging Mode: Data-Based Estimation of Antenna Pointing and Azimuth Steered Antenna Pattern, Proc. *EUSAR*, Berlin, Germany, Jun. 2014.

[RC-450] **Yague-Martinez, N.**, Fielding, E., Haghshenas Haghighi, M., Cong, X., Motagh, M., **Steinbrecher, U.**, Eineder, M., Fritz, T., Ground Displacement Measurement of the 2013 M7.7 and M6.8 Balochistan Earthquake with TerraSAR-X ScanSAR Data, Proc. *IGARSS*, Montreal, Canada, Jul. 2014.

[RC-451] **Younis, M.**, **Huber, S.**, **López-Dekker, F.**, **Krieger, G.**, Instrument Design and Performance for an L-Band Reflector-Based SAR Mission, Proc. *ARSI & Ka-Band Earth Observation Radar Missions Workshop (KEO)*, Noordwijk, The Netherlands, Nov. 2014.

[RC-452] **Younis, M.**, **Huber, S.**, **Tienda Herrero, C.**, **Krieger, G.**, **Moreira, A.**, Uematsu, A., Sudo, Y., Nakamura, R., Chishiki, Y., Shimada, M., Tandem-L Instrument Design and SAR Performance Overview, Proc. *IGARSS*, Québec City, Canada, Jul. 2014.

[RC-453] **Younis, M.**, **López-Dekker, F.**, **Krieger, G.**, MIMO SAR Operation Modes and Techniques, Proc. *EUSAR*, Berlin, Germany, Jun. 2014.

[RC-454] **Zink, M.**, **Moreira, A.**, TanDEM-X Mission Status: The New Topography of the Earth Takes Shape, Proc. *IGARSS*, Quebec City, Canada, Jul. 2014.

2013

[RC-455] **Aguilera, E.**, **Nannini, M.**, **Reigber, A.**, Wavelet-Based Compressed Sensing for Polarimetric SAR Tomography, Proc. *ESA POLinSAR Workshop*, Frascati, Italy, 2013.

[RC-456] **Al-Kahachi, N.**, **Papathanassiou, K.**, Modelling and Interpretation of Polarimetric Scattering from Sub-Arctic Lakes at L-Band, Proc. *ESA POLinSAR*, Frascati, Italy, 2013.

[RC-457] **Anglberger, H.**, **Speck, R.**, **Süß, H.**, Simulation of Imaging Effects of Very High Resolution SAR Systems, Proc. *SPIE Remote Sensing*, Dresden, Germany, Sep. 2013.

[RC-458] **Anglberger, H.**, **Speck, R.**, **Süß, H.**, Transforming Optical Image Data into a SAR System's Range Based Image Space, Proc. *SPIE Defense + Security*, Baltimore, USA, 2013.

[RC-459] **Anglberger, H.**, **Hager, M.**, **Speck, R.**, **Süß, H.**, Merging of Optical and SAR Data, Proc. *TerraSAR-X / TanDEM-X Science Team Meeting*, Oberpfaffenhofen, Germany, Jun. 2013.

[RC-460] **Bachmann, M.**, **Bräutigam, B.**, **Schulze, D.**, **Krieger, G.**, **Zink, M.**, TanDEM-X Acquisition Plan and DEM Performance in the Third Year of Operation, Proc. *Asia-Pacific Conference on Synthetic Aperture Radar (APSAR)*, Tsukuba, Japan, Sep. 2013.

[RC-461] Schaefer, C., **Baumgartner, S.**, Ka-Band Instrument for Ground Moving Target Indication with Low PRF Requirement, Proc. *Ka and Broadband Communications, Navigation and Earth Observation Conference*, Florence, Italy, vol. 3, Oct. 2013.

[RC-462] **Bertl, S.**, **Younis, M.**, **López-Dekker, F.**, **Krieger, G.**, Multi-Transmit Operation Scheme for a Reflector-Based SAR System, Proc. *IRS*, Dresden, Germany, Jun. 2013.

[RC-463] **Bordoni, F.**, **Laskowski, P.**, **Younis, M.**, **Krieger, G.**, Calibration Error Model for Multichannel Spaceborne SAR Systems Based on Digital Beamforming, Proc. *EuRAD*, Nuremberg, Germany, Oct. 2013.

[RC-464] **Borla Tridon, D.**, **Bachmann, M.**, **Schulze, D.**, **Ortega Miguez, C.**, **Polimeni, M.**, **Martone, M.**, TanDEM-X: DEM Acquisition in the Third Year Era, Proc. *International Conference on Spacecraft Formation Flying Missions and Technologies*, Munich, Germany, May 2013.

[RC-465] **Bräutigam, B.**, **Buckreuß, S.**, **Zink, M.**, Earth Observation in 2D and 3D: TerraSAR-X and TanDEM-X Mission Status, Proc. *Deutscher Luft- und Raumfahrtkongress (DLRK)*, Stuttgart, Germany, Sep. 2013.

[RC-466] Linck, R., Fassbinder, J., **Buckreuß, S.**, Palmyra Revisited from Space – High-Resolution Satellite Prospection of a UNESCO World Heritage Site, Proc. *Conference on Computer Applications and Quantitative Methods in Archaeology*, Perth, Australia, Mar. 2013.

[RC-467] **Buckreuß, S.**, Lehner, S., Schättler, B., New Wide ScanSAR Mode, Proc. *TerraSAR-X / TanDEM-X Science Team Meeting*, Oberpfaffenhofen, Germany, Jun. 2013.

[RC-468] Linck, R., Fassbinder, J., **Buckreuß, S.**, Palmyra Revisited from Space – High-Sesolution Satellite Prospection of the UNESCO World Heritage Site, Proc. *CAA Perth - Computer Applications and Quantitative Methods in Archaeology*, Perth, Australia, Mar. 2013.

[RC-469] **Buckreuß, S.**, **Zink, M.**, **Hajnsek, I.**, TerraSAR-X and TanDEM-X Mission Status, Proc. *Living Planet Symposium*, Edinburgh, UK, Sep. 2013.

[RC-470] Linck, R., Fassbinder, J., **Buckreuß, S.**, Integrated Geophysical Prospection by High-Resolution Optical Satellite Images, Synthetic Aperture Radar and Magnetometry at the Example of the UNESCO World Heritage Site of Palmyra (Syria), Proc. *Archaeology and Geoinformatics*, Moscow, Russia, vol. 7, May 2013.

[RC-471] **Börner, T.**, **López-Dekker, F.**, **Krieger, G.**, **Bachmann, M.**, Müller, H., **Moreira, A.**, Passive Interferometric Ocean Currents Observation Synthetic Aperture Radar (PICOSAR), Proc. *IAA Symposium on Small Satellites for Earth Observation*, Berlin, Germany, Apr. 2013.

[RC-472] **Castellanos Alfonzo, G.**, **Schwerdt, M.**, **Wollstadt, S.**, **Döring, B.**, **Bachmann, M.**, Geudtner, D., In-Flight Antenna Characterization of a SAR Instrument Operating in Complex TOPS Mode, Proc. *IRS*, Dresden, Germany, Jun. 2013.

[RC-473] Rocha, L., Junqueira, C., Gambin, E., Vicente, A., **Culhaoglu, A.**, **Kemptner, E.**, A Free Space Measurement Approach for Dielectric Material Characterization, Proc. *IMOC*, Rio de Janeiro, Brazil, Aug. 2013.

[RC-474] **De Zan, F.**, **Prats Iraola, P.**, Joint Coregistration of SAR Images with an Application to TerraSAR-X TOPS Mode Datasets, Proc. *Living Planet Symposium*, Edinburgh, UK, Sep. 2013.

[RC-475] **Di Maria, A.**, **Kosc, A.**, **Limbach, M.**, **Horn, R.**, **Reigber, A.**, Design and Measurements of a Double Ridged Guide Horn Feed for P-Band Direct Path Measurements, Proc. *European Conference on Antennas and Propagation (EUCAP)*, Gothenburg, Sweden, Apr. 2013.

[RC-476] **Di Maria, A.**, **Limbach, M.**, **Horn, R.**, **Reigber, A.**, Design and Measurements of a C-Band Array for High Power High Bandwidth SAR Application, Proc. *European Conference on Antennas and Propagation (EUCAP)*, Gothenburg, Sweden, Apr. 2013.

[RC-477] **Kosc, A.**, **Di Maria, A.**, **Limbach, M.**, **Horn, R.**, A 5 Way Lumped-Elements Wilkinson Power Divider, Proc. *European Conference on Antennas and Propagation (EUCAP)*, Gothenburg, Sweden, Apr. 2013.

[RC-478] **Dill, S.**, **Peichl, M.**, **Rudolf, D.**, SUMIRAD – A Fast Imaging MMW Radiometer for Security and Safety Applications, Proc. *EuMC*, Nuremberg, Germany, Oct. 2013.

[RC-479] **Dill, S.**, **Peichl, M.**, A Fast Imaging MMW Radiometer System for Security and Safety Applications, Proc. *SPIE Security, Defense + Sensing*, Dresden, Germany, Sep. 2013.

[RC-480] **Döring, B.**, **Schwerdt, M.**, DLR's Next Generating SAR Calibration Targets, Proc. *CEOS SAR CalVal Workshop*, St. Hubert, Canada, Oct. 2013.

[RC-481] **Döring, B.**, **Schwerdt, M.**, Learning from the Field of Photometry: The Way towards Better Radiometric Measurements, Proc. *CEOS SAR CalVal Workshop*, St. Hubert, Canada, Oct. 2013.

[RC-482] **Eilers, J.**, Observer Interface Analysis for Standardization to a Cloud-Based Realtime Space Situational Awareness (SSA), Proc. *Advanced Maui Optical and Space Surveillance Technologies Conference*, Maui, USA, Sep. 2013.

[RC-483] **Fischer, G.**, **Hajnsek, I.**, Temporal Pol-InSAR Signatures of Glaciers: First Concepts, Proc. *HGF Alliance Week*, Garmisch-Partenkirchen, Germany, Jul. 2013.

[RC-484] **Gabler, B.**, **Horn, R.**, **Limbach, M.**, **Di Maria, A.**, **Reigber, A.**, Calibration Techniques for Active RCS-Targets, Proc. *European Conference on Antennas and Propagation (EUCAP)*, Gothenburg, Sweden, vol. CFP137, Apr. 2013.

[RC-485] Macelloni, G., Brogioni, M., Montomoli, F., Lemmetyinen, J., Pulliainen, J., Rott, H., Voglmeier, K., **Hajnsek, I.**, **Scheiber, R.**, Rommen, B., On the Synergic Use of Sentinel-1 and CoReH2O SAR Data for the Retrieval of Snow Water Equivalent on Land and Glaciers, Proc. *Living Planet Symposium*, Edinburgh, UK, Sep. 2013.

[RC-486] Eckardt, R., Richter, N., Auer, S., Eineder, M., Roth, A., **Hajnsek, I.**, Walter, D., Braun, M., Motagh, M., Pathe, C., Schmullius, C., Thiel, C., SAR-EDU - Ein Webportal für die anwendungsorientierte SAR-Fernerkundungsausbildung, Proc. *3Wissenschaftlich-Technische Jahrestagung der DGPF,* Freiburg, Germany, Feb./Mar. 2013.

[RC-487] **Jagdhuber, T.**, **Hajnsek, I.**, **Papathanassiou, K.**, Derivation of Surface Soil Moisture under Vegetation Using Multiparametric SAR, Proc. *HGF Alliance Week*, Garmisch-Partenkirchen, Germany, Oct. 2013.

[RC-488] **Jagdhuber, T.**, **Hajnsek, I.**, Montzka, C., Wollschläger, U., Lausch, A., Itzerott, S., **Spengler, D.**, Kunstmann, H., Lorenz, C., Borg, E., Environmental Remote Sensing in TERENO Observatories, Proc. *HGF Alliance Week*, Garmisch-Partenkirchen, Germany, Oct. 2013.

[RC-489] **Jagdhuber, T.**, **Hajnsek, I.**, **Papathanassiou, K.**, Soil Moisture Estimation Using Dual-Polarimetric Coherent (HH/VV) TerraSAR-X and TanDEM-X Data, Proc. *TerraSAR-X / TanDEM-X Science Team Meeting*, Oberpfaffenhofen, Germany, Jun. 2013.

[RC-490] **Jagdhuber, T.**, **Hajnsek, I.**, **Papathanassiou, K.**, Polarimetric Decomposition for Soil Moisture Retrieval from Vegetated Soils in TERENO Observatories, Proc. *ESA POLinSAR Workshop*, Frascati, Italy, Jan./Feb. 2013.

[RC-491] **Jagdhuber, T.**, **Hajnsek, I.**, **Papathanassiou, K.**, Polarimetric Soil Moisture Retrieval at Short Wavelength, Proc. *ESA POLinSAR Workshop*, Frascati, Italy, Jan./Feb. 2013.

[RC-492] **Jörg, H.**, **Hajnsek, I.**, **Papathanassiou, K.**, A first Attempt on the Characterization of Crop Vegetation Volume and Structure Using Short Wavelength SAR Tomography, Proc. *HGF Alliance Week*, Garmisch-Partenkirchen, Germany, Oct. 2013.

[RC-493] **Jörg, H.**, **Jagdhuber, T.**, **Kugler, F.**, **Hajnsek, I.**, Interpretation of Single-Pass Pol-InSAR Vegetation Signatures at X-Band: Dual- vs. Quad-Pol Case, Proc. *POLinSAR*, Frascati, Italy, Feb. 2013.

[RC-494] **Kempf, T.**, **Anglberger, H.**, Image Fusion of Different Spaceborne SAR Sensors for Change Detection, Proc. *IEEE Radar Conference*, Ottawa, Japan, May 2013.

[RC-495] **Kim, J.**, **Papathanassiou, K.**, Correction of Ionospheric Effects on SAR Interferometry Using an Combined TEC Estimator, Proc. *URSI Commission F - Microwave Signatures*, Espoo, Finland, Oct. 2013.

[RC-496] **Kim, J.**, **Papathanassiou, K.**, Correction of Ionosphere for InSAR by the Combination of Differential TEC Estimators, Proc. *ESA POLinSAR Workshop*, Frascati, Italy, Jan./Feb. 2013.

[RC-497] **Kraus, T.**, **Bräutigam, B.**, **Grigorov, C.**, **Mittermayer, J.**, **Wollstadt, S.**, TerraSAR-X Staring Spotlight Mode Optimization, Proc. *Asia-Pacific Conference on Synthetic Aperture Radar (APSAR)*, Tsukuba, Japan, Sep. 2013.

[RC-498] **Kugler, F.**, **Toraño Caicoya, A.**, **Papathanassiou, K.**, **Hajnsek, I.**, POL-InSAR Forest Techniques and Applications by Means of TanDEM-X New Results and Experiments, Proc. *IGARSS*, Melbourne, Australia, Jul. 2013.

[RC-499] **Kugler, F.**, **Hajnsek, I.**, **Papathanassiou, K.**, Pol-InSAR Techniques for Forest Characterization with TanDEM-X, Proc. *POLinSAR2013*, Frascati, Italy, Jan./Feb. 2013.

[RC-500] **Laskowski, P.**, **Bordoni, F.**, **Younis, M.**, Error Analysis and Calibration Techniques for Multi-Channel SAR Instruments, Proc. *IGARSS*, Melbourne, Australien, Jul. 2013.

[RC-501] **Laskowski, P.**, **Bordoni, F.**, **Younis, M.**, Multi-Channel SAR Performance Analysis in the Presence of Antenna Excitation Errors, Proc. *IRS*, Dresden, Germany, Jun. 2013.

[RC-502] **Lee, S.**, **Kugler, F.**, **Papathanassiou, K.**, **Hajnsek, I.**, First Pol-InSAR Forest Height Inversion by Means of L-Band F-SAR Data, Proc. *ESA POLinSARWorkshop*, Frascati, Italy, Jan./Feb. 2013.

[RC-503] **Liebschwager, T.**, **Neff, T.**, **Süß, H.**, Förstner, R., Design of a Radar-Based Space Situational Awareness System, Proc. *AMOS*, Maui, USA, Sep. 2013.

[RC-504] **Limbach, M.**, **Di Maria, A.**, **Reigber, A.**, **Gabler, B.**, **Horn, R.**, **Kosc, A.**, S-Band Antenna for Airborne Polarimetric and Interferometric SAR-Applications, Proc. *European Conference on Antennas and Propagation (EUCAP)*, Gothenburg, Sweden, vol. CFP137, Apr. 2013.

[RC-505] **López-Dekker, F.**, **De Zan, F.**, **Rodríguez Cassolà, M.**, **Krieger, G.**, Correlating SAR (CoSAR): Concept, Performance Analysis, and Mission Concepts, Proc. *IGARSS*, Melbourne, Australia, Jul. 2013.

[RC-506] **Martone, M.**, **Bräutigam, B.**, **Rizzoli, P.**, **Krieger, G.**, Impact of SAR Raw Data Quantization on TanDEM-X Performance, Proc. *IGARSS*, Melbourne, Australia, Jul. 2013.

[RC-507] **Nannini, M.**, **Prats Iraola, P.**, **De Zan, F.**, Investigations of the DINSAR Performance in the TOPS Mode Using Experimental TerraSAR-X Data, Proc. *Living Planet*, Edinburgh, UK, Sep. 2013.

[RC-508] **Pardini, M.**, **Kugler, F.**, **Toraño Caicoya, A.**, **Hajnsek, I.**, **Papathanassiou, K.**, Spaceborne Single Pass Pol-InSAR for Monitoring Forest Vertical Structure: Recent TanDEM-X Experiments and Future Tandem-L Perspectives, Proc. *ESA Living Planet Symposium*, Edinburgh, UK, Sep. 2013.

[RC-509] **Pardini, M.**, **Toraño Caicoya, A.**, **Kugler, F.**, **Papathanassiou, K.**, Estimating and Understanding Vertical Structure of Forests from Multibaseline TanDEM-X Pol-InSAR Data, Proc. *IGARSS*, Melbourne, Australia, Jul. 2013.

[RC-510] **Pardini, M.**, **Kugler, F.**, **Papathanassiou, K.**, Towards Forest Vertical Structure Monitoring from Space: First Experiments with Multibaseline TandDEM-X Data, Proc. *ESA POLinSAR Workshop*, Frascati, Italy, Jan./Feb. 2013.

[RC-511] Leinss, S., **Parrella, G.**, **Hajnsek, I.**, Snow Height Determination by Polarimetric Phase Differences in X-Band SAR Data, Proc. *Swiss Geoscience Meeting*, Lausanne, Switzerland, Nov. 2013.

[RC-512] **Parrella, G.**, **Hajnsek, I.**, **Papathanassiou, K.**, Modelling of Polarimetric SAR Scattering Contributions from Glaciers Subsurface, Proc. *HGF Alliance Week*, Garmisch-Partenkirchen, Germany, Oct. 2013.

[RC-513] **Parrella, G.**, Marino, A., **Hajnsek, I.**, PolSAR-Ap: Exploitation of Fully Polarimetric Data for Glacier and Sea Ice Characterization, Proc. *ESA Living Planet Symposium*, Edinburgh, UK, Sep. 2013.

[RC-514] Leinss, S., **Parrella, G.**, **Hajnsek, I.**, Snow Depth Extraction Based on Polarimetric Phase Differences, Proc. *TerraSAR-X / TanDEM-X Science Team Meeting*, Oberpfaffenhofen, Germany, Jun. 2013.

[RC-515] **Parrella, G.**, **Hajnsek, I.**, **Papathanassiou, K.**, On the Interpretation of L- and P-Band PolSAR Signatures of Polythermal Glaciers, Proc. *ESA PolInSAR Workshop*, Frascati, Italy, Jan./Feb. 2013.

[RC-516] **Peichl, M.**, **Dill, S.**, **Rudolf, D.**, SUMIRAD – A Low-Cost Fast Millimeterwave Radiometric Imaging System, Proc. *SPIE SPIE Security, Defense + Sensing* , Baltimore, USA, Apr. 2013.

[RC-517] **Pinheiro, M.**, **Rodríguez Cassolà, M.**, **Prats Iraola, P.**, **Krieger, G.**, **Reigber, A.**, **Moreira, A.**, Reconstruction of Missing Data in Interferometric SAR Systems, Proc. *IGARSS*, Melbourne, Australia, Jul. 2013.

[RC-518] **Ponce Madrigal, O.**, **Prats Iraola, P.**, **Scheiber, R.**, **Reigber, A.**, **Moreira, A.**, First Demonstration of 3-D Holographic Tomography with Fully Polarimetric Multi-Circular SAR at L-Band, Proc. *IGARSS*, Melbourne, Australia, Jul. 2013.

[RC-519] Huang, Y., Ferro-Famil, L., **Reigber, A.**, Under-Foiliage Target Detection Using Multibaseline L-Band PolInSAR Data, Proc. *IRS*, Dresden, Germany, Jun. 2013.

[RC-520] **Rodríguez Cassolà, M.**, **Prats Iraola, P.**, **De Zan, F.**, **Scheiber, R.**, **Reigber, A.**, Doppler-Related Focusing Aspects in the TOPS Imaging Mode, Proc. *IGARSS*, Melbourne, Australia, Jul. 2013.

[RC-521] **Rodríguez Cassolà, M.**, **Prats Iraola, P.**, **Jäger, M.**, **Reigber, A.**, **Moreira, A.**, Estimation of Tropospheric Delays Using Synthetic Aperture Radar and Squint Diversity, Proc. *IGARSS*, Melbourne, Australia, Jul. 2013.

[RC-522] **Rommel, T.**, **Younis, M.**, **Krieger, G.**, Abbildendes MIMO-Radar mit modifizierten Chirp-Signalen, Proc. *URSI Kleinheubacher Tagung*, Miltenberg, Germany, Sep. 2013.

[RC-523] **Rommel, T.**, **Patyuchenko, A.**, **Laskowski, P.**, **Younis, M.**, **Krieger, G.**, An Orthogonal Waveform Scheme for Imaging MIMO-Radar Applications, Proc. *IRS*, Dresden, Germany, Jun. 2013.

[RC-524] **Sanjuan Ferrer, M.**, **Hajnsek, I.**, **Papathanassiou, K.**, Coherent Scatterer Detection Analysis over Different Test Sites Using TerraSAR-X Images, Proc. *ESA POLinSAR Workshop*, Frascati, Italy, Jan./Feb. 2013.

[RC-525] Morrison, K., Bennett, J., **Scheiber, R.**, Applying a Composite Pattern Scheme to Clutter Cancellation with the Airborne POLARIS Ice Sounder, Proc. *International Symposium on Radarglaciology*, Lawrence, USA, Sep. 2013.

[RC-526] **Scheiber, R.**, **Jäger, M.**, **De Zan, F.**, **Prats Iraola, P.**, Analysis of Speckle Tracking and Interferometric Coregistration for Non-Stationary Scenarios with TOPS SAR Data, Proc. *ESA Living Planet Symposium*, Edinburgh, UK, Sep. 2013.

[RC-527] **Schmidt, K.**, **Castellanos Alfonzo, G.**, **Bachmann, M.**, **Böer, J.**, **Polimeni, M.**, **Tous Ramon, N.**, **Schwerdt, M.**, **Schulze, D.**, Long Term System Monitoring of Performance Stability - Current Status of TerraSAR-X and TanDEM-X Satellites, Proc. *CEOS SAR CalVal Workshop*, St. Hubert, Canada, Oct. 2013.

[RC-528] **Schreiber, E.**, **Jirousek, M.**, **Peichl, M.**, **Süß, H.**, The Design of a Broadband Slotted Waveguide Antenna for Electronical Beam Steering Applications in MW Radiometry, Proc. *European Microwave Week*, Nuremberg, Germany, Oct. 2013.

[RC-529] **Schreiber, E.**, **Peichl, M.**, **Jirousek, M.**, A Calibration Concept for Passive MW Imaging Using Beam Steering by Frequency Shift and Aperture Synthesis, Proc. *SPIE Security, Defense + Sensing*, Dresden, Germany, vol. 8900, Sep. 2013.

[RC-530] **Schreiber, E.**, **Peichl, M.**, **Jirousek, M.**, **Süß, H.**, VESAS: A Novel Concept for Fully-Electronic Passive MW Imaging, Proc. *SPIE Security, Defense + Security*, Baltimore, USA, vol. 8715, Apr. 2013.

[RC-531] Navas-Traver, I., Østergaard, A., Ludwig, M., Snoeij, P., Schied, E., Rostan, F., Groci, R., Bauleo, A., Pietropaolo, A., Giudici, D., Belotti, M., Caccia, M., **Schwerdt, M.**, **Tous Ramon, N.**, Sentinel-1 C-SAR Internal Calibration Approach and its Evolution up to Flight Configuration, Proc. *ASAR & CEOS SAR CalVal Workshop*, Montreal, Canada, Oct. 2013.

[RC-532] **Schwerdt, M.**, **Schmidt, K.**, **Castellanos Alfonzo, G.**, **Tous Ramon, N.**, **Döring, B.**, **Prats Iraola, P.**, **Zink, M.**, Independent Verification of the Sentinel-1 System Calibration, Proc. *ASAR & CEOS SAR CalVal Workshop*, Montreal, Canada, Oct. 2013.

[RC-533] Østergaard, A., Navas-Traver, I., Snoeij, P., Rommen, B., Geudtner, D., Bibby, D., Torres, R., Schied, E., Rostan, F., **Schwerdt, M.**, **Zink, M.**, Bauleo, A., Groci, R., Pietropaolo, A., Sentinel-1 In-Orbit Calibration Approach, Proc. *ESA Living Planet Symposium*, Edinburgh, UK, Sep. 2013.

[RC-534] **Steinbrecher, U.**, **Zink, M.**, **Krieger, G.**, **Schulze, D.**, **Bachmann, M.**, **Moreira, A.**, TanDEM-X Mission: Overview, Current Situation and Future Prospects, Proc. *International Earth Observation Convoy and Constellation Concepts Workshop*, Noordwijk, The Netherlands, Oct. 2013.

[RC-535] **Steinbrecher, U.**, **Zink, M.**, **Moreira, A.**, **Bachmann, M.**, **Böer, J.**, **Schulze, D.**, **Krieger, G.**, TanDEM-X Mission: Overview, Status and Outlook, Proc. *International Society for Photogrammetry and Remote Sensing (ISPRS) Congress*, Hannover, Germany, vol. XL-1/W, May 2013.

[RC-536] **Stockamp, J.**, **Jagdhuber, T.**, **Parrella, G.**, **Hajnsek, I.**, Ludwig, R., Multi-Frequency Analysis of Snow-Covered Areas Using SAR Polarimetry, Proc. *POLinSAR*, Frascati, Italy, Jan./Feb. 2013.

[RC-537] **Tienda Herrero, C.**, **Patyuchenko, A.**, **Gabler, B.**, **Limbach, M.**, **Krieger, G.**, Measurements of a Multi Feed Reflector Antenna for SAR Systems Based on Digital Beamforming, Proc. *ESA Antenna Workshop*, Noordwiik, The Netherlands, Sep. 2013.

[RC-538] **Tienda Herrero, C.**, Jose Antonio, E., Manuel, A., Study of Different Multi-Beam Reflectarray Configurations, Proc. *EuCAP*, Gothenburg, Sweden, Apr. 2013.

[RC-539] **Toraño Caicoya, A.**, **Kugler, F.**, **Hajnsek, I.**, **Papathanassiou, K.**, Forest Vertical Structure Characterization for the Estimation of Above-Ground Forest Biomass towards its Application in Radar Remote Sensing, Proc. *HGF Alliance Week*, Garmisch-Partenkirchen, Germany, Oct. 2013.

[RC-540] **Toraño Caicoya, A.**, **Kugler, F.**, **Hajnsek, I.**, **Papathanassiou, K.**, Boreal Forest Biomass Classification with TanDEM-X Standard DEM Aquistions, Proc. *TerraSAR-X / TanDEM-X Science Team Meeting*, Oberpfaffenhofen, Germany, Jun. 2013.

[RC-541] **Toraño Caicoya, A.**, **Kugler, F.**, **Papathanassiou, K.**, **Hajnsek, I.**, Boreal Forest Biomass Classification with TanDEM-X, Proc. *ESA POLinSAR Workshop*, Frascati, Italy, Jan./Feb. 2013.

[RC-542] **Villano, M.**, **Krieger, G.**, **Moreira, A.**, The Staggered SAR Concept: Imaging a Wide Continuous Swath with High Resolution, Proc. *IRS*, Dresden, Germany, Jun. 2013.

[RC-543] **Villano, M.**, **Papathanassiou, K.**, SNR and Noise Variance Estimation in Polarimetric SAR Data, Proc. *ESA POLinSAR Workshop*, Frascati, Italy, Jan./Feb. 2013.

[RC-544] **Voormansik, K.**, **Jagdhuber, T.**, **Hajnsek, I.**, Olesk, A., Zalite, K., TerraSAR-X HH/VV Dual Polarimetric Signatures of Grassland, Proc. *TerraSAR-X / TanDEM-X Science Team Meeting*, Oberpfaffenhofen, Germany, Jun. 2013.

[RC-545] **Younis, M.**, **López-Dekker, F.**, **Patyuchenko, A.**, **Krieger, G.**, Digital Beamforming Architecture and Techniques for a Spaceborne Interferometric Ka-Band Mission, Proc. *RadarCon*, Ottawa, Canada, Apr./May 2013.

2012

[RC-546] **Anglberger, H.**, **Speck, R.**, **Süß, H.**, Application of Simulation Techniques for High-Resolution SAR Systems, Proc. *IGARSS*, Munich, Germany, Jul. 2012.

[RC-547] **Balkoski, J.**, **Bordoni, F.**, Nadir-Echo Properties, a Study Based on TerraSAR-X Data, Proc. *Telecommunications Forum TELFOR*, Belgrade, Serbia, Nov. 2012.

[RC-548] **Baumgartner, S.**, **López-Dekker, F.**, García Moliná, J., **Laux, C.**, **Börner, T.**, **Younis, M.**, Schäfer, C., Klein, R., Marques, P., Petrolati, D., Study of Multi-Channel Ka-Band SARs for Moving Target Indication, Proc. *Workshop on Ka-Band Earth Observation Radar Missions, KEO '12*, Noordwijk, The Netherlands, Nov. 2012.

[RC-549] **Baumgartner, S.**, **Krieger, G.**, Ship Detection and Motion Parameter Estimation with TanDEM-X in Large Along-Track Baseline Configuration, Proc. *SEASAR*, Tromsø, Norway, Jun. 2012.

[RC-550] **Baumgartner, S.**, **Krieger, G.**, A Priori Knowledge-Based Post-Doppler Stap for Traffic Monitoring Applications, Proc. *IGARSS*, Munich, Germany, Jul. 2012.

[RC-551] **Bertl, S.**, **López-Dekker, F.**, **Baumgartner, S.**, Garcia-Molina, J., **Younis, M.**, **Bordoni, F.**, **Tienda Herrero, C.**, Schaefer, C., **Krieger, G.**, Ka-Band Multibaseline ATI-SAR System for Ocean Surface Currents Measurements, Proc. *KEO Workshop (Ka-Band Earth Observation Radar Missions)*, Noordwijk, The Netherlands, Nov. 2012.

[RC-552] **Bianco, V.**, **Pardini, M.**, **Papathanassiou, K.**, Iodice, A., Phase-Calibration of Multibaseline SAR Data Stacks: A Minimum Entropy Approach, Proc. *GOLD*, Rome, Italy, Jun. 2012.

[RC-553] **Bordoni, F.**, **Younis, M.**, **Krieger, G.**, Performance Investigation on the High-Resolution Wide-Swath SAR System Operating in Multisubpulse Mode, Proc. *IGARSS*, Munich, Germany, Jul. 2012.

[RC-554] **Bräutigam, B.**, **Rizzoli, P.**, **Martone, M.**, **Bachmann, M.**, **Kraus, T.**, **Krieger, G.**, InSAR and DEM Quality Monitoring of TanDEM-X, Proc. *IGARSS*, Munich, Germany, Jul. 2012.

[RC-555] Gomez, B., Gonzalez, M., **Bräutigam, B.**, Vega, E., Garcia, M., Casal, N., **del Castillo, J.**, Cuerda, J., Alfaro, N., Alvarez, V., PAZ Mission: CALVAL Centre Activities, Proc. *EUSAR*, Nuremberg, Germany, Apr. 2012.

[RC-556] Linck, R., Fassbinder, J., **Buckreuß, S.**, The Application of High-Resolution Synthetic Aperture Radar for Detecting Buried Archaeology at the Example of the Roman Town of Palmyra (Syria), Proc. *EARSeL Workshop Ghent*, Ghent, Belgium, Sep. 2012.

[RC-557] **Bueso Bello, J.**, **Gonzalez, C.**, **Kraus, T.**, **Bräutigam, B.**, Characteristics of TanDEM-X Experimental Modes, Proc. *IGARSS*, Munich, Germany, Jul. 2012.

[RC-558] **Bueso Bello, J.**, **Grigorov, C.**, **Steinbrecher, U.**, **Kraus, T.**, **Gonzalez, C.**, **Schulze, D.**, **Bräutigam, B.**, System Commanding and Performance of TanDEM-X Scientific Modes, Proc. *EUSAR*, Nuremberg, Germany, Apr. 2012.

[RC-559] **Börner, T.**, **De Zan, F.**, **López-Dekker, F.**, On the Performance of Baseline Self-Calibration Using Intersecting Interferometric SAR Acquisitions, Proc. *IGARSS*, Munich, Germany, Jul. 2012.

[RC-560] **Castellanos Alfonzo, G.**, **Jirousek, M.**, **Peichl, M.**, Orthogonal Waveform Experiments with a Highly Digitized Radar, Proc. *EUSAR*, Nuremberg, Germany, Apr. 2012.

[RC-561] **Culhaoglu, A.**, **Osipov, A.**, Russer, P., Performance of a Metamaterial Absorber in Radar Cross Section Reduction, Proc. *URSI Kleinheubacher Tagung*, Kleinheubach, Germany, Sep. 2012.

[RC-562] Alitalo, P., **Culhaoglu, A.**, **Osipov, A.**, **Thurner, S.**, **Kemptner, E.**, Tretyakov, S., Experimental Characterization of Electromagnetic Cloaking Structures with Bistatic Measurements at X-Band, Proc. *EuCAP*, Prague, Czech Republic, Mar. 2012.

[RC-563] **De Zan, F.**, Parizzi, A., **Prats Iraola, P.**, A Proposal for a SAR Interferometric Model of Soil Moisture, Proc. *IGARSS*, Munich, Germany, Jul. 2012.

[RC-564] **De Zan, F.**, **Krieger, G.**, **López-Dekker, F.**, Observations and Discussions of TanDEM-X Interferogram Spectra over Rain Forest, Proc. *IGARSS*, Munich, Germany, Jul. 2012.

[RC-565] **Dill, S.**, **Peichl, M.**, **Rudolf, D.**, SUMIRAD – A Near Realtime MMW Radiometer Imaging System for Threat Detection in an Urban Environment, Proc. *SPIE Europe Security and Defense*, Edinburgh, UK, vol. 8544, Sep. 2012.

[RC-566] **Dill, S.**, **Peichl, M.**, **Rudolf, D.**, SUMIRAD - A Close to Real Time MMW Radiometer Imaging System, Proc. *IGARSS*, Munich, Germany, Jul. 2012.

[RC-567] **Döring, B.**, **Schwerdt, M.**, Are Pixel Intensities Proportional to Radar Cross Section In SAR Images?, Proc. *IGARSS*, Munich, Germany, Jul. 2012.

[RC-568] **Döring, B.**, **Looser, P.**, **Jirousek, M.**, **Schwerdt, M.**, Linking Reference Target Properties to its Perceived RCS in SAR Images, Proc. *EUSAR*, Nuremberg, Germany, Apr. 2012.

[RC-569] **Eilers, J.**, **Neff, T.**, Protection of Spaceborne Systems, Proc. *Future Security*, Bonn, Germany, Sep. 2012.

[RC-570] **Gonzalez, C.**, **Bräutigam, B.**, **Rizzoli, P.**, SAR Performance Enhancements Using Radar Backscatter Map of TerraSAR-X, Proc. *EUSAR*, Nuremberg, Germany, Apr. 2012.

[RC-571] **Hager, M.**, **Anglberger, H.**, **Speck, R.**, **Süß, H.**, Applications of Simulation Techniques for High-Resolution SAR Systems, Proc. *ISIS*, Bad Reichenhall, Germany, Oct. 2012.

[RC-572] Eckardt, R., Richter, N., Auer, S., Eineder, M., Roth, A., **Hajnsek, I.**, Thiel, C., Schmullius, C., SAR-EDU – A German Education Initiative for Applied Synthetic Aperture Radar Remote Sensing, Proc. *IGARSS*, Munich, Germany, Jul. 2012.

[RC-573] **Huber, S.**, **Younis, M.**, **Krieger, G.**, A Novel Reflector Based Digital Beamforming SAR System Robust Against Feed Failures, Proc. *IGARSS*, Munich, Germany, Jul. 2012.

[RC-574] **Hueso Gonzalez, J.**, **Walter Antony, J.**, **Bachmann, M.**, **Krieger, G.**, **Schwerdt, M.**, **Zink, M.**, Tests of the TanDEM-X DEM Calibration Performance, Proc. *IGARSS*, Munich, Germany, Jul. 2012.

[RC-575] Masseroli, G., **Jagdhuber, T.**, **Hajnsek, I.**, Iodice, A., Crop Volume Characterization Using Dual Polarimetric SAR in X-Band, Proc. *GOLD*, Rome, Italy, Jun. 2012.

[RC-576] **Jagdhuber, T.**, **Kohling, M.**, **Hajnsek, I.**, Montzka, C., **Papathanassiou, K.**, Validation of Distributed Soil Moisture: Airborne Polarimetric SAR vs. Ground-Based Sensor Networks, Proc. *European Geosciences Union (EGU) General Assembly*, Vienna, Austria, Apr. 2012.

[RC-577] **Jagdhuber, T.**, **Hajnsek, I.**, **Sauer, S.**, **Papathanassiou, K.**, Bronstert, A., Soil Moisture Retrieval Under Forest Using Polarimetric Decomposition Techniques at P-Band, Proc. *EUSAR*, Nuremberg, Germany, Apr. 2012.

[RC-578] **Jagdhuber, T.**, **Hajnsek, I.**, **Martone, M.**, **Busche, T.**, TanDEM-X: Coverage of the TERENO Observatories, Proc. *Tereno-Workshop*, Potsdam, Germany, Jan. 2012.

[RC-579] **Jagdhuber, T.**, **Hajnsek, I.**, **Papathanassiou, K.**, Bronstert, A., Soil Moisture Retrieval under Agricultural Vegetation Using Fully Polarimetric SAR, Proc. *IGARSS*, Munich, Germany, Jul. 2012.

[RC-580] Jirousek, M., **Döring, B.**, **Looser, P.**, **Schwerdt, M.**, First Measurement Results of a New Highly-Accurate SAR Calibration Target, Proc. *IGARSS*, Munich, Germany, Jul. 2012.

[RC-581] Jirousek, M., **Döring, B.**, **Looser, P.**, **Schwerdt, M.**, Linearity Measurements of an Accurate Transponder for Calibrating Future Spaceborne SAR Systems, Proc. *EUSAR*, Nuremberg, Germany, Apr. 2012.

[RC-582] Kemptner, E., **Peichl, M.**, **Osipov, A.**, **Dill, S.**, Berücksichtigung von Hochfrequenzeigenschaften bei Radomen, Proc. *Symposium WSE*, Mannheim, Germany, Nov. 2012.

[RC-583] Kemptner, E., **Thurner, S.**, Free Space Material Characterization for Microwave Frequencies, Proc. *EuCAP*, Prague, Czech Republic, Mar. 2012.

[RC-584] Kim, J., **Papathanassiou, K.**, Quegan, S., Rogers, N., Estimation and Correction of Scintillation Effects on Spaceborne P-Band SAR Images, Proc. *IGARSS*, Munich, Germany, Jul. 2012.

[RC-585] Kraus, T., **Bachmann, M.**, **Rizzoli, P.**, **Bräutigam, B.**, **Krieger, G.**, TanDEM-X Performance: Impact on Acquisition Planning Optimization, Proc. *IRS*, Warsaw, Poland, May 2012.

[RC-586] Krieger, G., **De Zan, F.**, **Bachmann, M.**, **Hueso Gonzalez, J.**, **Rodríguez Cassolà, M.**, **Zink, M.**, Unexpected Height Offsets in TanDEM-X: Explanation and Correction, Proc. *IGARSS*, Munich, Germany, Jul. 2012.

[RC-587] Lee, S., **Kugler, F.**, **Papathanassiou, K.**, **Hajnsek, I.**, Quantification and Compensation of Temporal Decorrelation Effects in Polarimetric SAR Interferometry, Proc. *IGARSS*, Munich, Germany, Jul. 2012.

[RC-588] Limbach, M., **Gabler, B.**, **Di Maria, A.**, **Horn, R.**, **Reigber, A.**, DLR-Compact Test Range Facility, Proc. *EuCAP*, Prague, Czech Republic, Mar. 2012.

[RC-589] Looser, P., **Döring, B.**, **Jirousek, M.**, **Schwerdt, M.**, Variations of the Transponder's RCS Due to Environmental Impacts on the Antennas, Proc. *EUSAR*, Nuremberg, Germany, Apr. 2012.

[RC-590] López-Dekker, F., **Younis, M.**, Garcia, J., **Börner, T.**, **Krieger, G.**, Advanced Digital Beamforming Architectures and Operation Modes for an Enhanced SIGNAL Mission Concept, Proc. *International Workshop on Ka-Band Earth Observation Radar Missions (KEO'12)*, Noordwijk, The Netherlands, Nov. 2012.

[RC-591] Schaefer, C., Völker, M., **López-Dekker, F.**, **Younis, M.**, Dagazo-Eusebio, E., Ludwig, M., Spaceborne Ka-Band Across-Track SAR Interferometer, Proc. *International Workshop on Ka-Band Earth Observation Radar Missions (KEO'12)*, Noordwijk, The Netherlands, Nov. 2012.

[RC-592] Martone, M., **Bräutigam, B.**, **Krieger, G.**, Decorrelation Effects in Bistatic TanDEM-X Data, Proc. *IGARSS*, Munich, Germany, Jul. 2012.

[RC-593] Mittermayer, J., **Prats Iraola, P.**, **Wollstadt, S.**, **Baumgartner, S.**, **López-Dekker, F.**, **Krieger, G.**, **Moreira, A.**, Approach to Velocity and Acceleration Measurement in the Bi-Directional SAR Imaging Mode, Proc. *IGARSS*, Munich, Germany, Jul. 2012.

[RC-594] Mittermayer, J., **Wollstadt, S.**, **Prats Iraola, P.**, **Scheiber, R.**, Koppe, W., Staring Spotlight Imaging with TerraSAR-X, Proc. *IGARSS*, Munich, Germany, Jul. 2012.

[RC-595] Moreira, A., Remote Sensing for a Dynamic Earth, Proc. *IGARSS*, Munich, Germany, Jul. 2012.

[RC-596] Ortega-Míguez, C., **Schulze, D.**, **Polimeni, M.**, **Böer, J.**, **Rizzoli, P.**, **Bachmann, M.**, TanDEM-X Acquisition Planner, Proc. *EUSAR*, Nuremberg, Germany, Apr. 2012.

[RC-597] Osipov, A., Kobayashi, H., Suzuki, H., An Improved Cylindrical NFFFT for Compact Measurement Facilities, Proc. *APMC*, Kaohsiung, Taiwan, Dec. 2012.

[RC-598] Osipov, A., Characteristic Features of Electromagnetic Scattering from Bodies with Unit Relative Surface Impedance, Proc. *URSI Kleinheubacher Tagung*, Miltenberg, Germany, Sep. 2012.

[RC-599] Pardini, M., **Bianco, V.**, **Papathanassiou, K.**, Iodice, A., Phase Calibration of Multibaseline SAR Data Based on a Minimum Entropy Criterion, Proc. *IGARSS*, Munich, Germany, Jul. 2012.

[RC-600] Pardini, M., **Papathanassiou, K.**, Sub-Canopy Topography Estimation: Experiments with Multibaseline SAR Data at L-Band, Proc. *IGARSS*, Munich, Germany, Jul. 2012.

[RC-601] Pardini, M., **Toraño Caicoya, A.**, **Kugler, F.**, **Lee, S.**, **Hajnsek, I.**, **Papathanassiou, K.**, On the Estimation of Forest Vertical Structure from Multibaseline Polarimetric SAR Data, Proc. *IGARSS*, Munich, Germany, Jul. 2012.

[RC-602] Parrella, G., **Al-Kahachi, N.**, **Jagdhuber, T.**, **Hajnsek, I.**, **Papathanassiou, K.**, Ice Volume Characterization Using Long-Wavelength Airborne PolSAR Data, Proc. *IGARSS*, Munich, Germany, Jul. 2012.

[RC-603] Parrella, G., **Della Corte, A.**, **Hajnsek, I.**, Iodice, A., Snow Properties Retrieval Using TerraSAR-X Dual-Polarization Data, Proc. *IGARSS*, Munich, Germany, Jul. 2012.

[RC-604] Parrella, G., **Al-Kahachi, N.**, **Jagdhuber, T.**, **Hajnsek, I.**, **Papathanassiou, K.**, Modelling PolSAR Scattering Signatures at Long Wavelengths of Glacier Ice Volumes, Proc. *ESA-CliC-EGU Earth Observation and Cryosphere Science Conference*, Frascati, Italy, Nov. 2012.

[RC-605] Parrella, G., **Kugler, F.**, **Hajnsek, I.**, Iodice, A., Validation of Pol-InSAR Derived Forest Height by Means of LiDAR Data, Proc. *IEEE GOLD*, Rome, Italy, Jun. 2012.

[RC-606] Patyuchenko, A., **Rommel, T.**, **Laskowski, P.**, **Younis, M.**, **Krieger, G.**, Digital Beamforming Reconfigurable Radar System Demonstrator, Proc. *IGARSS*, Munich, Germany, Jul. 2012.

[RC-607] Peichl, M., **Dill, S.**, Projektinhalte MikroVol, Proc. *Kick-off-Meeting MikroVol*, Oberpfaffenhofen, Germany, Feb. 2012.

[RC-608] Peichl, M., **Dill, S.**, **Rudolf, D.**, First Results for a Low-Cost Fast Millimeterwave Radiometric Imaging System, Proc. *SPIE Defense Security + Sensing*, Baltimore, USA, Apr. 2012.

[RC-609] Pinheiro, M., **Rodríguez Cassolà, M.**, **Prats Iraola, P.**, **Reigber, A.**, Analysis of Methods for Reconstructing Periodically Missed SAR Data Acquired Close to Nyquist, Proc. *IGARSS*, Munich, Germany, Jul. 2012.

[RC-610] Pinheiro, M., **Rodríguez Cassolà, M.**, Reconstruction Methods of Missing SAR Data: Analysis in the Frame of TanDEM-X Synchronization Link, Proc. *EUSAR*, Nuremberg, Germany, Apr. 2012.

[RC-611] Pisciottano, I., **Jagdhuber, T.**, **Hajnsek, I.**, Iodice, A., First Analysis on Snow Cover Change Using Polarimetric TerraSAR-X Data, Proc. *GOLD*, Rome,Italy, Jun. 2012.

[RC-612] Gutierrez-Nava, A., **Ponce Madrigal, O.**, **López-Dekker, F.**, **Patyuchenko, A.**, **Younis, M.**, **Krieger, G.**, **Reigber, A.**, **Moreira, A.**, Vicente-Vivas, E., Ocampo-Torres, F., Pacheco, E., TOPMEX-9 Distributed SAR Mission Employing Nanosatellite Cluster, Proc. *International Astronautical Congress (IAC)*, Naples, Italy, Oct. 2012.

[RC-613] Prats Iraola, P., **Rodríguez Cassolà, M.**, **Scheiber, R.**, **Reigber, A.**, Accommodation of Space-Variant Effects in Spaceborne SAR Image Formation, Proc. *IGARSS*, Québec, Canada, Jul. 2012.

[RC-614] Veci, L., **Prats Iraola, P.**, **Scheiber, R.**, Collard, F., Fomferra, N., Engdahl, M., The Sentinel-1 Toolbox, Proc. *IGARSS*, Québec, Canada, Jul. 2012.

[RC-615] **Prats Iraola, P.**, **Scheiber, R.**, **Rodríguez Cassolà, M.**, **Wollstadt, S.**, **Mittermayer, J.**, **Bräutigam, B.**, **Schwerdt, M.**, **Reigber, A.**, **Moreira, A.**, High-Precision SAR Focusing of TerraSAR-X Experimental Staring Spotlight Data, Proc. *IGARSS*, Munich, Germany, Jul. 2012.

[RC-616] **Marotti, L.**, **Prats Iraola, P.**, **Scheiber, R.**, **Wollstadt, S.**, **Reigber, A.**, Differential SAR Interferometry with TerraSAR-X TOPS Data: Mexico City Subsidence Results, Proc. *EUSAR*, Nuremberg, Germany, Apr. 2012.

[RC-617] **Prats Iraola, P.**, **Scheiber, R.**, **Mittermayer, J.**, **Wollstadt, S.**, **Baumgartner, S.**, **López-Dekker, F.**, **Schulze, D.**, **Steinbrecher, U.**, **Rodríguez Cassolà, M.**, **Reigber, A.**, **Krieger, G.**, **Zink, M.**, **Moreira, A.**, TanDEM-X Experiments in Pursuit Monostatic Configuration, Proc. *EUSAR*, Nuremberg, Germany, Apr. 2012.

[RC-618] **Que, R.**, **Ponce Madrigal, O.**, **Scheiber, R.**, **Reigber, A.**, Realtime Processing of SAR Images for Linear and Nonlinear Tracks, Proc. *IRS*, Krakow, Poland, May 2012.

[RC-619] **Reigber, A.**, **Jäger, M.**, **Pinheiro, M.**, **Scheiber, R.**, **Prats Iraola, P.**, **Fischer, J.**, **Horn, R.**, **Nottensteiner, A.**, Performance of the P-Band Subsystem and the X-Band Interferometer of the F-SAR Airborne SAR Instrument, Proc. *IGARSS*, Munich, Germany, Jul. 2012.

[RC-620] **Reigber, A.**, **Jäger, M.**, **Fischer, J.**, **Horn, R.**, **Scheiber, R.**, **Prats Iraola, P.**, **Nottensteiner, A.**, Performance of the L- and P-Band Subsystems of the F-SAR Airborne SAR Instrument, Proc. *EUSAR*, Nuremberg, Germany, May 2012.

[RC-621] **Rizzoli, P.**, **Bräutigam, B.**, Radar Backscatter Characterization Approach Combining Global TanDEM-X Data, Proc. *IGARSS*, Munich, Germany, Jul. 2012.

[RC-622] **Rizzoli, P.**, **Bachmann, M.**, **Bräutigam, B.**, Global Performance Monitoring from TanDEM-X Quicklook Data., Proc. *EUSAR*, Nuremberg, Germany, Apr. 2012.

[RC-623] **Rodríguez Cassolà, M.**, **Prats Iraola, P.**, **Schulze, D.**, **Steinbrecher, U.**, **Tous Ramon, N.**, **Younis, M.**, **López-Dekker, F.**, **Zink, M.**, **Reigber, A.**, **Moreira, A.**, **Krieger, G.**, Non-Nominal Experimental Bistatic SAR Acquisitions with TanDEM-X, Proc. *EUSAR*, Nuremberg, Germany, Apr. 2012.

[RC-624] **Rommel, T.**, **Patyuchenko, A.**, **Laskowski, P.**, **Younis, M.**, **Krieger, G.**, Development of a MIMO Radar System Demonstrator - Calibration and Demonstration of First Results, Proc. *International Radar Symposium (IRS')*, Warsaw, Poland, vol. 13, May 2012.

[RC-625] **Rudolf, D.**, **Peichl, M.**, **Dill, S.**, Sumirad - A High-Speed Imaging Millimetre-Wave Radiometer System, Proc. *ONERA-DLR Aerospace Symposium (ODAS)*, Brunswick, Germany, Jun. 2012.

[RC-626] **Sauer, S.**, **Jagdhuber, T.**, **Kugler, F.**, **Lee, S.**, **Papathanassiou, K.**, Orientation Angle Estimation over Forested Terrain Using P-Band POLSAR Data, Proc. *IGARSS*, Munich, Germany, Jul. 2012.

[RC-627] **Sauer, S.**, **Papathanassiou, K.**, Vertical Resolution Enhancement by Applying Polarimetric Spectral Analysis Techniques to Multibaseline InSAR Data, Proc. *IGARSS*, Munich, Germany, Jul. 2012.

[RC-628] **Schwerdt, M.**, **Schrank, D.**, **Bachmann, M.**, **Hueso Gonzalez, J.**, **Döring, B.**, **Tous Ramon, N.**, **Walter Antony, J.**, Calibration of the TerraSAR-X and the TanDEM-X Satellite for the TerraSAR-X Mission, Proc. *EUSAR*, Nuremberg, Germany, Apr. 2012.

[RC-629] **Tailhades, S.**, An End-to-End Simulation Framework for Optimizing the Design of Spaceborne Imaging Systems, Proc. *IGARSS*, Munich, Germany, Jul. 2012.

[RC-630] **Toraño Caicoya, A.**, **Kugler, F.**, **Papathanassiou, K.**, **Hajnsek, I.**, Boreal Forest Biomass Classification with TanDEM-X, Proc. *IGARSS*, Munich, Germany, Jul. 2012.

[RC-631] **Toraño Caicoya, A.**, **Kugler, F.**, **Pardini, M.**, **Hajnsek, I.**, **Papathanassiou, K.**, Forest Vertical Structure Characterization for Biomass Estimation with Remote Sensing Systems (Synthetic Aperture Radar): Spatial Scale Implications, Proc. *ForestSAT*, Corvallis, USA, Sep. 2012.

[RC-632] **Tous Ramon, N.**, **Schrank, D.**, **Bachmann, M.**, **Castellanos Alfonzo, G.**, **Polimeni, M.**, **Böer, J.**, **Schwerdt, M.**, Long-Term System Monitoring Status of the TerraSAR-X / TanDEM-X Satellites, Proc. *EUSAR*, Nuremberg, Germany, Apr. 2012.

[RC-633] **Villano, M.**, **Krieger, G.**, Accounting for Azimuth Ambiguities in Interferometric Performance Analysis, Proc. *IGARSS*, Munich, Germany, Jul. 2012.

[RC-634] **Villano, M.**, **Krieger, G.**, **Moreira, A.**, Staggered-SAR for High-Resolution Wide-Swath Imaging, Proc. *RADAR*, Glasgow, UK, Oct. 2012.

[RC-635] **Villano, M.**, **Krieger, G.**, **Moreira, A.**, Staggered-SAR: A New Concept for High-Resolution Wide-Swath Imaging, Proc. *IEEE GOLD Remote Sensing Conference*, Rome, Italy, Jun. 2012.

[RC-636] **Walter Antony, J.**, **Hueso Gonzalez, J.**, **Schwerdt, M.**, **Bachmann, M.**, **Krieger, G.**, **Zink, M.**, Results of Baseline Calibration for the TanDEM-X Mission, Proc. *URSI Kleinheubacher Tagung*, Miltenberg, Germany, Sep. 2012.

[RC-637] **Weigt, M.**, **Rizzoli, P.**, **Bachmann, M.**, **Bräutigam, B.**, **Schulze, D.**, TanDEM-X Mission - Interferometric Performance and Global DEM Acquisition Status, Proc. *RADAR - International Conference on Radar Systems*, Glasgow, UK, Oct. 2012.

[RC-638] **Wollstadt, S.**, **López-Dekker, F.**, **Prats Iraola, P.**, **De Zan, F.**, **Busche, T.**, **Krieger, G.**, 1 and 5 Day Differential INSAR under Crossing Orbits with TerraSAR-X, Proc. *IGARSS*, Munich, Germany, Jul. 2012.

[RC-639] **Younis, M.**, **López-Dekker, F.**, **Patyuchenko, A.**, Schaefer, C., **Krieger, G.**, Advanced Operation Mode Techniques for an Interferometric Synthetic Aperture Radar, Proc. *IGARSS*, Munich, Germany, Jul. 2012.

2011

[RC-640] **Aguilera, E.**, **Nannini, M.**, **Arthur, A.**, **Marotti, L.**, **Prats, P.**, **Reigber, A.**, Polarimetric SAR Tomography with TerraSAR-X by means of Distributed Compressed Sensing, Proc. *ESA FRINGE Workshop*, Frascati, Italy, Sep. 2011.

[RC-641] **Aguilera, E.**, **Nannini, M.**, **Reigber, A.**, Compressed Sensing for Polarimetric SAR Tomography, Proc. *URSI Commission F – Triennial Open Symposium on Radio Wave Propagation and Remote Sensing*, Garmisch-Partenkirchen, Germany, Mar. 2011.

[RC-642] **Al-Kahachi, N.**, **Papathanassiou, K.**, Polarimetric Characterisation of Two Layered Frozen Lakes, Proc. *Helmholtz Alliance Planetary Evolution and Life (PEL)*, Berlin, Germany, Mar. 2011.

[RC-643] **Al-Kahachi, N.**, **Papathanassiou, K.**, Polarimetric Investigation of a Two Surface Layer Structure Using L-Band PALSAR Data, Proc. *ESA POLinSAR Workshop*, Frascati, Italy, Jan. 2011.

[RC-644] **Anglberger, H.**, **Tailhades, S.**, **Süß, H.**, An Image Acquisition Planning Tool for Optimizing Information Content in Image Data of Spaceborne SAR Systems, Proc. *SPIE Remote Sensing Conference*, Prague, Czech Republic, vol. 8179, Oct. 2011.

[RC-645] Anglberger, H., **Süß, H.**, Fusion of High-Resolution Radar Images with Simulated Target Signatures, Proc. *International Conference of Space Technology (ICST)*, Athens, Greece, Sep. 2011.

[RC-646] Anglberger, H., **Süß, H.**, **Hager, M.**, Application of SAR Simulation for Signature Analysis and Identification of Complex Targets on TerraSAR-X Data, Proc. *TerraSAR-X Science Team Meeting*, Oberpfaffenhofen, Germany, Feb. 2011.

[RC-647] Bachmann, M., **Bräutigam, B.**, **Hueso Gonzalez, J.**, **Krieger, G.**, **Martone, M.**, **Rizzoli, P.**, **Schulze, D.**, **Schwerdt, M.**, **Walter Antony, J.**, **Zink, M.**, TanDEM-X DEM Performance and Calibration, Proc. *CEOS SAR CalVal Workshop*, Fairbanks, USA, Nov. 2011.

[RC-648] Baumgartner, S., **Krieger, G.**, Dual-Platform GMTI: First Results with the TerraSAR-X/TanDEM-X Constellation, Proc. *IRS*, Leipzig, Germany, Sep. 2011.

[RC-649] Baumgartner, S., **Krieger, G.**, Ground Moving Target Indication and Ship Surveillance with the German TerraSAR-X/TanDEM-X Radar Satellite Constellation, Proc. *Future Security*, Berlin, Germany, Sep. 2011.

[RC-650] Baumgartner, S., **Krieger, G.**, Large Along-Track Baseline SAR-GMTI: First Results with the TerraSAR-X/TanDEM-X Satellite Constellation, Proc. *IGARSS*, Vancouver, Canada, Jul. 2011.

[RC-651] Baumgartner, S., **Krieger, G.**, First GMTI Results with the TerraSAR-X/TanDEM-X Constellation, Proc. *URSI Commission F - Triennial Open Symposium on Radio Wave Propagation and Remote Sensing*, Garmisch-Partenkirchen, Germany, Mar. 2011.

[RC-652] Bordoni, F., **Younis, M.**, **Krieger, G.**, Performance Investigation on the High-Resolution Wide-Swath SAR System Operating in Stripmap Quad-Pol and Ultra-Wide Scansar Mode, Proc. *IGARSS*, Vancouver, Canada, Jul. 2011.

[RC-653] Bordoni, F., **Younis, M.**, **Krieger, G.**, Ambiguity Suppression by Azimuth Phase Coding in Multichannel SAR Systems, Proc. *IGARSS*, Vancouver, Canada, Jul. 2011.

[RC-654] Culhaoglu, A., **Osipov, A.**, Russer, P., Metamaterial Slab Excited by an Arbitrarily Oriented Dipole, Proc. *URSI General Assembly and Scientific Symposium (GASS)*, Istanbul, Turkey, Aug. 2011.

[RC-655] Danklmayer, A., Chandra, M., Propagation Effects for Satellite Mounted Radars and Remote Sensing by Active Microwave SAR Sensors for Frequencies of X-Band up to Ka-Band, Proc. *URSI Commission F – Triennial Open Symposium on Propagation and Remote Sensing*, Garmisch-Partenkirchen, Germany, Mar. 2011.

[RC-656] De Zan, F., **López-Dekker, F.**, Coherent Stacking of SAR Images for Efficient Interferometric Processing, Proc. *IGARSS*, Vancouver, Canada, Jul. 2011.

[RC-657] Döring, B., **Looser, P.**, **Jirousek, M.**, **Schwerdt, M.**, Point Target Correction Coefficients for Absolute SAR Calibration, Proc. *IEEE International Instrumentation and Measurement Technology Conference (I2TMC)*, Binjiang, Hanghzou, China, May 2011.

[RC-658] Hajnsek, I., **Pisciottano, I.**, **Jagdhuber, T.**, **Parrella, G.**, Analysis on Snow Cover Change Using Polarimetric TerraSAR-X Data, Proc. *EARSeL Land Ice and Snow Special Interest Group (LISSIG) Workshop*, Berne, Switzerland, Feb. 2011.

[RC-659] Huber, S., **Younis, M.**, **Patyuchenko, A.**, **Krieger, G.**, Digital Beamforming in Azimuth with Spaceborne Reflector SAR Systems, Proc. *URSI Commission F – Triennial Open Symposium on Radio Wave Propagation and Remote Sensing*, Garmisch-Partenkirchen, Germany, Mar. 2011.

[RC-660] Jagdhuber, T., **Hajnsek, I.**, **Papathanassiou, K.**, Bronstert, A., A Hybrid Decomposition for Soil Moisture Estimation under Vegetation Cover Using Polarimetric SAR, Proc. *ESA POLinSAR Workshop*, Frascati, Italy, Jan. 2011.

[RC-661] Jirousek, M., **Castellanos Alfonso, G.**, **Peichl, M.**, First Experiments Based on a Highly Digitized Radar, Proc. *IRS*, Leibzig, Germany, Sep. 2011.

[RC-662] Kemptner, E., RCS Simulations on Wet Corner Reflectors with SBR Code SIGRAY, Proc. *Progress in Electromagnetics Research Symposium (PIERS)*, Marrakesh, Morocco, Mar. 2011.

[RC-663] Kim, J., **Younis, M.**, **Gabele, M.**, **Prats Iraola, P.**, **Krieger, G.**, First Spaceborne Experiment of Digital Beamforming with TerraSAR-X Dual Receive Antenna Mode, Proc. *EuRAD*, Manchester, UK, Oct. 2011.

[RC-664] Kraus, T., **Schrank, D.**, **Rizzoli, P.**, **Bräutigam, B.**, In-Orbit SAR Performance of TerraSAR-X and TanDEM-X Satellites, Proc. *URSI Commission F – Triennial Open Symposium on Radio Wave Propagation and Remote Sensing*, Garmisch-Partenkirchen, Germany, Mar. 2011.

[RC-665] Kugler, F., **Hajnsek, I.**, **Papathanassiou, K.**, Forest Characterization by Means of TerraSAR-X and TanDEM-X Polarimetric Interferometric Data, Proc. *ESA POLinSAR Workshop*, Frascati, Italy, Jan. 2011.

[RC-666] Laskowski, P., **Bordoni, F.**, **Younis, M.**, Antenna Pattern Compensation in Multi-Channel Azimuth Reconstruction Algorithm, Proc. *ARSI*, Noordwijk, The Netherlands, Sep. 2011.

[RC-667] Lee, S., **Kugler, F.**, **Papathanassiou, K.**, **Hajnsek, I.**, Multibaseline Polarimetric SAR Interferometry Forest Height Inversion Approaches, Proc. *ESA POLinSAR Workshop*, Frascati, Italy, Jan. 2011.

[RC-668] Looser, P., **Döring, B.**, **Jirousek, M.**, **Schwerdt, M.**, Thermal Design of a Precise Transponder for Calibrating Future Spaceborne SAR Systems, Proc. *URSI Commission F – Triennial Open Symposium on Radio Wave Propagation and Remote Sensing*, Garmisch-Partenkirchen, Germany, Mar. 2011.

[RC-669] López-Dekker, F., **De Zan, F.**, **Wollstadt, S.**, **Prats Iraola, P.**, **Krieger, G.**, On the Tomographic Information in Single Pairs of Crossing-Orbits SAR Acquisitions, Proc. *IGARSS*, Munich, Germany, Jul. 2011.

[RC-670] López-Dekker, F., **García Molina, J.**, **De Zan, F.**, **Börner, T.**, **Younis, M.**, **Papathanassiou, K.**, Guardabrazo, T., Bourlon, V., Ramongassie, S., Taveneau, N., Ulander, L., Murdin, D., Rogers, N., Quegan, S., Franco, R., BIOMASS End-to-End Mission Performance Assessment, Proc. *IGARSS*, Munich, Germany, Jul. 2011.

[RC-671] López-Dekker, F., **Börner, T.**, **Younis, M.**, **Krieger, G.**, SIGNAL: A Ka-Band Digital Beamforming SAR System Concept to Monitor Topography Variations of Ice Caps and Glaciers, Proc. *ARSI*, Noordwijk, The Netherlands, Sep. 2011.

[RC-672] López-Dekker, F., **De Zan, F.**, **Börner, T.**, **Younis, M.**, **Papathanassiou, K.**, Guardabrazo, T., Bourlon, V., Ramongassie, S., Taveneau, N., Ulander, L., Murdin, D., Rogers, N., Quegan, S., Franco, R., BIOMASS End-to-End Mission Simulation and Performance Assessment, Proc. *ARSI*, Noordwijk, The Netherlands, Sep. 2011.

[RC-673] López-Dekker, F., **De Zan, F.**, **Börner, T.**, **Younis, M.**, **Papathanassiou, K.**, Guardabrazo, T., Bourlon, V., Ramongassie, S., Taveneau, N., Ulander, L., Murdin, D., Rogers, N., Quegan, S., Franco, R., BIOMASS End-to-End Mission Performance Simulator, Proc. *IGARSS*, Vancouver, Canada, Jul. 2011.

[RC-674] López-Dekker, F., **Prats Iraola, P.**, **De Zan, F.**, **Wollstadt, S.**, **Schulze, D.**, **Krieger, G.**, **Moreira, A.**, Demonstration of SAR Interferometry under Crossing Orbits Using TerraSAR-X and TanDEM-X, Proc. *IGARSS*, Vancouver, Canada, Jul. 2011.

[RC-675] Martone, M., **Krieger, G.**, **Rizzoli, P.**, **Bräutigam, B.**, First Interferometric Performance Results of TanDEM-X Commissioning Phase., Proc. *URSI Commission F – Triennial Open Symposium on Propagation and Remote Sensing*, Garmisch-Partenkirchen, Germany, Mar. 2011.

[RC-676] Moreira, A., **Krieger, G.**, **Younis, M.**, **Hajnsek, I.**, **Papathanassiou, K.**, Eineder, M., **De Zan, F.**, Tandem-L: A Mission Proposal for Monitoring Dynamic Earth Processes, Proc. *IGARSS*, Vancouver, Canada, Jul. 2011.

[RC-677] Osipov, A., Kobayashi, H., Suzuki, H., An Improved Image-Based Near-Field-to-Far-Field Transformation for Cylindrical Scanning Surfaces, Proc. *URSI GASS 2011*, Istanbul, Turkei, Aug. 2011.

[RC-678] Pardini, M., Lombardini, F., **Papathanassiou, K.**, Theoretical Performance Bounds on the Estimation of Forest Structure Parameters from Multibaseline SAR Data, Proc. *ESA FRINGE Workshop*, Frascati, Italy, Sep. 2011.

[RC-679] Pardini, M., **Papathanassiou, K.**, Sub-Canopy Topography Estimation with Multibaseline Pol-InSAR Data: A RELAX-Based Solution, Proc. *ESA FRINGE Workshop*, Frascati, Italy, Sep. 2011.

[RC-680] Pardini, M., **Papathanassiou, K.**, Robust Estimation of the Vertical Structure of Forest with Coherence Tomography, Proc. *ESA POLinSAR Workshop*, Frascati, Italy, Jan. 2011.

[RC-681] Pardini, M., **Kugler, F.**, **Lee, S.**, **Sauer, S.**, **Toraño Caicoya, A.**, **Papathanassiou, K.**, Biomass Estimation from Forest Vertical Structure: Potentials and Challenges for Multibaseline Pol-InSAR Techniques, Proc. *ESA POLinSAR Workshop*, Frascati, Italy, Jan. 2011.

[RC-682] Patyuchenko, A., **Younis, M.**, **Krieger, G.**, Digital Beamforming Antenna Optimization for Reflector-Based Space Debris Radar System, Proc. *ESA Antenna Workshop*, Noordwijk, The Netherlands, Oct. 2011.

[RC-683] Patyuchenko, A., **Younis, M.**, **Krieger, G.**, Weigel, M., A Concept for an Advanced Reflector-Based Space Surveillance Radar, Proc. *European Space Surveillance Conference (ESS)*, Madrid, Spain, Jun. 2011.

[RC-684] Peichl, M., **Dill, S.**, **Rudolf, D.**, Investigation of Fully Polarimetric Signatures from Targets with some Relevance to Security Applications, Proc. *SPIE Security, Defense + Sensing*, Orlando, USA, vol. s 8022, Apr. 2011.

[RC-685] Pisciottano, I., **Jagdhuber, T.**, **Parrella, G.**, **Hajnsek, I.**, First Analysis on Snow Cover Change Using Fully Polarimetric TerraSAR-X Data, Proc. *ESA POLinSAR Workshop*, Frascati, Italy, Jan. 2011.

[RC-686] Ponce Madrigal, O., **Prats Iraola, P.**, **Rodríguez Cassolà, M.**, **Scheiber, R.**, **Reigber, A.**, Processing of Circular SAR Trajectories with Fast-Factorized Back-Projection, Proc. *IGARSS*, Vancouver, Canada, Jul. 2011.

[RC-687] Ponce Madrigal, O., **Prats Iraola, P.**, **Reigber, A.**, **Pinheiro, M.**, Analysis of the Anisotropic Behaviour of Scatterers Using Polarimetric Circular SAR Data, Proc. *URSI Commission F – Triennial Open Symposium on Radio Wave Propagation and Remote Sensing*, Garmisch-Partenkirchen, Germany, Mar. 2011.

[RC-688] Marotti, L., **Prats Iraola, P.**, **Scheiber, R.**, **Wollstadt, S.**, **Reigber, A.**, TOPS Differential SAR Interferometry with TerraSAR-X, Proc. *ESA FRINGE Workshop*, Frascati, Italy, Sep. 2011.

[RC-689] Neumann, M., Hensley, S., Saatchi, S., Ferro-Famil, L., **Reigber, A.**, Michel, T., Lavalle, M., Ahmed, R., Siqueira, P., Potential and Limitations of Forest Remote Sensing from Polarimetric SAR Interferometry, Proc. *IGARSS*, Munich, Germany, Jul. 2011.

[RC-690] Ferro-Famil, L., Huang, Y., **Reigber, A.**, High-Resolution SAR Tomography Using Full-Rank Polarimetric Spectral Estimators, Proc. *IGARSS*, Munich, Germany, Jul. 2011.

[RC-691] Huang, Y., Ferro-Famil, L., **Reigber, A.**, Natural Environment Characterization Using Hybrid Tomographic Aproaches, Proc. *IGARSS*, Vancouver, Canada, Jul. 2011.

[RC-692] Ferro-Famil, L., Huang, Y., **Reigber, A.**, Polarimetric Methods for Tomographic Imaging of Natural Volumetric Media, Proc. *IGARSS*, Vancouver, Canada, Jul. 2011.

[RC-693] Neumann, M., Saatchi, S., Ferro-Famil, L., **Reigber, A.**, The Effect of Spatial and Temporal Forest Variability on Radar Observables, Proc. *IGARSS*, Vancouver, Canada, Jul. 2011.

[RC-694] Reigber, A., **Jäger, M.**, **Fischer, J.**, **Horn, R.**, **Scheiber, R.**, **Prats Iraola, P.**, **Nottensteiner, A.**, System Status and Calibration of the F-SAR Airborne SAR Instrument, Proc. *IGARSS*, Vancouver, Canada, Jul. 2011.

[RC-695] Rodríguez Cassolà, M., **Prats Iraola, P.**, **Schulze, D.**, **Tous Ramon, N.**, **Steinbrecher, U.**, **Marotti, L.**, **Nanninni, M.**, **Younis, M.**, **López-Dekker, F.**, **Zink, M.**, **Reigber, A.**, **Krieger, G.**, **Moreira, A.**, First Bistatic Spaceborne SAR Experiments with TanDEM-X, Proc. *IGARSS*, Vancouver, Canada, Jul. 2011.

[RC-696] Sanjuan Ferrer, M., **Hajnsek, I.**, **Papathanassiou, K.**, Characterization of Alpine Glaciers Using Fully-Polarimetric TerraSAR-X Data, Proc. *ESA POLinSAR Workshop*, Frascati, Italy, Jan. 2011.

[RC-697] Sauer, S., **Lee, S.**, **Kugler, F.**, **Papathanassiou, K.**, Assessment of Forest Biomass Retrieval Using Polarimetric Decompositions, Proc. *ESA POLinSAR Workshop*, Frascati, Italy, Jan. 2011.

[RC-698] Malz, E., **Scheiber, R.**, **Mittermayer, J.**, Snoeij, P., Attema, E., Sentinel-1 FDBAQ Performance Validation Using TerraSAR-X Data, Proc. *IGARSS*, Munich, Germany, Jul. 2012/Jul. 2011.

[RC-699] Scheiber, R., **De Zan, F.**, **Prats Iraola, P.**, Sant'Anna Araújo, L., **Künemund, M.**, Interferometric Sea Ice Mapping with TanDEM-X: First Experiments, Proc. *IGARSS*, Vancouver, Canada, Jul. 2011.

[RC-700] Schrank, D., **Schwerdt, M.**, **Hueso Gonzalez, J.**, **Bachmann, M.**, **Döring, B.**, **Tous Ramon, N.**, **Walter Antony, J.**, In-Orbit Calibration of both TanDEM-X Satellites, Proc. *CEOS SAR CalVal Workshop*, Fairbanks, USA, Nov. 2011.

[RC-701] Schreiber, E., **Anger, S.**, **Peichl, M.**, Design of an Integrated Ka-Band Receiver Module for Passive Microwave Imaging Systems, Proc. *IEEE Semiconductor Conference (SCD)*, Dresden, Germany, Sep. 2011.

[RC-702] Schwerdt, M., **Bachmann, M.**, **Schrank, D.**, **Hueso Gonzalez, J.**, **Döring, B.**, **Walter Antony, J.**, **Tous Ramon, N.**, Monostatic Calibration of both TanDEM-X Satellites, Proc. *URSI Commission F – Triennial Open Symposium on Radio Wave Propagation and Remote Sensing*, Garmisch-Partenkirchen, Germany, Feb. 2011.

[RC-703] Toraño Caicoya, A., **Kugler, F.**, **Hajnsek, I.**, **Papathanassiou, K.**, Biomass Estimation as a Function of Vertical Forest Structure and Forest Height. Potential and Limitations for Remote Sensing (Radar and LiDAR), Proc. *ESA POLinSAR Workshop*, Frascati, Italy, Jan. 2011.

[RC-704] Villano, M., **Papathanassiou, K.**, Differential Shift Estimation in the Absence of Coherence: Performance Analysis and Benefits of Polarimetry, Proc. *ESA POLinSAR Workshop*, Frascati, Italy, Jan. 2011.

[RC-705] **Walter Antony, J.**, **Hueso Gonzalez, J.**, **Döring, B.**, **Bachmann, M.**, **Schwerdt, M.**, First Results of Baseline Calibration for the TanDEM-X Mission, Proc. *URSI Commission F – Triennial Open Symposium on Radio Wave Propagation and Remote Sensing*, Garmisch-Partenkirchen, Germany, Mar. 2011.

[RC-706] **Weigt, M.**, **Steinbrecher, U.**, **Kraus, T.**, **Böer, J.**, **Bräutigam, B.**, TanDEM-X SAR System Verification, Proc. *CEOS SAR CalVal Workshop*, Fairbanks, USA, Nov. 2011.

[RC-707] **Wollstadt, S.**, **López-Dekker, F.**, **Prats Iraola, P.**, **De Zan, F.**, **Busche, T.**, **Krieger, G.**, Interferometric Crossing Orbit Experiment Using TerraSAR-X and TanDEM-X, Proc. *ESA FRINGE Workshop*, Frascati, Italy, Sep. 2011.

[RC-708] **Zink, M.**, TerraSAR-X / TanDEM-X Mission Status, Proc. *CEOS SAR CalVal Workshop*, Fairbanks, Alaska, Nov. 2011.

Technical and Project Reports

2017

[R-1] **Anglberger, H.**, **Kempf, T.**, **Profelt, J.**, **Villamil López, C.**, **Speck, R.**, RADIAN Version 2.04 Benutzerhandbuch, Technical Note, 2017.

[R-2] **Bachmann, M.**, Tandem-L Ground Segment Project Management Plan, Technical Note, 40 pages, TDL-GS-PL-0001, 2017.

[R-3] **Bachmann, M.**, Tandem-L Ground Segment Schedule, Technical Note, 1 page, TDL-GS-PL-0007, 2017.

[R-4] **Bachmann, M.**, Tandem-L Ground Segment Technical Readiness Level Assessment Report, Technical Note, 32 pages, TDL-GS-RP-0003, 2017.

[R-5] **Bachmann, M.**, Tandem-L Risk Assessment Report, Technical Note, 32 pages, TDL-GS-RP-0003, 2017.

[R-6] **Baris, I.**, Entwicklung von Rückstreumodellen zur Kombination von optischen und Radar-Daten, Technical Note, HR-AKS-003, 2017.

[R-7] **Baumgartner, S.**, **Scheiber, R.**, **Jäger, M.**, **Limbach, M.**, **Horn, R.**, **Nottensteiner, A.**, Jahresbericht 2016 für das Projekt EMS II HR - Flugzeuggetragenes Mehrkanal-SAR für die Maritime Sicherheit, Technical Note, 23 pages, 2017.

[R-8] **Baur, M.**, Physics-Based Data Integration for Estimation of Environmental Parameters and Security-Related Information, Technical Note, 2017.

[R-9] **Bojarski, A.**, **Bachmann, M.**, **Böer, J.**, **Rizolli, P.**, **Martone, M.**, **Tous Ramon, N.**, **Schmidt, K.**, **Schwerdt, M.**, **Steinbrecher, U.**, **Wecklich, C.**, **Schulze, D.**, **Walter Antony, J.**, Long-Term System Monitoring Report Q3/2016, Technical Note, 99 pages, TX-SEC-RP-4660, 2017.

[R-10] **Bojarski, A.**, **Bachmann, M.**, **Böer, J.**, **Rizzoli, P.**, **Martone, M.**, **Tous Ramon, N.**, **Schmidt, K.**, **Schwerdt, M.**, **Schulze, D.**, **Steinbrecher, U.**, **Wecklich, C.**, Long-Term System Monitoring Report Q2/2017, Technical Note, 100 pages, TX-SEC-RP-4660, 2017.

[R-11] **Bojarski, A.**, **Bachmann, M.**, **Böer, J.**, **Rizzoli, P.**, **Martone, M.**, **Tous Ramon, N.**, **Schulze, D.**, **Schwerdt, M.**, **Walter Antony, J.**, **Wecklich, C.**, Long-Term System Monitoring Report Q4/2015, Technical Note, 121 pages, TX-SEC-RP-4660, 2017.

[R-12] **Bojarski, A.**, **Bachmann, M.**, **Böer, J.**, **Rizzoli, P.**, **Martone, M.**, **Tous Ramon, N.**, **Schmidt, K.**, **Schulze, D.**, **Schwerdt, M.**, **Walter Antony, J.**, **Wecklich, C.**, Long-Term System Monitoring Report Q1/2017, Technical Note, 99 pages, TX-SEC-RP-4660, 2017.

[R-13] **Bojarski, A.**, **Bachmann, M.**, **Böer, J.**, **Rizzoli, P.**, **Martone, M.**, **Tous Ramon, N.**, **Schmidt, K.**, **Schulze, D.**, **Schwerdt, M.**, **Walter Antony, J.**, **Wecklich, C.**, Long-Term System Monitoring Report Q2/2016, Technical Note, 123 pages, TX-SEC-RP-4660, 2017.

[R-14] **Buckreuß, S.**, **Zink, M.**, Maurer, E., Schork, I., **Böer, J.**, Roth, A., **Hajnsek, I.**, Schättler, B., **Maier, M.**, **Bachmann, M.**, **Rizzoli, P.**, **Busche, T.**, Eger, C., TerraSAR-X/TanDEM-X Projektstatusbericht 3. Quartal 2017, Technical Note, 70 pages, TX-GS-2017-03, 2017.

[R-15] **Buckreuß, S.**, **Zink, M.**, Maurer, E., Schork, I., **Schulze, D.**, Roth, A., **Hajnsek, I.**, Schättler, B., **Maier, M.**, **Bachmann, M.**, **Rizzoli, P.**, **Busche, T.**, Eger, C., TerraSAR-X/TanDEM-X Projektstatusbericht 2. Quartal 2017, Technical Note, 65 pages, TX-GS-2017-02, 2017.

[R-16] **Buckreuß, S.**, **Zink, M.**, Maurer, E., Schork, I., **Schulze, D.**, Roth, A., **Hajnsek, I.**, Schättler, B., **Maier, M.**, **Bachmann, M.**, **Rizzoli, P.**, **Busche, T.**, Eger, C., TerraSAR-X/TanDEM-X Projektstatusbericht 1. Quartal 2017, Technical Note, 63 pages, TX-GS-2017-01, 2017.

[R-17] **Buckreuß, S.**, **Zink, M.**, Maurer, E., Schork, I., **Schulze, D.**, Roth, A., **Hajnsek, I.**, Schättler, B., **Maier, M.**, **Bachmann, M.**, **Rizzoli, P.**, TerraSAR-X/TanDEM-X Projektstatusbericht 4. Quartal 2016, Technical Note, 72 pages, TX-GS-2016-04, 2017.

[R-18] **Dietrich, B.**, **Iff, S.**, **Profelt, J.**, **Albers, T.**, **Blaschke, K.**, LOCASS Machbarkeitsstudie - Endbericht, Technical Note, 2017.

[R-19] **Fink, A.**, Estimation of Vegetation Water Content from Vegetation Optical Depth, Technical Note, 27 pages, 2017.

[R-20] **Fluhrer, A.**, Remote Sensing Based on Combination of Active and Passive Microwaves for Estimation of Vegetation and Soil Parameters, Technical Note, 27 pages, 2017.

[R-21] **Grigorov, C.**, **Bachmann, M.**, **Borla Tridon, D.**, **Böer, J.**, **Rizzoli, P.**, **Steinbrecher, U.**, Tandem-L IOCS System Requirements, Technical Note, 44 pages, TDL-IOCS-RS-0001, 2017.

[R-22] **Grigorov, C.**, **Schulze, D.**, Balzer, W., Lachaise, M., Matthias, D., Wörle, M., Maurer, E., Kahle, R., Schulze, D., Gnat, M., Tandem-L Ground Segment Functional Architecture, Technical Note, 25 pages, TDL-GS-TN-0001, 2017.

[R-23] **Grigorov, C.**, **Bachmann, M.**, **Borla Tridon, D.**, **Böer, J.**, **Reimann, J.**, **Rizzoli, P.**, **Steinbrecher, U.**, Tandem-L IOCS Functional Decomposition, Technical Note, 31 pages, TDL-IOCS-TN-0001, 2017.

[R-24] **Horn, R.**, **Geßwein, D.**, **Fischer, J.**, **Keller, M.**, **Jäger, M.**, **Scheiber, R.**, ATRSAR Airborne Campaign 2017 – Final Report, Technical Note, 41 pages, DLR-HR-ATRSAR-TR-002, 2017.

[R-25] **Horn, R.**, **Geßwein, D.**, **Fischer, J.**, **Keller, M.**, **Jäger, M.**, **Scheiber, R.**, ATRSAR Airborne Campaign 2017 – Data Acquisition Report, Technical Note, 21 pages, DLR-HR-ATRSAR-TR-001, 2017.

[R-26] **Jirousek, M.**, Hardware Inspection Report, Technical Note, 13 pages, RCM-DLR-PA-09_1, 2017.

[R-27] **Maier, M.**, Tandem-L GS Documentation and Information Management Plan, TDL-GS-PL-0008, Technical Note, 24 pages, 2017.

[R-28] **Maier, M.**, Tandem-L Ground Segment Product Assurance Plan, TDL-GS-PL-0009, Technical Note, 26 pages, 2017.

[R-29] **Maier, M.**, Tandem-L Ground Segment Risk Management Plan, TDL-GS-PL-0010, Technical Note, 19 pages, 2017.

[R-30] Mittermayer, J., **Zonno, M.**, **Krieger, G.**, **Huber, S.**, Breit, H., Earth-CON SAR Mission Concepts, Technical Note, ECON-DLR-TN-0002, 2017.

[R-31] Mittermayer, J., **del Castillo, J.**, **Queiroz de Almeida, F.**, **Villano, M.**, **Krieger, G.**, **Younis, M.**, HRWS Innovative SAR Systems and Techniques, Technical Note, HRWS-DLR-TN-0028, 2017.

[R-32] Pinheiro, M., Multi-Mode SAR Interferometry for High-Precision DEM Generation, DLR Forschungsbericht, 232 pages, DLR-FB-2017-2, 2017.

[R-33] Ponce Madrigal, O., Multicircular Holographic SAR Tomography over Forested Areas, DLR Forschungsbericht, 162 pages, DLR-FB-2016-59, 2017.

[R-34] Raab, S., **Döring, B.**, **Rudolf, D.**, Transponder Maintenance Manual, Technical Note, 13 pages, RCM-DLR-OPS-7_2, 2017.

[R-35] Raab, S., **Rudolf, D.**, **Weidenhaupt, K.**, Training Course Material, Technical Note, 32 pages, RCM-DLR-OPS-5_1, 2017.

[R-36] Reimann, J., **Klenk, P.**, **Schwerdt, M.**, Tandem-L: Overall SAR System Calibration Concept, Technical Note, 48 pages, 2017.

[R-37] Reimann, J., **Klenk, P.**, **Schwerdt, M.**, Tandem-L: Definition of Calibration Terms, Technical Note, 2017.

[R-38] Bölicke, A., **Rommel, T.**, Krstic, M., Boccia, L., Ho, A., Gao, S., Penkala, P., Quarterly Management Report EU Project DIFFERENT Q1-2017, Technical Note, 2017.

[R-39] Rudolf, D., Verification and Compliance Matrix, Technical Note, 7 pages, RCM-DLR-PA-8_1, 2017.

[R-40] Rudolf, D., End Item Data Package, Technical Note, 47 pages, RCM-DLR-PA-8_2, 2017.

[R-41] Rudolf, D., Technical Review Presentation: Delta-OSAT, Technical Note, 33 pages, RCM-DLR-PM-7-0007_1, 2017.

[R-42] Rudolf, D., **Böer, J.**, **Jirousek, M.**, **Raab, S.**, **Weidenhaupt, K.**, Test Report, Technical Note, 128 pages, RCM-DLR-EN-15_2.1, 2017.

[R-43] Rudolf, D., On-Site Acceptance Test Report, Technical Note, 51 pages, RCM-DLR-EN-19_3, 2017.

[R-44] Rudolf, D., Technical Review Presentation: OSAT, Technical Note, 43 pages, RCM-DLR-PM-7-0006_1, 2017.

[R-45] Rudolf, D., **Döring, B.**, Factory Acceptance Test Report, Technical Note, 34 pages, RCM-DLR-EN-17_1, 2017.

[R-46] Rudolf, D., **Döring, B.**, Technical Review Plan: OSAT, Technical Note, 13 pages, RCM-DLR-PM-6-0004_1, 2017.

[R-47] Schmidt, K., **Tous Ramon, N.**, **Klenk, P.**, **Schwerdt, M.**, DLR Calibration Support for Routine Operation of S-1A/B Constellation, Technical Note, 53 pages, S1-RP-DLR-0004, 2017.

[R-48] Schwerdt, M., **Tous Ramon, N.**, **Schmidt, K.**, **Klenk, P.**, Overall SAR System Calibration and Validation Plan (Sentinel-1C/D Cal/Val Plan), Technical Note, 109 pages, S1CD-PL-DLR-SY03-0001, Issue 1.2, 2017.

[R-49] Schwerdt, M., Kalibri – Next Generation – Fortschrittsbericht: 3. Quartal 2017, Technical Note, 3 pages, 2017.

[R-50] Schwerdt, M., SAR System Calibration Performance Analysis and Budgets (Sentinel-1C/D), Technical Note, 16 pages, S1CD-TN-DLR-SY05-0001, Issue 1.1, 2017.

[R-51] Schwerdt, M., SAR System Calibration Performance Analysis and Budgets (Sentinel-1C/D), *Published in Project Report*, Technical Note, 16 pages, S1CD-TN-DLR-SY05-0001, Issue 1.0, 2017.

[R-52] Schwerdt, M., **Tous Ramon, N.**, **Schmidt, K.**, **Klenk, P.**, Overall SAR System Calibration and Validation Plan (Sentinel-1C/D Cal/Val Plan), Technical Note, 108 pages, S1CD-PL-DLR-SY03-0001, Issue 1.0, 2017.

[R-53] Schwerdt, M., Kalibri – Next Generation – Fortschrittsbericht: 1. Quartal 2017, Technical Note, 2 pages, 2017.

[R-54] Tous Ramon, N., **Schwerdt, M.**, SAR Calibration Algorithms (Sentinel-1C/D), Technical Note, 86 pages, S1CD-DD-DLR-SY04-0001, Issue 1.1, 2017.

[R-55] Tous Ramon, N., Version Description Document, Technical Note, 48 pages, RCM-DLR-EN-12_2.2, 2017.

[R-56] Tous Ramon, N., **Schwerdt, M.**, SAR Calibration Algorithms (Sentinel-1C/D), Technical Note, 82 pages, S1CD-DD-DLR-SY04-0001, Issue 1.0, 2017.

[R-57] Weidenhaupt, K., **Rudolf, D.**, Technical Review Plan: Delta-OSAT, Technical Note, 13 pages, RCM-DLR-PM-6-0005_1, 2017.

[R-58] Weidenhaupt, K., **Rudolf, D.**, Transponder's User Manual, Technical Note, 61 pages, RCM-DLR-OPS-6_2.2, 2017.

[R-59] Wollstadt, S., HRWS Phase 0/A Misson Analysis - Bedarfsanalyse Verfahrensbezogene Wissenschaft, Technical Note, 34 pages, OSCMS-SYS-OHB-RP-0008, 2017.

2016

[R-60] Bachmann, M., Antenna Pattern Modeling and Calibration for Spaceborne SAR Systems, DLR Forschungsbericht, 227 pages, DLR-FB-2016-36, 2016.

[R-61] Baumgartner, S., Moving Point Target Raw Data Simulator with SAR / ISAR Focusing Module - Expansion Stage 1, Technical Note, 37 pages, D45521899-234-0010 Issue 0.3, 2016.

[R-62] Baumgartner, S., Study of Multi-Channel Ka-Band SARs for Moving Target Indication - Final Report, Technical Note, 57 pages, D7-4000105042 Issue 1.0, ESTEC Contract No. 4000105042, 2016.

[R-63] Baumgartner, S., Study of Multi-Channel Ka-Band SARs for Moving Target Indication - Executive Summary Report, Technical Note, 13 pages, D6-4000105042 Issue 1.0, ESTEC Contract No. 4000105042, 2016.

[R-64] Baumgartner, S., **Que, R.**, **Barros Cardoso da Silva, A.**, VABENE++ Meilensteinbericht MST 3304: Der kombinierte „A Priori Knowledge-Based STAP Verkehrsprozessor" läuft auf dem Onboard-Prozessor und ist präoperationell einsetzbar, Technical Note, 8 pages, DLR VABENE++ Meilensteinbericht MST3304_2016Q3, 2016.

[R-65] Baumgartner, S., Völker, M., Study of Multi-Channel Ka-Band SARs for Moving Target Indication - MTI-SAR: Technology Roadmap and Way Forward, Technical Note, 29 pages, D5-4000105042 Issue 1.1, ESTEC Contract No. 4000105042, 2016.

[R-66] Baumgartner, S., **Barros Cardoso da Silva, A.**, **Que, R.**, VABENE++ Meilensteinbericht MST 3303: Der STAP Verkehrsprozessor läuft auf dem Onboard-Prozessor und ist präoperationell einsetzbar, Technical Note, 7 pages, DLR VABENE++ Meilensteinbericht MST3303_2015Q4, 2016.

[R-67] Baumgartner, S., Völker, M., Study of Multi-Channel Ka-Band SARs for Moving Target Indication - MTI-SAR: Detailed Instrument Definition and Performance Assessment, Technical Note, 59 pages, D4-4000105042-Issue Draft, ESTEC Contract No. 4000105042, 2016.

[R-68] Baur, M., Active-Passive Microwave Covariability for Different Land Cover Types, Technical Note, 16 pages, 2016.

[R-69] **Bojarski, A.**, **Bachmann, M.**, Long-Term System Monitoring Tool User Manual and Functional Description, Technical Note, 37 pages, TX-IOCS-UM-4645, 2016.

[R-70] **Bojarski, A.**, **Bachmann, M.**, **Böer, J.**, **Rizzoli, P.**, **Castellanos Alfonzo, G.**, **Martone, M.**, **Tous Ramon, N.**, **Schmidt, K.**, **Schulze, D.**, **Schwerdt, M.**, **Walter Antony, J.**, **Wecklich, C.**, Long-Term System Monitoring Report Q1/2016, Technical Note, 172 pages, TX-SEC-RP-4660, 2016.

[R-71] **Bordoni, F.**, **Prats Iraola, P.**, Adamiuk, G., HRWS SAR System Capabilities Analysis, Issue 2, Technical Note, 61 pages, HRWS_APPS-D1 v2, 2016.

[R-72] **Borla Tridon, D.**, **Bachmann, M.**, Observation Concept, Technical Note, 27 pages, TL-SE-TN-0004, 2016.

[R-73] **Buckreuß, S.**, **Zink, M.**, Maurer, E., Schork, I., **Schulze, D.**, Roth, A., **Hajnsek, I.**, Schättler, B., **Maier, M.**, **Bachmann, M.**, **Rizzoli, P.**, TerraSAR-X/TanDEM-X Projektstatusbericht 3. Quartal 2016, Technical Note, 73 pages, TX-GS-2016-03, 2016.

[R-74] **Buckreuß, S.**, **Zink, M.**, Maurer, E., Schork, I., **Schulze, D.**, Roth, A., **Hajnsek, I.**, Schättler, B., **Maier, M.**, TerraSAR-X/TanDEM-X Projektstatusbericht 2. Quartal 2016, Technical Note, 73 pages, TX-GS-2016-02, 2016.

[R-75] **Buckreuß, S.**, **Zink, M.**, Maurer, E., Schork, I., **Schulze, D.**, Roth, A., **Hajnsek, I.**, Schättler, B., **Maier, M.**, TerraSAR-X/TanDEM-X Projektstatusbericht 1. Quartal 2016, Technical Note, 69 pages, TX-GS-2016-01, 2016.

[R-76] **Buckreuß, S.**, **Zink, M.**, Maurer, E., Pengler, I., **Schulze, D.**, Roth, A., **Hajnsek, I.**, Schättler, B., **Maier, M.**, TerraSAR-X/TanDEM-X Projektstatusbericht 4. Quartal 2015, Technical Note, 73 pages, TX-GS-2015-04, 2016.

[R-77] **Buckreuß, S.**, Erfolgskontrollbericht zum Vorhaben "Betrieb des Satelliten TerraSAR-X" vom 01.01.2013 bis 31.12.2015 (6.-8. Betriebsjahr), Technical Note, 3 pages, TD-GS-RP-0200, 2016.

[R-78] **Buckreuß, S.**, Schlussbericht Betrieb des Satelliten TerraSAR-X vom 01.01.2013 bis 31.12.2015 (6.-8. Betriebsjahr), Technical Note, 65 pages, TD-GS-RP-0199, 2016.

[R-79] **Börner, T.**, **Sanjuan Ferrer, M.**, **Borla Tridon, D.**, Völker, M., High-Resolution Wide-Swath SAR Applications Study – Analysis of Impact of HRWS SAR Instrument at System and Operation, Technical Note, 29 pages, D4-4000109920, 2016.

[R-80] **Dahme, C.**, **Börner, T.**, **Fischer, J.**, **Hager, M.**, Maier, MSE, M., **Posovszky, P.**, **Schulze, D.**, IKT-Konzept 2016, *Published in DLR IKT-Konzept*, Technical Note, 33 pages, DLR QMH_HR-UP_5_0_1, 2016.

[R-81] **Döring, B.**, RCM Transponder: Engineering Change Notice 1, Technical Note, RCM-DLR-PA-7-0001_v1, 2016.

[R-82] **Döring, B.**, RCM Transponder: Master Project Schedule, Technical Note, RCM-DLR-PM-2_v3, 2016.

[R-83] **Döring, B.**, RCM Transponder: Storage, Transport, and Handling Procedures, Technical Note, 16 pages, RCM-DLR-PA-6_v2, 2016.

[R-84] **Döring, B.**, RCM Transponder: Technical Review Plan -- FAT, Technical Note, RCM-DLR-PM-6-0003_v1, 2016.

[R-85] **Döring, B.**, Test Procedure, Technical Note, 40 pages, RCM-DLR-EN-14_v3, 2016.

[R-86] **Döring, B.**, **Böer, J.**, **Jirousek, M.**, **Raab, S.**, **Rudolf, D.**, **Weidenhaupt, K.**, RCM Transponder: Test Report, Technical Note, 131 pages, RCM-DLR-EN-15_v1, 2016.

[R-87] **Döring, B.**, **Böer, J.**, **Rudolf, D.**, **Raab, S.**, RCM Transponder: Video Documentation, Technical Note, RCM-DLR-EN-10-0005_v1, 2016.

[R-88] **Döring, B.**, **Rudolf, D.**, RCM Transponder: Transponder Maintenance Manual, Technical Note, RCM-DLR-OPS-7_v1, 2016.

[R-89] **Döring, B.**, **Rudolf, D.**, **Weigt, M.**, **Jirousek, M.**, **Raab, S.**, System Design Document, Technical Note, 185 pages, RCM-DLR-EN-6_v4, 2016.

[R-90] **Döring, B.**, Traceable Radiometric Calibration of Synthetic Aperture Radars, DLR Forschungsbericht, 200 pages, DLR-FB-2016-13, 2016.

[R-91] **Fischer, J.**, Simbach am Inn Flooding Disaster June 2016 - Digital Elevation Model, Technical Note, 3 pages, DLR-HR-STE-Simbach-DEM-2016-06-14-v1.02, 2016.

[R-92] **Kraus, T.**, Impact of TDX-1 Roll Steering on SAR Performance during TDM HDEM Phase, Technical Note, 24 pages, TD-SEC-TN-4282, 2016.

[R-93] **Kugler, F.**, Pol-InSAR Forest Height Estimation at Different Frequencies: Opportunities and Limitations, DLR Forschungsbericht, 154 pages, DLR-FB-2016-43, 2016.

[R-94] **Link, M.**, Auswertung von Modelldaten zur Simulation von aktiven und passiven Mikrowellen, Technical Note, 39 pages, 2016.

[R-95] **Nottensteiner, A.**, **Baumgartner, S.**, VABENE++ Meilensteinbericht MST2503 und MST2505: Labortests von Radar- und Digitalelektronik abgeschlossen und Fertigstellung Radarhardware X-Band und Digital-Rack, Technical Note, 12 pages, DLR VABENE++ Meilensteinbericht MST2503_MST2505_2016Q2, 2016.

[R-96] **Parrella, G.**, Characterization of Glacier Facies Using SAR Polarimetry at Long Wavelengths, DLR Forschungsbericht, 166 pages, DLR-FB-2016-05, 2016.

[R-97] **Prats Iraola, P.**, **Nannini, M.**, **Rodríguez Cassolà, M.**, SAOCOM/CS Study: Preliminary Definition of Processing Algorithms up to Level 1c, Technical Note, 33 pages, SAO-ST-RS-0009_1, 2016.

[R-98] **Raab, S.**, RCM Transponder: Installation Plan, Technical Note, 21 pages, RCM-DLR-EN-9_v3, 2016.

[R-99] **Reimann, J.**, **Schwerdt, M.**, TDX Phase Imbalance, Technical Note, TDX-IOCS-TN-4354, 2016.

[R-100] **Reimann, J.**, **Schwerdt, M.**, Tandem-L Calibration Approach, Technical Note, 33 pages, TDL-SE-TN-0002, 2016.

[R-101] **Rodríguez Cassolà, M.**, Breit, H., **Nannini, M.**, **Prats Iraola, P.**, SAOCOM/CS Study: Pre-Existing Elements for Re-Use in CS PDGS, Technical Note, 19 pages, SAO-ST-RS-0012_1, 2016.

[R-102] **Rodríguez Cassolà, M.**, **Nannini, M.**, **Prats Iraola, P.**, SAOCOM/CS Study: CS Calibration Needs and Strategy for On Ground Data Processing, Technical Note, 15 pages, SAO-ST-RS-0010_1, 2016.

[R-103] **Rodríguez Cassolà, M.**, **Nannini, M.**, **Prats Iraola, P.**, SAOCOM/CS Study: Preliminary Definition of Calibration Algorithms, Technical Note, 31 pages, SAO-ST-RS-0011_1, 2016.

[R-104] Bölicke, A., **Rommel, T.**, Krstic, M., Boccia, L., Ho, A., Gao, S., Penkala, P., Quarterly Management Report 3-2016 EU Project DIFFERENT, Technical Note, 26 pages, 606923_QMR-Q3-2016, 2016.

[R-105] Bölicke, A., **Rommel, T.**, Krstic, M., Boccia, L., Ho, A., Gao, S., Penkala, P., Quarterly Management Report 2-2016 EU Project DIFFERENT, Technical Note, 35 pages, 606923_QMR-Q2-2016, 2016.

[R-106] Bölicke, A., **Rommel, T.**, Krstic, M., Boccia, L., Ho, A., Gao, S., Penkala, P., Quarterly Management Report 1-2016 EU Project DIFFERENT, Technical Note, 53 pages, 606923_QMR-Q1-2016, 2016.

[R-107] **Ruess, T.**, Mitwirkung beim Design und Aufbau eines Radiometer-Radar-Kombi-Abbildungssystems für sicherheitsrelevante Mikrowellenabbildungen, Technical Note, 35 pages, 2016.

[R-108] **Sanjuan Ferrer, M.**, **López-Dekker, F.**, **Hajnsek, I.**, **Younis, M.**, **Bordoni, F.**, **Prats Iraola, P.**, Adamiuk, G., **Zonno, M.**, Hanssen, R., van Leijen, F., Skriver, H., Danielson, R., Nagler, T., Rott, H., Pedersen, L., Lang, O., **Borla Tridon, D.**, **Börner, T.**, High-Resolution Wide-Swath SAR Applications Study – Final Report: Conclusions and Recommendations, Technical Note, 36 pages, D5-4000109920, 2016.

[R-109] **Sanjuan Ferrer, M.**, **Zonno, M.**, **López-Dekker, F.**, van Leijen, F., Hanssen, R., Rott, H., Nagler, T., Lang, O., Danielson, R., Skriver, H., Pedersen, L., High-Resolution Wide-Swath SAR Applications Study – Applications Performance Algorithm-Definition and Performance-Analysis, Technical Note, 96 pages, D3-4000109920, 2016.

[R-110] **Schmidt, K.**, **Tous Ramon, N.**, **Schwerdt, M.**, DLR Calibration Support for S-1A Routine Operation: Calibration Report, Technical Note, 53 pages, S1-RP-DLR-0003, 2016.

[R-111] **Schmidt, K.**, **Castellanos Alfonzo, G.**, **Tous Ramon, N.**, **Yague-Martinez, N.**, **Klenk, P.**, **Schwerdt, M.**, **Prats Iraola, P.**, Sentinel-1B: Calibration Report, Technical Note, 123 pages, S1-TN-DLR-0007, Issue 1.0, 2016.

[R-112] **Schmidt, K.**, **Tous Ramon, N.**, **Castellanos Alfonzo, G.**, **Schwerdt, M.**, DLR Calibration Support for S-1A Routine Operation: Calibration Report, Technical Note, 48 pages, S1-RP-DLR-0003, 2016.

[R-113] **Schmidt, K.**, **Castellanos Alfonzo, G.**, **Tous Ramon, N.**, **Prats Iraola, P.**, Sentinel-1B: In-Orbit Commissioning Preparation, Technical Note, 141 pages, S1-TN-DLR-0006, Issue 1.0, 2016.

[R-114] **Schmidt, K.**, **Castellanos Alfonzo, G.**, **Tous Ramon, N.**, **Prats Iraola, P.**, Sentinel-1B: Pre-Launch Tools Description and Preparation, Technical Note, 48 pages, S1-TN-DLR-0005, Issue 1.0, 2016.

[R-115] **Schmidt, K.**, **Schwerdt, M.**, **Bräutigam, B.**, PAZ: External Calibration Tool. Verification and Validation Test Report, Technical Note, 24 pages, PZ-DLR-TR-1130, 2016.

[R-116] **Schreiber, E.**, **Jirousek, M.**, HALO Altimeter Radar: S-Parametermessungen der Anpassung und Durchgangsdämpfung der HALO Altimeterantennen und Verbindungskabel, Technical Note, 16 pages, DLR-HR-AKS-03-2016-ALTIMETER-HALO, 2016.

[R-117] **Schreiber, E.**, Interferenzmessungen im Bereich Robotik - Techlab, Technical Note, DLR-HR-AKS-01-2016-RFI-RM-Techlab, 2016.

[R-118] **Schulze, D.**, Diedrich, E., Maurer, E., Schulze, D., **Bachmann, M.**, **Steinbrecher, U.**, **Zink, M.**, Kahle, R., Kröger, S., Wörle, M., Molch, K., Wolfmüller, M., Figwer, F., Fritz, T., De Zan, F., Tandem-L Ground Segment Phase A Executive Summary, Technical Note, 30 pages, TDL-MD-RP-0001, 2016.

[R-119] **Schwerdt, M.**, **Schmidt, K.**, **Tous Ramon, N.**, **Klenk, P.**, **Yague-Martinez, N.**, **Prats Iraola, P.**, Sentinel-1B: Final Report, Technical Note, 134 pages, S1-RP-DLR-0003, Issue 1.0, 2016.

[R-120] **Schwerdt, M.**, Großinvestition Kalibri – Next Generation – Umsetzungsplan, Technical Note, 52 pages, 2016.

[R-121] **Schwerdt, M.**, Sentinel-1B: Contractor Calibration Campaign Plan, Technical Note, 19 pages, S1-PL-DLR-0002, Issue 1.1, 2016.

[R-122] **Schwerdt, M.**, Sentinel-1B: Contractor Calibration Campaign Plan, *Published in Project Report*, Technical Note, 17 pages, S1-PL-DLR-0002, Issue 1.0, 2016.

[R-123] **Toraño Caicoya, A.**, Allometric Estimation of Aboveground Forest Biomass Using Forest Structure Parameters Estimated by Means of Multibaseline SAR Measurements, DLR Forschungsbericht, DLR-FB-2016-39, 2016.

[R-124] **Tous Ramon, N.**, **Döring, B.**, RCM Transponder: Version Description Document, Technical Note, RCM-DLR-EN-12_v1, 2016.

[R-125] **Villano, M.**, Staggered Synthetic Aperture Radar, DLR Forschungsbericht, 181 pages, DLR-FB-2016-16, 2016.

[R-126] **Wecklich, C.**, TanDEM-X Voids Coverage Evaluation, Technical Note, 21 pages, TD-GS-TN-4014, 2016.

[R-127] **Weidenhaupt, K.**, **Döring, B.**, RCM Transponder: Transponder User Manual, Technical Note, RCM-DLR-OPS-6_v1, 2016.

[R-128] **Yelahanka Nagaraja, S.**, Multi-Dimensional SAR Data Visualization and Interpretation, Technical Note, 23 pages, DLR, 2016.

2015

[R-129] **Anglberger, H.**, Simulation und Analyse von SAR-Signaturen mit hoher Auflösung, DLR Forschungsbericht, DLR-FB-2015-30, 2015.

[R-130] **Baumgartner, S.**, **Que, R.**, **Ponce Madrigal, O.**, **Scheiber, R.**, VABENE++ Verkehrsmanagement bei Katastrophen und Großereignissen - Meilensteinbericht MST 3302 TP3000 - A Priori Knowledge-based Mehrkanal-Verkehrsprozessor läuft präoperationell auf dem Onboard-Prozessor, Technical Note, 7 pages, 2015.

[R-131] **Baumgartner, S.**, **Bordoni, F.**, **Ponce Madrigal, O.**, **Di Maria, A.**, **Scheiber, R.**, Eignungsuntersuchung von solarbetriebenen Stratosphären-Leichtflugzeugen für geo- bzw. topografische (Vermessungs-) Missionen und zur Stratosphären-Flugmessdatensammlung auf Basis des Demonstrators Zephyr: Teilbericht zur Eignung von Radarsystemen, Technical Note, 74 pages, RT-TN-0012, 2015.

[R-132] **Brand, B.**, Dietrich, A., **Eilers, J.**, **Neff, T.**, Ingenieurtechnisches Controlling von aktuellen Aufklärungssystemen, Technical Note, 27 pages, DLR-AS-AB-22, 2015.

[R-133] **Buckreuß, S.**, **Zink, M.**, Maurer, E., Pengler, I., **Schulze, D.**, Roth, A., **Hajnsek, I.**, Schättler, B., **Maier, M.**, TerraSAR-X/TanDEM-X Projektstatusbericht 3. Quartal 2015, Technical Note, 71 pages, TX-GS-2015-03, 2015.

[R-134] **Buckreuß, S.**, **Zink, M.**, Maurer, E., Pengler, I., **Schulze, D.**, Roth, A., **Hajnsek, I.**, Schättler, B., **Maier, M.**, TerraSAR-X/TanDEM-X Projektstatusbericht 2. Quartal 2015, Technical Note, 68 pages, TX-GS-2015-02, 2015.

[R-135] **Buckreuß, S.**, **Zink, M.**, Maurer, E., Pengler, I., **Schulze, D.**, Roth, A., **Hajnsek, I.**, Schättler, B., **Maier, M.**, TerraSAR-X/TanDEM-X Projektstatusbericht 1. Quartal 2015, Technical Note, 70 pages, TX-GS-2015-01, 2015.

[R-136] **Buckreuß, S.**, **Zink, M.**, Maurer, E., Pengler, I., **Schulze, D.**, Roth, A., **Hajnsek, I.**, Preuß, D., Schättler, B., **Maier, M.**, TerraSAR-X/TanDEM-X Projektstatusbericht 4. Quartal 2014, Technical Note, 71 pages, TX-GS-2014-04, 2015.

[R-137] **Bueso Bello, J.**, Characterization of TanDEM-X Quad Polarization Products, Technical Note, 72 pages, TD-SEC-TN-4280, 2015.

[R-138] **Börner, T.**, MAC-SAR: Executive Summary, Technical Note, 12 pages, D4-4000104960, 2015.

[R-139] **Döring, B.**, Product Tree, Technical Note, 19 pages, RCM-DLR-EN-2_4, 2015.

[R-140] **Döring, B.**, Test Procedure, Technical Note, 40 pages, RCM-DLR-EN-14_2, 2015.

[R-141] **Döring, B.**, **Rudolf, D.**, **Weigt, M.**, **Jirousek, M.**, **Raab, S.**, System Design Document, Technical Note, 187 pages, RCM-DLR-EN-6_3, 2015.

[R-142] **Döring, B.**, **Weigt, M.**, **Jirousek, M.**, **Raab, S.**, Verification, Validation, and Test Plan, Technical Note, 81 pages, RCM-DLR-EN-8_3, 2015.

[R-143] **Döring, B.**, Documentation Tree, Technical Note, 12 pages, RCM-DLR-EN-3_3, 2015.

[R-144] **Döring, B.**, Drawing Tree, Technical Note, 8 pages, RCM-DLR-EN-4_3, 2015.

[R-145] **Döring, B.**, FAT Procedure, Technical Note, 20 pages, RCM-DLR-EN-16_1, 2015.

[R-146] **Döring, B.**, OSAT Procedure, Technical Note, 15 pages, RCM-DLR-EN-18_1, 2015.

[R-147] **Döring, B.**, Product Tree, Technical Note, 11 pages, RCM-DLR-EN-2_3, 2015.

[R-148] **Döring, B.**, Project Management Plan, Technical Note, 28 pages, RCM-DLR-PM-1_3, 2015.

[R-149] **Döring, B.**, Storage, Transport and Handling Procedures, Technical Note, 16 pages, RCM-DLR-PA-6_1, 2015.

[R-150] **Döring, B.**, System Maintenance Concept, Technical Note, 15 pages, RCM-DLR-OPS-2_4, 2015.

[R-151] **Döring, B.**, Technical Review Plan – CDR, Technical Note, 14 pages, RCM-DLR-PM-6-0002_1, 2015.

[R-152] **Döring, B.**, The Three-Linearly-Polarized-Antenna Method for Determining the Directions of Polarization, Technical Note, 15 pages, RCM-DLR-EN-10-0004_1, 2015.

[R-153] **Döring, B.**, Training Plan, Technical Note, 14 pages, RCM-DLR-OPS-3_1, 2015.

[R-154] **Döring, B.**, Training Plan, Technical Note, 14 pages, RCM-DLR-OPS-3_2, 2015.

[R-155] **Döring, B.**, Training Plan, Technical Note, 14 pages, RCM-DLR-OPS-3_3, 2015.

[R-156] **Döring, B.**, **Weigt, M.**, **Jirousek, M.**, **Raab, S.**, System Requirements Specification, Technical Note, 67 pages, RCM-DLR-EN-1_3, 2015.

[R-157] **Döring, B.**, **Weigt, M.**, **Jirousek, M.**, **Raab, S.**, Verification, Validation, and Test Plan, Technical Note, 81 pages, RCM-DLR-EN-8_2, 2015.

[R-158] **Döring, B.**, Circuit Diagram for Outdoor Unit, Technical Note, 4 pages, RCM-DLR-EN-13-0001_1, 2015.

[R-159] **Döring, B.**, Comments on MDA ICD, Technical Note, 13 pages, RCM-DLR-TN-0003_1, 2015.

[R-160] **Döring, B.**, Crown Assets List, Technical Note, 6 pages, RCM-DLR-PM-11_1, 2015.

[R-161] **Döring, B.**, Documentation Tree, Technical Note, 10 pages, RCM-DLR-EN-3_2, 2015.

[R-162] **Döring, B.**, Drawing Tree, Technical Note, 8 pages, RCM-DLR-EN-4_2, 2015.

[R-163] **Döring, B.**, Product Tree, Technical Note, 10 pages, RCM-DLR-EN-2_2, 2015.

[R-164] **Döring, B.**, Project Management Plan, Technical Note, 27 pages, RCM-DLR-PM-1_2, 2015.

[R-165] **Döring, B.**, System Maintenance Concept, Technical Note, 17 pages, RCM-DLR-OPS-2_2, 2015.

[R-166] **Döring, B.**, Technical Review Plan – PDR, Technical Note, 14 pages, RCM-DLR-PM-6-0001_1, 2015.

[R-167] **Döring, B.**, Transponder System Dropbox Interface, Technical Note, 14 pages, RCM-DLR-EN-10-0001_1, 2015.

[R-168] **Döring, B.**, **Rudolf, D.**, **Weigt, M.**, **Jirousek, M.**, **Raab, S.**, System Design Document, Technical Note, 122 pages, RCM-DLR-EN-6_1, 2015.

[R-169] **Döring, B.**, Master Project Schedule, Technical Note, 1 pages, RCM-DLR-PM-2_1, 2015.

[R-170] **Döring, B.**, BIP/FIP Report, Technical Note, 13 pages, RCM-DLR-PM-12_1, 2015.

[R-171] **Döring, B.**, Documentation Tree, Technical Note, 8 pages, RCM-DLR-EN-3_1, 2015.

[R-172] **Döring, B.**, Drawing Tree, Technical Note, 6 pages, RCM-DLR-EN-4_1, 2015.

[R-173] **Döring, B.**, Product Tree, Technical Note, 10 pages, RCM-DLR-EN-2_1, 2015.

[R-174] **Döring, B.**, System Maintenance Concept, Technical Note, 15 pages, RCM-DLR-OPS-2_3, 2015.

[R-175] **Döring, B.**, **Weigt, M.**, **Jirousek, M.**, **Raab, S.**, Verification, Validation, and Test Plan, Technical Note, 74 pages, RCM-DLR-EN-8_1, 2015.

[R-176] **Döring, B.**, System Maintenance Concept, Technical Note, 16 pages, RCM-DLR-OPS-2_1, 2015.

[R-177] **Döring, B.**, Technical Review Plan, Technical Note, 13 pages, RCM-DLR-PM-6-SRR_1, 2015.

[R-178] **Döring, B.**, **Weigt, M.**, **Jirousek, M.**, **Raab, S.**, System Requirements Specification, Technical Note, 68 pages, RCM-DLR-EN-1_1, 2015.

[R-179] **Döring, B.**, **Weigt, M.**, **Jirousek, M.**, **Raab, S.**, System Requirements Specification, Technical Note, 67 pages, RCM-DLR-EN-1_2, 2015.

[R-180] **Eilers, J.**, **Neff, T.**, **Dietrich, B.**, **Speck, R.**, SAR-Aufklärungssystem Halbjahresbericht 2/2 2015, Technical Note, 10 pages, 2015.

[R-181] **Eilers, J.**, SAR-Aufklärungssystem Projektbericht 0010 2015, Technical Note, 19 pages, 2015.

[R-182] **Eilers, J.**, SAR-Aufklärungssystem Projektbericht 0011 2015, Technical Note, 13 pages, 2015.

[R-183] **Eilers, J.**, SAR-Aufklärungssystem Projektbericht 0006 2015, Technical Note, 2 pages, 2015.

[R-184] **Eilers, J.**, SAR-Aufklärungssystem Projektbericht 0005 2015, Technical Note, 27 pages, 2015.

[R-185] **Eilers, J.**, **Neff, T.**, **Dietrich, B.**, **Speck, R.**, SAR-Aufklärungssystem Halbjahresbericht 1/2 2015, Technical Note, 20 pages, 2015.

[R-186] **Eilers, J.**, SAR-Aufklärungssystem Projektbericht 0002 2015, Technical Note, 11 pages, 2015.

[R-187] **Eilers, J.**, SAR-Aufklärungssystem Projektbericht 0001 2015, Technical Note, 9 pages, 2015.

[R-188] **Eilers, J.**, SAR-Aufklärungssystem Projektbericht 0010 2015, Technical Note, 2015.

[R-189] **Horn, R.**, P2-Band TX Signal Characterization: Laboratory Test Report, Technical Note, 30 pages, TR-FSAR-P2-TX-DLR-2015-A, 2015.

[R-190] **Horn, R.**, The DLR F-SAR Radar System: A Technical Dossier to Obtain Authorisation for Temporary Use of Frequencies in Gabon, Technical Note, 12 pages, DLR-HR-AFRSAR-TR-001, 2015.

[R-191] **Horn, R.**, P2-band TX Signal Characterization: Test Plan for Laboratory Test, Technical Note, 12 pages, TP-FSAR-P2-TX-DLR-2015-A, 2015.

[R-192] **Jirousek, M.**, SAR-Aufklärungssystem Projektbericht 0004 2015, Technical Note, 10 pages, 2015.

[R-193] **Jochim, F.**, SAR-Aufklärungssystem Projektbericht 0007 2015, Technical Note, 11 pages, 2015.

[R-194] **Jochim, F.**, SAR-Aufklärungssystem Projektbericht 0008 2015, Technical Note, 10 pages, 2015.

[R-195] **Jochim, F.**, SAR-Aufklärungssystem Projektbericht 0009 2015, Technical Note, 10 pages, 2015.

[R-196] Huber, K., Loeser, T., Looye, G., Liersch, C., Lindermeir, E., **Kemptner, E.**, Klimmek, T., Koch, S., Kuchar, R., Nauroz, M., Paul, M., Rein, M., **Rode, G.**, Rohlf, D., Rütten, M., Schütte, A., Schwithal, J., Siggel, M., Voss, A., Zimper, D., Bewertung und Entwurf von agilen und hoch-gepfeilten Flugzeugkonfigurationen, DLR Interner Bericht, 120 pages, DLR-IB 124-2015/913, 2015.

[R-197] **Kraus, T.**, Ambiguity Performance Predictions for the TerraSAR-X Quad-Pol Mode, Technical Note, 19 pages, TD-SEC-TN-4281, 2015.

[R-198] **Kraus, T.**, Impact of TDX-1 Roll Steering on SAR Performance during TDM Science Phase, Technical Note, 51 pages, TD-SEC-TN-4274, 2015.

[R-199] **Laux, C.**, Digital Calibration Techniques, Technical Note, 22 pages, 2015.

[R-200] **López-Dekker, F.**, Völker, M., Chapron, B., **Börner, T.**, MAC-SAR: Final Report, Technical Note, 20 pages, D3-4000104960, 2015.

[R-201] **Maier, M.**, Safety Assessment Report, Technical Note, 18 pages, RCM-DLR-PA-4_2, 2015.

[R-202] **Maier, M.**, Quality Assurance Plan, Technical Note, 17 pages, RCM-DLR-PA-1_1.2, 2015.

[R-203] **Maier, M.**, Safety Assessment Report, Technical Note, 18 pages, RCM-DLR-PA-4_1, 2015.

[R-204] **Maier, M.**, Quality Assurance Plan, Technical Note, 17 pages, RCM-DLR-PA-1_1.1, 2015.

[R-205] **Martone, M.**, **Gonzalez, C.**, **Bräutigam, B.**, Duque, S., Fritz, T., Bandwidth Considerations in Range and Azimuth for Interferometric Applications, 43 pages, TD-GS-TN-4279, 2015.

[R-206] **Moreira, A.**, **Hajnsek, I.**, Huth, A., HGF Alliance: Mid-Term Review Report "Remote Sensing and Earth System Dynamics - EDA" Part I: Status Report, Technical Note, 2015.

[R-207] **Moreira, A.**, **Hajnsek, I.**, Huth, A., HGF Alliance: Mid-Term Review Report "Remote Sensing and Earth System Dynamics - EDA" Part II: Perspectives Report, Technical Note, 2015.

[R-208] **Moreira, A.**, **Hajnsek, I.**, Huth, A., HGF Alliance: Mid-Term Review Report "Remote Sensing and Earth System Dynamics - EDA" Part III: Resources, Technical Note, 2015.

[R-209] **Neff, T.**, Dietrich, A., **Peichl, M.**, **Speck, R.**, **Eilers, J.**, Wehrtechnische Forschungsarbeiten des DLR - Forschungsgebiet sicherheitsrelevante Erdbeobachtung Jahresbericht 2014, Technical Note, 31 pages, WTEB 0F263 HR, 2015.

[R-210] Bertolotti, M., Bilotti, F., Herbertz, K., Gonzalo, R., Laou, P., Maci, S., **Osipov, A.**, Ouslimani, H., Ozbay, E., Plaza del Olmo, J., Scafé, S., Meitzler, T., Metamaterials for Defence and Security Applications, Technical Note, 99 pages, STO-TR-SET-181, 2015.

[R-211] **Prats Iraola, P.**, **Nannini, M.**, **Scheiber, R.**, **Yague-Martinez, N.**, De Zan, F., Vecchioli, F., Minati, F., Costantini, M., Walter, T., Diao, F., Nikkhoo, M., Borgstrom, S., de Martino, P., Siniscalchi, V., Wright, T., Hooper, A., Gonzalez, P., INSARAP: Sentinel-1 InSAR Performance Study with TOPS Data, Technical Note, 144 pages, NSARAP-DLR-FR-01_1,1, 2015.

[R-212] **Prats Iraola, P.**, **Nannini, M.**, **Scheiber, R.**, **Yague-Martinez, N.**, Vecchioli, F., Minati, F., Costantini, M., Walter, T., Diao, F., Nikkhoo, M., Borgstrom, S., de Martino, P., Siniscalchi, V., SAR Interferometric Processing with Sentinel-1 TOPS Data and Validation, Technical Note, 116 pages, INSARAP-DLR-TN-05_1, 2015.

[R-213] **Raab, S.**, Development and Implementation of an Efficient Temperature Management System for SAR System Calibration Transponders – Project Documentation, Technical Note, 2015.

[R-214] **Raab, S.**, Installation Plan and Installation Procedure, Technical Note, 18 pages, RCM-DLR-EN-9_2, 2015.

[R-215] **Raab, S.**, Installation Plan and Installation Procedure, Technical Note, 19 pages, RCM-DLR-EN-9_1, 2015.

[R-216] **Rodríguez Cassolà, M.**, **López-Dekker, F.**, **Prats Iraola, P.**, **Nannini, M.**, SAOCOM-CS IN/TOMOSAR PERFORMANCE: Performance Evaluation, Technical Note, 69 pages, DD-02_1, 2015.

[R-217] **Rodríguez Cassolà, M.**, **López-Dekker, F.**, **Prats Iraola, P.**, **Nannini, M.**, SAOCOM-CS IN/TOMOSAR PERFORMANCE: Performance and Error Models, Technical Note, 80 pages, DD-01_2, 2015.

[R-218] **Rodríguez Cassolà, M.**, **López-Dekker, F.**, **Prats Iraola, P.**, **Nannini, M.**, SAOCOM-CS IN/TOMOSAR PERFORMANCE: Calibration Concept and Requirements, Technical Note, 23 pages, DD-03_1, 2015.

[R-219] **Rodríguez Cassolà, M.**, Balzer, W., SAOCOM/CS Study: Requirements on CS FOS, Technical Note, 11 pages, SAO-ST-RS-0002_1, 2015.

[R-220] **Scheiber, R.**, **Jäger, M.**, **Keller, M.**, **Ponce Madrigal, O.**, **Fischer, J.**, **Horn, R.**, Exploration of Possibilities with Advanced SAR Systems in the Arctic Region (DALO-ARCTIC), Technical Note, 88 pages, DLR-HR-DALO-ARCTIC-TR-001, 2015.

[R-221] **Schmidt, K.**, **Tous Ramon, N.**, **Castellanos Alfonzo, G.**, **Schwerdt, M.**, DLR Calibration Support for S-1A Routine Operation: Calibration Report, Technical Note, 43 pages, S1-RP-DLR-0003, 2015.

[R-222] **Schmidt, K.**, **Schwerdt, M.**, **Bräutigam, B.**, PAZ: External Calibration Tool. Verification and Validation Plan, Technical Note, 18 pages, PZ-DLR-PL-1110, 2015.

[R-223] **Schwerdt, M.**, SAOCOM TPM Calibration Needs and Plan for On-Ground Data Processing, *Published in Project Report*, Technical Note, 22 pages, SAO-STL-TN-0024, Issue 1.0, 2015.

[R-224] **Speck, R.**, SAR-Aufklärungssystem Projektbericht 0003 2015, Technical Note, 5 pages, 2015.

[R-225] **Tous Ramon, N.**, **Döring, B.**, RCMT Control System: Requirements Specification, Technical Note, 130 pages, RCM-DLR-EN-1-0001_3, 2015.

[R-226] **Tous Ramon, N.**, **Döring, B.**, RCMT Control System: Requirements Specification, Technical Note, 25 pages, RCM-DLR-EN-1-0001_1, 2015.

[R-227] **Weigt, M.**, Reliability, Maintainability, and Availability Report, Technical Note, 20 pages, RCM-DLR-PA-5_2, 2015.

[R-228] **Weigt, M.**, System Concept of Operations, Technical Note, 21 pages, RCM-DLR-OPS-1_3, 2015.

[R-229] **Weigt, M.**, Reliability, Maintainability, and Availability Report, Technical Note, 14 pages, RCM-DLR-PA-5_1, 2015.

[R-230] **Weigt, M.**, System Concept of Operations, Technical Note, 21 pages, RCM-DLR-OPS-1_2, 2015.

[R-231] **Weigt, M.**, System Concept of Operations, Technical Note, 21 pages, RCM-DLR-OPS-1_1, 2015.

[R-232] Ernst, R., **Wollstadt, S.**, **López-Dekker, F.**, **Younis, M.**, D'Aliesio, G., Ocean Surface Current Mission Study - Final Report, Technical Note, 106 pages, OSCMS-SYS-OHB-RP-0014, 2015.

[R-233] **Wollstadt, S.**, **Younis, M.**, **López-Dekker, F.**, D'Aliesio, G., Ernst, R., Ocean Surface Current Mission Study - Instrument Design, Technical Note, 71 pages, OSCMS-SYS-OHB-RP-0008, 2015.

2014

[R-234] **Al-Kahachi, N.**, Polarimetric SAR Modelling of a Two-Layer Structure: A Case Study Based on Subarctic Lakes, DLR Forschungsbericht, 163 pages, DLR-FB 2014-01, 2014.

[R-235] **Baumgartner, S.**, **Rosigkeit, D.**, VABENE++ Verkehrsmanagement bei Katastrophen und Großereignissen - Meilensteinbericht MST 5701 – Studie zu LTE-Datenlinks abgeschlossen, Technical Note, 83 pages, MST5701_2014Q4, 2014.

[R-236] **Baumgartner, S.**, **Scheiber, R.**, **Que, R.**, **Ponce Madrigal, O.**, **Nottensteiner, A.**, **Horn, R.**, **Di Maria, A.**, **Müller, G.**, **Fischer, J.**, **Jäger, M.**, VABENE++ Verkehrsmanagement bei Katastrophen und Großereignissen – Meilensteinbericht MST 3301 und MST 3401 TP3000 – Schnittstellen zum V-SAR Onboard-Prozessor für die Verkehrsdatenprozessierung und für die SAR-Bild-Prozessierung, Technical Note, 56 pages, MST3301_MST3401_2014Q4, 2014.

[R-237] **Baumgartner, S.**, Traffic Monitoring with Air- and Spaceborne Synthetic Aperture Radar, DLR Forschungsbericht, 242 pages, DLR-FB-2014-28, 2014.

[R-238] **Baumgartner, S.**, **Bertl, S.**, **López-Dekker, F.**, **Laskowski, P.**, Schaefer, C., Klein, R., MTI-SAR: Preliminary System Concepts Definition, Trade-Off and Performance Assessment for Land- and Ocean-Based MTI Applications, Technical Note, 126 pages, ESTEC Contract Number 4000105042, Document No. D2/D3-4000105042-Draft, 2014.

[R-239] **Bordoni, F.**, **Prats Iraola, P.**, Adamiuk, G., HRWS SAR System Capabilities Analysis, Technical Note, 2014.

[R-240] **Bordoni, F.**, **Younis, M.**, **López-Dekker, F.**, SAOCOM-CS SAR Performance, Technical Note, 2014.

[R-241] **Bräutigam, B.**, Instrument Calibration of Spaceborne SAR Systems, DLR Forschungsbericht, 221 pages, DLR-FB 2014-41, 2014.

[R-242] **Buckreuß, S.**, **Zink, M.**, Maurer, E., Pengler, I., **Schulze, D.**, Roth, A., **Hajnsek, I.**, Preuß, D., Schättler, B., TerraSAR-X/TanDEM-X Projektstatusbericht 3. Quartal 2014, Technical Note, 93 pages, TX-GS-2014-03, 2014.

[R-243] **Buckreuß, S.**, **Zink, M.**, Maurer, E., Pengler, I., **Schulze, D.**, Roth, A., **Hajnsek, I.**, Preuß, D., Schättler, B., TerraSAR-X/TanDEM-X Projektstatusbericht 2. Quartal 2014, Technical Note, 84 pages, TX-GS-2014-02, 2014.

[R-244] **Buckreuß, S.**, **Zink, M.**, Maurer, E., Pengler, I., **Schulze, D.**, Roth, A., **Hajnsek, I.**, Preuß, D., Schättler, B., TerraSAR-X/TanDEM-X Projektstatusbericht 1. Quartal 2014, Technical Note, 78 pages, TX-GS-2014-01, 2014.

[R-245] **Buckreuß, S.**, **Zink, M.**, Maurer, E., Pengler, I., **Schulze, D.**, Roth, A., **Hajnsek, I.**, Preuß, D., Schättler, B., TerraSAR-X/TanDEM-X Projektstatusbericht 4. Quartal 2013, Technical Note, 82 pages, TX-GS-2013-04, 2014.

[R-246] **Bueso Bello, J.**, TanDEM-X Experimental Modes Characterization, Technical Note, 91 pages, TD-SEC-TN-4258, 2014.

[R-247] **De Zan, F.**, Tesmer, V., Ernst, R., Ocean Surface Current Mission Study – System Requirements Analysis, Technical Note, 46 pages, OSCMS-SYS-DLR-RP-0001, 2014.

[R-248] **De Zan, F.**, **Scheiber, R.**, **Prats Iraola, P.**, **Reigber, A.**, Sentinel-1 InSAR Performance Study with TOPS Data: Assessment of the State of the Art and Consolidation of Scientific Goals (TN1), Technical Note, 36 pages, INSARAP-DLR-TN-01, 2014.

[R-249] **Fischer, J.**, **Jäger, M.**, **Horn, R.**, **Nottensteiner, A.**, **Di Maria, A.**, **Müller, G.**, **Que, R.**, **Scheiber, R.**, DBFSAR & V-SAR Naming Convention and On-Board Data Format Description: Interface Control Document, Technical Note, 27 pages, DBFSAR-ICD-0001, 2014.

[R-250] **Heinzel, A.**, Kalibration eines bodengebundenen Nahbereich-Radarsystems, Technical Note, 2014.

[R-251] **Huber, S.**, Spaceborne SAR Systems with Digital Beamforming and Reflector Antenna, DLR Forschungsbericht, 217 pages, DLR-FB--201409, 2014.

[R-252] **Jagdhuber, T.**, **Hajnsek, I.**, **Horn, R.**, Polarimetric SAR Soil Moisture Processing Report: SOIMEX 2013 L-Band Active / Passive Microwave Sensing, Technical Note, 26 pages, 2014.

[R-253] **Jochim, F.**, Satellitenbewegung, Band III: Natürliche und gesteuerte Bewegung, DLR Forschungsbericht, 572 pages, DLR-FB-2014-36, 2014.

[R-254] **Kaschke, M.**, Einheitliches GUI zu Mikrowellen-Materialcharakterisierungsmessungen und -simulationen, Praxisbericht Modul "Praxis I", Technical Note, 53 pages, 2014.

[R-255] Schütte, A., Huber, K., Liersch, C., Rütten, M., Rein, M., Koch, S., Jaffrezic, B., Zimper, D., Konrath, R., Wiggen, S., Voß, G., Lindermeir, E., Nauroz, M., **Kemptner, E.**, Steinhauser, R., Looye, G., Ehlers, J., Rohlf, D., Siggel, M., Abschlussbericht DLR Projekt FaUSST „Fortschrittliche aerodynamische UCAV Stabilitäts- und Steuerungs-Technologien", DLR Interner Bericht, 190 pages, DLR-IB 124-2014/907, 2014.

[R-256] **Laskowski, P.**, **Patyuchenko, A.**, DIFFERENT: Competitive Analysis Report, Technical Note, 21 pages, D2.3, 2014.

[R-257] **Link, M.**, Ground Measurements for Soil and Vegetation Characterization and for Comparison with Airborne SAR Data from the CROPEX 2014 Campaign, Technical Note, 2014.

[R-258] **Marull Paretas, G.**, **Baumgartner, S.**, **Sauer, S.**, **López-Dekker, F.**, **Börner, T.**, MAC-SAR: Modeling/Simulation of Processing Techniques of Multiple Azimuth Channels: for Ocean Currents & MTI, Technical Note, 144 pages, D2-4000104960, 2014.

[R-259] **Moreira, A.**, **Hajnsek, I.**, Huth, A., HGF Alliance: Remote Sensing and Earth System Dynamics – Intermediate Report, Technical Note, 2014.

[R-260] **Nannini, M.**, **Prats Iraola, P.**, **Scheiber, R.**, **Villano, M.**, Morrison, K., Bennett, J., Corr, H., Multi-Phase Center Processing of Ice Sounding Radar Signals for Across-Track Surface Clutter Cancellation: Final Report, Technical Note, 79 pages, MPC-104671-FR-DLR, 2014.

[R-261] **Neff, T.**, Wehrtechnische Forschung im DLR, Technical Note, 60 pages, D-04/14, 2014.

[R-262] **Neff, T.**, **Dietrich, B.**, **Peichl, M.**, **Speck, R.**, **Eilers, J.**, Wehrtechnische Forschungsarbeiten des DLR – Forschungsgebiet sicherheitsrelevante Erdbeobachtung Jahresbericht 2013, Technical Note, 31 pages, WTEB13 0F263 HR, 2014.

[R-263] **Pardini, M.**, **Bianco, V.**, **Papathanassiou, K.**, Phase Calibration of Multibaseline Pol-InSAR Data Stacks, DLR interner Bericht, 104 pages, DLR-HR-IB 551-1/2014, 2014.

[R-264] **Pardini, M.**, **Cantini, A.**, **Papathanassiou, K.**, Lombardini, F., 3-D Structure of Forests at L-Band: Experiments Towards a Spaceborne Implementation, DLR interner Bericht, 84 pages, DLR-HR-IB 551-2/2014, 2014.

[R-265] **Patyuchenko, A.**, Technical Notes – DBF SAR Performance Analysis, Technical Note, 16 pages, 2014.

[R-266] Patyuchenko, A., DIFFERENT: Radar Module Demonstrator Preliminary Design, Technical Note, 61 pages, D2.5, 2014.

[R-267] Patyuchenko, A., DIFFERENT: Preliminary Specifications for the Radar Module Demonstrator, Technical Note, 19 pages, D2.2, 2014.

[R-268] Patyuchenko, A., DIFFERENT: System Description, Technical Note, 27 pages, D2.1, 2014.

[R-269] Celton, E., Dominguez, A., **Patyuchenko, A.**, Boccia, L., DIFFERENT: Frequency Band Change, Technical Note, 21 pages, 2014.

[R-270] Pinheiro, M., **Scheiber, R.**, Flugzeuggestützte SAR-Interferometrie zur Erprobung der 3D-Erfassung trocken fallender Wattflächen und Küstenländer (3D-WATVOR – INSAR): Ergebnisbericht für die Daten der F-SAR Befliegung vom Juli 2013, Technical Note, 22 pages, DLR-FSAR-EB3-3DWATT, 2014.

[R-271] Polimeni, M., **Bachmann, M.**, **Castellanos Alfonzo, G.**, **Schulze, D.**, **Bräutigam, B.**, **Tous Ramon, N.**, **Weigt, M.**, **Böer, J.**, **Martone, M.**, **Wecklich, C.**, **Schmidt, K.**, **Schwerdt, M.**, Long-Term System-Monitoring Report – Quarter Q3/2014, Technical Note, 108 pages, 2014.

[R-272] Polimeni, M., **Bachmann, M.**, **Castellanos Alfonzo, G.**, **Schulze, D.**, **Bräutigam, B.**, **Tous Ramon, N.**, **Weigt, M.**, **Böer, J.**, **Martone, M.**, **Wecklich, C.**, **Schmidt, K.**, **Schwerdt, M.**, Long-Term System-Monitoring Report – Quarter Q2/2014, Technical Note, 108 pages, 2014.

[R-273] Polimeni, M., **Bachmann, M.**, **Castellanos Alfonzo, G.**, **Schulze, D.**, **Bräutigam, B.**, **Tous Ramon, N.**, **Weigt, M.**, **Böer, J.**, **Martone, M.**, **Wecklich, C.**, **Schmidt, K.**, **Schwerdt, M.**, Long-Term System-Monitoring Report – Quarter Q1/2014, Technical Note, 109 pages, 2014.

[R-274] Polimeni, M., **Bachmann, M.**, **Castellanos Alfonzo, G.**, **Schulze, D.**, **Bräutigam, B.**, **Tous Ramon, N.**, **Weigt, M.**, **Böer, J.**, **Martone, M.**, **Wecklich, C.**, **Schmidt, K.**, **Schwerdt, M.**, Long-Term System-Monitoring Report – Quarter Q4/2013, Technical Note, 110 pages, 2014.

[R-275] Prats Iraola, P., **Reigber, A.**, Radarsat-2 Tops Stack (dp2 Part I), Technical Note, 15 pages, INSARAP-DLR-DP-02, 2014.

[R-276] Minati, F., Costantini, M., **Prats Iraola, P.**, **Reigber, A.**, ENVISAT PSI Processing over the Selected Pilot Sites (TN3), Technical Note, 83 pages, INSARAP-DLR-TN-03, 2014.

[R-277] Prats Iraola, P., **Nannini, M.**, **Reigber, A.**, RADARSAT-2 TOPS PSI Processing over Mexico City (TN4), Technical Note, 25 pages, INSARAP-DLR-TN-04, 2014.

[R-278] Prats Iraola, P., **Reigber, A.**, TOPS InSAR Pseudo-Code (DP2 Part II), Technical Note, 32 pages, INSARAP-DLR-DP-02, 2014.

[R-279] Prats Iraola, P., **Schwerdt, M.**, **Zink, M.**, Experimental TanDEM-X Interferometric Processor (TAXI) SLC Product Description, Technical Note, 16 pages, S1-TN-DLR-DP1, 2014.

[R-280] Walter, T., Borgstrom, S., **Prats Iraola, P.**, **Reigber, A.**, Sentinel-1 InSAR Performance Study with TOPS Data: Definition of Pilot Sites (TN2), Technical Note, 29 pages, INSARAP-DLR-TN-02, 2014.

[R-281] Prats Iraola, P., **Reigber, A.**, Sentinel-1 Toolbox Development: TOPS InSAR Processing Chain Description (TN2), Technical Note, 29 pages, S1TD-DLR-TN-0002, 2014.

[R-282] Raab, S., Transponderausrichtung bei der Drei-Transponder-Methode: Anleitung und Protokoll zur Kampagne im Dezember 2013, Technical Note, 10 pages, Kalibr-TN-DLR-0003_ausrichtungZiele3TM_2014_v1.4.pdf, 2014.

[R-283] Raab, S., Untersuchungen zur Temperaturstabilität des Kalibri-Transponders, Technical Note, 12 pages, Kalibr-TN-DLR-0004_UntersuchungTempstabilitätKalibriTrsp_2014_v1.2.pdf, 2014.

[R-284] Reimann, J., Beschreibung der Polarisationseinstellungen und der Streumatrix der Kalibri-Transponder, Technical Note, 10 pages, Kalibr-TN-DLR-0002_ Polarisationsdefinition_2014_v1.0, 2014.

[R-285] Reimann, J., **Raab, S.**, Kalibri Corner Reflector Alignment and Phase Center Estimation, Technical Note, 11 pages, Kalibr-TN-DLR-0001_Corner_Reflector_Alignment_2014_v1.0, 2014.

[R-286] Sanjuan Ferrer, M., Detection of Coherent Scatterers in SAR Data: Algorithms and Applications, DLR Forschungsbericht, 166 pages, DLR-FB 2014-02, 2014.

[R-287] Scheiber, R., **Jäger, M.**, Korean Airborne SAR Consulting: Phase 1 - Review Result Report, Technical Note, 21 pages, LIGNEX1-DLR-RRR-01, 2014.

[R-288] Scheiber, R., **Prats Iraola, P.**, **Reigber, A.**, Sentinel-1 Toolbox Development: TOPS InSAR Requirements Analysis (TN1), Technical Note, 17 pages, S1TD-DLR-TN-0001, 2014.

[R-289] Scheiber, R., **Prats Iraola, P.**, **Nannini, M.**, Multi-Phase Center Processing of Ice Sounding Radar Signals for Across-Track Surface Clutter Cancellation: MPC Processing Tool User Manual, Technical Note, 18 pages, MPC-104671-DD6-DLR, 2014.

[R-290] Scheiber, R., **Prats Iraola, P.**, **Nannini, M.**, **Villano, M.**, **Walter Antony, J.**, Multi-Phase Center Processing of Ice Sounding Radar Signals for Across-Track Surface Clutter Cancellation: Assessment of MVDR Beamformer, High-Resolution DEM and DoA Methods for Improved Surface Clutter Cancellation, Technical Note, 89 pages, MPC-104671-DD7-DLR, 2014.

[R-291] Schmidt, K., **Tous Ramon, N.**, **Castellanos Alfonzo, G.**, **Prats Iraola, P.**, **Schwerdt, M.**, GMES Sentinel-1A Commissioning Campaign: Compliance Table, Issue 1.0, Technical Note, 112 pages, S1-TN-DLR-0003, 2014.

[R-292] Schmidt, K., **Tous Ramon, N.**, **Castellanos Alfonzo, G.**, **Prats Iraola, P.**, **Schwerdt, M.**, GMES Sentinel-1A Commissioning Campaign: Tool Test Plan, Issue 1.0, Technical Note, 56 pages, S1-TP-DLR-0001, 2014.

[R-293] Schwerdt, M., **Schmidt, K.**, **Tous Ramon, N.**, **Castellanos Alfonzo, G.**, **Prats Iraola, P.**, GMES Sentinel-1A Commissioning Campaign: Final Report, *Published in Project Report*, Technical Note, 99 pages, S1-RP-DLR-0002, Issue 1.0, 2014.

[R-294] Schwerdt, M., **Schmidt, K.**, **Tous Ramon, N.**, **Castellanos Alfonzo, G.**, **Prats Iraola, P.**, Independent Assessment of the Sentinel-1A Calibration - IOCR Status, *Published in Project Report*, Technical Note, 91 pages, S1-RP-DLR-0001, Issue 1.0, 2014.

[R-295] Schwerdt, M., **Schmidt, K.**, **Castellanos Alfonzo, G.**, **Prats Iraola, P.**, Test Report for: S1-A Commissioning Rehearsal #2 – Execution 1, *Published in Project Report*, Technical Note, 52 pages, S1-RP-ESA-GS-0454, 2014.

[R-296] Schwerdt, M., **Tous Ramon, N.**, Test Report for: S1-A Commissioning Rehearsal #1 – Execution 1, *Published in Project Report*, Technical Note, 32 pages, S1-RP-ESA-GS-0453, 2014.

[R-297] Schwerdt, M., GMES Sentinel-1 Commissioning Campaign: Contractor Calibration Campaign Plan, *Published in Project Report*, Technical Note, 11 pages, S1-PL-DLR-0001, Issue 1.0, 2014.

[R-298] Speck, R., **Hager, M.**, **Rode, G.**, Analyse der Fähigkeiten von Software-Werkzeugen zur Erstellung von Interferometrieprodukten, Technical Note, 64 pages, AFESI-DLRAS-AB-0001, 2014.

[R-299] **Speck, R.**, **Anglberger, H.**, **Kempf, T.**, Realisierbarkeits- und Systemverträglichkeitsuntersuchungen RADIAN, Technical Note, 27 pages, RADIAN-DLRAS-AB-0001, 2014.

[R-300] **Tous Ramon, N.**, Internal Calibration Tool User Manual and Functional Description – Issue 1.4, Technical Note, 48 pages, 2014.

[R-301] **Tous Ramon, N.**, Internal Calibration Tool Verification and Validation Plan – Issue 1.5, Technical Note, 32 pages, 2014.

[R-302] **Ulrich, R.**, Erweiterung des DLR_School_Lab Experiments "Mikrowellen im Einsatz", Technical Note, 19 pages, 2014.

[R-303] **Weiß, T.**, Multi-Temporal F-SAR Campaign over Agricultural Crops, Technical Note, 2014.

[R-304] **Wollstadt, S.**, **López-Dekker, F.**, **Börner, T.**, Technical Note on Hybrid-Polarization, Technical Note, 20 pages, OSCMS-DLR-TN-0001, 2014.

[R-305] **Wollstadt, S.**, **Younis, M.**, **De Zan, F.**, **López-Dekker, F.**, Ernst, R., Ocean Surface Current Mission Study – Instrument Architecture Options, Technical Note, 85 pages, OSCMS-SYS-DLR-RP-0003, 2014.

2013

[R-306] **Bachmann, M.**, **Polimeni, M.**, **Böer, J.**, **Bräutigam, B.**, **Castellanos Alfonzo, G.**, **Martone, M.**, **Tous Ramon, N.**, **Schmidt, K.**, **Schulze, D.**, **Schwerdt, M.**, **Walter Antony, J.**, **Weigt, M.**, Long-Term System Monitoring Report – Quarter Q1/2013, Technical Note, 96 pages, 2013.

[R-307] **Bachmann, M.**, **Polimeni, M.**, **Böer, J.**, **Bräutigam, B.**, **Castellanos Alfonzo, G.**, **Martone, M.**, **Tous Ramon, N.**, **Schmidt, K.**, **Schulze, D.**, **Schwerdt, M.**, **Walter Antony, J.**, **Weigt, M.**, Long-Term System Monitoring Report – Quarter Q2/2013, Technical Note, 96 pages, 2013.

[R-308] **Bachmann, M.**, **Polimeni, M.**, **Böer, J.**, **Bräutigam, B.**, **Castellanos Alfonzo, G.**, **Martone, M.**, **Tous Ramon, N.**, **Schmidt, K.**, **Schulze, D.**, **Schwerdt, M.**, **Walter Antony, J.**, **Weigt, M.**, Long-Term System Monitoring Report – Quarter Q3/2013, Technical Note, 96 pages, 2013.

[R-309] **Brand, B.**, **Dietrich, B.**, **Eilers, J.**, **Neff, T.**, Ingenieurtechnisches Controlling von aktuellen Aufklärungssystemen, Technical Note, DLR-AS-AB-0020, 2013.

[R-310] **Buckreuß, S.**, **Zink, M.**, Maurer, E., Pengler, I., **Schulze, D.**, Roth, A., **Hajnsek, I.**, Preuß, D., Schättler, B., TerraSAR-X/TanDEM-X Projektstatusbericht 3. Quartal 2013, Technical Note, 88 pages, TX-GS-2013-03, 2013.

[R-311] **Buckreuß, S.**, Fritz, T., Schättler, B., **Kraus, T.**, **Schulze, D.**, **Steinbrecher, U.**, Breit, H., **Grigorov, C.**, TerraSAR-X Staring Spotlight Implementation, Status Report Phase-2, Technical Note, 18 pages, 3008170-ST2, 2013.

[R-312] **Buckreuß, S.**, Fritz, T., Schättler, B., **Kraus, T.**, **Schulze, D.**, **Steinbrecher, U.**, Breit, H., TerraSAR-X Wide ScanSAR Implementation, Status Report Phase-2, Technical Note, 17 pages, 3008170-Ph2, 2013.

[R-313] **Buckreuß, S.**, **Zink, M.**, Maurer, E., Pengler, I., **Schulze, D.**, Roth, A., **Hajnsek, I.**, Preuß, D., Schättler, B., TerraSAR-X/TanDEM-X Projektstatusbericht 2. Quartal 2013, Technical Note, 88 pages, TX-GS-2013-02, 2013.

[R-314] **Buckreuß, S.**, Fritz, T., Schättler, B., **Kraus, T.**, **Steinbrecher, U.**, Breit, H., TerraSAR-X Staring Spotlight and Wide ScanSAR Implementation, Results Report Phase-1, Technical Note, 20 pages, 3008170-Ph1, 2013.

[R-315] **Buckreuß, S.**, **Zink, M.**, Maurer, E., Pengler, I., **Schulze, D.**, Roth, A., **Hajnsek, I.**, Preuß, D., Schättler, B., TerraSAR-X/TanDEM-X Projektstatusbericht 1. Quartal 2013, Technical Note, 75 pages, TX-GS-2013-01, 2013.

[R-316] **Buckreuß, S.**, **Zink, M.**, Maurer, E., Pengler, I., **Schulze, D.**, Roth, A., **Hajnsek, I.**, Preuß, D., Schättler, B., TerraSAR-X/TanDEM-X Projektstatusbericht 4. Quartal 2012, Technical Note, 74 pages, TX-GS-2012-04, 2013.

[R-317] **Böer, J.**, **Steinbrecher, U.**, Impact of Formation Flying with a Minimum Separation of 120m, Technical Note, 11 pages, TD-GS-TN-0171, 2013.

[R-318] **Castellanos Alfonzo, G.**, Antenna Model Tool Verification and Validation Plan. Issue 1.4, Technical Note, 28 pages, PZ-DLR-PL-1210, 2013.

[R-319] **Castellanos Alfonzo, G.**, Antenna Model Tool User Manual and Functional Description. Issue 1.2, Technical Note, 44 pages, PZ-DLR-UM-1220, 2013.

[R-320] **De Zan, F.**, **Nannini, M.**, **Prats Iraola, P.**, GMES Sentinel-1 Interferometric Wide-Swath Mode Implementation Study: TOPS-Time-Series Evaluation, Technical Note, 66 pages, IWSM-DLR-TN_0003, 2013.

[R-321] **Dill, S.**, **Peichl, M.**, **Kempf, T.**, **Anglberger, H.**, Results of TerraSAR-X Datatake at NATO MCG8 Trial 2013, Technical Note, 11 pages, HR-AKS-MWS-NATO_TSXNov2013, 2013.

[R-322] **Dill, S.**, **Peichl, M.**, **Schreiber, E.**, Ka-Band Radiometer Weilheim – Theoretische Betrachtungen zur Bandbreite eines Ka-Band Radiometers zur Messung der atmosphärischen Dämpfung am DLR-Standort Weilheim, Technical Note, 9 pages, HR-AKS-MWS-KaSpecs-1, 2013.

[R-323] **Döring, B.**, **Zink, M.**, **Schwerdt, M.**, GMES Sentinel-1 Calibration and Performance Budget, Technical Note, 17 pages, S1-TN-DLR-SY-0003, Issue 1.5, 2013.

[R-324] **Döring, B.**, KalibriC/Radarsat-2 Campaign: Analysis and Results, Technical Note, 37 pages, TC-TN-0020, 2013.

[R-325] **Döring, B.**, **Jirousek, M.**, **Schmidt, K.**, Standortbeschreibung: Standorte für die Sentinel-1-Kalibrierziele, Technical Note, 2013.

[R-326] **Grigorov, C.**, Rodriguez Gonzalez, F., Customization Proposal of DLR Tools, Technical Note, 27 pages, PZ-DLR-TN-0040, 2013.

[R-327] **Hajnsek, I.**, **Jagdhuber, T.**, Investigation of Snow Backscatter at a Boreal Environment for the ESA CoReH20 Mission Related NoSREx Campaign, Technical Note, 8 pages, SOAR-ID 5071, 2013.

[R-328] **Hajnsek, I.**, **Jagdhuber, T.**, **Stockamp, J.**, ALGOSNOW: Algorithms for Snow and Land Ice Retrieval Using SAR Data: DLR-HR-Contribution – WP 310, Technical Note, 19 pages, 2013.

[R-329] **Hepner, C.**, Erstellung dreidimensionaler Radarsignaturen der Turm-Drehstands-Messkampagne von 2007, Technical Note, 2013.

[R-330] **Jochim, F.**, Satellitenbewegung Band IV: Die Verknüpfung von Bewegung und Beobachtungsgeometrie, DLR Forschungsbericht, 555 pages, DLR-FB-2013-12, 2013.

[R-331] **Jäger, M.**, **Pinheiro, M.**, **Horn, R.**, **Keller, M.**, **Scheiber, R.**, Flugzeuggestützte SAR-Interferometrie zur Erprobung der 3D-Erfassung trocken fallender Wattflächen und Küstenländer (3D-WATVOR – INSAR): Ergebnisbericht für die Daten der F-SAR Befliegung vom April 2013, Technical Note, 29 pages, DLR-FSAR-EB2-3DWATT, 2013.

[R-332] Jäger, M., **Pinheiro, M.**, **Horn, R.**, **Scheiber, R.**, Flugzeuggestützte SAR-Interferometrie zur Erprobung der 3D-Erfassung trocken fallender Wattflächen und Küstenländer (3D-WATVOR – INSAR): Ergebnisbericht für die Daten der F-SAR Befliegung vom November 2012, Technical Note, 32 pages, 2013.

[R-333] Jäger, M., **Scheiber, R.**, **Prats Iraola, P.**, GMES Sentinel-1 Interferometric Wide-Swath Mode Implementation Study: TOPS Image Coregistration/2D Tracking for Non-Stationary Scenarios, Technical Note, 44 pages, IWSM-DLR-TN-0001, 2013.

[R-334] Kraus, T., Wide ScanSAR Mode Design and Performance Analysis, Technical Note, 36 pages, TX-SEC-TN-4265, 2013.

[R-335] Kraus, T., SAR Performance Inputs of Staring Spotlight and Wide ScanSAR for the Basic Product Specification, Technical Note, 25 pages, TX-SEC-TN-4266, 2013.

[R-336] Kraus, T., Performance Optimization for the Staring Spotlight Mode, Technical Note, 33 pages, TX-SEC-TN-4268, 2013.

[R-337] Laskowski, P., **Younis, M.**, Integrated Tile Demonstrator: Design Definition File, Technical Note, 76 pages, ITD_D3_40000103316_DDF, 2013.

[R-338] Laskowski, P., **Younis, M.**, Integrated Tile Demonstrator: Design Justification File, Technical Note, 62 pages, ITD_D4_4000103316_DJF, 2013.

[R-339] Laskowski, P., **Younis, M.**, Integrated Tile Demonstrator: Technical Requirements and Interface Requirements Specification, Technical Note, 5 pages, ITD_D1_40000103316_TS, 2013.

[R-340] Lee, S., Forest Parameter Estimation Using Polarimetric SAR Interferometry Techniques at Low Frequencies, DLR Forschungsbericht, 137 pages, DLR-FB--2013-09, 2013.

[R-341] Muhammad Abu, T., **López-Dekker, F.**, **De Zan, F.**, Formation Flying Concept, Technical Note, 2013.

[R-342] Nannini, M., **Prats Iraola, P.**, **Scheiber, R.**, **Villano, M.**, Morrison, K., Bennett, J., Corr, H., Multi-Phase Center Processing of Ice Sounding Radar Signals for Across-Track Surface Clutter Cancellation: Final Report, Technical Note, 64 pages, MPC-104671-FR-DLR, 2013.

[R-343] Neff, T., **Dietrich, B.**, **Speck, R.**, **Peichl, M.**, Wehrtechnische Forschungsarbeiten des DLR – Forschungsgebiet sicherheitsrelevante Erdbeobachtung Jahresbericht 2012, Technical Note, 27 pages, WTEB12 0F263 HR, 2013.

[R-344] Polimeni, M., **Bachmann, M.**, **Böer, J.**, **Bräutigam, B.**, **Castellanos Alfonzo, G.**, **Martone, M.**, **Tous Ramon, N.**, **Schmidt, K.**, **Schulze, D.**, **Schwerdt, M.**, **Walter Antony, J.**, **Weigt, M.**, Long-Term System Monitoring Report – Quarter Q4/2012, Technical Note, 89 pages, 2013.

[R-345] Pollner, A., DEM Based Shadow & Layover Detection Using Python (Praktikantenbericht von Anita Pollner), Technical Note, 2013.

[R-346] Prats Iraola, P., **De Zan, F.**, **Jäger, M.**, **Nannini, M.**, **Rodríguez Cassolà, M.**, **Scheiber, R.**, **Wollstadt, S.**, GMES Sentinel-1 Interferometric Wide-Swath Mode Implementation Study: Final Report, Technical Note, 132 pages, IWSM-DLR-FR-0001, 2013.

[R-347] Rodríguez Cassolà, M., **Wollstadt, S.**, **Prats Iraola, P.**, GMES Sentinel-1 Interferometric Wide-Swath Mode Implementation Study: TOPS Doppler Spectrum Analysis and Antenna Mis-Pointing, Technical Note, 42 pages, IWSM-DLR-TN-0002, 2013.

[R-348] Rudolf, D., **Schwerdt, M.**, Abnahme der zentralen Steuereinheit Corner Reflektor, Technical Note, 9 pages, ZES-TN-0002-1.0, 2013.

[R-349] Rudolf, D., **Schwerdt, M.**, Abnahme der zentralen Steuereinheit Transponder, Technical Note, 8 pages, ZES-TN-0003-1.0, 2013.

[R-350] Scheiber, R., **Prats Iraola, P.**, Multi-Phase Center Processing of Ice Sounding Radar Signals for Across-Track Surface Clutter Cancellation: MPC Processing Tool User Manual, Technical Note, 19 pages, MPC-104671-DD4-DLR, 2013.

[R-351] Scheiber, R., **Prats Iraola, P.**, **Nannini, M.**, **Villano, M.**, Multi-Phase Center Processing of Ice Sounding Radar Signals for Across-Track Surface Clutter Cancellation: POLARIS Processing Results and Optimisation Report, Technical Note, 49 pages, MPC-104671-DD5-DLR, 2013.

[R-352] Schmidt, K., **Döring, B.**, Anforderungskatalog für Baumaßnahmen: Kalibri-Standorte in Süddeutschland, Technical Note, 2013.

[R-353] Schmidt, K., **Schwerdt, M.**, **Bräutigam, B.**, PAZ: External Calibration Tool, User Manual and Functional Description, Technical Note, 25 pages, PZ-DLR-UM-1120, 2013.

[R-354] Schwerdt, M., **Tous Ramon, N.**, **Bachmann, M.**, GMES Sentinel-1: SAR Calibration Algorithms, Part A of IN-11, *Published in Project Report*, Technical Note, 88 pages, S1-DD-DLR-SY-0002, Issue 3.0, 2013.

[R-355] Schwerdt, M., **Bräutigam, B.**, **Döring, B.**, GMES Sentinel-1: Overall SAR System Calibration and Validation Plan and End-to-End Performance Budgets, *Published in Project Report*, Technical Note, 95 pages, S1-PL-DLR-SY-0001, Issue 1.6, 2013.

[R-356] Speck, R., **Tailhades, S.**, Untersuchung von Artefakten bei aktuellen Aufklärungssystemen, Technical Note, 24 pages, DLR-AS-TB-0021, 2013.

[R-357] Tous Ramon, N., Internal Calibration Tool User Manual and Functional Description – Issue 1.3, Technical Note, 43 pages, PZ-DLR-UM-1320, 2013.

[R-358] Tous Ramon, N., Internal Calibration Tool Verification and Validation Plan – Issue 1.4, Technical Note, 30 pages, PZ-DLR-PL-1310, 2013.

[R-359] Tous Ramon, N., Automatic TRM Monitoring Tool User Manual and Functional Description – Issue 1.1, Technical Note, 30 pages, PZ-DLR-UM-2220, 2013.

[R-360] Tous Ramon, N., Automatic TRM Monitoring Tool Verification and Validation Plan – Issue 1.2, Technical Note, 20 pages, PZ-DLR-PL-2210, 2013.

[R-361] Villano, M., **Nannini, M.**, **Prats Iraola, P.**, **Scheiber, R.**, Multi-Phase Center Processing of Ice Sounding Radar Signals for Across-Track Surface Clutter Cancellation: Validation Test Report, V1.0, Technical Note, 42 pages, MPC-104671-DD3-DLR, 2013.

[R-362] Villano, M., **Nannini, M.**, **Prats Iraola, P.**, **Scheiber, R.**, Multi-Phase Center Processing of Ice Sounding Radar Signals for Across-Track Surface Clutter Cancellation: Validation Test Report, V2.0, Technical Note, 42 pages, MPC-104671-DD3-DLR, 2013.

2012

[R-363] Ariza Redondo, J., Development of a Graphic User Interface for Managing the TanDEM-X Backscatter Map Using Python, Technical Note, 20 pages, 2012.

[R-364] Bachmann, M., **Bueso Bello, J.**, **Polimeni, M.**, Long-Term System-Monitoring Tool – Verification and Validation Plan, Technical Note, 10 pages, PZ-DLR-PL-2410, 2012.

[R-365] Bachmann, M., **Ortega-Míguez, C.**, Auxiliary Data Formatter – User Manual and Functional Description, Technical Note, 14 pages, 2012.

[R-366] García Molina, J., **Baumgartner, S.**, **Bordoni, F.**, **López-Dekker, F.**, **Börner, T.**, MAC-SAR: Processing Techniques Survey, Technical Note, 88 pages, D1-4000104960, 2012.

[R-367] **Baumgartner, S.**, **Laux, C.**, García Molína, J., **Bordoni, F.**, **López-Dekker, F.**, Schaefer, C., Marques, P., MTI-SAR: MTI Multi-Channel Techniques Survey and Scenario Definition, Technical Note, 180 pages, D1-4000105042, 2012.

[R-368] **Bordoni, F.**, **Younis, M.**, Performance Parameters: Definitions and Numerical Analysis, Technical Note, 65 pages, DLR-HRWS-TB-1002, 2012.

[R-369] **Bräutigam, B.**, **Gonzalez, C.**, SAR Study: The Technical Survey and Analysis for Image Quality Parameters, Technical Note, 30 pages, KARI-DLR-RP-2000, 2012.

[R-370] **Buckreuß, S.**, **Zink, M.**, Maurer, E., Pengler, I., **Schulze, D.**, Roth, A., **Hajnsek, I.**, Preuß, D., Schättler, B., TerraSAR-X/TanDEM-X Projektstatusbericht 3. Quartal 2012, Technical Note, 75 pages, TX-GS-2012-03, 2012.

[R-371] **Buckreuß, S.**, **Zink, M.**, Maurer, E., Bollner, M., **Schulze, D.**, Roth, A., **Hajnsek, I.**, Preuß, D., Schättler, B., TerraSAR-X/TanDEM-X Projektstatusbericht 2. Quartal 2012, Technical Note, 74 pages, TX-GS-2012-02, 2012.

[R-372] **Buckreuß, S.**, **Zink, M.**, Maurer, E., Bollner, M., **Schulze, D.**, Roth, A., **Hajnsek, I.**, Preuß, D., Schättler, B., TerraSAR-X/TanDEM-X Projektstatusbericht 1. Quartal 2012, Technical Note, 72 pages, TX-GS-2012-01, 2012.

[R-373] **Buckreuß, S.**, **Zink, M.**, Maurer, E., Bollner, M., **Schulze, D.**, Roth, A., **Hajnsek, I.**, Preuß, D., Schättler, B., TerraSAR-X/TanDEM-X Projektstatusbericht 4. Quartal 2011, Technical Note, 70 pages, TX-GS-2011-04, 2012.

[R-374] **Bueso Bello, J.**, SAR Toolbox User Manual and Functional Description, Technical Note, 73 pages, PZ-DLR-PL-5320, 2012.

[R-375] **Bueso Bello, J.**, SAR Toolbox Verification and Validation Plan, Technical Note, 29 pages, PZ-DLR-PL-5310, 2012.

[R-376] **Böer, J.**, Expert Request to Command Converter Tool User Manual and Functional Description, Technical Note, 34 pages, 2012.

[R-377] **Böer, J.**, Expert Request to Command Converter Verification and Validation Plan, Technical Note, 21 pages, PZ-DLR-PL-5210, 2012.

[R-378] **Börner, T.**, BIOMASS End-to-End Mission Performance Simulator – Modules Verification Test Report – Product Generation Module, Technical Note, 31 pages, BIOMASS_E2ES_MVTR-PGM_2.0, 2012.

[R-379] **Börner, T.**, **De Zan, F.**, **López-Dekker, F.**, BIOMASS End-to-End Mission Performance Simulator – Modules Verification Plan – Product Generation Module, Technical Note, 21 pages, BIOMASS_E2ES_MVP-PGM_2.0, 2012.

[R-380] **Castellanos Alfonzo, G.**, **Prats Iraola, P.**, **Scheiber, R.**, **Döring, B.**, Pre-Launch Preparatory Study. Issue 1.0, Technical Note, 44 pages, S1-TN-DLR-0001, 2012.

[R-381] **Culhaoglu, A.**, Microwave Metamaterials: Superlensing and Design of Low Reflection Coatings, Technical Note, 124 pages, DLR-Forschungsbericht 2012-11, 2012.

[R-382] **Dill, S.**, **Peichl, M.**, **Rudolf, D.**, SUM, C., SUM Demonstration Experiments Completed, *EDA JIP FP Project A-0444-RT-GC*, Technical Note, 24 pages, SUM-DEC-10, 2012.

[R-383] **Dill, S.**, **Peichl, M.**, **Rudolf, D.**, SUM, C., SUM Demonstration Results, *EDA JIP FP Project A-0444-RT-GC*, Technical Note, 56 pages, SUM-DRT-10, 2012.

[R-384] **Dill, S.**, **Peichl, M.**, **Rudolf, D.**, SUM, C., SUM Executive Summary, *EDA JIP FP Project A-0444-RT-GC*, Technical Note, 5 pages, SUM-EPS-10, 2012.

[R-385] **Dill, S.**, **Peichl, M.**, **Rudolf, D.**, SUM, C., SUM Integration Report, *EDA JIP FP Project A-0444-RT-GC*, Technical Note, 25 pages, SUM-INR-10, 2012.

[R-386] **Dill, S.**, **Peichl, M.**, **Rudolf, D.**, SUM, C., SUM MMI and Human factors definition, *EDA JIP FP Project A-0444-RT-GC*, Technical Note, 33 pages, SUM-MHF-10, 2012.

[R-387] **Dill, S.**, **Peichl, M.**, **Rudolf, D.**, SUM, C., SUM Project Results Review, *EDA JIP FP Project A-0444-RT-GC*, Technical Note, 28 pages, SUM-PRR-10, 2012.

[R-388] **Dill, S.**, **Peichl, M.**, **Rudolf, D.**, SUM, C., SUM Roadmap, *EDA JIP FP Project A-0444-RT-GC*, Technical Note, 23 pages, SUM-RMP-10, 2012.

[R-389] **Dill, S.**, **Peichl, M.**, **Rudolf, D.**, SUM, C., SUM Integration Plan, *EDA JIP FP Project A-0444-RT-GC*, Technical Note, 33 pages, SUM-INP-10, 2012.

[R-390] **Dill, S.**, **Peichl, M.**, **Rudolf, D.**, SUM, C., SUM Overall System Integration and Tests Completed, *DA JIP FP Project A-0444-RT-GC*, Technical Note, 36 pages, SUM-OSITC-10, 2012.

[R-391] **Döring, B.**, **Schwerdt, M.**, Absolute Radiometric Bias Budget Update, Technical Note, Version 1.0, 15 pages, 2012.

[R-392] **Döring, B.**, **Schwerdt, M.**, Absolute Radiometric Bias Budget Update, Technical Note, Version 2.0, 15 pages, 2012.

[R-393] **Gonzalez, C.**, Data Take Quality Monitor User Manual and Functional Description, Technical Note, 28 pages, PZ-DLR-UM-2320, 2012.

[R-394] **Gonzalez, C.**, Data Take Quality Monitor Verification and Validation Plan, Technical Note, 14 pages, PZ-DLR-PL-2310, 2012.

[R-395] **Hepner, C.**, Erstellung dreidimensionaler Radarsignaturen der Turm-Drehstands-Messkampagne mit ausgedünnter Apertur, Technical Note, [DLR-IB 551-1/2012], 2012.

[R-396] **Huber Garcia, V.**, Untersuchung der physischen Gründe für Ausreißer in TanDEM-X DEMs, Technical Note, 43 pages, 2012.

[R-397] **Jagdhuber, T.**, Soil Parameter Retrieval under Vegetation Cover Using SAR Polarimetry, DLR Forschungsbericht, 236 pages, DLR-FB 2012-24, 2012.

[R-398] **Jirousek, M.**, Abbildendes Mikrowellen-Spektrometer mit Apertursynthese, DLR Forschungsbericht, 244 pages, DLR-FB-2012-04, 2012.

[R-399] **Jochim, F.**, Satellitenbewegung Band II: Mathematische und astronomische Grundlagen, DLR Forschungsbericht, 570 pages, DLR-FB-2012-13, 2012.

[R-400] **Jochim, F.**, Satellitenbewegung Band I: Der Bewegungsbegriff, DLR Forschungsbericht, 548 pages, DLR-FB-2012-12, 2012.

[R-401] Walker, N., **Jäger, M.**, IMAS: ISTAR Using Multi-Aspect SAR – Final Report, Technical Note, 42 pages, DSTL X 10000 6294, 2012.

[R-402] **Nannini, M.**, **Prats Iraola, P.**, **Scheiber, R.**, **Villano, M.**, Morrison, K., Bennett, J., Multi-Phase Center Processing of Ice Sounding Radar Signals for Across-Track Surface Clutter Cancellation: Processor Algorithm and Software Architeture Specification, Technical Note, 49 pages, MPC-104671-DD2-DLR, 2012.

[R-403] **Nannini, M.**, **Prats Iraola, P.**, **Scheiber, R.**, **Villano, M.**, Morrison, K., Bennett, J., Multi-Phase Center Processing of Ice Sounding Radar Signals for Across-Track Surface Clutter Cancellation: Comparison of Surface Clutter Cancellation Techniques and Processor Concept Description, Technical Note, 64 pages, MPC-104671-DD1-DLR, 2012.

[R-404] **Neff, T.**, **Brand, B.**, **Calaminus, B.**, **Eilers, J.**, **Tailhades, S.**, **Speck, R.**, **Peichl, M.**, Technisches Controlling während der Analysephase und Projektierung eines zukünftigen raumgestützten Aufklärungssystems, Technical Note, DLR-AB-SARah-2012, 2012.

[R-405] Neff, T., **Brand, B.**, **Dietrich, B.**, **Eilers, J.**, **Speck, R.**, **Peichl, M.**, Ingenieurtechnisches Controlling von aktuellen raumgestützten Aufklärungssystemen im Jahr 2012, Technical Note, 19 pages, SL-DLRAS-AB-0019-V3, 2012.

[R-406] Ortega-Míguez, C., Long-Term Data Base User Manual and Functional Description, Technical Note, 25 pages, PZ-DLR-UM-5520, 2012.

[R-407] Ortega-Míguez, C., Auxiliary Data Formatter. Verification and Validation Plan, Technical Note, 9 pages, 2012.

[R-408] Peichl, M., **Schreiber, E.**, Marques, L., TIRAMISU – Close-in Detection Tool Description, Technical Note, 109 pages, D310.1, 2012.

[R-409] Polimeni, M., Long-Term System Monitoring Tool User Manual and Functional Description, Technical Note, 27 pages, PZ-DLR-UM-2420_1, 2012.

[R-410] Polimeni, M., Long-Term System Monitoring User Manual and Functional Description, Technical Note, 27 pages, PZ-DLR-UM-2420_2, 2012.

[R-411] Polimeni, M., **Bachmann, M.**, Long-Term System Monitoring Tool Verification and Validation Plan, Technical Note, 10 pages, PZ-DLR-PL-2410, 2012.

[R-412] Prats Iraola, P., **Rodríguez Cassolà, M.**, **Bräutigam, B.**, **Baumgartner, S.**, SAR Study: The Technical Survey and Analysis for SAR Processing, *Published in Final Report*, Technical Note, 40 pages, KARI-DLR-RP-3000, 2012.

[R-413] Rott, H., Voglmeier, K., **Scheiber, R.**, Development of Snow Retrieval Algorithms for CoReH2O CCN1 – Processing and Analysis of March 2011 Data: Report on SSG Modifications for SnowSAR, Technical Note, 12 pages, 22830/09/NL/JC-CCN1-D-C02, 2012.

[R-414] Schmidt, K., **Tous Ramon, N.**, **Castellanos Alfonzo, G.**, **Prats Iraola, P.**, **Schwerdt, M.**, GMES Sentinel-1A Commissioning Campaign: S1-TN-DLR-0002 Tool Description, Technical Note, 29 pages, S1-TN-DLR-0002, 2012.

[R-415] Schwerdt, M., **Döring, B.**, CoReH2O: SAR Payload Calibration Analysis and Design, *Published in Project Report*, Technical Note, 53 pages, CRH.DLR.TN.00001, 2012.

[R-416] Schwerdt, M., SAR Study: The Technical Survey and Analysis for Calibration, *Published in Final Report*, Technical Note, 30 pages, KARI-DLR-RP-4000, 2012.

[R-417] Thiemer, P., Aufbau und messtechnische Verifikation eines breitbandigen digitalen Pulsradars, Technical Note, 83 pages, 2012.

[R-418] Weigt, M., Data Take Verification Unit–User Manual and Functional Description, Technical Note, 35 pages, PZ-DLR-UM-2120, 2012.

[R-419] Weigt, M., Data Take Verification Unit - Verification and Validation Plan, Technical Note, 29 pages, PZ-DLR-PL-2110, 2012.

2011

[R-420] Antonello, A., Implementation of Compressed Sensing Algorithms in Python, Technical Note, 90 pages, 2011.

[R-421] Bordoni, F., **Younis, M.**, HRWS SAR System Calibration, *Published in Technische Berichte*, Technical Note, 33 pages, DLR-HRWS-TB-1003, 2011.

[R-422] Brand, B., **Dietrich, B.**, **Eilers, J.**, **Neff, T.**, Ingenieurtechnisches Controlling von aktuellen raumgestützten Aufklärungssystemen, Technical Note, 25 pages, DLR-AB-SAR-Lupe_2011, 2011.

[R-423] Buckreuß, S., **Zink, M.**, Maurer, E., Bollner, M., **Schulze, D.**, Roth, A., **Hajnsek, I.**, Preuß, D., Schättler, B., TerraSAR-X /TanDEM-X Projektstatusbericht 3. Quartal 2011, Technical Note, 68 pages, TX-GS-2011-03, 2011.

[R-424] Buckreuß, S., **Zink, M.**, Hofmann, H., Bollner, M., **Schulze, D.**, Roth, A., **Hajnsek, I.**, Preuß, D., Schättler, B., TerraSAR-X/TanDEM-X Projektstatusbericht 2. Quartal 2011, Technical Note, 70 pages, TX-GS-2011-02, 2011.

[R-425] Buckreuß, S., **Zink, M.**, Hofmann, H., Bollner, M., **Schulze, D.**, Roth, A., **Hajnsek, I.**, Preuß, D., TerraSAR-X/TanDEM-X Projektstatusbericht 1. Quartal 2011, Technical Note, 74 pages, TX-GS-2011-01, 2011.

[R-426] Buckreuß, S., Hofmann, H., Bollner, M., **Schulze, D.**, Roth, A., Preuß, D., TerraSAR-X Projektstatusbericht 4. Quartal 2010, Technical Note, 51 pages, TX-GS-2010-04, 2011.

[R-427] Börner, T., SIGNAL - SAR for Ice, Glacier aNd globAL Dynamics - Schlussbericht, *Published in Schlussbericht*, Technical Note, 15 pages, HR-55114-SG-01/11, 2011.

[R-428] Börner, T., **López-Dekker, F.**, Cian, F., Kuntz, S., Ka-InSAR: Application and System Requirement Analysis Report, Technical Note, 82 pages, D1-4000102378, 2011.

[R-429] Börner, T., **López-Dekker, F.**, **De Zan, F.**, **Younis, M.**, **Hajnsek, I.**, **Papathanassiou, K.**, **Villano, M.**, **Danklmayer, A.**, **Krieger, G.**, **Moreira, A.**, Rott, H., Nagler, T., Dierking, W., Fügen, T., Völker, M., Klein, R., SIGNAL – SAR for Ice, Glacier and Global Dynamics – Mission Description Document, Technical Note, 88 pages, HR-55114-SG-02/10, 2011.

[R-430] Börner, T., **López-Dekker, F.**, **De Zan, F.**, **Younis, M.**, **Hajnsek, I.**, **Papathanassiou, K.**, **Villano, M.**, **Danklmayer, A.**, **Krieger, G.**, **Moreira, A.**, Rott, H., Nagler, T., Dierking, W., Fügen, T., Völker, M., Klein, R., SIGNAL - SAR for Ice, Glacier and Global Dynamics – System Functional Specification, Technical Note, 24 pages, HR-55114-SG-04/10, 2011.

[R-431] Börner, T., **López-Dekker, F.**, Soccorsi, M., SIGNAL – SAR for Ice, Glacier and Global Dynamics – Ocean and ATI Technical Note, Technical Note, 24 pages, HR-55114-SG-05/10, 2011.

[R-432] De Zan, F., Guardabrazo, T., **Börner, T.**, Biomass End-to-End Mission Performance Simulator: Algorithm Theoretical Baseline Documentation (ATBD), Technical Note, 43 pages, 2011.

[R-433] De Zan, F., **García Molina, J.**, Guardabrazo, T., Biomass End-to-End Mission Performance Simulator: System Verification Report (SVR), Technical Note, 31 pages, 2011.

[R-434] Dill, S., **Peichl, M.**, **Rudolf, D.**, SUM, C., SUM Demonstration Definition report, *EDA JIP FP Project A-0444-RT-GC*, Technical Note, 21 pages, SUM-DEDEF-10, 2011.

[R-435] Dill, S., **Peichl, M.**, **Rudolf, D.**, SUM Data collection report (Version 2) Part: Imaging Radiometer System, *EDA JIP FP Project A-0444-RT-GC*, Technical Note, 74 pages, SUM-DCR-20, 2011.

[R-436] Dill, S., **Peichl, M.**, **Rudolf, D.**, SUM Feature Selection and Preparation for Fusion (Part: Radiometer Characterization), *EDA JIP FP Project A-0444-RT-GC*, Technical Note, 29 pages, SUM-FSL-10, 2011.

[R-437] Dill, S., **Peichl, M.**, **Rudolf, D.**, SUM Registration Report (Part: Radiometer image registration), *EDA JIP FP Project A-0444-RT-GC*, Technical Note, 37 pages, SUM-RGT-10, 2011.

[R-438] Dill, S., **Peichl, M.**, **Rudolf, D.**, SUM Radiometer System Software and Test Report (Version 2), *EDA JIP FP Project A-0444-RT-GC*, Technical Note, 37 pages, SUM-RDMSWTR-20, 2011.

[R-439] **Dill, S.**, **Peichl, M.**, **Rudolf, D.**, SUM Ground Vehicle Data Processing Report – Final Version Part: Imaging Radiometer System, *EDA JIP FP Project A-0444-RT-GC*, Technical Note, 56 pages, SUM-GVDP-Final, 2011.

[R-440] **Dill, S.**, **Peichl, M.**, **Rudolf, D.**, SUM Radiometer System Software and Test Report (Version 1), *EDA JIP FP Project A-0444-RT-GC*, Technical Note, 19 pages, SUM-TR011-prelim, 2011.

[R-441] **Grigorov, C.**, **Bueso Bello, J.**, Instrument Operations and Calibration/Verification Tools External Interface Description, Technical Note, 94 pages, PZ-DLR-ID-9002, 2011.

[R-442] **Grigorov, C.**, **Bueso Bello, J.**, Instrument Operations and Calibration/Verification Tools Internal Interface Description, Technical Note, 311 pages, PZ-DLR-ID-9001, 2011.

[R-443] **Grigorov, C.**, **Bueso Bello, J.**, Nominal Request To Command Converter Tool User Manual and Functional Description, Technical Note, 41 pages, PZ-DLR-UM-5120, 2011.

[R-444] **Grigorov, C.**, **Bueso Bello, J.**, Nominal Request To Command Converter Tool Verification and Validation Plan, Technical Note, 24 pages, PZ-DLR-UM-5110, 2011.

[R-445] **Jochim, F.**, Die Verwendung von Hansen-Systemen in Himmelsmechanik und Astrodynamik, DLR Forschungsbericht, 221 pages, DLR-FB 2011-04, 2011.

[R-446] **Jochim, F.**, Einige Anmerkungen zum Bearbeiten astrodynamischer Problemstellungen mit MAPLE, Technical Note, 152 pages, DLR-HR-IB-551- 1/2011, 2011.

[R-447] **Kim, J.**, Multiple-Input Multiple-Output Synthetic Aperture Radar (SAR) for Multimodal Operation, DLR Forschungsbericht 2011, 210 pages, 2011.

[R-448] **Laskowski, P.**, Multi-Channel Processing: Antenna Pattern Compensation, Technical Note, 43 pages, DLR-HRWS-TB-1004, 2011.

[R-449] **López-Dekker, F.**, Guardabrazo, T., BIOMASS End-to-End Mission Performance Simulator – Modules Verification Plan – Interface Control Document, Technical Note, 102 pages, 2011.

[R-450] **López-Dekker, F.**, Guardabrazo, T., **De Zan, F.**, BIOMASS End-to-End Mission Performance Simulator – Modules Verification Plan – Simulator Architecture Design Document, Technical Note, 62 pages, 2011.

[R-451] Guardabrazo, T., **López-Dekker, F.**, **De Zan, F.**, Biomass End-to-End Mission Performance Simulator: System Verification Plan (SVP), Technical Note, 32 pages, 2011.

[R-452] **Martone, M.**, Quantization Effects on Interferometric Performance – TanDEM-X Commissioning Phase Results, Technical Note, 61 pages, 2011.

[R-453] **Malz, E.**, **Marotti, L.**, **Mittermayer, J.**, **Prats Iraola, P.**, **Sauer, S.**, **Scheiber, R.**, **Wollstadt, S.**, TOPS Image Quality and Processor Verification Study – Final Report, Technical Note, 87 pages, DLR-HR-SSE-FR-TOPS09-02, 2011.

[R-454] **Neff, T.**, **Brand, B.**, **Calaminus, B.**, **Eilers, J.**, **Tailhades, S.**, Technisches Controlling während der Analysephase und Projektierung eines zukünftigen raumgestützten Aufklärungssystems, Technical Note, 71 pages, DLR-AB-SARah-2011, 2011.

[R-455] **Peichl, M.**, **Dill, S.**, **Kempf, T.**, **Jirousek, M.**, **Schreiber, E.**, **Rudolf, D.**, 2.4.7 Ground-Based Radar Systems, 2.4.8 Radiometry and Security Applications, *Published in Status Report 2006-2011*, Technical Note, vol. Volume 1, 177 pages, 2011.

[R-456] **Pisciottano, I.**, First Analysis on Snow Cover Change Using Polarimetric TerraSAR-X Data, DLR Interner Bericht, 128 pages, DLR-IB 551-4/2011, 2011.

[R-457] **Marotti, L.**, **Prats Iraola, P.**, **Sauer, S.**, **Wollstadt, S.**, TOPS Image Quality and Processor Verification Study: TOPS Time Series Part 2: Mexico City – Coherent Scatterers and Differential SAR Interferometry, Technical Note, 35 pages, HR-SSE-TN4-TOPS09-02, 2011.

[R-458] **Rode, G.**, Radardetektionswahrscheinlichkeiten aus Rückstreuquerschnitts-Verteilungen, Technical Note, 6 pages, 2011.

[R-459] Rott, H., Nagler, T., Heidinger, M., Müller, F., **Scheiber, R.**, **Hajnsek, I.**, Flach, D., Pulliainen, J., Malnes, E., Etchevers, P., Development of Snow Retrieval Algorithms for CoReH2O: Final Report, Technical Note, 25 pages, 22830/09/NL/JC-D14, 2011.

[R-460] **Scheiber, R.**, **Wollstadt, S.**, TOPS Image Quality and Processor Verification Study: TOPS Time Series – Part 1: Flevoland Flashing Fileds Analysis, Technical Note, 19 pages, HR-SSE-TN4-TOPS09-01, 2011.

[R-461] **Schiller-Lorande, M.**, Estimation of Moving Target Velocity Parameters with Air- and Spaceborne Multi-Channel SAR Systems, Technical Note, 2011.

[R-462] **Schwerdt, M.**, **Döring, B.**, CoReH2O: SAR Payload Calibration Analysis and Design, *Published in Project Report*, Technical Note, 51 pages, CRH.DLR.TN.00001, 2011.

[R-463] **Schwerdt, M.**, **Schulz, C.**, **Bachmann, M.**, **Schrank, D.**, GMES Sentinel-1: SAR Calibration Algorithms, Part A of IN-11, *Published in Project Report*, Technical Note, 56 pages, S1-DD-DLR-SY-0002, 2011.

[R-464] **Speck, R.**, **Anglberger, H.**, **Hager, M.**, 2.4.4 SAR Simulation, Microwaves and Radar Institute Status Report 2006-2011, vol. Volume 1, 177 pages, 2011.

[R-465] **Tous Ramon, N.**, **Hueso González, J.**, **Bueso Bello, J.**, Internal Calibration Tool User Manual and Functional Description, Technical Note, 16 pages, PZ-DLR-UM-1320, 2011.

[R-466] **Tous Ramon, N.**, **Hueso González, J.**, **Bueso Bello, J.**, Internal Calibration Tool Verification and Validation Plan, Technical Note, 18 pages, PZ-DLR-PL-1310, 2011.

[R-467] **Tous Ramon, N.**, TDX-1 Panel PN-Gating DTs Analysis, Technical Note, 40 pages, TX-IOCS-TN-4357, 2011.

[R-468] **Wollstadt, S.**, Analysis on TerraSAR-X Spotlight Scene Size and Sliding Spotlight Azimuth Ambiguity Ratio, Technical Note, 20 pages, HR-RK-TN-SW01, 2011.

Doctoral Theses

2017

[PhD-1] **Jörg, H.**, Multi-Frequency Polarimetric SAR Tomography for the 3-D Characterization and Monitoring of Agricultural Crops, Dissertation, 100 pages, ETH Zurich, Institute of Environmental Engineering, Dec. 2017.

[PhD-2] **Dexin, L.**, Advanced Processing Techniques for GeoSAR Missions, Dissertation, National University of Defense Technology (NUDT), Changsha, Nov. 2017.

[PhD-3] **Queiroz de Almeida, F.**, Multichannel Staggered SAR for High-Resolution Wide-Swath Imaging, Dissertation, 273 pages, Karlsruher Institut für Technologie (KIT), Fakultät für Elektrotechnik und Informationstechnik, Dec. 2017.

2016

[PhD-4] Döring, B., Traceable Radiometric Calibration of Synthetic Aperture Radars, Dissertation, 200 pages, Karlsruher Institut für Technologie (KIT), Fakultät für Elektrotechnik und Informationstechnik, Feb. 2016.

[PhD-5] Eilers, J., Planning Procedures for SAR Satellite Systems for Interferometric Product Generation, Dissertation, 181 pages, Universität der Bundeswehr München, Apr. 2016.

[PhD-6] Gramini Ganesan, P., Retrieval of Soil Moisture Using Polarimetric SAR Remote Sensing, Dissertation, 178 pages, Indian Institute of Technology Bombay, Centre of Studies in Resources Engineering, Jul. 2016.

[PhD-7] Pinheiro, M., Multi-Mode SAR Interferometry for High-Precision DEM Generation, Dissertation, 232 pages, Karlsruher Institut für Technologie (KIT), Fakultät für Elektrotechnik und Informationstechnik, Dec. 2016.

[PhD-8] Ponce Madrigal, O., Multicircular Holographic SAR Tomography over Forested Areas, Dissertation, 162 pages, ETH Zurich, Departement Bau, Umwelt und Geomatik (D-BAUG), Dec. 2016.

[PhD-9] Toraño Caicoya, A., Allometric Estimation of Aboveground Forest Biomass Using Forest Structure Parameters Estimated by Means of Multibaseline SAR Measurements, Dissertation, Technische Universität München (TUM), Lehrstuhl für Waldwachstumskunde, Apr. 2016.

[PhD-10] Villano, M., Staggered Synthetic Aperture Radar, Dissertation, 181 pages, Karlsruher Institut für Technologie (KIT), Fakultät für Elektrotechnik und Informationstechnik, Feb. 2016.

2015

[PhD-11] Anglberger, H., Simulation and Analysis of SAR Signatures with High Resolution, Dissertation, 249 pages, Universität der Bundeswehr München, Fakultät für Luft- und Raumfahrttechnik, Dec. 2015.

[PhD-12] Bachmann, M., Antenna Pattern Modeling and Calibration for Spaceborne SAR Systems, Dissertation, 217 pages, Karlsruher Institut für Technologie (KIT), Fakultät für Elektrotechnik und Informationstechnik, Jul. 2015.

[PhD-13] Kugler, F., Pol-InSAR Forest Height Estimation at Different Frequencies: Opportunities and Limitations, Dissertation, 154 pages, Technical University Munich (TUM), Chair in Forest Growth and Yield Science, Dec. 2015.

[PhD-14] Parrella, G., Characterization of Glacier Facies Using SAR Polarimetry at Long Wavelengths, Dissertation, 166 pages, ETH Zurich, Institue of Environmental Engineering, Nov. 2015.

[PhD-15] Zonno, M., SAR Images Processing: Advancements in GB-SAR Data Focusing and InSAR Applications, Dissertation, 160 pages, Politecnico di Bari, Department of Electrics and Information Engineering, Mar. 2015.

2014

[PhD-16] Aguilera, E., Synthetic Aperture Radar Tomography – Compressed Sensing Models and Algorithms, Dissertation, 120 pages, Technical University of Berlin, Sep. 2014.

[PhD-17] Baumgartner, S., Traffic Monitoring with Air- and Spaceborne Synthetic Aperture Radar, Dissertation, 242 pages, Karlsruher Institut für Technologie (KIT), Fakultät für Elektrotechnik und Informationstechnik, Jul. 2014.

[PhD-18] Bräutigam, B., Instrument Calibration of Spaceborne SAR Systems, Dissertation, 221 pages, Karlsruher Institut für Technologie (KIT), Fakultät für Elektrotechnik und Informationstechnik, Jul. 2014.

[PhD-19] Huber, S., Spaceborne Reflector SAR Systems with Digital Beamforming, Dissertation, 159 pages, Karlsruher Institut für Technologie (KIT), Fakultät für Elektrotechnik und Informationstechnik, Feb. 2014.

[PhD-20] Schreiber, E., Fully Electronic Passive Microwave Imaging System Using Beam Steering by Frequency Shift and Aperture Synthesis, Dissertation, 234 pages, Karlsruher Institut für Technologie, Fakultät für Elektrotechnik und Informationstechnik, Jun. 2014.

2013

[PhD-21] Al-Kahachi, N., Polarimetric SAR Modelling of a Two-Layer Structure: A Case Study Based on Subarctic Lakes, Dissertation, 163 pages, Technische Universität München (TUM), Elektrotechnik und Informationstechnik, Dec. 2013.

[PhD-22] Gabele, M., SAR/GMTI for Space-Based Radar with Two-Dimensional Antenna Arrays, Dissertation, 198 pages, Karlsruher Institut für Technologie (KIT), Institut für Hochfrequenztechnik und Elektronik, May 2013.

[PhD-23] Kim, J., Development of Ionosphere Estimation Techniques for the Correction of SAR Data, Dissertation, 130 pages, ETH Zurich, Department of Civil, Environmental and Geomatic Engineering (D-BAUG), Oct. 2013.

[PhD-24] Sanjuan Ferrer, M., Detection of Coherent Scatterers in SAR Data: Algorithms and Applications, Dissertation, 166 pages, ETH Zurich, Department of Civil, Environmental and Geomatic Engineering, Oct. 2013.

2012

[PhD-25] Culhaoglu, A., Microwave Metamaterials: Superlensing and Design of Low Reflection Coatings, Dissertation, 124 pages, Technische Universität München (TUM), Sep. 2012.

[PhD-26] Jagdhuber, T., Soil Parameter Retrieval under Vegetation Cover Using SAR Polarimetry, Dissertation, 236 pages, University of Potsdam, Faculty of Mathematics and Natural Sciences, Jul. 2012.

[PhD-27] Lee, S., Forest Parameter Estimation Using Polarimetric SAR Interferometry Techniques at Low Frequencies, Dissertation, 109 pages, ETH Zurich, Chair of Earth Observation and Remote Sensing, Oct. 2012.

[PhD-28] Rodríguez Cassolà, M., Bistatic Synthetic Aperture Radar Data Processing, Dissertation, 182 pages, Karlsruher Institut für Technologie (KIT), Fakultät für Elektrotechnik und Informationstechnik, Dec. 2012.

2011

[PhD-29] Jirousek, M., Imaging Microwave Spectrometer with Aperture Synthesis, Dissertation, 100 pages, Karlsruher Institut für Technologie (KIT), Faculty of Electrical Engineering and Information Technology, Jul. 2011.

[PhD-30] Jochim, F., The Application of Hansen-Systems in Celestial Mechanics and Astro Dynamics, Dissertation, 221 pages, Universität der Bundeswehr München, Fakultät für Luft- und Raumfahrt, Apr. 2011.

[PhD-31] **Kim, J.**, Multiple-Input Multiple-Output Synthetic Aperture Radar (SAR) for Multimodal Operation, Dissertation, 210 pages, Karlsruher Institut für Technologie (KIT), Faculty of Electrical Engineering and Information Technology, Dec. 2011.

Diploma and Master Theses

2017

[MaT-1] **Bischeltsrieder, F.**, Untersuchung zu einem abbildenden harmonischen Radar mit digitaler Strahlformung, Master Thesis, 84 pages, Technische Universität München (TUM), Fakultät für Elektrotechnik und Informationstechnik, 2017.

[MaT-2] **Heiderich, L.**, Performance Analysis of Multi-Static SAR Satellite Data, Master Thesis, 127 pages, Hochschule für angewandte Wissenschaften München, Fakultät für Elektrotechnik und Informationstechnik, May 2017.

[MaT-3] **Kousidis, K.**, Multi-Dimensional SAR Imaging Based on Compressive Sensing, Master Thesis, 80 pages, Technische Universität München (TUM), Fakultät für Informatik, Apr. 2017.

[MaT-4] **Link, M.**, Potential and Limitations of Soil Moisture Induced Active-Passive Microwave Covariation: A Modeling Study for the Mono- and Dual-Frequency Case, Master Thesis, 103 pages, Ludwig-Maximilians-Universität (LMU) München, Department für Geographie, Sep. 2017.

[MaT-5] **Mouthaan, K.**, Digital Beamforming for Spaceborne Reflector SAR Systems via FIR Filter Networks in the Presence of Uncertainties, Master Thesis, 70 pages, Technische Universität Berlin, Institut für Luft- und Raumfahrt, Feb. 2017.

[MaT-6] **Pawar, B.**, Concept and Demonstration of a SAR Receiver with Intra-Drift Correction, Master Thesis, 76 pages, Ernst-Abbe-Hochschule Jena, Jun. 2017.

[MaT-7] **Pulella, A.**, An Analysis of the Potentials of TanDEM-X Data to Characterize Tropical Forest Horizontal Heterogeneity, Master Thesis, 80 pages, Università di Pisa, Jun. 2017.

[MaT-8] **Weber, C.**, Development of Innovative Processing Methods for Monostatic and Bistatic SAR Data, Master Thesis, 65 pages, Technische Universität München (TUM), Fakultät für Elektrotechnik und Informationstechnik, Mar. 2017.

[MaT-9] **Yelahanka Nagaraja, S.**, Visualization, Detection and Reconstruction of Trees in Fully Polarimetric Long Wavelength SAR Imagery, Master Thesis, 89 pages, Technische Universität Chemnitz, Fakultät für Elektrotechnik und Informationstechnik, Oct. 2017.

2016

[MaT-10] **Aitha, S.**, Development, Manufacturing, and Testing of a P- and L-Band Outdoor Horn Antenna, Master Thesis, 99 pages, Universität Kassel, Fachgebiet Mikrowellenelektronik, Oct. 2016.

[MaT-11] **Dirscherl, M.**, Topographic Change Quantification and DEM Uncertainty Assessment Using TanDEM-X and F-SAR DEM Time Series and Quality Maps: Application to the 2014-2015 Bárðarbunga Volcanic Eruption, Iceland, Master Thesis, 77 pages, University College London, Department of Geography, Aug. 2016.

[MaT-12] **Freitas Carvalho, R.**, A Posteriori Knowledge Based Digital Beamforming Concepts Demonstrated with Multi-Channel SAR Data, Diploma Thesis, 69 pages, Instituto Tecnológico de Aeronáutica (ITA), Nov. 2016.

[MaT-13] **Kraus, L.**, Theoretische und experimentelle Untersuchungen zur Bestimmung von Bodenfeuchte mit breitbandigem Radar, Master Thesis, 72 pages, Universität Augsburg, Institut für Geographie, Dec. 2016.

[MaT-14] **Kroll, J.**, Untersuchung und Modellierung von Hardwareeinflüssen auf Mehrkanal-SAR-Systeme, Master Thesis, 91 pages, Karlsruher Institut für Technologie (KIT), Fakultät für Elektrotechnik und Informationstechnik, Sep. 2016.

[MaT-15] **Möhring, B.**, Modular Simulation of a Compact Antenna Test Range, Master Thesis, 100 pages, Technische Universität München (TUM), Lehrstuhl für Hochfrequenztechnik, Sep. 2016.

[MaT-16] **Pozza, D.**, Analysis of Vertical Structure of Forests at X-Band and Synergies with Lidar, Master Thesis, 100 pages, Università degli Studi di Trento, May 2016.

[MaT-17] **Raab, S.**, Development and Implementation of an Efficient Temperature Management System for SAR System Calibration Transponders, Master Thesis, 86 pages, Hochschule für angewandte Wissenschaften Würzburg-Schweinfurt, Fakultät Elektrotechnik, Apr. 2016.

[MaT-18] **Valdo, P.**, Detection of Changes in Agricultural Scenarios by Means of TanDEM-X Data, Master Thesis, 100 pages, Università degli Studi di Trento, May 2016.

2015

[MaT-19] **Bertoluzza, M.**, Monitoring Forest Height Dynamics by Means of L-Band Multibaseline PolInSAR Data, Master Thesis, 54 pages, Università degli Studi di Trento, Jan. 2015.

[MaT-20] **Haas, A.**, Entwicklung einer breitbandigen Speiseantenne für ein Cassegrain-Antennensystem in der Radarfernerkundung, Diploma Thesis, 62 pages, Karlsruher Institut für Technologie (KIT), Institut für Hochfrequenztechnik und Elektronik (IHE), May 2015.

[MaT-21] **Heinzel, A.**, Untersuchung von Fokussierungsmöglichkeiten einer SAR-Abbildung bei Halbräumen unterschiedlicher Permittivität, Master Thesis, 63 pages, Technische Universität München (TUM), Fakultät für Elektrotechnik und Informationstechnik, Sep. 2015.

[MaT-22] **Marongiu, S.**, Estimation of Vertical Structure of Forests from Multibaseline SAR Data: A Performance Analysis, Master Thesis, 85 pages, Università di Pisa, Mar. 2015.

[MaT-23] **Severino, C.**, Compact Feeding System for a P-Band Circular Horn Antenna, Diploma Thesis, 80 pages, Instituto Tecnológico de Aeronáutica (ITA), Nov. 2015.

[MaT-24] **Tiwari, S.**, Spaceborne-Airborne Bistatic SAR: Data Processing and Calibration of an Experimental Acquisition between TanDEM-X and F-SAR, Master Thesis, 50 pages, Universität Kassel, Fachgebiet Nachrichtentechnik, Mar. 2015.

[MaT-25] **Wallner, D.**, Untersuchungen zur radartechnischen Erweiterung eines radiometrischen Abbildungssystems, Master Thesis, 102 pages, Technische Universität München (TUM), Fakultät für Elektrotechnik und Informationstechnik, Oct. 2015.

[MaT-26] **Weiß, T.**, Polarimetric Analyses of SAR Data towards Plant Moisture Estimation, Master Thesis, 70 pages, Ludwig-Maximilians-Universität (LMU) München, Department für Geographie, Aug. 2015.

2014

[MaT-27] Albers, T., Aufbau eines Radarsystems zur Detektion von Verunreinigungen, Master Thesis, 71 pages, Hochschule für angewandte Wissenschaften Würzburg-Schweinfurt, Fakultät Elektrotechnik, Nov. 2014.

[MaT-28] Axt, H., Vergleichende Analyse von Antennenkonzepten für P-Band Kalibriertransponder, Diploma Thesis, 77 pages, Hochschule für angewandte Wissenschaften Würzburg-Schweinfurt, Sep. 2014.

[MaT-29] Gehrig, S., Untersuchung zur Abbildungsqualität und Absolutwertgenauigkeit eines hochauflösenden Pulsradars, Diploma Thesis, 85 pages, Hochschule für angewandte Wissenschaften Würzburg-Schweinfurt, Fakultät Nachrichtentechnik, Sep. 2014.

[MaT-30] Grill, J., Analyse von SAR-Bildmaterial in der Umgebung von Minenfeldern in semiariden Gebieten, Master Thesis, 146 pages, Universität der Bundeswehr München, Aug. 2014.

[MaT-31] Iff, S., Untersuchungen zum Nachweis von SAR-Bildqualitätsparametern, Master Thesis, 87 pages, Hochschule für angewandte Wissenschaften Würzburg-Schweinfurt, Sep. 2014.

[MaT-32] Lloredo, J., Joint Phase Unwrapping for Multi-Frequency SAR Interferometry, Master Thesis, 76 pages, Ecole nationale supérieure de l'électronique et de ses applications ENSEA, Aug. 2014.

[MaT-33] Melo Galvao Machado, B., Performance Analysis of Rotating SAR (RoSAR), Diploma Thesis, 80 pages, Instituto Tecnológico de Aeronáutica (ITA), Dec. 2014.

[MaT-34] Özis, E., Metamaterial Technologies for Microwave Radomes, Master Thesis, 88 pages, Technische Universität München (TUM), Fakultät für Elektrotechnik und Informationstechnik, Jan. 2014.

[MaT-35] Rosigkeit, D., Verwendbarkeit von LTE im DLR Forschungsflugzeug DO 228-212, Master Thesis, Fachhochschule Lübeck, Dec. 2014.

[MaT-36] Sorrentino, A., Investigation of Polarimetric Active/Passive Microwave Scattering towards Soil Moisture Estimation, Master Thesis, 84 pages, Università degli Studi di Napoli Federico II, Dipartimento di Ingegneria Elettrica e Tecnologie dell'Informazione, Jul. 2014.

2013

[MaT-37] Brancato, V., Electromagnetic Modeling of P-Band Polarimetric SAR Signatures of Polythermal Ice Cap, Master Thesis, 95 pages, University of Naples, Italy, Sep. 2013.

[MaT-38] Cantini, A., 3-D Structure of a Forest at L-Band: Experiments Towards a Spaceborne Implementation, Master Thesis, 110 pages, Università di Pisa, Italy, Department of Information Engineering, Sep. 2013.

[MaT-39] Caputo, M., Soil Moisture Retrieval under a Changing Vegetation Cover Using Dual Polarimetric Data at X-Band, Master Thesis, 110 pages, University of Naples, Italy, Sep. 2013.

[MaT-40] Iff, S., Untersuchungen zur Fehleranalyse und zu Kalibrationsmethoden für ein breitbandiges Pulsradar, Diploma Thesis, 92 pages, Hochschule für angewandte Wissenschaften Würzburg-Schweinfurt, Oct. 2013.

[MaT-41] Kötschau, C., Frequency Analysis of Radar Backscatter in X-Band Using F-SAR Data, Diploma Thesis, 68 pages, Karlsruhe Institut für Technologie (KIT), Institut für Hochfrequenztechnik und Elektronik, Dec. 2013.

[MaT-42] Liebschwager, T., Erste Untersuchungen zu einem radarbasierten SSA-Systemverbund, Master Thesis, 82 pages, Universität der Bundeswehr München, Sep. 2013.

[MaT-43] Lopes Melo, R., Hardware Extension and Experiments for the Digital Beamforming Radar Ground Demonstrator, Diploma Thesis, 100 pages, Instituto Tecnológico de Aeronáutica (ITA), Electronics Engineering, Dec. 2013.

[MaT-44] Madanahalli Jai Prakash, A., Investigations of OFDM Signals for Imaging Radar Applications, Master Thesis, 76 pages, Technische Universität München (TUM), Fakultät für Elektrotechnik und Informationstechnik, Oct. 2013.

[MaT-45] Raab, S., Planung und Durchführung einer Freifeld-RCS-Messreihe zur genauen Kalibrierung von Referenzzielen, Diploma Thesis, 66 pages, Hochschule für angewandte Wissenschaften Würzburg-Schweinfurt, Fakultät Elektrotechnik, Apr. 2013.

[MaT-46] Stockamp, J., Multi-Frequency Analysis of Snow-Covered Areas Using SAR Polarimetry, Master Thesis, 113 pages, Ludwig-Maximilians-Universität (LMU) München, Department für Geographie, Mar. 2013.

[MaT-47] Wiese, T., Potentielle Anwendungen moderner Inpainting-Algorithmen für die Verarbeitung von Höhenmodellen in der Fernerkundung, Diploma Thesis, 145 pages, Technische Universität Dresden, Fakultät für Umweltwissenschaften, Institut für Kartographie, Feb. 2013.

2012

[MaT-48] Albers, T., Optimierung und messtechnische Verifikation eines Millimeterwellen-FMCW-Radars, Diploma Thesis, 83 pages, Hochschule für angewandte Wissenschaften Würzburg-Schweinfurt, Fakultät Elektrotechnik, Sep. 2012.

[MaT-49] Anger, S., Experimenteller Aufbau und Untersuchung integrierter Empfangsmodule für die Apertursynthese, Master Thesis, 80 pages, Universität Ulm, Institut für Mikrowellentechnik, May 2012.

[MaT-50] Balkoski, J., Nadir Echo Properties and Suppression in Spaceborne Synthetic Aperture Radar Systems - A Study Based on TerraSAR-X Data, Master Thesis, 81 pages, University of Belgrad, Faculty of Electrotechnics, Nov. 2012.

[MaT-51] Dabrowski, S., Untersuchung der Auswirkungen block-adaptiver Quantisierung (BAQ) von SAR-Rohdaten auf die Bildqualität, Diploma Thesis, 68 pages, Karlsruher Institut für Technologie (KIT), Institut für Hochfrequenztechnik und Elektronik, Sep. 2012.

[MaT-52] Della Corte, A., Snow Properties Retrieval Using TerraSAR-X Dual-Polarization Data, Master Thesis, University of Naples, Dipartimento di Ingegneria Biomedica, Elettronica e delle Telecomunicazioni (DIBET), Mar. 2012.

[MaT-53] Festi, G., Development and Implementation of a Digital Internal Calibration Strategy for Precise SAR Reference Targets, Master Thesis, 65 pages, Università degli Studi di Trento, Ingegneria delle Telecomunicazioni, Sep. 2012.

[MaT-54] Kant, P., Systemanalysen und Verfahren zur Kalibrierung eines breitbandigen digitalen Pulsradars, Diploma Thesis, 80 pages, Karlsruher Institut für Technologie (KIT), Institut für Hochfrequenztechnik und Elektronik (IHE), Jun. 2012.

[MaT-55] Massaroli, G., Crop Volume Characterization Using Dual Polarimetric SAR in X-Band, Master Thesis, Universita' degli Studi di Napoli Federico II, Dipartimento di Ingegneria Elettronica e delle Telecomunicazioni, Apr. 2012.

[MaT-56] Profelt, J., Anwendung elastischer Koregistrierungsverfahren auf hoch auflösende Radar-Bildpaare, Master Thesis, 76 pages, Technische Universität München (TUM), Lehrstuhl für Datenverarbeitung, Dec. 2012.

[MaT-57] Queiroz de Almeida, V., Performance Analysis of Medium Earth Orbit and Geosynchronous Synthetic Aperture Radar, Diploma Thesis, 107 pages, Instituto Tecnológico de Aeronáutica (ITA), Jul. 2012.

[MaT-58] Rückel, T., Signaturanalysen polarimetrischer SAR-Daten von Radarsat-2 und F-SAR, Diploma Thesis, 161 pages, Universität der Bundeswehr München, Mar. 2012.

[MaT-59] Simon, D., Weiterentwicklung einer Hohlleiterschlitzantenne für elektronisches Schwenken der Antennenkeule bei radiometrischen Abbildungen, Master Thesis, 95 pages, Universität Kassel, Institut für Mikrowellenelektronik, 2012.

[MaT-60] Thiemer, P., Aufbau und messtechnische Verifikation eines breitbandigen digitalen Pulsradars, Diploma Thesis, 83 pages, Hochschule für angewandte Wissenschaften Würzburg - Schweinfurt, Fakultät Elektrotechnik / Nachrichtentechnik, Aug. 2012.

2011

[MaT-61] Antonello, A., Implementation of Compressed Sensing Algorithms in Python, Diploma Thesis, 90 pages, Instituto Tecnológico de Aeronáutica (ITA), Brazil, Dec. 2011.

[MaT-62] Bianco, V., Phase Calibration of Multibaseline PolInSAR Data Stacks, Master Thesis, 100 pages, Universita' degli studi di Napoli 'Federico II', Ingegneria elettronica e delle telecomunicazioni, Dec. 2011.

[MaT-63] Eyssartier, K., Monitoring the Petermann Ice Island (2010) Using TanDEM-X Satellites, Diploma Thesis, 34 pages, Institute National Polytechnique de Grenoble, Sep. 2011.

[MaT-64] Helbig, D., Genauigkeitsanalyse der Georeferenzierung für SAR Bildprodukte, Diploma Thesis, 86 pages, Universität der Bundeswehr München, Institut für Photogrammetrie und Kartografie, Mar. 2011.

[MaT-65] Hepner, C., Erstellung dreidimensionaler Radarsignaturen aus Turm-Drehstands-Messungen mit ausgedünnter Apertur, Master Thesis, 116 pages, Hochschule Ulm, Fakultät Elektrotechnik und Informationstechnik, Mar. 2011.

[MaT-66] Illner, S., Charakterisierung und Untersuchungen zur Fehlerkorrektur eines Millimeterwellen-FMCW-Radars, Diploma Thesis, 91 pages, Fachhochschule Würzburg-Schweinfurt, Fachbereich Elektrotechnik-Nachrichtentechnik, Aug. 2011.

[MaT-67] Pereira Vicente, L., Correlating SAR: Concepts and Simulation, Diploma Thesis, 50 pages, Instituto Tecnológico de Aeronáutica (ITA), Oct. 2011.

[MaT-68] Pisciottano, I., First Analysis on Snow Cover Change Using Polarimetric TerraSAR-X Data, Master Thesis, 128 pages, Università degli Studi di Napoli Federico II, Mar. 2011.

[MaT-69] Rommel, T., Aufbau eines Radars, auf Basis eines FMCW-Radars, zur Untersuchung der Eignung orthogonaler Signale für die SAR-Prozessierung, Diploma Thesis, 73 pages, Hochschule für angewandte Wissenschaften Würzburg - Schweinfurt, Fakultät Elektrotechnik, Aug. 2011.

[MaT-70] Scheuerer, L., Integration eines Mehrkanal-Analog-Digital-Wandlers in das Apertursynthese-Radiometer ANSAS, Diploma Thesis, 73 pages, Hochschule für angewandte Wissenschaften Würzburg - Schweinfurt, Fachbereich Elektrotechnik-Nachrichtentechnik, Aug. 2011.

[MaT-71] Simon, D., Untersuchung möglicher Leitungsübergänge von Hohlleiter auf Streifenleitung für radiometrische Anwendungen, Diploma Thesis, Universität Kassel, Fachgebiet Mikrowellenelektronik, Jul. 2011.

Bachelor Theses

2017

[BaT-1] Baris, I., Physikalische Integration von Streumodellen für Mikrowellen und optische Wellenlängen, Bachelor Thesis, 109 pages, Georg-August-University Göttingen, Sep. 2017.

[BaT-2] Engel, M., Entwicklung und Anaylse von Teilkomponenten eines Ultraleicht-UWB-Radars, Bachelor Thesis, Hochschule für angewandte Wissenschaften Würzburg-Schweinfurt, Fakultät Elektrotechnik, 2017.

[BaT-3] van Kempen, M., Refokussierungsverfahren für Schiffe in flugzeuggestützten SAR Bildern, Bachelor Thesis, 51 pages, Duale Hochschule Baden-Württemberg Mannheim, Informationstechnik, Sep. 2017.

2016

[BaT-4] Kaschke, M., Charakterisierung mehrschichtiger Materialien für Mikrowellenfrequenzen mit Hilfe eines evolutionären Algorithmus, Bachelor Thesis, 108 pages, Duale Hochschule Baden-Württemberg Mannheim, Informationstechnik, Sep. 2016.

2015

[BaT-5] Braun, S., An Integer Linear Programming Approach to Multi-Satellite Mission Planning, Bachelor Thesis, 58 pages, Technische Universität München (TUM), Lehrstuhl für angewandte Geometrie und Diskrete Mathematik, Oct. 2015.

[BaT-6] Linde Cerezo, A., Performance Assessment and Design of Advance Processing Techniques for Innovative SAR Acquisitions, Bachelor Thesis, 100 pages, Universidad de Alcalá, Signal Theory and Telecommunications Department, Sep. 2015.

[BaT-7] Ditton, B., Parametrische Abschätzung der zu erwartenden Bildqualität für flugzeuggestützte SAR Sensoren, Bachelor Thesis, 78 pages, Duale Hochschule Baden-Württemberg Mannheim, Informationstechnik, Sep. 2015.

[BaT-8] Marcinkowski, B., Investigation in Basic Micro Doppler Analysis with a High Resolution Pulse Radar, Bachelor Thesis, 50 pages, Karlsruher Institut für Technologie (KIT), Institut für Hochfrequenztechnik und Elektronik (IHE); Gdansk University of Technology, Department of Electronics, Telecommunication and Informatics, Jan. 2015.

[BaT-9] Szulc, Z., Development of a Broadband Slotted-Waveguide Antenna at X-Band for Radiometric Applications, Bachelor Thesis, 55 pages, Karlsruher Institut für Technologie, Fakultät für Elektrotechnik und Informationstechnik, Jan. 2015.

[BaT-10] Telega, M., Parametrische Berechnung der Einflüsse von Verformungen bei Corner Reflektoren auf den RCS, Bachelor Thesis, 50 pages, Karlsruher Institut für Technologie (KIT), Institut für Hochfrequenztechnik und Elektronik, Jan. 2015.

[BaT-11] Trumpp, J., Untersuchung zu Techniken der elektronischen Strahlformung für abbildende Mikrowellenradiometer, Bachelor Thesis, 61 pages, Karlsruher Institut für Technologie (KIT), Institut für Hochfrequenztechnik und Elektronik, Oct. 2015.

2014

[BaT-12] Bischeltsrieder, F., Untersuchungen von Verfahren zur Bewegungskompensation bei höchstauflösenden SAR-Systemen, Bachelor Thesis, 60 pages, Hochschule für angewandte Wissenschaften München, Angewandte Naturwissenschaften und Mechatronik, Nov. 2014.

[BaT-13] Rauh, L., Entwicklung und Optimierung einer Wendelantenne für den Einsatz in einem Mikrowellen-Autoklav, Bachelor Thesis, Hochschule für angewandte Wissenschaften München, Physikalische Technik, Elektronik und Numerische Physik, Apr. 2014.

[BaT-14] de Sousa Rego, E., Theoretical Investigation of High-Resolution SAR for Buried Object Detection, Bachelor Thesis, 57 pages, Instituto Tecnológico de Aeronáutica (ITA), Divisão de Engenharia Eletrônica, Nov. 2014.

[BaT-15] Stambouli, F., Digitale Kalibrierung mehrkanaliger SAR-Systeme, Bachelor Thesis, 45 pages, Karlsruher Institut für Technologie (KIT), Fakultät für Elektrotechnik und Informationstechnik, Oct. 2014.

2013

[BaT-16] Heinzel, A., Untersuchungen über die Verwendung von UHF-SAR im Nahbereich zur Detektion verborgener Objekte, Bachelor Thesis, Technische Universität München (TUM), Lehrstuhl für Hochfrequenztechnik, Sep. 2013.

[BaT-17] Posovszky, P., Entwicklung einer 3D-Animations-Bibiliothek für Java zur Darstellung von Flugobjekten und Flugtrajektorien, Duale Hochschule Baden-Württemberg Mannheim, Bachelor Thesis, 72 pages, Oct. 2013.

2011

[BaT-18] Künemund, M., Hochauflösende Prozessierung flugzeuggestützter SAR Daten auf GPU, Bachelor Thesis, 91 pages, Duale Hochschule Baden-Württemberg Mannheim, Studiengang Informationstechnik, Sep. 2011.

Internship Theses

2017

[InT-1] Beitler, D., Konzeption, Implementierung und Inbetriebnahme einer postgreSQL-Datenbank – Bericht zum Modul Praxis I, Project Thesis, Duale Hochschule Baden-Württemberg Mannheim, Informationstechnik, Oct. 2017.

[InT-2] van Kempen, M., Echtzeitfähige Analyse und Zuordnung von AIS-Signalen zu SAR-Bildinformation, Praxisbericht "Modul III", Project Thesis, 21 pages, Duale Hochschule Baden-Württemberg Mannheim, Informationstechnik, 2017.

2016

[InT-3] Bischeltsrieder, F., Systemaufbau eines abbildenden harmonischen Radars, Project Thesis, Technische Universität München (TUM), Fakultät für Elektrotechnik und Informationstechnik, 2016.

[InT-4] Haque, A., Praktikumsbericht, Project Thesis, 43 pages, Karlsruher Institut für Technologie (KIT), Institut für Hochfrequenztechnik und Elektronik, May 2016.

[InT-5] Kaschke, M., Erweiterungen des Regressionsmodells zur Materialparameterbestimmung basierend auf Mikrowellen-Transmissions- und Reflexionsmessdaten, Project Thesis, 63 pages, Duale Hochschule Baden-Württemberg Mannheim, Informationstechnik, Mar. 2016.

[InT-6] Pawar, B., Entwicklung eines Prototypen für einen Mehrkanaltransponder, Project Thesis, Ernst-Abbe-Hochschule Jena, 2016.

[InT-7] Schreiber, E., **Bischeltsrieder, F.**, Voruntersuchungen zum nichtlinearen Verhalten von elektronischen Bauteilen und Geräten zur Entwicklung eines harmonischen Radars, Project Thesis, 16 pages, Technische Universität München (TUM), Fakultät für Elektrotechnik und Informationstechnik, Mar. 2016.

[InT-8] van Kempen, M., SAR-Rohdatensimulation von fahrenden Schiffen, Praxisbericht Modul "Praxis II", Project Thesis, 23 pages, Duale Hochschule Baden-Württemberg Mannheim, Informationstechnik, Sep. 2016.

[InT-9] van Kempen, M., Analyse von Interpolationsverfahren zur Georeferenzierung von SAR Daten, Praxisbericht Modul "Praxis II", Project Thesis, 21 pages, Duale Hochschule Baden-Württemberg Mannheim, Informationstechnik, 2016.

2015

[InT-10] Kaschke, M., Mikrowellenreflexion und Transmission an dispersiven Schichten, Project Thesis, 81 pages, Duale Hochschule Baden-Württemberg Mannheim, Informationstechnik, Sep. 2015.

[InT-11] Marahrens, S., **Rommel, T.**, Praktikumsbericht, Project Thesis, 32 pages, Karlsruher Institut für Technologie (KIT), Institut für Hochfrequenztechnik und Elektronik, Jul. 2015.

[InT-12] van Kempen, M., Schnittstellen Implementierung für ein SAR-Daten Analysewerkzeug in Python – Auswahl von Interessengebieten in F-SAR Produkten: Konzeption und Implementierung in Python, Praxisbericht Modul "Praxis I", Project Thesis, 55 pages, Duale Hochschule Baden-Württemberg Mannheim, Informationstechnik, Sep. 2015.

2014

[InT-13] Ditton, B., Implementierung der SAR-Rohdatenanalyse als Teil einer Transkriptionssoftware für Flugzeug-SAR-Rohdaten, Praxisbericht Modul "Praxis II", Project Thesis, 45 pages, Duale Hochschule Baden-Württemberg Mannheim, Informationstechnik, Sep. 2014.

[InT-14] Gehrig, S., Praktikumsbericht, Project Thesis, Hochschule Würzburg-Schweinfurt, Fakultät Elektrotechnik, Feb. 2014.

[InT-15] Haas, A., Weiterentwicklung eines Apertursynthese-radiometer-Demonstrators zur Verbesserung der räumlichen Auflösung, Project Thesis, Karlsruher Institut für Technologie (KIT), Institut für Hochfrequenztechnik und Elektronik (IHE), 2014.

[InT-16] Heinzel, A., Durchführung und Analyse von Messungen mit einem bodengebunden Nahbereichs-Radarsystem, Project Thesis, Technische Universität München (TUM), Elektro- und Informationstechnik, Oct. 2014.

2013

[InT-17] Ditton, B., F-SAR Rohdaten-Transkription via Phyton, Praxisbericht Modul "Praxis I", Project Thesis, 30 pages, Duale Hochschule Baden-Württemberg Mannheim, Informationstechnik, Sep. 2013.

[InT-18] Kirschner, F., Praktikumsbericht (Systemtechnik), Project Thesis, Technische Universität München (TUM), 2013.

[InT-19] Liebschwager, T., Studie über die Fähigkeiten globaler Space Situational Awareness Systeme, Project Thesis, 63 pages, Universität der Bundeswehr München, Jan. 2013.

2012

[InT-20] Heinzel, A., Untersuchung und Verifikation der Rauschleistungsmessung unterschiedlicher Leistungsmessgeräte, Project Thesis, Technische Universität München (TUM), Jun. 2012.

[InT-21] Madanahalli Jai Prakash, A., **Rommel, T.**, Softwareentwicklung für den DBF-Hardware Demonstrator, Project Thesis, 28 pages, Technische Universität München (TUM), Fakultät für Elektrotechnik und Informationstechnik, May 2012.

[InT-22] Pipaud, F., Erstellen von TanDEM-X DEMs für geomorphologische Fragestellungen, Project Thesis, Rheinisch-Westfälische Technische Hochschule Aachen, Lehrstuhl für Physische Geographie und Geoökologie, May 2012.

[InT-23] Wiese, T., Entwicklung von erweiterten Darstellungswerkzeugen für digitale Höhenmodelle im Rahmen der TanDEM-X-Mission, Project Thesis, 97 pages, Technische Universität Dresden, Fakultät Forst-, Geo- und Hydrowissenschaften, Institut für Kartographie, Feb. 2012.

2011

[InT-24] Zobel, G., Untersuchung von ausgedünnten Aperturen auf die SAR Bildqualität, Project Thesis, Hochschule für angewandte Wissenschaften Würzburg-Schweinfurt, 2011.

Patents

2017

[P-1] Baumgartner, S., Schaefer, C., Synthetic Aperture Radar for Simultaneous Imaging and Moving Target Detection, Priority establishing European Patent EP000002725382B1, prio. est. on 26 October 2012, granted on 18 January 2017.

[P-2] Mittermayer, J., **López-Dekker, F.**, **Prats Iraola, P.**, **Kraus, T.**, **Krieger, G.**, **Moreira, A.**, Verfahren zur Erstellung eines Erdbeobachtungsbildes einer Region mittels eines Radars mit synthetischer Apertur, Priority establishing German Patent DE102016209803B3, prio. est. on 03 June 2016, granted on 12 October 2017.

[P-3] Queiroz de Almeida, F., **Younis, M.**, **Krieger, G.**, **López-Dekker, F.**, **Moreira, A.**, Synthetik-Apertur-Radarverfahren und Synthetik-Apertur-Radarvorrichtung, Priority establishing German Patent DE102016208899B3, prio. est. on 23 May 2016, granted on 08 June 2017.

[P-4] Reimann, J., **Döring, B.**, **Schwerdt, M.**, **Rudolf, D.**, **Raab, S.**, Verfahren zur Kalibrierung eines aktiven Sensorsystems, Priority establishing German Patent DE102016101898B3, prio. est. on 03 February 2016, granted on 13 April 2017.

2016

[P-5] Huber, S., **Krieger, G.**, **Younis, M.**, Reflector Antenna for a Synthetic Aperture Radar, Priority establishing European Patent EP000002735055B1, prio. est. on 20 July 2011, granted on 10 February 2016.

[P-6] Huber, S., **Krieger, G.**, **Younis, M.**, Reflector Antenna for a Synthetic Aperture Radar, Subsequent US Patent US000009531081B2, based on EP000002735055B1, prio. est. on 20 July 2011, granted on 27 December 2016.

[P-7] Martone, M., **Krieger, G.**, **Bräutigam, B.**, Verfahren und Vorrichtung zur rechnergestützten Verarbeitung von SAR-Rohdaten, Priority establishing German Patent DE102012209113B4, prio. est. on 30 May 2012, granted on 02 June 2016.

[P-8] Villano, M., **Krieger, G.**, **Moreira, A.**, Synthetik-Apertur-Radarverfahren und Synthetik-Apertur-Radarvorrichtung, Priority establishing German Patent DE102012219225B4, prio. est. on 22 October 2012, granted on 04 August 2016.

2015

[P-9] Döring, B., **Schwerdt, M.**, **Jirousek, M.**, **Rudolf, D.**, **Reimann, J.**, **Raab, S.**, Method for Absolute Radiometric Calibration of the Radar Cross-Section of Radar Targets, Priority establishing German Patent DE102014110079B3, prio. est. on 17 July 2014, granted on 09 July 2015.

[P-10] Hounam, D., **Limbach, M.**, Method for Localizing Objects by Means of an Imaging Radar System and Transponder for Localizing Objects by Means of such Radar Systems, Priority establishing European Patent EP000002018578B1, prio. est. on 12 May 2006, granted on 09 September 2015.

[P-11] Peichl, M., **Dill, S.**, **Albers, T.**, Inverses Synthetisches Apertur Radar (ISAR) und Verfahren zur Erfassung von Verunreinigungen in einem Material, Priority establishing German Patent DE102014106892B3, prio. est. on 15 May 2014, granted on 22 October 2015.

2014

[P-12] de Florio, S., Monitoring Data Delivery System for Earth Monitoring Satellite, has Small/Micro Courier Satellite Provided as Inter Satellite Connection for Delivery of Command from Earth Station to Monitoring Satellite or for Bridging Satellites, Priority establishing German Patent DE102008006432B4, prio. est. on 28 January 2008, granted on 31 December 2014.

[P-13] Rodríguez Cassolà, M., **Pinheiro, M.**, **Prats Iraola, P.**, **Krieger, G.**, Method for the Computer-Assisted Processing of SAR Data, Priority establishing German Patent DE102013213304B3, prio. est. on 08 July 2013, granted on 04 September 2014.

[P-14] **Younis, M.**, **Bordoni, F.**, **Krieger, G.**, **López-Dekker, F.**, **De Zan, F.**, Synthetic Aperture Radar Method, Priority establishing German Patent DE102013221756B3, prio. est. on 25 October 2013, granted on 16 October 2014.

2013

[P-15] **Brand, B.**, **Zehetbauer, T.**, Method for Reducing the Data Age of Image Products Obtained by Earth Observation Satellites , Subsequent French Patent FR000002893794B1, based on DE102005055918B3, prio. est. on 22 November 2005, granted on 15 February 2013.

[P-16] **Lopez Martinez, C.**, **Papathanassiou, K.**, Method for Estimating the Topography of the Earth's Surface in Areas with Plant Cover, Priority establishing Spanish Patent ES000002384922B1, prio. est. on 07 June 2010, granted on 11 June 2013.

[P-17] **Peichl, M.**, **Dill, S.**, **Jirousek, M.**, Berthel , D., Device for Two-Dimensional Imaging of Scenes by Microwave Scanning, Subsequent European Patent EP000002099095B1, based on DE102008013066B3, prio. est. on 06 March 2008, granted on 20 November 2013.

2012

[P-18] **Gebert, N.**, **Krieger, G.**, Synthetic Aperture Radar Process, Subsequent US Patent US000008134490B2, based on DE102007041373B3, prio. est. on 30 August 2007, granted on 13 March 2012.

[P-19] **Scheiber, R.**, Method for Examining an Ice Region or Dry Region Using Radar Echo Sounding, Subsequent US Patent US000008159384B2, based on DE102007015561B3, prio. est. on 29 March 2007, granted on 17 April 2012.

2011

[P-20] **Gebert, N.**, **Krieger, G.**, Synthetic Aperture Radar Process, Subsequent European Patent EP000002191297B1, based on DE102007041373B3, prio. est. on 30 August 2007, granted on 02 March 2011.

[P-21] **Krieger, G.**, **Gebert, N.**, **Moreira, A.**, High-Resolution Synthetic Aperture Side View Radar System Used By Means of Digital Beamforming, Subsequent US Patent US000007944390B2, based on EP000002018577B1, prio. est. on 13 May 2006, granted on 17 May 2011.

[P-22] **Krieger, G.**, **Gebert, N.**, **Moreira, A.**, High-Resolution Synthetic Aperture Side View Radar System Used By Means of Digital Beamforming, Priority establishing European Patent EP000002018577B1, prio. est. on 13 May 2006, granted on 27 April 2011.

[P-23] **Peichl, M.**, **Dill, S.**, **Jirousek, M.**, Berthel , D., Device for Two-Dimensional Imaging of Scenes by Microwave Scanning, Subsequent US Patent US000008009116B2, based on DE102008013066B3, prio. est. on 06 March 2008, granted on 30 August 2011.

[P-24] **Prats Iraola, P.**, **Mittermayer, J.**, **Scheiber, R.**, **Moreira, A.**, Method for Processing TOPS (Terrain Observation by Progressive Scan)-SAR (Synthetic Aperture Radar)-Raw Data, Subsequent US Patent US000008049657B2, based on DE102007031020B3, prio. est. on 04 July 2007, granted on 01 November 2011.

[P-25] **Scheiber, R.**, Method for Examining an Ice Region or Dry Region Using Radar Echo Sounding, Subsequent European Patent EP000002130062B1, based on DE102007015561B3, prio. est. on 29 March 2007, granted on 31 August 2011.

Acronyms and Abbreviations

Acronym	Expansion
2-D	Two-dimensional
3-D	Three-dimensional
4-D	Four-dimensional
A/D	Analog/Digital
AASR	Azimuth Ambiguity-to-Signal Ratio
ABOSCA	Abbildender BOdenSCAnner (ground based imaging radiometer system)
ACAE	Permanent station within cGPS Campi Flegrei network
ACRAS	Advanced Concept for RAdar Sounder (ESA project)
ACROSS	Advanced Remote Sensing - Ground Truth Demo and Test Facilities
ADC	Analog-to-Digital Converter
AIS	Automatic Identification System
ALOS	Advanced Land Observing Satellite, JAXA, Japan
AM	Antenna Model
AMP	Mean AMPlitude (mask)
ANSAS	Abbildendes Niederfrequenz-Spektrometer mit Apertur-Synthese
AO	Announcement of Opportunity
ARGOS	Airborne wide area high altitude monitoring system (DLR project)
ASAR	Advanced Synthetic Aperture Radar on-board ENVISAT
ASI	Italian Space Agency (Agenzia Spaziale Italiana)
ASR	Ambiguity-to-Sidelobe Ratio
ATI	Along-Track Interferometry
AWG	Arbitrary Waveform Generator
AWI	Alfred Wegener Research Institute, Germany
BAQ	Block Adaptive Quantization
BAS	British Antarctic Survey
BAS Algorithm	Baseband Azimuth Scaling Algorithm
BEEPS	BIOMASS End-to-End Performance Simulator
BEEPS-FE	BIOMASS End-to-End Performance Simulator Front End
BEES	BIOMASS End-to-End Simulator
BiDi	BiDirectional synthetic aperture radar
BIOMASS	ESA Earth Explorer Mission (P-Band SAR for forest biomass estimation)
BISTRO	BIstatische STReufeldberechnung einfacher Objekte (software tool)
BLU	Best Linear Unbiased
BMBF	German Federal Ministry of Education and Research (Bundesministerium für Bildung und Forschung)
BMVg	Bundesministerium der Verteidigung (German Ministry of Defence)
BNA	Bundesnetzagentur (German Federal Network Agency)
BP	Back-Projection
CAD	Computer-Aided Design
CAN	Controller Area Network bus
CASA	Construcciones Aeronáuticas SA (Spanish member of the Airbus Consortium)
C-BEEPS	Complete BIOMASS End-to-End Performance Simulator
CEOS	Committee on Earth Observation Satellites
CFRP	Carbon Fiber Reinforced Plastic
CMG	Controlled Momentum Gyroscopes
CNES	Centre National d'Études Spatiales, France

Acronym	Expansion
CONAE	Comisión Nacional de Actividades Espaciales (National Space Activities Commission of Argentina)
CoReH2O	ESA Earth Explorer Mission Candidate (Cold Regions Hydrology High-Resolution Observatory)
CoSAR	Correlating SAR
COSMO-SkyMed	Constellation of Small Satellites for Mediterranean Basin Observation (Italian Satellite System)
Counter-UAS	Counter Unmanned Aerial System
COV	Coverage mask
CP	Commissioning Phase
CPACS	Common Parametric Aircraft Configuration Standard
cGPS	continuous GPS
CPU	Central Processing Unit
CR	Corner Reflector
CSA	Canadian Space Agency
CSAR	Circular SAR
CTR	Compact Test Range
CW	Continuous Wave
DAT	Defence Against Terrorism
DBF	Digital Beamforming
DBFRAM	Digital Beamforming Receive Antenna Module
DBFSAR	Digital Beamforming SAR
DEM	Digital Elevation Model
DFD	German Remote Sensing Data Center
D-GPS	Differential Global Postioning System (GPS)
Diabolo	Technologies and concept of next generation fighters
DIMS	Data Information and Management System for Earth Observation
D-InSAR	Differential Interferometric SAR
DLR	German Aerospace Center
D.MoVe	Data-Driven Mobility and Traffic Management
DO228	Dornier DO228-212 aircraft used for the E-SAR & F-SAR systems
DoA	Direction of Arrival
DPCA	Displaced Phase Center Antenna
DRA	Dual Receive Antenna mode
Dronar	DRONne rAdaR system
DSCC	DLR SAR Calibration Center
DSTL	Defence Science and Technology Laboratory, UK
DT	Data Take
DTM	Digital Terrain Model
DTU	Technical University of Denmark
dual-pol	Radar operation mode with two polarizations (e.g., HH and HV)
DuoLIM	Duo L-band SAR IMager
E2E	End-to-End
EADS	European Aeronautic Defence and Space Company (now Airbus Defence and Space)
EarthCARE	Earth Clouds, Aerosols and Radiation Explorer
ECCS	European Cooperation for Space Standardization
ECV	Essential Climate Variable
EDA	European Defence Agency
EE-10	ESA's 10th Earth Explorer
EMS-II	Mulitchannel airborne SAR for maritime security applications
ENVISAT	Environmental Satellite, ESA

Acronym	Expansion
EO	Earth Observation
EOWEB	User Interface for Earth Observation on the WEB
ERS-1/2	European Remote Sensing Satellites, ESA
ESA	European Space Agency
E-SAR	Experimental airborne SAR system of DLR (1988-2009)
ESD	Enhanced Spectral Diversity
EU	European Union
EUSAR	European Conference on Synthetic Aperture Radar
EW	Extra Wide-Swath
FaUSST	Advanced aerodynamic unmanned combat aerial vehicle stability and steering technologies
FDR	Frequency Domain Reflectometer
FDTD	Finite-Difference Time-Domain method
FEM	Finite-Element Method
FFBP	Fast Factorized Back-Projection
FFT	Fast Fourier Transform
FFT-2	DLR project dealing with UCAVs
FIS	Research Infrastructure (Forschungsinfrastruktur)
FMCW	Frequency Modulated Continuous Wave
ForestGEO	Smithsonian Tropical Forest Institute Network
FOS	Flight Operations Segment
FPGA	Field Programmable Gate Array
FR4	FR4 is a glass-reinforced epoxy laminate material
F-SAR	New airborne SAR system being developed at the Microwaves and Radar Institute of DLR
FSS	Frequency Selective Surface
FT	Fourier Transform
FTP	File Transfer Protocol
FZJ	Jülich Research Centre
GEO	Geostationary Earth Orbit
GEOMAR	Helmholtz Centre for Ocean Research Kiel
GFZ	GeoForschungsZentrum Potsdam, Germany
GHz	Gigahertz
Gigarad	Digital radar system
GMTI	Ground Moving Target Indication
GNSS	Global Navigation Satellite System
GPP	Ground Processor Prototype
GPS	Global Positioning System
GPU	Graphics Processing Unit
GS	Ground Segment
GSOC	German Space Operations Center
GTC	Geocoded Terrain Corrected
GTD	Geometrical Theory of Diffraction
Gtom	Gebäudetomograph (Tomography of buildings)
GUF	Global Urban Footprint
GUI	Graphical User Interface
HAARP	High Frequency Active Auroral Research Program
HAPS	High-Altitude Pseudo-Satellite
HE	Height Error
HEM	Height Error Map

Acronym	Expansion
HGF	Helmholtz Association (Helmholtz-Gemeinschaft Deutscher Forschungszentren e.V.)
HH	Horizontal transmit polarization, Horizontal receive polarization
HMGU	German Research Centre for Environmental Health, Helmholtz Zentrum München
HoA	Height of Ambiguity
HR	Microwaves and Radar Institute of DLR
HRTI	High-Resolution Terrain Information
HRWS	High-Resolution Wide-Swath
HS	High-Resolution Spotlight
HV	Horizontal transmit polarization, Vertical receive polarization
HZG	Helmholtz-Zentrum Geesthacht Center for Materials and Coastal Research
I/Q	Inphase/Quadrature phase detector
ICESat	Ice, Cloud and Land Elevation Satellite
IED	Improvised Explosive Device
IHE	Institute of Radio Frequency Engineering and Electronics at Karlsruhe Institute of Technology (KIT)
IF	Intermediate Frequency
IFT	Inverse Fourier Transform
IGARSS	IEEE International Geoscience & Remote Sensing Symposium
IGI	Ingenieur-Gesellschaft für Interfaces
IGOR	Integrated GPS Occultation Receiver
IMF	Remote Sensing Technology Institute of DLR
IMU	Inertial Measurement Unit
INGV	National Institute of Geophysics and Volcanology, Vesuvius Observatory Naples
INS	Inertial Navigation System
InSAR	Interferometric SAR
InSARap	Sentinel-1 INSAR Performance Study with TOPS Data
INTA	National Institute of Aerospace Technology (Spanish space agency)
IOCS	Instrument Operations and Calibration Segment
IoSiS	Imaging of Satellites in Space
IPCC	Intergovernmental Panel on Climate Change
IRF	Impulse Response Function
IRIS	Interferometric Radar for Ice, glaciers and permafrost dynamicS
ISAR	Inverse SAR
ISLR	Integrated Sidelobe Ratio
ISS	International Space Station
ITEM-FK	Innovative missile technologies and methods
ITU	International Telecommunication Union
IW	Interferometric Wide-Swath
JAXA	Japan Aerospace Exploration Agency
JPL	Jet Propulsion Laboratory
K&C	JAXA's Kyoto and Carbon initiative
KABUL	Concept for the detection and neutralisation of unmanned aerial vehicles
KARI	Korea Aerospace Research Institute
KIT	Karlsruhe Institute of Technology
LC	Liquid Crystal
LDR	Large Deployable Reflector
LEO	Low Earth Orbit
LIDAR	LIght Detection And Ranging
LLB	Institute of Lightweight Construction, TUM

Acronym	Expansion
LNA	Low-Noise Amplifier
LO	Local Oscillator
LOCASS	LOcal Air Surveillance System for Security purposes
LOEWE-STT	Landes-Offensive zur Entwicklung Wissenschaftlich-ökonomischer Exzellenz - Sensors Towards Terahertz
LoS	Line of Sight
LPAS	Laborsystem zur Personen-Abbildung mit Scanner
LRC	Low-Reflection Coating
LSB	Lower Side-Band
LTDB	Long-Term Data Base
LVIS	Land Vegetation and Ice Sensor
MAPS	Multiple Azimuth Phase Centers
Mephisto	Military research on techniques and technologies for a UAV master plan
MEO	Medium Earth Orbit
MIMO	Multiple-Input Multiple-Output
MirrorSAR	A novel fractionated radar concept developed at the Institute
MMIC	Monolithic Microwave Integrated Circuit
MMTI	Maritime Moving Target Indication
MMV	Multiple-Measurement-Vectors
MMW	MilliMeterWave
MoD	Ministry of Defense
MoM	Method of Moments
MOS	Mission Operations Segment
MOSES	Modular Observation Solutions for Earth Systems
MSMP	Multi-Satellite Mission Planner
MTI	Moving Target Indication
MTM	MeTaMaterial
MVDR	Minimum Variance Distortionless Response
NASA	National Aeronautics and Space Administration
NESZ	Noise Equivalent Sigma Zero
NORAD	North American Aerospace Defense Command
ONERA	Office National d'Études et de Recherches Aérospatiales, France
PALSAR	Phased Array L-band Synthetic Aperture Radar on board ALOS
PASTA	Post-Processing Algorithm for Squint and Topography Accommodation
PAZ	A TerraSAR-X-like satellite which has been developed for Hisdesat in Spain and launched in 2018
PCC	Pulse-Coded Calibration
PCT	Polarization Coherent Tomography
PDF	Probability Density Function
PDGS	Payload and Data Ground Segment
PDR	Preliminary Design Review
PGS	Payload Ground Segment
PICOSAR	Passive Interferometric Ocean Currents Observation Synthetic Aperture Radar
PN	Pseudo Noise
PO	Physical Optics
Pol-InSAR	Polarimetric SAR Interferometry
PPP	Public Private Partnership
PPS	Pulse Per Second
PRF	Pulse Repetition Frequency
PRISMA	Hyperspectral PRecursor of the Application Mission

Acronym	Expansion
PS	Permanent Scatterer (processing technique)
PSI	Persistent Scatterer Interferometry
PSLR	Peak-to-Sidelobe Ratio
PTD	Physical Theory of Diffraction
quad-pol	Fully polarimetric radar operation mode (HH, HV, VV, VH)
R&D	Research and Development
Radarsat-2	Second Canadian SAR satellite
RADIAN	RADar Image Analysis
RAM	Radar Absorbing Material
RASR	Range Ambiguity-to-Signal Ratio
RCM	RADARSAT Constellation Mission (Canadian Spaceborne SAR mission)
RCMC	Range Cell Migration Correction
RCMT	RCM Transponder (transponder developed by DLR for the Canadian RCM project)
RCS	Radar Cross Section
RF	Radio Frequency
RFI	Radio Frequency Interference
RGB	Red-Green-Blue
RGI	Radar Geometry Image
rms	Root Mean Square
RP	Repeat-Pass
RSE	Space-based surveillance and security (DLR project)
RVoG	Random Volume over Ground
Rx	Receive
SAOCOM	Satélite Argentino de Observación COn Microondas (Argentine Microwaves Observation Satellite)
SAOCOM-CS	SAOCOM Companion Satellite
SAR	Synthetic Aperture Radar
SARah	SAR-Lupe follow on mission
SARah NG	SARah follow on mission (Next Generation)
SAREF	SAR EFfects simulator
SAR-Lupe	Constellation of 5 high-resolution X-band SAR satellites (Germany)
SATA	Sub-Aperture Topography- and aperture-dependent Algorithm
SBAS	Small BASeline (processing technique)
SBR	Shooting and Bouncing Rays
SCORE	SCan-On-REceive
SD	Spectral Diversity
Sentinel-1	C-band SAR satellites developed by ESA in the scope of the European Copernicus program
SEPIA	Special filter of RADIAN, filtering method for despeckling and sidelobe reduction without loss of resolution
SESAME	SEntinel-1 SAR Companion Multistatic Explorer
SETES	SAR End-To-End Simulation
SETHI	ONERA's airborne SAR system
SGP4	Simplified General Perturbation model
SIGNAL	SAR for Ice, Glacier, aNd globAL dynamics
SIR-C	Shuttle Imaging Radar-C
SLC	Single Look Complex
SM	Strimap
SNR	Signal-to-Noise Ratio
SRTM	Shuttle Radar Topography Mission
SSA	Space Situational Awareness

Acronym	Expansion
SSD	Solid State Disk
SSN	Space Surveillance Network
ST	Staring-spotlight
STAP	Space-Time Adaptive Processing
STEP	SAR TEchnology Processor
STRATOSAR	STRATOspheric Synthetic Aperture Radar
STSO	Short-Term Shift-Orthogonal
SUM	Surveillance in an Urban environment using Mobile sensors
SUMIRAD	SUM Imaging RADiometer
SVD	Singular Value Decomposition
TAD	Topography adaptive and Aperture Dependent motion compensation
TanDEM-X	TerraSAR-X add-on for Digital Elevation Measurement mission
TAP	TanDEM-X Acquisition Planner
TASR	Total Ambiguity-to-Signal Ratio
TAXI	TanDEM-X interferometric processor
TDX	TanDEM-X spacecraft
TEC	Total Electron Content
TechLab	Facility for microwave sensor development with laboratories and large-scale measurement test sites
TERENO	TERestrial ENvironmental Observatories (HGF project)
TerraSAR-X	German high-resolution X-band radar mission
TimeDAT	Time-Domain Analysis Tool
TIRAMI-SAR	Toolbox Implementation for Removal of Anti-personnel MInes – Synthetic Aperture Radar (sensor system)
TIRAMISU	Toolbox Implementation for Removal of Anti-personnel MInes, Sub-Munitions and UXO (EU project)
TLE	Two-Line Elements
TomoSAR	Tomographic SAR
TOPS	Terrain Observation by Progressive Scans
TRAMRAD	TRAffic Monitoring with RADar (former DLR project)
TRL	Technological Readiness Level
TRM	Transmit/Receive Module
TSX	TerraSAR-X spacecraft
TUM	Technical University of Munich
TWT	Travelling Wave Tube
Tx	Transmit
UAV	Unmanned Aerial Vehicle
UCAV	Unmanned Combat Aerial Vehicle
UFZ	Helmholtz Center for Environmental Research
UHF	Ultra-High Frequency
UNFCCC	United Nations Framework Convention on Climate Change
Unirad	Universal radar system
USB	Upper Side-Band
UTD	Uniform geometrical Theory of Diffraction
UTM	Universal Transverse Mercator
UXO	Unexploded Ordnance
VABENE ++	Traffic monitoring for major events and disasters (DLR project)
VAC	Volts Alternating Current
VBS	Virtual Beam Synthesis
VDC	Volts Direct Current
VeGA	Verkürzte Gauß Antenne (shortened Gauss antenna)

Acronym	Expansion
VENI	Visibility, Ephemeris and Numerous other Investigations for satellite orbit analysis
VERITAS	Venus Emissivity, Radio Science, In-SAR, Topography, And Spectroscopy mission
VESAS	VollElektronischer Scanner mit AperturSynthese (fully electronic scanner using aperture synthesis)
VH	Vertical transmit polarization, Horizontal receive polarization
VHF	Very High Frequency
VISAR	Venus Interferometric Synthetic Aperture Radar payload on-board VERITAS
VNA	Vector Network Analyzer
VV	Vertical transmit polarization, Vertical receive polarization
WAM	WAter indication Mask
WGS	World Geodetic System
WGS84	World Geodetic System 1984
Wi-Fi	Wireless local area network
WM	Wave Mode
WRLageZ	Weltraumlagezentrum (space situational awareness center operated by the German Federal Army)
X-SAR	X-band Synthetic Aperture Radar
XTI	Across-Track Interferometry

Acknowledgements

A large team of Institute's members contributed to this report and their names are recognized below:
(A = Author, R = Reviewer)

Anger, Simon (A)
Anglberger, Harald (A)
Antesberger, Klara (A, R)
Bachmann, Markus (A, R)
Baumgartner, Stefan (A, R)
Börner, Thomas (A)
Bojarski, Allan (R)
Buckreuss, Stefan (A)
Chiari, Martin Freiherr von (A)
Dietrich, Björn (A)
Dill, Stephan (A)
Eilers, Jan (A, R)
Fischer, Jens (A)
Gabler, Bernd (A)
Gracheva, Valeria (R)
Grigorov, Christo (A, R)
Hajnsek, Irena (A)
Heistser, Anton (A)
Horn, Ralf (A)
Huber, Sigurd (R)
Iff, Sebastian (A)
Jäger, Marc (A, R)
Jagdhuber, Thomas (R)
Jirousek, Matthias (A, R)
Kaschke, Markus (A)
Kim, Jun Su (A)
Keller, Martin (A)
Kempf, Timo (A)
Kemptner, Erich (A, R)
Klämke, Juliane (R)
Klenk, Patrick (A, R)
Kraus, Thomas (A, R)
Krieger, Gerhard (A, R)
Laux, Christopher (R)
Limbach, Markus (A)
Lützner, Mark (R)
Martín del Campo Becerra, Gustavo (R)
Martone, Michele (R)
Middeler, Sandra (A, R)
Mittermayer, Josef (A)
Nannini, Matteo (A, R)
Neff, Thomas (A, R)
Nottensteiner, Anton (A)
Osipov, Andrey (A)
Papathanassiou, Konstantinos (A)
Pardini, Matteo (A, R)
Peichl, Markus (A, R)
Pinheiro, Muriel Aline (R)
Prats, Pau (A)
Profelt, Juliane (R)
Queiroz de Almeida, Felipe (R)
Reigber, Andreas (A, R)
Reigber, Sandra (R)
Reimann, Jens (A, R)
Rizzoli, Paola (A, R)
Rodríguez-Cassolà, Marc (A)
Sanjuan Ferrer, Maria Jose (R)
Scheiber, Rolf (A, R)
Schmidt, Kersten (R)
Schreiber, Eric (A, R)
Schwerdt, Marco (A, R)
Sica, Francescopaolo (R)
Speck, Rainer (A, R)
Umrath, Stefan (A)
Yague-Martinez, Nestor (R)
Younis, Marwan (A, R)
Villamil López, Carlos (A,R)
Villano, Michelangelo (R)
Weidenhaupt, Klaus (A)
Zink, Manfred (A, R)
Zonno, Mariantonietta (A, R)

I would also like to recognize the entire Institute's staff for their exemplary engagement, hard work and outstanding research results. The complete list of the Institute's members is given in the second volume of this report.

Alberto Moreira

DLR at a glance

DLR is the national aeronautics and space research center of the Federal Republic of Germany. Its extensive research and development work in aeronautics, space, energy, transport and security is integrated into national and international cooperative ventures. In addition to its own research, as Germany's space agency, DLR has been given responsibility by the federal government for the planning and implementation of the German space program.

DLR is also the umbrella organization for the nation's largest project management agency. DLR has approximately 8000 employees at 20 locations in Germany: Cologne (headquarters), Augsburg, Berlin, Bonn, Braunschweig, Bremen, Bremerhaven, Dresden, Goettingen, Hamburg, Jena, Juelich, Lampoldshausen, Neustrelitz, Oberpfaffenhofen, Oldenburg, Stade, Stuttgart, Trauen, and Weilheim. DLR also has offices in Brussels, Paris, Tokyo and Washington D.C.

Microwaves and Radar Institute

With its know-how and expertise in passive and active microwave remote sensing, the Microwaves and Radar Institute contributes to the development and advancement of ground-based, airborne and spaceborne sensors with applications in Earth observation, aeronautics, traffic monitoring, and reconnaissance and security. The focus of its research work is on the conception and development of innovative synthetic aperture radar (SAR) techniques and systems, as well as new sensor-specific applications for Earth observation. In the last 15 years, the Institute has provided major contributions to several SAR missions like TerraSAR-X, TanDEM-X, Sentinel-1A/B, and SAR-Lupe. It is also working on future remote sensing and reconnaissance systems, such as Tandem-L, HRWS, Sentinel-1C/D, BIOMASS and SARah. The mission TanDEM-X, initiated and led by the Institute, has generated a global, high-resolution digital elevation model of the Earth with unprecedented accuracy. By means of these projects and scientific programs the Institute provides an essential contribution to existing and future SAR missions towards the vision of a radar observatory in space for continuous observation of dynamic processes on the Earth surface.

Imprint

Publisher:
German Aerospace Center (DLR)
Microwaves and Radar Institute

Address:
Münchener Straße 20
82234 Weßling
Germany
Phone + 49 (0) 8153 28-2305
e-mail DLR-HR@dlr.de

DLR.de

Images DLR (CC-BY 3.0), unless otherwise stated.

Printed on chlorine-free bleached and PEFC certified paper

Deutsches Zentrum
für Luft- und Raumfahrt
German Aerospace Center